PACIFIC EARTHQUAKE ENGINEERING
RESEARCH CENTER

Seismic Performance of Reinforced Concrete Bridges Allowed to Uplift during Multi-Directional Excitation

Andres Oscar Espinoza
Stephen A. Mahin
Department of Civil and Environmental Engineering
University of California, Berkeley

PEER 2012/02
JULY 2012

Seismic Performance of Reinforced Concrete Bridges Allowed to Uplift during Multi-Directional Excitation

Andres Oscar Espinoza

Stephen A. Mahin

Department of Civil and Environmental Engineering
University of California, Berkeley

PEER Report 2012/02
Pacific Earthquake Engineering Research Center
Headquarters at the University of California, Berkeley

July 2012

ABSTRACT

The behavior of bridges subjected to recent moderate and large earthquakes has led to bridge design detailed for better seismic performance, particularly through wider bridge foundations to handle larger expected design forces. Foundation uplift, which is not employed in conventional bridge design, has been identified as an important mechanism, in conjunction with structural yielding and soil-structure interaction that may dissipate energy during earthquakes. Preventing uplift through wider foundations looks past the technical and economic feasibility of allowing foundation uplift during seismic events. The research presented in this study is part of a larger experimental and analytical investigation to develop and validate design methods for bridge piers on shallow foundations allowed to uplift during seismic events.

Several analytical and some experimental studies have been performed to assess rocking and or uplift of shallow foundation systems, however they have evaluated systems with a limited range of footing dimensions and seismic excitations. As such, there is an uncertainty in the information needed to base a performance evaluation and develop design methods. The purpose of this study is to investigate through experimental and analytical studies the seismic performance of uplifting bridge piers on shallow foundations when considering different ground motions and footing dimensions, as well as identifying key differences in performance evaluation criteria for conventional and uplifting bridge pier systems.

The experimental study dynamically tested a single reinforced concrete bridge column specimen with three adjustable footing configurations grouped by footing dimension, and tested for various combinations of one, two, and three components of seismic excitation. Groups one and two evaluated uplifting systems where the column was limited to elastic loading levels while group three considered inelastic column loading levels. All test groups remained stable and exhibited some rocking and or uplift during testing. Analytical models were developed and validated using the experimental testing results to predict local and global footing and column response. Reliable estimates of forces and displacements during elastic and inelastic response were achieved. To assess the seismic performance of a range of bridge pier systems allowed to uplift a parametric investigation using the validated analytical models was performed in which the column was modeled per conventional design criteria to ensure adequate strength and flexural ductility. The parameters varied include footing width, ground motion excitation, and elastic or inelastic column response. Response of the uplifting bridge pier systems was found to be sensitive to the structural periods, magnitude of excitation, and footing width.

ACKNOWLEDGMENTS

Financial support for this research project was provided by the California State Department of Transportation under Contract No. 59A0433. The title of the overall project, which also involved researchers from the University of California, Davis, was "Design Guidelines for Foundation Rocking of Bridge Piers (STAP13)." The findings, observations, and conclusions contained herein are those of the authors and do not necessarily represent those of the sponsors. The thoughtful advice and encouragement provided by the Craig Whitten and Fadel Alameddine of Caltrans in planning and carrying out this work is greatly appreciated.

We would like to thank the laboratory staff at the Earthquake Engineering Research Center where much of this research work was performed: Wesley Neighbour, Don Clyde, David Maclam, and Shakhzod Takhirov. In particular, Charles James of the PEER Library was helpful in preparing this work. Graduate students at U.C. Berkeley whose help was invaluable include Kevin Mackie, Michael Scott, Gabriel Hurtado, Hyungil Jeong, Janise Rodgers, and Patxi Uriz. We also thank Dr. Frank McKenna of PEER for his assistance. Special thanks are also due to Professors Bozidar Stojadinovic and Douglas Dreger for their support and review of this work. The active collaboration of Professors Bruce Kutter and Boris Jeremic, their students, and the laboratory staff from University of California, Davis, was also instrumental in developing and carrying out the research described herein.

CONTENTS

ABSTRACT ..... **iii**
ACKNOWLEDGMENTS ..... **v**
TABLE OF CONTENTS ..... **vii**
LIST OF FIGURES ..... **xiii**
LIST OF TABLES ..... **xxi**

1 INTRODUCTION **1**
1.1 BACKGROUND 1
1.2 RESEARCH PROGRAM OBJECTIVES 3
1.3 ORGANIZATION OF REPORT AND SCOPE 4

2 LITERATURE REVIEW **5**
2.1 INTRODUCTION 5
2.2 STRUCTURAL SYSTEMS WITH UPLIFTING FOUNDATION 5
2.2.1 Analytical Investigations 5
2.2.2 Experimental Studies 10
2.3 DESIGN OF UPLIFTING FOUNDATION SYSTEMS 10
2.4 SUMMARY 18

3 EXPERIMENTAL TEST PROGRAM **19**
3.1 INTRODUCTION 19
3.2 PROTOTYPE COLUMN 20
3.3 DESIGN OF SPECIMENS 21
3.3.1 Model Scaling 21
3.3.2 Design of Test Specimens 22
3.3.3 Footing 24
3.3.4 Elastomeric Pad 25
3.3.5 Steel Brackets 26
3.3.6 Mass Blocks 26
3.4 SPECIMEN CONSTRUCTION 27
3.5 MEASURED MATERIAL PROPERTIES 30
3.5.1 Steel Reinforcement Properties 30
3.5.2 Concrete Properties 31

3.5.3 Elastomeric Pad 33
3.6 TEST SET UP 34
3.7 INSTRUMENTATION 37
3.7.1 Shaking Table Instrumentation 39
3.7.2 Accelerometers 40
3.7.3 Linear Potentiometers 40
3.7.4 Direct Current Displacement Transducers 41
3.7.5 Strain Gauges 45
3.7.6 Novotechniks (NOVOs) 45
3.8 DATA ACQUISITION 47
3.9 TEST SPECIMEN DOCUMENTATION 47
3.10 GROUND MOTIONS 47
3.10.1 Preprocessing of the Recorded Motions 47
3.10.2 1989 Loma Prieta Earthquake (Loma Prieta Record) 48
3.10.3 1978 Tabas, Iran, Earthquake 48
3.11 TEST SEQUENCE 52
3.11.1 Pullback (Free Vibration) Test 52
3.11.2 Shake Table Test 52

4 EXPERIMENTAL RESULTS 55

4.1 INTRODUCTION 55
4.2 ROCKING SYSTEM RESPONSE QUANTITIES 56
4.2.1 Displacements 56
4.2.2 Forces and Moments 58
4.3 OBSERVED COLUMN RESPONSE 60
4.4 RECORDED RESULTS 71
4.5 TEST SPECIMEN WITH DESIGN AXIAL LOAD AND 3DC X 3DC FOOTING 71
4.5.1 Global Displacement 71
4.5.2 Local Response 86
4.5.3 Force-Displacement Hysteresis Curves 90
4.6 TEST SPECIMEN WITH DESIGN AXIAL LOAD AND 5DC X 3DC FOOTING 98
4.6.1 Global Displacement 98
4.6.2 Local Response 107

4.6.3 Force-Displacement Hysteresis Curves 108
4.7 APPLIED MOMENT VERSUS RESTORING MOMENT 114
4.8 INTERACTION OF PRINCIPAL DISPLACEMENTS 116
4.9 NATURAL PERIOD AND DAMPING 118
4.10 CONCLUSIONS 118

5 VALIDATED ANALYSIS OF EXPERIMENTAL RESULTS 121
5.1 INTRODUCTION 121
5.2 MATERIAL MODELING 122
5.2.1 Reinforcing Steel 122
5.2.2 Concrete 122
5.2.3 Elastomeric Pad 124
5.3 MODELING OF REINFORCED CONCRETE BRIDGE PIER 127
5.3.1 Fiber Element Modeling 128
5.3.2 Column 130
5.3.3 Footing - Soil Structure Interaction 133
5.3.4 Damping 137
5.4 ELASTIC FOOTING ANALYSIS 137
5.4.1 3Dc x 3Dc Square Footing Configuration 142
5.4.2 5Dc x 3Dc Square Footing Configuration 144
5.5 COMPARISON OF LINEAR ANALYSIS AND EXPERIMENTAL RESULTS 145
5.5.1 Design Axial Load and 3Dc × 3Dc Footing 146
5.5.2 Accelerations 156
5.5.3 Design Axial Load and 5Dc x 3Dc Footing 161
5.5.4 Displacements 161
5.5.5 Accelerations 161
5.6 COMPARISON OF NONLINEAR ANALYSIS AND EXPERIMENTAL RESULTS 164
5.6.1 Design Axial Load and 5Dx x 3Dc Footing 164
5.7 SUMMARY AND CONCLUSIONS 175
5.7.1 Summary 175
5.7.2 Conclusions 176

6 PARAMETRIC INVESTIGATION OF UPLIFTING BRIDGE PIERS 179

6.1 INTRODUCTION 179

6.2 SUMMARY OF OBJECTIVES 180

6.3 UPLIFTING BRIDGE PIER SYSTEM 180

6.3.1 Notation 181

6.3.2 Column and Superstructure 181

6.3.3 Footing 182

6.3.4 Soil 182

6.3.5 Soil Springs 183

6.3.6 Natural Period 184

6.3.7 Damping 184

6.3.8 Ground Motions 184

6.4 PERFORMANCE EVALUATION OF UPLIFTING BRIDGE PIER SYSTEM 187

6.4.1 Pushover Analysis 187

6.4.2 Dynamic Analysis 192

6.4.3 Spectral Analysis 198

6.5 SPECTRAL ACCELERATION RESPONSE OF UPLIFTING BRIDGE PIER SYSTEM 203

6.5.1 Elastic Column and Soil 203

6.5.2 Inelastic Column and Elastic Soil 209

6.5.3 Elastic Column and Soil 212

6.5.4 Inelastic Column and Elastic Soil 221

6.6 DISPLACEMENT DUCTILITY RESPONSE OF UPLIFTING BRIDGE PIER SYSTEM 226

6.7 SPECTRAL RELATIONSHIP OF UPLIFTING TO FIXED BASE SYSTEMS 228

6.7.1 Acceleration 229

6.7.2 Displacement 229

6.7.3 Ductility 230

6.8 UPLIFTING BRIDGE PIER GUIDELINE RECOMMENDATIONS 236

6.8.1 Design Guidance 236

6.8.2 Benefits 236

6.8.3 Negative Consequences 237

6.8.4 Recommendations 238

7 CONCLUSIONS 241
7.1 EXPERIMENTAL INVESTIGATION OF UPLIFTING SYSTEMS 241
7.2 ANALYTICAL MODELING OF UPLIFTING SYSTEMS 242
7.3 PARAMETRIC STUDY 243
7.4 FUTURE RESEARCH 246

REFERENCES 247

APPENDIX A EXPERIMENTAL TEST SCHEDULE 251

APPENDIX B EXPERIMENTAL TEST RESULTS 255

APPENDIX C TCL CODE – 3D SHALLOW FOUNDATIONS ALLOWED TO UPLIFT 293

LIST OF FIGURES

Figure 1.1 Generalized bridge with spread footings. 3

Figure 2.1 Uplifting elastic column models on spread footing. 7
Figure 2.2 Base shear spectra uplifting system with $h/b = 10$. 7
Figure 2.3 M-ϕ column response of RC bridge column. 9
Figure 2.4 Uplifting column model. 12
Figure 2.5 Nonlinear Winkler foundation. 13
Figure 2.6 C_1 ratio of maximum lateral displacement with/without footing uplift. 15
Figure 2.7 Two-column bridge bent column and footing rotations. 17

Figure 3.1 Prototype column. 20
Figure 3.2 Specimen with mass blocks. 23
Figure 3.3 Column reinforcement details. 24
Figure 3.4 Footing reinforcement details. 25
Figure 3.5 Footing configuration for $3D_c \times 5\ D_c$. 25
Figure 3.6 Elastomeric pad and footing edges. 26
Figure 3.7 Footing forms (rocking column at top right). 28
Figure 3.8 Column cage and footing steel. 28
Figure 3.9 Casting footing. 29
Figure 3.10 Footing and blocks before column casting (rocking column center of specimens). 29
Figure 3.11 Threaded rods for measuring column curvature. 30
Figure 3.12 Column and top block (rocking specimen in center). 30
Figure 3.13 Stress-strain curve for grade 60 ASTM 706 bars. 31
Figure 3.14 Stress-strain curve of concrete cylinders at test date. 33
Figure 3.15 Column concrete compressive strength versus age. 33
Figure 3.16 Stress-strain curve of compression test of 2 in.-thick elastomeric pad sample. 34
Figure 3.17 Group 2 specimen set up. 35
Figure 3.18 Specimen configuration for Test Group 1. 36
Figure 3.19 Group 2 specimen. 37
Figure 3.20 Footing configuration with safety restraints. 37

Figure 3.21 Specimen global sign convention. 39
Figure 3.22 Shaking table instrumentation. 40
Figure 3.23 DCDT configuration along column height. 41
Figure 3.24 Group 1 ($3D_c$x$3D_c$ footing) instrumentation details. 42
Figure 3.25 Group 2 (3Dc×3Dc footing) elevation of instrumentation details. 43
Figure 3.26 Group 3 (3Dc×5Dc footing) elevation of instrumentation details. 44
Figure 3.27 Locations of strain gauges. 45
Figure 3.28 Novotechnik locations (Test Groups 1 and 2). 46
Figure 3.29 Novotechnik locations (Test Group 3). 46
Figure 3.30 NF01 and NF02 horizontal filtered ground motion. 49
Figure 3.31 NF03 and NF04 horizontal filtered ground motion. 50
Figure 3.32 Vertical filtered ground motion. 51

Figure 4.1 Displacement response quantities. 57
Figure 4.2 Free body diagram. 59
Figure 4.3 Footing free body diagram. 60
Figure 4.4 Test Group 1 with footing 3Dc × 3Dc and low axial load following final run. 62
Figure 4.5 Specimen damage condition with 3Dc × 3Dc footing after run D5S. 66
Figure 4.6 Damage condition of specimen with 3Dc×5Dc footing following run A3R. 68
Figure 4.7 Damage condition of specimen with 3Dc × 5Dc footing following Run A4R (safety chains tightened subsequent to testing). 69
Figure 4.8 Damage condition of specimen with 3Dc × 5Dc footing following Run A4R. 70
Figure 4.9 Illustration of terminology used to describe total displacements. 72
Figure 4.10 Displacement response: 1, 2, 3 components of excitation (Test Set AS). 74
Figure 4.11 Displacement response: 1, 2, 3 components of excitation (Test Set DS). 75
Figure 4.12 Displacement response: 1, 2, 3 components of excitation (Test Set FS). 76
Figure 4.13 Test Group 2: rocking contribution to maximum center mass lateral displacement. 78
Figure 4.14 Test Group 2: rocking and flexure contribution to peak lateral displacement. 79
Figure 4.15 Illustration of terminology for footing vertical displacement. 80
Figure 4.16 AS centerline edge footing uplift response 82
Figure 4.17 DS centerline edge footing uplift response. 83
Figure 4.18 DS centerline envelope footing uplift response. 84
Figure 4.19 DS contour footing uplift response. 85

Figure 4.20 Test Set DS and FS twisting about vertical axis. 87
Figure 4.21 Recorded column curvatures along column height. 88
Figure 4.22 Reinforcing steel strain for south rebar (Test D5S). 89
Figure 4.23 Cumulative strain time history test D5S. 90
Figure 4.24 DS column base moment time history. 91
Figure 4.25 FS column base moment time history. 91
Figure 4.26 Lateral force versus lateral displacement (Tests AS, DS, FS). 93
Figure 4.28 Moment-footing rotation characteristics. 96
Figure 4.29 D3S footing rotation. 96
Figure 4.30 Column base moment footing rotation response (Tests AS, DS, FS). 97
Figure 4.31 Elastic level Test A1R displacement response. 100
Figure 4.32 Yield level Test A2R displacement response. 100
Figure 4.33 Design level Test A3R displacement response. 101
Figure 4.34 Maximum level Test A4R displacement response. 101
Figure 4.35 AR test set ratio of rocking to total displacement. 102
Figure 4.36 AR test set - footing uplift response (centerline edges). 104
Figure 4.37 AR test set – envelope of peak footing uplift (centerlines). 105
Figure 4.38 AR test set – contours of max/min footing uplift. 106
Figure 4.39 Test set AR twisting about vertical axis. 107
Figure 4.40 Column curvatures (Tests A3R and A4R). 108
Figure 4.41 Lateral force versus lateral displacement (Test A2R, A3R, A4R). 110
Figure 4.42 Column base moment-curvature response (Test A2R, A3R, A4R). 111
Figure 4.43 Column base moment-footing rotation (Test A2R, A3R, A4R). 113
Figure 4.44 Normalized interaction displacements for Test Groups 1 and 2 ($3D_c \times 3D_c$). 117

Figure 5.1 Analytic material modeling for analysis. 124
Figure 5.2 OpenSees Neoprene material model characteristics. 126
Figure 5.3 Fiber section representation of column. 129
Figure 1.1 Column element with fiber sections. 129
Figure 5.5 Moment-curvature relationship of column section. 130
Figure 5.6 General column model. 131
Figure 5.7 Elastic column model. 132
Figure 5.8 Force-based beam column models. 133

Figure 5.9 Beam on Nonlinear Winkler Foundation model. 135
Figure 5.10 Discretization of 3D footing model. 135
Figure 5.11 Beam-On-Nonlinear-Winkler-Foundation three-dimensional model. 136
Figure 5.12 Analytic model of uplifting bridge pier system. 136
Figure 5.13 Footing force deformation relationship formulation. 138
Figure 5.14 Analytic model moment rotation relationship of footing (ENT springs). 141
Figure 5.15 M-θ analytic envelope of 3Dc square footing (test D5S ENT springs). 143
Figure 5.16 M-θ analytic envelope of 3Dc square footing (test F5S ENT springs). 143
Figure 5.17 M-θ analytic envelope 3Dc square footing (test D5S neoprene springs). 144
Figure 5.18 M-θ analytic envelope of 3Dc square footing (test F5S neoprene springs). 144
Figure 5.19 M-θ analytic envelope $3D_c \times 5D_c$ footing (test A2R ENT springs). 145
Figure 5.20 M-θ analytic envelope of $3D_c \times 5D_c$ footing (test A2R neoprene springs). 145
Figure 5.21 Center mass displacement – elastic column ENT springs (D1S). 149
Figure 5.22 Center mass displacement – elastic column neoprene springs (D1S). 149
Figure 5.23 Center mass displacement – elastic column ENT springs (F1S). 149
Figure 5.24 Center mass displacement – elastic column neoprene springs (F1S). 150
Figure 5.25 Center mass displacement – distributed plasticity column ENT springs (D1S). 150
Figure 5.26 Center mass displacement – distributed plasticity column neoprene springs (D1S). 150
Figure 5.27 Center mass displacement – lumped plasticity column ENT springs (D1S). 151
Figure 5.28 Center mass displacement – lumped plasticity column neoprene springs (D1S). 151
Figure 5.29 Elastic column neoprene springs – displacements comparison (D1S). 152
Figure 5.30 Elastic column neoprene springs – displacements comparison (D3S). 153
Figure 5.31 Elastic column neoprene springs – displacements comparison (D5S). 154
Figure 5.32 Elastic column neoprene springs – displacements comparison (F5S). 155
Figure 5.33 Center mass acceleration – elastic column neoprene springs (D1S). 156
Figure 5.34 Center mass acceleration – elastic column neoprene springs (D3S). 156
Figure 5.35 Center mass acceleration – elastic column neoprene springs (D5S). 157
Figure 5.36 Center mass acceleration – elastic column neoprene springs (F5S). 157
Figure 5.37 Column base M-ϕ – elastic column neoprene springs (D1S) 158
Figure 5.38 Column base M-ϕ – elastic column neoprene springs (D3S) 158
Figure 5.39 Column base M-ϕ – elastic column neoprene springs (D5S) 159
Figure 5.40 Column base M-ϕ – elastic column neoprene springs (F5S). 159

Figure 5.41 Footing moment rotation M-ϕ – elastic column neoprene springs (D1S)..... 159
Figure 5.42 Footing moment rotation M-ϕ – elastic column neoprene springs (D3S)..... 160
Figure 5.43 Footing moment rotation M-ϕ – elastic column neoprene springs (D5S)..... 160
Figure 5.44 Footing moment rotation M-ϕ – elastic column neoprene springs (F5S). 160
Figure 5.45 Center mass total displacement – elastic column neoprene springs (A2R). 161
Figure 5.46 Center mass flexural displacement – elastic column neoprene springs (A2R)... 162
Figure 5.47 Footing rotation – elastic column neoprene springs (A2R). 162
Figure 5.48 Center mass acceleration – elastic column ENT springs (A2R). 162
Figure 5.49 Column base M-ϕ – elastic column ENT springs (A2R). 163
Figure 5.50 Footing moment rotation M-θ – elastic column ENT springs (A2R). 164
Figure 5.51 Design .level earthquake – distributed plasticity column with neoprene springs CG displacements, bilinear steel (A3R). 166
Figure 5.52 Design-level earthquake - distributed plasticity column with neoprene springs CG displacements, reinforcing steel (A3R). 166
Figure 5.53 Design-level earthquake concentrated plasticity column with neoprene springs CG displacements, bilinear steel (A3R). 167
Figure 5.54 Design-level earthquake concentrated plasticity column with neoprene springs CG displacements, reinforcing steel (A3R). 167
Figure 5.55 Design-level earthquake concentrated plasticity column with neoprene springs column flexural displacements (A3R). 168
Figure 5.56 Design-level earthquake concentrated plasticity column with neoprene springs footing rotation (A3R). 168
Figure 5.57 Maximum-level earthquake concentrated plasticity column with neoprene springs CG displacements (A4R)..... 169
Figure 5.58 Maximum-level earthquake concentrated plasticity column with neoprene springs column flexural displacements (A4R). 169
Figure 5.59 Maximum-level earthquake concentrated plasticity column with neoprene springs footing rotation (A4R). 170
Figure 5.60 Design-level earthquake concentrated plasticity column with neoprene springs CG accelerations (A3R). 171
Figure 5.61 Maximum-level earthquake concentrated plasticity column with neoprene springs CG accelerations (A4R). 171
Figure 5.62 Design-level earthquake concentrated plasticity column with neoprene springs column base M-ϕ (A3R). 173
Figure 5.63 Maximum-level earthquake concentrated plasticity column with neoprene springs column base M-ϕ (A4R). 173

Figure 5.64 Design-level earthquake concentrated plasticity column with neoprene springs footing moment rotation M-θ (A3R). 174
Figure 5.65 Maximum-level earthquake concentrated plasticity column with neoprene springs footing moment rotation M-θ (A4R). 174

Figure 6.1 Prototype column. 181
Figure 6.2 Pushover analysis (elastic or nonlinear column – elastic soil). 188
Figure 6.3 Pushover analysis (nonlinear column-soil). 189
Figure 6.4 Footing moment rotation (elastic or nonlinear column – elastic soil). 190
Figure 6.5 Footing moment rotation (nonlinear column-soil). 190
Figure 6.6 Soil springs versus rotation (elastic or nonlinear column – elastic soil). 191
Figure 6.7 Soil springs versus rotation (nonlinear column-soil). 191
Figure 6.8 Acceleration time history (elastic column and soil). 192
Figure 6.9 Acceleration time history (nonlinear column-elastic soil). 193
Figure 6.10 Displacement rime history (elastic column and soil). 194
Figure 6.11 Displacement time history (nonlinear column-elastic soil). 195
Figure 6.12 Moment time history (elastic column and soil). 196
Figure 6.13 Moment time history (nonlinear column-elastic soil). 196
Figure 6.14 Moment-footing rotation (elastic column and soil). 197
Figure 6.15 Moment curvature (nonlinear column-elastic soil). 198
Figure 6.16 Spectral acceleration; elastic column and soil 1D excitation (Oak_10_50_6). .. 199
Figure 6.17 Spectral acceleration; nonlinear column-elastic soil 1D excitation. (Oak_10_50_6). 199
Figure 6.18 Spectral displacement; elastic column-soil 1D excitation (Oak_10_50_6). 201
Figure 6.19 Spectral displacement; nonlinear column-elastic soil 1D excitation (Oak_10_50_6). 202
Figure 6.20 S_A representative mean response (10% in 50 years 1D). 204
Figure 6.21 S_A mean response; elastic column-soil (all ground motions 1D). 206
Figure 6.22 S_A mean response; elastic column-soil (near fault 3D). 207
Figure 6.23 S_A mean response; elastic column-soil (2% in 50 years 3D). 207
Figure 6.24 S_A mean response; elastic column-soil (10% in 50 years 3D). 208
Figure 6.25 S_A mean response; elastic column-soil (50% in 50 years 3D). 208
Figure 6.26 S_A mean response; nonlinear column-elastic soil (all ground motions 3D). 210
Figure 6.27 S_A mean response; nonlinear column-elastic soil (near fault 3D). 211
Figure 6.28 S_A mean response; nonlinear column-elastic soil (2% in 50 years 3D). 211

Figure 6.29 S_A mean response; nonlinear column-elastic soil (10% in 50 years 3D). 211
Figure 6.30 S_D representative mean response (10% in 50 years 1D). 213
Figure 6.31 S_D mean response; elastic column-soil (near fault 1D). 215
Figure 6.32 S_D mean response; elastic column-soil (2% in 50 years 1D). 215
Figure 6.33 S_D mean response; elastic column-soil (10% in 50 years 1D). 216
Figure 6.34 S_D mean response; elastic column-soil (50% in 50 years 1D). 216
Figure 6.35 S_D Mean response; elastic column-soil (near fault 3D). 217
Figure 6.36 S_D mean response; elastic column-soil (2% in 50 years 3D). 218
Figure 6.37 S_D mean response; elastic column-soil (10% in 50 years 3D). 219
Figure 6.38 S_D mean response; elastic column-soil. (50% in 50 years 3D). 220
Figure 6.39 S_D mean response; nonlinear column-elastic soil. (near fault 1D)..... 222
Figure 6.40 S_D mean response; nonlinear column-elastic soil. (2% in 50 years 1D). 222
Figure 6.41 S_D mean response; nonlinear column-elastic soil. (10% in 50 years 1D). 223
Figure 6.42 S_D mean response; nonlinear column-elastic soil (near-fault 3D). 224
Figure 6.43 S_D mean response; nonlinear column-elastic soil (2% in 50 years 3D). 225
Figure 6.44 S_D mean response; nonlinear column-elastic soil (10% in 50 years 3D). 226
Figure 6.45 Displacement ductility response. 228
Figure 6.46 R_R elastic column-elastic soil. 231
Figure 6.47 R_R nonlinear column-elastic soil. 232
Figure 6.48 γ_R and γ_{RF} elastic column-elastic soil. 233
Figure 6.49 γ_R and γ_{RF} nonlinear column-elastic soil. 234
Figure 6.50 μ_R ductility ratio. 235

LIST OF TABLES

Table 2.1 Lateral displacement comparison of shear wall model using various methods ... 15

Table 2.2 Base shear comparison of shear wall model using various methods. ... 16

Table 3.1 Similitude requirements and scale factors for column test. ... 22

Table 3.2 Concrete mix design. ... 32

Table 3.3 Compressive strength of column concrete cylinders. ... 32

Table 3.4 Testing schedule of rocking column. ... 53

Table 3.5 Summary of peak ground motion values for all test groups. ... 53

Table 4.1 Summary of Test Group 1 response footing size 3Dc × 3Dc with low axial load. ... 63

Table 4.2 Summary of Test Group 2 response footing size 3Dc × 3Dc ... 65

Table 4.3 Summary of test Group 3 response footing size 3Dc × 5Dc. ... 67

Table 4.4 Column and footing moment characteristic values. ... 114

Table 4.5 Ratio of applied to restoring moment (β uplift likelihood) ... 116

Table 4.6 Natural period and damping of test specimens. ... 118

Table 5.1 Footing vertical stiffness values ... 142

Table 5.2 Linear analysis modeling options. ... 147

Table 6.1 Parametric soil spring model parameters. ... 183

Table 6.2 Parametric investigation ground motions. ... 186

Table 6.3 Uplifting system response values ... 189

Table 6.4 Uplifting system ratios of response parameters. ... 237

1 Introduction

1.1 BACKGROUND

Recent moderate to large earthquakes have caused significant damage to bridge structures around the world. Such examples include the 1989 Loma Prieta, 1994 Northridge, and 1995 Kobe earthquakes. These events subjected many types of bridges to intense ground motions that resulted in a wide range of damage states, from little to no damage, to catastrophic failures in some cases. Newer bridges that have been detailed for better performance during seismic events did particularly well. Nonetheless, the wide range of damage created a need to reevaluate the design and rehabilitation procedures of new and existing structures.

In many cases, bridges are being designed or retrofitted to withstand higher seismic design forces, resulting in larger bridge foundations. The current inclination to design larger foundations may have overlooked the potential benefits of allowing foundation systems to uplift during seismic events. Foundation rocking has been identified as an important mechanism, along with structural yielding and soil-structure interaction, that may explain why some engineered structures suffer less damage during strong earthquake ground shaking than might be predicted based on elastic methods of dynamic analysis (e.g., Rutenberg et al. [1982]; Werner [1992]).

The California Department of Transportation (Caltrans) has investigated several mechanisms for absorbing and dissipating energy during intense earthquake ground motions. However, to date, rocking of foundations is one of the few design strategies for which Caltrans has yet to develop and validate design guidelines. Development of design and analysis guidelines could be beneficial for the assessment of existing and new construction by identifying situations where allowing foundation uplift could, at a minimum, and possibly not degrade bridge performance during ground shaking.

Conventional design methods required large and expensive foundations so that a bridge achieves a "fixed-base" condition that dissipates energy in response to intense earthquake shaking through ductile plastic hinging in the columns. For instance, the Seismic Design Criteria (SDC) [Caltrans 2004a] assumes that a rigid footing response will occur if the width of a regular spread footing on competent soil is six or more times the column diameter. Significant experimental and analytical evidence suggests that adequate seismic performance can be achieved on competent soil at less cost if the foundation of the bridge pier is narrower and allowed to uplift. It appears that there may be circumstances under which improved performance can be obtained by allowing bridge foundations to rock. The lack of information and guidelines related to intended foundation uplift leads most engineers to avoid rocking all together through the use of costly widened spread footings or foundations supported by piles. The state-of-the-art information on seismic performance of rocking foundations has yet to be integrated and

evaluated to determine conditions where rocking might be dependably permitted, or which design procedures might be most appropriate.

The behavior of even simple bridge foundations that are allowed to rock is quite complex and highly nonlinear. There is a worry that bridge piers might become globally unstable and simply overturn if their foundations are allowed to uplift. Some studies suggest that short-period structures supported on rocking foundations may not perform as well as conventionally designed structures. However, other studies indicate that the nonlinearity associated with uplift and the energy dissipation added by the supporting soil may be sufficient to improve response compared to a fixed-base bridge pier.

A significant concern in the evaluation of rocking foundations is the performance of the supporting soil. If the demand for soil yielding becomes excessive, significant permanent vertical and lateral displacements of the bridge could occur due to permanent deformations of the supporting soil. Thus, assessment of the rocking mechanism and development of reliable design guidelines requires a methodology that carefully integrates structural and geotechnical engineering expertise.

To date, most experimental and analytical studies of rocking foundations have considered cases that are simpler than encountered in actual bridges, and analytical models have generally not been validated in terms of experimental data, raising concern when considering more complex systems. For example, when a bridge column is subjected to multiple components of motion or intense near-fault pulse-like motions, the accuracy of analytical predictions may be uncertain. Thus, a critical review of the structural and geotechnical engineering issues involved with allowing bridge pier foundations to rock during strong earthquake ground motions is needed.

The performance of systems allowed to uplift has been studied in systems ranging from rigid bodies to deformable systems resting on tension carrying or compression-only media with a wide array of assumptions regarding soil behavior. For example, in an early study, Chopra and Yim [1983] analyzed flexible single-degree-of-freedom systems subjected to one horizontal component of ground shaking. The model in these studies assumed the soil to be elastic and unable to resist tension. The soil was modeled as either a two-spring/dashpot or Winkler spring/dashpot model. The benefit of foundation uplift illustrated in this work was a reduction in lateral force acting on the structure. This reduction could be used to effectively reduce the damage to existing structures in seismic events without the need to strengthen or otherwise retrofit. This investigation also identified appropriate parameters that could be used to objectively ascertain those distinct conditions where no rocking, rocking and no yielding, or simultaneous rocking and yielding would occur during seismic shaking.

Modeling of soil behavior during system uplift is a key aspect of capturing the complexity of soil-structure interaction. Many studies have investigated the performance of soil response during uplift both experimentally and numerically (e.g., Rosebrook [2001]; Harden et al. [2005]). The experimental studies investigated the rocking of scale models in centrifuge tests where the supporting soil was sand and saturated clay. Analysis modeling assumptions for foundations on soil have varied from the two-spring model to the Winkler-spring model that incorporates a significant number of soil springs. Harden et al. [2005] investigated the nonlinear cyclic response of shallow foundations under building shear walls, which suggested that the

behavior of soil and foundations during rocking could be reasonably predicted using nonlinear Winkler foundations for a given soil.

To date, few analytical or experimental studies have investigated the performance of systems allowed to uplift in more than one direction. While experimental and analytical predictions have been done for one-dimensional excitation, many concerns remain for multi-directional dynamic response:

1. Modeling of the foundation and underlying soil has been generally limited to one-dimension analytical models. This may be significant when considering non-linear soil behavior, which may be affected by interaction of displacements along the principal directions.
2. The type of input excitation has been primarily limited to one dimension. There has not been much investigation into the behavior of uplifting systems loaded in two or three dimensions for a rectangular footing configuration. The effective width of the footing is larger when considering a section of the footing along the diagonal axis and may affect the rocking characteristics of the system.
3. Interaction and force redistribution for a system that may uplift and then yield or vice versa.
4. The global performance and residual displacements of a system is a concern. Allowances for total displacement demand may be a concern. A system may rock, not yield, yet exceed the allowable displacement and thereby perform negatively.

Tests that assess the dynamic behavior of a simple bridge system (See Figure 1.1) could be used to identify key characteristic of uplifting systems. In turn, the results could be used to identify conditions of incipient rocking, yielding, or both. The behavior of these systems under moderate and significant near-fault ground motions could be useful in designing systems in regions of high seismicity.

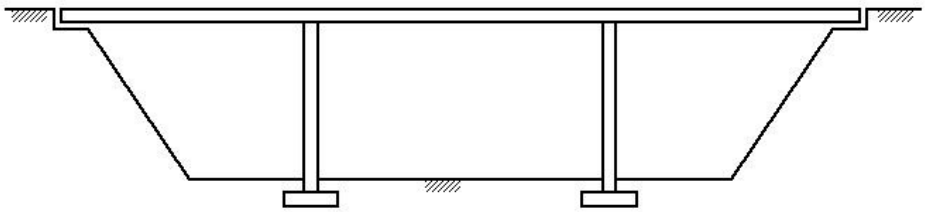

Figure 1.1 Generalized bridge with spread footings.

1.2 RESEARCH PROGRAM OBJECTIVES

This report addresses the key aspects involved in assessing the performance bridge piers allowed to uplift during seismic events. Specifically, single column reinforced concrete (RC) bridge piers were considered. The thrust of the research program aimed to address knowledge gaps identified for uplifting foundations with the following specific objectives:

1. Gather and review available information about structural behavior, analysis, and design of bridge column foundations that rock and uplift during seismic response.
2. Perform shake table experiments to obtain data to better understand rocking behavior under multiple components of motion and fill in knowledge gaps.
3. Validate analytic models using experimental results.
4. Perform numerical studies to identify situations where rocking foundations can be utilized with confidence and meet acceptable bridge pier performance expectations.

The scope of this effort is limited to individual bridge piers supported on competent soil using rectangular shallow spread footings. Potential issues concerning marginal soil conditions and the response of complete bridge systems are not addressed herein.

1.3 ORGANIZATION OF REPORT AND SCOPE

This research focused on conducting a series of shake table tests of moderate-scale bridge piers subject to one, two, or three components of base shaking. Soil behavior was not believed to have been reduced properly for reduced scale 1g shake table tests; therefore, the supporting soil for these tests was idealized using an elastomeric sheet. To compare the response of bridge piers with fixed and rocking foundations, the test specimens used in these tests were similar to ones previously tested with fixed bases [Hachem et al. 2003]. Typically, Caltrans will design a spread footing width of 4 column diameters in plan dimension, and if fixed-base conditions are assumed, then a footing width of 6 column diameters. To assess impact of smaller than normal footing dimensions, the test specimens were chosen to be 3 and 5 times the column diameter.

The following chapters address the assessment, observation, and prediction of spread footing bridge piers allowed to uplift. In the course of conducting this research, a knowledge base was developed that may provide the basis for formulating design guidelines for uplifting bridge piers. Chapter 2 discusses the literature currently available for systems allowed to uplift and discusses current design practices of RC bridge columns and their footings. The experimental test program, design, and physical test set up are explained in Chapter 3. The experimental results—including global response and the overall damage state experienced by the specimens—are described in Chapter 4. Chapter 5 presents a comparison of the experimental and analytical results. Simple methods used in design as well as refined inelastic dynamic analyses were used to compare the observed and predicted response. Based on the analytic models presented in Chapter 5, ranges of parametric analyses were performed in Chapter 6. The analyses present the effects of varying the physical dimensions and loading conditions of uplifting bridge piers. Conclusions and recommendations are summarized in Chapter 7.

Also included are several appendices. Appendix A explains the experimental test schedule, instrumentation, and location associated with testing. Appendix B presents further experimental test data for all the three groups of testing. Appendix C includes the code used to represent uplifting foundations in the simulation software.

2 Literature Review

2.1 INTRODUCTION

Much research has been done to date that investigates the dynamic rocking or uplift of rigid bodies. There has also been research conducted on various types of steel and RC bridges allowed to experience unrestrained or controlled uplift. In addition, some studies have investigated simple frame-type structures where column uplift relative to the footing is unrestrained or where some type of energy dissipation device has been installed between the column and foundation connection. The studies have indicated that, in general, allowing a structure to uplift may reduce forces and damage in a structure when compared to a similar structure with a fixed base. There has been relatively little analytical and even less experimental research on the behavior of deformable bodies resembling bridge piers where the footing is allowed to rock or uplift on the supporting soil.

Some analytical and experimental studies investigating the characteristics and response of structural systems allowed to uplift are described in Section 2.2. Studies that have attempted to determine or validate design-oriented procedures for structural systems that may rock and or uplift are described in Section 2.3. A summary of the findings of this literature review is presented in Section 2.4.

2.2 STRUCTURAL SYSTEMS WITH UPLIFTING FOUNDATION

The studies described here identify the characteristics of rocking and uplifting systems and the effects on structural response, including the global and local response related to deformation, acceleration, and force. The types of systems reviewed include: elastic and inelastic columns, shear walls, elastic and inelastic soil response, spread footing foundations, and systems subjected to uni- or multi-directional earthquake input excitation. Analytical investigations are reviewed in Section 2.2.1, and experimental investigations are described in Section 2.2.2.

2.2.1 Analytical Investigations

Meek [1975] studied the dynamic in-plane response of flexible single degree-of-freedom elastic columns connected to a rigid spread footing supported only at the outer edges (two locations);the soil was modeled as rigid assuming elastic impact. Basic equations of motion for a flexible superstructure were developed and used to determine the dynamic response of tipping and fixed-base systems. Tipping or rocking was found to significantly reduce the lateral shear force acting

on the structure, especially for cases with large ratios of super structure mass height to footing half width. Tipping or rocking mechanisms were found to be a viable option that effectively reduced base shear without designing a strong structure. Further clarification was required for the potential negative effects on nonlinearity of the soil for cases where the footing uplifts and subsequently impacts the ground.

Yim and Chopra [1983] investigated a system similar to that proposed by Meek with a simple elastic single- or multiple-degree-of-freedom model considered in combination with a more complex soil model. The column foundation was supported on either a two-spring/dashpot model (at each edge) or a Winkler model with springs and dashpots uniformly distributed along the entire width of the footing (Figure 2.1). Nonlinear soil springs were modeled as being elastic in compression only, with no tension resistance. Additional soil nonlinearity and inelastic impact damping qualities were modeled using viscous dampers.

In general, the peak base shear (in comparison to a fixed-base system) is reduced if the foundation uplifts for either foundation model. The most important factors determined to influence structural response were:

- Fixed base period (T_n)
- Structure slenderness (h/b)
- Ratio of foundation weight to superstructure weight (W/W_{footing})
- Vertical period of fixed base system
- Damping ratio of a fixed-base structure with rigid soil to damping ratio of a fixed-base structure considering soil dynamic characteristics

The authors developed simple equations to predict the critical base shear—which occurs at incipient footing uplift—assuming the soil springs had no tension carrying abilities and were fully elastic in compression. The critical base shear equation (V_c) for the two-spring soil model is given in Equation (2.1) and Equation (2.2) for the Winkler foundation model.

Two Spring Model:

$$V_c = \left(m + m_o\right) g \frac{b}{h} \tag{2.1}$$

Winkler Foundation

$$V_c = \left(m + m_o\right) g \frac{b}{3h} \tag{2.2}$$

The lateral force-displacement relation for the system is bilinear for the two-spring model. In comparison, the Winkler-foundation response differs due to the distribution of vertical springs along the footing length. After initial edge uplift, the base shear continues to increase gradually with applied lateral force as the rotational stiffness of the footing decreases as additional springs lose contact with the uplifting footing. This repeats until only one spring is in contact with the footing, at which point the Winkler model calculated base shear has converged on the two-spring model calculation. Rotational flexibility of the uplifting foundation contributes

to the lengthening the natural period of the system compared to a fixed-base system. The critical base shear formulation indicates there is a limited value of base shear, which may be induced in a structure that is independent of the applied excitation and dependent only on the structural weight and the geometry of the system (*h* and *b*).

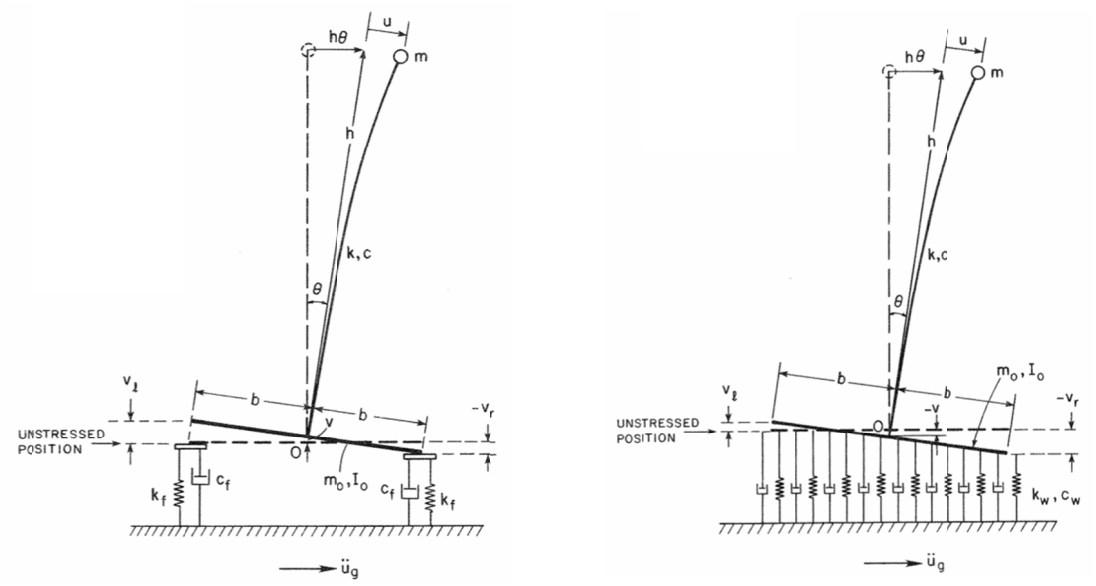

(a) two-spring model **(b) Winkler Foundation Model**

Figure 2.1 Uplifting elastic column models on spread footing [Yim and Chopra 1984a, 1984b].

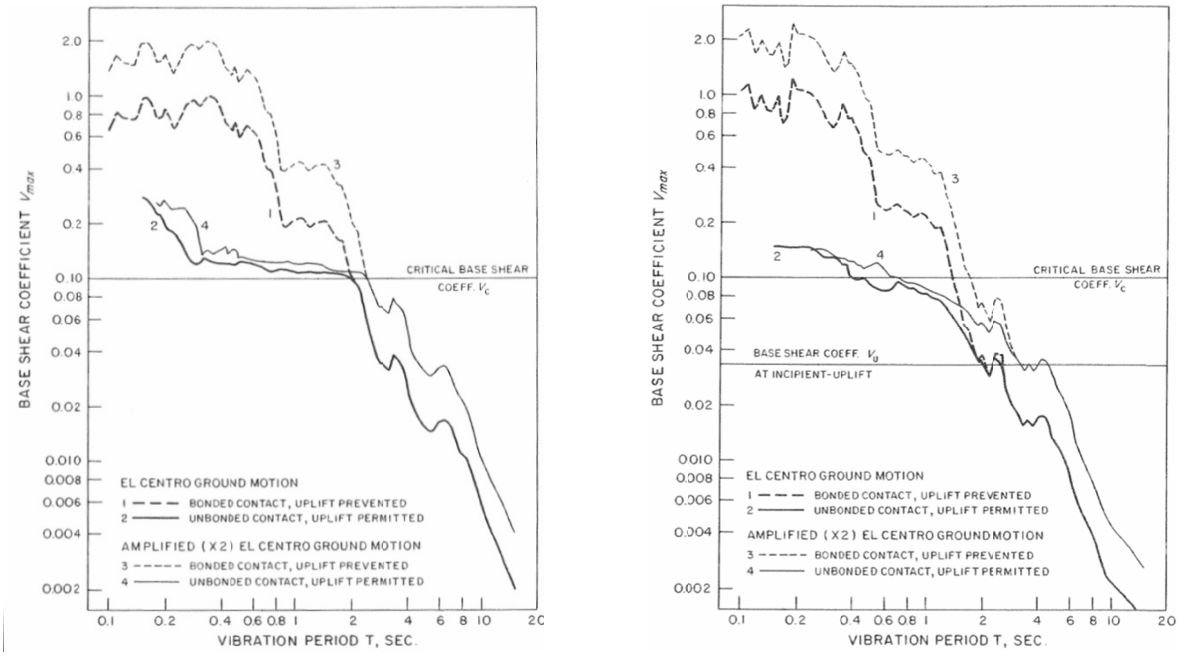

(a) two-spring model **(b) Winkler Foundation Model**

Figure 2.2 Base shear spectra uplifting system with *h*/*b* = 10 [Yim and Chopra 1983].

Results for the numerical models subjected to several earthquake ground motion records are shown in Figure 2.2 for both foundation types. The Winkler-spring model uplifts earlier than the two-spring model. In the short period range, however, where significant uplift is expected, the base shear demand approaches that for the two spring model.

Yim and Chopra [1984a] developed a simplified two-spring model to represent the behavior exhibited by the Winker model. From these studies, Yim and Chopra reached several conclusions:

1. Base shear in long-period range may be equal for structures allowed or prevented from uplifting as a result of a seismic demand less than that required to initiate uplift for a given axial load and column height to footing width ratio h/b.
2. Uplift expected in short-period range.
3. Base shear for uplifting systems is reduced compared to elastic column fixed-base systems.
4. Maximum base shear is relatively independent of the intensity and dynamic characteristics of the ground motion.
5. Uplift is more likely in slender column systems (i.e., large h/b), resulting in larger reductions in base shear for columns with narrower foundations.

Yim and Chopra [1984a] concluded there was no need to prevent uplift, as it had a positive effect on structural deformations and forces and that the critical base shear [Equation (2.1)] could be used as a guide in designing a column that would not yield or be damaged in an earthquake. Note that global displacements of systems with fixed or uplifting foundations were not compared in this study nor were the effects of multi-directional ground motions. Lateral displacements of bridge piers are important is estimating P-Δ effects and assess displacement demands at abutments and expansion joints.

Priestley et al. [1978] conducted an experimental and analytical study on rocking and uplifting of a simple cantilever column system. The experimental program performed a series of small shake table tests of the system allowed to rock and uplift. A rigid foundation was provided that rested upon a rubber pad supported uniformly or only at the four corners. The analytical investigation estimated peak lateral displacements of the system and the amount of deformation due to column flexibility by utilizing Housner's method [1963] developed for rocking of rigid bodies. This modified Housner methodology was also used in subsequent analytical investigations by Priestley and Seible [1991] and Priestley et al. [1996]. Maximum lateral displacement of the rocking system was estimated using a conventional elastic response spectrum and equivalent elastic characteristics of the system allowed to rock.

To determine the maximum lateral displacement, the authors developed an iterative method. This method used an initial prediction of total lateral displacement (Δ_1) with an assumed viscous damping ratio ξ_1 of the rocking system to determine an effective equivalent period, T_1. The values T_1 and ξ_1 were used with the elastic response spectrum to determine a new lateral displacement, Δ_2. The process was repeated i times until the maximum lateral displacement converged on $\Delta_i = \Delta_{total}$. With a converged solution, the computed shear force [Equation (2.3)] was used with the lateral stiffness of the fixed-base bridge pier to estimate the contribution of

column flexural displacement to the total system displacement [Equation (2.4)]. The rocking displacement was then calculated by subtracting total displacement from column flexural displacement [Equation (2.5)].

$$V_{base} = S_A\left(T_i, \xi_i\right)\left(\frac{W}{g}\right) \tag{2.3}$$

$$\Delta_{flexure} = \frac{V_{base}}{k_{column}} \tag{2.4}$$

$$\Delta_{rock} = \Delta_{total} - \Delta_{flexure} \tag{2.5}$$

The methodology proposed by Priestley et al. [1996] is susceptible to inaccuracy owing in part to the assumptions of rigid body rocking, perfect inelastic impact, equivalent linearization, etc. The software program WINROCK [2005] has implemented this method despite not being substantially validated by more thorough analytic or experimental methods.

Kawashima and Hoisori [2003] investigated the uplift response of an existing bridge pier system using nonlinear dynamic analysis that indicated the bridge pier system performed well when uplift was allowed. A Takada degrading stiffness model was used to characterize the moment-rotation response of the plastic hinge region of the bridge column along with a nonlinear Winkler-spring foundation model based on uplift and elastic properties of the soil properties. The ground motion used was a one-dimensional strong-motion near-fault recorded by the JMA Observatory during the 1995 Kobe earthquake.

Kawashima and Hoisori [2003] found that allowing uplift significantly reduced the moment-rotation response compared to a fixed-base assumption (Figure 2.3). Global displacements increased 27% for the case considered in spite of allowing uplift. However, the contribution of column flexure to total displacement was only 20%, corresponding to the reduction in inelastic column behavior and damage. No residual displacements were observed when the column was allowed to uplift. The authors concluded that allowing inelastic rocking and uplift essentially created an isolation mechanism that increases as the footing width decreases.

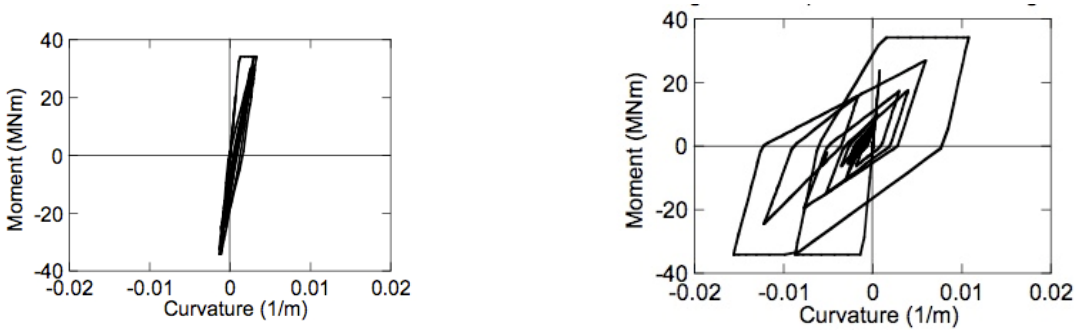

(a) uplifting system **(b) fixed-base system**

Figure 2.3 *M-ϕ* column response of RC bridge column [Kawashima and Hoisori 2003].

2.2.2 Experimental Studies

Sakellaraki et al. [2005] performed a shake table test of an idealized bridge column with uplifting foundation. The system was a steel column with a mass at the top and a metal footing resting upon a rubber pad with footing translation prevented. The mass was varied to achieve a system with natural periods (fixed-base assumption) ranging from 0.3 to 1.2 sec. Additional analytic studies were performed to gauge rocking response and validate analytic modeling techniques of the experimental tests [Sakellaraki et al. 2005; Sakellaraki and Kawashima 2006]. The uplifting foundation model consisted of an elastic column and footing resting upon elastic (compression only) Winkler springs.

Rocking was found to affect the system by increasing the effective natural period and viscous damping ratio as the amount of rotation increased. Typically, the rocking response increased as the mass increased, footing width decreased, and/or soil stiffness decreased. Specimen performance under rocking and uplifting footing conditions had both positive and negative effects. The column flexural deformation decreased, as did the center of mass accelerations. The acceleration reduction correlated to a reduction in the base shear; however, the total displacement increased due to rocking. Large vertical accelerations were recorded at the footing edges during impact of foundation with the soil.

The recorded vertical accelerations suggested to the authors of the study a risk of soil yielding in actual bridges due to uplifting systems. The inelastic Winkler-spring model provided good correlation between predicted and experimental results at small and medium rotations of the footing, but less so at large values, indicating the need for an improved numerical model of foundation springs.

Nagai and Kawashima [2006] built upon this study and performed an analysis on the effect of two-horizontal components of excitation on the behavior of bridge piers on foundations allowed to uplift. A typical bridge on spread footing foundation was analyzed under uni- and bi-directional excitation. The columns were modeled using inelastic behavior assumptions. As previously shown [Sakellarki et al. 2005; Sakellaraki and Kawashima 2006], under unidirectional excitation, foundation rocking significantly reduced the plastic deformation of the column. The authors found that bi-directional excitation increased the uplift of the footing by comparison, but also increased the isolation effect, thereby reducing the potential yielding behavior in the column.

Kawashima et al. [2007] followed up on their earlier work and considered three-directional input excitation. The findings indicate that the soil stress induced at the corners of the foundation significantly increased. In general, they found that although foundation rocking provided a positive benefit in the seismic design of bridges, they expressed concern that underlying soil may need enhancement at foundation corners to fully realize the benefits of rocking systems.

2.3 DESIGN OF UPLIFTING FOUNDATION SYSTEMS

The design-oriented studies reviewed in this section investigated the case when rocking is an acceptable response mode and determined or assessed design guidelines for evaluating new and

existing systems allowed to uplift. The evaluation was based on the local response (forces, deformations, etc.) and global response (displacements).

An investigation by Alameddine and Imbsen [2002] suggested that the iterative solution methodology by Priestley et al. [1996] may not converge on a total displacement solution that agrees with analyses based on nonlinear dynamic analysis. Comparisons of results of studies of equivalent elastic systems (such as the iterative methodology used) with those from simpler direct methods based on empirically modified elastic response spectrum suggest that comparable accuracy can be obtained in the moderate and long-period range. However, reliability of the iterative equivalent elastic approach decreases substantially for short-period structures [Chopra and Goel 1999; Miranda and Ruiz-Garcia 2002]. Chopra and Goel [1999] found that iterative methods may not converge or converge on erroneous solutions.

Alameddine and Imbsen [2002] investigated a retrofit strategy for older bridges where columns might have inadequate lap splices in discontinuous reinforcement or inadequate confinement of continuous reinforcement at the column footing connection. They examined the seismic response when the column foundations were allowed to rock. The systems considered all had a footing to column width ratio of 3 and were supported by spread footings on dense soil subjected to low, moderate, and high intensity ground motions. Analysis was performed using either WINROCK [2005], based on the iterative method by Priestley and Seible [1991] or a nonlinear dynamic analysis incorporating a Winkler-spring model for the soil with a nonlinear beam-column element for modeling the inelastic response of the column. A total of 24 column systems were subjected to six ground motions.

The nonlinear dynamic analysis model found that for existing columns with relatively high flexural strength and narrow footing widths, allowing uplift resulted in acceptable total lateral displacement and elastic column response for a majority of cases. Columns with weak flexural strength exhibited significant yielding and a 30% increase in total lateral displacement compared to stronger columns. Rocking and uplifting did not significantly contribute to the response of these weaker systems, and in some cases no rocking occurred. It was observed that larger ductility demands occurred for columns with larger footing width to column height (b/H) ratios.

A comparison of nonlinear analysis results with results predicted by WINROCK showed large discrepancies. Stronger columns with limited flexural demands due to significant uplift had very different results compared to weaker columns where less rocking and more flexural yielding occurred. For example, the peak ratio (nonlinear analysis to WINROCK) of flexural column displacements predicted by the two methods varied by a factor of 0.71 to 1.95 for each ground motion on average for the stronger column and 0.56 to 4.01 for the weaker column system. Larger discrepancies were found for low footing width to column height ratios. Using both methods, they found that rocking and uplifting was not a cause of instability in any of the analyses, leading to the conclusion that enlarging the footing as part of a retrofit scheme was not warranted. Some of the weak column systems with little or no rocking collapsed due to inadequate flexural ductility.

Based on nonlinear dynamic analyses, Alameddine and Imbsen [2002] developed design guidelines, , identifying acceptable conditions of rocking and uplifting systems for new design and existing column retrofit The criteria for allowing rocking in the design process was primarily based on the calculated ratio of overturning moment to restoring moment β . The overturning

moment was defined as column axial load P times the center of column mass displacement (Δ_{demand}). The restoring moment is calculated as the minimum of the factored column plastic moment capacity (1.2Mp) or the moment resisting uplift calculated as the total structure and soil weight (W_t) times the distance from the centroid of W_t to the centroid of the soil force generated by uplift. Figure 2.4 is a schematic of the forces developed in the uplifting and deforming system. Relationships between β and drift, ductility and column width to height ratios (D/H) were developed to identify acceptable response criteria.

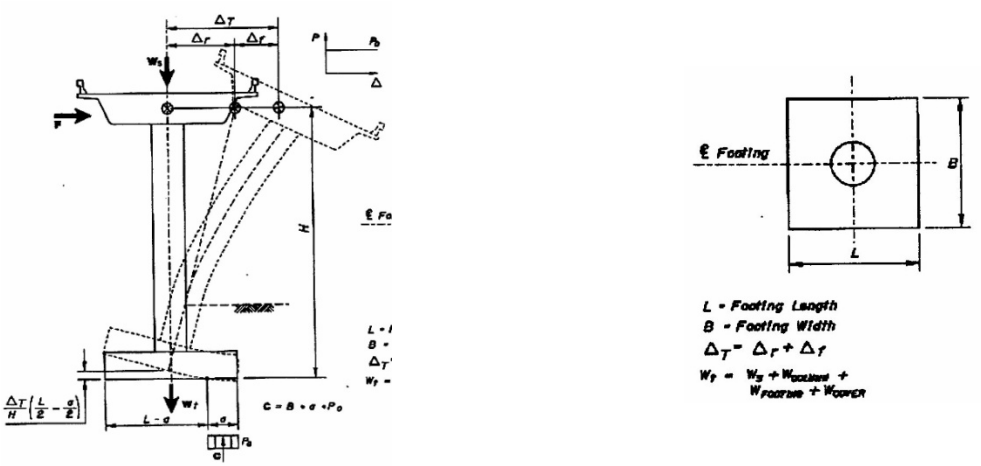

Figure 2.4 Uplifting column model [Alameddine and Imbsen 2002].

To evaluate the acceptability of rocking, the authors developed a decision making flowchart with β as the primary decision variable. They then determined the footing dimension required by service loading or the minimum footing width of 3 column diameters and estimated the lateral flexural displacement of the column (Δ_{demand}) using WINROCK [2005], although alternative methods could have been used. The overturning and restoring moments were then determined and these were used to evaluate β [Equation (2.6)]. Based on the analysis conducted, Alameddine and Imbsen determined acceptable values of β for design based on the column fixed base ductility [Equation (2.7)]. When β was larger than $\beta_{\text{allowable}}$, they re-evaluated the design process using a larger footing dimensions. They iterated on the footing dimensions until an acceptable value of β was achieved.

$$\beta = \frac{P \cdot \Delta_{demand}}{\min\left(1.2M_p, W_t\left(L-a\right)/2\right)} \tag{2.6}$$

Criteria for accepting rocking in design:

$$\begin{aligned} \mu < 6 \qquad & \beta_{\text{allowable}} \le 0.3 \\ \mu = 6-8 \qquad & \beta_{\text{allowable}} \le 0.2 \end{aligned} \tag{2.7}$$

In the design procedure, the column is required to be ductile regardless of the amount of rocking. This is to prevent against column failure in the event of modeling uncertainty or an unanticipated increase in footing strength (e.g., additional soil surcharge). While the study is useful, it only considers a limited number of soil conditions, does not include damping effects of the soil and foundation (which means elastic rebound would occur upon contact), and limits the seismic excitation to one direction.

Harden et al. [2005] studied methods for numerical modeling of nonlinear cyclic response of shallow foundations similar to those used for shear walls in building structures. Using the developed numerical modeling methods, the authors investigated the ability of several design-oriented analysis procedures to predict lateral displacements and bases shears of uplifting systems. A simple method was developed based on a refined FEMA 356 [2000] prediction methodology that could be used to estimate peak displacements and base shears. They concluded by performing a case study of a shear wall and highlighting accuracy between the methods as well as the benefits in allowing uplift.

Work done by Rosebrook [2001] and Phalen [2003] was reviewed by Harden et al. to develop their numerical models. The works reviewed investigated the effect of foundation rocking on the inelastic behavior of soils and overall dynamic response of structures on rocking and uplifting foundations. Rosebrook summarized tests of small-scale pairs of coupled walls supported on sand and saturated clay. Phalen summarized tests of single strips footings on dry sand having different sizes and design vertical factors of safety.

Based on the recent quasi-static and dynamic tests, Harden et al. developed a nonlinear Winkler foundation model that modeled the underlying soil of a shear wall on a strip footing. The primary input parameters are shown in Figure 2.5. Three types of material models were used for the supporting springs: elastic-perfectly plastic combined with gap elements, general hysteretic materials, and the QzSimple1 material model developed by Boulanger et al. [1999]. Dashpots were excluded since Wang et al. [1998] previously showed that including rate-dependent damping in parallel with hysteretic spring elements overestimates the damping force.

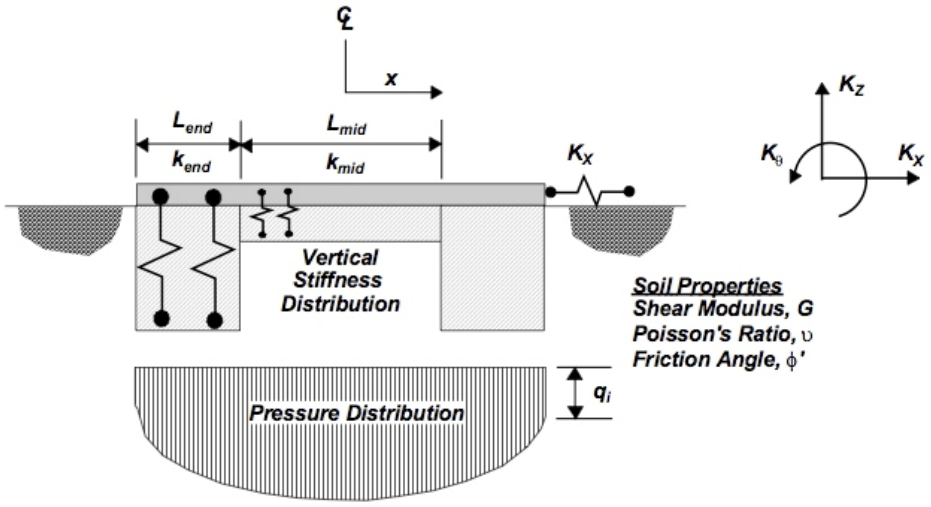

Figure 2.5 Nonlinear Winkler foundation [Harden et al. 2005].

In investigating the ability of the design analysis procedures to predict lateral displacements and bases shears of uplifting systems, the authors compared their numerical models to four simplified analysis methods included in FEMA 356 [2000]. The design methods were evaluated for three foundation assumptions: elastic springs with tension allowed, inelastic springs with uplift (no tension) allowed, and a fixed-base assumption that ignored soil-structure interaction. The four simplified methods included the Capacity Spectrum approach, a method similar to Priestley and Seible [1991], the Nonlinear Static Procedure (NSP) (method of coefficients), and the time-history method.

The subsequent investigation of the simplified methods improved on the parameter C_1 used in the NSP, which is the ratio of predicted peak displacements for the nonlinear time-history analysis using inelastic spring models with uplift to that of a similar system with elastic springs with elastic tension/compression springs where uplift is prevented. The estimation of C_1 depends on the period of the elastic structure (on a Winkler foundation) and the Harden et al. parameter R, which is defined as the ratio of base shear developed for the structure if the foundation remained elastic (uplift prevented) to the base shear at incipient uplift [Equation (2.2)]. This definition provides an upper bound on R. In the cases considered, the supported structures had yielding forces much larger than those required to cause uplift of the foundation.

Harden et al. [2005] investigated directly measured values of C_1 for preselected R values using an elastic cantilever column structure model on a Winkler foundation. The foundation was modeled as nonlinear soil with uplift allowed and entirely elastic without uplift. Figure 2.6 shows the simulation data points, best-fit curves, and FEMA 356 recommended values of C_1. For structural periods greater than T_S, C_1 is typically around 1 (i.e., no amplification in lateral displacements due to soil model) but increases for structural periods less than or equal to T_S, especially with increasing values of R. By comparison, FEMA 356 limits C_1 to 1.5 in the short-period range, which is unconservative for all the cases shown, except R=1.5. As another example, the Newmark and Rosenblueth [1971] energy conserved method for calculating C_1 gives a value of 2.13 when R=4.0 for a structural period of approximately $T_S/2$. A lower value of R might be warranted since the footing strength incrementally increases as it continues to uplift.

Harden et al. [2005] also investigated the peak structural lateral displacements and base shears predicted by their model using inelastic time-history analysis with uplift and compared their results to the simplified methods in FEMA 356 [2000]. The structural system used was a reinforced concrete shear wall on a shallow strip footing supported on soil with a bearing capacity factor of safety of 4. The seismic hazard level was selected as 10% probability of exceedance in 50 years, with a site specific characteristic period T_S = 0.367 sec. The structural period was 0.03 sec for a fixed-base assumption and 0.44 sec on an elastic Winkler foundation. The computed R value was 3.97. The results for peak lateral displacement and base shear are given in Table 2.1and Table 2.2.

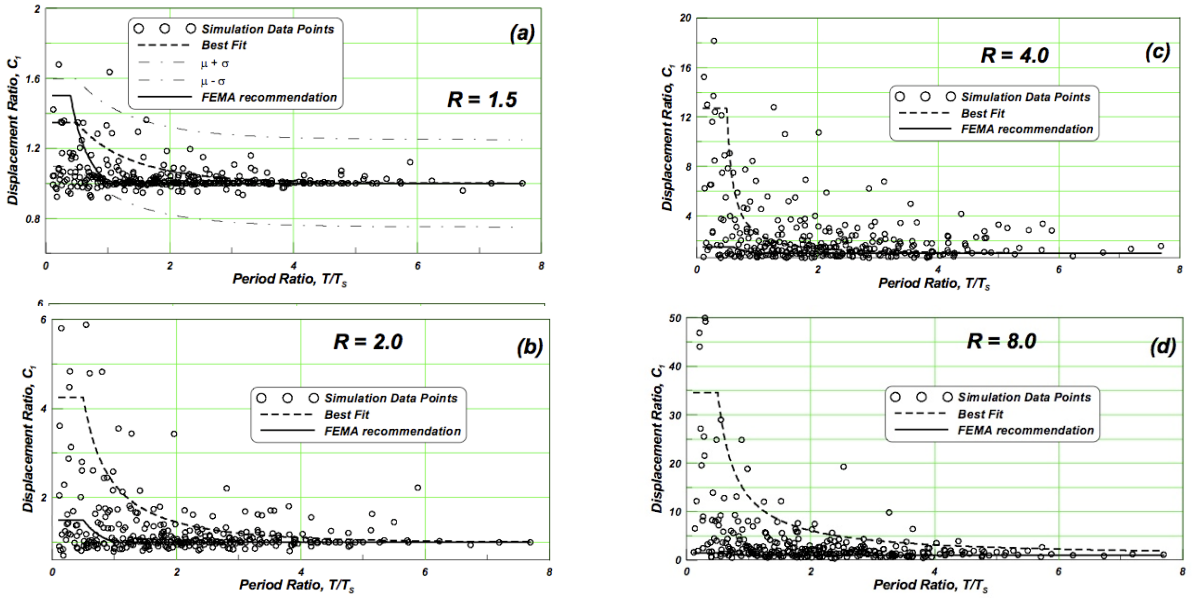

Figure 2.6 **C_1 ratio of maximum lateral displacement with/without footing uplift [Harden et al. 2005].**

Table 2.1 **Lateral displacement comparison of shear wall model using various methods [Harden et al. 2005].**

	Soil Structure Interaction (SSI) Included			*SSI Not Included*
	Uplift Allowed		*Elastic*	*Fixed Base*
	Nonlinear Soil Springs	*Elastic Soil Springs*	*Method 1*	
Natural Period, T (sec)	0.555	0.424	0.424	0.033
Analysis Method	u_{top} (mm)	u_{top} (mm)	u_{top} (mm)	u_{top} (mm)
LDP (Capacity Spectrum)	280	178	38	0.14
Housner Model	206	202	202	0.16
FEMA NSP - C_1 defined by FEMA 356 (2000)	91	57	57	0.27
FEMA NSP - C_1 based on uplifting foundation (values from this study)	414	308	62	0.27
Time History Method (envelope of three ground motions)	385	102	237	0.0003

Table 2.2 Base shear comparison of shear wall model using various methods [Harden et al. 2005].

	Soil Structure Interaction (SSI) Included			*SSI Not Included*
	Uplift Allowed		*Elastic*	*Fixed Base*
	Nonlinear Soil Springs	*Elastic Soil Springs*	*Method 1*	
Natural Period, T (sec)	0.555	0.424	0.424	0.033
Analysis Method	*V* (kN)	*V* (kN)	*V* (kN)	*V* (kN)
LDP (Capacity Spectrum)	211	331	1181	728
Housner Model	284	291	291	723
FEMA NSP - C_1 defined by FEMA 356 (2000)	162	240	1024	793
FEMA NSP - C_1 based on uplifting foundation (values from this study)	170	265	1108	793
Time History Method (envelope of three ground motions)	169	251	4245	1341

Comparing the displacements shows that the simplified methods all underestimate the peak response. The least accurate method is the NSP [FEMA 2000], followed by the modified Housner model, and the Capacity Spectrum Method. Using the C_1 defined by the best fit curve in Figure 2.6, the peak displacement is slightly overestimated using the more complex inelastic time-history analysis. Base shear results had much less scatter than the peak lateral displacements. The modified Housner method [1963] and the Capacity Spectrum Method overestimated the base shear by 70% and 25%, respectively. The NSP or Harden et al. [2005] calculation of C_1 predicted a base shear within 5% of that from the inelastic time-history analyses. The design shear for a fixed base system is 7.9 times larger than the case allowing uplift.

The improved calculation of C_1 using the NSP shows much larger displacements than predicted by the simplified methods, which advocates against allowing uplift. However, typically displacements for short-period structures are very small; therefore, a large percentage increase still may be a small displacement. The RC shear wall investigation shows that allowing uplift significantly reduced base shear but increased global displacements of the system. For the shear wall, assuming the system could accommodate increased displacements, allowing foundation uplift would be very beneficial because there would be a significant reduction in base shear and deformation of the wall. The studies by Harden et al. are promising, but do not directly address the concerns of longer period structures like bridges where bi-directional bending is also of greater concern.

Algie et al. [2008] performed dynamic centrifuge testing of rocking bridge spread footing foundations with cantilevered columns allowed to yield and variable footing dimensions. Experimental results found footing moment-capacity could be reliably predicted when allowed to rock. The results also identified a reduction in column plastic rotation demand that was

consistent with a reduction in foundation moment-capacity, highlighting a potential design benefit.

Deng et al. [2010] utilized methods similar to those by Algie et al. [2008] to predict foundation moment-capacity and perform dynamic centrifuge modeling of a bridge system with rocking footings. The experimental testing validated a design method that allows rocking of bridge spread footings to protect columns from excessive ductility demands. Two 2-column bents systems, with columns designed to Caltrans standards and pinned at the top, and small or large footings were evaluated. They were designed such that one bent (small footings) had less moment capacity than the column and the other (large footing) had more moment capacity than the column. For the seven input motions considered, column peak and permanent rotations of the smaller footing with yielding soil were typically less, , relative to the larger footing with column yield and little rocking, which had little yielding of the soil (Figure 2.7). Soil yielding caused settlements that may cause permanent rotation of the system not related to column yielding. Algie et al. [2008] also identified soil settlement as a potential negative effect when allowing rocking.

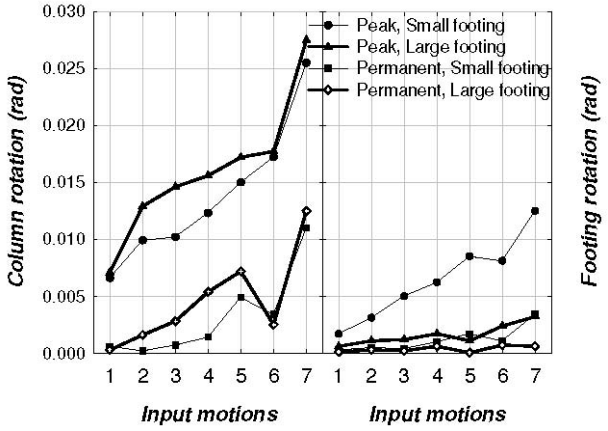

Figure 2.7 Two-column bridge bent column and footing rotations [Deng et al. 2010].

Deng and Kutter [2011] investigated the settlements associated with bridge piers on spread footings allowed to rock on dry sand through centrifuge testing. The aim was to mitigate settlements due to rocking foundations while still allowing rocking to reliably dissipate energy through soil-structure interaction. Placement of localized concrete pads beneath footing edges was found to reduce settlements associated with rocking, but still allowed the foundations to reliably rock. One of the important factors found for acceptable combination of energy dissipation and re-centering (minimized soil yielding) ability was the ratio of footing length to critical length required to support axial loads only, L_f / L_c . The studies by Algie et al. [2008], Deng et al. [2010], and Deng and Kutter [2011] are encouraging, providing an example of the benefits of allowing bridge piers to rock during seismic events and the potential negative effects rocking piers might have on re-centering abilities post-seismic event. However, they do not consider a large sample of bridge column dimensions and footings sizes or seismic excitations.

2.4 SUMMARY

From a review of the analytical and experimental studies, there appears to be credible evidence that suggests that soil-structure interaction and uplifting of a spread foundation from the supporting soil can significantly diminish the base shear of a bridge column when compared to a fixed-based elastic structure. Inelastic deformation and shear force demands on the column can be significantly reduced when competent soil is provided and the foundation restoring capacity is smaller than the column strength. Force demands on columns supported on uplifting foundations can be reasonably estimated from existing relationships.

Much less certain, however, is estimating with acceptable accuracy the total displacement of the column supported on an uplifting foundation and the contribution of uplift to total displacement. Although suitable for design purposes, the approximate simplified methods , for estimating displacements are less well developed and appear to vary significantly compared to nonlinear dynamic analyses. More robust numerical models have been developed, but there is a lack of experimental data necessary to calibrate the material and kinematic properties. Additional research is warranted related to the behavior of bridge columns supported on foundations that can rock and uplift during severe earthquake ground motions.

3 Experimental Test Program

3.1 INTRODUCTION

A review of the available literature on rocking columns demonstrated the need for better physical understanding of uplifting RC columns. Sakellaraki et al. [2005] performed experimental testing and analysis of a small-scale elastic column that experienced no inelastic loading during shaking. Representative modeling of elastic soil was done via a rubber pad. The testing did not explore the behavior of uplifting systems when there is a transition to inelastic response of the supporting column. A study presented by Nagai and Kawashima [2006] assessed the effect of two horizontal components of excitation on the behavior of piers supported on foundations allowed to rock. The work illustrated analytically that foundation rocking significantly reduced the plastic deformation of the column for one component of excitation and even more when considering two components of excitation.

To date there has been little work published on the experimental testing of uplifting RC columns resting on spread footings. Better understanding of the characteristics of uplifting systems would identify when the already-known potential benefits of rocking systems would occur and under what conditions allowing a system to uplift could be detrimental to performance. There are several response modes to consider for uplifting bridge piers: rocking on flexible soil without uplift and elastic column response, rocking and uplift on the flexible soil with elastic column response, rocking without uplift and inelastic column response, and the simultaneous occurrence of rocking, uplift and inelastic column response.

Through a series of earthquake simulator tests, the specimen presented herein investigates the seismic performance of a conventional RC bridge column with varying footing widths under near-field forward-directivity strong ground motion excitations. A single specimen was tested for three different types of footing width and axial load combination. The prototype column used as the basis of the test specimen is described in Section 3.2. The design of the specimen including scaling laws, column, footing, elastic soil representation, steel brackets, and mass blocks are described in Section 3.3. The construction sequence is described in Section 3.4. Measured material properties for elastomeric pad, concrete, and steel are described in Section 3.5. The test set up for investigating uplifting columns is described in Section 3.6. The instrumentation, data acquisition system, and test documentation are described in Sections 3.7, 3.8, and 3.9, respectively. Grounds motions used in testing are described in Section 3.10. Finally, the testing sequence for all runs of the specimen is described in Section 3.11.

3.2 PROTOTYPE COLUMN

To simplify the investigation, a cantilever reinforced concrete bridge column considered in previous shake table studies conducted at the University of California, Berkeley (UC Berkeley) (Hachem et al [2003]; Sakai and Mahin [2006]; Jeong et al. [2008]) was selected as the prototype (see in Figure 3.1). The column was designed in accordance with the Caltrans SDC [2004a]. The prototype column used had a circular cross section 6 ft in diameter. In order to achieve a target aspect ratio of 6, the column was specified as 36 ft high, as measured from the bottom of the column to the center-of-mass of the superstructure. The axial load was taken to be 0.10 $f'_{co}A_g$ based on a typical nominal strength of unconfined concrete of 3.25 ksi.

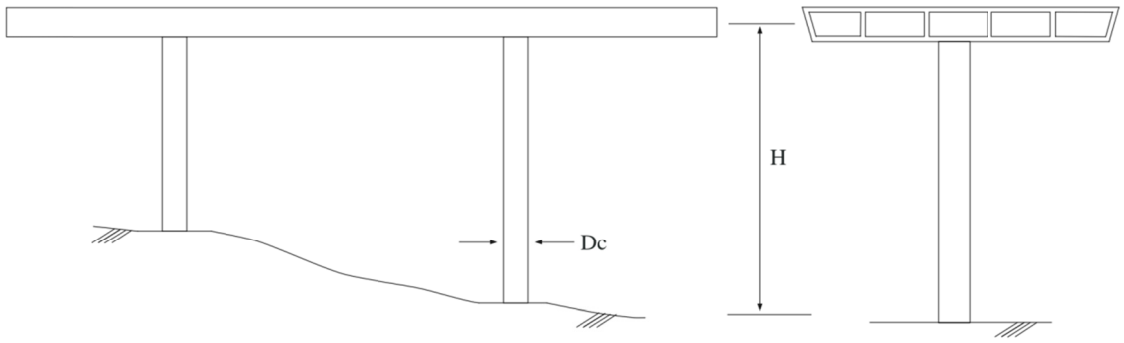

Figure 3.1 Prototype column.

The prototype column was reinforced longitudinally with forty-eight No. 9 deformed bars, providing a longitudinal reinforcement ratio (ρ_l) of 1.18%. Confinement of the concrete core was achieved using No. 5 spirals spaced at a 3 in. pitch, resulting in a volumetric ratio (ρ_s) of 0.61%. Nominal yield strength of the longitudinal and spiral reinforcement was considered to be 60 ksi.

Column strength per the SDC [Caltrans 2004a] is independent of the specified footing dimensions. Thus, there is no effect on column strength for varying the footing. Based on typical Caltrans analysis assumptions and procedures, the ultimate lateral load capacity of the fixed-base column was 290 kip, with a corresponding yield and ultimate displacement of 4.3 in and 22.8 in, respectively. Thus, the column has a displacement ductility capacity of 5.2. The effective natural period of the prototype column is 1.26 sec.

Once the dimensions and geometry of the prototype column were determined, a subsequent analysis was performed to assess the effect of ground motion and footing size on global displacements and local column flexural and shear demands. The prototype was modeled using a detailed fiber element model for the column, nonlinear Winkler beam foundation for the soil, and rigid beams for footing elements. Several hundred analyses were run for multiple footing widths, ground motions, and amplitude scales. The results were used to select appropriate footing dimensions and ground motions for consideration in these tests.

3.3 DESIGN OF SPECIMENS

Many experimental tests are not conducted at full-scale size due to the lack of available equipment and the relatively high cost of fabricating specimens. Additionally, shake table tests are limited by the physical table size and the range of displacement, velocity, and acceleration values the simulator can impose. The combination of these factors, in addition to many others, often requires specimens be built at a reduced scale.

Based on work done by Hachem et al. [2003], described in Section 3.2, the diameter of the column was set at 16 in., corresponding to a model length scale factor of 4.5. The length-scale factor was used as the basis for computing other necessary quantities for scaling of the test specimen.

3.3.1 Model Scaling

Dimensional analysis provides a methodology for how to scale the dimensions, material properties, and loads for the model specimen. The rules of scaling for dynamic tests include time-dependent parameters such as strain rate, velocity, and acceleration in addition to those for statically loaded specimens. Dimensional analysis of the dynamic tests was performed considering the scale-length factor [Equation (3.1)] the acceleration of gravity be maintained [Equation (3.2)] and the modulus of elasticity of materials be identical [Equation (3.3)]. By stipulating that the acceleration of gravity be maintained, the strains in the test specimen and prototype were identical. Furthermore, if the same materials are used in the model and prototype, then the same stress levels would be expected for each specimen. Table 3.1 summarizes the dimensional similitude requirements for the dynamic test under the condition that acceleration of gravity is maintained. For further discussion of dimensional analyses, see Krawinkler and Moncarz [1982].

$$L = 4.5 \tag{3.1}$$

$$LT^{-2} = 1 \tag{3.2}$$

$$ML^{-1}T^{-2} = 1 \tag{3.3}$$

To scale all quantities appropriately, imitations exist. For instance in the case of scaling concrete, small-scale models are problematic as the aggregate and sand dimensions do not have the same mechanical properties as the full-sized material. To avoid this phenomenon, typically a regular concrete mix design utilizing slightly reduced aggregate size is employed for moderately-reduced scale specimens.

Table 3.1 Similitude requirements and scale factors for column test.

Quantity	Scale Symbol	Target Scale Factor	Scale Factor Value Used
Length	S_d	S_d	4.50
Time	S_t	$S_d^{1/2}$	2.12
Frequency	S_ω	$S_d^{-1/2}$	0.47
Displacement	S_d	S_d	4.50
Velocity	S_v	$S_d^{1/2}$	2.12
Acceleration	S_a	1	1
Mass Density	S_ρ	S_E/S_d	0.22
Strain	S_ε	1	1
Stress	S_σ	S_E	1
Modulus of Elasticity	S_E	S_E	1
Force	S_F	$S_E S_d^2$	20.25
Moment	S_M	$S_E S_d^3$	91.13
Energy	S_W	$S_E S_d^3$	91.13

3.3.2 Design of Test Specimens

Based on the design of the earlier RC bridge column specimens [Hachem et al. 2003; Sakai and Mahin 2006], a single 16-in.-diameter RC column specimen was designed. The clear cover to the spiral reinforcement was set at 1/2 in. The footing design was altered to investigate the effects of footing width on foundation uplift. The footing was cast monolithically with the column and had square dimensions of 48 in. × 48 in. that were three times the column diameter ($3D_c$). Horizontally oriented post-tensioning ducts were provided to facilitate the widening of the footing in some tests.

The general specimen design was nearly identical to the design of specimens in previous studies of fixed-base columns, except for the footing width and supports provided for supporting the top mass block. To facilitate construction, reusable steel brackets were designed to support the top mass blocks. Reinforced concrete slabs were used as the mass blocks and attached to the top of the column via the steel brackets. Figure 3.2 shows the effective height of the specimen with mass blocks installed to represent the weight and inertial mass of the superstructure.

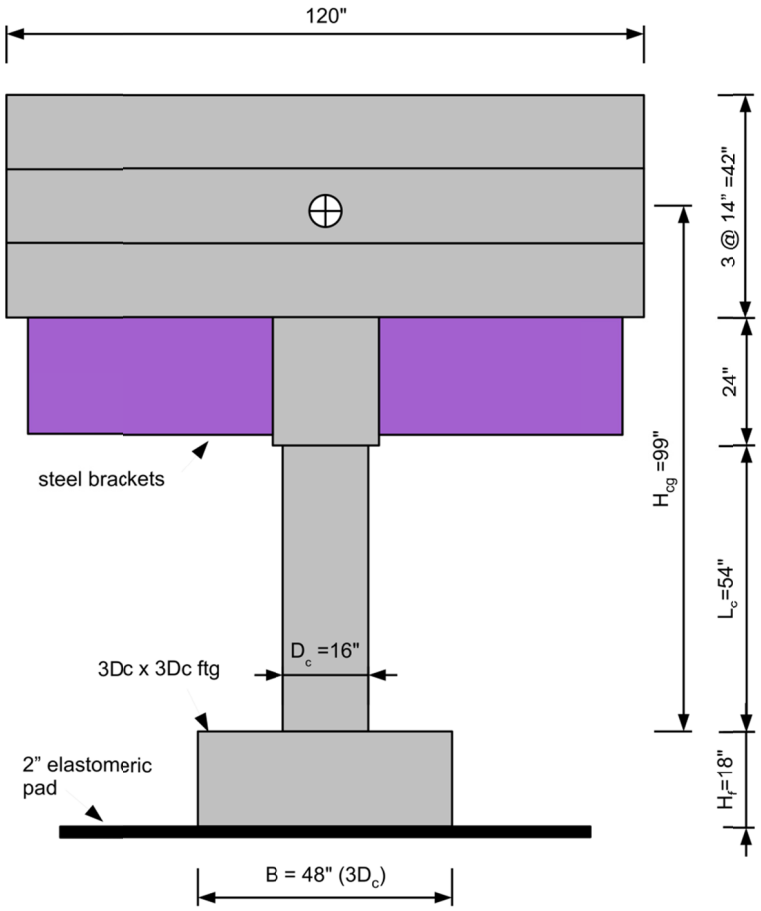

Figure 3.2 Specimen with mass blocks.

To provide the specimen with representative *in situ* concrete properties, normal density hard rock concrete was specified with a design strength of concrete $f_{co} = 5\,\text{ksi}$. The axial dead load from the combination of steel brackets and three weight blocks was 54 kip, which when combined with the measured column concrete strength of 5.25 ksi resulted in an axial force ratio $\left(\alpha_{DL} = P/f_{co}A_g\right)$ of 5.7%.

Following the static pushover analysis procedures recommended by Caltrans [2004a], the yield and ultimate displacement capacities and the lateral strength of the specimen were evaluated for a fixed-base condition to be 1.02 in, 8.26 in, and 15 kip, respectively. When expressed as a drift ratio (displacement divided by column height measured from bottom of column to center of gravity of mass blocks), the yield and ultimate displacement occurred at drift ratios of 1.02% and 8.3%, respectively. Using procedures developed by Priestley et al. [1996], the plastic hinge length was calculated as 12.9 in.

3.3.2.1 Column Reinforcement

The column was reinforced with twelve No. 4 deformed grade 60 (A706) reinforcing bars. This resulted in a longitudinal reinforcement (ρ_l) ratio of 1.18%. The design axial load was calculated to have a moment capacity of about 1400 kip-in.. The amount of steel was selected based on

satisfying the SDC [Caltrans 2004a]. At footing end of the bar, 90° hooks with a bend radius of 6 bar diameters (d_b) were used. See Figure 3.3 for a graphical depiction.

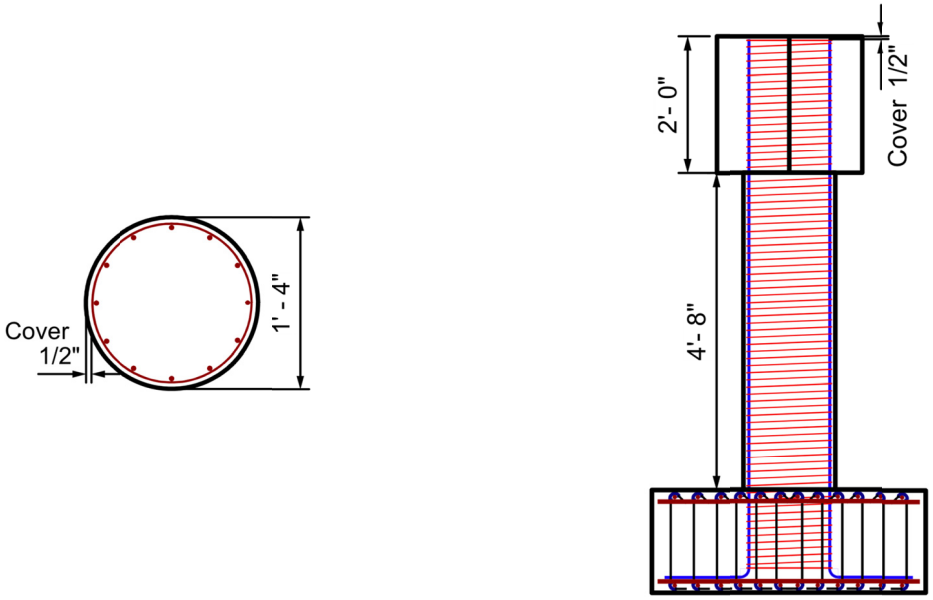

(a) column cross-section (12 No. 4 Grade 60 longitudinal bars; W3.5 smooth Grade 80 wire spirals with a 1-1/4 in. pitch)

(b) specimen

Figure 3.3 Column reinforcement details.

3.3.2.2 Spiral Reinforcement

Although the 6-ft-diameter prototype column was used to calculate a required volumetric ratio of spiral reinforcement equal to 0.54% [Caltrans 2004a], smooth wire with a diameter small enough to satisfy the volumetric ratio was not available. A larger diameter continuous W3.5 Grade 80 (ASTM 82) smooth wire with d_{sp}= 0.211 in. and A_{sp}= 0.035 in.^{2} was used, resulting in a volumetric ratio of spiral reinforcement (ρ_s) of 0.61%.

3.3.3 Footing

The footing was designed to remain elastic and as rigid as possible during the tests to avoid additional deformation caused by flexure or shear loading in the system. Design forces for the footing were evaluated based on a safety factor of 4, the plastic moment capacity of the column when the plastic hinge was fully developed. The Caltrans Bridge Design Specifications (BDS) [Caltrans 2004b] require that the footing be capable of developing the full plastic moment capacity of the column. Regulations on footing thickness are limited to the ability to develop the mentioned column capacity. Reinforcement ratios for the designed specimen footing exceeded those required [Caltrans 2004b] .The footing was directly connected to the bottom of the column and rested on top of the elastomeric pads that were centered on the earthquake simulator platform.

The 4-ft-square, 18-in.-thick footing was reinforced longitudinally with No. 6 deformed bars. Transverse reinforcing consisted of No. 3 stirrup ties. See Figure 3.4 for footing details. To widen the footing from $3D_c$ square to $3D_c$ x $5D_c$, 1-1/8-in.-diameter high-strength post-tensioning rods were used to fasten concrete blocks to the existing footing. The blocks were cast from the same concrete batch and had the same height as the existing footing, with a plan depth of 1Dc such that when attached to both sides would create a new width of $5D_c$. To expand the footing, blocks which had the same reinforcement ratio as the footing were connected to the square footing using high-strength grout and post-tensioning rods. See Figure 3.5. The weight of the footing was 3.6 kip for the $3D_c$ x $3D_c$ configuration. Expanding the footing to $3D_c \times 5D_c$ created an additional weight of 2.4 kip for a total of 6.0 kips.

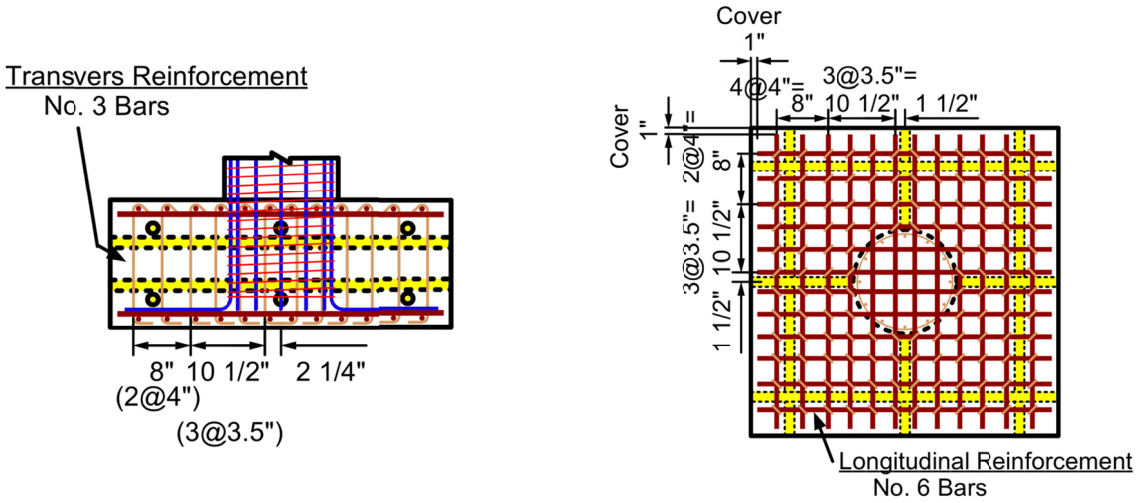

Figure 3.4 Footing reinforcement details.

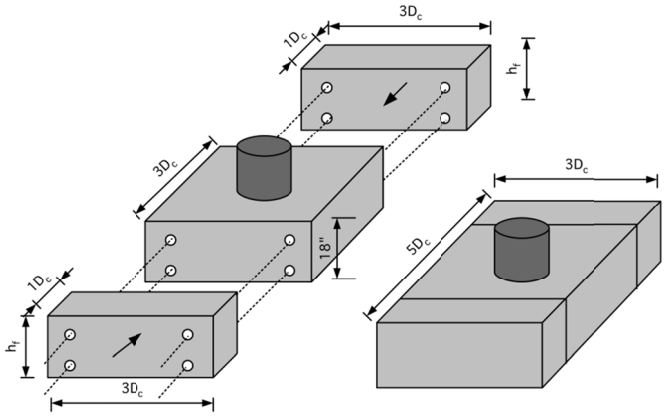

Figure 3.5 Footing configuration for $3D_c \times 5\ D_c$.

3.3.4 Elastomeric Pad

The elastomeric pad was chosen such that the initial stiffness was similar to that of a competent dense sandy soil. A thorough review of available material types and thickness found that the target properties that best matched the initial stiffness of sand soil were a 2 in. thick commercial

Neoprene Duro 80 that satisfied ASTM D-2000 standards. Single pieces of Duro 80 were not available in the size needed to extend beyond the footing edges. Instead, two separate pieces (8 ft × 2 ft-6 in.) were used to support the 3Dc square footing and the 3Dc x 5Dc footing, and still maintain a minimum of 6 in. pad clearance from the footing on all sides (Figure 3.6). Bearing properties of the pad were determined from uniaxial compression tests of a 12-in.-square sample of the same material. The results are presented in Chapter 4.

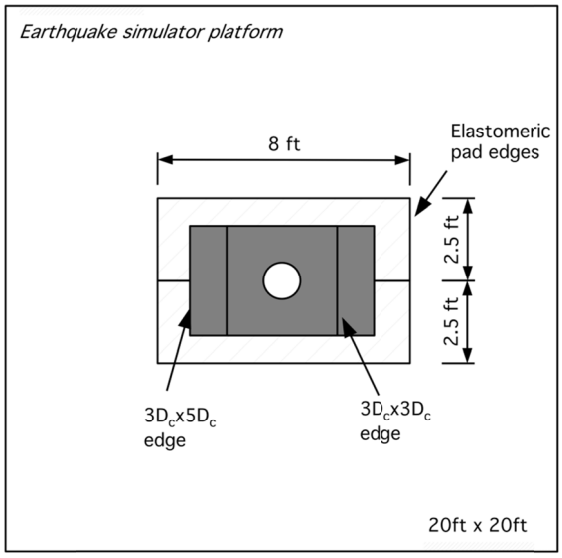

Figure 3.6 Elastomeric pad and footing edges.

3.3.5 Steel Brackets

Four steel brackets connected to the top of the column via 1-1/8-in. high-strength post-tensioning rods supported the mass blocks. The steel brackets were checked using an appropriate factor of safety for bending and shear due to the supported dead load of the weight blocks. The steel bracket weight for all four was 1.84 kip. Excluding the mass blocks, the total weight of the steel brackets, column, and $3D_c$ square footing was 7.12 kip.

3.3.6 Mass Blocks

Three 10 ft × 10 ft × 14 in. concrete blocks were used to represent the weight and mass of the superstructure of the bridge. The blocks were post-tensioned to the steel brackets via 1-1/8-in high-strength steel rods to ensure they acted as a unit. The weight of each block was approximately 17.1 kip, resulting in a total weight of 54 kip for the mass blocks and steel brackets.

3.4 SPECIMEN CONSTRUCTION

To model the simple inverted pendulum, several options were considered. The design was governed by several factors including cost, ease of construction and use, safety, and method reusability for future testing of additional single column cantilevers. The design considered options previously erected for shake table tests (e.g., Hachem et al. [2003]) before deciding on a system where steel brackets would be post-tensioned to the top of the column thereby creating a support frame that would support mass blocks to achieve the desired axial stress.

The construction site used an existing level platform but modified it appropriately. Formwork was erected for the footing as well as the blocks that would be used to widen the footing during testing (Figure 3.7). During this time, the four longitudinal bars that were to have strain gauges attached were prepared and instrumented. The bottom layer of steel for the footings was placed as well as the steel necessary for the widening blocks of the footing.

The column cage was constructed next using twelve No. 4, bars including the four instrumented bars with strain gauges (two per bar along the bar height for a total of eight gauges). Next, the cage was spirally reinforced along the column height with W3.5 wire (0.21 in diameter) at a pitch of 1.25 in. At the top of the column where the post-tensioned steel brackets were connected, the pitch of spiral reinforcing was reduced to 0.5 in. The column cage was installed at the center of the footing and tied to the bottom steel layer (Figure 3.8). Next, the top layer of footing reinforcement and the 2-in.-diameter PVC ducts used for widening the footing were installed. The PVC pipes extended along the entire length of the footing in each direction to create a connection for the widened blocks (Figure 3.9). The No 3. hooked bars for transverse reinforcement were then placed, and the footing and blocks were ready to be cast.

The specified design strength of the footing was larger than the column, requiring that the footing and blocks to be cast separately (Figure 3.10). Several 6 in. diameter × 12-in. long cylinders were cast for testing the compressive strength of the concrete at 7 and 28 days, and the testing date as necessary. The slump of concrete, which had been specified as 5 in., was measured to be 3.5 in. for the footing. After casting, the footing and blocks were covered with plastic sheathing and allowed to cure. Following the necessary curing time, the joint area at the column-footing interface was sand blasted and cleaned in preparation for casting the column. A circular column form was placed that had holes cut in it to allow installation of additional instrumentation equipment. Threaded 1/2-in.-diameter rods were installed transversely through the holes in the column to provide a method of measuring curvature distribution along the column height (Figure 3.11). For monitoring the strain gauge readings, wiring guided along the longitudinal bars to an exit point at the column mid-height. At the top of the column, formwork was added to create the block to which the steel brackets would be connected. The PVC ducts and additional No. 3 transverse reinforcement were added as necessary for the design objective. The column and top block were then cast and allowed to cure for 28 days before removal of the formwork (Figure 3.12). Again, several 6 in. x 12 in. concrete cylinders were cast for measuring the concrete compressive strength at 7 and 28 days, and the shake table test date. The specified slump for the column was 5 in. and measured as 9.5 in.

Figure 3.7 Footing forms (rocking column at top right).

Figure 3.8 Column cage and footing steel.

Figure 3.9 Casting footing.

Figure 3.10 Footing and blocks before column casting (rocking column center of specimens).

Figure 3.11 Threaded rods for measuring column curvature.

Figure 3.12 Column and top block (rocking specimen in center).

3.5 MEASURED MATERIAL PROPERTIES

3.5.1 Steel Reinforcement Properties

The column longitudinal steel was specified as ASTM A706, Grade 60 steel. Mechanical properties of the reinforcing bars were determined using tensile tests of sample steel coupons. The average values for three sample coupons for yield strength, ultimate strength, and modulus of elasticity of the No. 4 bars was 69.1 ksi, 90.9 ksi, and 29,090 ksi, respectively. See Figure

3.13. The spiral reinforcement was specified as ASTM 82, Grade 80. No tensile tests were performed due to the absence of coupons for spiral samples. No certified mill test report was available for the spirals.

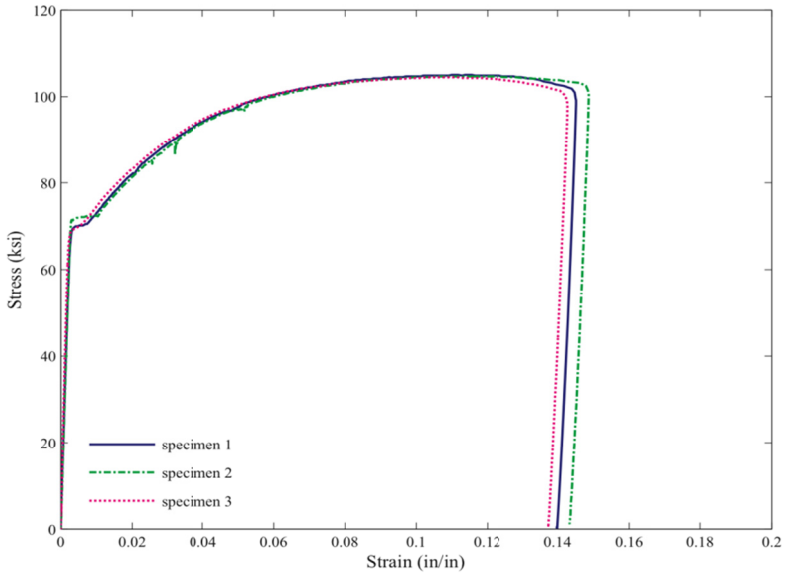

Figure 3.13 Stress-strain curve for grade 60 ASTM 706 bars.

3.5.2 Concrete Properties

To represent the actual properties of concrete used in modern RC bridges, the concrete for the columns was specified as normal weight with a 28-day strength of no less than 4 ksi and no more than 5.5 ksi. Mix design details are presented in Table 3.2. Twenty seven, 6 in. x 12 in. standard cylinders were prepared at the casting of the column and were used to measure the concrete compressive strength and stress-strain relationship. When the forms from the footing and columns were removed, so were the casings of the corresponding cylinders. Compressive strength tests were performed at 8 and 29 days after casting of the footing. Column concrete compressive strength tests were performed at 7, 14, 21, and 28 days after the column casting date. Additional cylinders of each group were tested the day following their respective shake table test.

At each test date, three cylinders were tested. The column concrete had a 28-day strength of 3.9 ksi, while the footing concrete had a strength of 5.25 ksi. The average strength of column concrete on testing day was about 4.7 ksi. The average tangent and secant modulus of elasticity of concrete for the specimen—defined by Equation (3.4) and Equation (3.5)—were calculated to be 2753 ksi and 2453 ksi, respectively. Values from testing of the cylinders are presented in Table 3.3 and shown plotted in Figure 3.14 and Figure 3.15.

$$E_{c-\tan} = \frac{f_{c-50}}{\varepsilon_{c-50}} \tag{3.4}$$

$$E_{c-\tan} = \frac{f_{c-50} - f_{c-25}}{\varepsilon_{c-50} - \varepsilon_{c-25}} \tag{3.5}$$

Table 3.2 Concrete mix design.

Mix Specifications	Cement	ASTM C-150 TYPE II
	Fly ash	ASTM C-618 CLASS F, 15%
	Admixture (water reducer)	ASTM C-494 TYPE A
	Minimum 28-day strength	3850 psi
	Maximum 28-day strength	4350 psi
	Cementitious sacks/yd^3	5.60
	Maximum size aggregate	3/8 in.
	Slump	5 in.
	Water/cement ratio	0.603

	Material	**Specific gravity**	**Absolute volume**	**SSD weight**
Mix Design and Quantities	3/8in. × #8 gravel	2.68	5.98 ft^3	1000 lb
	Regular top sand	2.67	9.02 ft^3	1503 lb
	SR blend sand	2.60	3.69 ft^3	599 lb
	Cement Type II	3.15	2.27 ft^3	447 lb
	Fly ash	0.00	0.55 ft^3	79 lb
	Water	1.00	5.08 ft^3	317 lb
	Water reducer	-----	0.41 ft^3	26.3 fl oz
	Total	-----	27 ft^3	3945 lb

Table 3.3 Compressive strength of column concrete cylinders.

Day	No. 1 (ksi)	No. 2 (ksi)	No. 3 (ksi)	Average (ksi)
7	2.20	2.52	2.18	2.30
14	2.93	2.88	2.97	2.93
21	3.53	3.60	3.49	3.54
28	3.86	3.88	3.97	3.90

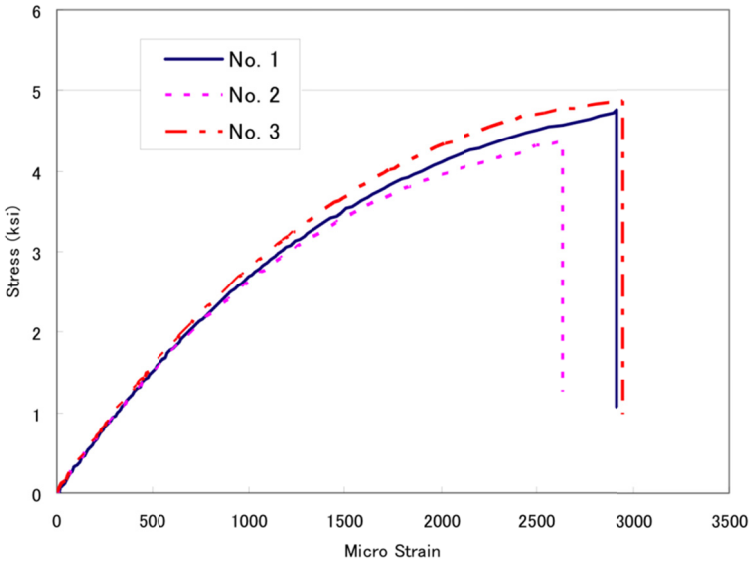

Figure 3.14 Stress-strain curve of concrete cylinders at test date.

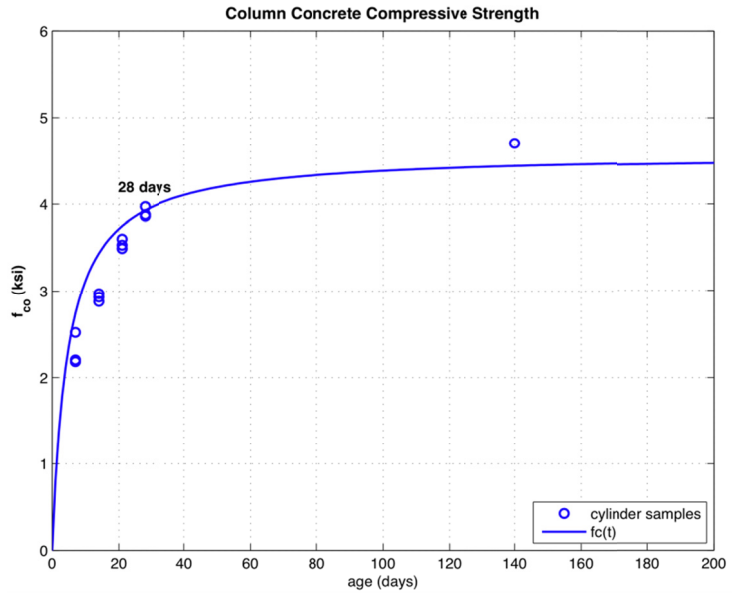

Figure 3.15 Column concrete compressive strength versus age.

3.5.3 Elastomeric Pad

The elastomeric pad was tested uniaxially at a cyclically increasing amplitude with only force compression. The load behavior was determined by an initial application of a small force, removal of the load, and then application of a larger force. This was repeated until the final load considered had reached a strain value that corresponded to a deflection equal to 7% of the pad thickness. See Figure 3.16. From compression data, the modulus of elasticity E_{pad} during the loading phase was calculated to be approximately 3000 psi $\left(\sigma = E_{\text{pad}}\varepsilon\right)$ from best fit data [Equation (3.6].

$$E_{\text{pad}} = \frac{\sigma_2 - \sigma_1}{\varepsilon_2 - \varepsilon_1} \tag{3.6}$$

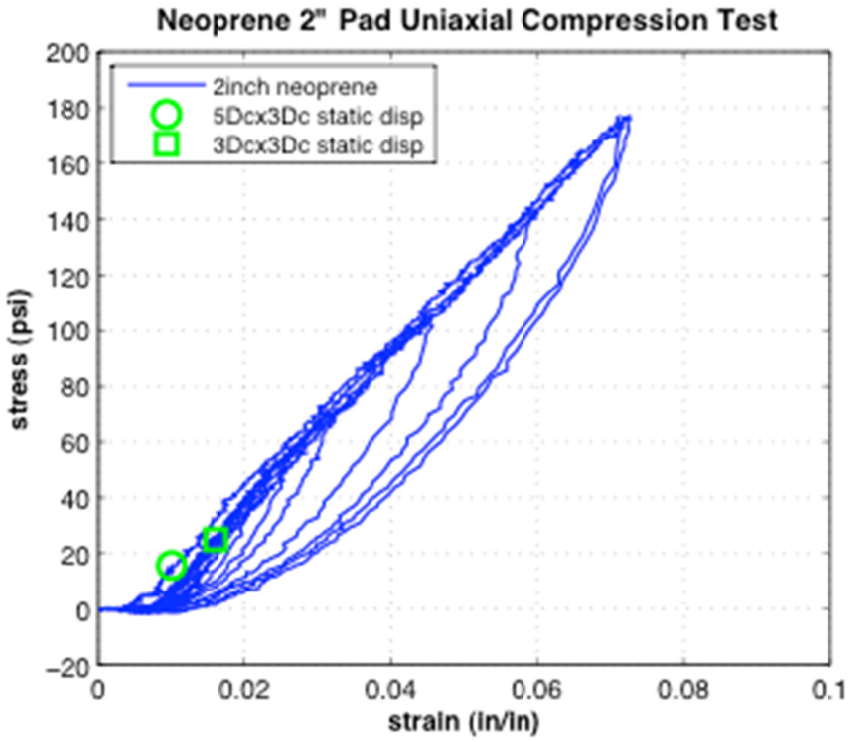

Figure 3.16 Stress-strain curve of compression test of 2 in.-thick elastomeric pad sample.

3.6 TEST SET UP

A series of shake table tests was performed at the Earthquake Simulation Laboratory, located at the Richmond Field Station of UC Berkeley. Three test group geometric configurations were selected for testing on the earthquake simulator: (1) a footing width of $3D_c \times 3D_c$ with one weight block with a nominal axial load ratio of 3% $f_c' A_g$; (2) a footing width of $3D_c \times 3D_c$ with three weight blocks with a nominal axial load ratio of 10% $f_c' A_g$, and (3) a footing width of $3D_c \times 5D_c$ with three weight blocks with a nominal axial load ratio of 10% $f_c' A_g$. Figure 3.17 shows the specimen set up on the table for the second test group.

To simulate a rocking base at the bottom of the footing, two 2 in. thick, 8 ft long × 2.5 ft wide elastomeric pads were laid down initially side-by-side and centered on the platform. No material was placed between the top of the table and the bottom of the pads. The pads were not fastened to the table; instead they were kept in place by utilizing friction from the normal load of the weight blocks, column, and footing. Away from the platform, the steel brackets were connected to the specimen at the top of the column. The brackets were placed in pairs along each diagonal direction and fastened to each other using 1-1/8-in.-high-strength steel rods that passed through the steel connection plate, the concrete block at the top of column, and through the steel

connection plate of the parallel bracket. For each face, a layer of grout was poured between the steel plate and concrete block to ensure uniform bearing stress and prevention of movement during testing. The column and steel brackets were then lifted and placed directly on top of the pads, and centered on the table using a 20 kip capacity bridge crane. Transfer to the table was done carefully to prevent any cracking in the column. No material was placed between the top of the pad and the bottom of the footing.

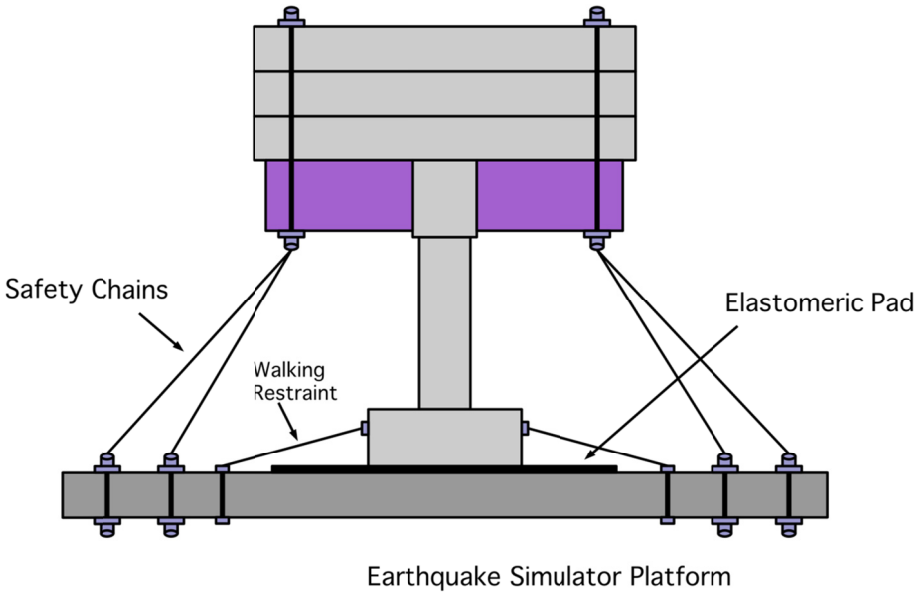

Figure 3.17 Group 2 specimen set up.

The mass blocks were then placed on top of the steel brackets and connected using 1-1/8-in.high-strength post-tensioning rods. Each bracket had a duct that corresponded with holes in the weighted blocks that allowed a rod to pass completely through all of the elements. A total of four rods were used to make the weighted block to steel bracket connections. At the interface between each block, block and steel bracket, and connection hardware, high-strength grout was used to ensure a uniform bearing stress and no-slip between the elements.

The initial test group used only one weighted block to validate test set up, verify instrumentation, and calibrate the analytic models used to plan the subsequent tests. The test set up for Test Group 1 is shown in Figure 3.18. For Test Group 2, the same procedure was followed as for Test Group 1, except that three weighted blocks were added to achieve the desired axial load ratio. Figure 3.19 shows the test specimen on the shake table. Upon completion of the second test group, all instrumentation was left in place with the exception of the footing instrumentation. For safety reasons, the weighted blocks were removed before lifting the specimen. The entire specimen was then lifted up 2 in using hydraulic jacks as measured from the top of the pad to the bottom of the footing, and then shored in place for installation of the footing widening blocks. Two blocks measuring $1D_c$ wide by $3D_c$ long and 18 in. thick were connected to opposing footing faces using high-strength rods and grout to create a wider footing size of $3D_c$ x $5D_c$. See Figure 3.20(b). The specimen was then reset back to the original position and the three weight blocks were reinstalled.

To prevent collapse of the specimen during testing, two steel chains were connected to each corner of the steel brackets. The length of each chain was adjusted to accommodate at least 10 in. (10% drift) of lateral column displacement, corresponding to the maximum displacement experienced in previous tests of fixed-based columns. The safety chains were used to prevent overturning of the column and mass blocks. To prevent excessive movement by the footing from "walking" while up uplifting, turnbuckles were used to allow approximately 2 in. of lateral displacement during each test. The details of footing restraint are shown in Figure 3.20.

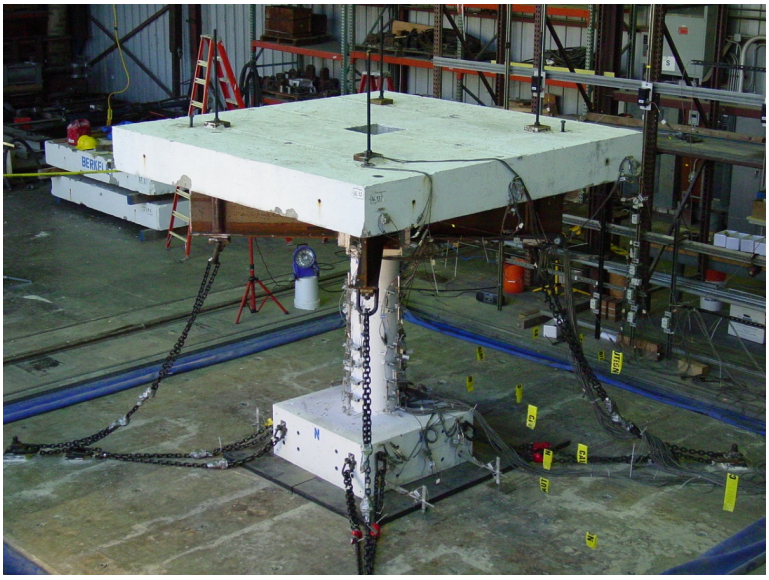

(a) specimen for Test Group 1

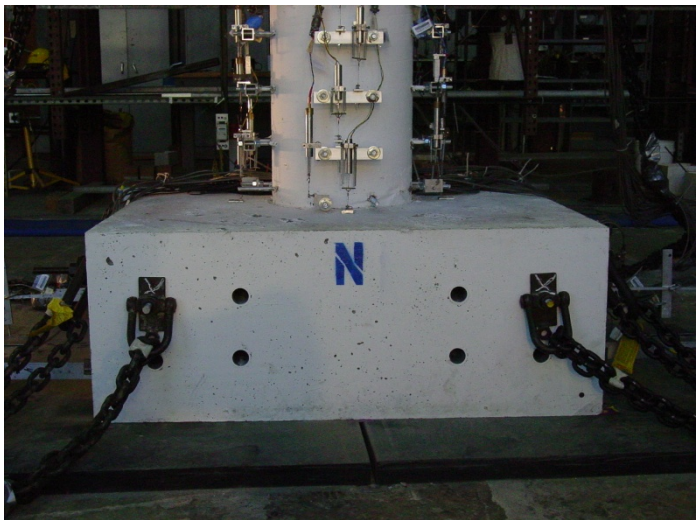

(b) footing and elastomeric pad

Figure 3.18 Specimen configuration for Test Group 1.

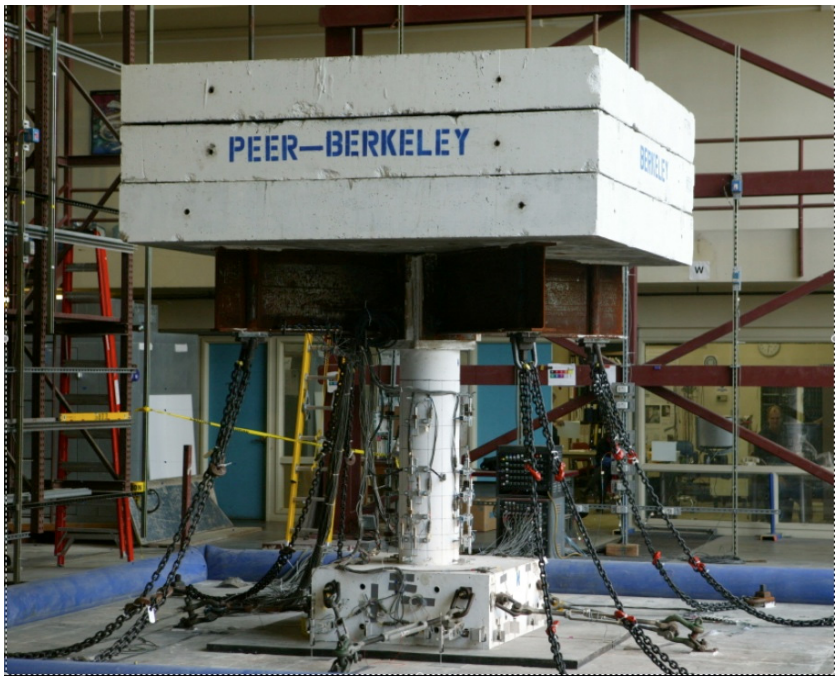

Figure 3.19 Group 2 specimen.

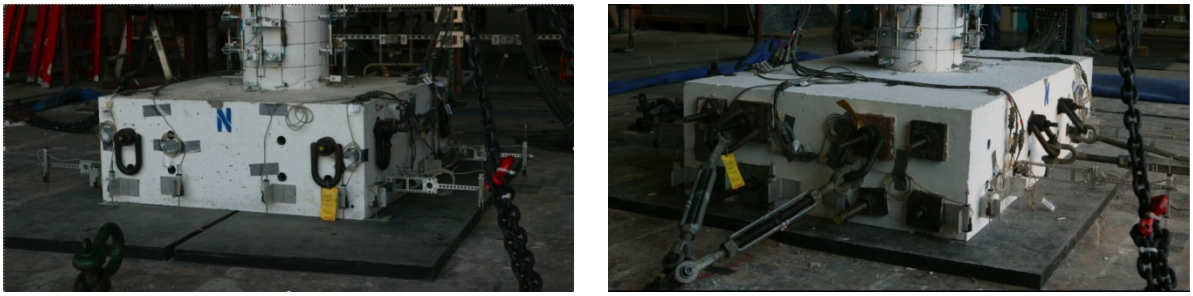

(a) Group 2 footing $3D_c$ x $3D_c$ **(b) Group 3 footing 3Dc x 5Dc**

Figure 3.20 Footing configuration with safety restraints.

3.7 INSTRUMENTATION

A vast instrumentation scheme was used to record the global response of the column, footing, and local deformations and strain at specific locations. A total of up to 118 channels were used in each of the shake table tests. The channels were recorded by a variety of instruments for measuring displacements, accelerations, strains, and forces. The 118 channels were distributed as follows:

- 16 channels for monitoring the accelerations and displacements of the shake table
- 21 channels for accelerometers at weight blocks and footings
- 28 channels for linear displacement potentiometers (LPs) monitoring global displacement
- 24 channels for direct current displacement transducers (DCDTs) monitoring local column deformation
- 8 channels for strain gauges measuring longitudinal reinforcing strain
- 20 channels for Novotechniks (NOVO) monitoring footing uplift displacement
- 1 channel for a linear voltage displacement transducer (LVDT) monitoring the displacement at center-of-gravity during free vibration test
- 1 channel for load cell monitoring of the pullback force during the pullback test

A more detailed overview of the distribution on the three test groups is presented below. The data was sampled at a rate of 200 Hz (0.005 sec). The sign convention for the global system is presented in Figure 3.21. The origin of the coordinate system was located in the *xy* plane at the center of the column. The origin of the *z*-axis was assumed at the bottom of the footing.

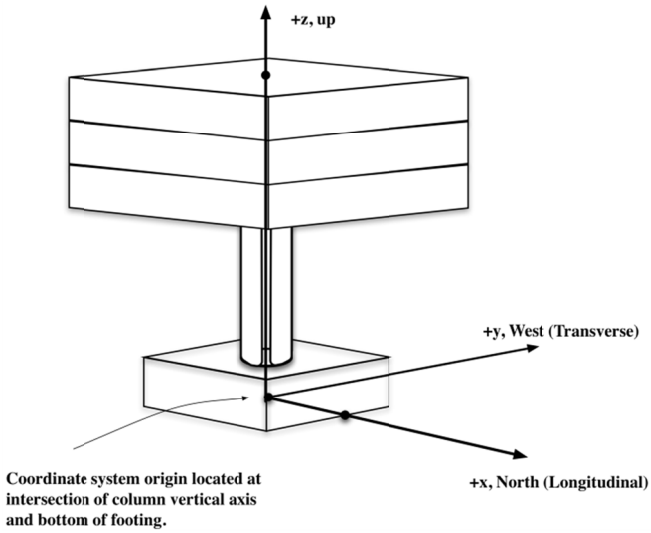

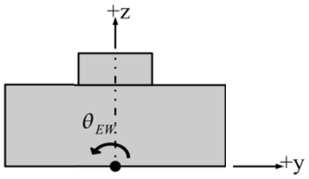

(b) *yz* plane of footing

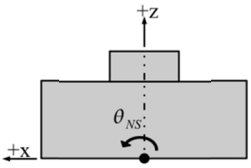

(c) *xz* plane of footing

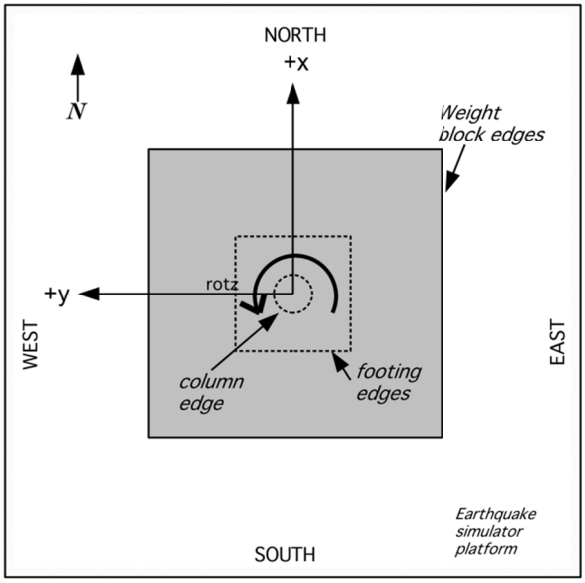

(d) table in plan view

Figure 3.21 Specimen global sign convention.

3.7.1 Shaking Table Instrumentation

A total of 16 channels was used to capture the movement of the shake table. Horizontal accelerations and displacements were monitored through four accelerometers placed on the stiffening beams under the table and four displacement transducers acting along the outer horizontal actuators. Vertical accelerations and displacements were monitored through four accelerometers and four displacement transducers placed near the four corners of the table. This instrumentation allows for computation of acceleration and displacement components in all 6

degrees-of-freedom of the shake table motion. See Figure 3.22 for a diagram of the shake table instrumentation.

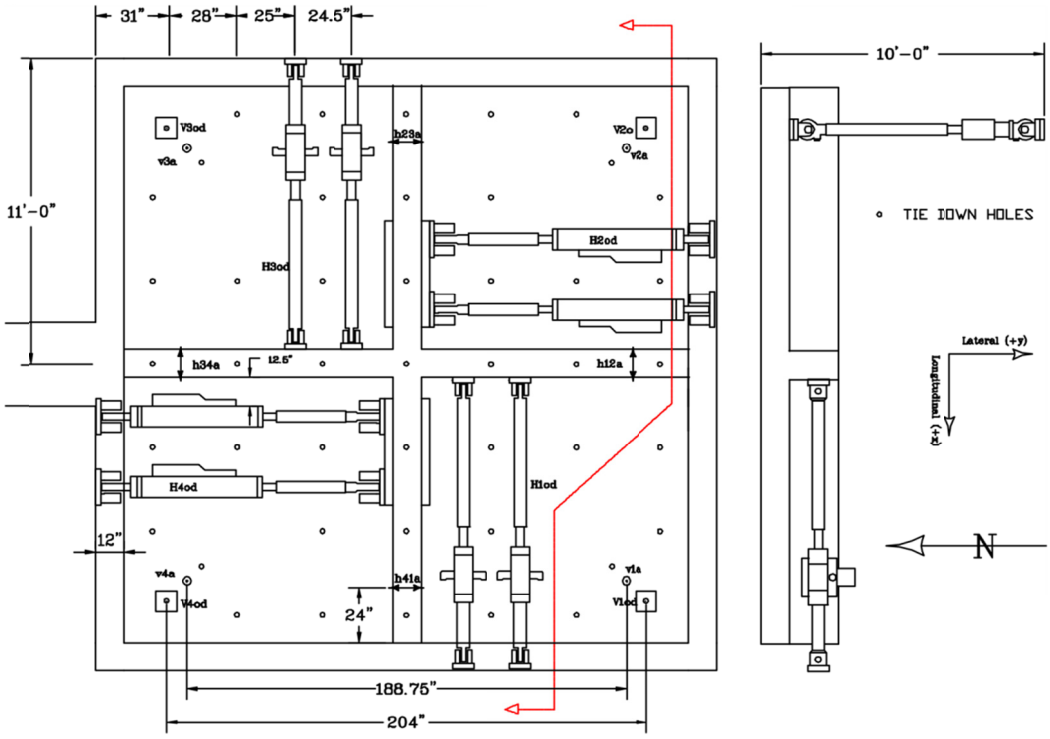

Figure 3.22 Shaking table instrumentation.

3.7.2 Accelerometers

Accelerations were measured by 21 accelerometers mounted at seven separate locations on the specimen and weighted blocks. Each location had a cluster of 3 one-dimensional accelerometers that were oriented in the *x*, *y*, and *z* orthogonal directions. Three groups were located on the weighted blocks at the center-of-gravity elevation on the west and south faces and on top of the blocks. The remaining four groups were located on the west and south footing faces. See Figure 3.24 through Figure 3.26 for depiction of the accelerometer locations of the three test groups. Each accelerometer group was positioned to coincide with a global displacement measurement using an LP.

3.7.3 Linear Potentiometers

Global displacements were directly measured by LPs installed on stiff frames located off the shaking table at the west and south faces. A total of up to 28 LPs shown in Figure 3.24 through Figure 3.26 were used for the three test groups. Five LPs were used for each face of the weights blocks: one at the center-of gravity of the weighted block assembly, two along the top near the corner edges and two more along the bottom near the corner edges. Rotational movement of the weighted block assembly was captured by the pairs located near the edges. The movement of

footing, including rotation about the vertical axis of the column, was monitored using three LPs on each footing face along the top edge: one at the center and two at the outer corners.

Local deformation of the column was captured by six LPs on the West and South faces. Used to measure the shape of the column during testing, they were located along the center line of each face at heights of 6 in., 12 in., 18 in., 24 in., 38 in., and 44 in. from the bottom of the column.

3.7.4 Direct Current Displacement Transducers

Twenty-four DCDTs were used to measure the relative vertical displacement between different sections along the height of the column. The data was then used to measure the approximate curvature over a region of height *h*. Figure 3.23 shows an expanded view of the typical DCDT column configuration. Figure 3.24 through Figure 3.26 show the locations of the DCDTS along the column height for each of the test groups.

Implementation of DCDT instrumentation used the 1/2-in.threaded rods installed through the column during construction. The rods were located at heights of approximately 1 in., 6 in., 12 in., 18 in., 24 in., and 38 in. The DCDTs were connected to aluminum tubing and fastened to the threaded rod such that they were located approximately 3-1/2 in. from the column surface. Actual horizontal distance between the DCDTs and the column surface, and vertical distance between the rods and the surface of the footing or top slab were measured prior to each test. The readings from the pairs of DCDTs located at the 1 in. and 6 in. heights were used to estimate the amount of rebar pullout from the footing.

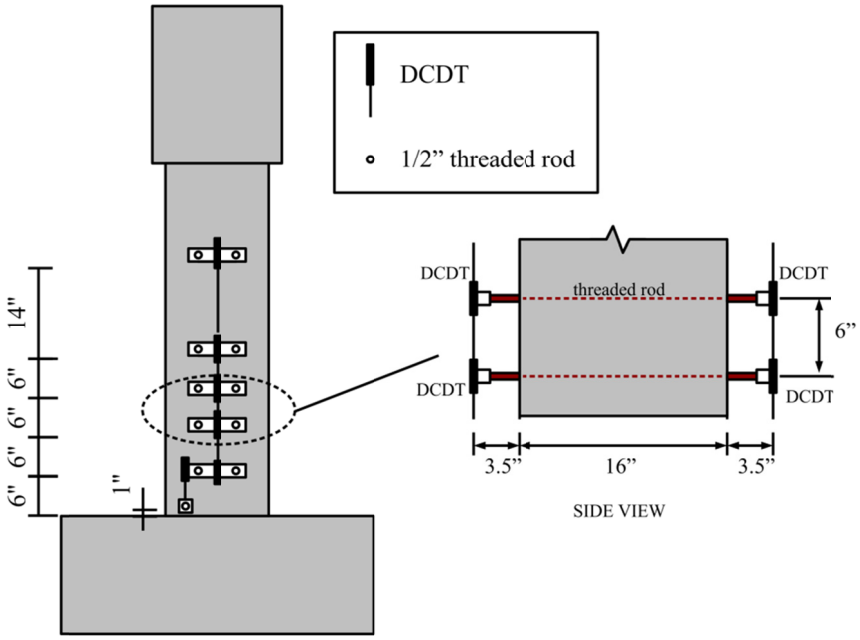

Figure 3.23 DCDT configuration along column height.

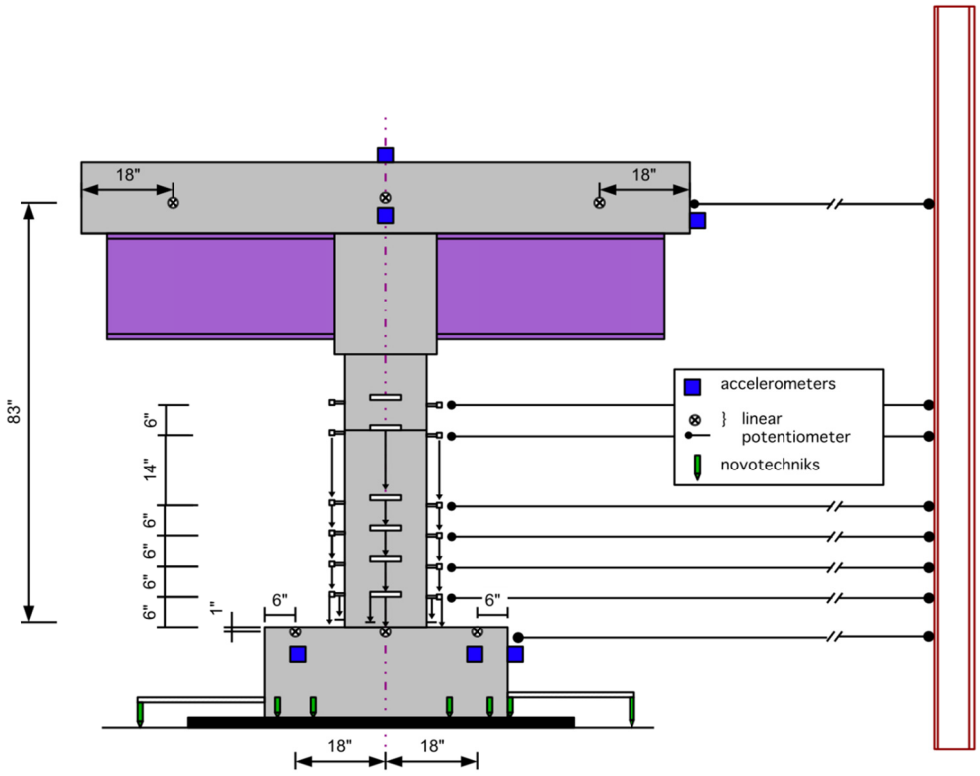

(a) specimen instrumentation elevation details

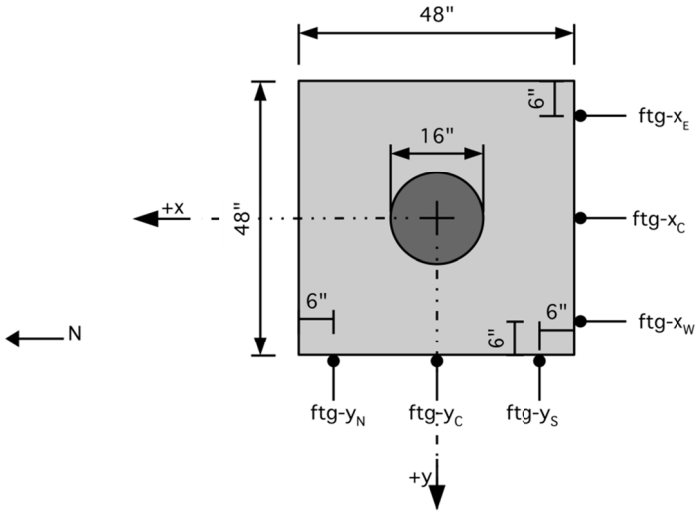

(b) footing linear potentiometer locations

Figure 3.24 Group 1 ($3D_c$x$3D_c$ footing) instrumentation details.

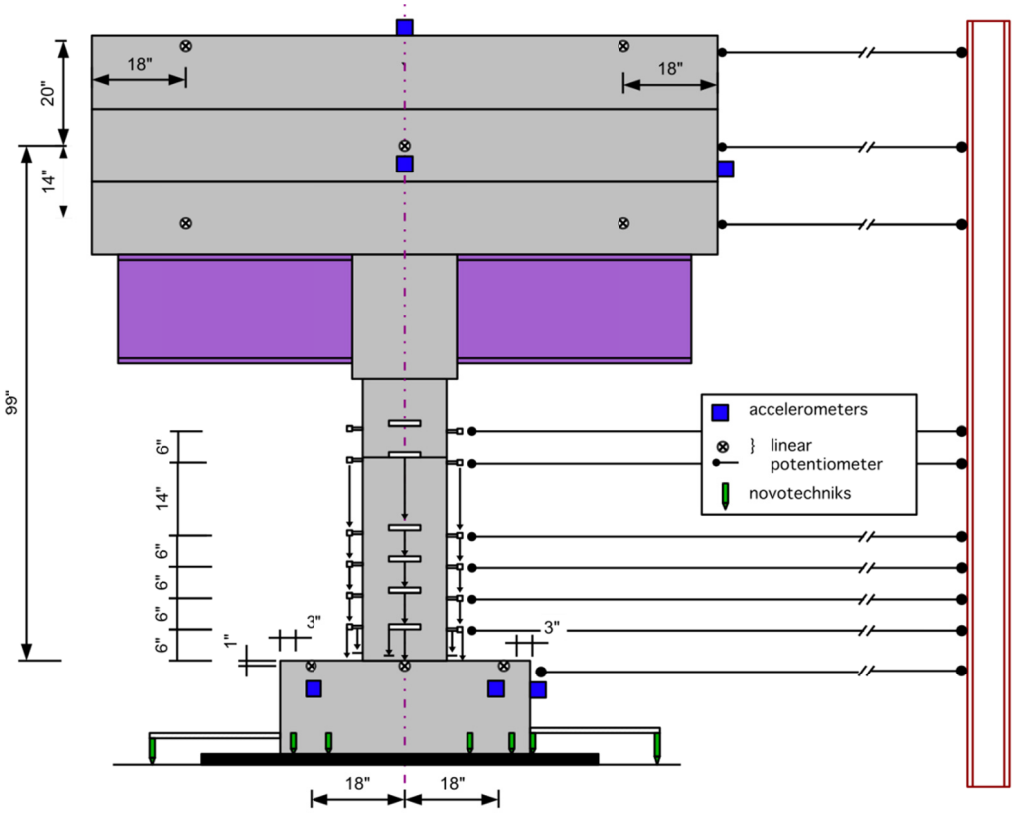

(a) specimen instrumentation elevation details

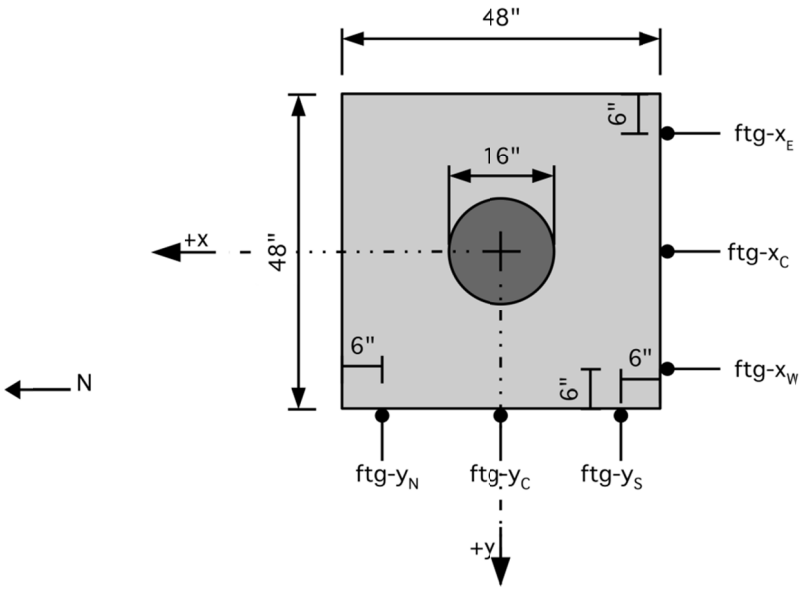

(b) footing linear potentiometer locations

Figure 3.25 Group 2 (3Dc×3Dc footing) elevation of instrumentation details.

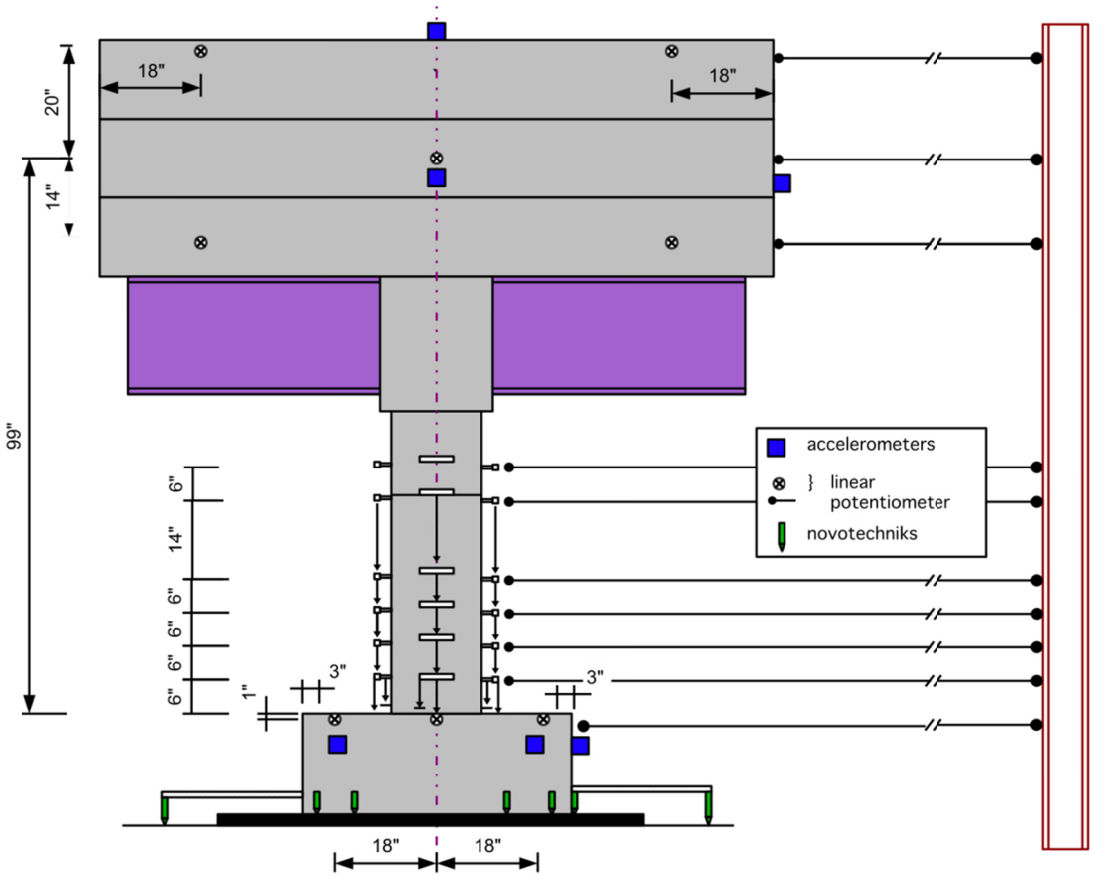

(a) specimen instrumentation elevation details

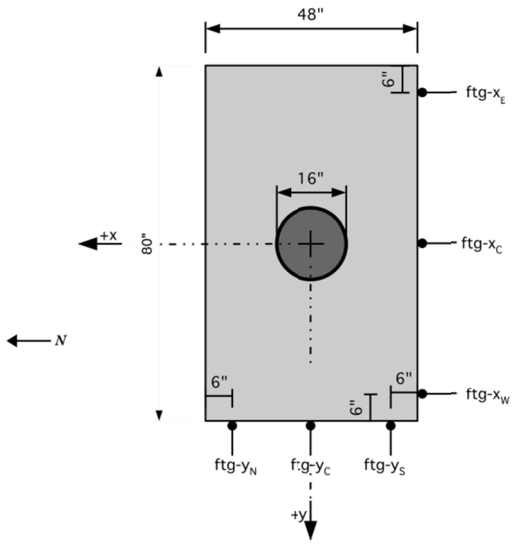

(b) footing linear potentiometer locations

Figure 3.26 Group 3 (3Dc×5Dc footing) elevation of instrumentation details.

3.7.5 Strain Gauges

A total of eight strain gauges were used to monitor strain of longitudinal reinforcement in the specimen. Four reinforcing bars, located at the north, east, south, and west sides, were gauged and protected with coating materials prior to construction. The gauges were positioned on the outside face of the rebar, located slightly above the top of the footing and 16 in above the top of footing. See Figure 3.27 for the typical strain gauge location. These locations were chosen to approximate the expected plastic hinge length per Priestley et al. [1996].

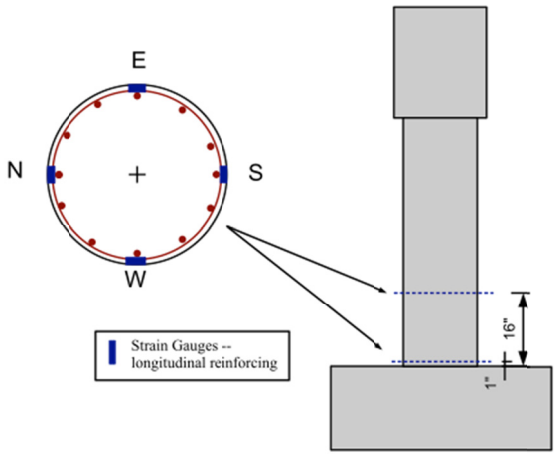

Figure 3.27 Locations of strain gauges.

3.7.6 Novotechniks (NOVOs)

A total of 20 NOVOs were used to monitor uplift displacement of the footing during testing. Measuring uplift during testing was critical to determining the rocking behavior of the system. To do this, four NOVOs were placed on each face of the footing to measure the relative displacement between the footing and the pad. In addition, two pairs of outrigger arms were rigidly attached to the footing and used to support NOVOs that measured the relative displacement between the tip of the outrigger and rigid slab of the simulator. Figure 3.28 and Figure 3.29 show the locations of the NOVOs for each test group and configuration. To accurately capture the pad displacement before each test, snapshot readings were taken as each new load was applied. This information was used to distinguish when the system was simply rocking or also uplifting from the pad.

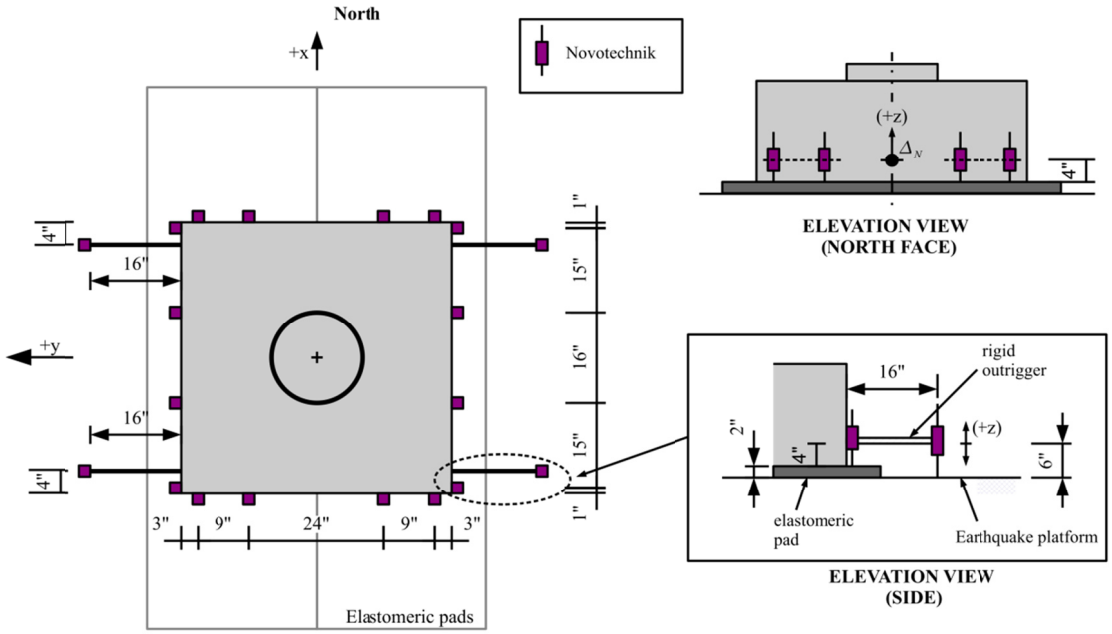

Figure 3.28 Novotechnik locations (Test Groups 1 and 2).

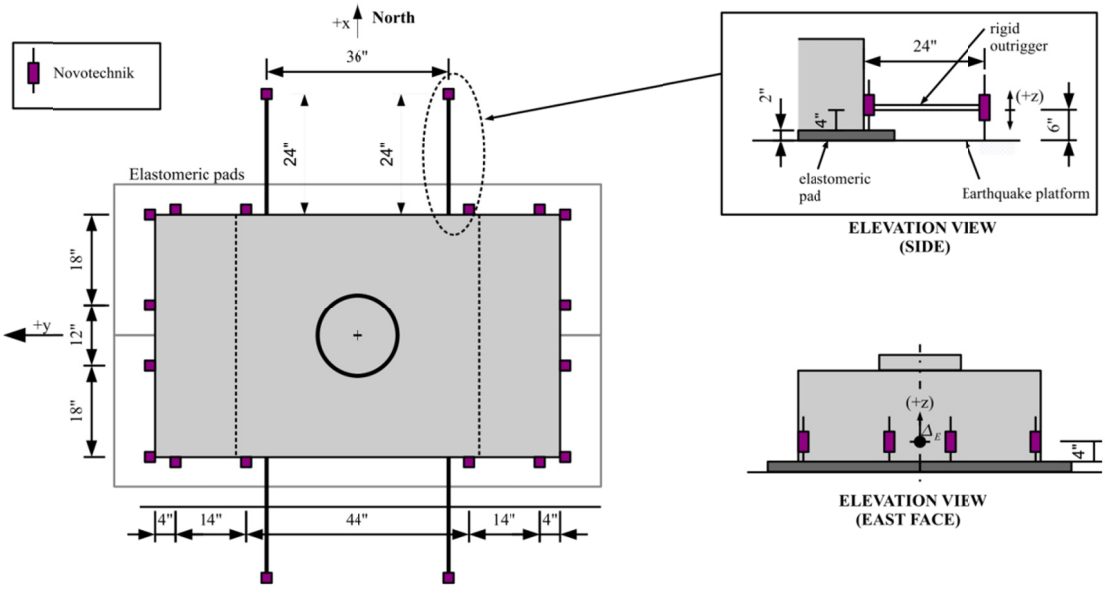

Figure 3.29 Novotechnik locations (Test Group 3).

3.8 DATA ACQUISITION

During the tests, data was recorded by the shaking table data acquisition software system. Each instrument of the system was calibrated using distinct cables. Data was recorded at a 200 Hz interval (0.005 sec) and saved to a text file. Each text file began with a header row. The first entry was the date and time stamp followed by a unique column entry for each instrument name. The text file was recorded as a MxN array, where M equaled one (for the header row) plus the number of time samples and N equaled one (for the time stamp) plus the number of instruments. Data recording was initiated a few seconds prior to the beginning of each earthquake signal and continued for several seconds following the end of each record to capture the free-vibration response.

3.9 TEST SPECIMEN DOCUMENTATION

In addition to the digital data recorded, digital videos were taken during the tests to document specimen behavior and the progression of localized damage. Five video cameras were used simultaneously: two focused on the bottom portion of the column—where the plastic hinge was expected to be developed at the east and north faces and capture uplift—and two cameras were used to capture the global response of the specimen from the east and north sides. The last camera was set along the diagonal axis to capture global movements. Digital photographs were taken prior to and after each test to document localized damage of the column. In the interim between tests, new concrete cracks that occurred during the tests were traced by hand and color coded for easy representation.

The specimens were painted white prior to testing, and a grid was drawn in black marker on the column to sub-divide and readily identify regions. The grid resolution was drawn by sub-dividing the column into 4-in.-tall segments, approximately 30° wide (~4.2 in). Each footing face, column face, and weighted block face were marked with a W, S, E, and N, respectively.

3.10 GROUND MOTIONS

As mentioned in Section 1.3, two ground motions were used for testing each of the three group configurations. Each test group was subjected to one, two, and three directions of excitations of the two ground motions.

3.10.1 Preprocessing of the Recorded Motions

Processing was done on both of the records to accommodate the displacement, velocity, and acceleration thresholds that could be delivered by the shake table. The three-dimensional components of each record were processed in a similar manner. First, the recorded time step was reduced by the square root of the length-scale factor (See Table 3.1). The magnitude of the amplitude was left unchanged. Next the ground motion was band-passed filtered to remove unwanted frequency components. The frequency characteristics of the band-pass filter included two cut-off points and two corner points. Finally, the amplitude of acceleration was scaled to meet the desired testing level. The design level was scaled such that the spectral acceleration of the record matched the target design spectrum at the period of the specimen.

3.10.2 1989 Loma Prieta Earthquake (Loma Prieta Record)

Each of the test groups was subjected to a modified version of the Los Gatos (PEER NGA Database [2005]) record of the 1989 Loma Prieta earthquake. The record was representative of a strong intensity near-fault forward-directivity ground motion. The specific records used were the two horizontal plus vertical components for the NF03 and NF04 motions of the SAC Steel project [2006]. The Loma Prieta earthquake had a moment magnitude of M_w=6.9. The Los Gatos records were recorded at a distance of 2.4 miles from fault rupture and a hypocentral distance of 15.9 miles. The soil conditions were classified as "soft rock," with a shear wave velocity of approximately V_{s30}= 1560 ft/sec. The record peak values were measured as PGA 0.78g, PGV 30.4 in/sec and PGD 16.8 in. Fault-normal and fault=parallel components were defined by NF03 and NF04, respectively. The vertical component was from the record NF03_04v. The ground motion—chosen because in preliminary analysis it was shown to cause large permanent displacements—was considered useful in determining the characteristics of systems allowed to uplift and yield. The records were scaled assuming a length-scale factor of 4.5. Thus, the time duration was scaled by √4.5 (~2.12). The original records were band pass filtered using cutoff frequencies of 0.4 Hz and 15 Hz and corner frequencies of 0.5 Hz and 12 Hz.

Figure 3.31 and Figure 3.32 show the horizontal and vertical components before and after band pass filtering. Each figure includes a plot of the (a) Fourier Spectrum, (b) acceleration time history, (c) velocity time history, and (d) displacement time history. For test groups 1 and 2 the fault normal (stronger direction) and fault parallel (weaker direction) components were oriented along +*x*-axis (north-south) and +*y*-axis (east-west) directions, respectively. For Test Group 3, the orientation of components was rotated 90° to place the strongest ground motion component in line with the wider footing dimension. The peak ground acceleration, velocity, and displacement of the filtered records were 0.74*g*, 29.1 in./sec and 4.8 in., respectively.

3.10.3 1978 Tabas, Iran, Earthquake

Test Groups 1 and 2 were subjected to a modified version of the 1978 Tabas, Iran, earthquake. The site was located 1.25 miles from the epicenter and had a moment magnitude of Mw=7.4. The ground motions used were from the SAC-Steel Project records NF01, NF02, and NF01_02v, which were the fault-normal, fault-parallel, and vertical components, respectively. These records were representative of a strong intensity near-fault forward-directivity ground motion. The soil was described as "rock" and had a shear wave velocity of approximately V_s=2520 ft/sec. The records were scaled assuming a length-scale factor of 4.5, thus the time duration was scaled by √4.5 (~2.12). The original records were band-pass filtered using cutoff frequencies of 0.1 Hz and 15 Hz and corner frequencies of 0.2 Hz and 14 Hz. The record peak values were measured as PGA 0.84*g*, PGV 42.5 in/sec and PGD 26.8 in.

Figure 3.30 through Figure 3.32 show the horizontal and vertical components before and after band-pass filtering. Each figure includes a plot of the (a) Fourier Spectrum, (b) acceleration time history, (c) velocity time history, and (d) displacement time history. For Test Groups 1 and 2, the fault-normal (stronger direction) and fault-parallel (weaker direction) components were oriented along +*x*-axis (north-south) and +*y*-axis (east-west) directions, respectively. The peak ground acceleration, velocity, and displacement of the filtered records were 0.84*g*, 18.6 in./sec, and 4.8 in., respectively.

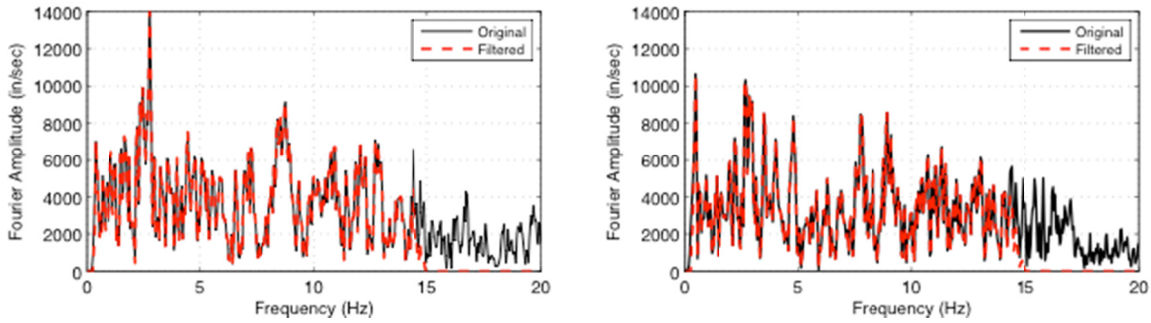

(a) Fourier spectra

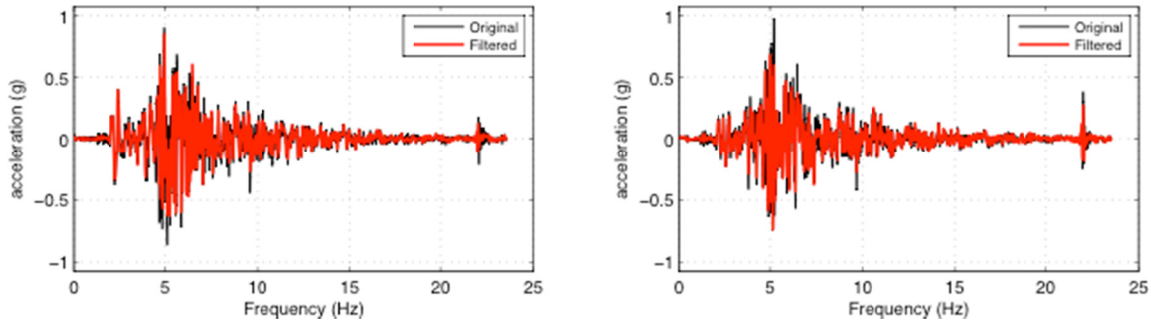

(b) acceleration time history

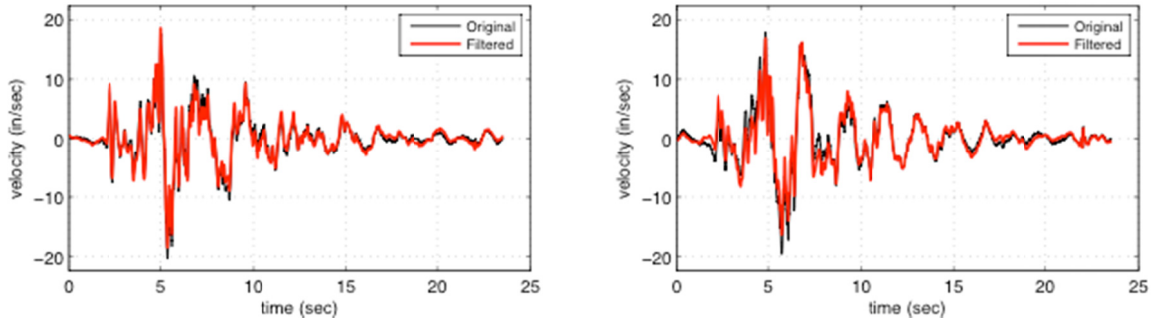

(c) velocity time history

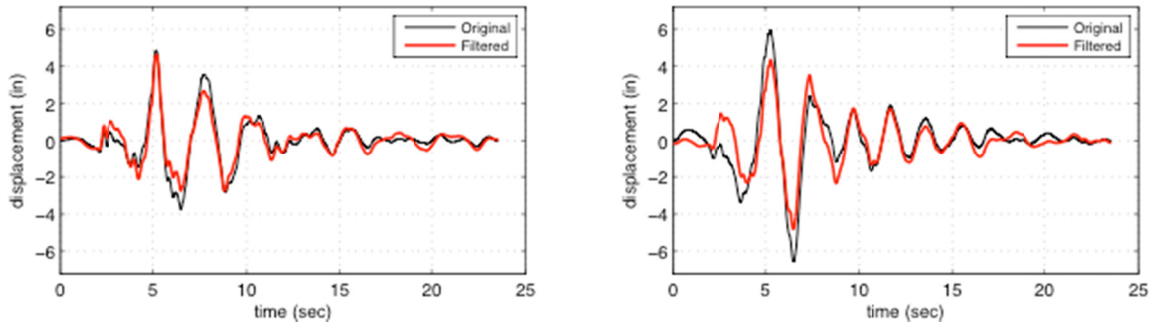

(d) displacement time history

fault-normal component **fault-parallel component**

Figure 3.30 NF01 and NF02 horizontal filtered ground motion.

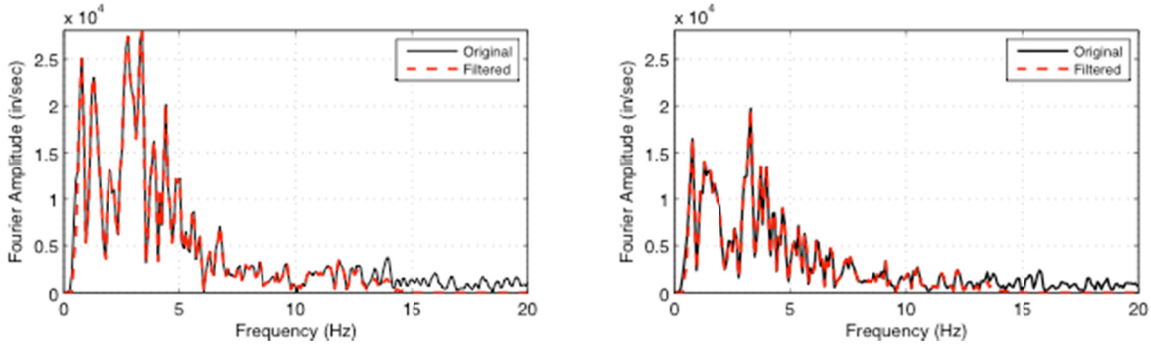

(a) Fourier spectra

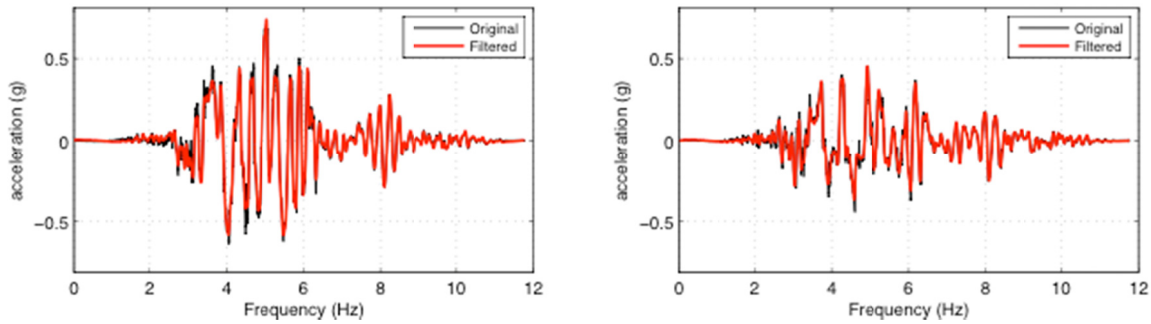

(b) acceleration time history

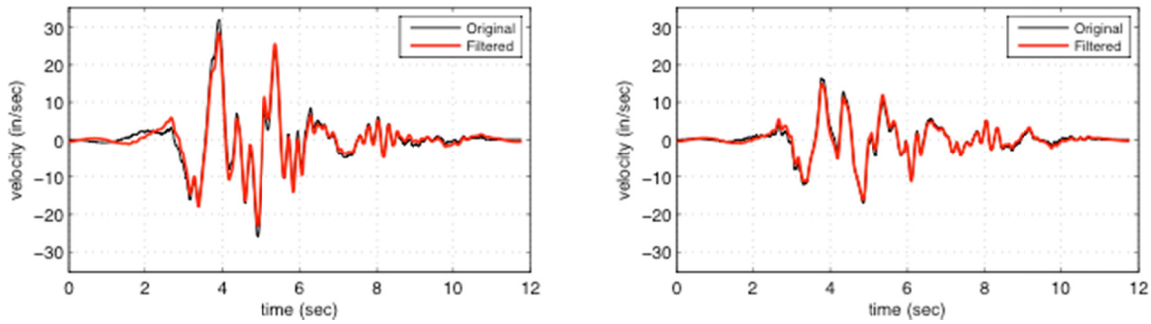

(c) velocity time history

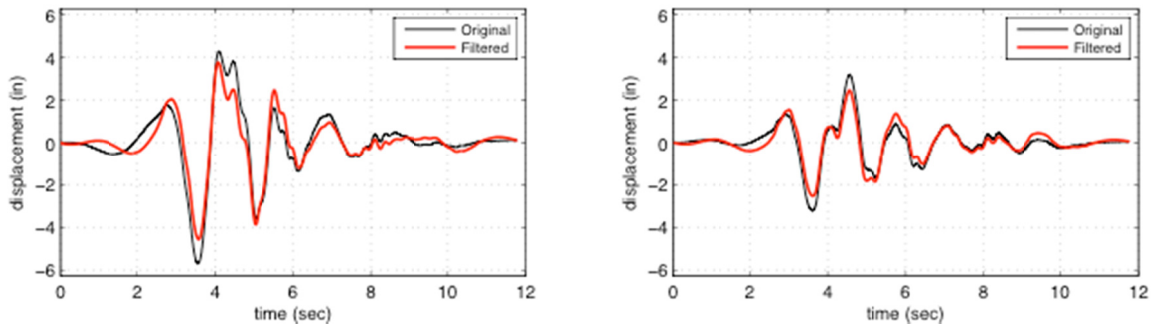

(d) displacement time history

fault-normal component **fault-parallel component**

Figure 3.31 NF03 and NF04 horizontal filtered ground motion.

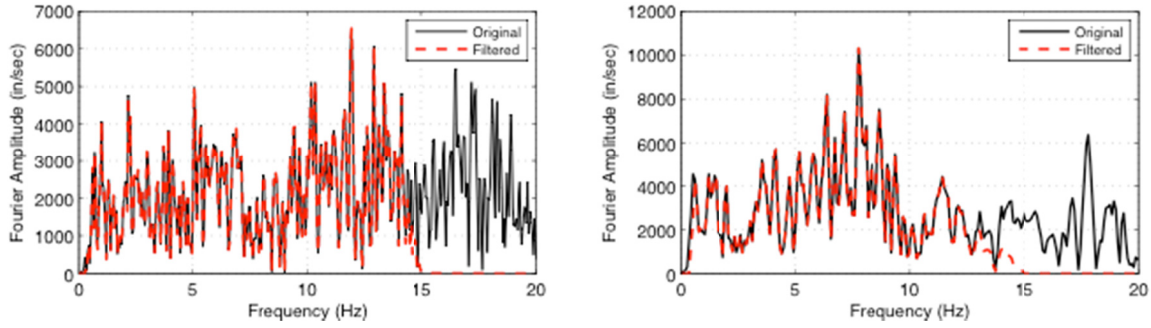

(a) Fourier spectra

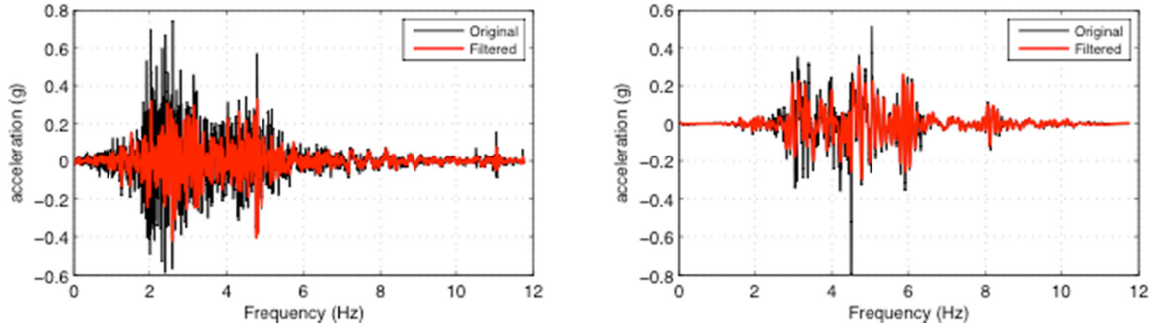

(b) acceleration time history

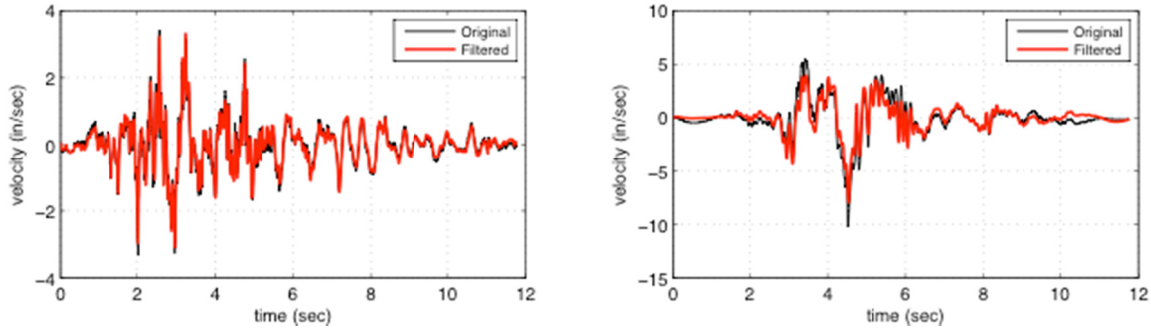

(c) velocity time history

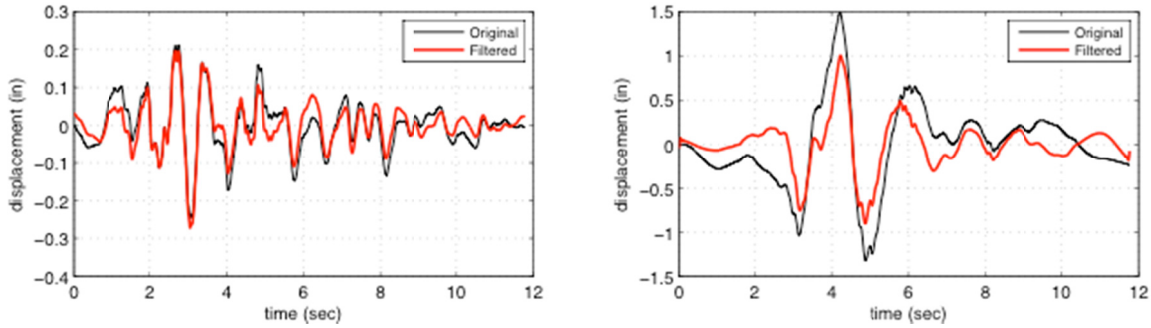

(d) displacement time history

NF01/NF02 vertical **NF03/NF04 vertical**

Figure 3.32 Vertical filtered ground motion.

3.11 TEST SEQUENCE

3.11.1 Pullback (Free Vibration) Test

Prior to the shake table tests, each specimen was subjected to pullback tests to investigate dynamic properties of the specimen in the *x*- and *y*-directions. A cable was attached on both ends at an anchor on the laboratory floor and the center-of-mass of the weighted blocks. The cable assembly included a come-along winch for pulling back the specimen, a load cell to measure the corresponding force at the anchor end, and a small diameter machine bolt at the other end to be cut. An LP was placed at the center-of-mass on the opposing face (connected to the instrumentation frame) to measure displacement. A 1.0 kip force was applied to the mass blocks using the come-along winch, and the bolt was then cut to initiate free vibration motion. To prevent the table from moving, wood blocks were placed in the gap between the simulator platform and outer edges. Displacement and accelerations were recorded to determine the natural period and damping ratios of the systems.

3.11.2 Shake Table Test

Following the free vibration test, a series of shake table tests were conducted. There were three selected test groups that varied the footing size, axial load, and earthquake intensity Presented previously and shown again in Table 3.4, each test group varied the input excitation for the one-dimensional, two-dimensional, and three-dimensional components of motion. Test Groups 1 and 2 were expected to remain elastic during all testing levels. Because Test Group 1 was an evaluation of the rocking set up and instrumentation, the axial load was one-third the designed for load to avoid damaging the column. The footing dimension was 48 in. × 48 in. ($3D_c$ x $3D_c$). For the two ground motions, five earthquake directional combinations were conducted at different earthquake intensity amplitudes: 1D-X, 1D-Y, 2D-X+Y, 2D-X+Z, and 3D-X+Y+Z. In total, approximately thirty runs were done for Test Group 1. A complete list of dynamic test runs can be found in Appendix A.

Test Group 2, for which the footing size remained three times the column diameter ($3D_c$) square, the axial load was increased to 5.7% $f_c' A_g$, and the column was tested within the elastic range. Similarly to the first group, approximately 5 types of earthquakes were run for five different input excitations. A total of approximately 30 runs were conducted (see Appendix A).

Test Group 3 was designed to initiate inelastic behavior and rocking/uplifting of the system. The footing was widened to five times the column diameter ($5D_c$) in the strong component loading direction and left at three times the column diameter ($3D_c$) in the opposite direction. The interaction of fixed-base behavior in one direction with rocking-uplift behavior was of particular interest. Each of the earthquake runs was a three-dimensional excitation. First the specimen loading was done at an elastic level. Next, the loading was increased to the yield and then design and maximum credible earthquake (MCE) loading levels. At the conclusion of testing, the damaged accrued by the column prevented any further testing. A total of four runs were conducted for Test Group 3 (see Appendix A). Table 3.5 lists the type of earthquakes run for each test group and some of their input characteristics.

Table 3.4 Testing schedule of rocking column.

Test Group	Axial Load	Footing Size[1]	Earthquake Loading	Testing Levels[2]	Input Motions
1	Nominal $3\%f'_cA_g$	$3D_c \times 3D_c$	Los Gatos (1989 Loma Prieta) Tabas, Iran (1977)	Elastic 90% Yield	1D - X 1D - Y 2D-X+Y 2D-X+Z 3D-X+Y+Z
2 Square Footing (S)	Nominal $10\%f'_cA_g$	$3D_c \times 3D_c$	Los Gatos (1989 Loma Prieta) Tabas, Iran (1977)	Elastic 90% Yield	1D - X 1D - Y 2D-X+Y 2D-X+Z 3D-X+Y+Z
3 Rectangular Footing (R)	Nominal $10\%f'_cA_g$	$5D_c \times 3D_c$	Los Gatos (1989 Loma Prieta)	Elastic Yield Design MCE	1D - X 1D - Y 2D-X+Y 2D-X+Z 3D-X+Y+Z

[1]multiple of column diameter (D_c)
[2]loading level defined by flexural ductility demands

Table 3.5 Summary of peak ground motion values for all test groups.

	Run	Record	Level	PGA (*g*)	PGV (in./sec)	PGD (in.)
Test Group 1	A	Los Gatos	Elastic	0.08	2.4	0.4
	B	Los Gatos	Elastic	0.25	8.5	1.3
	C	Tabas	Elastic	0.08	7.0	0.3
	D	Tabas	Elastic	0.22	10.3	1.3
	E	Los Gatos	Elastic	0.15	7.4	1.4
	F	Tabas	Elastic	0.30	10.4	1.9
Test Group 2	AS	Los Gatos	Elastic	0.11	4.0	0.6
	BS	Tabas	Elastic	0.20	3.6	0.6
	CS	Los Gatos	Elastic	0.20	5.6	0.7
	DS	Los Gatos	Elastic	0.30	10.2	1.1
	ES	Los Gatos	Elastic	0.28	8.2	1.1
	FS	Tabas	Elastic	0.25	6.8	0.8
	GS	Tabas	Elastic	0.14	0.14	6.1
	HS	Los Gatos	Elastic	0.30	9.1	1.1
Test Group 3	AR	Los Gatos	Elastic, Yield, Design, MCE	1.1	16.8	4.6

4 Experimental Results

4.1 INTRODUCTION

Sample results from the test program described in Chapter 3 are presented here to illustrate the performance of bridge piers that are supported by rectangular spread footings, and which uplift during strong ground shaking. The results are categorized by global and local response measures. The results of the shaking table specimens are very useful because they provide an indication of the magnitude of response of an uplifting bridge pier and column, which can be compared to previous tests of fixed-base bridge piers. The results presented show the response of the test specimen using metrics similar to those used in previous tests [Sakai and Mahin 2006] and those specified in the SDC for designing bridge piers [Caltrans 2004a]. Rocking and uplift of the test specimen footing and center mass displacement and rotation was investigated in depth, which is described in the following sections.

Several calculations are necessary to efficiently analyze the recorded data. These include the amount of rotation of the footing, translation of the top of the column due to footing uplift, the column base moment, average curvature at various regions along the column, and the column shear. These response quantities then are used to develop an index that assesses the likelihood of foundation rocking. The index is described as the ratio of applied moment to restoring moment.

The shake table test program conducted nearly 70 tests on the single column specimen with variable loads and footing dimensions. Except for the final two test runs—which were anticipated to undergo inelastic deformations—virtually no damage occurred. Hence, there was negligible change in structural periods or damping during most of the tests. As mentioned previously, each test group was subjected to modified versions of the Los Gatos (1989 Loma Prieta) and Tabas (1977 Iran) ground motions. Test Groups 1 and 2 were conducted in the elastic range and had a maximum demand equal to incipient yielding of the column. Test Group 3 was designed to test into the inelastic demand range. A total of four runs were conducted for the last group, of which the final two runs damaged the column.

Because of the lack of horizontal restraint, using a rectangular footing created interaction between the principal directions and caused rotation of the footing about the vertical axis. Included are plots that show the amount of rotation compared to the overall displacements.

See Appendix A for a complete list of test runs, along with specimen configuration, run identification number, ground motion records and scaling used.. A more complete series of plots showing time histories of specimen lateral and uplift displacements, and computed column moment-average curvature relations are available in Appendix B.

4.2 ROCKING SYSTEM RESPONSE QUANTITIES

All three of the test groups had similar instrumentation configurations, thus determining the response for all test groups was similar. For each test group minor changes were made to instrumentation position, but the process was not radically altered. For all test runs, displacement and force time histories were calculated as well as force-deformation relationships. Global displacement, local displacement, and acceleration recordings were used to calculate the response. The next two sections describe the process for calculating the rocking system response quantities.

4.2.1 Displacements

4.2.1.1 External Displacements

Using the instrumentation described in Chapter 3, the displacement response quantities of interest were calculated. The total relative lateral translation $\left(u_{\text{rel}}\right)$ in each direction (east-west and north-south) was computed as the difference between the lateral displacement at the center of mass and at the base of the footing in that direction [Equation (4.1)].

$$u_{\text{rel}} = u_{\text{total}} - u_{\text{footing}} \tag{4.1}$$

The uplift of the footing from the elastomeric pad was measured at four locations offset from the edge of the footing, as shown in Figure 3.28 and Figure 3.29. The average vertical displacements from the two vertical displacement transducers on the east side of the footing were subtracted from corresponding value for the transducers on the west side of the footing. Dividing the resultant by the east-west horizontal distance between the pairs of transducers, the base rotation θ_{ftg} of the footing is estimated [Equation (4.3)]. The lateral displacement Δr of the center of the top mass associated with rigid body rotation of the footing is then estimated as the base rotation of the footing times the height of the center mass measured from the center of mass to the bottom of the footing [Equation (4.4)]. Figure 4.1 depicts the displacements of interest of the rocking system. The total relative lateral translation $\left(u_{\text{rel}}\right)$ is also noted as ΔT for convenience in reporting the results. The total displacement is a combination of the lateral rigid body translation (Δr) due to uplift of the footing and the flexural displacement (Δf) of the column due to input excitation.

$$\Delta T = u_{\text{rel}} \tag{4.2}$$

$$\theta_{ftg} = \frac{Z_L - Z_R}{2B} \tag{4.3}$$

$$\Delta r = H \sin\theta \approx H\theta \tag{4.4}$$

The contribution of flexural displacement (Δf) is assumed to include the contribution of flexure, bar pullout, shear, and similar internal deformations in the column. At the center of mass, the contribution due to flexural displacement is estimated by Equation (4.5) as the total relative

displacement minus the rigid body translation. For Test Group 3, where the footing was widened to $3D_c \times 5D_c$, the outriggers with vertical displacement transducers were shifted to the north-south faces and a similar process was used for the calculations.

$$\Delta f = \Delta T - \Delta r \tag{4.5}$$

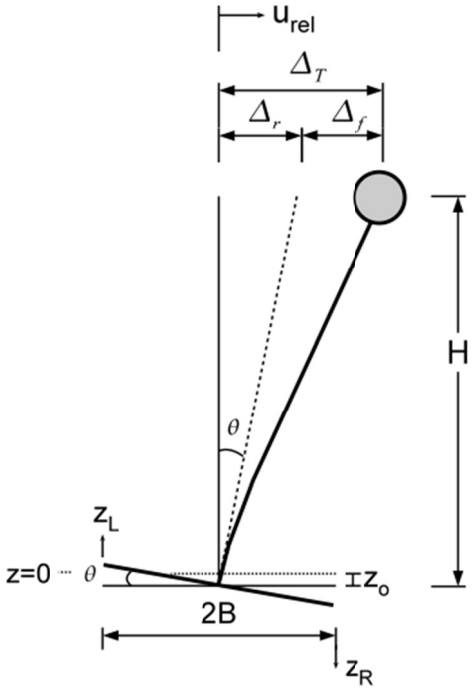

Figure 4.1 Displacement response quantities.

4.2.1.2 Footing Vertical Uplift

The estimated footing rotation was used to calculate the vertical uplift at any point along the footing. The shear and flexure deformations of the footing were assumed to be negligible in comparison to the footing uplift. Hence the footing was assumed to behave as a rigid block. By assuming rigid motion of the footing, the vertical uplift at any point could be estimated using the footing rotation along both principle directions (θ_{ftg-NS} and θ_{ftg-EW}) and the initial displacement (z_o) due to gravity load [Equation (4.6)].

$$z_{xy} = \left(\theta_{ftg-NS}\right)x + \left(\theta_{ftg-EW}\right)y + z_o \tag{4.6}$$

4.2.1.3 Column Curvatures

The DCDT instrumentation along the column height (see Chapter 3) was used to estimate the average curvature along the column. The DCDTs were located on the north, south, east and west column faces and connected to rods running through the column along the north-south and east-west directions. Each instrument was located a small horizontal distance away from the column

face. At each elevation (h_i), the horizontal distance, $S_{N\text{-}S}$, was recorded as the distance between the DCDT instruments on opposing faces. The rotation (θ_i) of each region at each elevation (h_i) was determined by dividing the extension (Δ_i) of the DCDT on each face by the horizontal distance between them [Equation (4.7)]. The average curvature (ϕ_i) of each region was then estimated by dividing the rotation by the region height measured as the vertical distance between the adjacent set of rods at elevation $h_{i\text{-}1}$ [Equation (4.8)].

$$\theta_i = \frac{\Delta_S - \Delta_N}{S_{N-S}} \tag{4.7}$$

$$\phi_i = \frac{\theta_i}{h_i - h_{i-1}} \tag{4.8}$$

4.2.2 Forces and Moments

The shear and moment along the column were estimated using the recorded accelerations and center-of-mass relative displacements. The shear force was approximated as the total acceleration of the mass block times the mass (m) of the block, excluding the contribution from damping. The rotational force was estimated by multiplying the rotational acceleration by the rotational mass (m_R) moment of inertia of the mass block. At the base of the column, moments were determined using equilibrium and neglecting damping forces again. The base column moment is a product of the lateral acceleration, rotational acceleration, and the lateral displacement. Equations (4.9) and (4.10) illustrate the equation of motion for the x-direction. The process was similar for the y-direction.

$$m\ddot{u}_x + F_{dx} + F_{sx} = -m\ddot{u}_{gx} \tag{4.9}$$

$$m_R\theta_y + M_{d\theta} + M_{s\theta} = 0 \tag{4.10}$$

The quantities of interest are:

m = mass of weight block

m_R = rotational mass moment of inertia

$\ddot{u}$ = total relative acceleration of the center of mass

$\ddot{u}_{gx}$ = table acceleration

θ_y = rotational acceleration of mass block about y-axis

F_{dx} = damping force

F_{sx} = hysteretic force

$M_{d\theta}$ = damping moment about y-axis

$M_{s\theta}$ = hysteretic moment about *y*-axis

The total displacement and acceleration can be written as $u_t = u_{\text{rel}} + u_g$ and $\ddot{u}_t = \ddot{u}_{\text{rel}} + \ddot{u}_g$, respectively, where $\ddot{u}_g$ is the ground acceleration. The forces in the system can be determined by rewriting the above equations to solve for the hysteretic force (F_{sx}) in the *x*-direction and the hysteretic moment $(M_{s\theta})$ about the *y*-axis.

$$F_{sx} = -m\ddot{u}_x - m\ddot{u}_{gx} - F_{dx} = -m\ddot{u}_t - F_{dx} \approx -m\ddot{u}_t \tag{4.11}$$

$$M_{s\theta} = -m_R\theta_y - M_{d\theta} \approx -m_R\theta_y \tag{4.12}$$

Figure 4.2 depicts the quantities described and calculation of base shear and moment. If we neglect the contribution of damping, then $F_{s\theta}$ and $M_{s\theta}$ can be calculated as shown in Equations (4.11) and (4.12). With the shear and moment at the center of mass now determined and using equilibrium, the moment at each point along the column can be calculated. Equation (4.13) shows the calculation for moment at the base of the column. When the damping force is small, the approximation provides a reasonable approximation of the system forces.

$$M_b = \left(m\ddot{u}_t + F_{dx}\right)H_c - M_{d\theta} - M_{s\theta} + Pu_{\text{rel}} \approx F_{sx} * H_c - M_{s\theta} + Pu_{\text{rel}} \tag{4.13}$$

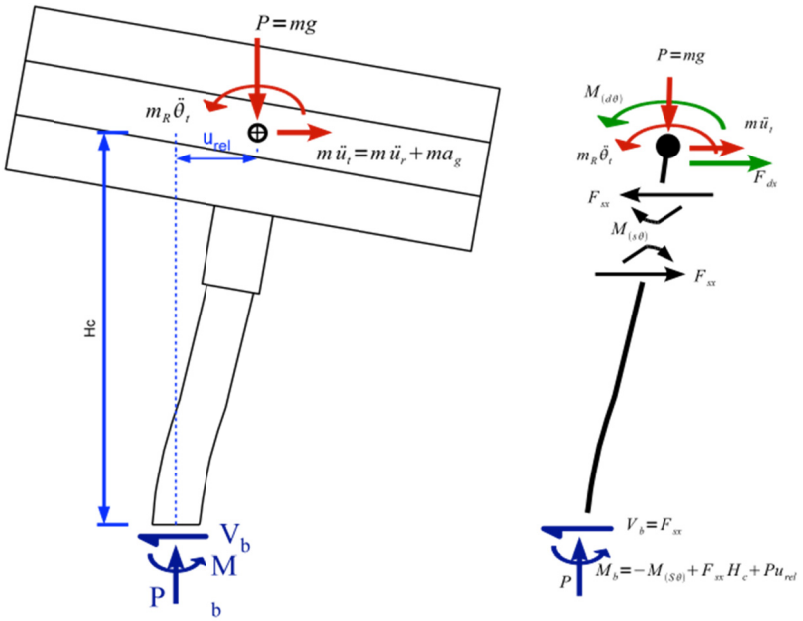

Figure 4.2 Free body diagram.

The footing free body diagram (Figure 4.3) illustrates the force transfer at the base of the footing. Instrumentation to clarify the magnitude of compression force developed in the pad was not used. The shear and vertical reaction of the pad can be approximated using the relationships for the base shear and moment already developed. Using equilibrium, the shear across the pad

was approximated as the base shear plus the total acceleration of the footing. The vertical reaction R_{pad} and its eccentricity from the column center can be determined using equilibrium and the column axial force, shear and moment at the base.

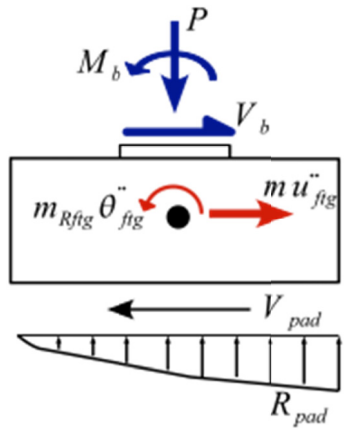

Figure 4.3 Footing free body diagram.

4.3 OBSERVED COLUMN RESPONSE

The response of the specimen, with varying footing widths and axial load, to several types of excitation is next. Prior to the start of each test group, a pullback and a free-vibration test were conducted to determine the stiffness, natural period, and damping of the system. Except for the final two runs of Test Group 3 all dynamic runs were conducted at a nominal elastic demand level of the column. The final two runs were conducted at the nominal design and maximum levels for the column.

Test Groups 1 and 2 were designed to remain elastic so that a large number of tests could be conducted to determine the response of the system to varying footing sizes and axial loads. Test Group 3 was designed to sustain damage by increasing the amplification of excitation such that the column reached design and maximum loading levels. In general, Groups 1 and 2 followed a similar testing protocol. Typically, for each ground motion, amplification scale, and time step combination, five runs with varied input excitation were conducted. The input excitation sequence was usually two one-directional excitations (*X*, *Y*), two two-directional excitations (*X*+*Y*, *X*+*Z*) and 1 three-directional excitation (*X*+*Y*+*Z*). For example, Appendix A lists the five runs for the Los Gatos input signal scaled to 25% of the original amplitude and a modified time step of 0.094 sec for Test Group 2 Sequence DS.

The principal objective of these rocking tests was to assess the behavior of a system when allowed to simultaneously rock, uplift, and deform under typical earthquake loading levels. These loading levels were determined by corresponding systems with the same configuration, except for a fixed-base assumption that prevents uplift of the footing. Typical performance levels for fixed-base bridge systems were design (displacement ductility equal to 4) and the MCE (displacement ductility equal to 6–8). Assessing the behavior of uplifting systems allows for

drawing a correlation between columns of identical design and axial load, and the effect of footing restraint on column performance for seismic loading.

The response of Test Group 1, for low axial load was used for the preliminary analysis of the more relevant system with the design axial load. Prior to dynamic testing, the stiffness, natural frequency, and damping of the system were determined using pullback and free vibration tests. Following this, a total of 30 runs were conducted to assess the dynamic response. As shown in Figure 4.4, no physical damage or cracking of the specimen occurred although the specimen was observed to twist about a vertical axis and translate. Table 4.1 summarizes some of the response values for Test Group 1. The low axial load is not typical of bridge design, so its usefulness here is only for characterizing the behavior of rocking systems and modeling of the elastomeric pad for subsequent dynamic analysis.

(a) global view

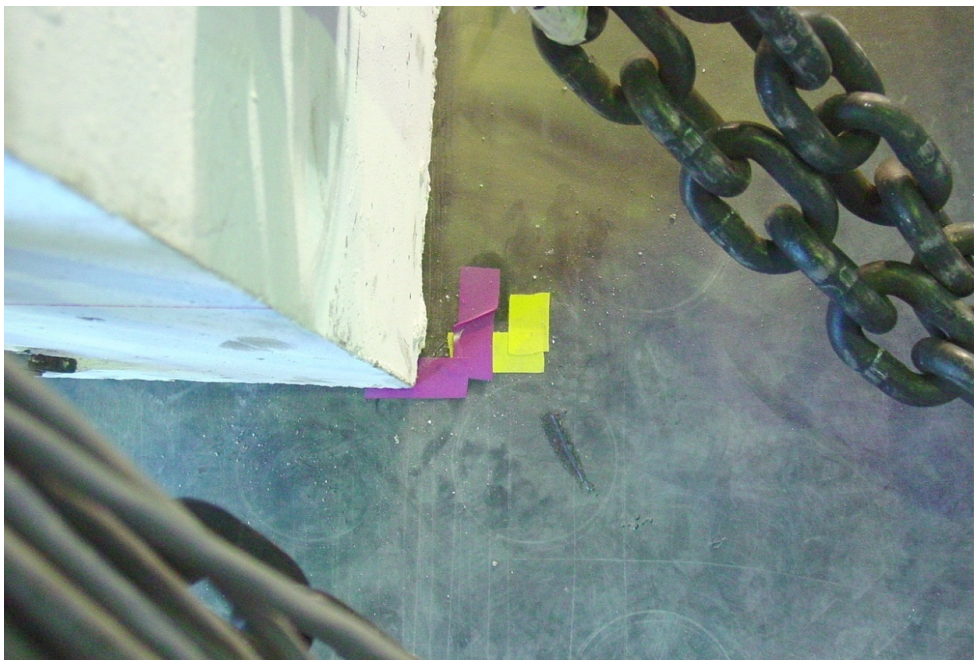

(b) rotation about vertical axis indicated by distance from tape attached to elastomeric pad

Figure 4.4 Test Group 1 with footing 3Dc × 3Dc and low axial load following final run.

Table 4.1 Summary of Test Group 1 response footing size 3Dc × 3Dc with low axial load.

Run	Performance Level	Table Acceleration And Displacement				Relative Displacement				Base Shear and Moment				Observations
		u_{gx}	u_{gy}	$\ddot{u}_{gx}$	$\ddot{u}_{gy}$	Peak Lateral		Peak Uplift		Shear		Moment		
		(in.)	(in.)	(g)	(g)	x (in.)	y (in.)	θ_y (%)	θ_x (%)	V_{bx} kip	V_{by} kip	M_{by} kip-in.	M_{bx} kip-in.	
A1	Elastic	0.33	0.00	0.08	0.01	0.16	0.08	0.04	0.11	2.4	1.0	194	84	Stiffness, Free Vibration test Performed prior to dynamic runs.
A3	Elastic	0.33	0.16	0.08	0.04	0.11	0.13	0.02	0.20	2.3	1.4	186	111	
A5	Elastic	0.34	0.16	0.07	0.03	0.12	0.14	0.02	0.20	2.2	1.5	177	121	
B1	Elastic	1.42	0.06	0.23	0.04	0.52	0.32	0.15	0.56	4.4	2.6	359	206	Large amount of uplift and rocking.
B3	Elastic	1.43	0.92	0.23	0.21	1.11	1.14	0.42	2.37	4.6	4.0	365	317	
B5	Elastic	1.46	0.97	0.24	0.20	1.39	1.13	0.54	2.41	4.9	4.1	389	321	
C1	Elastic	0.37	0.00	0.08	0.01	0.09	0.05	0.01	0.04	1.2	0.6	99	48	Little to no uplift.
C3	Elastic	0.36	0.22	0.06	0.02	0.10	0.07	0.01	0.06	1.5	0.9	120	73	
C5	Elastic	0.37	0.22	0.07	0.02	0.09	0.07	0.01	0.07	1.3	0.9	109	74	
D1	Elastic	1.36	0.03	0.23	0.04	0.49	0.28	0.12	0.53	3.7	2.1	300	171	No observed damage.
D3	Elastic	1.36	0.94	0.25	0.09	0.42	0.35	0.10	0.60	3.8	2.8	310	230	
D5	Elastic	1.38	0.97	0.23	0.09	0.42	0.36	0.10	0.60	3.9	2.7	312	221	
E1	Elastic	1.45	0.07	0.17	0.05	0.66	0.44	0.18	0.58	4.5	3.1	364	245	Significant amount of uplift.
E3	Elastic	1.46	0.96	0.18	0.10	0.68	0.63	0.19	1.08	4.4	3.8	356	304	
E5	Elastic	1.46	0.94	0.18	0.10	0.71	0.67	0.19	1.12	4.4	3.8	357	305	
F1	Elastic	1.95	0.06	0.28	0.05	0.74	0.47	0.21	0.81	4.2	2.9	338	236	Significant amount of uplift.
F3	Elastic	2.02	1.42	0.27	0.15	0.70	0.52	0.21	0.97	4.0	3.4	320	272	
F5	Elastic	2.01	1.45	0.25	0.13	0.73	0.52	0.21	1.01	3.9	3.4	318	275	

The total number of dynamic tests for Group 2 was 34. Section 4.5 discusses some of the important response parameters for the system. During testing, rocking easily occurred for the square footing 3Dc × 3Dc in size. No yielding or damage was noted during the test. Some cracking was observed; however, the cracks closed completely by the conclusion of the testing and could not be located. Table 4.2 lists some of the response values for Test Group 2. During testing, some rotation of the footing around the vertical axis was observed. Figure 4.5 shows the condition of the specimen following dynamic test D5S. During testing a significant amount of rocking was observed. For the testing of group DS, the amount of lateral translation due to rigid body rotation was up to one-half of the total displacement. At the conclusion of Test Group 2, the column had no observable damage and some minor period lengthening from softening of the system after repeated test deformation cycles. Following Test Group 2, the footing of the specimen was widened in the *y*-direction for a new size of 3Dc × 5Dc. In addition, the ground motion was rotated 90° to align the strongest component with the wider footing dimension.

The four tests conducted for Group 3 (Table 4.3) used all three components of excitation. The yield level test (A2R) was conducted at the same amplitude as test D5S and resulted in less uplift and total displacement than the smaller footing dimension. The footing dimensions clearly have an impact on the total uplift of the system. The design and maximum level tests were scaled to cause inelastic behavior in both directions. The observed response showed there was less relative uplift to total displacement in both directions than the smaller footing size. The column was damaged on the north-west face where spalling occurred during the design and maximum level tests. A plastic hinge formed over approximately the bottom 16 in. of the column height. Also the large deformations of the center of mass induced a permanent displacement in both directions of the column, about 1 in. for the design level and 9 in. and 13 in. for the *x*- and *y*-direction after the maximum level test. At the conclusion of the maximum level tests, testing was terminated because the column was deemed to be badly damaged and unsafe for any subsequent runs. Figure 4.6 shows photos of the damaged column condition following the design level test A3R. Figure 4.7 and Figure 4.8 show the damaged condition of the column following the maximum level test.

Test Group 3 revealed that vertical restraint of the footing was unnecessary to develop the plastic hinge moment of the column, and that the desired design goal could be achieved without the restraint. It should be stressed that it is important to detail columns to be ductile—even if they are expected to rock—due to effects of bi-directional bending on the footing and column, and in the event of accidental restraint being placed on the footing such as by overburden pressures.

Table 4.2 Summary of Test Group 2 response footing size 3Dc × 3Dc

Run	Performance Level	Table Acceleration and Displacement				Relative Displacement				Base Shear and Moment				Observations
		u_{gx}	u_{gy}	$\ddot{u}_{gx}$	$\ddot{u}_{gy}$	Peak Lateral		Peak Uplift		Shear		Moment		
		(in.)	(in.)	(g)	(g)	x (in.)	y (in.)	θ_y (%)	θ_x (%)	V_{bx} kip	V_{by} kip	M_{by} kip-in.	M_{bx} kip-in.	
A1S	Elastic	0.33	0.00	0.08	0.01	0.16	0.08	0.04	0.11	2.4	1.0	194	84	Stiffness and free vibration test performed prior to dynamic runs.
A3S	Elastic	0.33	0.16	0.08	0.04	0.11	0.13	0.02	0.20	2.3	1.4	186	111	
A5S	Elastic	0.68	0.35	0.09	0.09	1.10	0.60	0.34	0.25	7.2	3.7	775	380	
B1S	Elastic	0.56	0.02	0.17	0.03	0.65	0.46	0.08	0.07	5.2	3.5	559	353	Negligible amount of uplift.
B3S	Elastic	0.56	0.56	0.16	0.18	0.65	0.70	0.12	0.18	5.4	5.0	557	450	
B5S	Elastic	0.56	0.57	0.17	0.17	0.64	0.67	0.12	0.17	4.9	4.7	543	444	
C1S	Elastic	0.68	0.03	0.14	0.03	1.17	0.51	0.30	0.16	7.2	3.4	847	356	More observable uplift in footing. Footing rotation about vertical axis.
C3S	Elastic	0.68	0.39	0.14	0.12	1.24	0.77	0.40	0.30	7.2	3.9	820	388	
C5S	Elastic	0.70	0.38	0.14	0.12	1.24	0.77	0.40	0.30	7.0	4.2	834	391	
D1S	Elastic	1.16	0.07	0.23	0.07	2.15	0.74	0.98	0.28	9.7	4.1	1078	428	Test reached nominal yield level. Some minor cracks that closed at end of test.
D3S	Elastic	1.15	0.67	0.24	0.15	2.19	1.62	1.06	0.57	9.9	8.3	1047	802	
D5S	Elastic	1.14	0.67	0.27	0.18	2.21	1.87	0.98	0.72	9.8	8.9	1042	858	
E1S	Elastic	0.80	0.02	0.22	0.03	0.97	0.63	0.14	0.09	6.9	3.9	727	411	Frequency content altered small amount of uplift.
E3S	Elastic	0.79	0.77	0.18	0.19	0.91	0.67	0.19	0.16	6.6	4.9	624	411	
E5S	Elastic	0.80	0.76	0.21	0.20	0.91	0.68	0.20	0.17	6.7	5.3	631	409	
F1S	Elastic	0.79	0.01	0.14	0.02	0.53	0.22	0.04	0.03	4.4	1.6	414	146	Frequency content altered small amount of uplift.
F3S	Elastic	0.80	0.75	0.14	0.18	0.40	0.59	0.05	0.09	3.8	4.0	298	379	
F5S	Elastic	0.80	0.77	0.12	0.21	0.41	0.59	0.05	0.09	3.5	3.7	305	370	

(a) global view

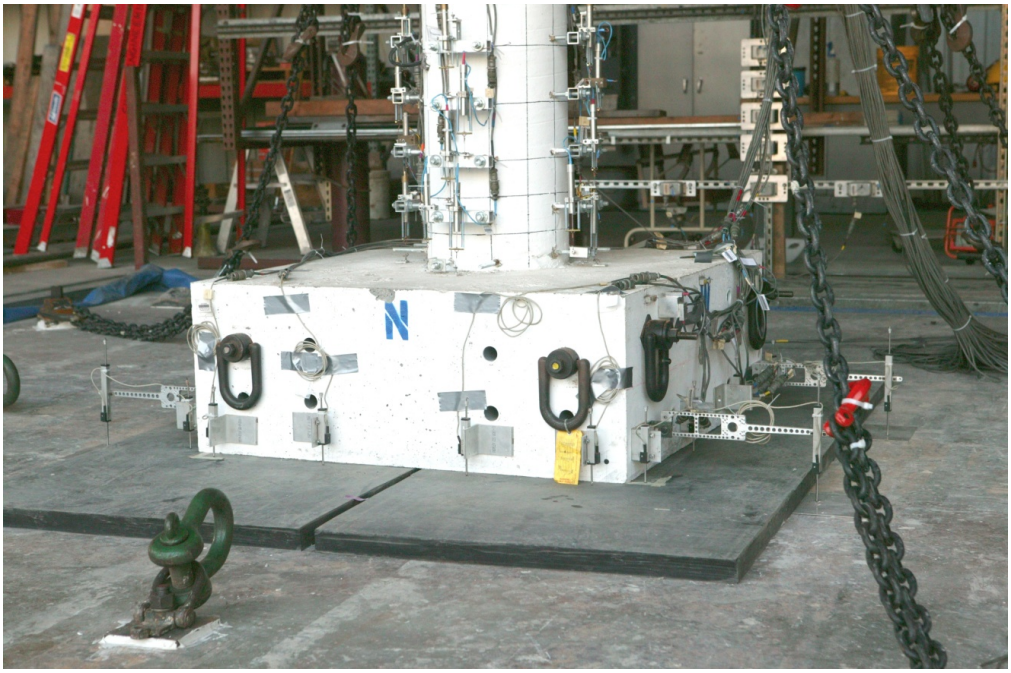

(b) column base

Figure 4.5 Specimen damage condition with 3Dc × 3Dc footing after run D5S.

Table 4.3 Summary of test Group 3 response footing size 3Dc × 5Dc.

Run	Performance Level	Table Acceleration and Displacement				Relative Displacement				Base Shear and Moment				Observations
		u_{gx}	u_{gy}	$\ddot{u}_{gx}$	$\ddot{u}_{gy}$	Peak Lateral		Peak Uplift		Shear		Moment		
		(in.)	(in.)	(g)	(g)	x (in.)	y (in.)	θ_y (%)	θ_x (%)	V_{bx} kip	V_{by} kip	M_{by} kip-in.	M_{bx} kip-in.	
A1R	Elastic	0.18	0.34	0.10	0.13	0.33	0.70	0.03	0.04	3.3	4.7	287	467	Small amount of uplift. No cracking in column.
A2R	Yield	0.33	0.62	0.13	0.16	0.61	1.28	0.13	0.10	4.9	8.2	495	810	Cracking observed in column. Small uplift recorded.
A3R	Design	1.74	3.16	0.42	0.71	4.31	5.78	0.50	0.16	10.5	14.6	1236	1194	Cracking at column base in plastic hinge zone. Some spalling on NW column face. Residual drift of ~1% in both directions.
A4R	Maximum	2.51	4.54	0.55	1.03	9.86	14.17	0.61	0.27	12.2	18.8	1623	1133	Significant spalling on NW face at plastic hinge zone. Large cracks on SE face. Residual drift of 8% and 12% in x-y-directions

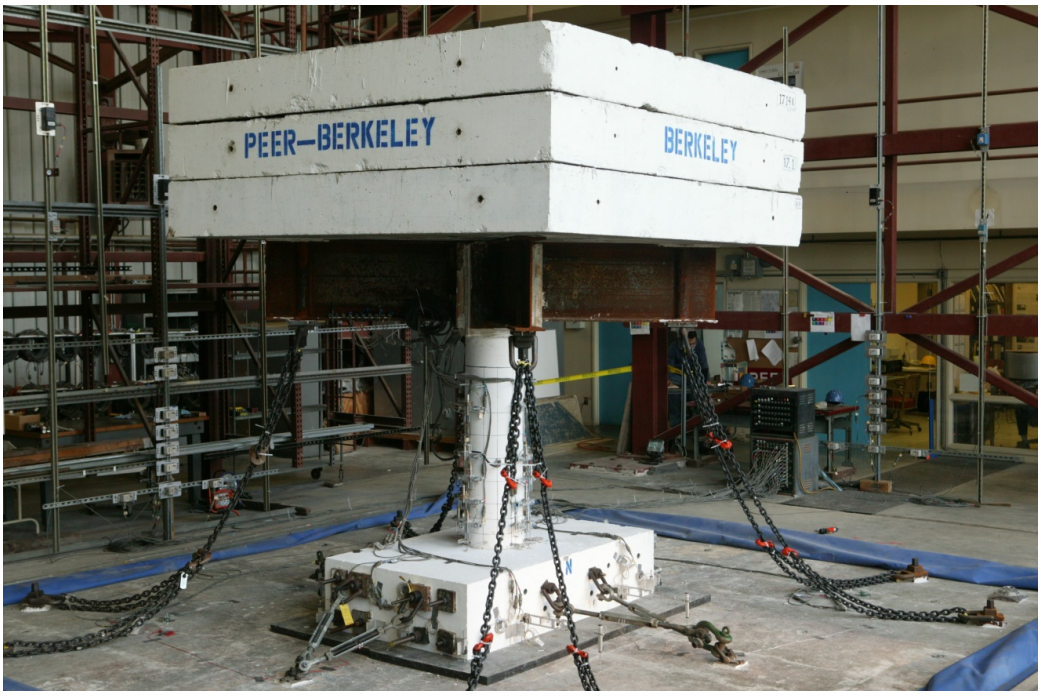

(a) global view

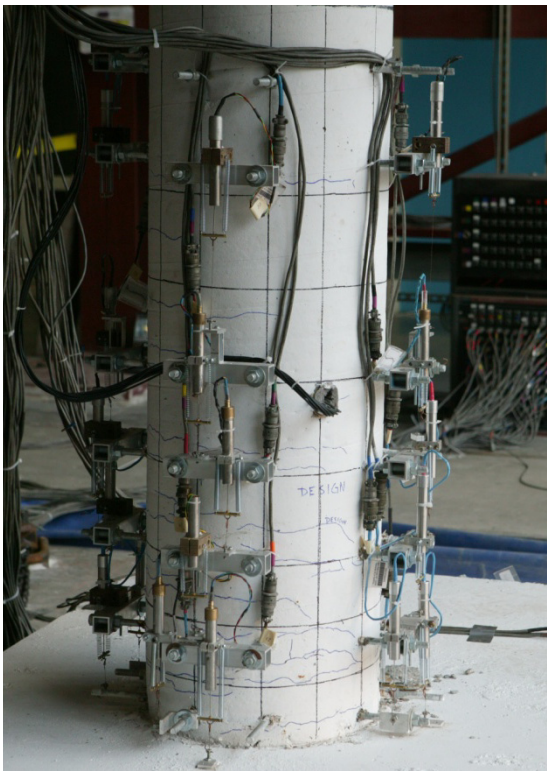

(b) slight residual drift observed

(c) local spalling of concrete cover and cracking at NW face

Figure 4.6 Damage condition of specimen with 3Dc×5Dc footing following run A3R.

(a) global view north direction

(b) global view north east direction

Figure 4.7 **Damage condition of specimen with 3Dc × 5Dc footing following Run A4R (safety chains tightened subsequent to testing).**

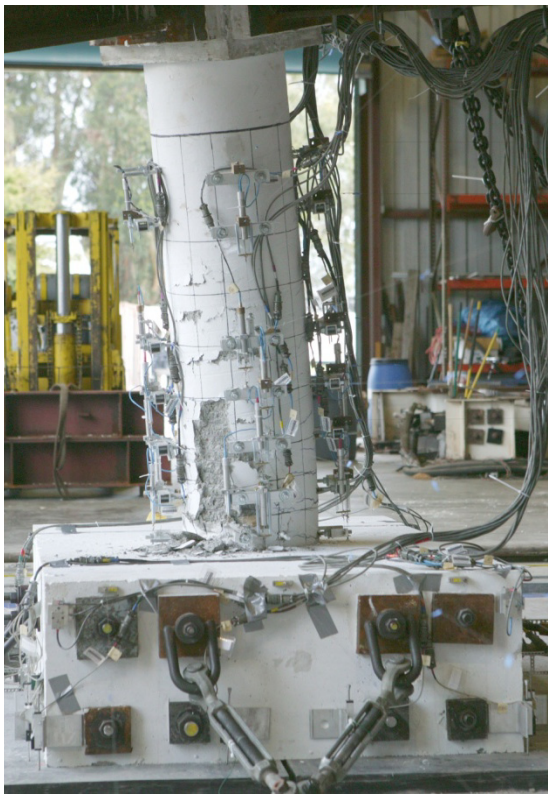

(a) plastic hinge formation on west side

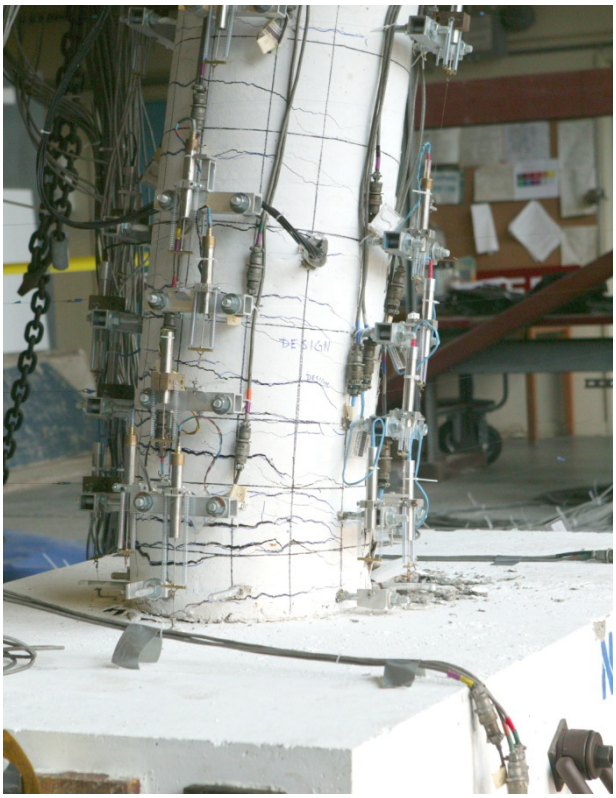

(b) plastic hinge formation on north-east side

(c) plastic hinge formation on north side (after removal of instrumentation)

Figure 4.8 Damage condition of specimen with 3Dc × 5Dc footing following Run A4R.

4.4 RECORDED RESULTS

Response histories are presented in Sections 4.5, 4.6, 4.7, and 4.8. The specimen variables of interest are presented for all tests of Group 3, and selected results of the elastic runs of Test Group 2. These include comparisons among one-dimensional, two-dimensional, and three-dimensional components of excitation. See Appendix B for a more comprehensive review of all the tests conducted.

The response quantities described in Section 4.2 and some simple calculations are presented next. Each test run includes a description of the following response quantities: (a) relative lateral displacement of center mass and resulting contribution from rocking translation and flexure; (b) amount of footing uplift, which includes peak contours and envelopes of displacement; (c) base moment histories; and (d) the hysteretic plots for column base moment versus curvature of the column and rotation of the footing. Additionally, the (e) displacement interaction and the (f) footing rotation about a vertical axis are shown when relevant.

4.5 TEST SPECIMEN WITH DESIGN AXIAL LOAD AND 3DC X 3DC FOOTING

For the footing configuration $3D_c$ x $3D_c$, rocking easily occurred during low levels of seismic excitation. No yielding or damage was noted during any of the tests. Cracks may have opened during testing; however, they had closed completely by the end of the test and their location could not be identified. See Appendix A for a complete list of the test runs for Test Group 2. The two ground motions were scaled to meet target objectives for the desired rocking amplitude and the displacement demand of the column. Interaction between the orthogonal directions was detected even when only one direction of excitation was implemented. During testing it was noted that the specimen would tend to twist about a vertical axis. There was no restraint against horizontal movement of the footing between the specimen and elastomeric pad other than friction.

For these tests the results showed a linear relationship between the lateral force hysteresis and displacement. However, some inelastic behavior was observed for the moment about the column base and the rotation of the footing due to uplift. The inelastic behavior observed likely produced significant damping for the system.

4.5.1 Global Displacement

Some of the key descriptors of global displacement are shown in Figure 4.9, including the response quantities described in Section 4.2. The total displacement at which rocking will occur is shown, as well as the displacement at which the footing will uplift from the elastomeric pad.

4.5.1.1 Column Response

The test set AS was subjected to a low-level seismic excitation intended to be at the onset of uplifting behavior. Analysis determined that this was also the amplitude that would cause incipient yielding in a similar column and axial load when restrained against uplift. Designed with a 3Dc x 3Dc footing plan dimension, the specimen was subjected to a single component of

the Los Gatos record, amplitude scaled to 15% of its initial intensity, and time scaled by a factor of $1/\sqrt{4.5}$.

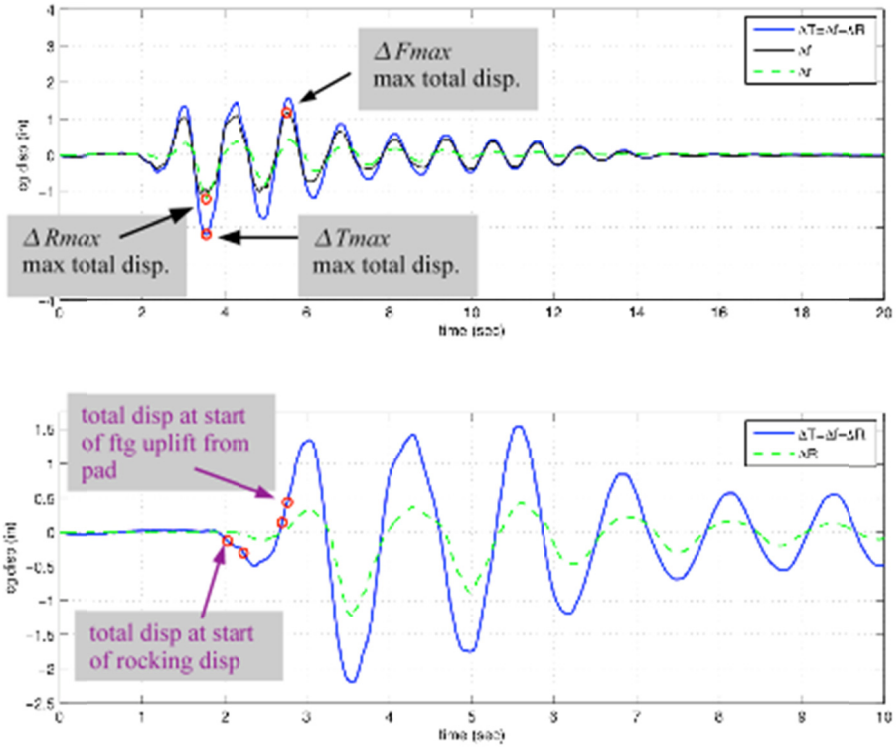

Figure 4.9 Illustration of terminology used to describe total displacements.

Selected results for one horizontal component of excitation for test runs A1S and A2S are shown in Figure 4.10. Also shown is the response of the specimen to two horizontal components of excitation, A3S, and three components of excitation A5S. It can be seen from the time histories of lateral displacement at the center of mass of the top mass blocks that rigid body rotations due to rocking contributed to the response, but not significantly. The rocking contributions appeared to lag behind the overall response. This may be influenced by higher mode response of the specimen.

It is clear that in spite of one direction of only one component of excitation being imposed, the specimen had significant response in the orthogonal direction. This is likely due to two factors: (1) the difficulty of aligning the specimen perfectly with the axis of excitation, and (2) small movements of the table in the direction perpendicular to the direction of specified excitation.

Figure 4.11shows some selected results from testing set DS, which was for the same Los Gatos ground motion scaled to 25% of the original amplitude. This test sequence was intended to induce about two-thirds of the yield displacement of the column under unidirectional excitation. The DS test group included five different combinations of excitation. Figure 4.11 presents the

lateral displacement at the center of mass of the top mass block for runs D1S, D3S, and D5S, which have *X*, *X*+*Y*, and *X*+*Y*+*Z* excitation components. As noted before, there is significant movement in the *Y*-direction during the test, even if excitation was imposed only in the *X*-direction. The basic character of the response in the *X*-direction did not change when the *Y* or *Y*+*Z* components were added. However, the response for the *Y*-direction increased significantly when the *Y*-direction excitation was added.

Results similar to the Los Gatos records are shown in Figure 4.12 for the Tabas record. These records are for test set FS scaled to 25% of the original amplitude and time scaled by a factor of $1/\sqrt{4.5}$. These results indicate that the response is less severe for this test specimen than for the Los Gatos record test set DS, which is associated with the different spectral characteristics of the ground motion. Interaction between the orthogonal directions occurred even when only one horizontal component of excitation was applied. When only the *X*-direction was excited (F1S), the *Y*-direction responded with significant motion, including up to 15% of which is due to rocking. See Appendix B for additional test results.

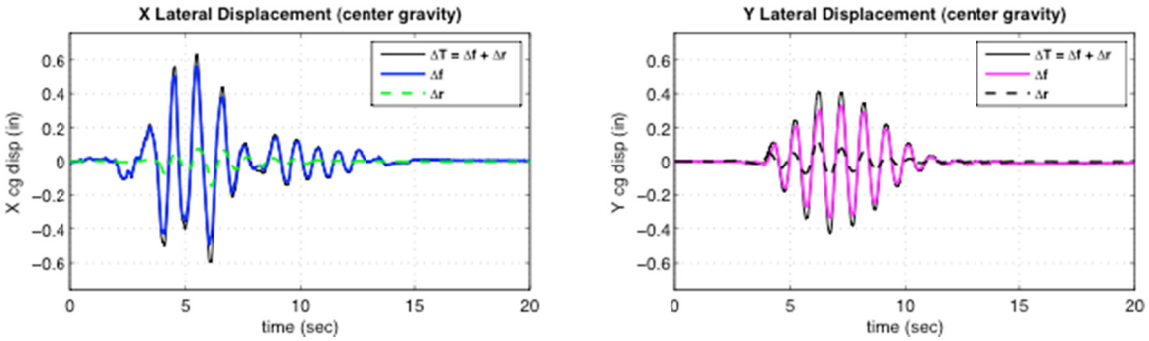

(a) orthogonal displacement response for 1D-*X* input excitation. (Test A1S)

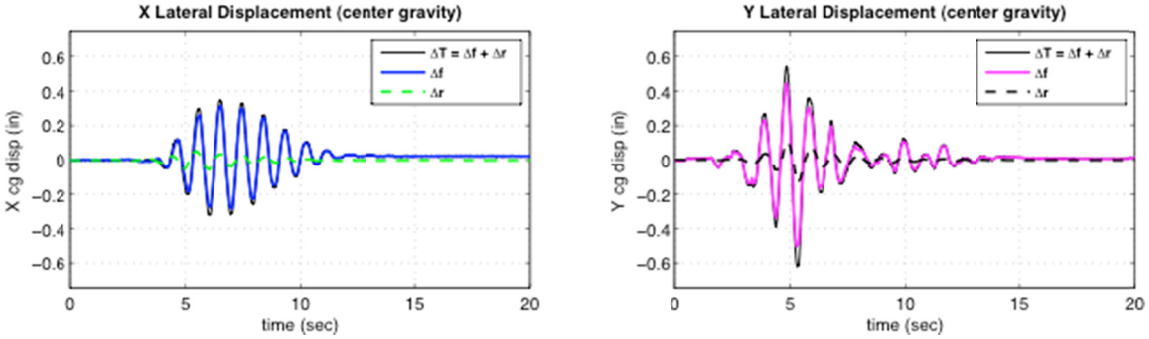

(b) orthogonal displacement response for 1D-*Y* input excitation. (Test A2S)

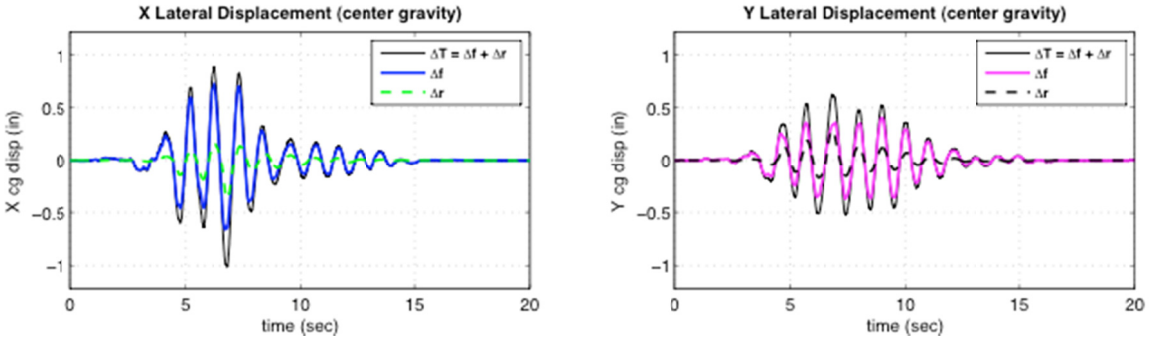

(c) orthogonal displacement response for 2D-*X*+*Y* input excitation. (Test A3S)

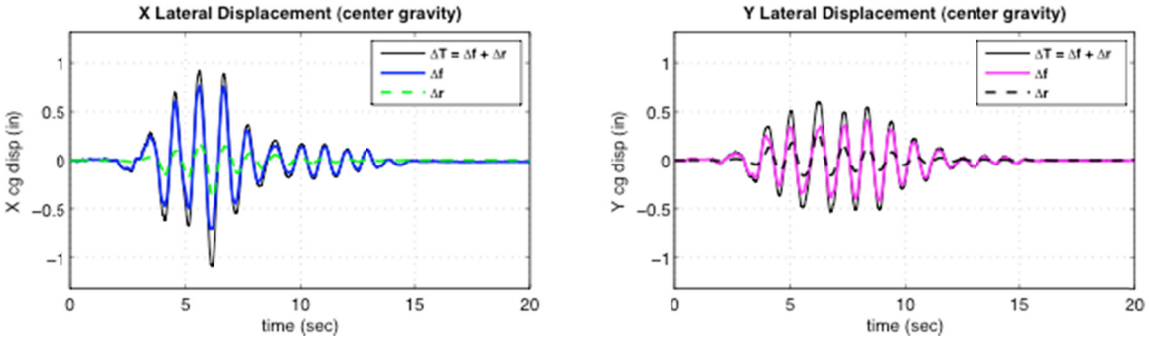

(d) orthogonal cisplacement response for 3D-*X*+*Y*+*Z* input excitation. (Test A5S)

Figure 4.10 Displacement response: 1, 2, 3 components of excitation (Test Set AS).

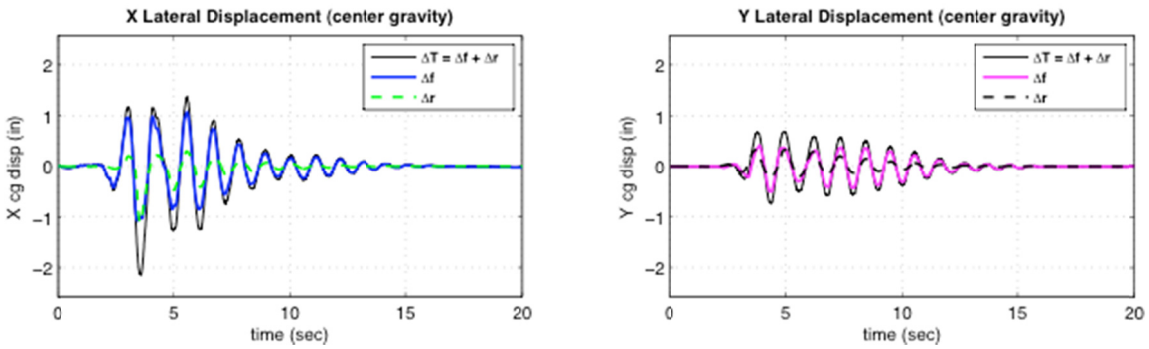

(a) orthogonal displacement response for 1D-*X* input excitation. (Test D1S)

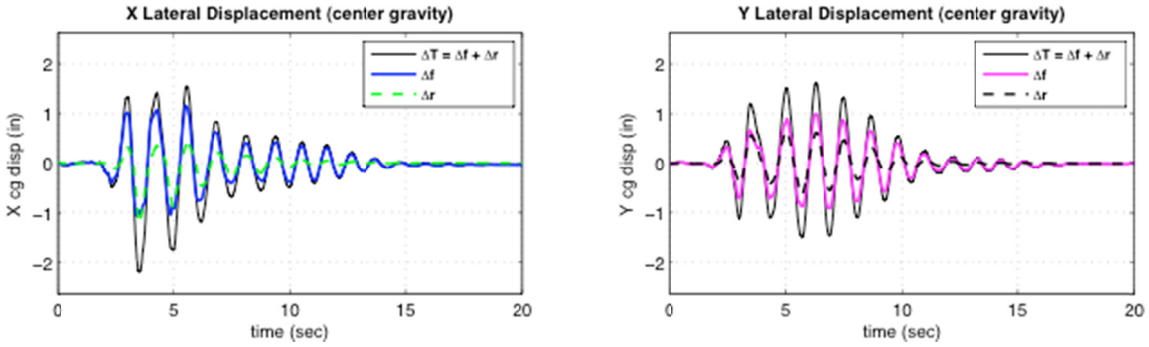

(b) orthogonal displacement response for 2D-*X*+*Y* input excitation. (Test D3S)

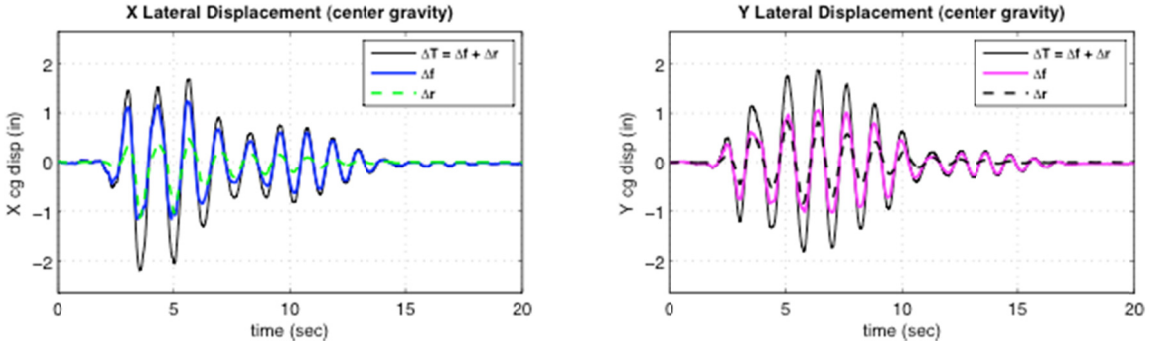

(c) orthogonal displacement response for 3D-*X*+*Y*+*Z* input excitation. (Test D5S)

Figure 4.11 Displacement response: 1, 2, 3 components of excitation (Test Set DS).

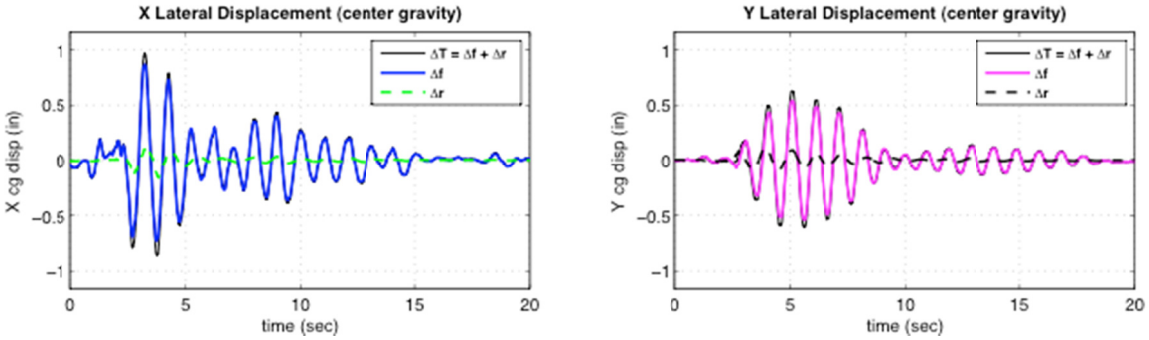

(a) orthogonal displacement response for 1D-*X* input excitation. (Test F1S)

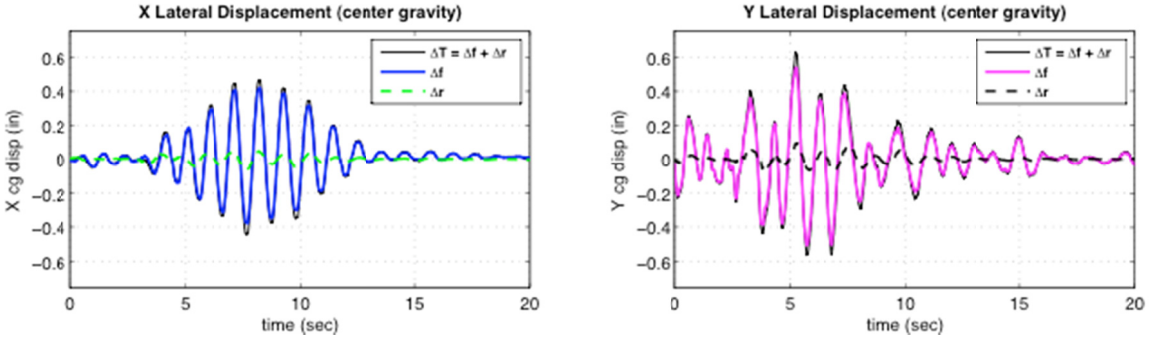

(b) orthogonal displacement response for 1D-*Y* input excitation. (Test F2S)

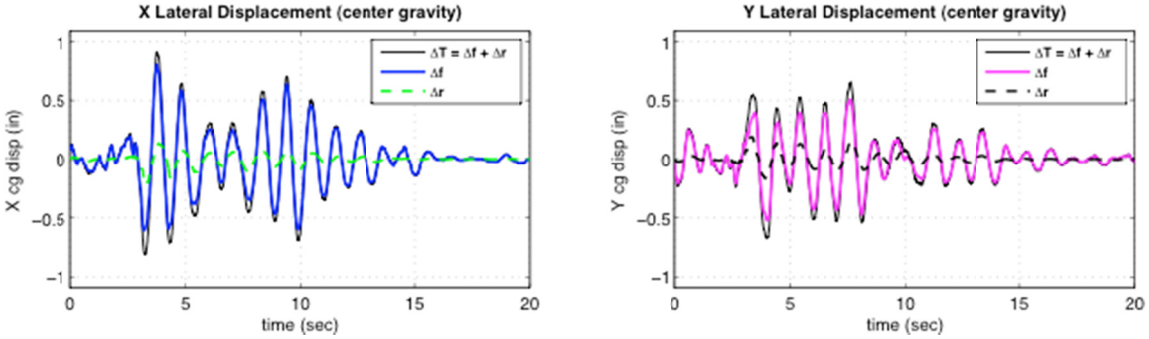

(c) orthogonal displacement response for 2D-*X*+*Y* input excitation. (Test F3S)

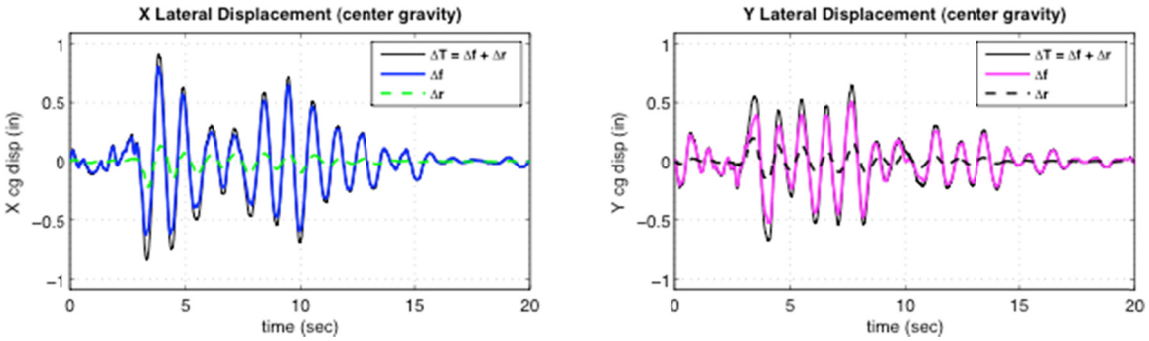

(d) orthogonal displacement response for 3D-*X*+*Y*+*Z* input excitation. (Test F5S)

Figure 4.12 Displacement response: 1, 2, 3 components of excitation (Test Set FS).

The amount of rocking that comprises the total displacement indicates how susceptible the specimen is to uplift. Inspection of the displacement time histories showed that consistently the peak lateral displacement due to rigid body translation from uplift occurred during the peak total displacement of the system or a fraction of second afterwards (as noted previously by the lag of the overall rocking response). Essentially, the peak rocking displacement occurs at the same moment as the peak total displacement.

The comparison of peak total displacement and the contribution of rocking displacement to the total are shown in Figure 4.13 for test sets AS, DS, and FS. These are the amplitude and time scaled records for Los Gatos and Tabas, as described previously. The bar on the left is the maximum lateral displacement of the center of mass, and the bar on the right is the contribution of rocking to the maximum displacement. The system had a significant contribution from rocking to the total displacement for test sets AS and DS. For these tests the peak displacements from the rocking contribution were upwards of one-half of the total displacement. Test set FS was more resistant to uplift, owing likely to the spectral characteristics of the input excitation.

The ratio of rocking (ΔR) and flexural displacement (ΔF) to the total displacement was calculated by dividing the individual contributions by the total displacement. Assuming that the peaks for rocking and total displacement occur almost simultaneously, the ratios can be described by $\Delta R_{t_i} / \Delta T_{t_i}$ and $\Delta F_{t_i} / \Delta T_{t_i}$, where t_i is time of maximum total displacement. Figure 4.14 shows the described ratios for test sets AS, DS, and FS. The first two sets show that rocking displacement comprises up to one-half of the total displacement. For test set FS rocking displacement is no more than one-fifth of the total displacement.

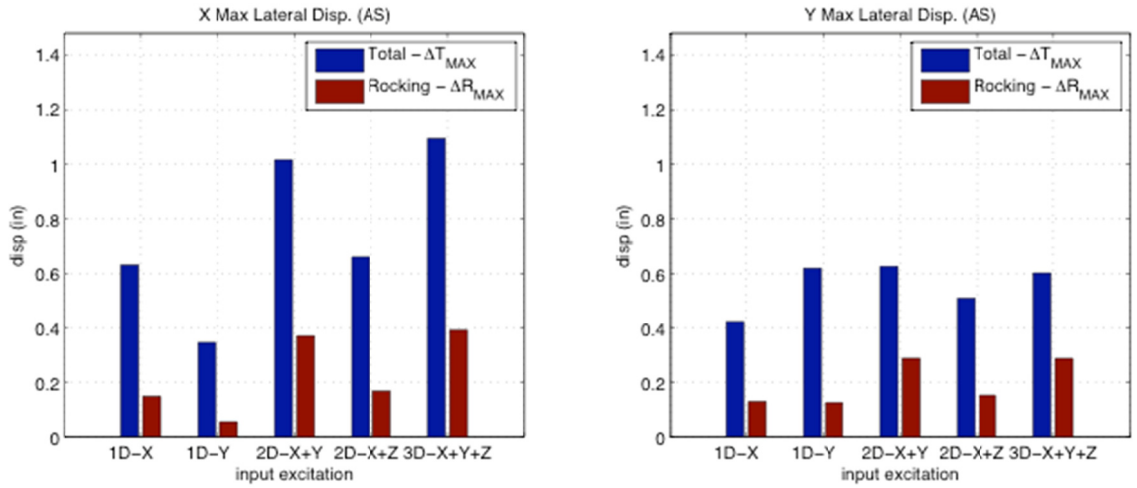

(a) test set AS

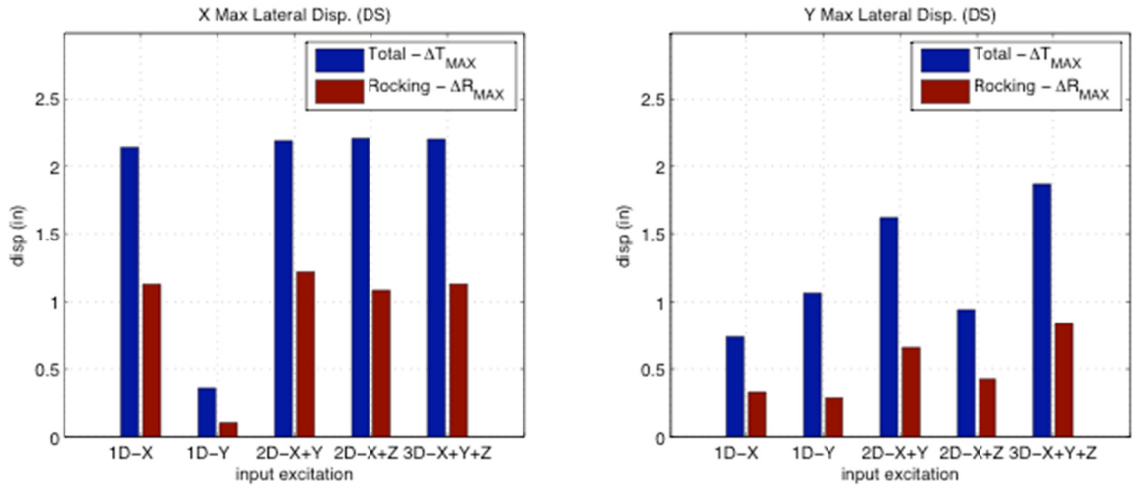

(b) test set DS

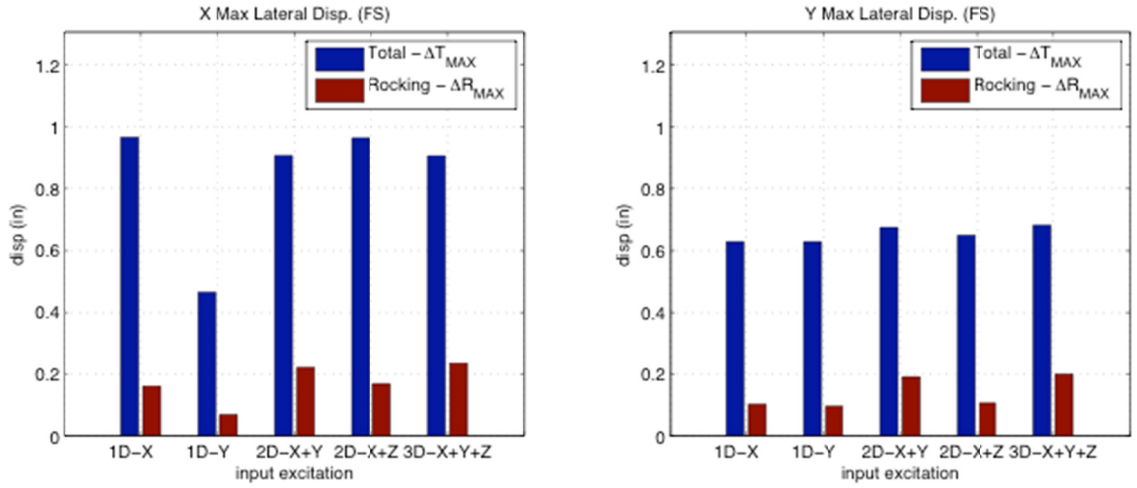

(c) test set FS

Figure 4.13 Test Group 2: rocking contribution to maximum center mass lateral displacement.

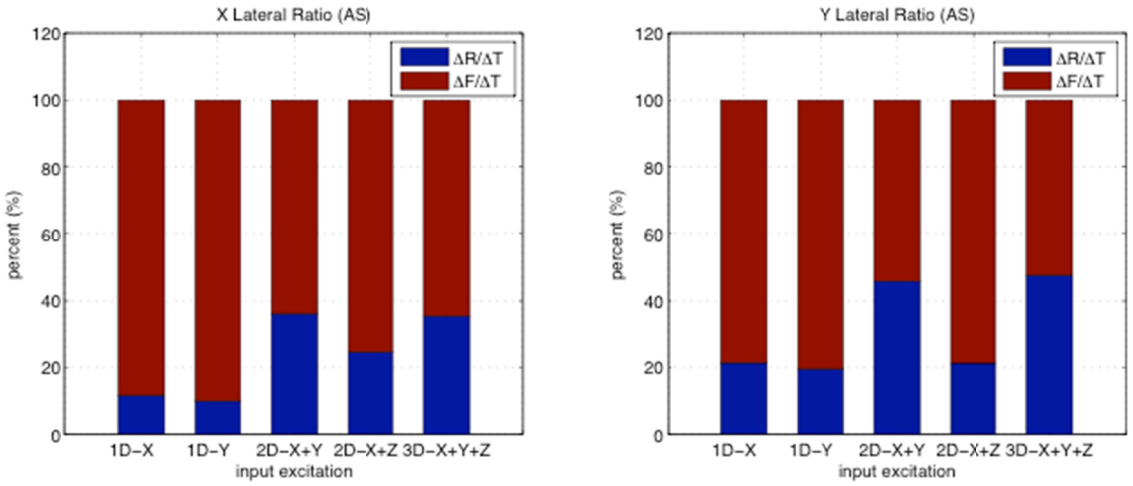

(a) test set AS

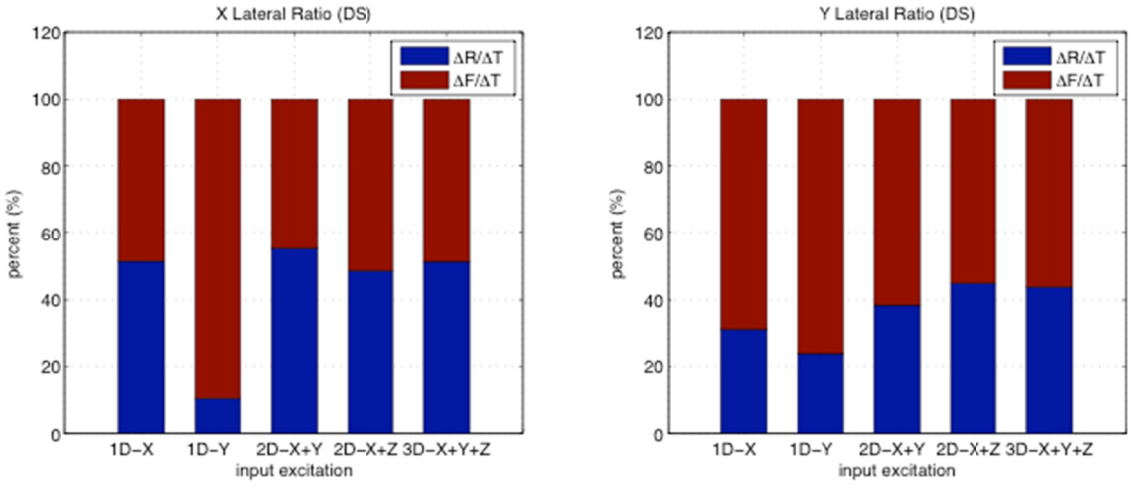

(b) test set DS

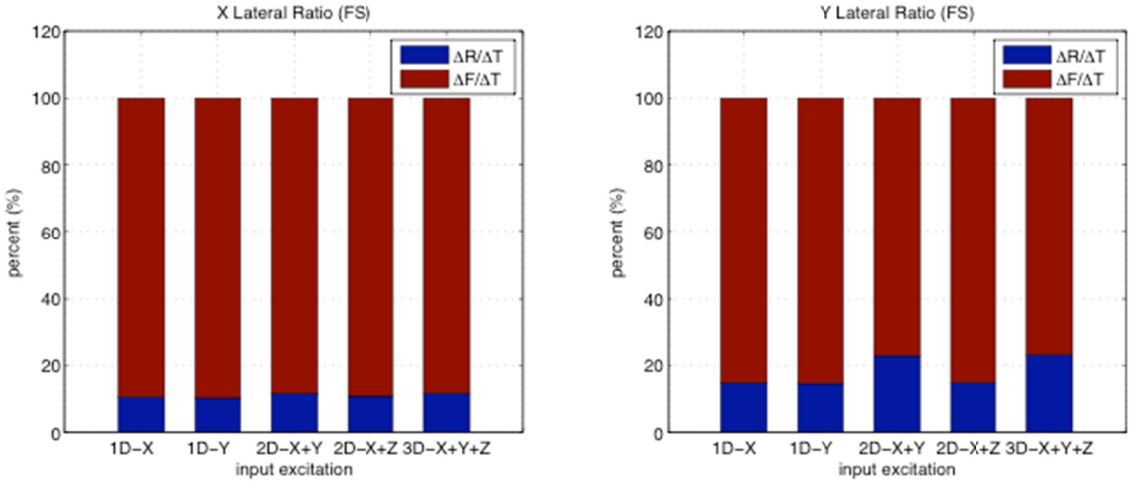

(c) test set FS

Figure 4.14 Test Group 2: rocking and flexure contribution to peak lateral displacement.

4.5.1.2 Footing Uplift

The uplift of the footing was determined as follows. The initial vertical displacement of the footing was recorded due to axial load, and then the dynamic vertical uplift of the footing was determined using the four NOVOS to record the dynamic footing vertical displacement relative to the rigid table surface. The footing vertical displacement was calculated for the entire footing by assuming a rigid body, a reasonable approach. The vertical displacement of the footing can be described as uplift when the footing physically separates from the elastomeric pad. It can be described as rocking when the footing remains in contact with the pad, but rotates due to the flexibility of the pad. Figure 4.15 illustrates the terminology for footing vertical displacement.

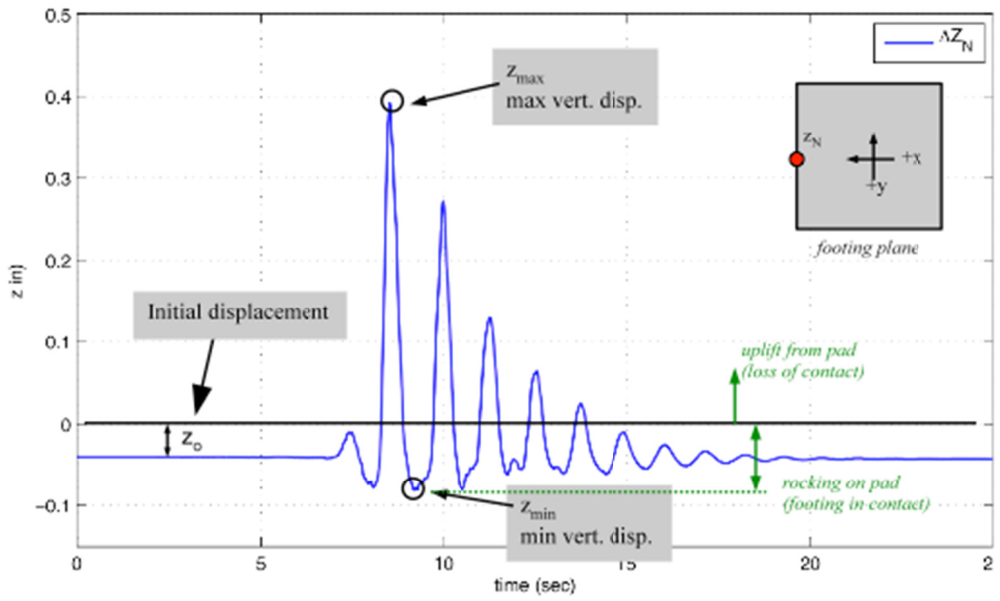

Figure 4.15 Illustration of terminology for footing vertical displacement.

The recorded vertical displacements were used to calculate the rotation about the centerline in the *X*-direction (θ_{NS}) and the *Y*-direction (θ_{EW}). The rotations were then used to calculate the edge vertical displacements along the centerlines in the *X*-direction at the north edge (ΔZ_N) and south edge (ΔZ_S) as for the *Y*-direction for the east (ΔZ_E) and west (ΔZ_W) edges. A rigid body assumption allowed for calculating vertical displacements of all locations in the horizontal plane of the footing. The entire footing uplift profile was then used to assess the envelope of displacements along the *X*- and *Y*-directions and the peak contours of vertical displacement for the entire footing.

The measured static displacement due to weight of the top mass, column, and footing was approximately $z_o = 0.03\,\mathrm{in.}$ The edge displacements for test set AS are shown in Figure 4.16. The amount of uplift of this level of excitation was quite small, on the order of 0.08 in., which

was similar to the amount of indentation on the compression side. This is consistent with the intent of this test.

Selected uplift vertical displacements for tests D1S, D3S, and D5S are shown in Figure 4.17, Figure 4.18, and Figure 4.19. At this level of excitation the amount of uplift is small about 0.4 in., but not insignificant. This is consistent with the intent of this test, which was to cause uplift and rocking of the specimen. The envelopes of displacement are presented. Interestingly the peak uplift values take a linear shape and the peak indentation values take a nonlinear shape indicating nonlinear displacement response of the elastomeric pad when compressed. The contours for peak uplift and indentation are also shown for the entire footing. As the column response results illustrate, the addition of the *Y*-component of excitation significantly contributed to the uplift in that direction. The additional component increased the peak displacement by approximately 50%.

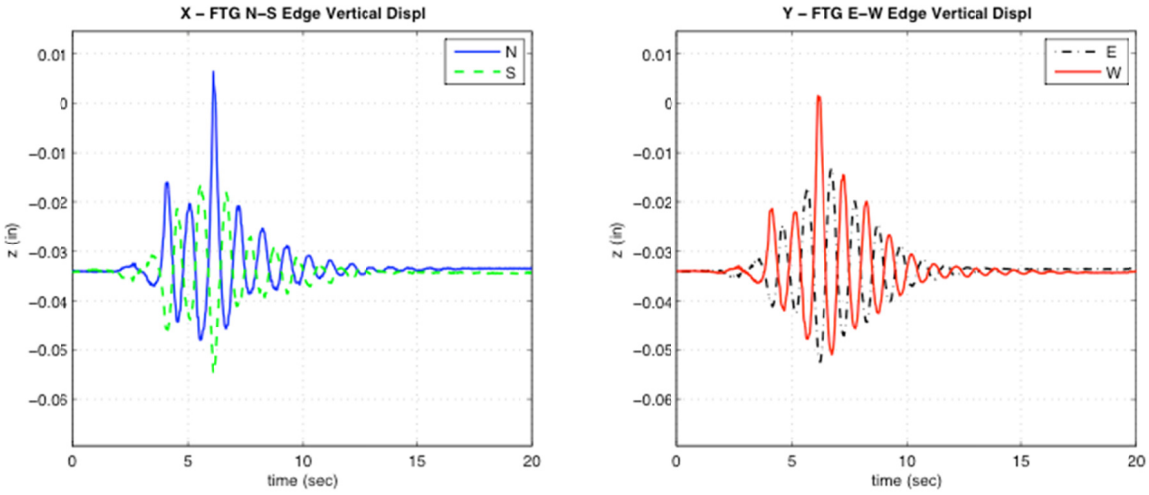

(a) test Run A1S

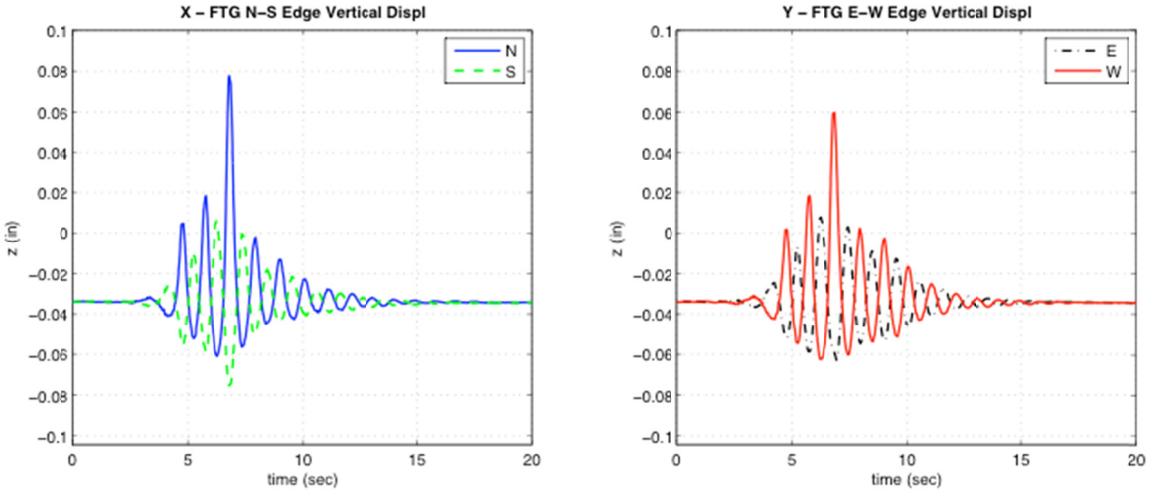

(b) test run A3S

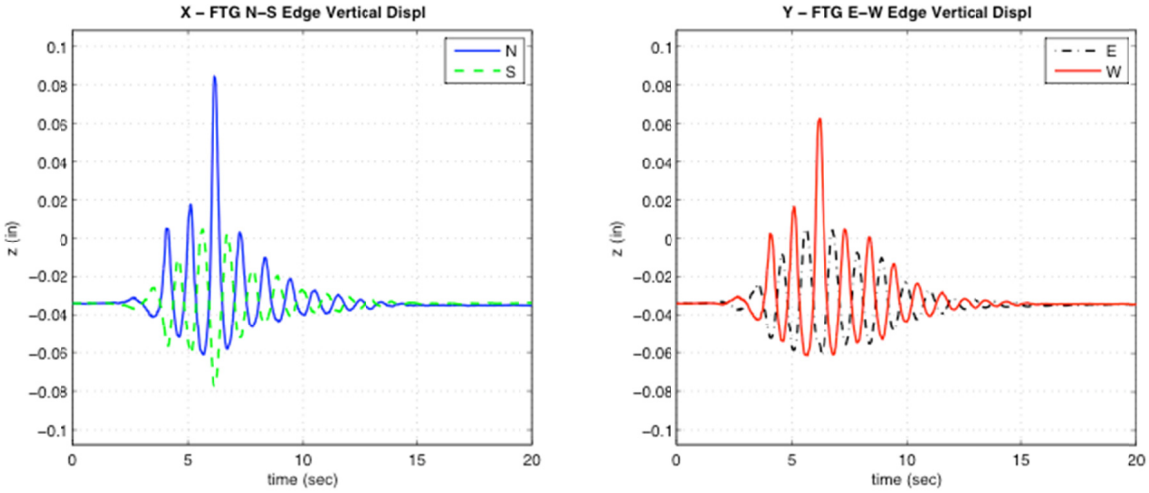

(c) test run A5S

Figure 4.16 AS centerline edge footing uplift response

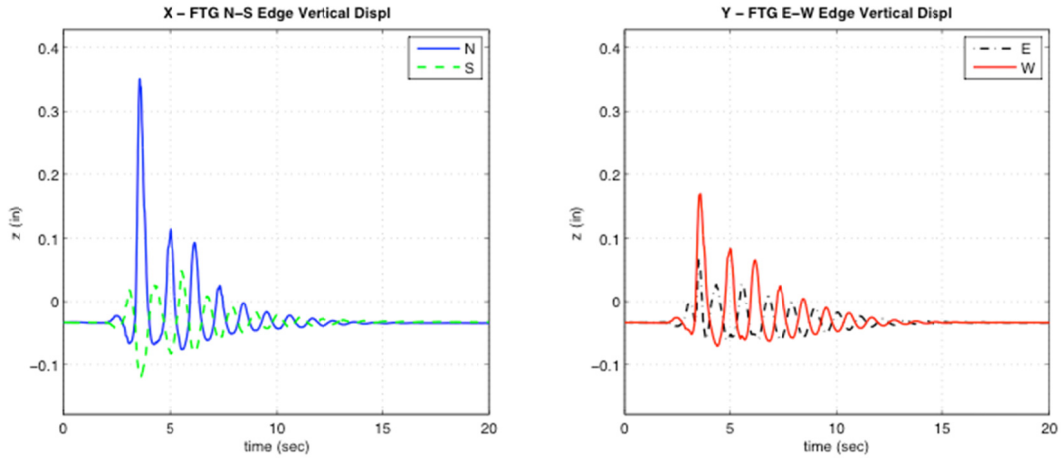

(a) test run D1S

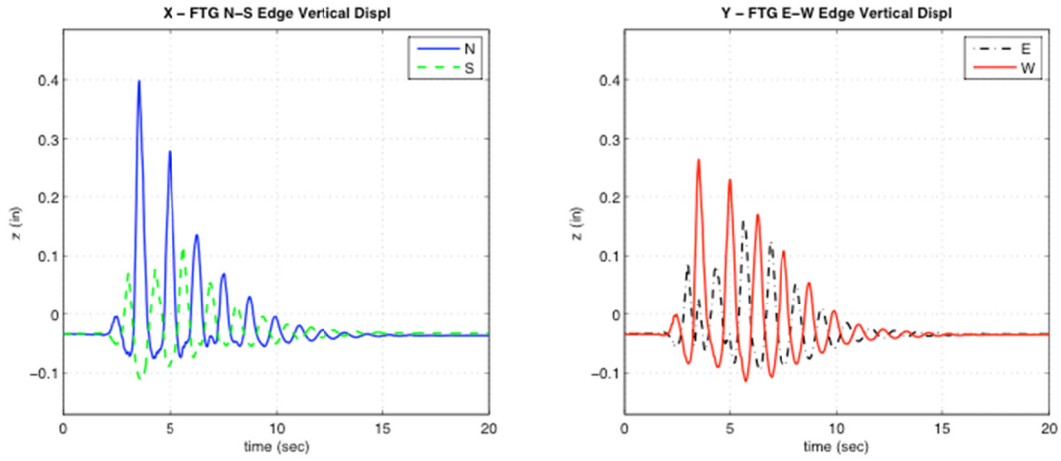

(b) test run D3S

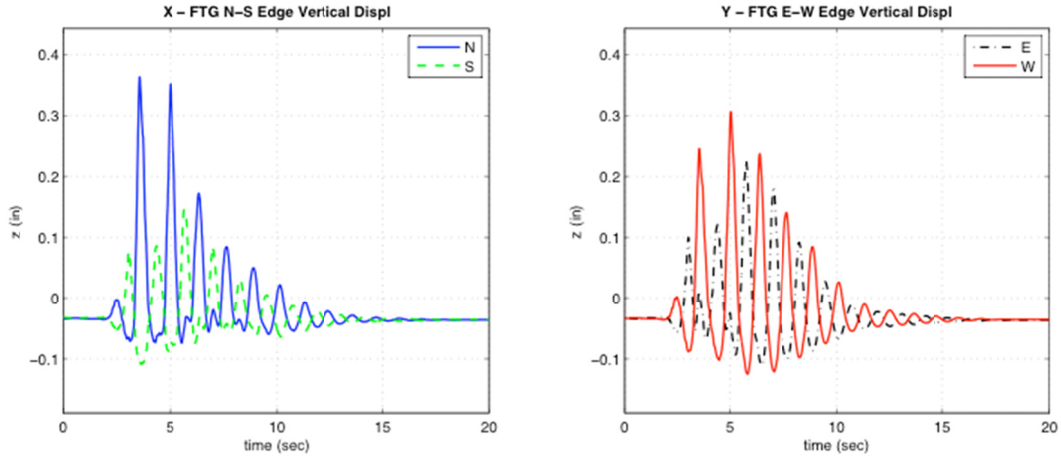

(c) test run D5S

Figure 4.17 DS centerline edge footing uplift response.

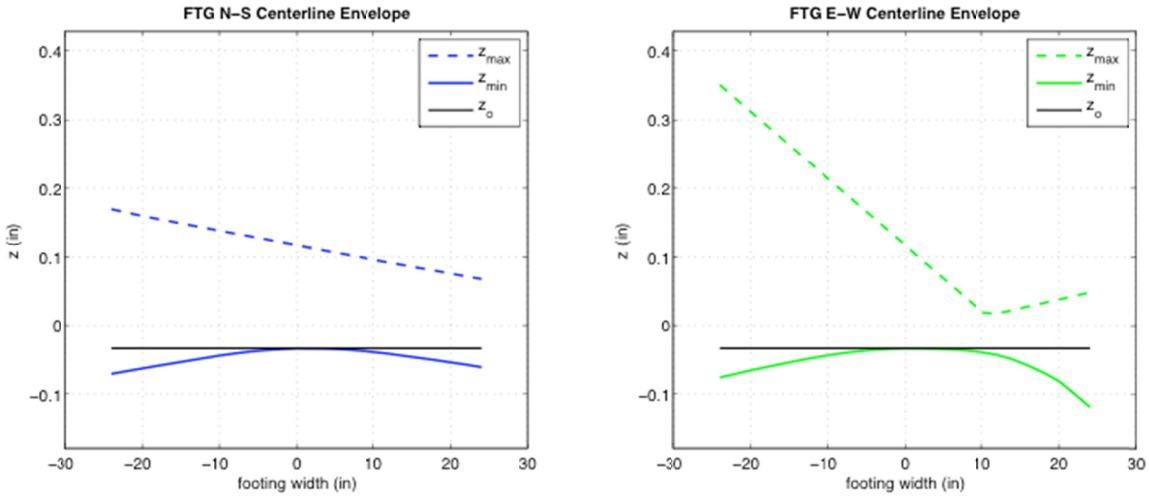

(a) test run D1S

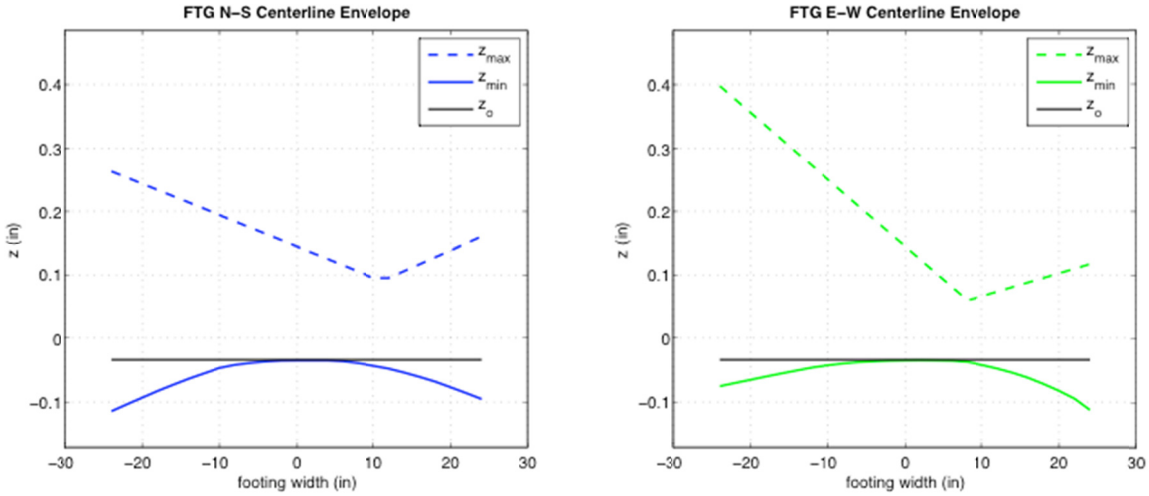

(b) test run D3S

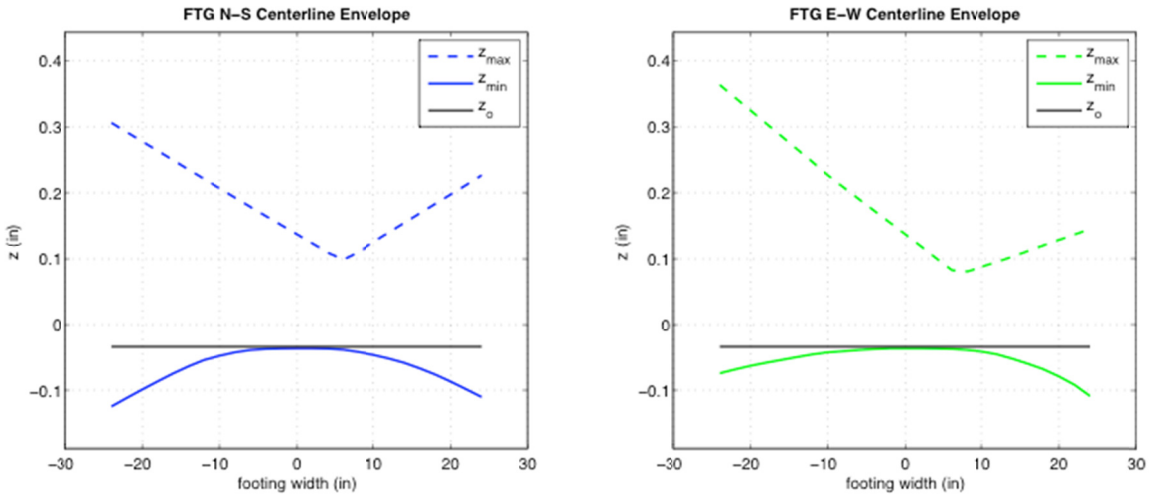

(c) test run D5S

Figure 4.18 DS centerline envelope footing uplift response.

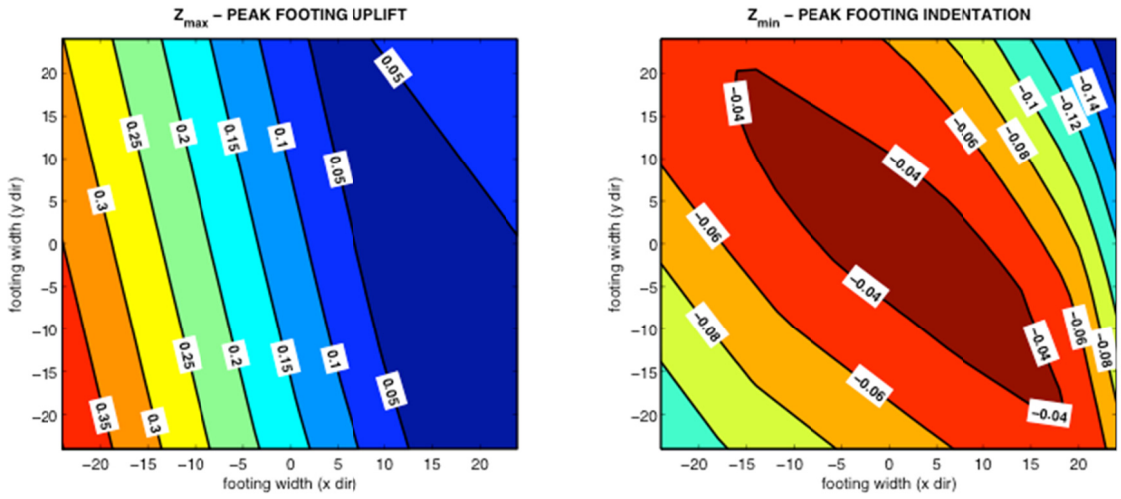

(a) test run D1S

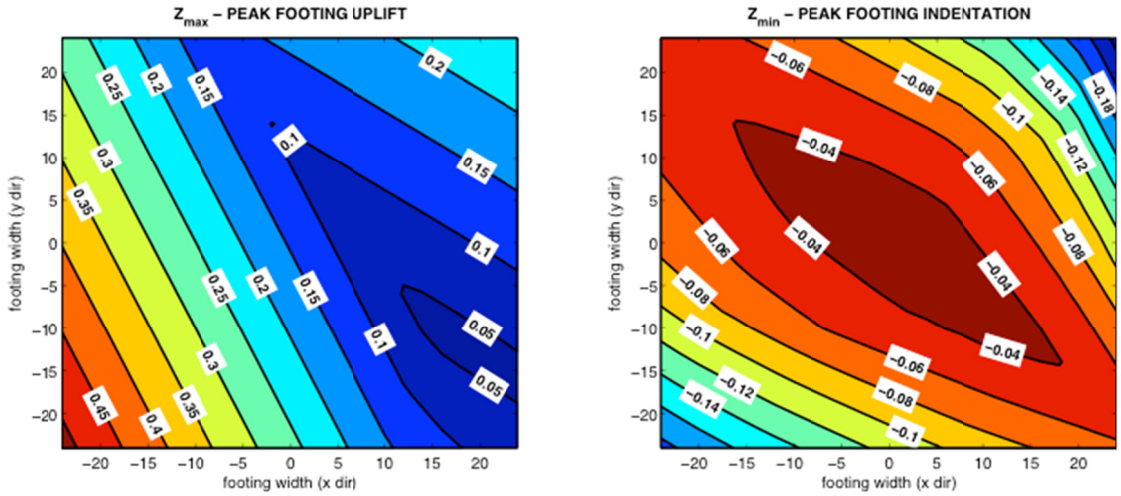

(b) test run D3S

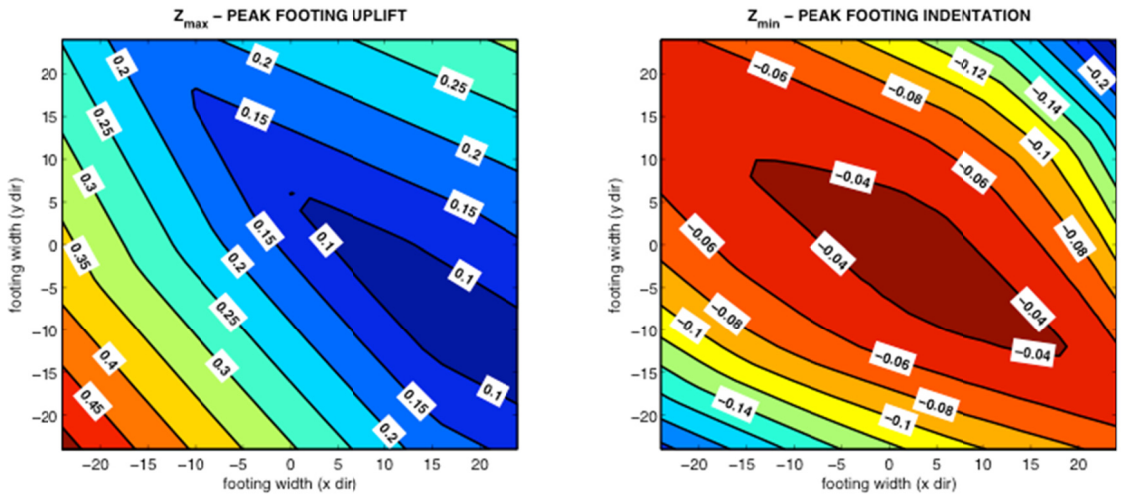

(c) test run D5S

Figure 4.19 DS contour footing uplift response.

4.5.1.3 Rotations about Vertical Axis

During testing the unrestrained footing was observed to rotate about a vertical axis especially during strong bi-directional response. An explanation for why twisting occurred is readily available, considering a situation where the footing was lifting due to excitation in the *X*-direction, and then was subjected to an inertial force in the *Y*-direction. Here there was a tendency to rock in the *Y*-direction, and an eccentricity between the center of mass and the center of lateral resistance between the footing and the soil occurred. This eccentricity will tend to twist the specimen and tends to pivot around the corner of the footing still in contact with the elastomeric pad.

As a result of repeated occurrences of this phenomenon, the test results show a permanent lateral movement in the *X*- and *Y*-directions and rotation about the vertical axis. Figure 4.20 shows the results for test sets DS and FS. The cumulative displacement at the conclusion of the test set was 0.5 in. and 0.0 in., respectively. As noted, the amount of uplift for FS was very small, so it would be expected that a negligible amount of rotation would occur because of the phenomenon of rotation, which is the case for this test set. In an actual footing, passive pressure of the soil against the sides of the footing and the attachment of the top of the column to the bridge deck would tend to minimize this motion. Because of the higher weight of the test specimen relative to the capacity of the laboratory crane, no attempt was made to align the specimen with the principle axes of the table following each test run.

The calculation of rotation about the vertical axis was done using recorded displacement on the corners of one footing face and dividing by the horizontal distance between the locations. Test sets DS and FS had a maximum rotation of approximately 0.012 rads and 0.0015 rads, which for the 48 in. square footing is approximately 0.27 in. and 0.03 in. of twists of the corner edges.

4.5.2 Local Response

Measuring curvatures and strains in critical locations provided insight to global response measures and observed damage of the systems. Curvature distributions within the column plastic hinge length were of particular interest, as were the strains of reinforcing within this region. Reinforcing slip complicates the analysis of the system, and so an attempt was made to quantify the amount of slip in the system. This section describes the average column curvature over several regions of column height, the amount slip or bar pull-out measured at the base of the column, and the reinforcing strains in rebar within the plastic hinge zone.

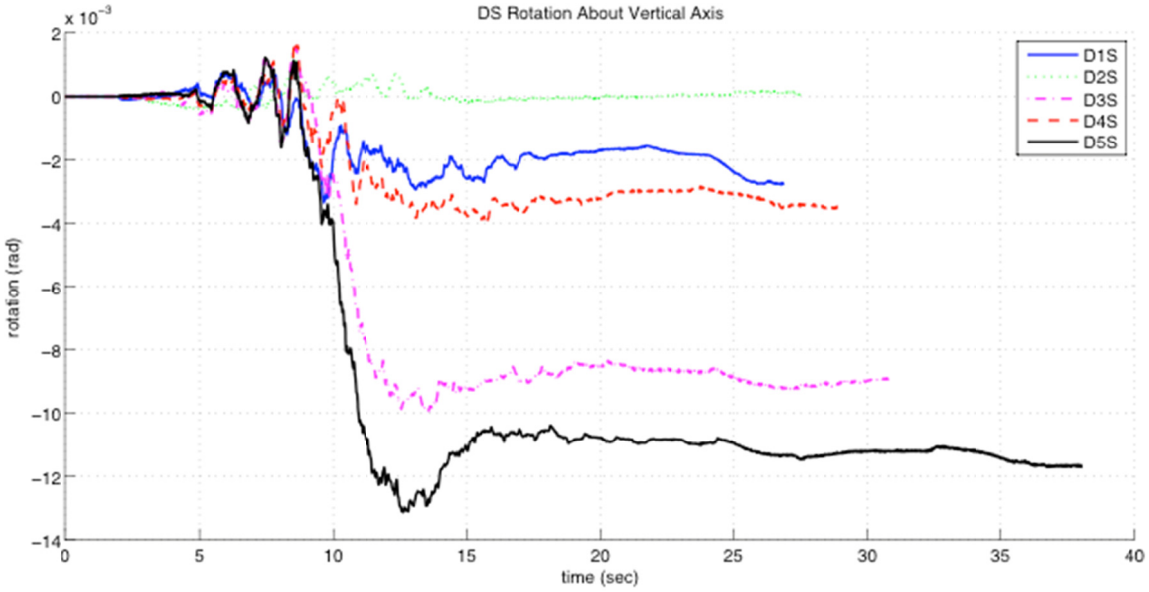

(a) test set DS

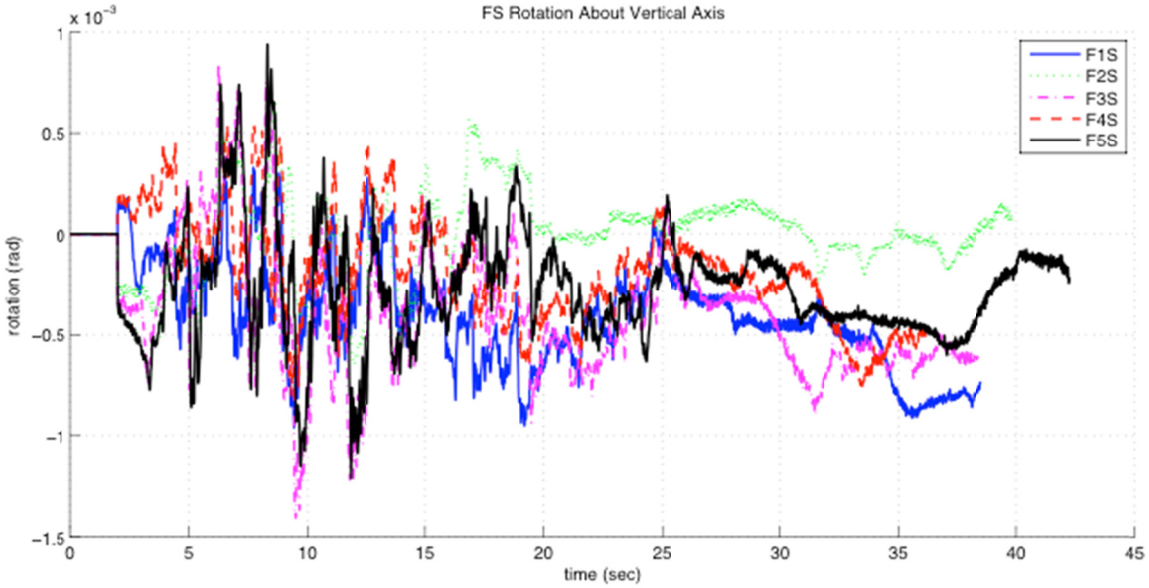

(b) test set FS

Figure 4.20 Test Set DS and FS twisting about vertical axis.

4.5.2.1 Column Curvature Distribution

Average curvatures were estimated over regions of the column extending between the locations of DCDT instruments attached to the face of column. Section 4.2.1.3 illustrates the method of column curvature calculation and Figure 3.24 highlights the locations of the DCDTs. The curvature recordings for tests D3S and F3S are shown in Figure 4.21. The results show that there was less curvature demand for the FS group, which is consistent with global displacements measures shown in Figure 4.11 and Figure 4.12.

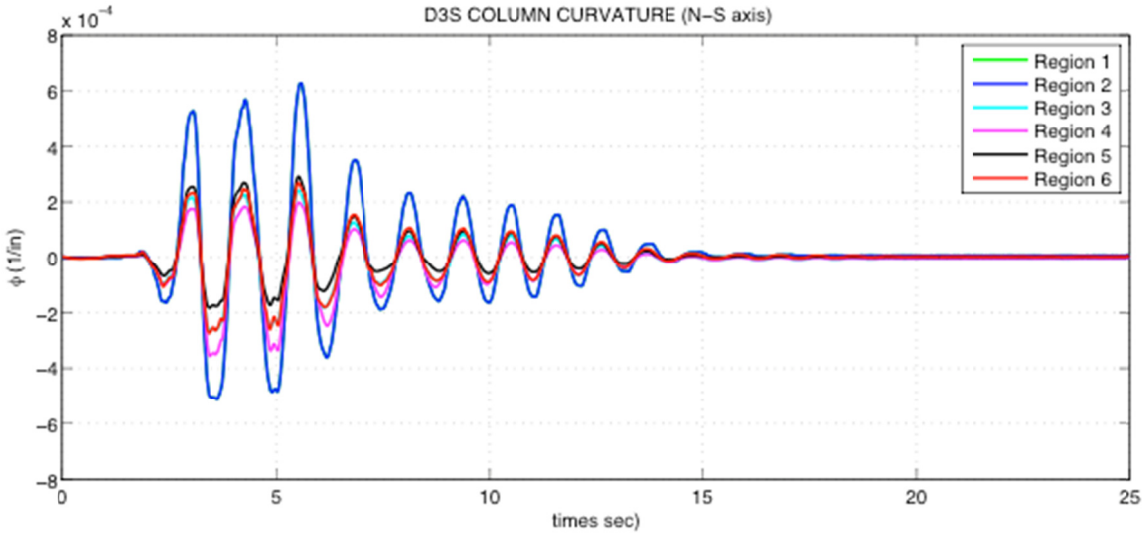

(a) D3S column curvature

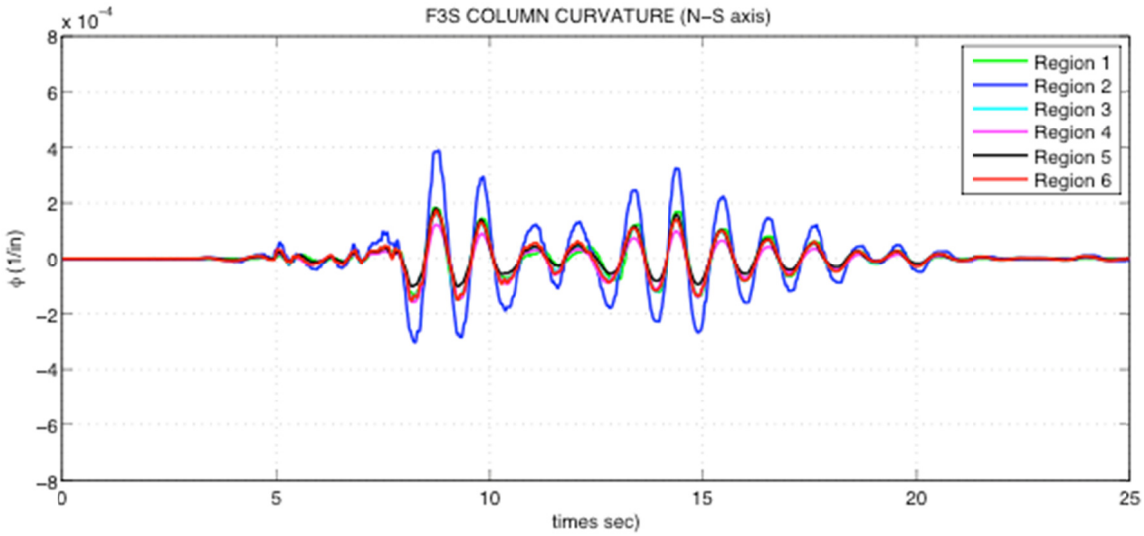

(b) F3S column curvature

Figure 4.21 Recorded column curvatures along column height.

Region 1 and 2 were used to determine bar pullout measuring elongation at the same column height to distinct locations at or above the footing. Pullout of the longitudinal reinforcing from the footing was measured using a similar method to the curvature calculations. At the region adjacent to the footing (for each face), a pair of DCDTs was connected 6 in. above the footing. One of the pair measured elongation between the connection and the footing, and the other measured elongation between the connection and a rod attached to the column approximately 1/2 in. above the footing. The difference between the two readings is an estimate of the pullout the bar for that face. Using the same process for the opposing face, the slip rotation could be calculated and the displacement of the center of mass due to anchorage slip could be determined. For Test Group 2 the amount of slip measured was on average between 20–30% of the total flexural displacement of the column.

4.5.2.2 Strains

Strain gauges were mounted on four of the twelve longitudinal reinforcing bars. The measured strains provided insight into the behavior to the bars during loading, particularly when the strains in the reinforcement reach the inelastic demand level. The four locations of strain measurement were the bars that coincided with the north, south, east and west column faces. The gauges were mounted on the outer face of the reinforcement and located at two elevation points that corresponded to the top and bottom of the plastic hinge zone. Although information from the gauges is very useful in determining when yielding begins, beyond that the information they provide can be unreliable because the gauges often fail when strains reach excessive demands (such as those from large deformations and rotations of the column).

Figure 4.22 shows the strains on the south-most reinforcing bar for test D5S, which is a three-dimensional input excitation. The peak value of tensile strain was 1200 μS, which is approximately 60% of the yield strain. Clearly, the strains did not reach an inelastic level. The two locations of recording were at the base (0 in. height) and the top of the expected plastic hinge zone (16 in. height) above the base. The cumulative time history for test set DS is shown in Figure 4.23 for the south and east reinforcing steel; the strain gauge was located at the bottom of the column.

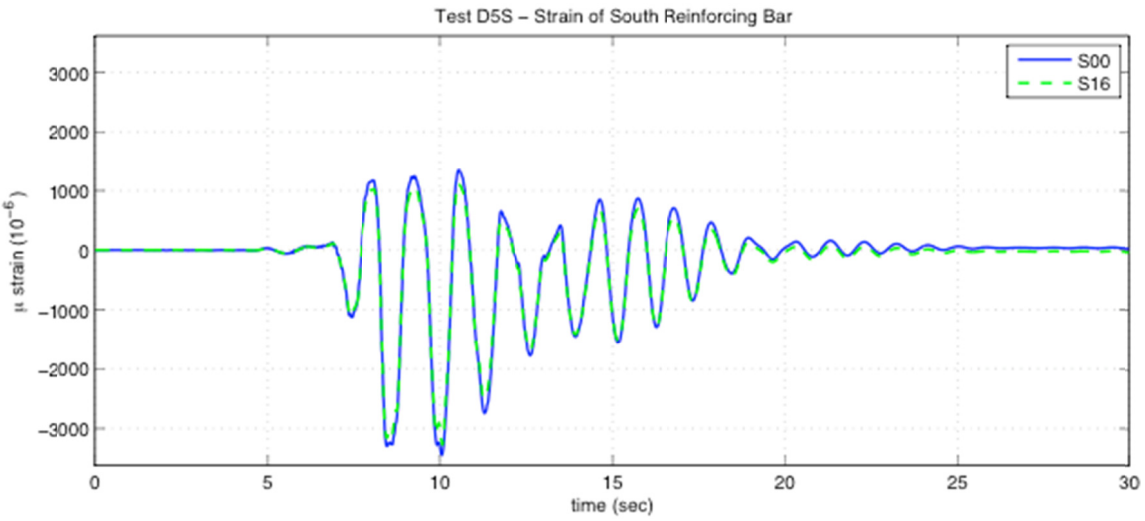

Figure 4.22 Reinforcing steel strain for south rebar (Test D5S).

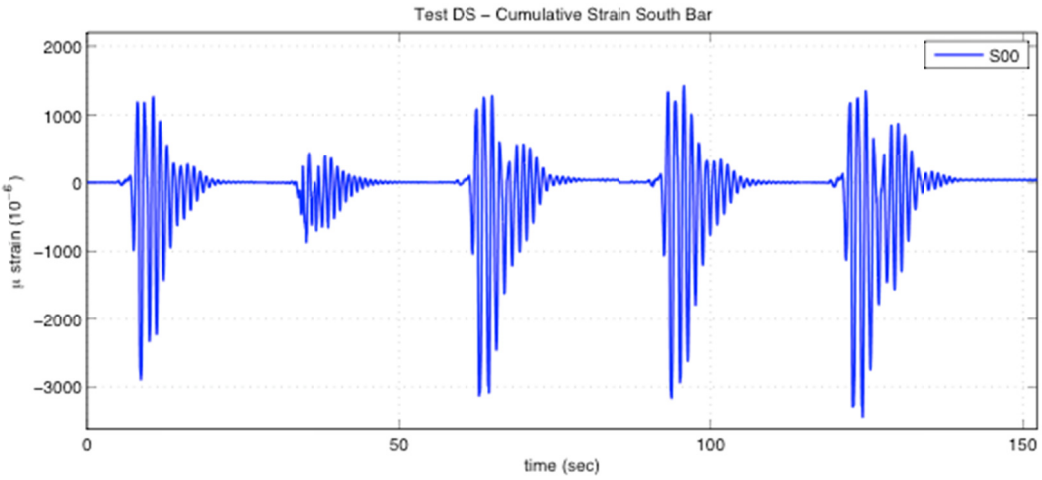

(a) south bar strain gauge @ 0 in. height

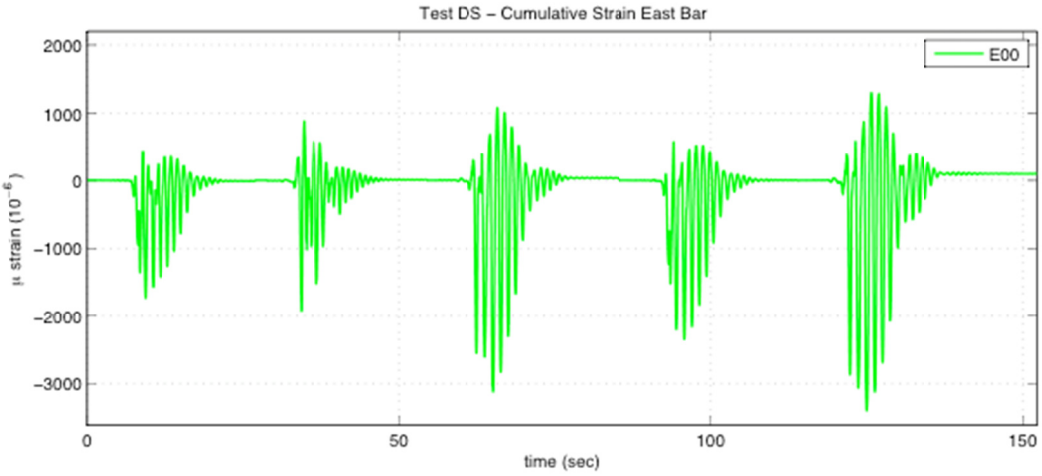

(b) east bar strain gauge @ 0 in. height

Figure 4.23 Cumulative strain time history test D5S.

4.5.3 Force-Displacement Hysteresis Curves

The force-displacement relationships of the specimen highlight the behavior during shaking and provide particular insight into how the specimen behaves when allowed to uplift. When a well-confined RC column is restrained from uplift at the base, the moment-curvature relationship at the base of the column is essentially linear until the point where inelastic demands are reached and exceeded. Significant energy dissipation occurs due to nonlinear behavior associated with yielding of the reinforcement and concrete crushing. The inclusion of an uplifting foundation with flexible supporting medium adds considerable hysteretic energy dissipation from uplift and interaction of the soil. The addition of this energy dissipation mode may draw away some of the energy dissipated by the deformation along the column height.

The force-displacement relationships of particular interest for uplifting footings are the base moment-column curvature and the base moment versus footing rotation. This section illustrates the magnitude of response for both of these relationships. Calculations of the moment

time histories were done by the methods described in Section 4.2.2. Figure 4.24 shows the calculated base moment time histories for test D1S, D3S, and D5S. The results between the two and three components of excitation are similar but not exact owing to the inclusion of the vertical component of excitation. As the number of input excitations increased, the response at the 8 sec mark became out of phase, more so for each component of excitation. Although this could be due to a lengthening of the natural period due to softening during testing, more likely it was caused by the interaction between orthogonal directions when considering additional excitations. The moment time history of test F1S, F3S, and F5S are compared in Figure 4.25, which had less demand at the column base than the DS test set. Although test F1S appears out of phase, in reality it was time shifted to start earlier.

The peak moment for tests DS was calculated as 1078 kip-in., 1047 kip-in., and 1041 kip-in. for the DS tests shown. The approximate ratio between peak moments was approximately 1. For tests FS, the peak moments are 726 kip-in., 624 kip-in., and 631 kip-in., respectively. Note the larger demand for the one component of excitation, which is approximately 115% greater.

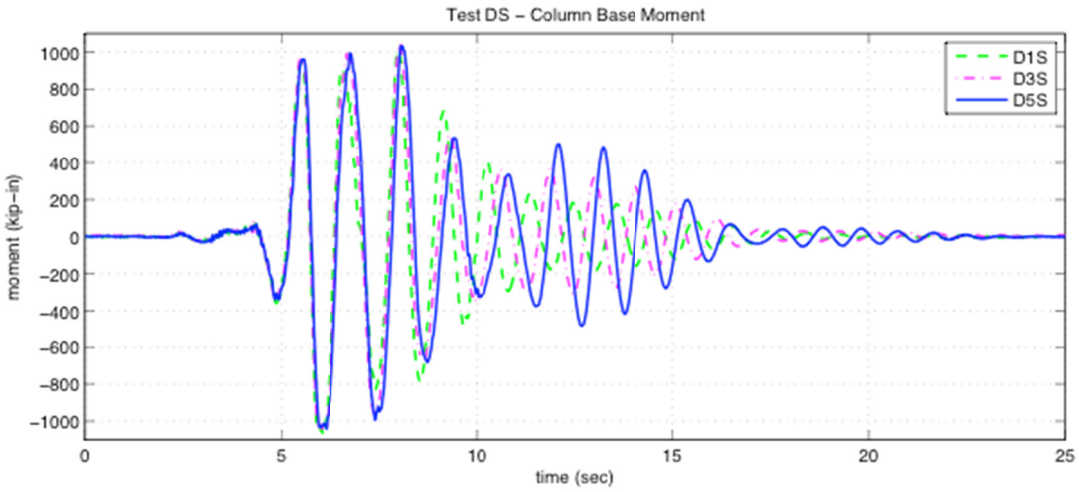

Figure 4.24 DS column base moment time history.

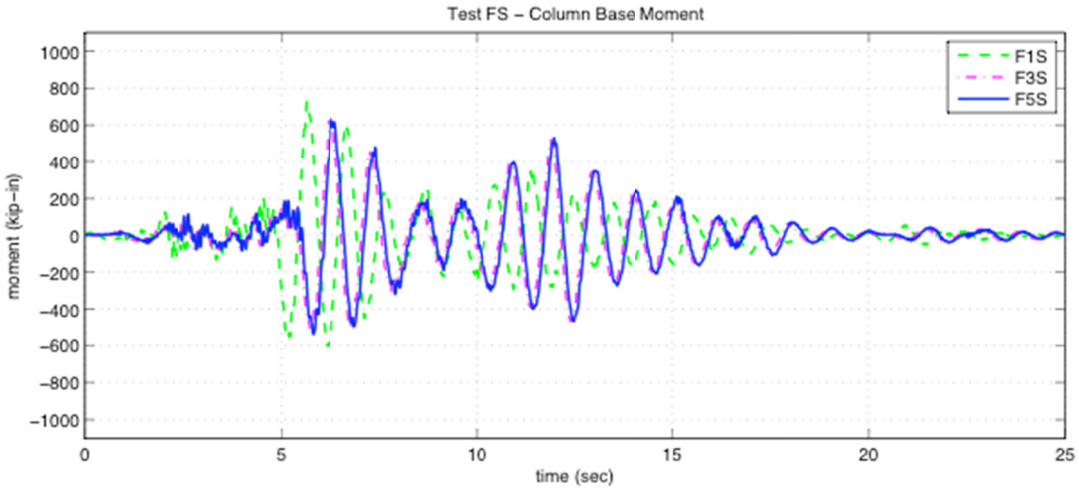

Figure 4.25 FS column base moment time history.

The lateral force versus lateral displacement hysteresis of the column base shear and center of mass of the top block is shown in Figure 4.26 for tests AS, DS, and FS, whose displacements are shown in Figure 4.10 through Figure 4.12. No significant nonlinear behavior was observed, which was consistent with the testing objective. High-frequency response was observed in the shears. Hachem et al. [2003] discussed this phenomenon, and found that it was related to high mode vibrations of the specimen involving rotation of the center of mass about the local horizontal axes.

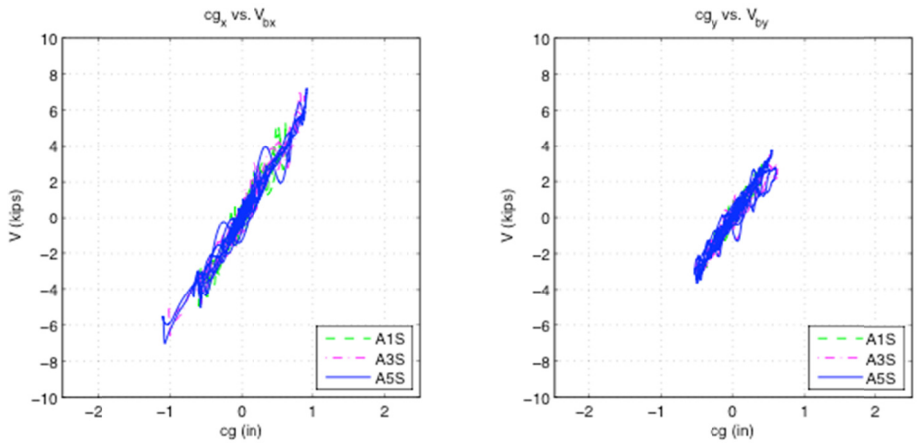

(a) AS – 1D-*X*, 2D-*X*+*Y*, 3D-*X*+*Y*+*Z*

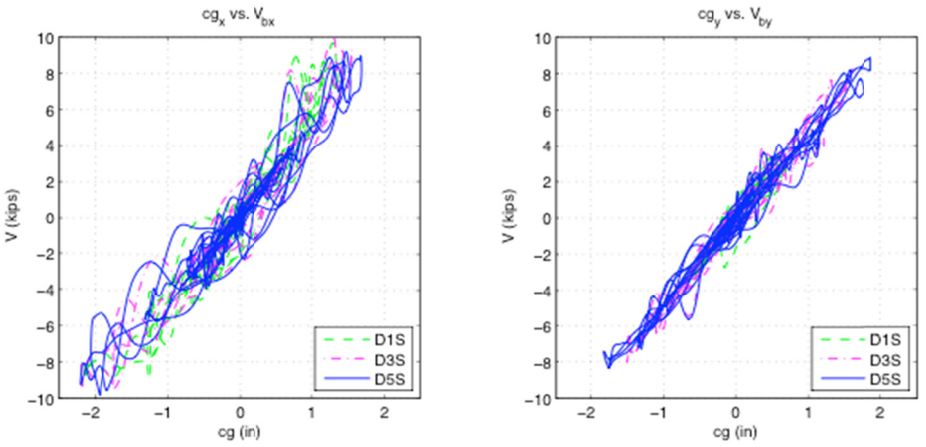

(b) DS – 1D-*X*, 2D-*X*+*Y*, 3D-*X*+*Y*+*Z*

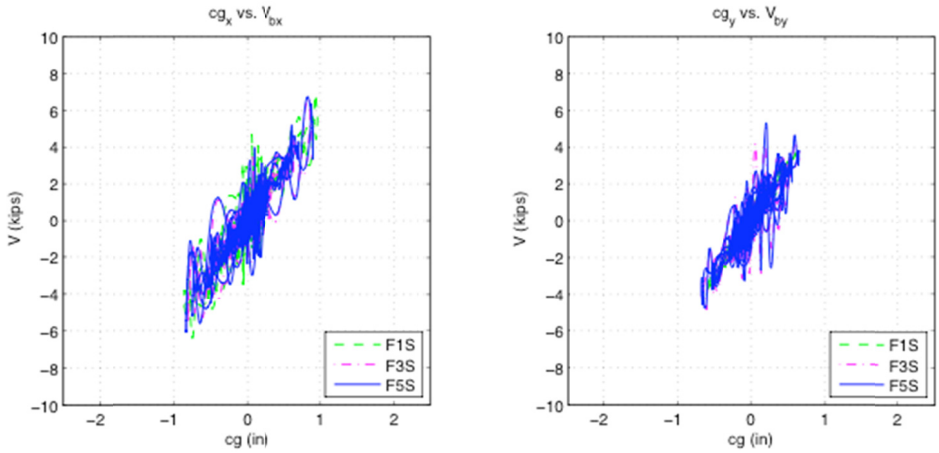

(c) FS – 1D-*X*, 2D-*X*+*Y*, 3D-*X*+*Y*+*Z*

Figure 4.26 Lateral force versus lateral displacement (Tests AS, DS, FS).

4.5.3.1 Moment-Curvature Column Response

Average column curvatures at the base are plotted in Figure 4.21 against the calculated column base moment. A highly linear relationship exists between the moment and curvature, indicating that the specimens behaved as desired. Figure 4.27 shows the average curvature versus column moment for tests AS, DS, and FS. In Figure 4.27(b) note that the observed that the stiffness of the system as described by the slope of the curvature-moment plot seems to be more gradual than the other plots. This may be an anomaly due to loading or recording instruments, because plots from the subsequent test FS matched well with the others.

4.5.3.2 Moment-Rotation Footing Response

The column moment-footing rotation relationship indicates the relationship of rocking and uplift on energy dissipation via hysteresis. Figure 4.28 illustrates some of the important characteristics of a rocking and/or uplifting footing. For low levels of excitation it is likely that the relationship would be essentially linear while rocking and that as uplift occurs, the behavior would become nonlinear. At the value of moment the footing loses contact with the pad and the response softens, indicating an essentially linear response while rocking and a nonlinear elastic response while rocking and uplifting. The literature review (see Chapter 2) indicated that there is likely a value of overturning moment, at which point the footing response to applied moment softens and essentially behaves as a bilinear curve with smaller overturning post-yield stiffness.

The footing uplift described in Section 4.5.1.2 was used to calculate rotation along the centerline for both the north-south axis and the east-west axis. Rotations were calculated by subtracting the relative uplift between opposing footing edges and dividing by the footing width [Equation (4.4)]. Figure 4.29 shows an example of the calculated rotation for the test D3S for each direction. Figure 4.30 shows the footing rotation versus column moment for tests AS, DS, and FS. The values for moment at which uplift from the footing and rotation about the outer edge would occur were the same for each direction and were measured to be approximately M_{upNS}=M_{upEW} = 600 kip-in. and M_{rotNS}=M_{rotEW}=1100 kip-in., respectively.

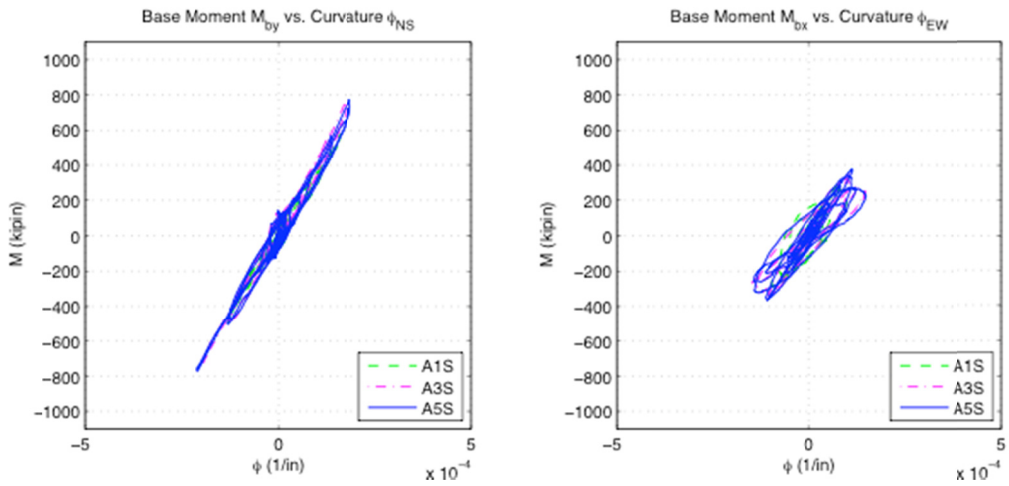

(a) AS – 1D-*X*, 2D-*X*+*Y*, 3D-*X*+*Y*+*Z*

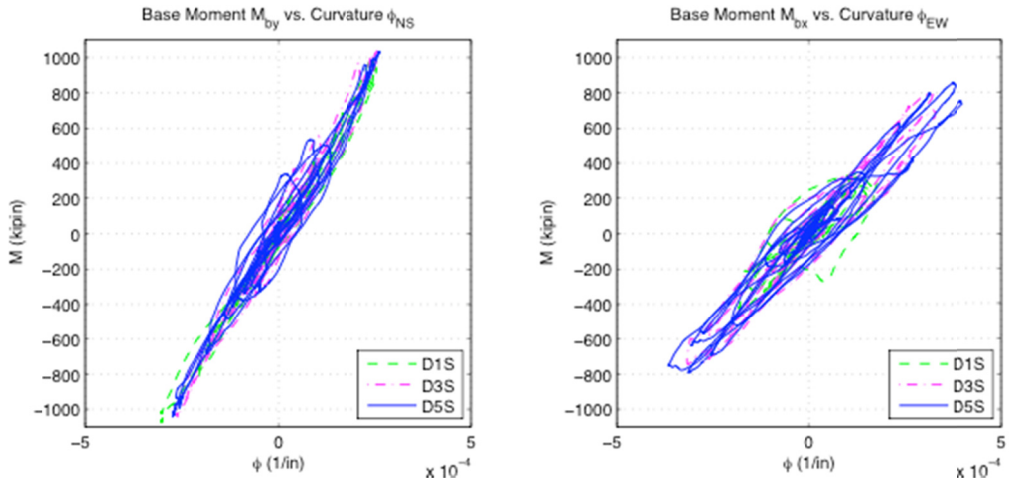

(b) DS – 1D-*X*, 2D-*X*+*Y*, 3D-*X*+*Y*+*Z*

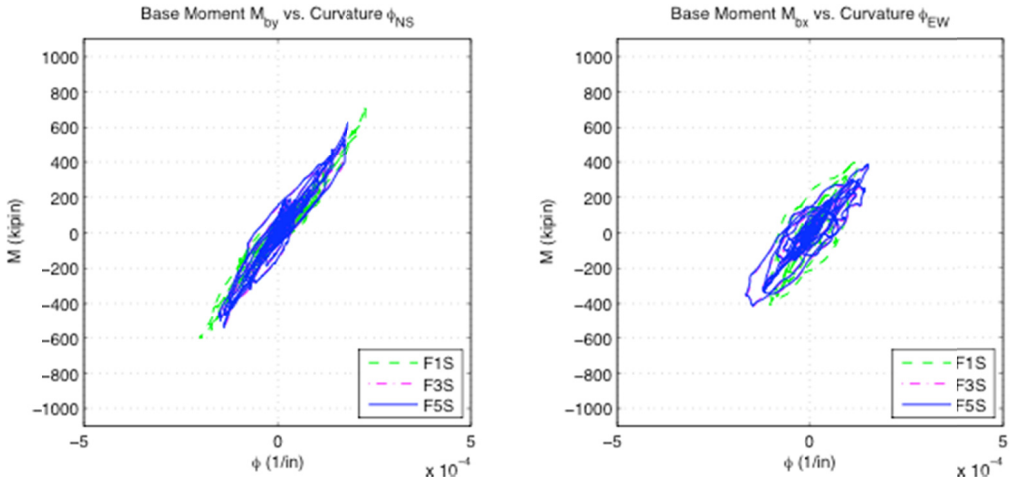

(c) FS – 1D-*X*, 2D-*X*+*Y*, 3D-*X*+*Y*+*Z*

Figure 4.27 Column base moment curvature response (Tests AS, DS, FS).

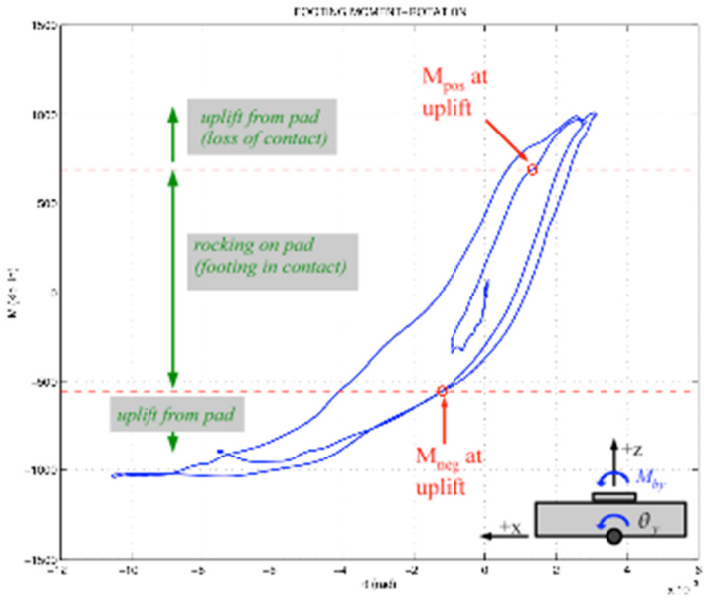

Figure 4.28 Moment-footing rotation characteristics.

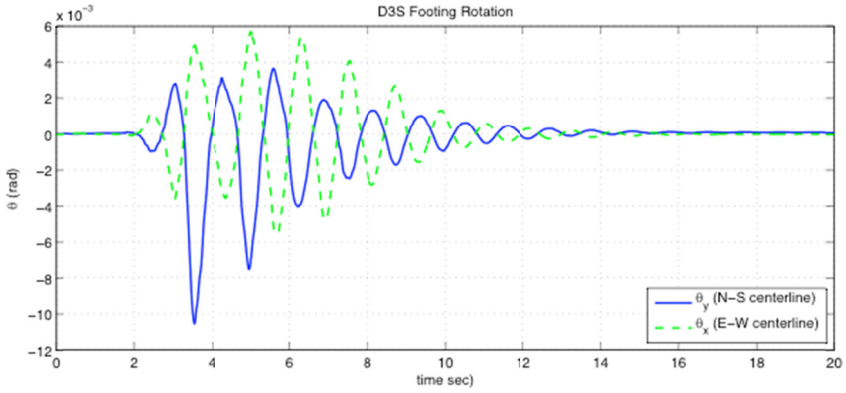

Figure 4.29 D3S footing rotation.

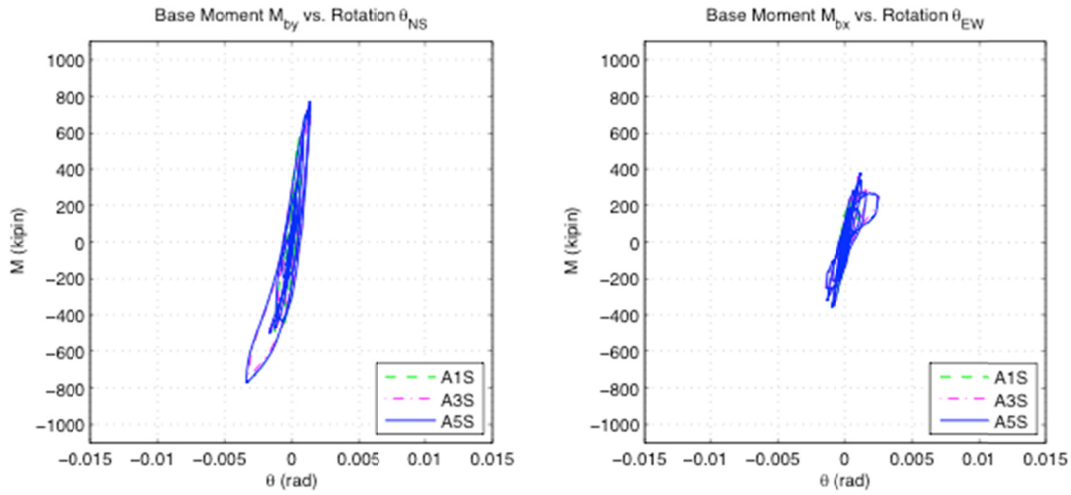

(a) AS – 1D-*X*, 2D-*X*+*Y*, 3D-*X*+*Y*+*Z*

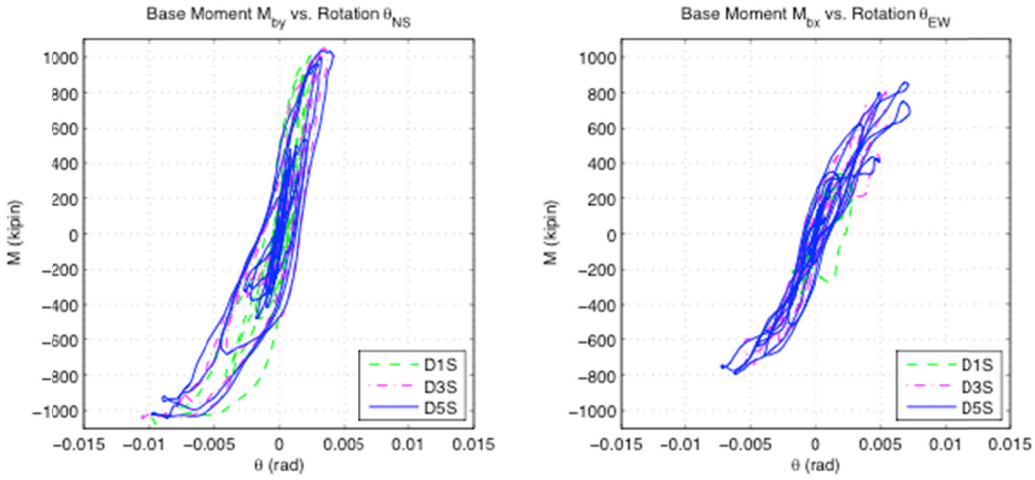

(b) DS – 1D-*X*, 2D-*X*+*Y*, 3D-*X*+*Y*+*Z*

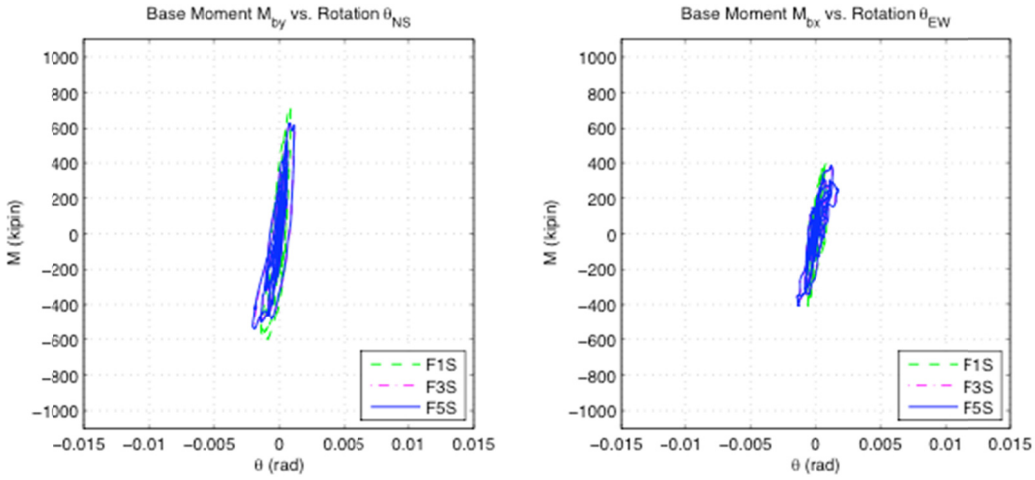

(c) FS – 1D-*X*, 2D-*X*+*Y*, 3D-*X*+*Y*+*Z*

Figure 4.30 Column base moment footing rotation response (Tests AS, DS, FS).

4.6 TEST SPECIMEN WITH DESIGN AXIAL LOAD AND 5DC X 3DC FOOTING

The final test group widened the footing in one direction to $5D_c \times 3D_c$, and the intensity of the motions were increased to the point where the column would be loaded into the inelastic range. For this test series, all three components of excitation were used for all runs. The test set AR includes all four tests conducted for Test Group 3. Only the Los Gatos record was used for testing. In the smaller footing dimension direction, the rocking response was preferred over yielding in all cases. Section 4.7 will compare the applied versus restoring moment to correlate the observations of increased inelastic demand and reduced uplift for the test set.

Time histories for global displacement, local response, and force-displacement response are included below. The instrumentation protocol described in Chapter 3 was again used to measure the global and local response. Positioning of the instruments was unchanged with the exception of using the NOVOS to record footing uplift. The devices had to be repositioned to accommodate the wider footing direction; however, the calculation of response was done in a similar manner.

The amplitude scale of ground motions was set at a level that would cause an elastic, yield, design, and maximum displacement ductility response for the rocking system as determined by the column. The magnitude of scaling was 10%, 25%, 90%, and 120% of the original scale. A direct correlation on the effect of footing width on total response can be made between test A2R and D5S, both of which had a three-dimensional input excitation at 25% amplitude scale.

Only the first test run A1R was conducted in the elastic range of the column. All subsequent tests illustrated a nonlinear relationship of the lateral force-displacement response. Additionally permanent displacements occurred in the column due to the damage of nonlinear loading. This test group clearly shows that vertical restraint of the footing was unnecessary to develop the plastic hinge moment of the column and achieved the desired design goal as determined by the Caltrans SDC, which is to confine damage in a bridge system to the plastic hinge region of the column. It also shows that it is prudent to detail columns to be ductile—even if they are expected to rock—due to the effects of bi-directional bending on the footing and column.

The results for Test Group 3 are presented in a similar fashion as those of Test Group 2 (Section 4.5).

4.6.1 Global Displacement

The global displacements of the system are described in this section. Three types of displacement were calculated to describe the response: (1) The total center of mass displacement is a combination of the rocking from rigid body translation due to footing uplift and the flexural displacement of the column due to inertial loading; (2) the uplift of the footing due to inertial loading; and (3) the rotation of the footing about a vertical axis due to uplift and simultaneous lateral loading.

4.6.1.1 Column Response

The set AR includes all four tests conducted for Test Group 3. Time histories of lateral displacement of the center of mass are presented in Figure 4.31 to Figure 4.34. The results for the wider footing suggest less rocking behavior in the orthogonal directions than for the smaller footing size of Test Group 2, and less total displacement for the elastic and yield level tests than the similar amplitude-scaled ground motions of Group 2.

Test A2R and D5S both had three-dimensional input excitations scaled to 25% of the Los Gatos record. Figure 4.32 and Figure 4.11(c) show the response for each and suggest that the overall lateral displacement of the center of top mass is considerably smaller for the $3D_c \times 5D_c$ footing than for the $3D_c \times 3D_c$ footing in either direction. Little rocking was measured for the $3D_c \times 5D_c$ case, but rocking and uplift contributed to about one-half of the lateral displacement response for the $3D_c \times 3D_c$ case. The response of the $3D_c \times 5D_c$ footing was similar to that of the $3D_c \times 3D_c$ if the rocking and uplift displacements are deducted. A comparison of Figure 4.32 and Figure 4.11(c) suggests that limiting rocking in one direction (by increasing the footing width to $5D_c$) can reduce its effect in the other direction.

During testing, inelastic behavior occurred following test runs A3R and A4R (see Figure 4.33 and Figure 4.34), as evidenced by the permanent lateral(?) displacement,. Following the A3R run there was approximately 1 in. of permanent displacement for the *X*- and *Y*-direction, respectively, which was approximately a 1% permanent drift. The incremental permanent displacement for run A4R in the *X*- and *Y*-directions are about 9 and 13 in., respectively; giving a cumulative residual displacement in the *X*- and *Y*-directions of 10 in. and 15 in., respectively. Thus, even though the base was not restrained against rocking in either direction, and rocking would be expected on the basis of a simple one-dimensional analysis in the $3D_c$ direction, ductile yielding of the column dominated the response of the column with the $3D_c \times 5D_c$ footing.

A comparison of peak total displacement and the contribution of rocking displacement to the total is shown in Figure 4.35(a) for tests A1R, A2R, A3R, and A4R. The bar on the left is the maximum lateral displacement of the center of mass, and the bar on the right is the contribution of rocking to the maximum displacement. As shown in Figure 4.35(b), the ratio of rocking and flexural displacement to the total displacement was calculated by dividing the individual contribution to the total displacement. The assumption for these calculations is described in Section 4.5.1.1. The yield level test experienced the most amount of uplift and rocking, with approximately 25% and 10% for the short- and wide-footing directions, respectively. The design and elastic level tests each had no more than a peak of 10% uplift and rocking in either direction.

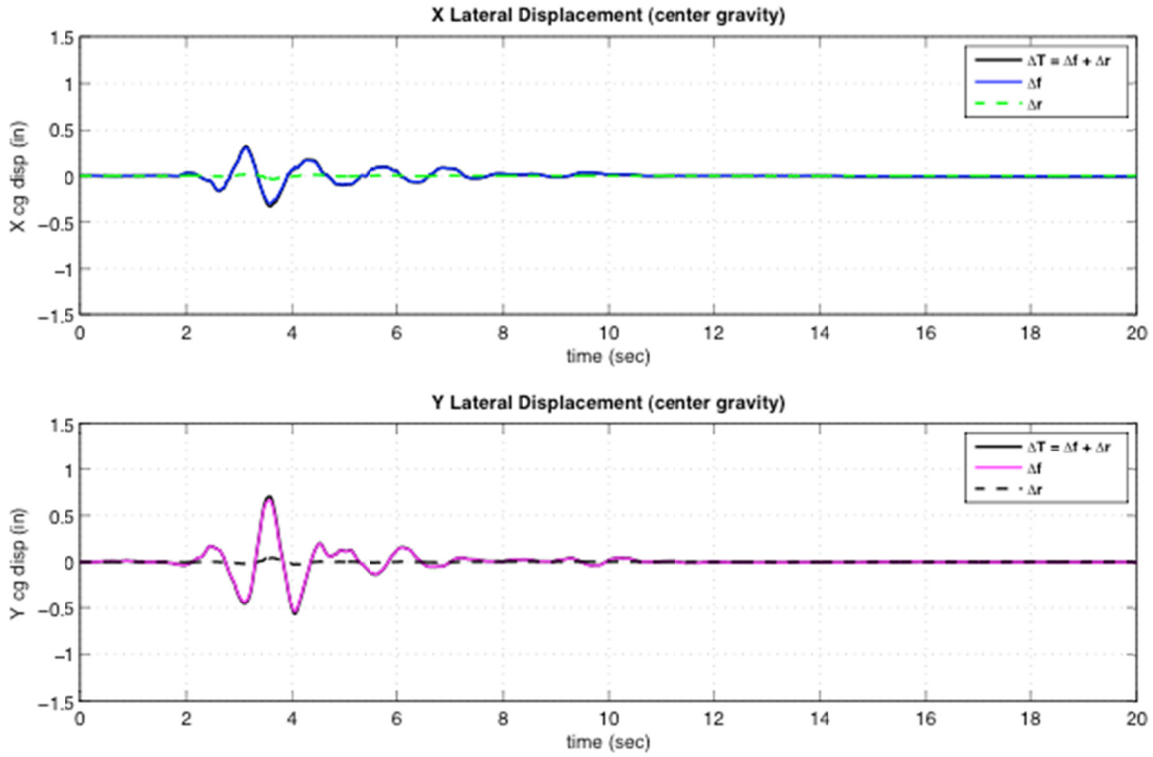

Figure 4.31 Elastic level Test A1R displacement response.

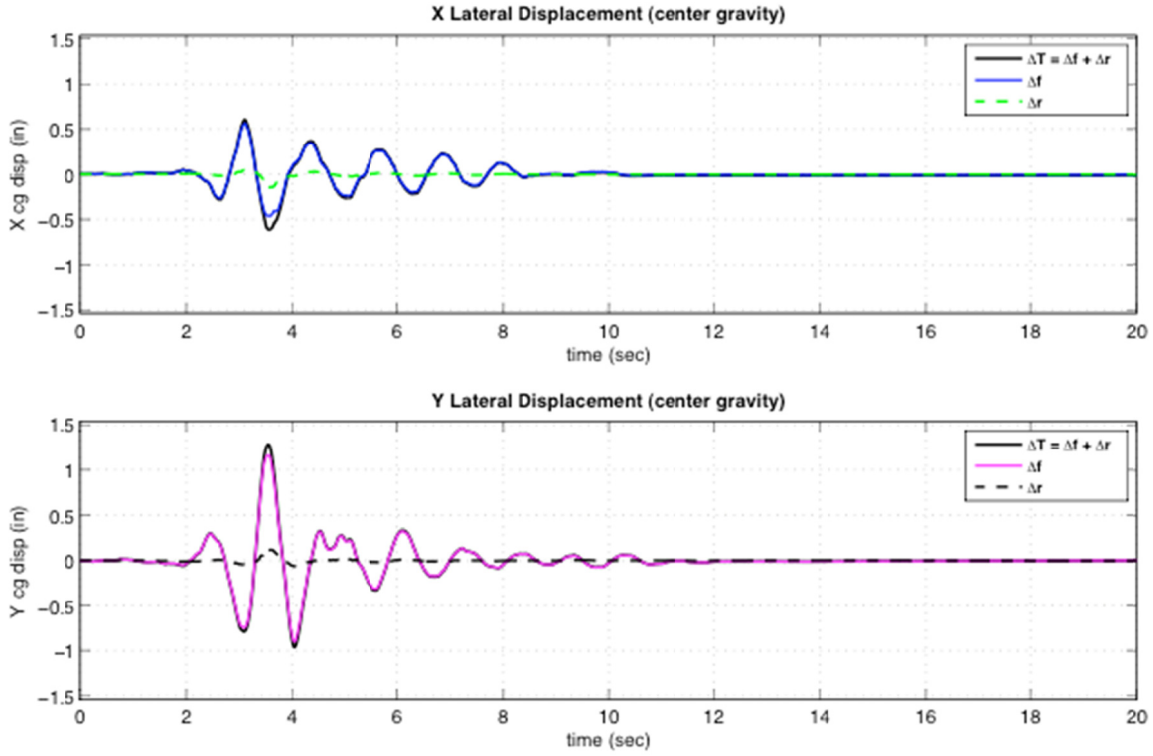

Figure 4.32 Yield level Test A2R displacement response.

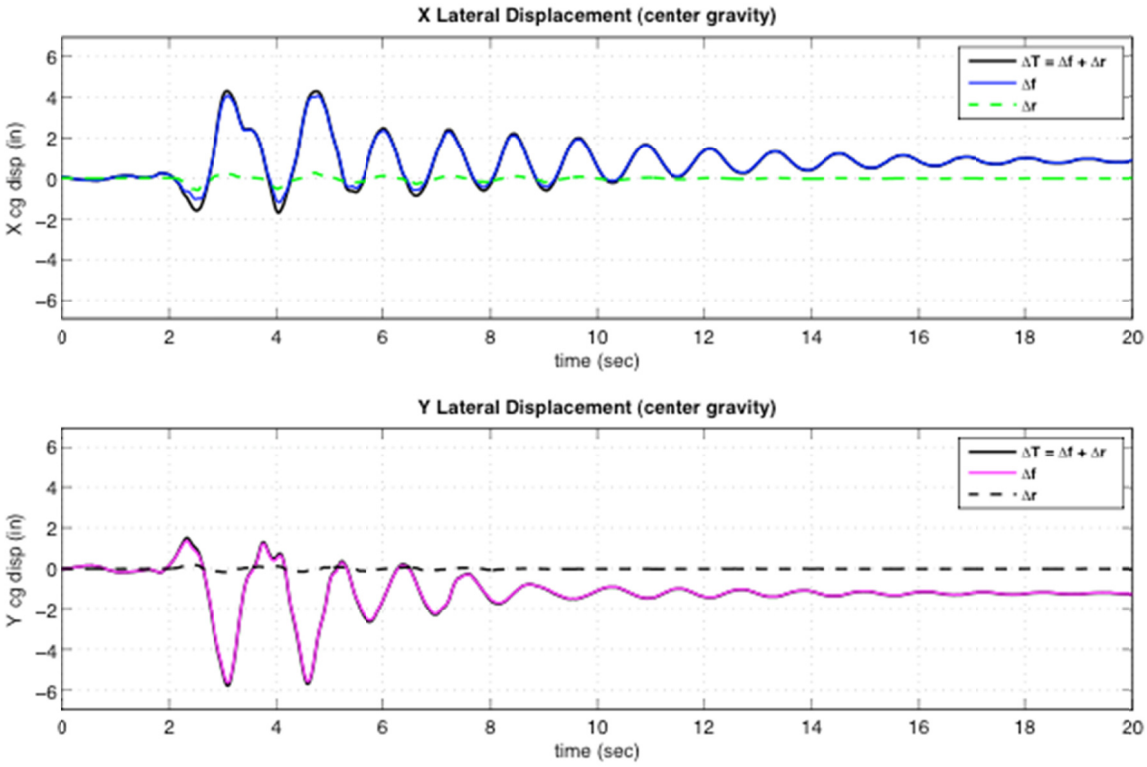

Figure 4.33 Design level Test A3R displacement response.

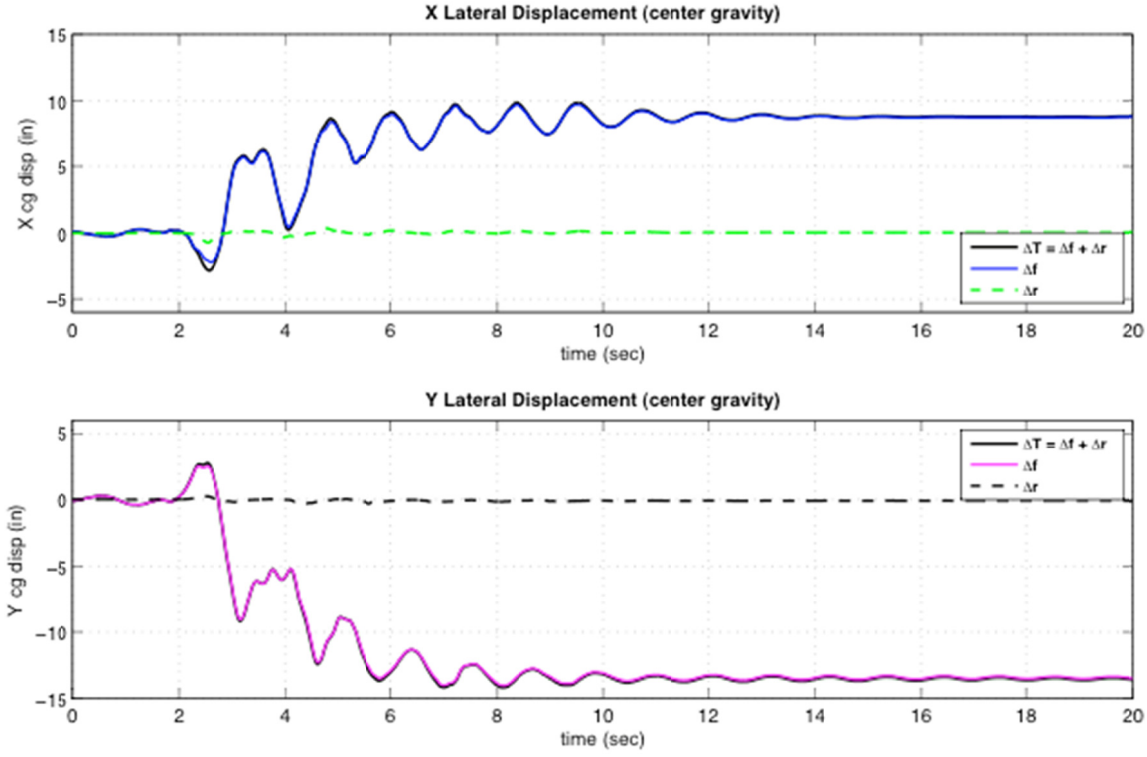

Figure 4.34 Maximum level Test A4R displacement response.

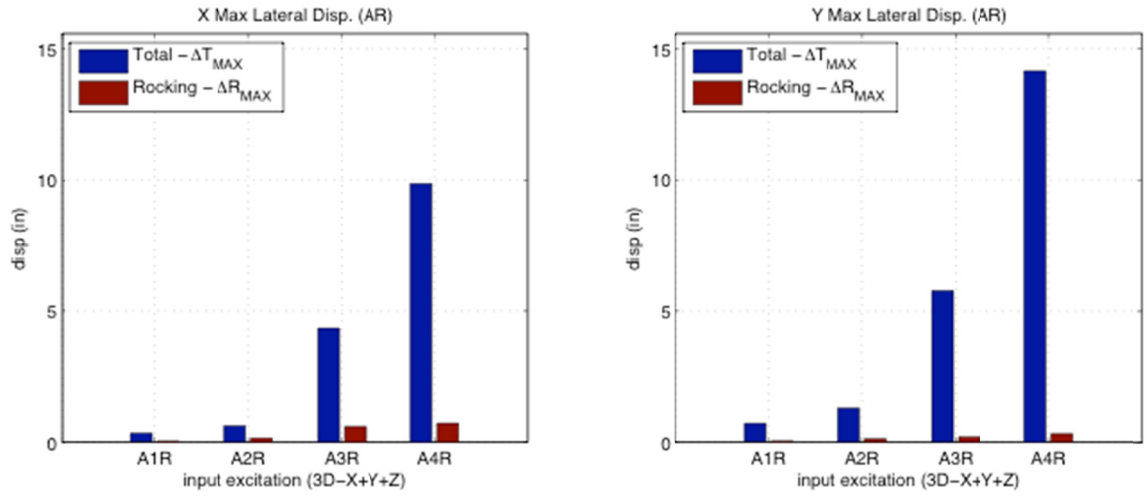

(a) maximum total versus rocking displacement

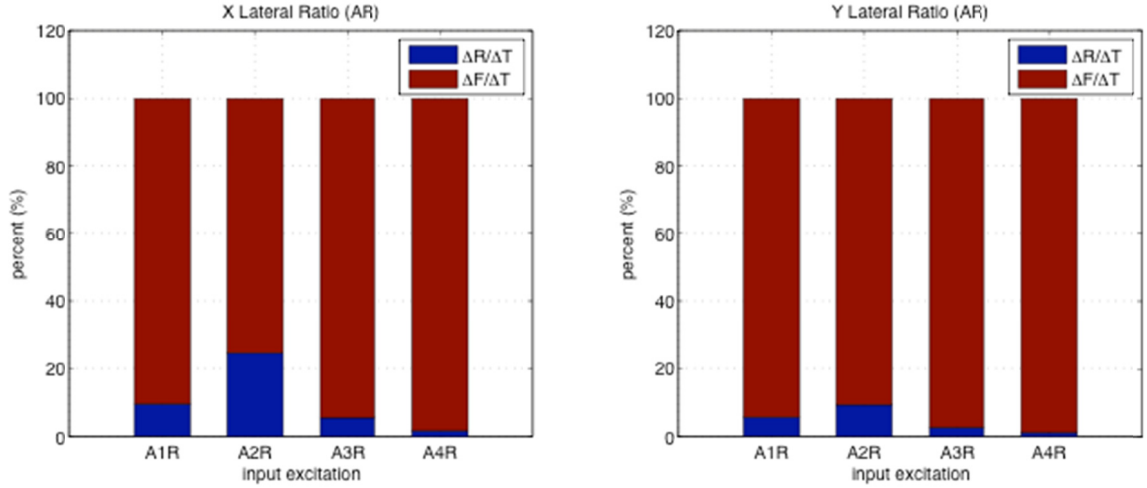

(b) ratio of rocking and flexural displacement to maximum total displacement

Figure 4.35 AR test set ratio of rocking to total displacement.

4.6.1.2 Footing Uplift

Footing uplift was determined by the procedures described in Section 4.2.1.2. The uplift response for Test Group 2 is described in Section 4.5.1.2, and some of the pertinent terminology for uplift is described in Figure 4.15. As described for the footing uplift of Test Group 2, the vertical displacement was calculated for the entire footing by assuming as a rigid body. The vertical displacement of the footing can be described as uplift when the footing physically loses contact with the elastomeric pad. Rocking is defined as when the footing remains in contact with the pad but is rotating due to flexibility of the pad.

The results of center of top mass lateral displacement demonstrated that rocking contributed less than 25% of the total displacement for all four tests. In the *X*-(north-south) direction, the shorter footing dimension experienced more uplift as would be expected. However for even the larger tests of 90% and 120% of the original amplitude, the amount of maximum uplift was small, approximately 0.2 in., which is one-half of the measured 0.4 in. for the DS test.

It is assumed that this is due to the bi-directional aspect of the response under tri-directional excitation, leading to a larger effective footing width than assumed in a simple uni-directional analysis.

For the $3D_c \times 3D_c$ footing with the Los Gatos record scaled to 25%, the peak amount of uplift was measured to be approximately 0.4 in. For Run A2R, the uplift was reduced to about 0.03 in. [Figure 4.36(a)] for the wider $5D_c$ direction and only 0.02 in. for the narrow $3D_c$ direction for this level of excitation. Note that for Test A3R, the amount of peak indentation into the elastomeric pad was greater than the amount of uplift. When the amplitude was increased, the amount of uplift increased moderately (to about 0.2 in.). As shown in Figure 4.36(c) for the last run A4R, the specimen retained a considerable permanent lateral displacement due to column yielding, which resulted in permanent rotation and uplift of the footing in the at-rest state due to the P-Δ moments created by the permanent lateral displacements. Figure 4.37 illustrates the enveloped uplift displacements of the footing along the main axes of the footing.

The contour plots of peak uplift and indentation in Figure 4.38 are useful in demonstrating the directional response of the footing while rocking and uplifting. Each individual test had different magnitudes of response, but a dominant direction is apparent along the diagonal from lower right to upper left (north-west footing corner to south-east corner). Figure 4.38(c) supports this suggestion because it appears the dominant direction of uplift occurs along the diagonal axis.

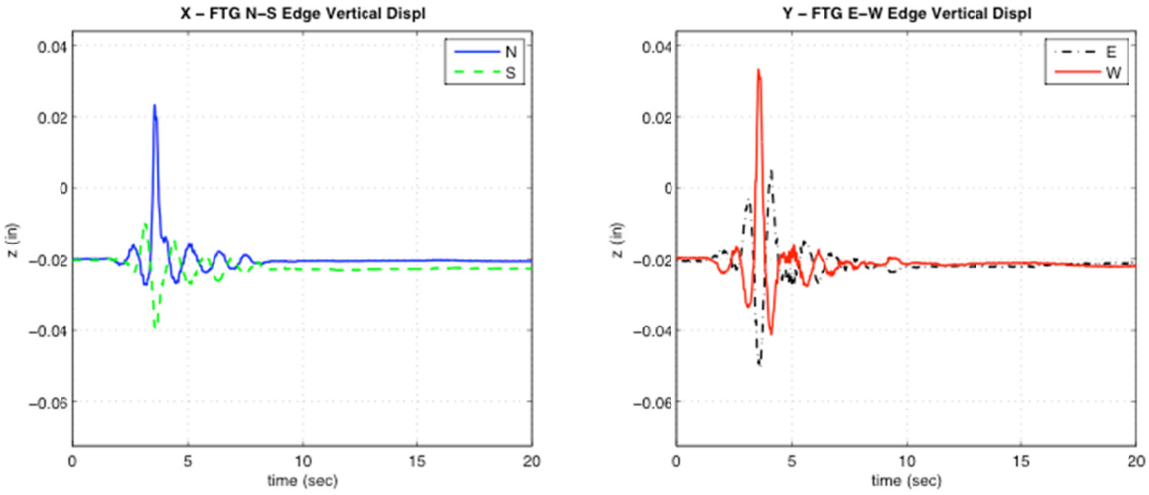

(a) A2R yield level

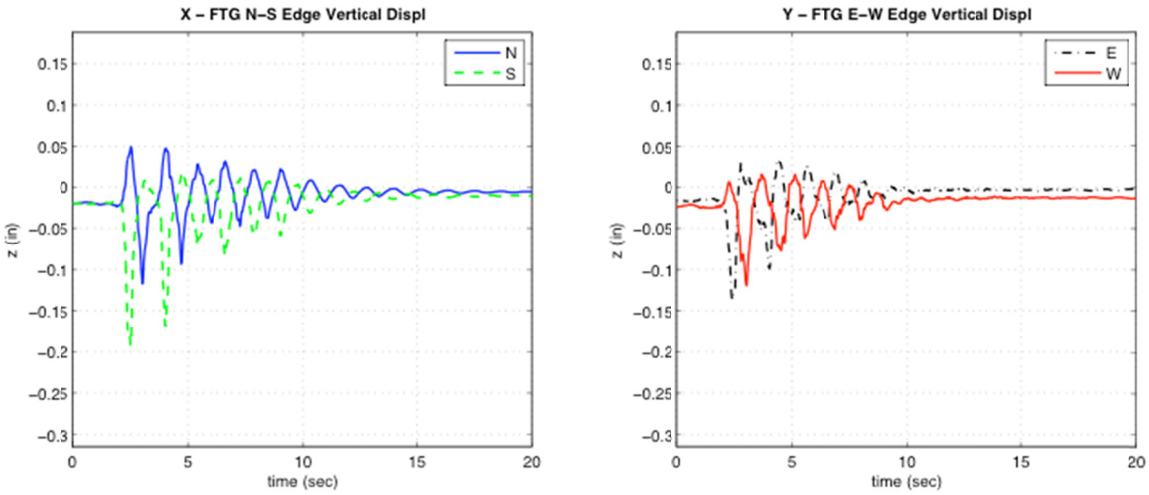

(b) A3R design level

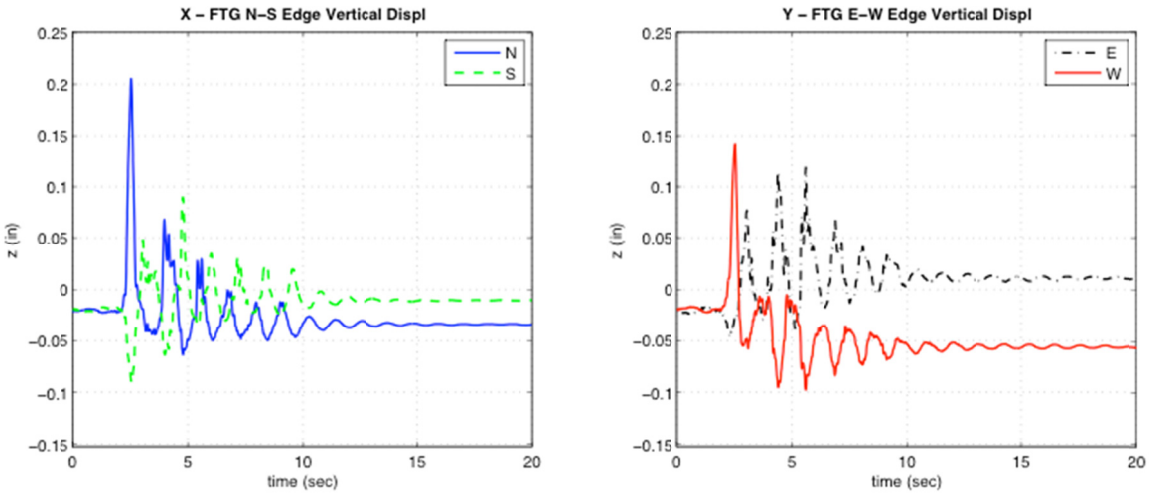

(c) A4R maximum level

Figure 4.36 AR test set - footing uplift response (centerline edges).

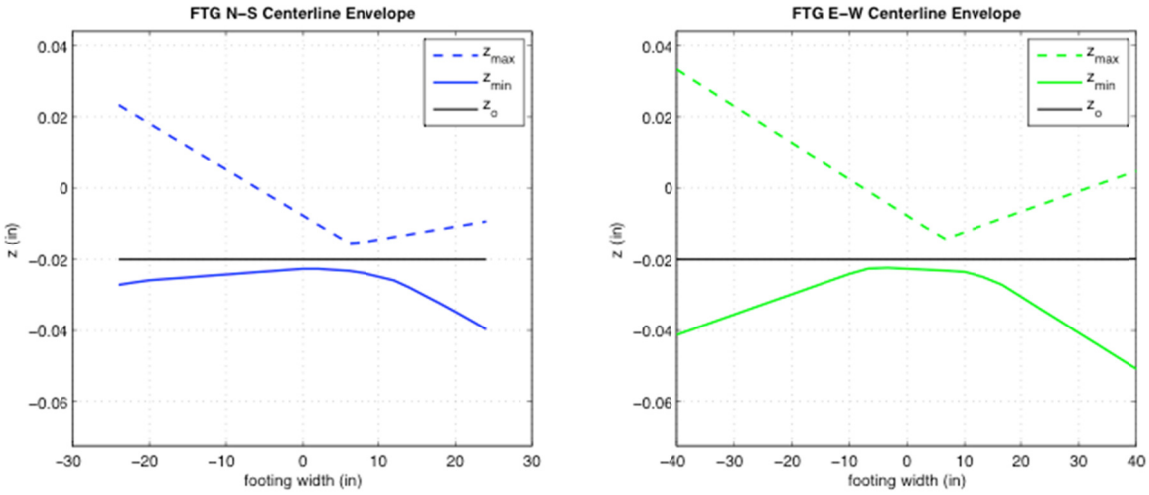

(a) A2R yield level

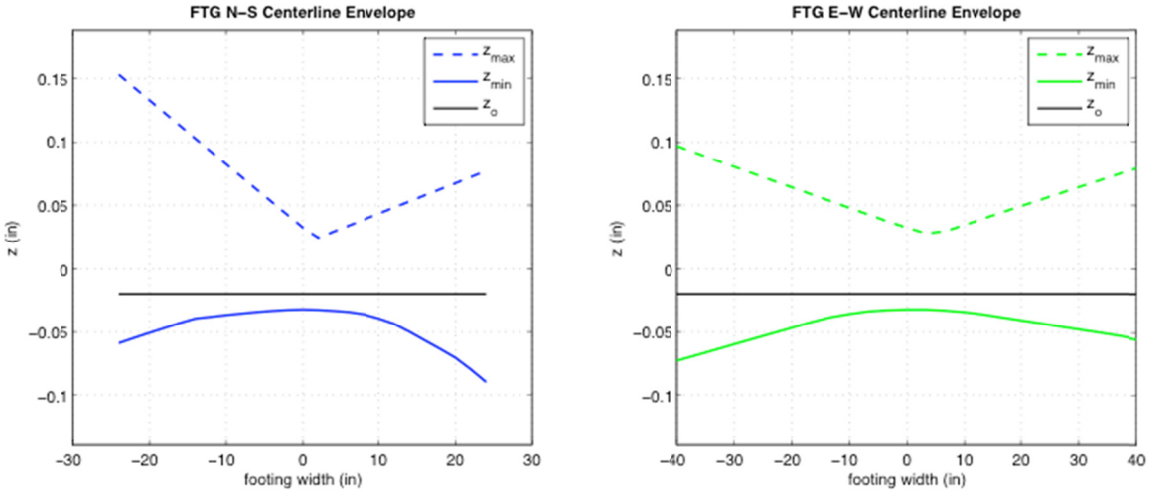

(b) A3R design level

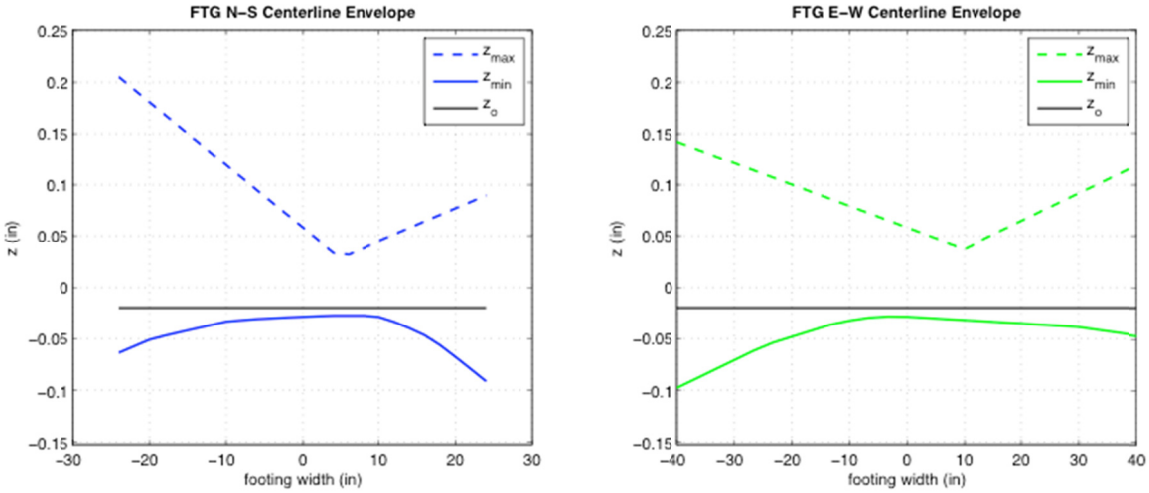

(c) A4R maximum level

Figure 4.37 AR test set – envelope of peak footing uplift (centerlines).

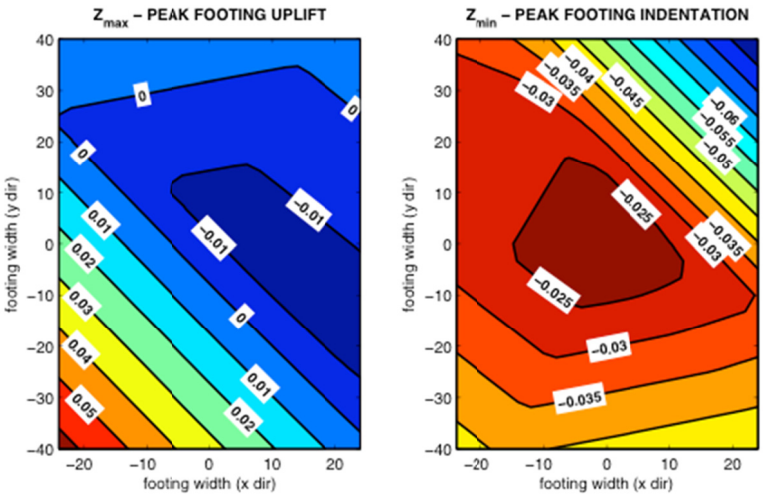

(a) A2R yield level

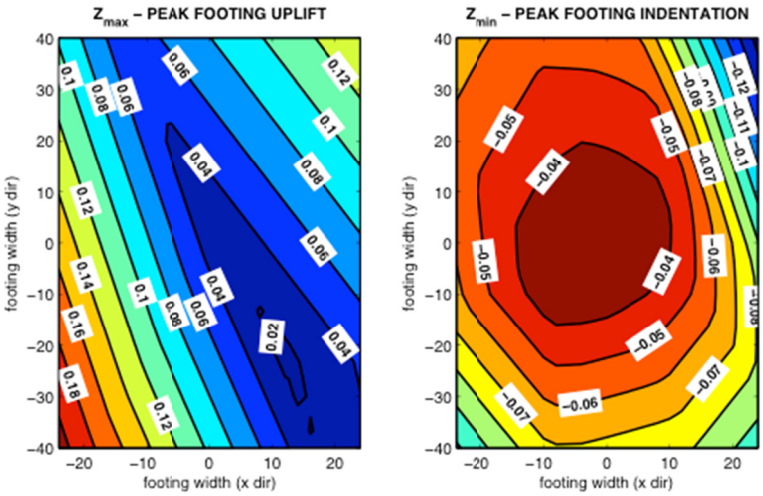

(b) A3R design level

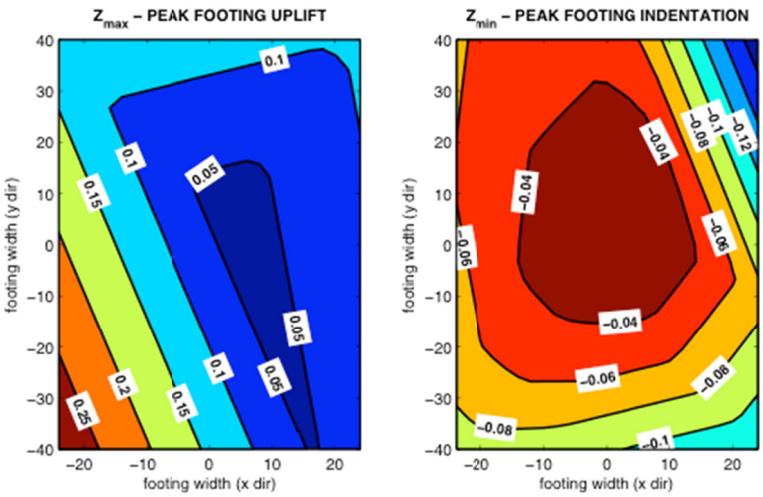

(c) A4R maximum level

Figure 4.38 AR test set – contours of max/min footing uplift.

4.6.1.3 Rotations about Vertical Axis

Section 4.5.1.3 discussed the propensity of the specimen to rotate about a vertical axis because of the lack of restraint. When the footing uplifts in one direction and experiences an inertial load in the opposite direction, it will want to rotate about the corner of footing still in contact. Less rocking and uplift occurred for Test Group 3 compared to Test Group 2, hence less rotation would be expected. Figure 4.39 verifies that the rotation about the vertical axis occurred, especially for tests A3R and A4R. The cumulative permanent displacement was estimated to be approximately 0.5 in. at the corners.

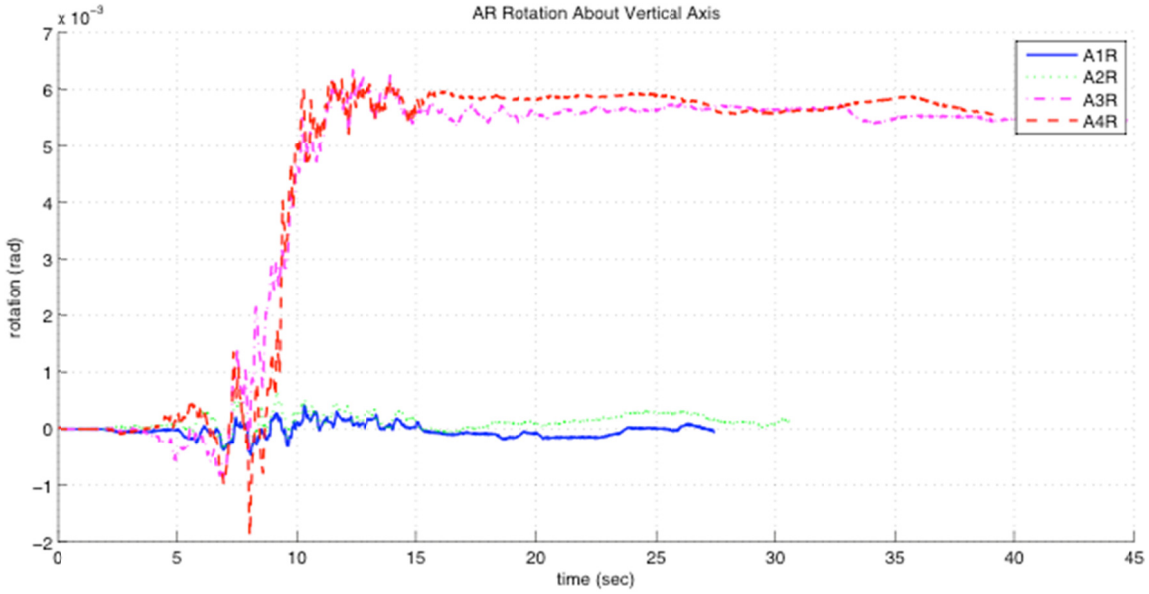

Figure 4.39 Test set AR twisting about vertical axis.

4.6.2 Local Response

Test Group 3 experienced large inelastic displacements as well as significant permanent lateral displacements (see Section 4.6.1.1). The cause of permanent displacement was mostly due to damage in the plastic hinge region at the base of the column. The curvature demands and strains highlight the response of the specimen in this region.

4.6.2.1 Curvature Distribution

Section 4.5.2.1 described how the average curvature and their characteristics were calculated including bar pullout for all tests performed. The curvature recordings and principal column directions for tests A3R and A4R are shown in Figure 4.40 Column curvatures (Tests A3R and A4R). Following test A3R some permanent rotation was observation over regions 1, 2, and 3, which comprise the plastic hinge zone. At the conclusion of test A4R (the 120% maximum level), there was permanent curvature distribution along the column height that was not solely restricted to the plastic hinge region. Much of this permanent rotation above the plastic hinge region was due to P-Δ effects of the lateral displacement and not associated with inelastic

response above the expected plastic hinge region. The peak curvature demand for test A4R was in the *y*-direction and was approximately ϕ_{EWmax}=0.012 (1/in.).

4.6.2.2 Strains

The strain gauges described in Section 4.5.2.2 were used for all of Test Group 3. The reliability and accuracy of gauges is reduced when subjected to strains beyond the yield point. For this reason they are used only to determine when yielding in the bar and column has occurred and any results beyond this level are discounted.

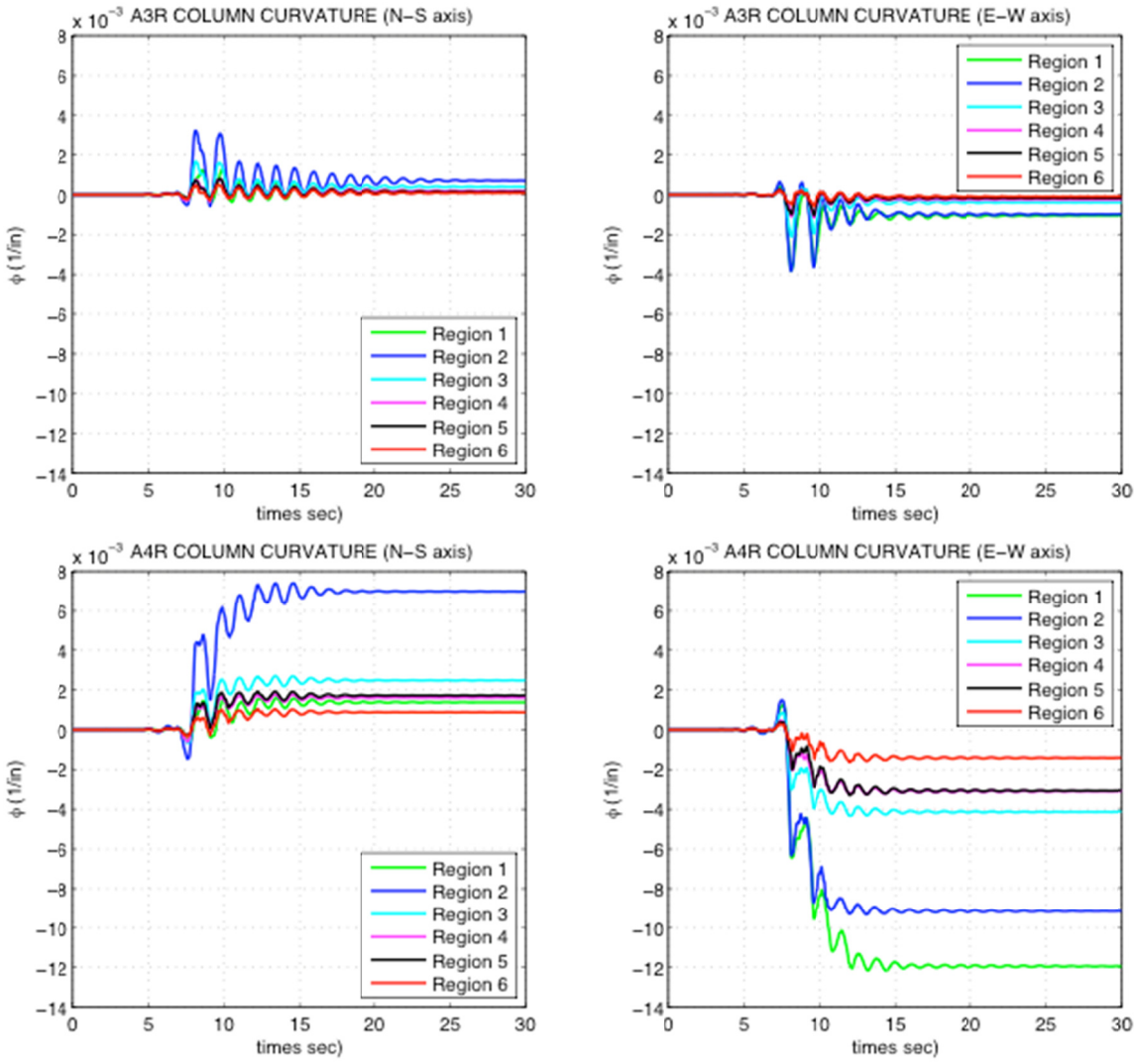

Figure 4.40 Column curvatures (Tests A3R and A4R).

4.6.3 Force-Displacement Hysteresis Curves

The force-displacement relationship calculation method was described in Section 4.5.3. Test Group 3 was designed such that inelastic behavior would occur while the footing was

simultaneously rocking and/or uplifting. The combination of the two was expected to produce an alternative method of energy dissipation to a column solely fixed at the base. The behavior of the column while uplifting had several points of transition during the response, which affected the observed behavior. For the moment demand at the column base, this included the several points related to the footing displacement: the moment at which rocking will occur (M_{rock}), first uplift of the footing (M_{up}), and total uplift of the footing so it is rotating about an edge point (M_{edge}). For column displacement, the moment values of interest are the curvatures at which yielding of the column occur (M_y) and the nominal strength level will be reached (M_n).

The lateral force versus lateral displacement hysteresis of the column base shear and center of mass of the top block is shown in Figure 4.41 for tests A2R, A3R, and A4R whose displacements are shown in Figure 4.32 through Figure 4.34. The plots for test levels A3R and A4R are very noisy however, they do illustrate the presence of nonlinear inelastic demands as well a significant amount of higher mode response as described by the noise in the plot.

4.6.3.1 Moment-Curvature Column Response

The nonlinearity of the column response and system can be best observed by studying Figure 4.42. For Run A2R (25% of original amplitude), the column base moment-average curvature relation was nearly elastic, especially for the direction associated with the $3D_c$ footing width. Significant hysteresis was noted for the column base for Run A3R (90% of original amplitude), especially for the direction parallel with the $5D_c$ footing dimension. For Run A4R (120% of original amplitude), the hysteresis for both directions is pronounced, especially for the $5D_c$ footing direction. For the east-west (5Dc) direction, considerable P-Δ effects resulted in a negative post-yield stiffness in the moment-average curvature relations for runs A3R and A4R.

During testing it was observed that at the yield displacement the moment demand was M_y= 1050 kip-in. The nominal strength at which the column response plateaued was approximately M_u= 1200 kip-in.

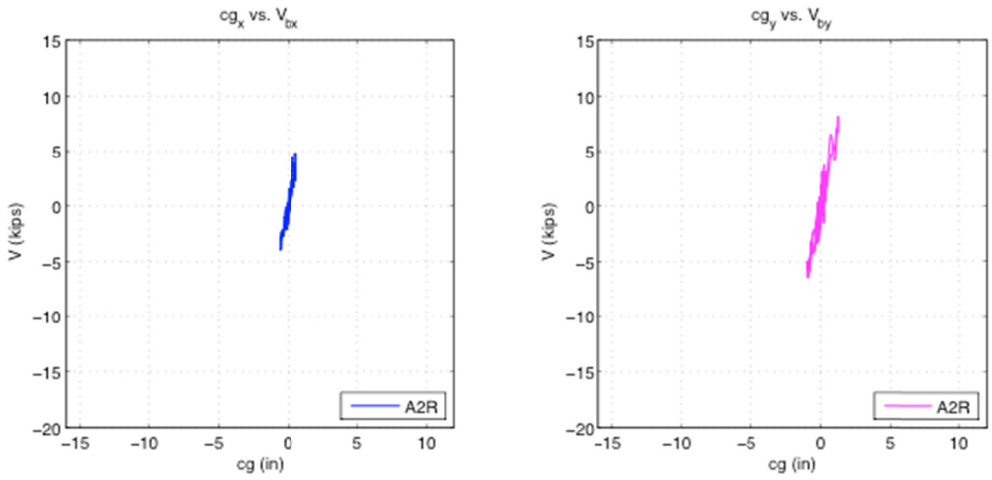

(a) Test A2R (yield level)

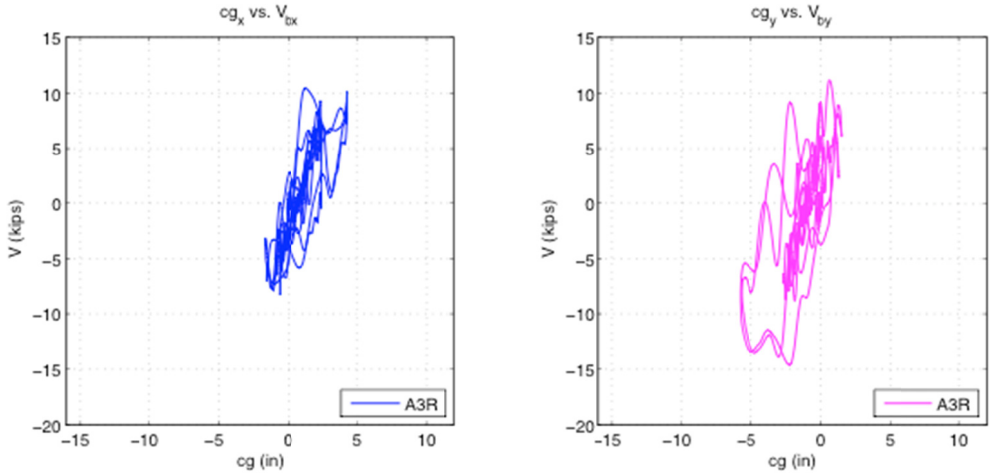

(b) Test A3R (design level)

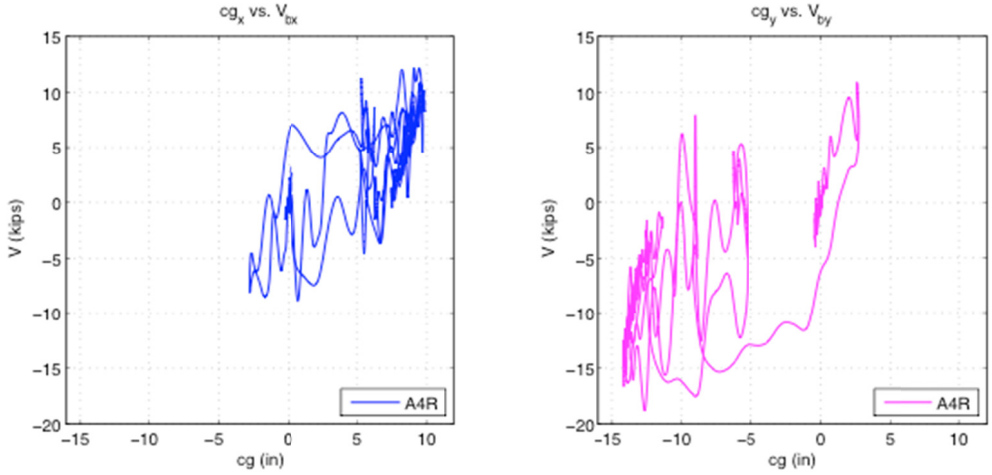

(c) Test A4R (maximum level)

Figure 4.41 Lateral force versus lateral displacement (Test A2R, A3R, A4R).

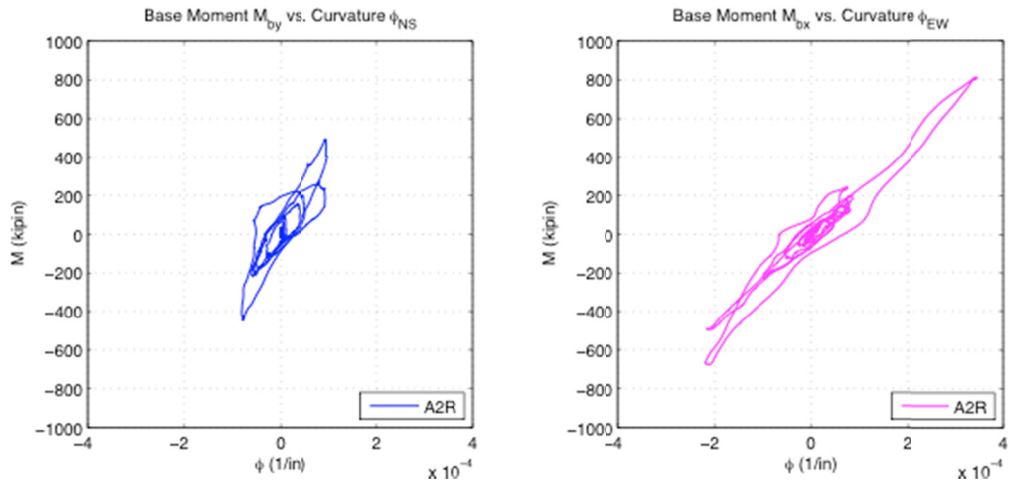

(a) Test A2R (yield level)

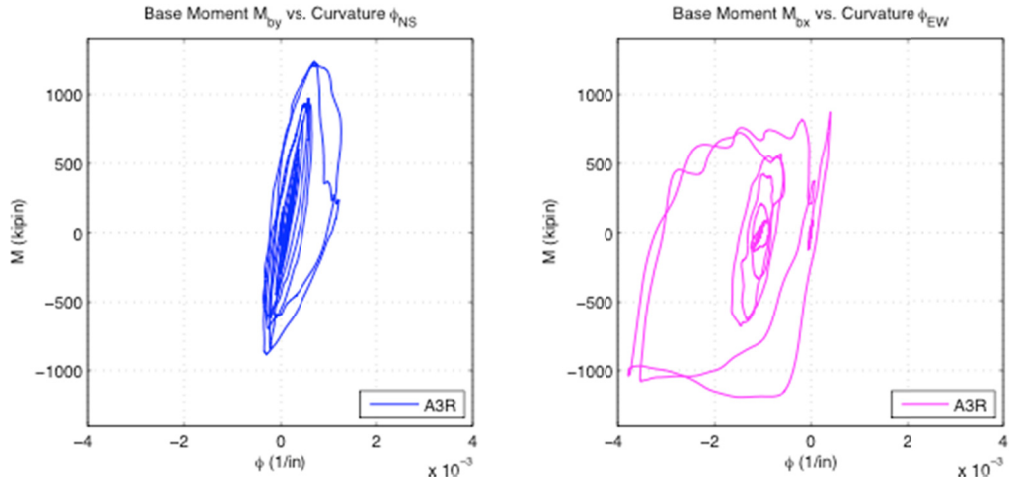

(b) Test A3R (design level)

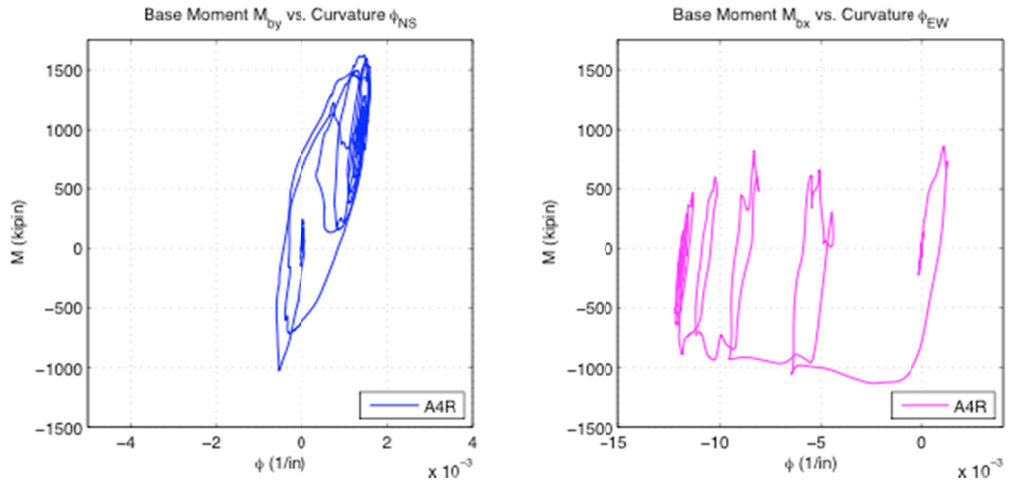

(c) Test A4R (maximum level)

Figure 4.42 Column base moment-curvature response (Test A2R, A3R, A4R).

4.6.3.2 Moment-Rotation Footing Response

Figure 4.43 plots the moment-rotation response of the footing. In spite of previous comments regarding the lower level of rocking and uplift for this column, it is clear from the plots of the base moment-footing rotation that there was considerable energy dissipation at the footing elastomeric pad interface. Considerable moment-footing rotation nonlinearity was noted in the north-south ($3D_c$) direction, while there was little nonlinearity associated with uplift in the orthogonal direction. It is clear from Figure 4.42(b) and (c) that the forces developed in the base of the column in the north-south (3Dc) direction due to rocking were sufficient to initiate yielding in the column. In the east-west ($5D_c$) direction, the column yielded before significant uplift could occur.

As shown in Figure 4.43(b), for Run A2R, the footing started to uplift (resulting in nonlinearity of the moment rotation relationship) prior to yielding of the column in the *Y*= ($3D_c$) direction. The wider ($5D_c$) footing produced a greater restoring force in this direction, but it was still not sufficient to yield the column. However, for Run A3R [Figure 4.43 (c)], the strength of the column increased to the point where the column could yield slightly (under the effects of bi-directional excitation where in the case of a uni-directional excitation, the yield capacity would be sufficient to prevent column yielding in this direction). For the other direction ($5D_c$), the column reached its yield point before much rocking could occur. As expected, the effects of bi-directional excitation, stiffness deterioration, and P-Δ effects further weakened the column such that rocking/uplift was largely avoided in this direction. The moment at footing uplift was measured M_{upNS}= 350 kip-in. and M_{upEW} = 575 kip-in. The footing did not uplift enough to rotate about the outer edge.

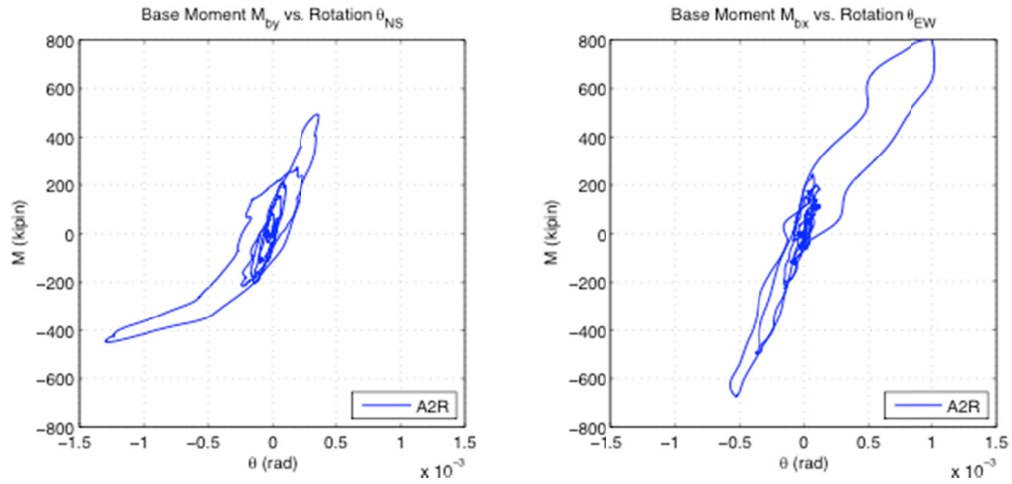

(a) Test A2R (yield level)

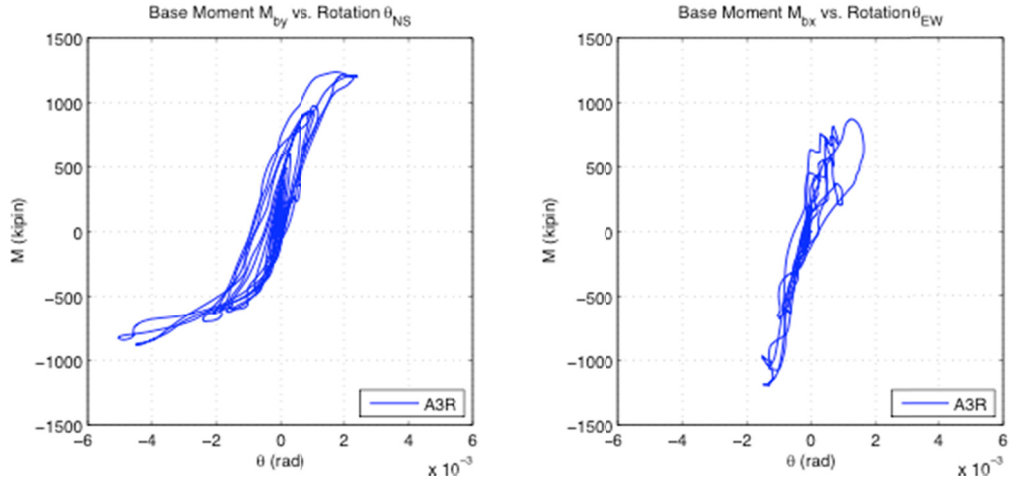

(b) Test A3R (design level)

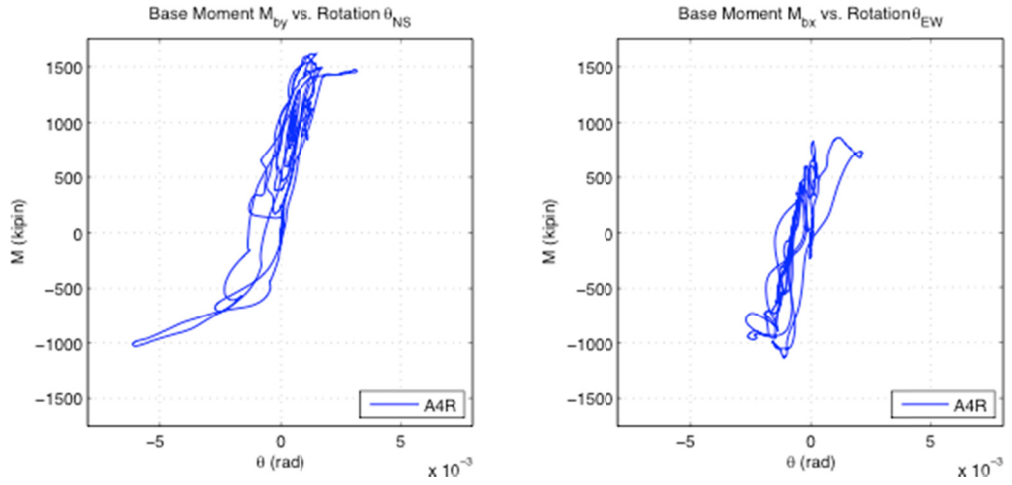

(c) Test A4R (maximum level)

Figure 4.43 Column base moment-footing rotation (Test A2R, A3R, A4R).

4.7 APPLIED MOMENT VERSUS RESTORING MOMENT

A key parameter for assessing the likelihood of foundation rocking and uplift would be the ratio of applied moment to restoring moment due to gravity load. When the ratio of applied to restoring moment is greater than or equal to unity, the footing of the column would be expected to uplift. Transition points in the moment-deformation relationship of the column and footing were described in Section 4.5.3. Key values of transition for the footing include when the moment at which rocking, uplift, and uplift about the corner point occurs. For the column relationship, key values of response were described in Section 4.6.3 and include the yield moment, nominal strength, and ultimate moment. The moment values determined experimentally for the column and footing quantities are as follows:

Table 4.4 Column and footing moment characteristic values.

Column:	
M_y =	950 kip-in.
M_n =	1050 kip-in.
M_u =	1200 kip-in.

Footing	**3Dc × 3Dc**		**3Dc × 5 Dc**	
	X (N-S)	**Y (E-W)**	**X (N-S)**	**Y (E-W)**
M_{up}	600 kip-in.	600 kip in.	350 kip-in.	575 kip-in.
M_{upu}	1100 kip-in.	1100 kip-in.	n/a	n/a

In Chapter 2 the lateral shear at incipient uplift of a cantilever column was described by Yim and Chopra [1984] for a two-spring model and a continuous Winkler foundation with uniform spring stiffness and spacing. The lateral shear applied to the top of a cantilever column at initiation of uplift was given for a two-spring model by Equation (4.14) as:

$$V_c = (m+m_o)gb/h \tag{4.14}$$

For a continuous Winkler foundation, the load at incipient uplift changes to:

$$V_i = (m+ m_o)gb/(3h) \tag{4.15}$$

Parameter β can be described as an indication of the tendency of the foundation to uplift due to the applied lateral shear V_{col}. Inserting a value for general footing stiffness K_θ obtains:

$$\beta = V_{col}/ V_c \tag{4.16}$$

where M_{col} is the measured experimental column moment, and h_{col} is column base to top mass center of mass height:

$$V_{\text{col}} = M_{\text{col}}/h_{\text{col}} \tag{4.17}$$

The columns considered here in had footing widths of 3Dc and 5Dc. The nominal column axial loads were 10% $f'_c A_g$ for Test Groups 2 and 3 and 3% $f'_c A_g$ for Test Group 1. Using the measured concrete strengths, the calculated weights of Test Groups 1, 2, and 3 specimens were 0.027, 0.055, and 0.060 times $f'_c A_g$, respectively.

It is desirable to represent the likelihood of foundation uplift parameter β [Equation (4.16)]] to applied moment M_{col} in terms derived from the physical dimensions of the column and footing system. The gross area of the column A_g equals $\pi D_c^2/4$, and the axial load $(m+m_o)g$ equals $\gamma f'_c A_g$. The ratio of footing width to column width is $\rho = 2b/D_c$. Inserting these values into the equations for V_c obtains:

$$V_c = \gamma f'_c A \gamma \rho D_c/2h_{\text{col}} = \gamma\rho\pi D_c^3 f'_c/8h_{\text{col}} \tag{4.18}$$

or V_i

$$V_i = \gamma\rho\pi D_c^3 f'_c/24h_{\text{col}} \tag{4.19}$$

Thus the parameter β_c becomes:

$$\beta_c = 8M_{\text{col}}h_{\text{col}}\Big/\left(\gamma\rho\pi D_c^3 f'_c/h_{\text{col}}\right) = 8M_{\text{col}}\Big/\left(\gamma\rho\pi D_c^3 f'_c\right) \tag{4.20}$$

and β_i is:

$$\beta_i = 24M_{\text{col}}h_{\text{col}}\Big/\left(\gamma\rho\pi D_c^3 f'_c/h_{\text{col}}\right) = 24M_{\text{col}}\Big/\left(\gamma\rho\pi D_c^3 f'_c\right) \tag{4.21}$$

where M_{col} represents the moment induced by a particular earthquake (M_{eqk}), or the yield (M_y), nominal (M_n), or factored nominal (M_u) of the column.

Computed ratios for various tests are shown in Table 4.5, based on β_i for the column moment demand for each run (for the maximum component), and for the computed values of yield and nominal moment capacities of the column. If any of the values of β are greater than unity, the footing would be expected to uplift when M_{col} developed during the earthquake. If the value of β_{eqk} is greater than β_y, the column would be expected to uplift before yielding could

occur. If uplift occurs, the moment demand on the column will increase such that β increases up to β_c (the condition for which the footing is rotating about a corner point only). If β_n is less than β_c, the column might be expected to yield while uplifting. Note that some yielding during uplift may occur temporarily under bi-directional excitation since the effective width of the footing increases.

Table 4.5 Ratio of applied to restoring moment (β uplift likelihood).

Test Group	ρ	γ	Record	Amplitude Scale	Time Scale	β_{eqk}	β_y	β_n
1	3	0.027	Los Gatos	0.08	2.12	0.56	3.90	4.56
1	3	0.027	Los Gatos	0.32	2.12	1.72	3.90	4.56
1	3	0.027	Los Gatos	0.32	1.50	0.56	3.90	4.56
1	3	0.027	Tabas	0.08	2.12	1.41	3.90	4.56
1	3	0.027	Tabas	0.32	2.12	1.32	3.90	4.56
1	3	0.027	Tabas	0.42	2.12	1.50	3.90	4.56
2	3	0.055	Los Gatos	0.15	1.50	1.44	1.98	2.30
2	3	0.055	Los Gatos	0.15	2.12	1.05	1.98	2.30
2	3	0.055	Los Gatos	0.25	2.12	1.54	1.98	2.30
2	3	0.055	Tabas	0.15	2.12	1.91	1.98	2.30
2	3	0.055	Tabas	0.25	2.12	1.96	1.98	2.30
2	3	0.055	Tabas	0.25	1.50	1.35	1.98	2.30
3	3 5	0.060	Los Gatos	0.10	2.12	0.49 0.54	1.82 1.09	2.11 1.26
3	3 5	0.060	Los Gatos	0.25	2.12	0.84 0.95	1.82 1.09	2.11 1.26
3	3 5	0.060	Los Gatos	0.90	2.12	1.54 1.40	1.82 1.09	2.11 1.26
3	3 5	0.060	Los Gatos	1.20	2.12	1.52 1.32	1.82 1.09	2.11 1.26

4.8 INTERACTION OF PRINCIPAL DISPLACEMENTS

The use of a square or rectangular footing raised the question of whether there would be interaction between the principal axis directions, especially for lateral displacement of the top in the *Y*-direction when the input excitation is restricted to one dimension in the *X*-direction (see Section 4.5.1). See Figure 4.13 for a plot of peak rocking displacement versus total displacement. The results may be slightly influenced by rotation of the footing because of the lack of horizontal restraint. Investigation of the footing rotation during testing (Section 4.5.1.3 and 4.6.1.3) showed

that there was a negligible amount compared to the overall displacements. However, it was difficult to perfectly align the specimen with the direction of excitation due to this rotation.

Figure 4.44 shows the peak displacement for the five directional load cases of each earthquake run for Test Group 1 and 2 ($3D_c \times 3D_c$). These results are normalized to the peak displacement of the three-dimensional (X+Y+Z) loading case. If interaction were not an issue, there would no response in the opposing direction for the 1D-X, 1D-Y, and 2D-X+Z input excitations. The figure clearly shows that there was a significant amount of displacement in the direction not being loaded.

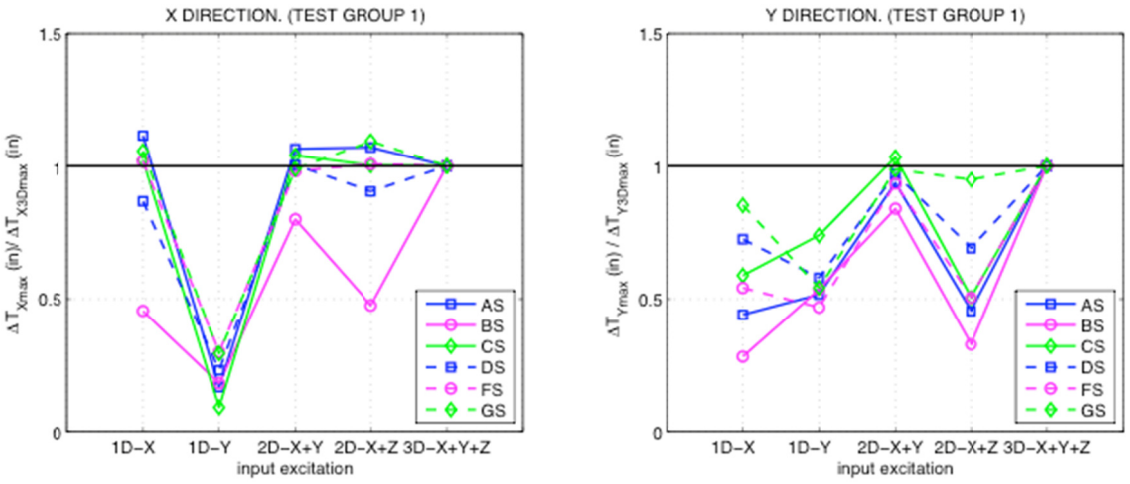

(a) Test Group 1

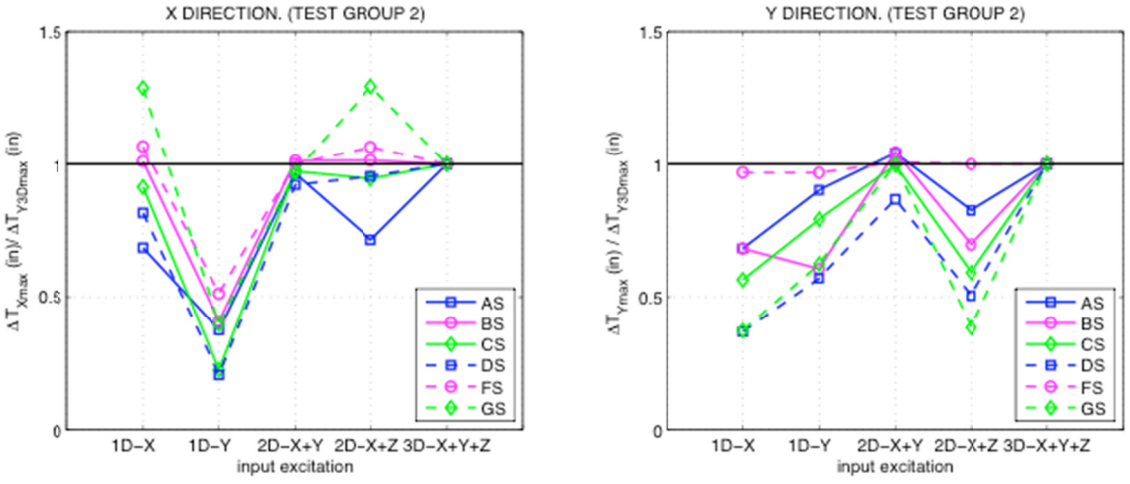

(b) Test Group 2

Figure 4.44 Normalized interaction displacements for Test Groups 1 and 2 ($3D_c \times 3D_c$).

4.9 NATURAL PERIOD AND DAMPING

Prior to each test group the shake table was blocked to prevent movement, and a series of pullback tests were performed to estimate the free vibration characteristics of the specimen. The response to the free vibration was used to estimate the period of vibration and viscous damping properties at low amplitude motion. Pullback tests were not performed between runs due to time and practical constraints. Instead the free-vibration characteristics for each run were determined during free vibration of the specimen (after earthquake excitation had ended). Both the natural period and damping were determined.

Table 4.6 shows the natural period and damping for the specimen at the listed phase. As expected, at the conclusion of the elastic level tests the period changed very little from beginning to the end. Test Group 2 had approximately the same initial characteristics in each direction because of the equal footing dimensions. For the *X*- and *Y*-directions the fundamental period was approximately 0.9 sec in each direction. Test Group 3 had a shorter period in the direction with the wider footing because it was more resistant to displacement. At the start of the test, the natural period in the *X*- and *Y*-directions was approximately 0.8 and 0.7 sec, respectively. After incurring damage during Test Group 3, the natural period was lengthened to approximately 1.2 and 1.1 sec in the *X*- and *Y*-direction, respectively.

The inclusion of a nonlinear elastic neoprene pad to represent the soil created nonlinear damping behavior in the system. Essentially there were two values of damping: that associated with significant footing rotation (composed of elastomeric damping plus column damping) and that associated with column damping only (when the footing rotation was very small). The elastomeric pad damping of footing motion was predominant and only disappeared at the very end of the motions when the displacement amplitude was very small. At this point, the motion was eliminated by the column damping qualities. For the test set up, the damping value was approximately 8.0% and 2.5% for significant footing rotation and column damping only, respectively.

Table 4.6 Natural period and damping of test specimens.

	T_{nx} (sec)	T_{ny} (sec)	ζ_{nx} (%)	ζ_{ny} (%)
Test Group 2 – Free Vibration	0.85	0.95	7.6	7.4
Test Group 2 – Conclusion	0.95	0.95	8.2	7.8
Test Group 3 – Free Vibration	0.9	0.75	8.1	7.8
Test A1R free vibration	0.82	0.76	7.6	7.9
Test A2R free vibration	0.82	0.70	7.9	8.1
Test A3R free vibration	1.16	1.06	8.2	7.6
Test A4R free vibration	1.12	1.08	8.1	7.9

4.10 CONCLUSIONS

Test Groups 1 and 2 were expected to remain elastic during all testing levels. Test Group 1 was designed to evaluate of the test set up and instrumentation; therefore, the axial load was designed

to be only one-third to avoid damaging the column. Five earthquake directional combinations were conducted at different earthquake intensity amplitudes: 1D-*X*, 1D-*Y*, 2D-*X*+*Y*, 2D-*X*+*Z*, and 3D-*X*+*Y*+*Z*. In total, approximately thirty runs were done for Test Group 1.

For Test Group 2, the footing size remained the same at three times the column diameter (3Dc) square. The axial load was increased to $0.057\, f'_c A_g$, and the column was tested within the elastic range. Similar to the first test group, approximately five types of earthquakes were run for five different input excitations. Again, a total of approximately 30 runs were conducted.

Test Group 3 was designed to have a wider footing in one direction and was tested under simultaneous rocking and yielding. The interaction of fixed-base behavior in one direction with rocking/uplifting behavior in the other direction was of interest. The footing was widened to 5Dc in one direction, and the more intense component of shaking was oriented in that direction. The first earthquake run was a three-dimensional input at the elastic level. Next, the loading was increased to the yield level, and then design and maximum earthquake loading levels. At the conclusion of test, the column was significantly damaged and no further tests were feasible.

The measured base moment versus footing rotation behavior for the footings generally followed the behavior expected based on simple analyses of Winkler foundation models of spread-footing supported bridge piers. For sufficiently narrow footings, uplift occurred, exhibiting a nonlinear elastic type hysteresis with some energy dissipation. In this case, the restoring capacity of the footing was less than the moment capacity of the column, and the column responded elastically with no damage. The damage performance of the square footing with a width of $3D_c$ illustrated that flexural displacement demands may be reduced in comparison to a fixed-based column design, with inelastic behavior confined to the footing soil interface.

It was observed that rocking foundations lengthened the fundamental period of a system, thereby reducing expected acceleration demands. However, this can lead to larger total displacement demands for the system. Two and three components of excitation introduced more complex behavior where based on analyses of uni-directional excitations the footing may not rock as much as expected. For the boundary conditions considered in these tests, the footing may twist about its vertical axis and translate from its initial position.

In Test Group 3, wider foundations and larger excitations were imposed such that yielding of the column would be expected slightly before uplift of the foundation in the direction of the 5Dc footing width. It was noted that bi-directional moments in the column reduced the effective moment capacity of the column in the narrow footing direction during the design and maximum level tests; therefore, column yielding occurred in this direction though it would not be expected on the basis of loading only in the narrow footing direction. Similarly, multi-directional response appeared to increase the effective width of the footing (due to skew); as such, rocking and uplift may not occur as much as expected. One important beneficial observation noted from Test Group 3 was the lack of need to tie-down the foundation in the following cases: (1) where competent soils are available; (2) the column has standard Caltrans axial loads applied; and the footing width is on the order of 3Dc or above, avoiding the need to enlarge footings or install a pile foundation. The final test run of a MCE illustrated that the column was able to develop a full plastic hinge, dissipate earthquake energy, and remain stable *and* undergo small uplift without the need for vertical restraint. These limited test runs show the design performance may be met without the added cost of piles or alternative methods.

However, it should be pointed out that these shake table tests used an elastomeric pad beneath the footing instead of soil. Consequently, the test results will be used subsequently to validate a numerical model for spread footings under multiple components of excitation, and these will be used in parametric studies to assess the behavior of bridge piers supported on footings resting on competent soil.

5 Validated Analysis of Experimental Results

5.1 INTRODUCTION

One of the primary objectives of this report is to develop analytical models that can predict with reliable accuracy the seismic performance of RC bridge piers allowed to uplift. In turn, these analytical models can be used to develop design guidelines for bridge piers allowed to uplift can be created by considering the wide range of values for these parameters that are most relevant to bridge design. Robust guidelines depend on the accuracy of the analytic tools and modeling capabilities. Some of the results described in the previous results sections are compared with analysis results obtained using several analysis methods and modeling approaches. Previous work in modeling guidelines for RC bridge columns [Berry and Eberhard 2006] were used as an initial reference. Comparisons of the results in this chapter were done by using these initial recommendations and including a foundation Winkler-spring model approach for the elastomeric pad and footing, and by calibrating the response to the observed experimental data.

The analysis package Open System for Earthquake Engineering Simulation (OpenSees), was used to create analytic models and perform linear and nonlinear dynamic analyses. OpenSees, an object-oriented framework, is open-source software used for structural and geotechnical earthquake analysis of structures. The analysis platform was developed by researchers at the Pacific Earthquake Engineering Research (PEER) center and collaborated on by many affiliated researchers. The open-source concept allows for easy additions and modifications to improve and enhancement material and element modeling analysis of structures.

To develop the analytic model requires addressing two phenomena observed during testing: (1) the significant residual displacement from column damage to accurately describe the simultaneously uplifting and yielding system; and (2) the nonlinearity of the elastomeric pad and how it affected the energy dissipation qualities of the system.

First considered are material modeling assumptions described in Section 5.2, including the reinforcing steel, concrete, and elastomeric pad. The analytic model creation including column, footing, and soil model assumptions are described in Section 5.3. The results of the linear and nonlinear dynamic analysis performed using the soil, footing, and column specifications are compared to the experimental results and presented in Sections 5.5 and 5.6. Global response parameters including peak lateral displacement, residual displacements, footing rotation, peak lateral shear, and overturning and restoring moments are presented herein. The effect of varying the model for damping, soil, and column properties are also discussed. These effects include the damping value associated with elastomeric pad plus column viscous damping, soil spring rotational, and vertical stiffness values, and values for the column concrete and

reinforcing steel materials. A summary and conclusions of the modeling and results is presented in Section 5.7. This includes best practices for the soil structure interaction (SSI) with the footing and column for the elastomeric pad. With the experimentally validated models, a more broad range of bridge piers and underlying soil can be considered. Chapter 6 presents a parametric investigation using the validated models presented in this chapter. Varying the footing, column, and soil properties in addition to the ground motion excitation will lead to better understanding of bridge piers allowed to simultaneously uplift and yield. This more complete understanding of uplifting behavior will in turn lead to the development of guidelines for when uplifting of bridge piers is practical and beneficial in the overall structural design philosophy.

5.2 MATERIAL MODELING

Accurate modeling of material stress-strain behavior is essential to predicting the observed member response. Hysteretic response—including under seismic loading—requires careful examination and replication of the unloading and reloading response of the materials in question. A brief discussion on the material models used in this study is presented here and then compared to the observed physical response of sample specimens. Materials used and modeled in this test program include concrete, steel, and neoprene.

5.2.1 Reinforcing Steel

Modeling of the mild longitudinal reinforcing steel was done using two different steel models: (1) The Giuffre-Menegotto-Pinto [Taucer et al. 1991] constitutive model; and (2) the model developed by Chang and Mander [1994].

Steel02

The material model **Steel02**—based on principles developed by Giuffre-Menegotto-Pinto—is a bilinear curve that transitions at the yield stress and strain but does not include the post-yield plateau typically observed in the stress-strain relationship of mild steel. The model includes the Bauschinger effect, which is the contribution to the gradual stiffness degradation of RC members under cyclic response. Figure 5.1(a) shows the coupon test data and the steel material model calibrated to the test data.

ReinforcingSteel

The **ReinforcingSteel** model uses a shifted nonlinear backbone curve to account for isotropic hardening, as described by Chang and Mander (1994). Although several buckling options are available for modeling the material, , they were excluded because no buckling of the rebar was observed during testing. The complexity of the material model requires several inputs: yield stress, ultimate stress, initial elastic tangent, tangent at initial strain-hardening, and strain at peak stress. Figure 5.1(a) shows the response of the material calibrated to the observed coupon test, showing. a very good correlation between observed and predicted response.

5.2.2 Concrete

For this test program, two types of concrete behavior were modeled as uni-axial materials. They were confined concrete (core concrete) and unconfined concrete (cover concrete). The

Concrete02 model implemented by OpenSees uses the Kent-Park model to represent the concrete compressive stress-strain curve and linear behavior for the tension zone. Unloading in the compressive region is based on Karsa and Jirsa [1969]. The material models were able to control the descending slope as well as the residual strength. Figure 5.1(b) shows the compressive strength of the cylinder tests compared to the material model for unconfined concrete, showing reasonably good correlation between the material model and the cylinder tests. The compressive behavior of the confined concrete was not directly measured. Instead, the Mander equations for confined concrete were used as inputs to calibrate the confined concrete model. The ultimate stress and strain equations from Mander are shown in Equations (5.1) and (5.2). The stress-strain response of the material model for unconfined versus confined concrete is shown in Figure 5.1(c). Note that the confined concrete offers much more strength in compression.

$$f'_{cc} = f'_{co}\left(-1.254 + 2.254\sqrt{1 + \frac{7.94 f'_{l}}{f'_{cc}}} - 2\frac{f'_{cc}}{f'_{co}}\right) \tag{5.1}$$

$$\varepsilon_{cu} = 0.004 + \frac{1.4\rho_{sp} f_{yh} \varepsilon_{su}}{f'_{cc}} \tag{5.2}$$

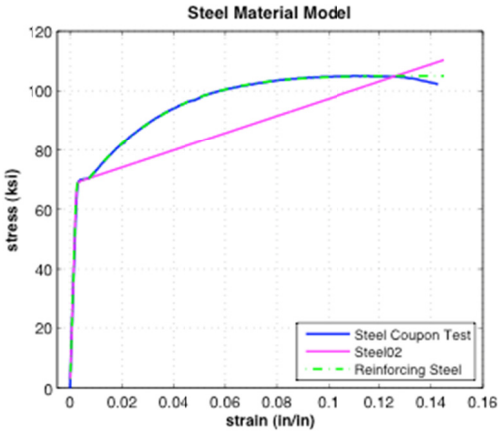

(a) steel material model

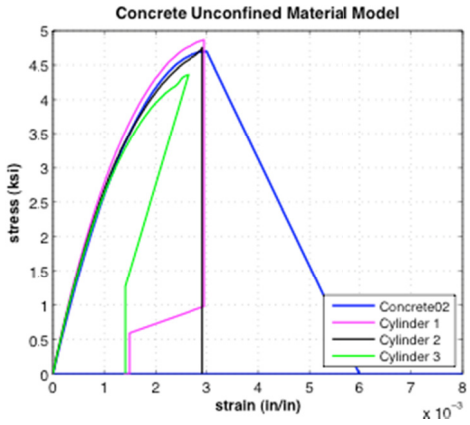

(b) unconfined concrete model

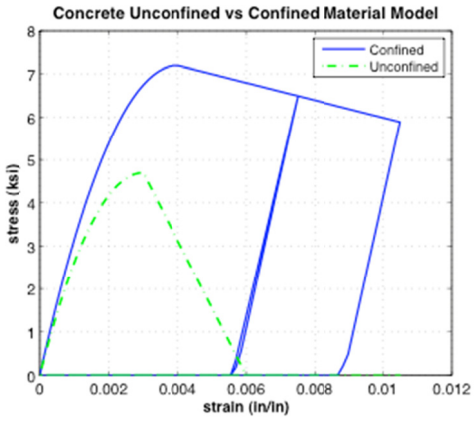

(c) confined vs unconfined concrete

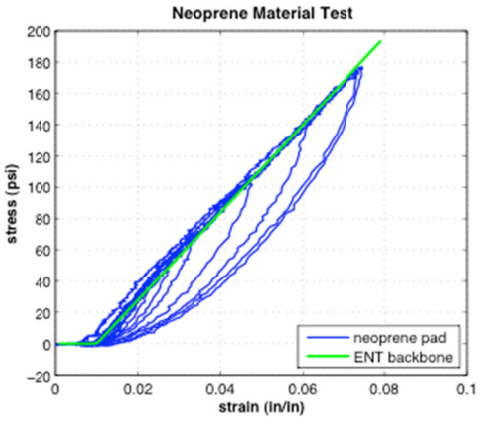

(d) neoprene modelconfined vs. unconfined concrete

Figure 5.1 Analytic material modeling for analysis.

5.2.3 Elastomeric Pad

Modeling of the elastomeric pad was a challenge due to the lack of any materials explicitly developed in OpenSees for neoprene or rubber. The observed uniaxial test response of a sample 2 in. thick × 1 ft square piece of material showed an initial gap strain of 0.008 in. per inch followed by a linear elastic loading modulus of elasticity equal to 2.8 ksi. The material followed a nonlinear-elastic curve back to its origin and in the process dissipated some energy.

Capturing the nonlinear elastic behavior proved to be a difficult task. To initially calibrate the model to the observed structure response, the analysis omitted the damping qualities of the neoprene. The backbone curve was modeled using a bilinear elastic curve that loaded and unloaded along the same path. To do this a new material was created in OpenSees, which combined an **Elastic-No-Tension (ENT)** material with an initial gap strain. Figure 5.1(d) shows the recorded pad response compared to the OpenSees material backbone curve with no hysteretic qualities.

To better model the hysteretic energy dissipation of the neoprene using OpenSees, a new material model, **Neoprene,** was developed. The material is Elastic-No-Tension and loads along the same backbone curve as the **ENT** material with a gap strain. During unloading the material follows a nonlinear elastic curve that closely follows the measured unloading path before returning to the origin in an undamaged state.

Figure 5.2(a) shows the **Neoprene** material model response compared to the measured compressive behavior. When a compressive strain cycle was applied, the **Neoprene** material closely followed the same loading path. During unloading, the nonlinear curve was similar; however, the material slightly under predicted the hysteretic energy dissipation of the neoprene pad. Equally important is the material response when the material cycled through compressive and tensile loads. Figure 5.2(b) shows the response of the material under this condition. Clearly, the **Neoprene** material is compression only. Figure 5.2(c). shows the material behavior for **Neoprene** when it is loaded, partially unloaded, and then reloaded several times before the load is completely removed. In this case, the reloading path is the initial stiffness. When the load is completely removed, the material returns to its original undamaged stress-strain state.

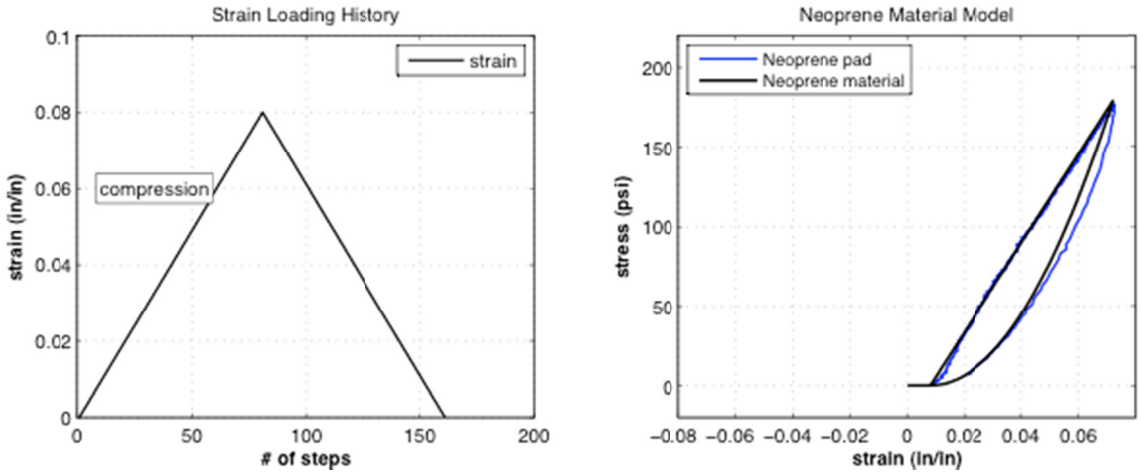

(a) one compression cycle response

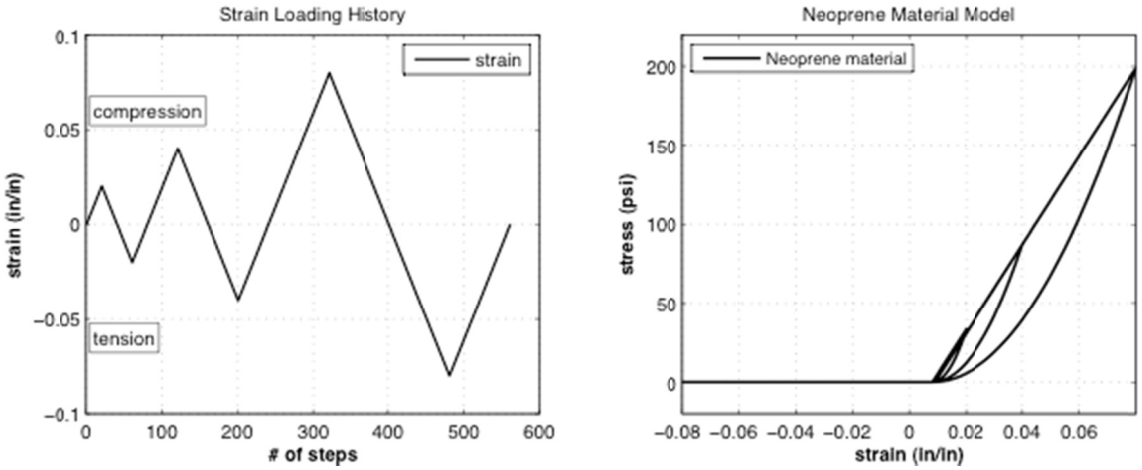

(b) tension/compression cyclic response

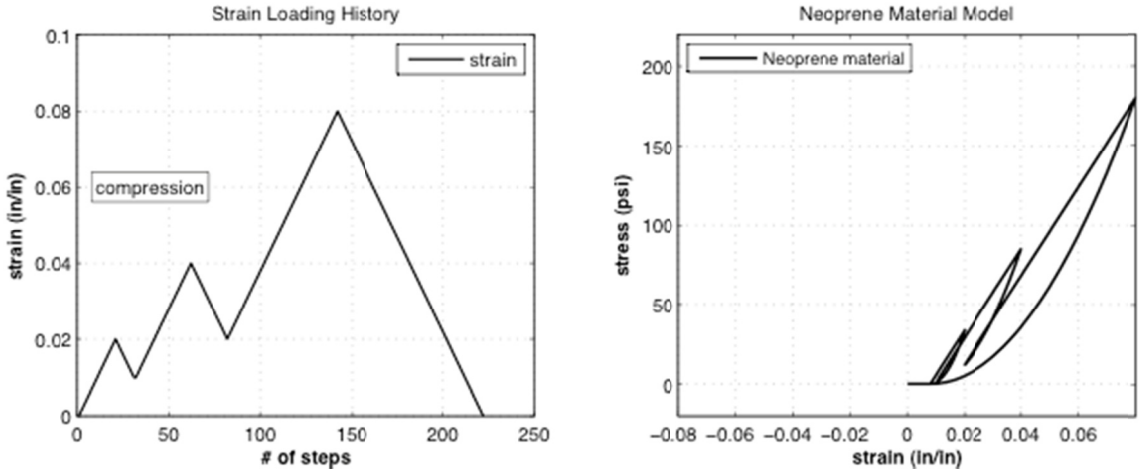

(c) compressive unloading/reloading response

Figure 5.2 OpenSees Neoprene material model characteristics.

5.3 MODELING OF REINFORCED CONCRETE BRIDGE PIER

Predicting the observed behavior of RC bridges allowed to uplift is essential to furthering the understanding of uplifting bridge piers in general. The experimental results reported in Chapters 3 and 4 described the response of a single column with two footing sizes and varying multi-directional excitations. Historically, the type of analysis done to predict the demand response of uplifting bridge piers used linear response spectrums and employed equivalent systems using static procedures, using the physical footing and column dimensions but typically do not incorporate the soil characteristics or the potential inertial effects and yielding of the columns. To more accurately capture the behavior of uplifting bridge piers, it is recommended that dynamic time-history analysis be conducted. Although much dynamic time-history analysis has been done to determine the response of uplifting systems [Kawashima et al. 2007], few research investigations have experimental data as a justification for the models. The analysis included herein attempts to fill the gap between the dynamic analysis research performed to date but which lacks the experimental data as verification of the behavior of uplifting systems.

Selecting the appropriate modeling technique involves several considerations. Care should be given to the complexity, reliability, and accessibility of the analysis model. A priority in developing analytic models is to simplify where possible to make the model less complex and more obvious without sacrificing accuracy of the desired response quantities. Ideally, a simple model that captured all of the relevant behavior modes of the system would be optimum. Equivalent static methods do not accomplish this. This research program selected OpenSees as the analysis platform to conduct dynamic time-history analyses. It is an open source model that allows many users to contribute various materials and elements. For this reason it is well suited to model uplifting bridge piers.

When necessary the column, footing, and elastomeric pad can be represented using previously defined elements or user-specified elements. The modes of response critical for the modeling of the uplifting bridge piers include elastic pad response, footing uplift, elastic footing response, and both elastic and inelastic behavior of the column. The elastic column response levels can be utilized to determine the effect that uplift has on the system response without the complexity of simultaneous yielding of the column. The absence of yielding at these levels allows for calibrating the footing response. With this understanding of uplifting behavior, attention can then be turned to the system response when the column is yielding concurrently with footing uplift.

The footing and pad response was modeled using Beam-on-Nonlinear Winkler Foundation (BNWF) method, which assumed that the response was nonlinear elastic for the pad and linear elastic for the footing. The pad is discretized into small rectangular sections whose vertical and rotational stiffness is simulated using a vertical spring at each sub-section. The footing behavior was assumed to be rigid elastic because of the very small footing flexural and shear deformations.

Fiber element modeling of RC bridge column can be divided into two categories: elastic columns and inelastic columns. Both of these methods used the BNWF method previously described. Elastic column models utilized the concept of effective sectional stiffness. The effect of cracking was estimated using the typical element formulation with an equivalent cracked stiffness under the axial load along the entire length of the column. Often the cracked stiffness of a section was estimated as one half of the gross section properties. In this case, it was $EI_{\text{eff}} =$

$EI_{gross}/2$. While useful for low-level excitation with no yielding, this method did not capture the inelastic action of the column.

Inelastic action in the reinforced column can be modeled several ways. The choice here was to use fiber sections at discrete points along the column to represent the inelastic yielding behavior. Two fiber section approaches used here to model the columns were flexibility based beam-column elements:

- Distributed Plasticity Element – yielding may propagate along the column length. Each integration point is assigned a fiber section. Location of the integration points is important in modeling all of the observed inelastic behavior.
- Concentrated Plasticity Element – a region of finite length at each end of the element is assumed to contain all of the inelastic action. This region is known as the plastic hinge length. Each plastic hinge has two integration points at the ends with a fiber section model assigned. The rest of the element is assumed to be elastic with effective sectional properties.

Damping of the system will be carefully considered also. Systems allowed to uplift typically have more observed damping due to energy dissipation within the supporting soil during rocking and uplift. Standard RC columns use a mass and stiffness dependent Rayleigh approach to calculate damping. The damping of the column will be modeled this way. The effect of a Rayleigh damping assumption for the footing and elastomeric pad was investigated to see if this was appropriate or if there was a more suitable alternative.

In summary, a series of analyses were done to determine the ability of three types of analytic models to predict observed response. Each of the models used the BNWF method to model the footing and elastomeric pad. The models used were as follows:

1. Elastic Column that predicted system response for varying multi-directional excitations when no yielding occurs in the column.
2. Distributed Plasticity Column that allowed for a progression of inelastic behavior along the column length with no restrictions.
3. Concentrated Plasticity Column that assumed inelastic behavior is restricted to the plastic hinge region at the ends of the column.

A comprehensive diagram of the analysis model showing the column and footing options is shown in Figure 5.12.

5.3.1 Fiber Element Modeling

Fiber section models were used for sectional moment-curvature analysis and section assignment at integration points of flexibility based elements. Fiber models were used to predict the moment curvature relationship at the integration points over member lengths. The ability of fiber models to predict elastic or inelastic behavior allows for using one element to model members; for example, in the case where they are yielding at the ends but behaving elastically in the center region.

A fiber model is built by dividing the cross-section of the desired member into a collection of fibers. Each fiber is assigned a uniaxial constitutive material model corresponding to the discretization location. For the experimental test program, the column cross-section was discretized using confined concrete, unconfined concrete, and longitudinal steel. The uniaxial material models of the fibers are described in Section 5.2. The fiber section representation is shown in Figure 5.3. The section is comprised of 200 confined concrete fibers, 40 unconfined concrete fibers, and 12 longitudinal steel fibers. Figure 5.4 shows an example of a column element with four integration points and the associated fiber sections.

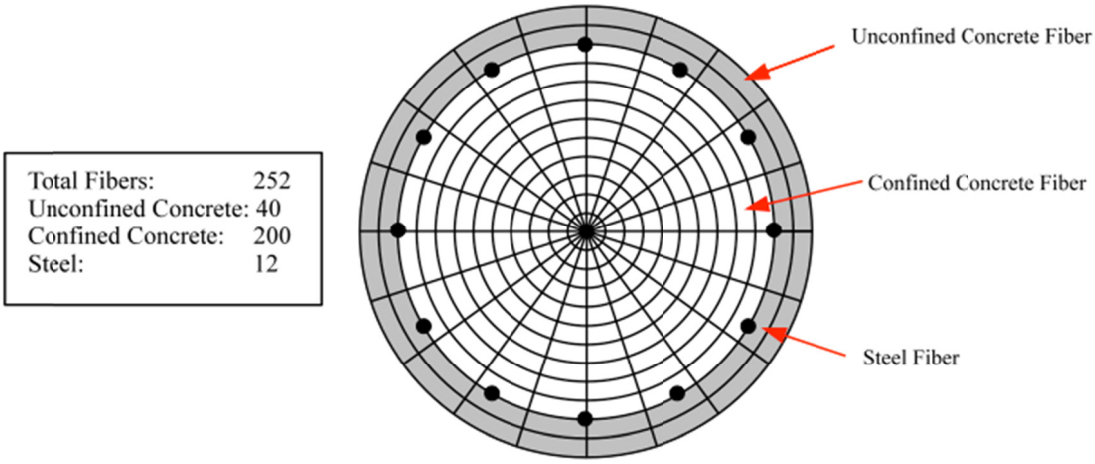

Figure 5.3 Fiber section representation of column.

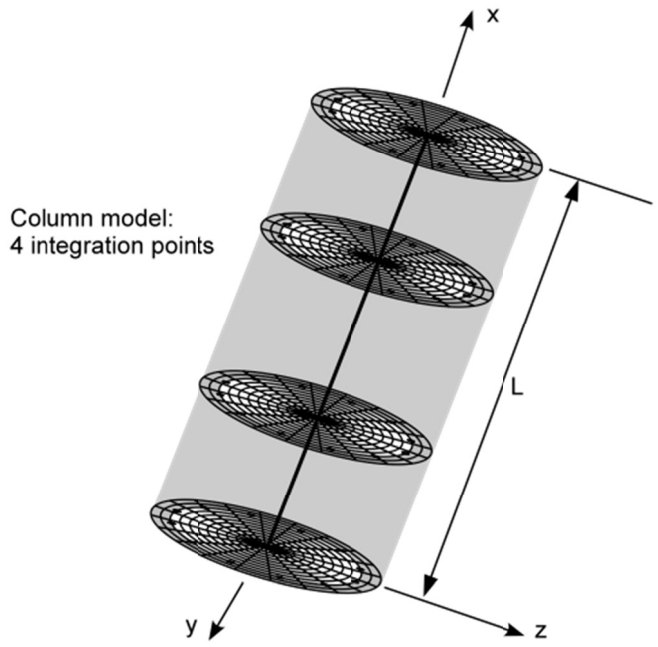

Figure 5.4 Column element with fiber sections.

5.3.1.1 Moment-Curvature

It is possible to perform sectional analysis on the fiber section alone without having to build the entire model by using OpenSees. This proved useful in calibrating the analysis to the observed moment-curvature response during the testing. To perform a moment-curvature analysis, a moment was calculated based on an imposed curvature and axial load. This was accomplished by iterating on the neutral axis depth until axial load equilibrium was satisfied. Per the Bernoulli-Navier beam theory, plane sections were assumed to remain plane during deformation. For RC structures, the confined concrete within the core was modeled using the enhanced properties as described in Section 5.2.2. The moment-curvature relationship used for these tests is shown in Figure 5.5. The analysis used the concrete properties described in Section 5.2.2 and varied the steel models as either the bilinear model **Steel02** or the **ReinforcingSteel** model (Section 5.2.1).

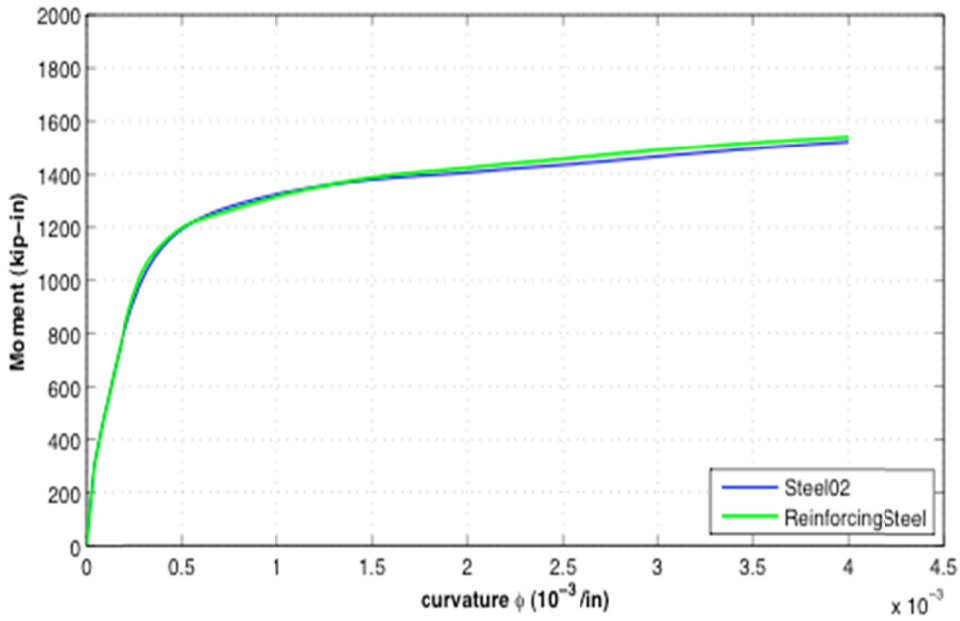

Figure 5.5 Moment-curvature relationship of column section.

5.3.2 Column

As described previously, three options were used to model the RC column: as elastic, distributed plasticity, or concentrated plasticity element. The elastic column model should only be used to predict the observed results when no yielding occurred. It utilizes effective section properties to predict observed response. The other two options are force-based beam column elements that can be used to model elastic or inelastic behavior. The distributed plasticity model has no restrictions on the spread of inelastic behavior over the member length. By comparison, the concentrated plasticity model limits inelastic behavior to the ends of the column over a user specified length. This length is commonly known as the plastic hinge length. This section briefly describes the implementation of the column model assumption and the associated theory for each column type.

For each of the column models, the weight block assembly was modeled as a lumped mass with rotational mass moment of inertia specified at the center of gravity of the blocks. A

rigid offset was used from the top of the column to the center of gravity of the blocks and at the base from the bottom of the footing to the bottom of the column. The lengths of the offsets were 56 in. and 18 in., respectively, for the top and bottom. The P-Δ effects associated with lateral displacements dues to gravity loads were also included for the system, because measured P-Δ ratios were greater than $0.20M_u$ as specified by the Caltrans SDC.

In summary, one column element with lumped mass and rotational mass moment of inertia at the center of gravity with rigid end offsets at both ends was used to model the RC column for any of three column model assumptions. The idealized three-dimensional column model is shown in Figure 5.6.

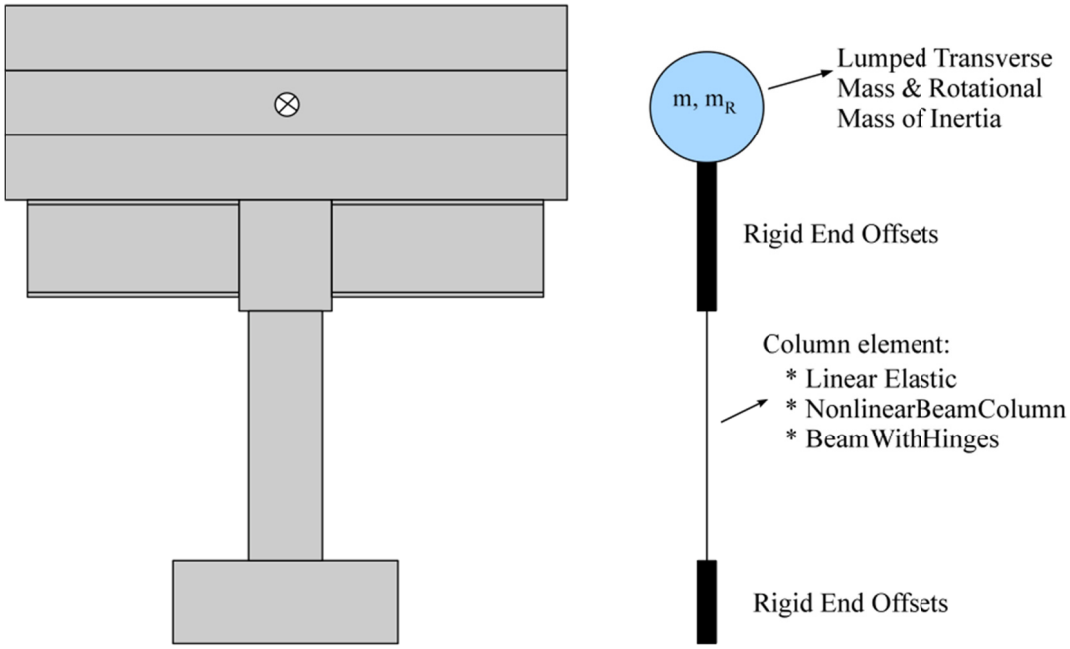

Figure 5.6 General column model.

5.3.2.1 Elastic

Typically, the elastic column element is the simplest to implement in any type of analysis. In this case, it was a three-dimensional line element with uniform cross-section properties along the length. The mechanical (E, G) and physical properties (L, A, I_y, I_z) were the specified from the outset, with both ends having rigid end offsets. Figure 5.7 shows a depiction of the elastic column element. The accuracy of linear elements response depends on the specified initial stiffness. Usually, the effective initial stiffness is assumed to be $EI_{\text{eff}} = 0.5EI_g$. From the observed test results, it appears the effective stiffness ratio is closer to 0.2–0.3 EI_g.

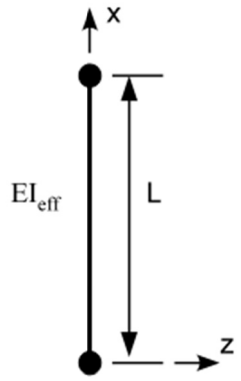

Figure 5.7 Elastic column model.

5.3.2.2 Distributed Plasticity (NonlinearBeamColumn)

A distributed plasticity beam-column element is one of the two force-based flexibility elements used to model column response. Implemented via OpenSees as a ***nonlinearBeamColumn*** element, the line element moment-curvature and axial load-deformation response is determined by the fiber sections assigned to each integration point. To predict the observed column response, five integration points were used. Figure 5.8(a) shows the ***nonlinearBeamColumn*** element used in the analysis.

The flexibility based formulation estimates the inelastic behavior along the length of the member using integration points. A moment and axial force distribution, which is in equilibrium with the forces at the end of the member, is assumed along the member length. Curvatures and axial deformations are then estimated via iteration given the moment and axial load. Weighted integration of the section deformations at each integration point along the length [Taucer et al. 1991] is used to determine the column response. Because most of the inelastic action is expected to occur at the member ends, it is critical to have integration points there. The Gauss-Lobatto integration scheme places weighted integration points at the ends of the elements as well as along the column length when more than two integration points are used. For this scheme, the weights and location of the integration points are predetermined. The user specifies only the number of integration points.

5.3.2.3 Concentrated Plasticity (BeamWithHinges)

The other force based flexibility element uses a concentrated plasticity beam-column element to model column response. It is implemented in OpenSees as ***beamWithHinges.*** The fiber based element has nonlinear constitutive behavior limited to user specified lengths at the ends known as plastic hinge lengths. Fiber sections are assigned to the integration points at the end of each plastic hinge. There are several methods available to estimate the plastic hinge length. Equation (5.3) shows the method by Priestly et al. [1996] to determine the plastic hinge length of a circular column. Away from the plastic hinge zones the element behaves linearly elastic with user specified effective stiffness properties EI_{eff}. Figure 5.8(b) shows the column modeled using a ***beamWithHinges*** approach. The cantilever column tested only had inelastic action at the base of

the column; therefore a plastic hinge was specified only there. The estimated plastic hinge length was 13.0 in.

$$l_p = 0.08L + 0.15 f_y d_b \tag{5.3}$$

The concentrated plasticity element restricts the integration points to the hinge regions. By comparison, the distributed plasticity element distributes integration points along the entire member length. Two integration points per hinge are used to model the curvature distribution. The formulation of the flexibility based element uses a modified Gauss-Radau quadrature rule for integrating element stiffness to eliminate objectivity in the nonlinear region while still maintaining the exact response under linear conditions. A full description of the element formulation can be found in Scott and Fenves [2006]. The primary inputs for the column model are fiber sections, plastic hinge lengths, and effective stiffness of the elastic portion of the column.

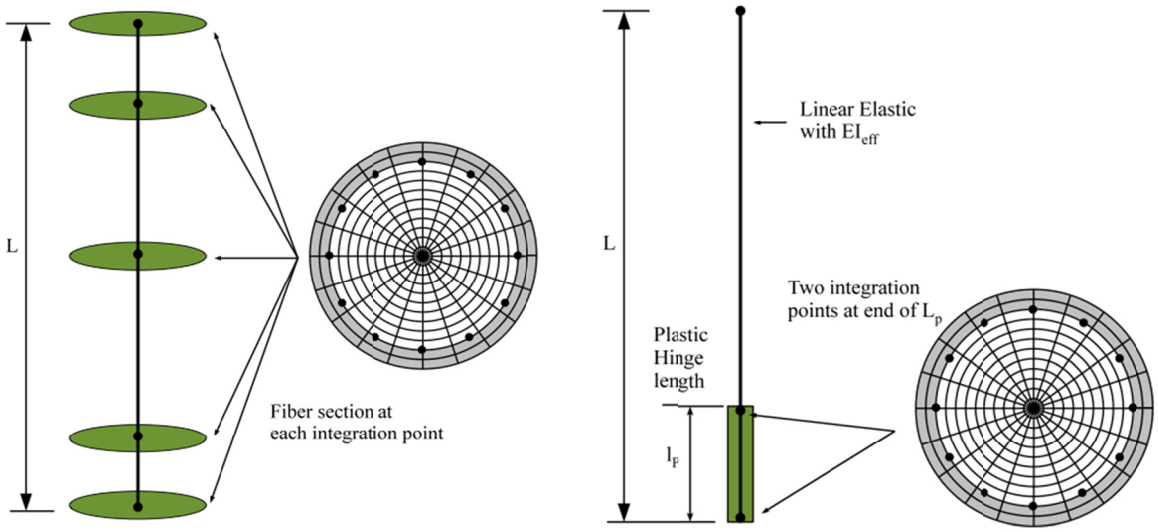

(a) NonlinearBeamColumn **(b) BeamWithHinges**

Figure 5.8 Force-based beam column models.

5.3.3 Footing - Soil Structure Interaction

Work by Harden et al. [2005] illustrates that Winkler spring foundations may be able to provide results with a sufficient degree of accuracy. Because of the two- and three- dimensional character of excitations considered for the experimental testing program (Chapter 3 and 4), it was not viewed as suitable to use more simplified two-spring models or simplified methods based on rocking response of rigid blocks, i.e., those adapted from the procedures developed by Housner [1963]. The model originally developed by Harden et al. [2005] was calibrated for two-

dimensional analysis. This model was extended to consider three-dimensional response based on calibration to the experimental results.

The Winkler foundation model has several key parameters that affect the global response of the system. These include modeling of the rotation and vertical stiffness of the foundation. The rotational stiffness was calibrated by varying the stiffness of the end-region springs and the length of the end region (Figure 5.9). The material used to represent elastic soil response for the specimens on the shake table was an elastomeric pad (see Section 5.2.3). The vertical stiffness characteristics of the pad were explicitly measured.

From the outset a few simplifying assumptions were made for the purposes of analysis. It was assumed that the footing was rigid, and that its horizontal translational movement on the pad was negligible. Some horizontal movement was detected; however, it was very small in comparison to the overall lateral displacements of the specimen. Material damping of the elastomeric pads was also considered negligible, so the vertical dashpots were not included in the Winkler foundation model.

The BNWF method was chosen to model the shallow spread footing response. Analytically, it was simple to implement via OpenSees. The base of the column connected to the BNWF footing beam elements. The BNWF model linked the footing and underlying soil response at each discretization point. Everywhere the footing is discretized, the soil below is also discretized in the same size and shape. For the testing program the elastomeric pad beneath the sub-section was modeled using a vertical stiffness spring and a dashpot. The footing was modeled using rigid line elements. Figure 5.9 shows a two-dimensional cross section through the BNWF footing model. The footing elements were considered to be rigid-elastic. The springs and dashpots were modeled as a combination of linear and nonlinear elastic elements (Section 5.2.3). A plan view of the discretization scheme is shown in Figure 5.10. The spacing and number and nodes can be varied in each direction, which proved useful in calibrating the footing and pad response to observed results. Figure 5.11 shows the three-dimensional BNWF model used to predict the observed test results.

The physical properties needed to model the soil include ultimate bearing capacity (q_{ult}), soil type, vertical stiffness (K_z), rotational stiffness (K_θ), damping, etc. Modeling assumptions include the ratio-of-end length (L_{end}) to total length (L), the spacing of the springs for each region, and the spring stiffness in the middle and end regions. Also, the type of uniaxial material hysteresis model used for the individual soil springs needs to be determined.

For the purposes of this research, the distribution of pressure for each spring across the foundation was assumed to be uniform. Appendix C contains the Tcl script for implementation of a shallow foundation allowed to uplift in the analysis framework OpenSees. The coding is such that for systems with more than one footing, the command can be looped and called as many times as necessary. The resulting foundation model connects to the specified node of the superstructure and does not need spring or other coordinates to be implemented. For the analyses of the shake table tests, the soil springs were assumed to be linear elastic and unable to resist tension.

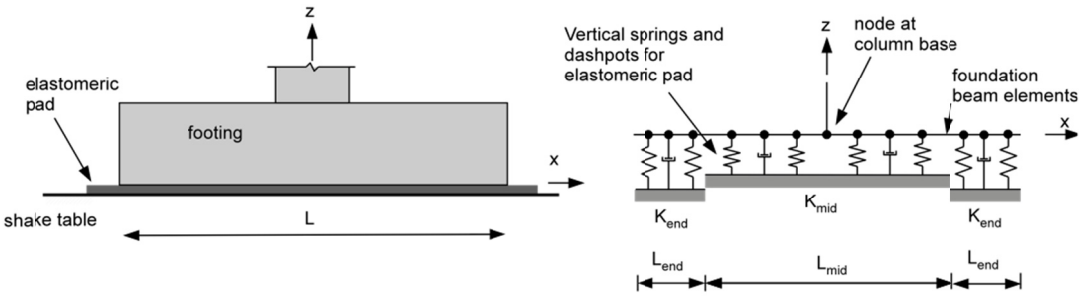

Figure 5.9 Beam on Nonlinear Winkler Foundation model.

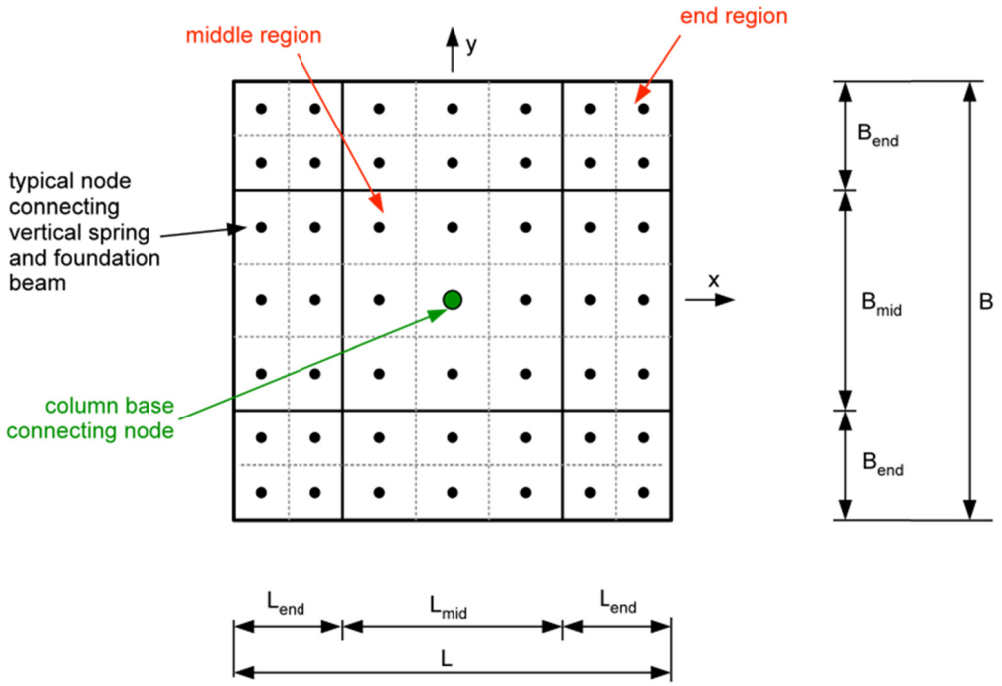

Figure 5.10 Discretization of 3D footing model.

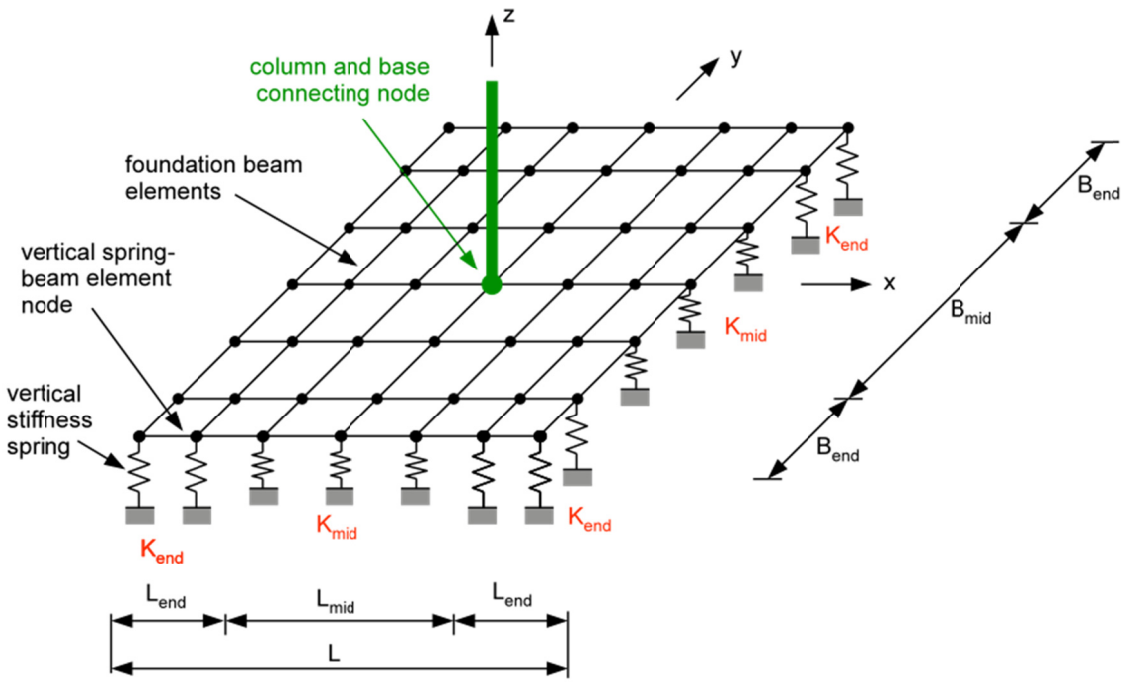

Figure 5.11 Beam-On-Nonlinear-Winkler-Foundation three-dimensional model.

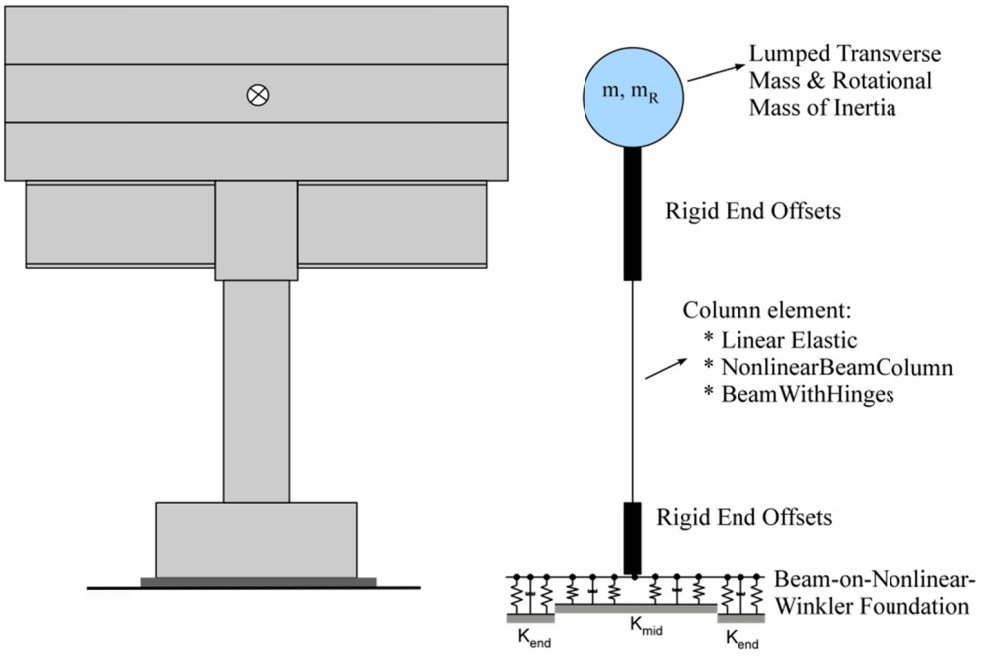

Figure 5.12 Analytic model of uplifting bridge pier system.

5.3.4 Damping

Damping modes not associated with hysteretic energy dissipation are usually combined together and idealized as pure viscous damping. This may include SSI, friction, material damping, and non-structural components. Rayleigh damping is often used for multi-degree-of-freedom structures because damping at two natural frequencies ω_i and ω_j may be specified. Damping is most conveniently expressed in terms of the ratio ξ, defined as the damping coefficient c relative to the critical damping coefficient c_{cr}. Equation (5.4) shows the relationship for a single-degree-of-freedom structure.

$$\xi = \frac{c}{c_{cr}} = \frac{c}{2m\omega} \tag{5.4}$$

For a multi-degree-of-freedom structure the damping matrix is computed as a linear combination of the mass and stiffness matrices [Equation (5.5)]. The coefficients α and β are determined by solving the system of equations [Equation (5.6)]. The estimation of damping can be mass proportional only, stiffness proportional only, or a combination of mass and stiffness damping.

$$c = \alpha \cdot m + \beta \cdot k_t \tag{5.5}$$

$$\frac{1}{2}\begin{bmatrix} 1/\omega_i & \omega_i \\ 1/\omega_j & \omega_j \end{bmatrix} \cdot \begin{bmatrix} \alpha \\ \beta \end{bmatrix} = \begin{bmatrix} \xi_i \\ \xi_j \end{bmatrix} \tag{5.6}$$

Damping ratios for RC structures typically range from 3–7%. In designing structures, 5% is common. However, this is for fixed-base systems that do not include SSI. The presence of soil deformation and yielding tends to increase the amount of damping in the system. The viscous damping associated with SSI is a complex phenomenon that goes beyond the focus of this research work. A study by Housner [1963] determined the equivalent viscous damping of rigid blocks allowed to rock. Work by Chopra and Goel [1999] also may be useful in determining the equivalent viscous damping of an uplifting system.

For the purposes of this investigation, only the effects of mass, stiffness and mass-stiffness proportional damping were investigated. The analysis done also shows the effect that varying the damping ratio has on the damping force within the system. Based on the observed results (Chapter 4) of the shake table tests, the initial Rayleigh damping parameters α and β were selected based on a damping ratio of 7.8%. The damping matrix was formed at each analysis step using the current tangent stiffness matrix.

5.4 ELASTIC FOOTING ANALYSIS

Each of the analytic model options for the column was paired with an elastic footing model whose formulation is described in this section. Both footing sizes used in the test configurations are described here analytically. Best modeling values for the global vertical stiffness of the elastomeric pad and spring spacing were developed to most accurately capture the observed

footing rotational stiffness and uplift. The footing analytic model is an approximation of the footing. Although more accuracy may be possible with smaller discretization segments of the footing, this comes at the expense of more nodes and longer analysis run times. In general, decreasing the node spacing by a half (for example) increases the number of nodes by a power of two. Damping of the elastomeric pad may be an additional source of uncertainty. The effects of the type of damping assumptions on footing response are described in the column analysis (Section 5.3.4).

The footing analysis is accomplished by calibrating the analytic model to the observed moment-rotation relationship. The BNWF approach described in Section 5.3.3 requires specifying several parameters. The inputs for modeling are the middle region global stiffness K_{zm} and end-region global stiffness K_{ze}. Additionally the footing length L, width B, end lengths, and node spacing are specified.

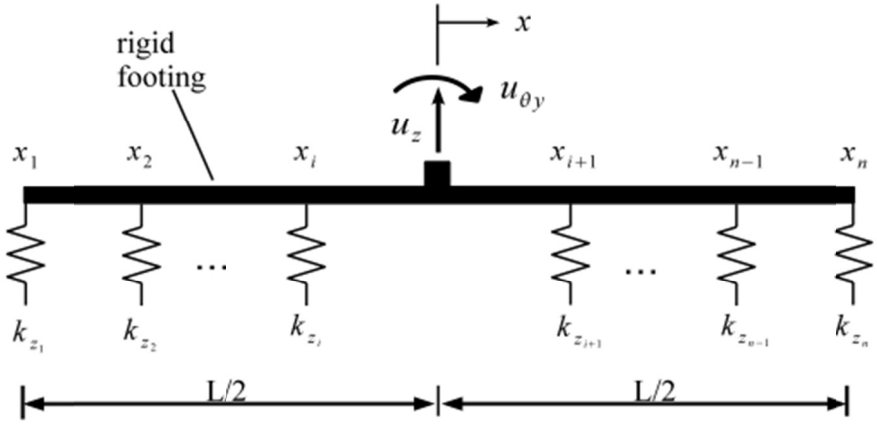

Figure 5.13 Footing force deformation relationship formulation.

The force deformation relationship can be formed by assuming a rigid footing assumption supported on vertical springs. This is the method used by the BNWF footing mesh generator described in Section 5.3.3. Although the formulation method described here is based on a two-dimensional plane, the three-dimensional formulation is very similar. For all analysis cases the footing is restrained from translating laterally in the *x*- or *y*-axis direction. The footing is allowed to uplift in the *z*-axis direction and rotate about all three axes. Using a rigid footing assumption, the entire footing uplift along the length can be described by two degrees-of-freedom at the center node of the footing; the vertical displacement, and the rotation about the centerline of the footing. Figure 5.13 depicts the footing, displacement degrees-of-freedom, and generalized vertical spring stiffness and locations. The force deformation relationship is described by Equation (5.8) expressed in terms of vertical footing force and overturning moment as a function of footing displacement degrees of freedom. The uplift at a given spring location is determined by Equation (5.9).

Footing Force Deformation Relationship [Equation (5.7)].

$$F = K_{ftg} \cdot u \tag{5.7}$$

Expressed in matrix form as individual forces and displacements:

$$\begin{bmatrix} F_z \\ M_{\theta_y} \end{bmatrix} = \begin{bmatrix} k_z & k_{z\theta} \\ k_{z\theta} & k_\theta \end{bmatrix} \cdot \begin{bmatrix} u_z \\ u_{\theta y} \end{bmatrix} \tag{5.8}$$

Individual spring uplift displacement:

$$z_i = z_o + x_i \cdot \theta \tag{5.9}$$

The general footing stiffness matrix is given in Equation (5.10).

$$k_{ftg} = \begin{bmatrix} k_z & k_{z\theta} \\ k_{z\theta} & k_\theta \end{bmatrix} \tag{5.10}$$

The individual components of the footing stiffness matrix as a function of the vertical spring stiffness and relative spring locations are given by Equations (5.11) through (5.13). The formulations as shown are for when no uplift of the footing at the springs has occurred.

$$k_z = \sum_{i=1}^{n} k_{zi} \tag{5.11}$$

$$k_{z\theta} = \sum_{i=1}^{n} k_{zi} \cdot x_i \tag{5.12}$$

$$k_\theta = \sum_{i=1}^{n} k_{zi} \cdot x_i^{\,2} \tag{5.13}$$

The individual spring stiffness k_{zi} at each location x_i along the footing length L is the sum of the individual springs distributed along the width B of the footing at the x_i coordinate. In general the individual spring stiffness k_{zi} at x_i is the sum of each spring kz_{ij} for j=1:m, Where m = number of nodes in the y-direction. The footing length segment is expressed as fL_x [Equation (5.14)].The stiffness k_{zi} in the x-direction can be expressed as Equation (5.15) for the middle region of the footing and Equation (5.16) for the end region of the footing. The procedure is the same for the y-direction but substituting the width terms B, B_{ep}, and fL_y for length terms L, L_{ep}, and fL_x.

fL_x = length of foot segment (5.14)

The spring stiffness at middle footing region:

$$k_{zi} = \left[\frac{fL_x\left(1 - 2B_{ep}\right)}{L} \right] \cdot K_{zm} + \left[\frac{fL_x B_{ep}}{L} \right] \cdot K_{ze} \tag{5.15}$$

The spring stiffness at end footing region:

$$k_{zi} = \left[\frac{fL_x}{L}\right] \cdot K_{ze} \tag{5.16}$$

Under a static vertical load with zero rotation the footing stiffness matrix is uncoupled owing to the symmetry of the springs locations and stiffness values. The force-deformation relationship simplifies to Equation (5.17):

$$\begin{bmatrix} F_z \\ M_{\theta_y} \end{bmatrix} = \begin{bmatrix} k_z & 0 \\ 0 & k_\theta \end{bmatrix} \cdot \begin{bmatrix} u_z \\ u_{\theta y} \end{bmatrix} \tag{5.17}$$

The initial static displacement [Equation (5.18)] of all the springs under a vertical load with no rotation is:

$$u_z = z_o = \frac{F_z}{k_z} = \frac{F_z}{\sum_{i=1}^{n} k_{zi}} \tag{5.18}$$

The rotation of the footing and the corresponding moment when the first spring loses contact with the footing are given by Equation (5.19) and Equation (5.20):

$$\theta_{up1} = \frac{u_z}{x_1} = \frac{z_o}{x_1} \tag{5.19}$$

$$M_{\theta up1} = k_\theta \cdot \theta_{up1} = \left[\sum_{i=1}^{n} k_{zi} \cdot x_i^{\,2}\right] \cdot \frac{z_o}{x_1} \tag{5.20}$$

The footing stiffness while rocking, when no uplift occurs along the footing length at the springs, is described by Equation (5.17). As the footing uplifts with increasing rotation, the footing stiffness matrix is redefined as subsequent springs lose contact with the footing. The moment-rotational stiffness relationship becomes a multi-linear curve with transition points defined by the uplift of individual springs. In reality, as the footing continues to uplift, there is a continuous decrease in the length of footing resisting the uplift, and, therefore, a continuous change in the vertical and rotational stiffness, whether it be small or large magnitude, resulting in a smooth moment-rotation relationship.

The individual components of the footing stiffness matrix K_{ftg} as footing uplift occurs can be described by modifying Equations (5.11) through (5.13). When uplift occurs at the first spring i=1, the force is eliminated, and the individual spring stiffness k_{z1} is removed from the determination of k_z, $k_{z\theta}$, and k_θ. As the footing loses contact with the spring at location x_i, the footing stiffness components are a function of the spring stiffnesses from k_{zi} for i= *i+1:n* [Equations (5.21) to (5.23)]. This is the case until the next spring uplifts, when the footing stiffness matrix is recalculated for contributing springs k_{zi} for i= *i+2:n*.

The individual footing stiffness K_{ftg} components when uplift has occurred at spring location x_i are:

$$k_z = \sum_{i=i+1}^{n} k_{zi} \tag{5.21}$$

$$k_{z\theta} = \sum_{i=i+1}^{n} k_{zi} \cdot x_i \tag{5.22}$$

$$k_{\theta} = \sum_{i=i+1}^{n} k_{zi} \cdot x_i^{\,2} \tag{5.23}$$

The representative moment rotation relationship for a footing with dimensions L long and B wide are shown in Figure 5.14. The applied rotation θ is one full cycle from zero to $+\theta_{max}$ to $-\theta_{max}$ and back to zero. The M-θ relationship for the two vertical spring analysis options—Elastic-No-Tension (ENT) and neoprene—is shown in Figure 5.14a and Figure 5.14b, respectively. The end length ratios L_{ep} and B_{ep} and global vertical stiffness K_{zm} and K_{ze} are specified and the node spacing is set so there are 6 nodes in each direction (symmetric about the centerlines). Before first uplift the footing rotational stiffness K_{θ} may be calculated using Equation (5.17). The corresponding moment at first uplift is M_{up1}, as given by Equation (5.20). As the footing rotation increases, the footing loses contact with the vertical springs and the rotational stiffness decreases. The plots show the transitions in rotational stiffness as each subsequent vertical spring loses contact with the footing. During unloading, the ENT springs follow the same path while the neoprene springs dissipate some energy (see Section 5.2.3).

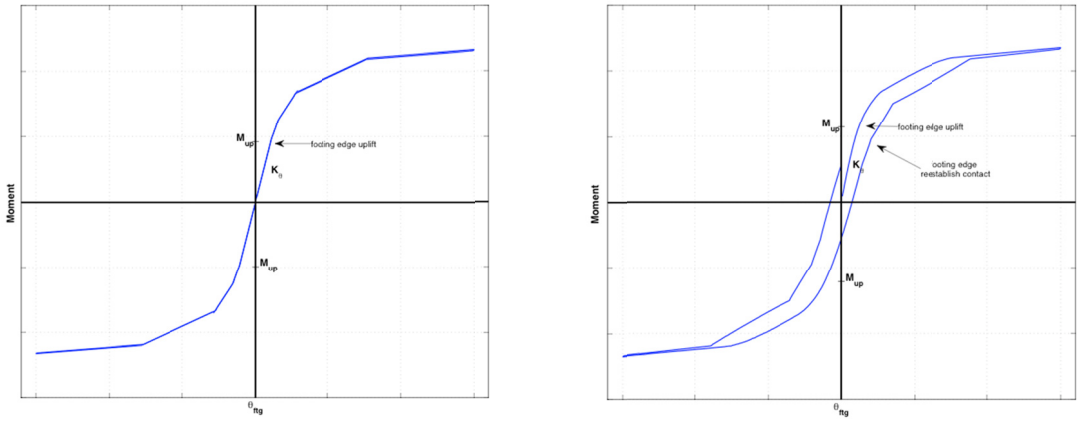

(a) Elastic-No-Tension springs **(b) neoprene springs**

Figure 5.14 Analytic model moment rotation relationship of footing (ENT springs).

The methods described above can be used to calibrate the footing stiffness and spring spacing to best match the observed response. The comparison of results focused on the two footing configurations when the column had a nominal design axial load applied. The less than design axial load experimental test was used to assess the viability of rocking systems and is not

investigated further. The first test group was the $3D_c \times 3D_c$ square footing configuration, which had only elastic response of the column. The second test group was the $5D_c \times 3D_c$ rectangular footing configuration that had elastic and inelastic response of the column.

5.4.1 3Dc x 3Dc Square Footing Configuration

The best values of global vertical stiffness for the square configuration footing were in the range of K_{zm} = 600–800 kip/in. for the middle region and K_{ze} = 2000–2200 kip/in. for the end region. The stiffness of the neoprene vertical spring material needed to be slightly higher than the ENT material due to the gap strain creating more deflection with less force on the footing springs. The range of end-length ratio for the $3D_c$ square footing configuration was approximately L_{ep}, B_{ep} = 0.20–0.30. Figure 5.15 shows the moment-rotation envelope from an applied cyclic rotation using ENT springs for the $3D_c$ square footing compared to the recorded DS test group data (3D *X*+*Y*+*Z* input), which had the most significant uplift. Dynamic effects were not included in this envelope analysis. The recorded FS test group data (3D *X*+*Y*+*Z* input) is shown Figure 5.16 for the ENT springs. The response using neoprene springs and an applied cyclic rotation was very similar to that shown for the ENT springs with the addition of energy dissipation during unloading, as shown in Figure 5.17 and Figure 5.18 for the 3D-*X*+*Y*+*Z* input of the DS and FS experimental tests.

The ranges of K_{zm} and K_{ze} best match the recorded vertical displacement $\Delta_z = z_o$ under static load, the initial rotational stiffness K_θ, the moment at first uplift M_{up1}, and an approximation of the softening of the footing rotational stiffness as the footing uplifts with increasing rotation. The values of global vertical stiffness and end-length ratio, which best approximated the vertical and rotational stiffness of the $3D_c \times 3D_c$ footing for all experimental tests of the square footing, are given in Table 5.1. The square configuration did not exhibit identical rotational stiffness and first uplift moment about the *X* and *Y* axes because of the variable spring spacing in each direction.

Table 5.1 Footing vertical stiffness values.

	$3D_c$ x $3D_c$		$3D_c$ x $5D_c$	
	ENT Spring	**Neoprene Spring**	**ENT Spring**	**Neoprene Spring**
K_{zm} (kip/in.)	600	600	600	600
K_{ze} (kip/in.)	2200	2200	2200	2200
L_{ep}	0.24	0.24	0.24	0.24
B_{ep}	0.26	0.26	0.26	0.26
z_o (in.)	0.033	0.041	0.033	0.04
$K_{\theta Y}$ (kip-in.)	427,750	427,750	312,680	427,745
$K_{\theta X}$ (kip-in.)	438,900	438,900	890,430	1,219,170
M_{up1Y} (kip-in.)	580.0	720.0	594.0	730
M_{up1X} (kip-in.)	595.0	740.0	1095.0	1260

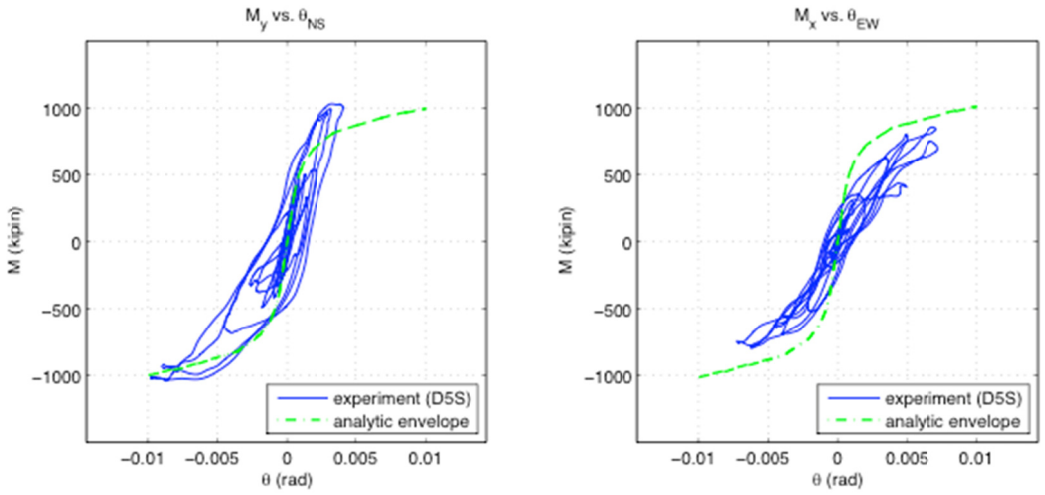

Figure 5.15 ***M-θ*** **analytic envelope of 3Dc square footing (test D5S ENT springs).**

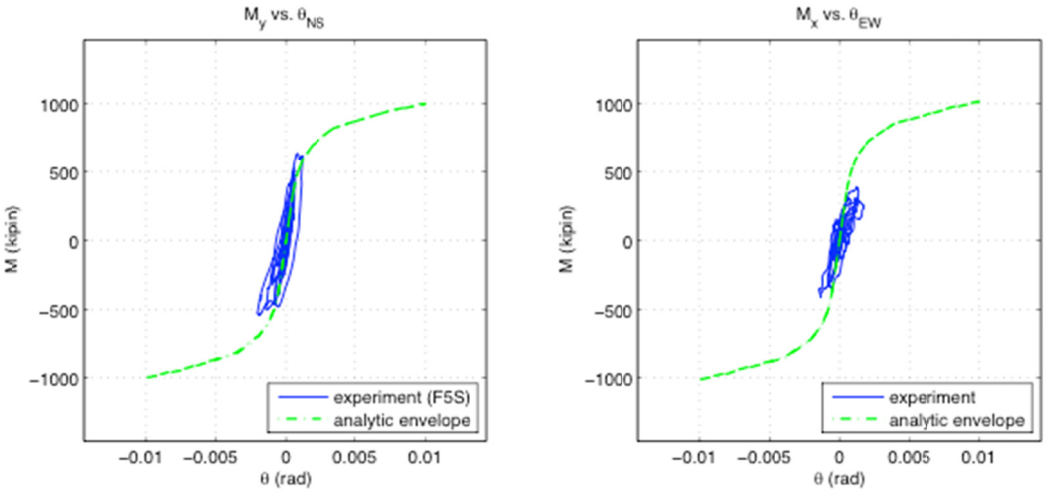

Figure 5.16 ***M-θ*** **analytic envelope of 3Dc square footing (test F5S ENT springs).**

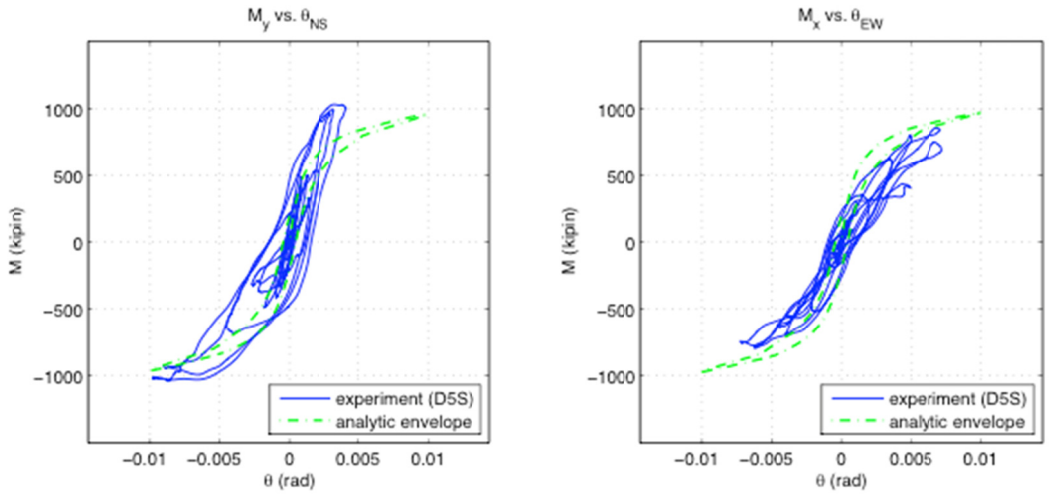

Figure 5.17 ***M-θ*** **analytic envelope 3Dc square footing (test D5S neoprene springs).**

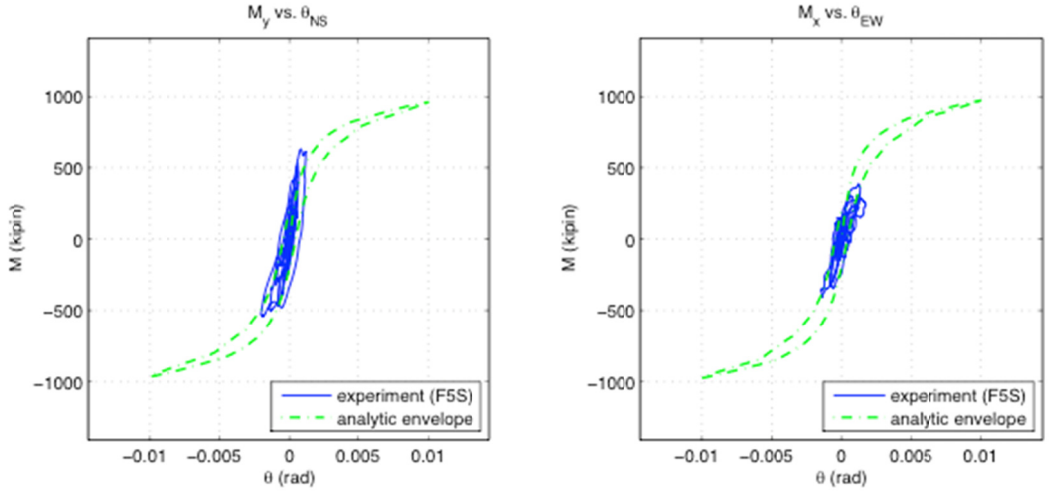

Figure 5.18 ***M-θ*** **analytic envelope of 3Dc square footing (test F5S neoprene springs).**

5.4.2 5Dc x 3Dc Square Footing Configuration

The best values of global vertical stiffness for the rectangular configuration footing were in the range of K_{zm} = 600–800 kip/in. for the middle region and K_{ze} = 2000–2200 kip/in. for the end region. The range of end-length ratio for the $3D_c$ (*X*) direction and the $5D_c$ (*Y*) direction is approximately L_{ep}, B_{ep} = 0.20–0.30, respectively. Figure 5.19 and Figure 5.20 show the moment-rotation envelope from an applied cyclic rotation using ENT springs and neoprene springs for the $3D_c \times 5D_c$ rectangular footing compared to the recorded A2R test group data (3D *X*+*Y*+*Z* input). Some uplift occurred and was not influenced by residual displacements, which caused a shifted moment-rotation origin due to permanent overturning moment. Dynamic effects were not included in this envelope analysis. The footing values of K_{zm} and K_{ze} that best match the initial displacement z_o, rotational stiffness K_θ, the moment at first uplift M_{up1}, and an approximation of the softening of the footing rotational stiffness as the footing uplifts with increasing rotation are given in Table 5.1.

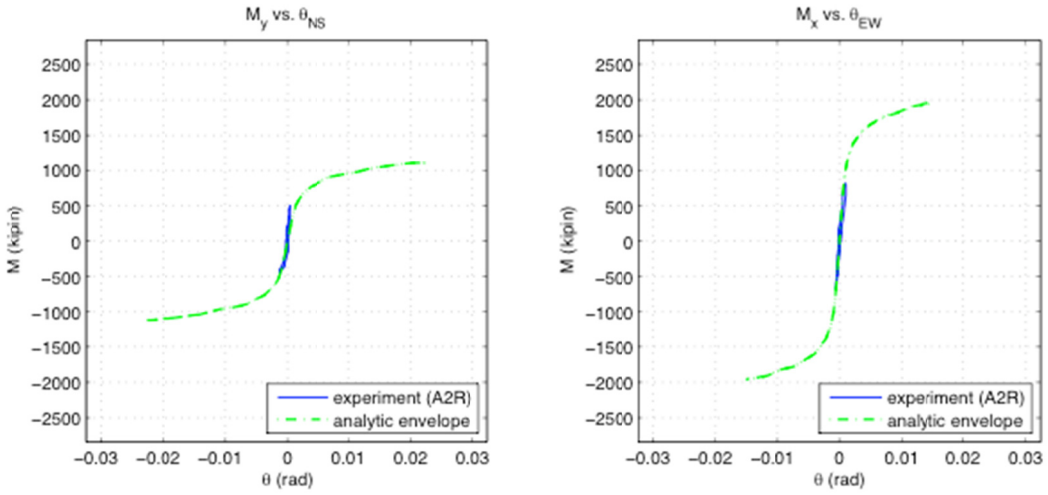

Figure 5.19 ***M-θ*** **analytic envelope $3D_c \times 5D_c$ footing (test A2R ENT springs).**

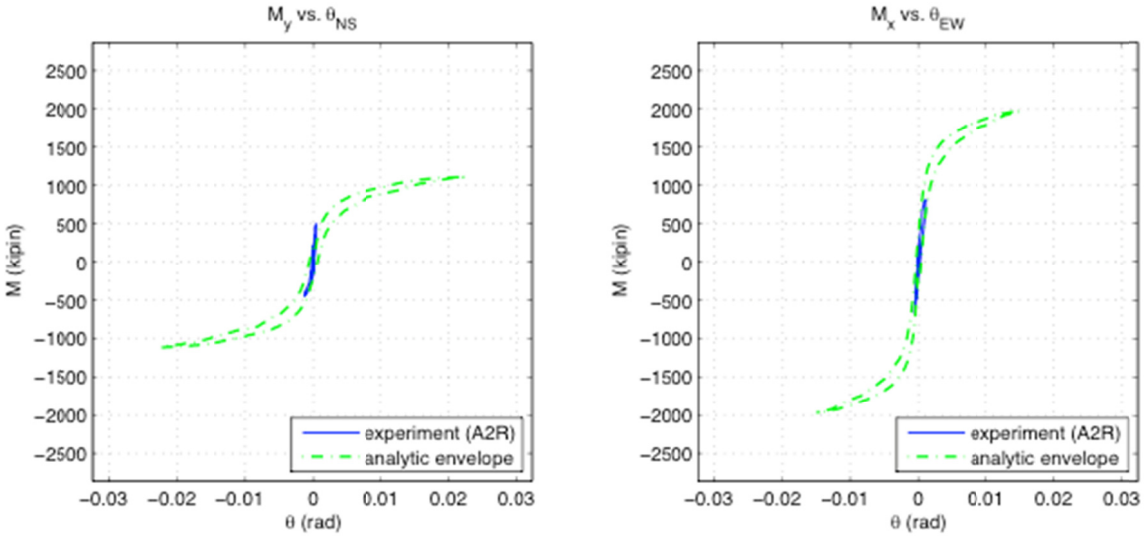

Figure 5.20 ***M-θ*** **analytic envelope of $3D_c \times 5D_c$ footing (test A2R neoprene springs).**

5.5 COMPARISON OF LINEAR ANALYSIS AND EXPERIMENTAL RESULTS

Several analytical models were evaluated for their ability to predict the observed specimen response. The analysis models considered had elastic footing response and column response that is linear or nonlinear. The tests performed were monitored for displacement, acceleration, and strains, which were used to validate the analysis models. The recorded natural modes of vibration, damping values of the system, and material properties were used to calibrate and conduct the analysis (see Chapter 4 for a summary of the experimental results). The material modeling assumptions for concrete, steel, and neoprene are described in Section 5.2. Element modeling options and assumptions for the neoprene pad, footing, column and superstructure weight blocks are described in Section 5.3.

The quantities of interest that were compared comprised key response parameters of an uplifting bridge system. The displacement quantities of interest include the footing uplift (or footing rotation) and the column center of mass displacement. The acceleration response of the center of mass was compared. Force quantities included the lateral force at center of mass, moment-curvature response at the column base, and the moment-footing rotation response.

The two ground motions used in the testing program varied combinations of the amplitude, time scale, and input directions; footing widths were also varied. A comprehensive list of all the test runs can be found in Appendix A. Because the volume of test results is too vast to present here, only the most relevant test runs and analytic comparisons are discussed. For all analyses the input accelerations used were those recorded by the shake table instrumentation and directly felt by the uplifting bridge pier system.

First, the simplest possible model was considered, which is the linear column coupled with the elastic footing model. After comparison and calibration of the footing and column for linear response, the model was enhanced to include nonlinear column response. The footing response was modeled as elastic for all column model assumptions (see Section 5.4). Linear column analysis for the two-column footing width test groups ($3D_c \times 3D_c$ and $5D_c \times 3D_c$) is described in Sections 5.5.1 and 5.5.3. Nonlinear column analysis is described in Section 5.6 for the $5D_c \times 3D_c$ footing width test group. Summaries and conclusions on the various column and footing analysis models are described in Section 5.7.

5.5.1 Design Axial Load and 3Dc × 3Dc Footing

The linear column response analysis compared analytic model predictions to experimental tests when the column behaved linearly. This includes all of the tests using a square footing configuration. Subsequently, the best model properties that captured displacements, forces, and accelerations were determined. The modeling options included the column type, which may be elastic, concentrated plasticity, or distributed plasticity models and either an ENT or neoprene vertical spring model for the footings. To calibrate the models to the observed response, the effective column stiffness, damping ratios, and spring spacing were adjusted.

Next, the analytic results were compared to the experimental results for the DS and FS test groups. The two groups exhibited the largest magnitudes of elastic column response for the Los Gatos and Tabas input earthquake excitations, respectively. Three types of input acceleration were compared: 1D-*X*, 2D-*X*+*Y*, and 3D-*X*+*Y*+*Z*. The center of mass and footing displacements are compared in Section 5.5.1.1. A comparison of the center of mass acceleration is presented in Section 5.5.1.2. The comparison of the column moment-curvature response and footing moment rotations is described Section 5.7. The initial model used had an elastic column assumption, with ENT vertical springs for the footing. Table 5.2 summarizes the combinations of models used for the uplifting system when in the elastic range.

Table 5.2 Linear analysis modeling options.

Column	Footing Vertical Springs	Materials
Elastic	Elastic-No-Tension (ENT) Neoprene (NEO)	-
Distributed Plasticity (DIST)	Elastic-No-Tension (ENT) Neoprene (NEO)	Concrete02 Steel02 Reinforcing Steel
Concentrated Plasticity (BWH)	Elastic-No-Tension (ENT) Neoprene (NEO)	Concrete02 Steel02 Reinforcing Steel

5.5.1.1 Displacements

The linear analysis displacement histories were compared to measured displacement for the square configuration footing subjected to the one-dimensional input excitation for the Los Gatos (D1S) and Tabas (F1S) test runs. Figure 5.21 and Figure 5.22 show the center-of-mass displacement response for an elastic column model with ENT or neoprene vertical springs subjected to D1S. The center-of-mass displacement response for an elastic column model with ENT or neoprene vertical springs are presented in Figure 5.23 and Figure 5.24 for F1S.

The analysis was repeated using the alternate distributed plasticity or lumped plasticity column model assumptions. Figure 5.25 and Figure 5.26 show the center-of-mass displacement of test D1S using a distributed plasticity column model with either vertical spring material. This analysis was repeated using the lumped plasticity column model. Figure 5.27 and Figure 5.28 show the corresponding center-of-mass displacement for test D1S. Because of space limitations, the test F1S results that varied the column models are not shown.. The response in general was very similar to that shown for D1S.

Inspection of the one-dimensional input excitation results shows the elastic column model approximated very well the observed center-of-mass displacement response as did the lumped plasticity column model, which was expected since the behavior of the column was elastic. The distributed plasticity model did not predict the observed response as well due to difficulty in matching the initial stiffness of the column. To simplify the presentation, the contribution of column total displacement due to flexural and rocking was not shown in the column modeling and vertical spring material comparisons. In general, the accuracy of the various column models and vertical spring materials on flexure and rocking column displacement was in agreement with the observed center-of-mass displacement response. The ability to predict the flexural and rocking column displacement was investigated thoroughly for all combinations of column and vertical spring options presented herein and used as an evaluator.

Review of the relevant response quantities found that the best model available in determining for the elastic response of the test system for a one-dimensional input excitation is an elastic column model assumption with a neoprene vertical spring material. The elastic column model and lumped plasticity column model yielded similar results, but the elastic option is preferred because of its analytic simplicity. The hysteretic damping qualities of the neoprene vertical spring made it the preferred option because of its ability to capture observed damping of

the neoprene pad. The analytic damping options that best predicted the column and footing response was Rayleigh mass proportional only with 5–6% damping ratio.

The relevant displacement results for the one-dimensional input excitation D1S using the most appropriate model available are presented in Figure 5.29. The total center-of-mass displacement is shown in Figure 5.29(a). The contribution of column flexural displacement is shown in Figure 5.29(b). The lateral displacement of the center of mass due to rocking was represented by the footing rotation since they are analogous [see Section 4.2 and Equation (4.3)]. For test D1S, the comparison is shown in Figure 5.29(c). Figure 5.29 shows the initial stiffness and free vibration phase at the end of the signal tracking reasonably well, as does the damping, which is indicated by the signal attenuating after the forced vibration phase ends. The peak column displacements seemed to track reasonably well given the complexity of the uplifting and deforming column system. The peak total displacement, flexural displacement, and rocking displacement all occurred at the peaks as those recorded. Their magnitude was within 15%, 27%, and 26%, respectively, of the recorded results. The acceleration and moment-deformation results are discussed in Sections 5.5.1.2 and 5.5.2.3, demonstrating that they also approximated with acceptable accuracy the observed response.

Using the most appropriate model developed for the one-dimensional input analytic comparisons the column model was investigated for two-dimensional and three-dimensional input excitation. The center-of-mass displacement results for the Los Gatos tests are shown in Figure 5.30(a)-(c) for the two-dimensional input excitation test D3S and Figure 5.31(a)-(c) for the three-dimensional input excitation test D5S. Inspection of the results shows that test D3S approximated the results reasonably well. The peaks occurred at the same time and were within 22%, 20%, and 20% for the peak column total, flexural, and rocking displacement, respectively. The forced vibration phase tracked very well, deviating during the free vibration phase (approximately 15 sec and beyond). Although the system appears to be slightly over damped for the two-dimensional input excitation,, attempts to reduce the damping and lengthen the period in the free vibration phase negatively affected the peak displacements. The test results indicate that the two-directional input excitation affects the natural period of the system along the diagonal.

Inspection of the results for test D5S show the analysis predicted the peak displacements reasonably well, within 15%, 9%, and 11% for the peak column total displacement, flexural displacement, and rocking displacement, respectively. Although the stiffness of the system during the forced vibration phase of the signal also tracked reasonably well, the analytic model is over damped during the free vibration phase. Again, attempting to reduce the damping overestimated the peak displacements significantly for the three-dimensional input excitation.

Comparison of the analytic versus experimental displacement results are given in Figure 5.36 using the most appropriate column model. The peak column displacements were within 17%, 5%, and 11% of the observed column total, flexural, and rocking values, respectively. Note that in the *Y*-direction the analytic prediction deviated from the observed response, which is due mostly to filtering of the recorded input signal for high-frequency content; when the original signal was used the analysis tracked well. The noise generated in the analytic prediction, however, was significant and affected the ability to evaluate the model. Therefore, the results using the filtered signal are presented, because the overall clarity outweighs the distorted signal at this time step.

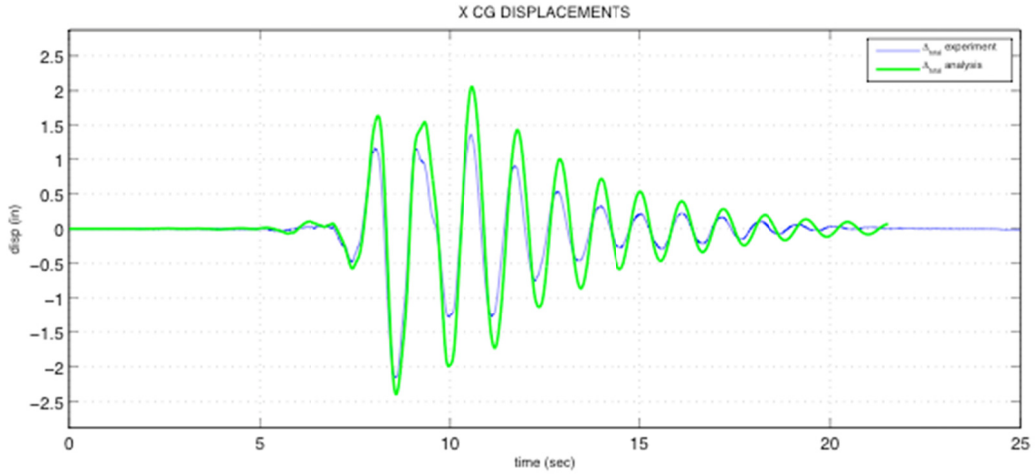

Figure 5.21 Center mass displacement – elastic column ENT springs (D1S).

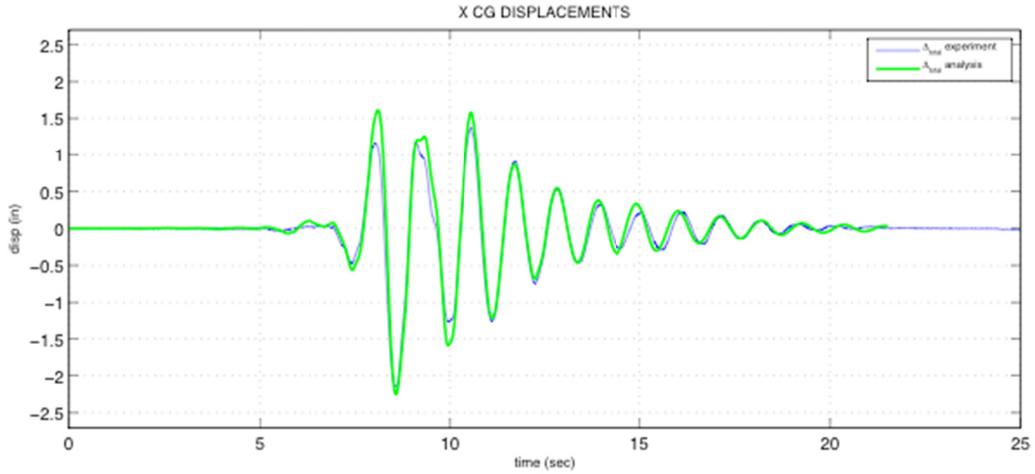

Figure 5.22 Center mass displacement – elastic column neoprene springs (D1S).

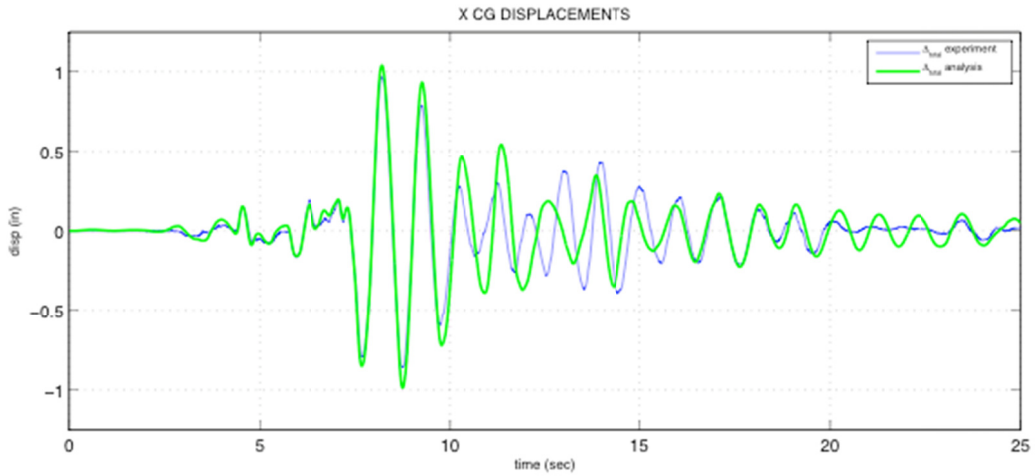

Figure 5.23 Center mass displacement – elastic column ENT springs (F1S).

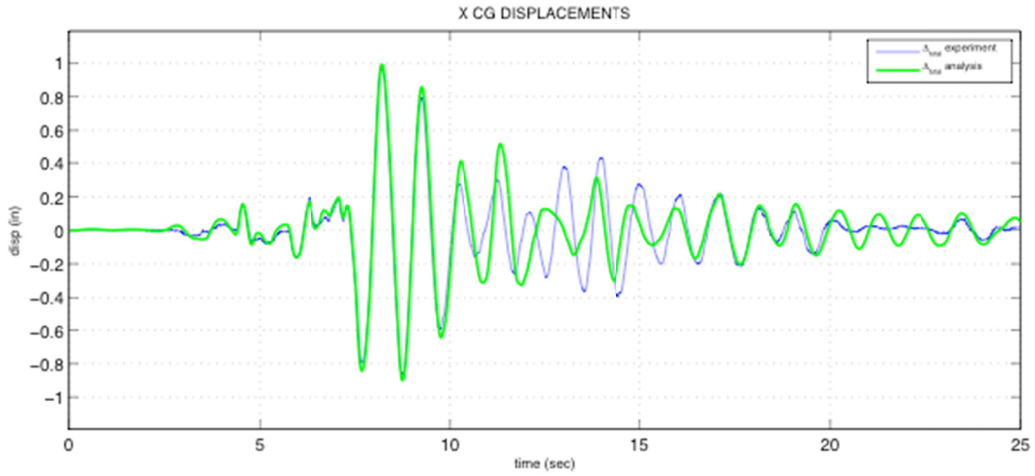

Figure 5.24 Center mass displacement – elastic column neoprene springs (F1S).

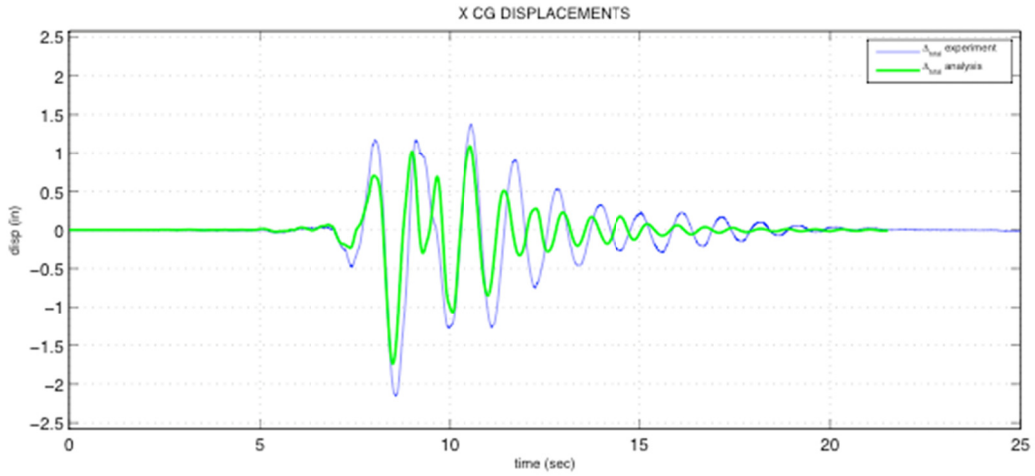

Figure 5.25 Center mass displacement – distributed plasticity column ENT springs (D1S).

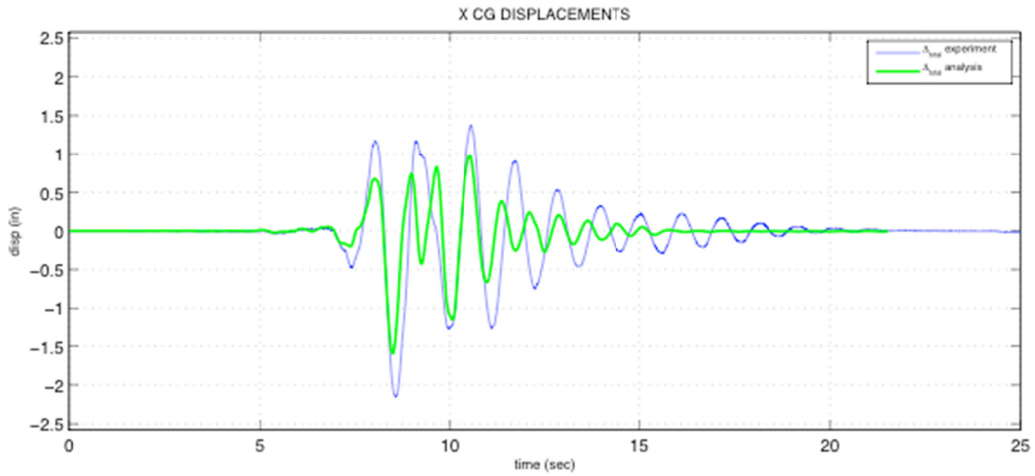

Figure 5.26 Center mass displacement – distributed plasticity column neoprene springs (D1S).

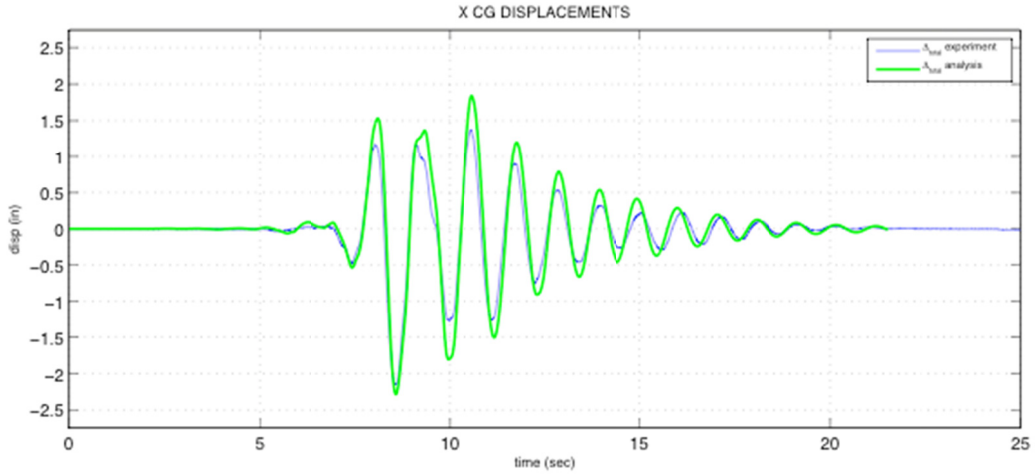

Figure 5.27 Center mass displacement – lumped plasticity column ENT springs (D1S).

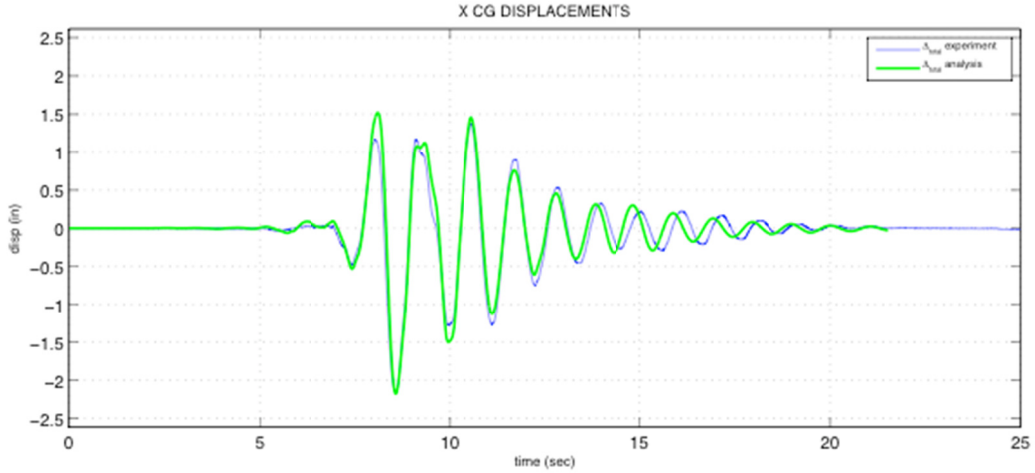

Figure 5.28 Center mass displacement – lumped plasticity column neoprene springs (D1S).

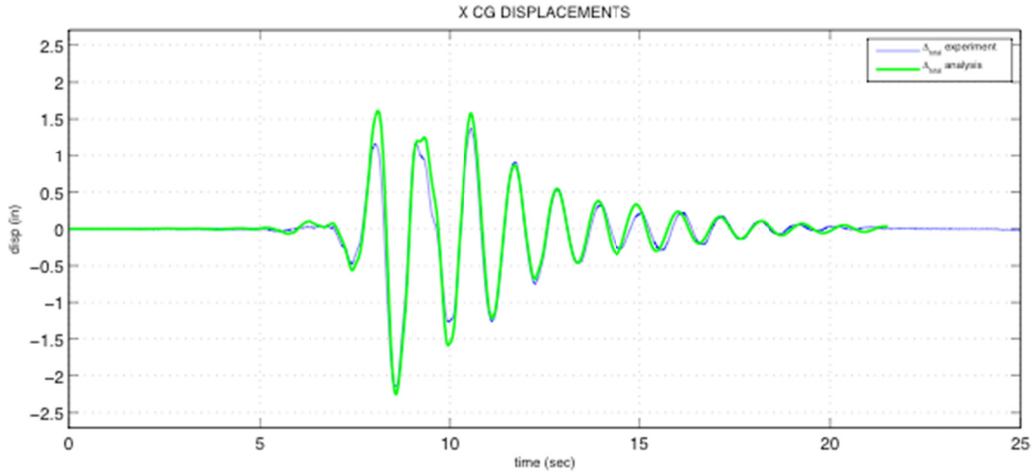

(a) column rotal center of mass displacements

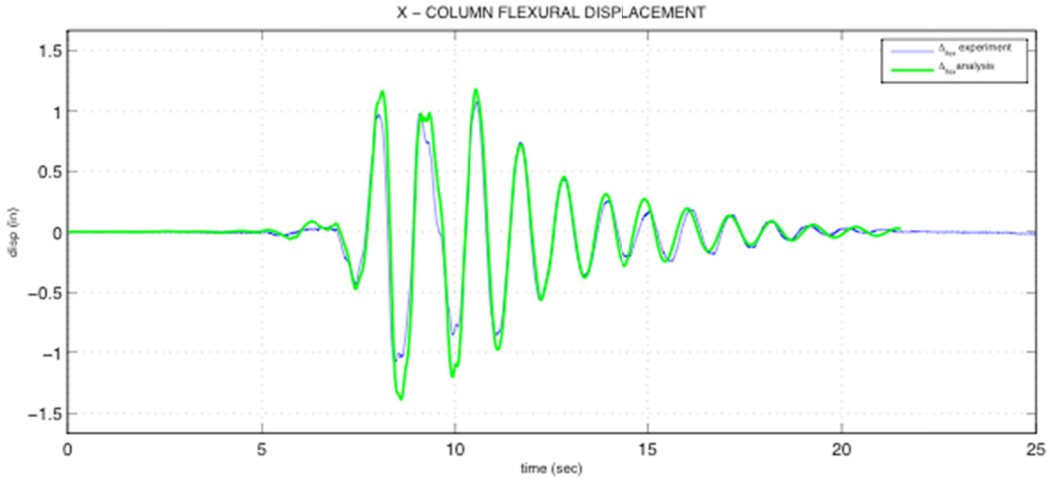

(b) column flexural displacements

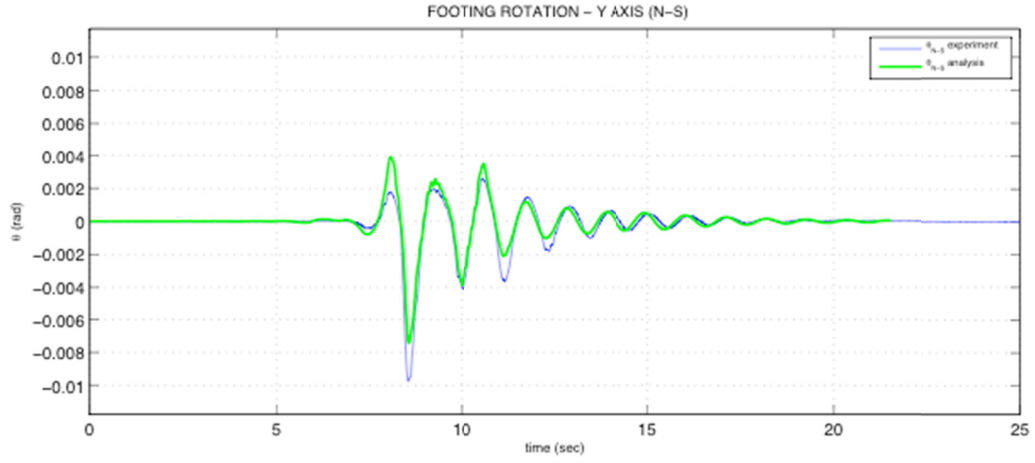

(c) footing rotation

Figure 5.29 Elastic column neoprene springs – displacements comparison (D1S).

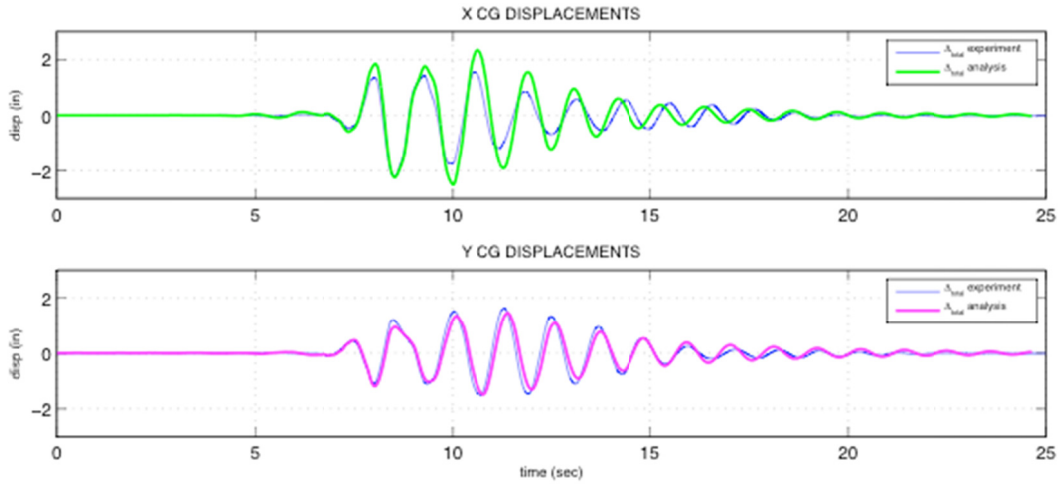

(a) column total center of mass displacements

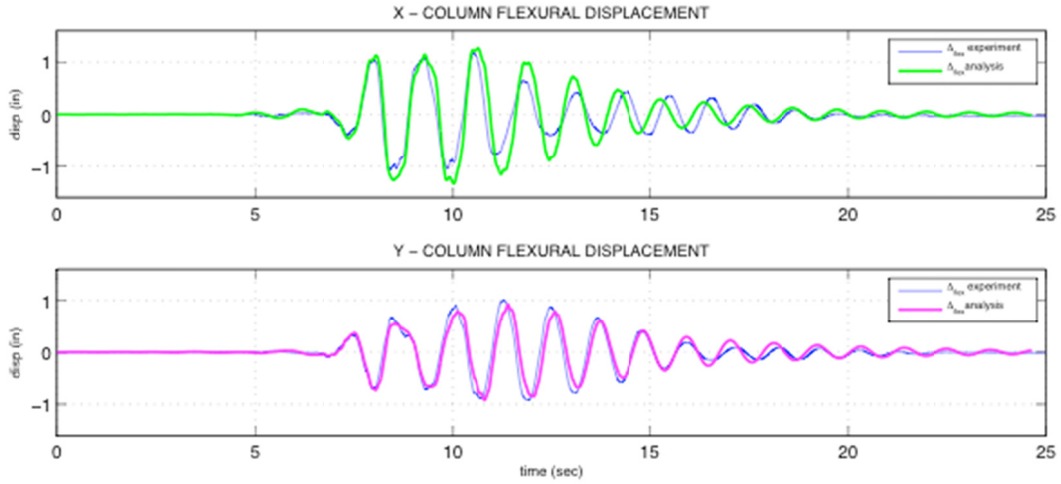

(b) column flexural displacements

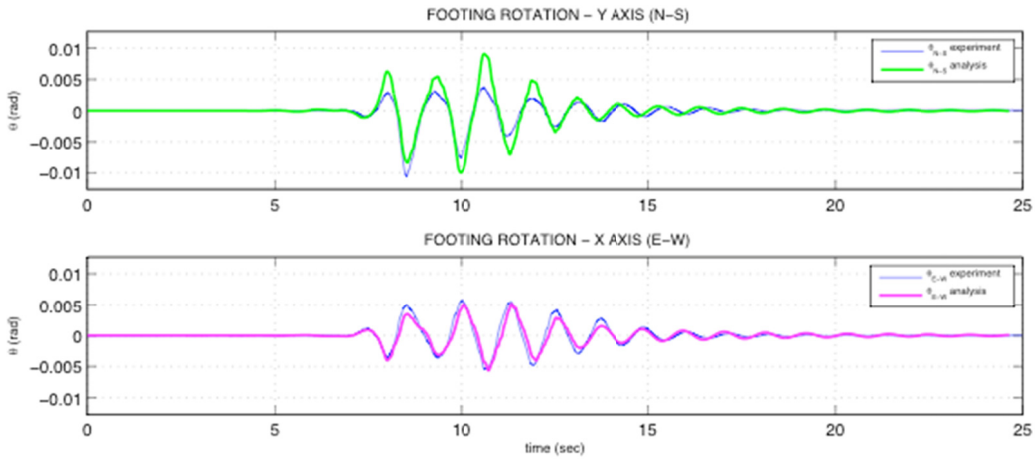

(c) footing rotation

Figure 5.30 Elastic column neoprene springs – displacements comparison (D3S).

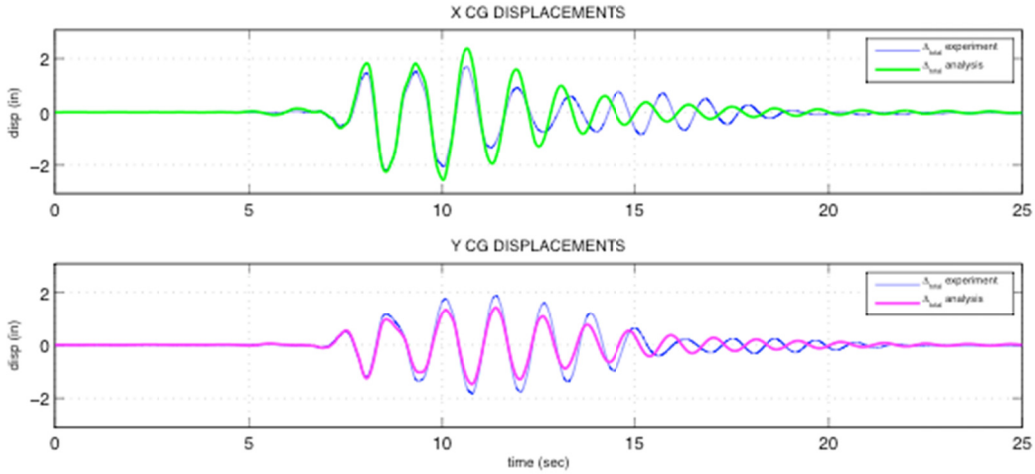

(a) column rotal center of mass displacements

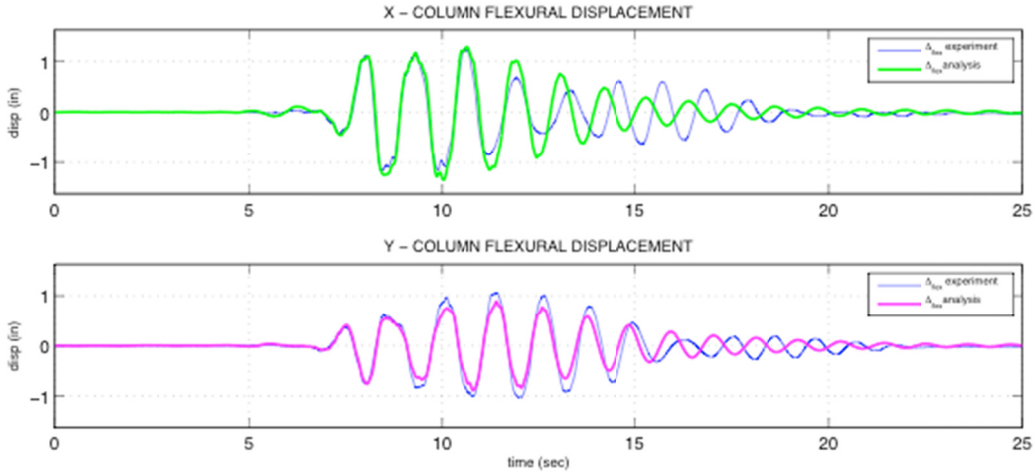

(b) column flexural displacements

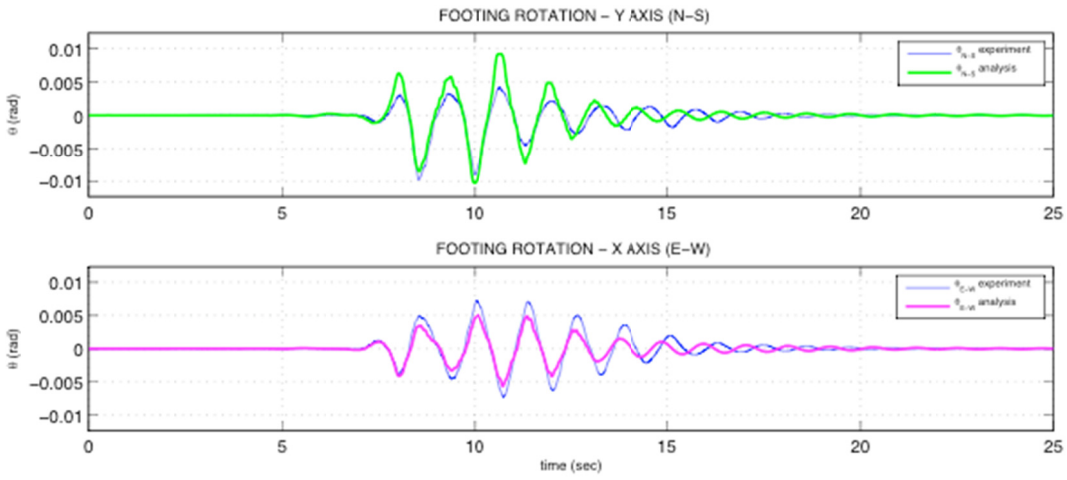

(c) footing rotation

Figure 5.31 Elastic column neoprene springs – displacements comparison (D5S).

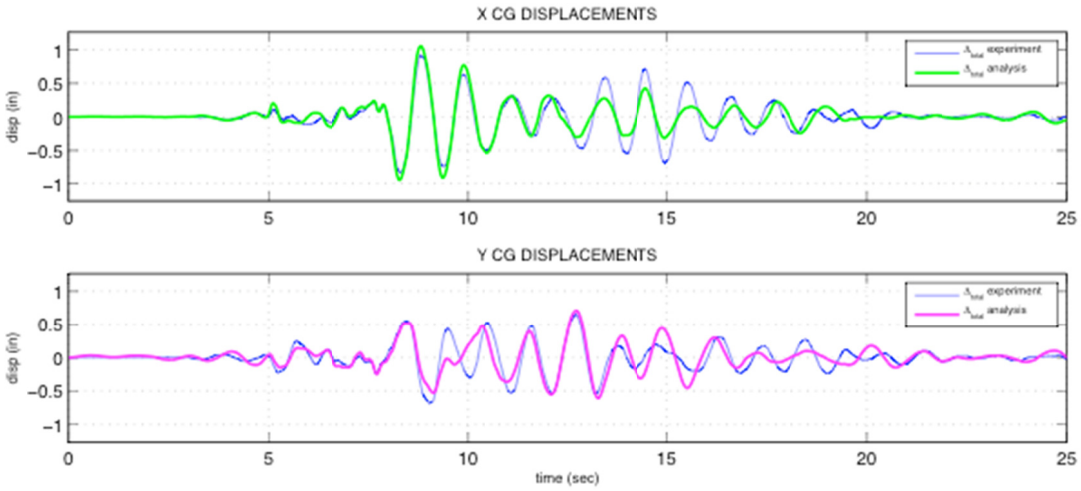

(a) column total center of mass displacements

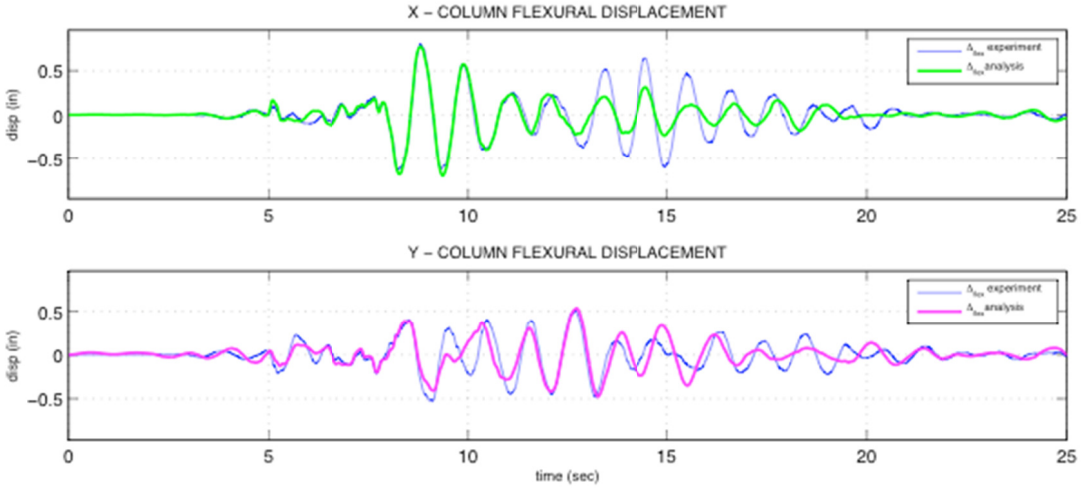

(b) column flexural displacements

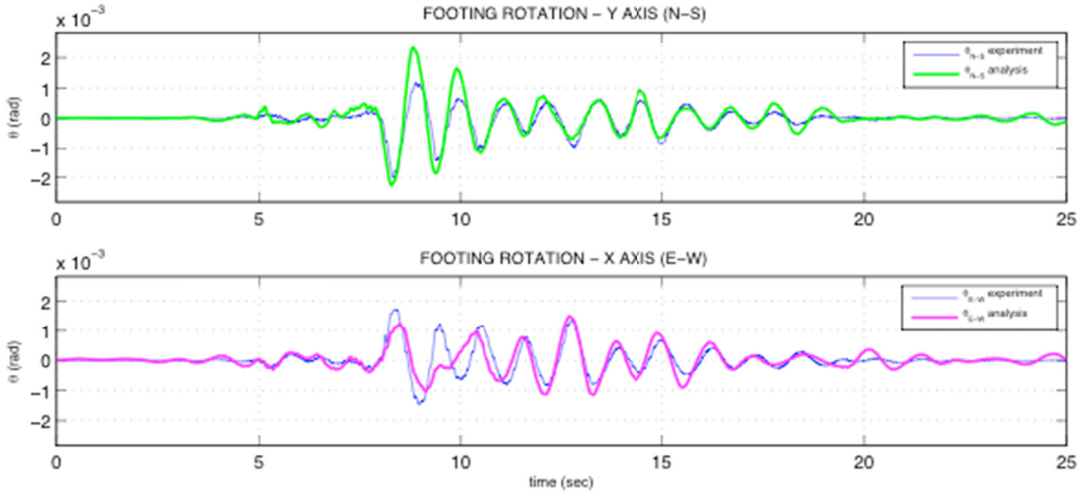

(c) footing rotation

Figure 5.32 Elastic column neoprene springs – displacements comparison (F5S).

5.5.2 Accelerations

The acceleration time histories for tests D1S, D3S, D5S, and F5S described in the displacement evaluations (Section 5.5.1.1) are shown in Figure 5.33 through Figure 5.36, In general, the accuracy of the analytic predictions tracked very well. The peak values appeared to occur at the same cycle and were within 25% of the recorded values. For test D3S and D5S the signal deviated during the free vibration phase, as discussed in the displacement comparison section. Test F5S tracked reasonably well and again deviated from the observed response in the *Y*-direction around the 9 sec mark.

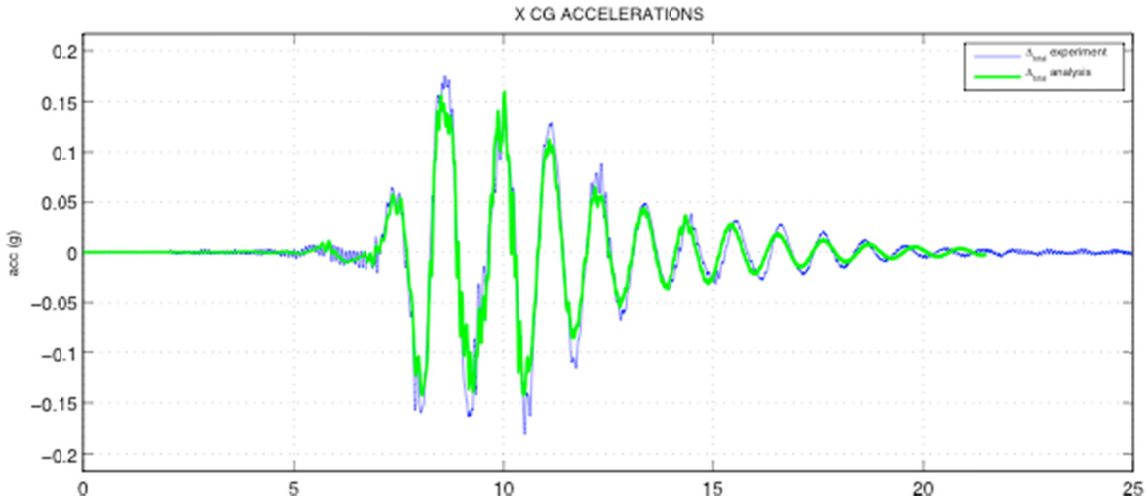

Figure 5.33 Center mass acceleration – elastic column neoprene springs (D1S).

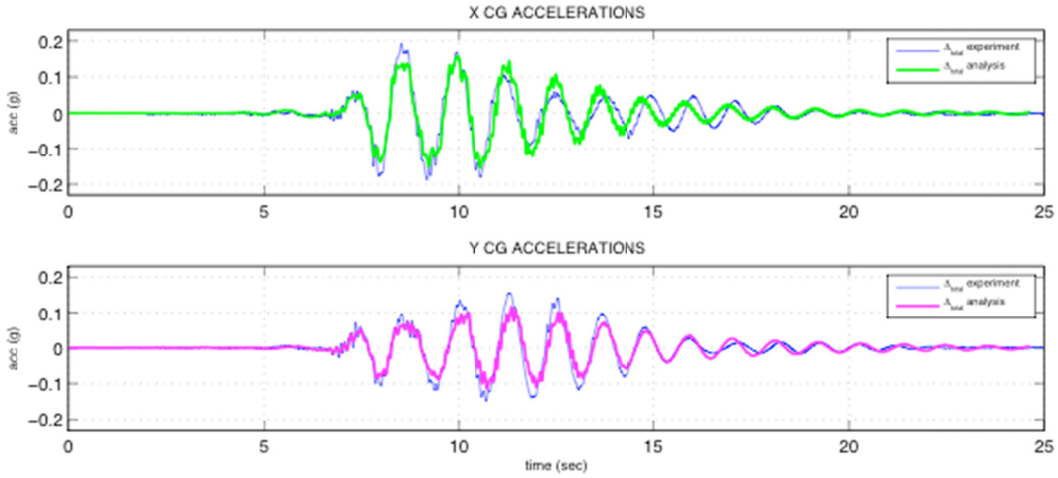

Figure 5.34 Center mass acceleration – elastic column neoprene springs (D3S).

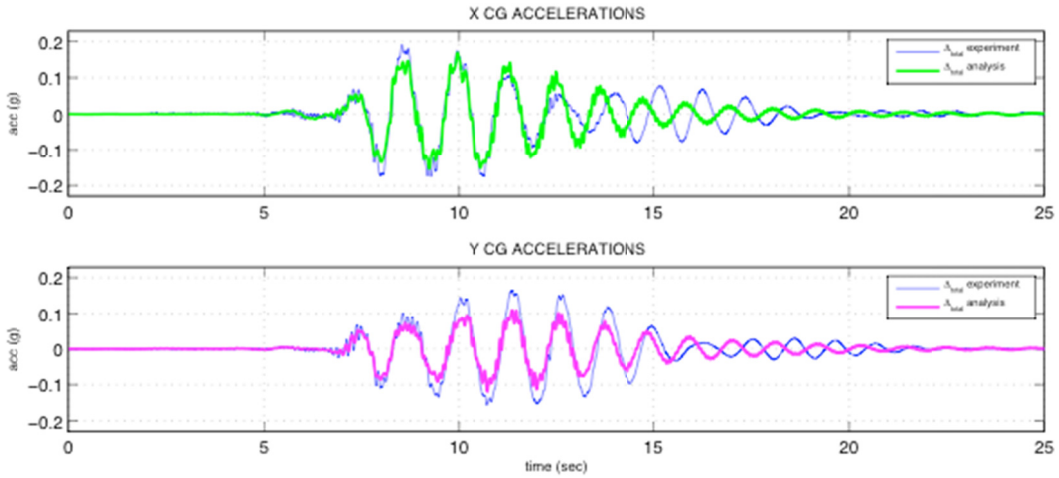

Figure 5.35 Center mass acceleration – elastic column neoprene springs (D5S).

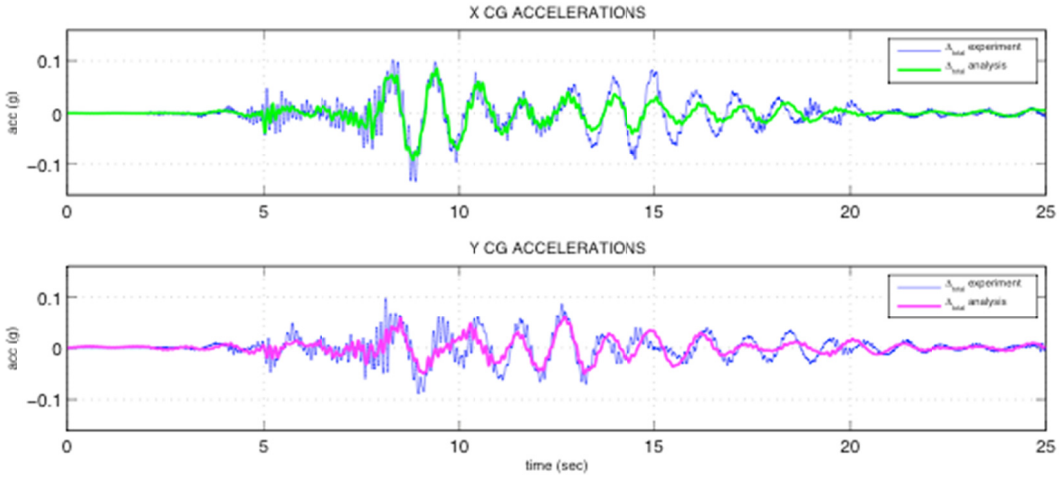

Figure 5.36 Center mass acceleration – elastic column neoprene springs (F5S).

5.5.2.1 Forces and Moments

Column base moment versus curvature (M-ϕ) and column base moment versus footing rotation (M-θ) comparisons are presented below for the relevant tests described in the displacement analysis (Section 5.5.1.1). The base shear versus center of mass displacement is not shown here.

Column Moment-Curvature: Figure 5.37 through Figure 5.40 compared the results of analytical models of the column base moment curvature test results for D1S, D3S, D5S, and F5S he with the observed response. In general, the prediction was reasonably good; the peak values of moment and curvature appear to match.

Column Moment- Footing Rotation: The column base moment footing rotation analytic prediction was compared to the experimental results and is shown in Figure 5.41 through Figure 5.44 for the tests D1S, D3S, D5S, and F5S. In general, the prediction agreed reasonably well with what was observed in the displacement comparison; the peak values of moment and

curvature appeared to match. Note that the observed rotational stiffness of the footing for F5S was higher than that predicted by the model. It is unclear if this is an aberration in the calculated results or a discrepancy in the model.

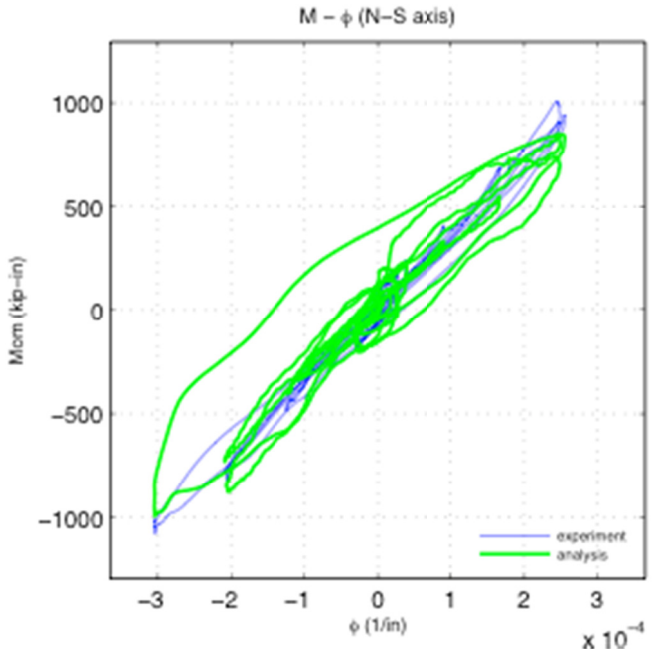

Figure 5.37 Column base *M-ϕ* – elastic column neoprene springs (D1S).

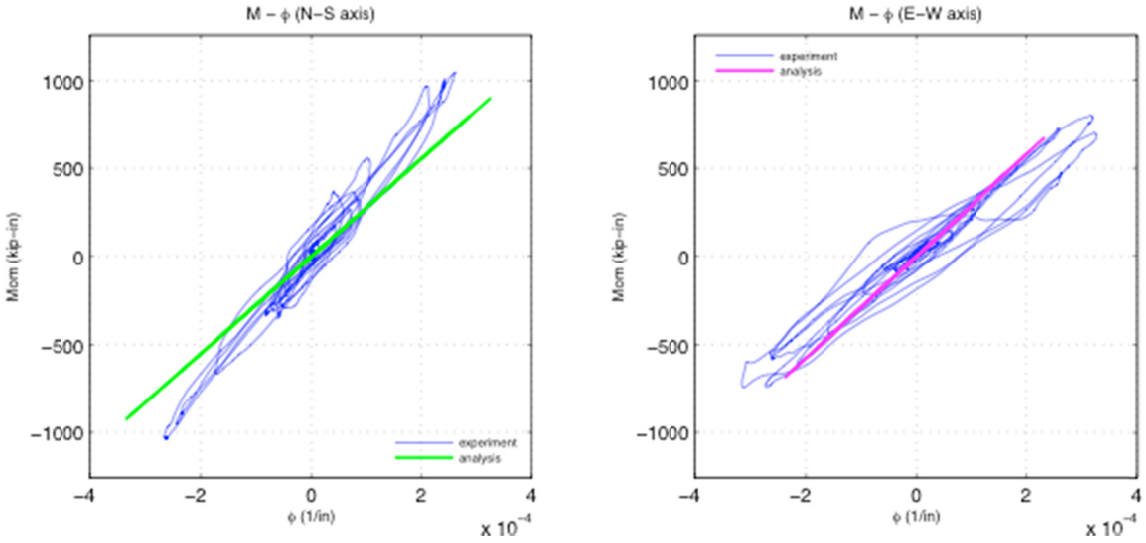

Figure 5.38 Column base *M-ϕ* – elastic column neoprene springs (D3S).

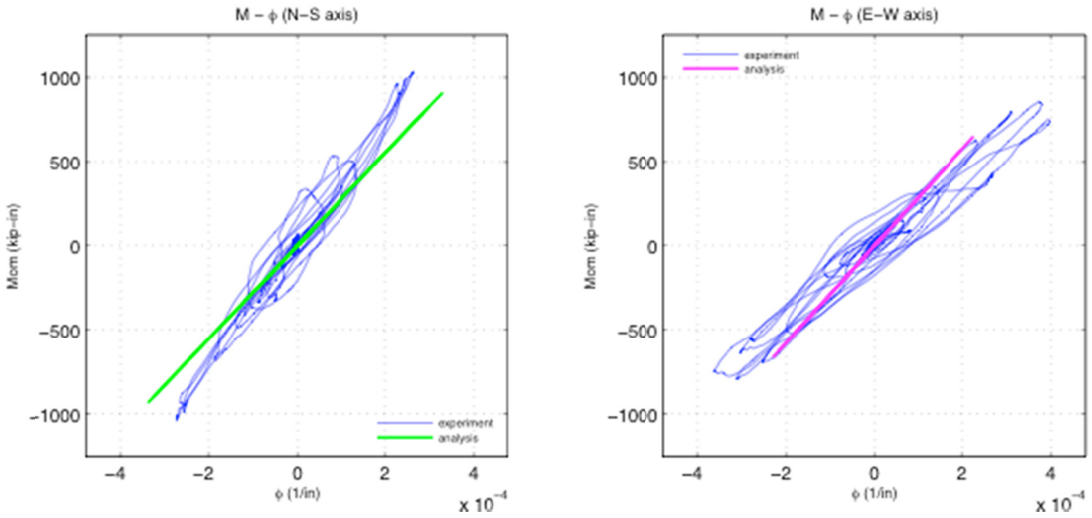

Figure 5.39 Column base *M-ϕ* – elastic column neoprene springs (D5S).

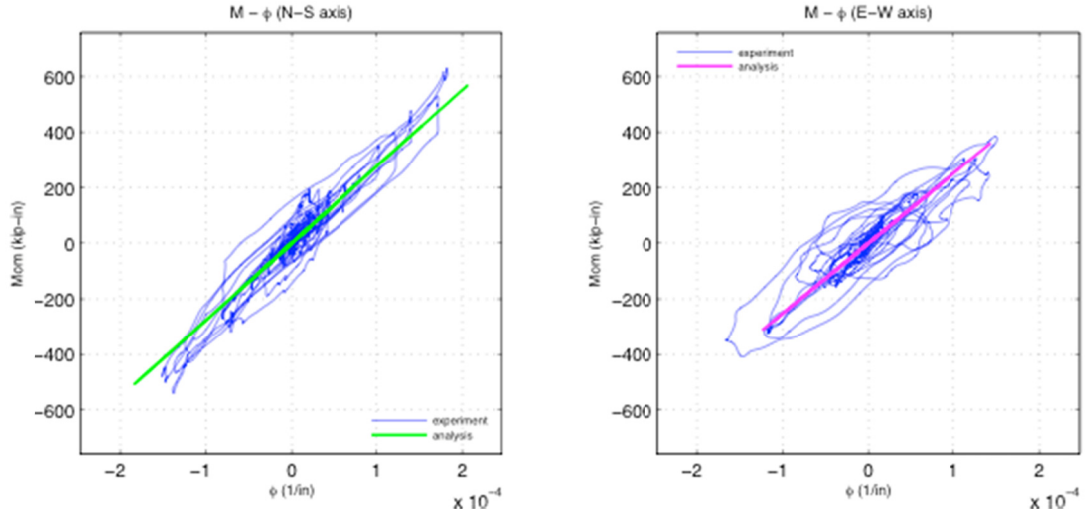

Figure 5.40 Column base *M-ϕ* – elastic column neoprene springs (F5S).

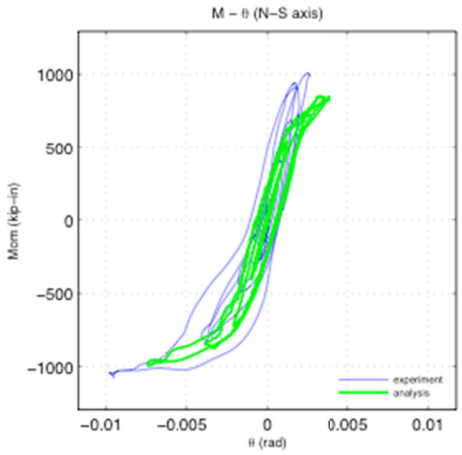

Figure 5.41 Footing moment rotation *M-ϕ* – elastic column neoprene springs (D1S).

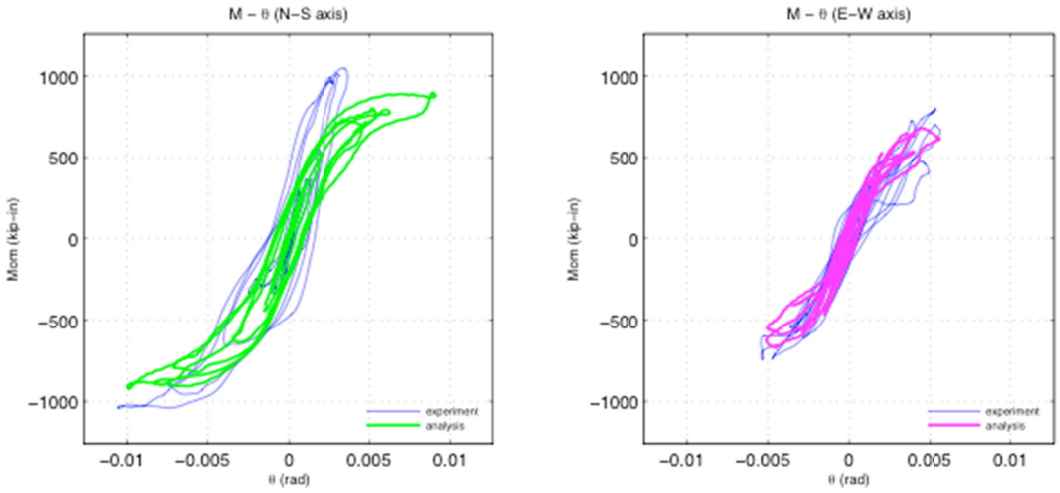

Figure 5.42 Footing moment rotation *M-ϕ* – elastic column neoprene springs (D3S).

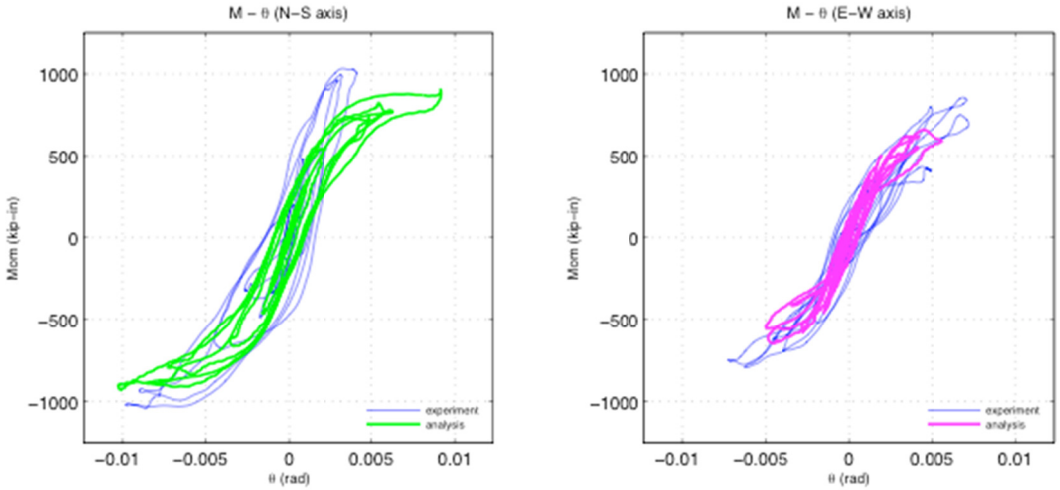

Figure 5.43 Footing moment rotation *M-ϕ* – elastic column neoprene springs (D5S).

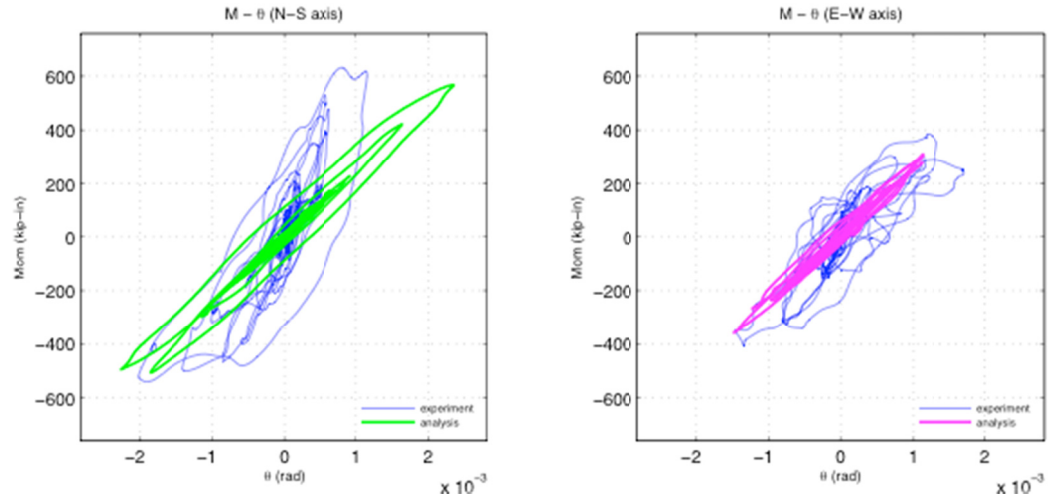

Figure 5.44 Footing moment rotation *M-ϕ* – elastic column neoprene springs (F5S).

5.5.3 Design Axial Load and 5Dc x 3Dc Footing

The test group AR has the widened footing (see Section 5.4.2). This test group had a widened footing in the *Y*-direction ($5D_c$ width) while the *X*-direction remained the same ($3D_c$ width). A discussion of the results for displacement, acceleration, and moment-deformation response is presented below. Of the two elastic tests done for this footing only configuration A2R is presented since it contained more significant column and footing response.

5.5.4 Displacements

Test A2R tested the column to incipient yielding. In general, the analytic models predicted the experimental results very well. The column total displacements, flexural displacements, and footing rotation are shown in Figure 5.45, Figure 5.46, and Figure 5.47. The peak values were within 5%, 5%, and 27% of the observed peak total, flexural and rotational column displacements, respectively. The stiffness and damping matched the observed response during the forced and free vibration phase of the bridge pier system.

5.5.5 Accelerations

Figure 5.48 compares the accelerations predicted by the analytical model versus the observed response In general, the peaks and natural periods matched very well. The analytic model prediction was within 20% of the observed peak values.

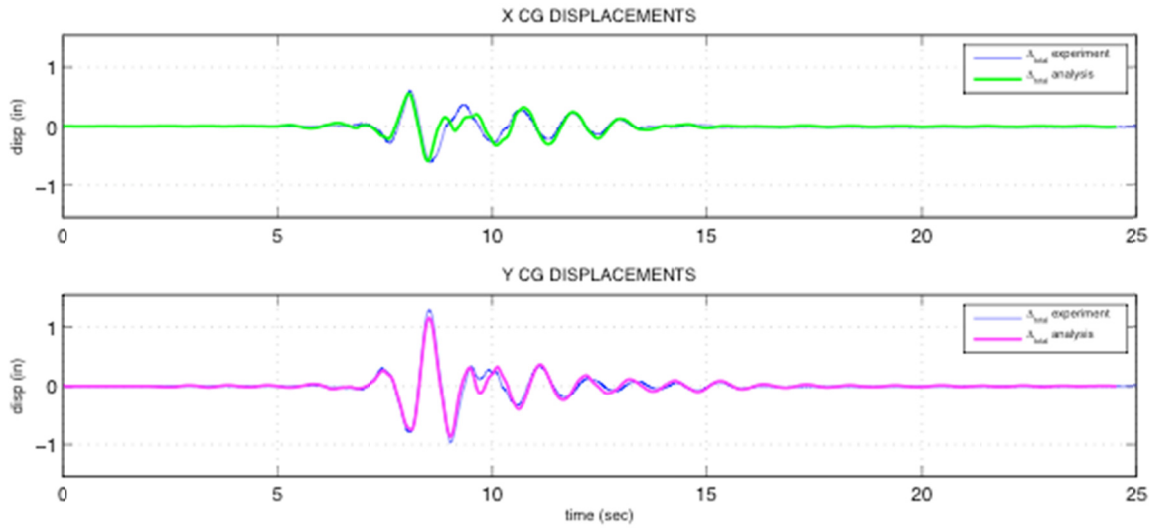

Figure 5.45 Center mass total displacement – elastic column neoprene springs (A2R).

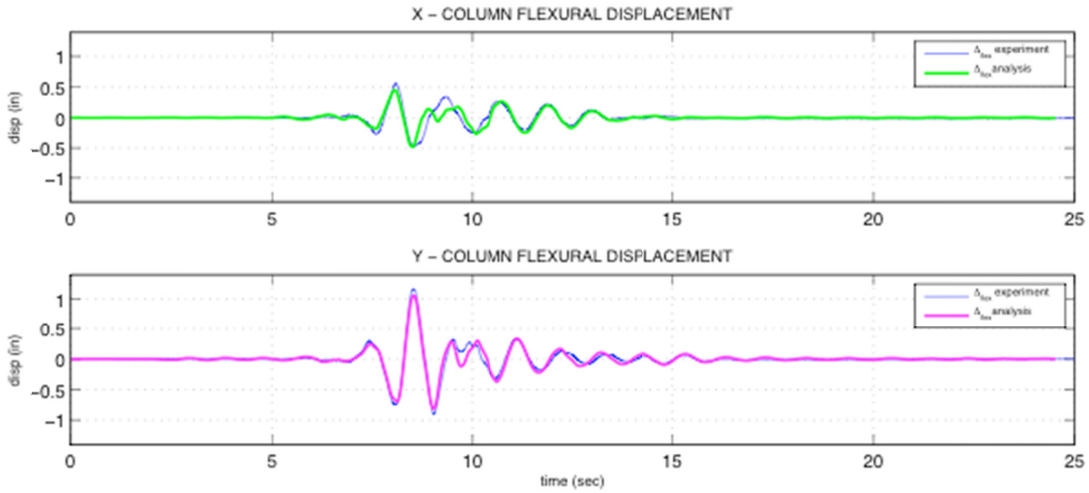

Figure 5.46 Center mass flexural displacement – elastic column neoprene springs (A2R).

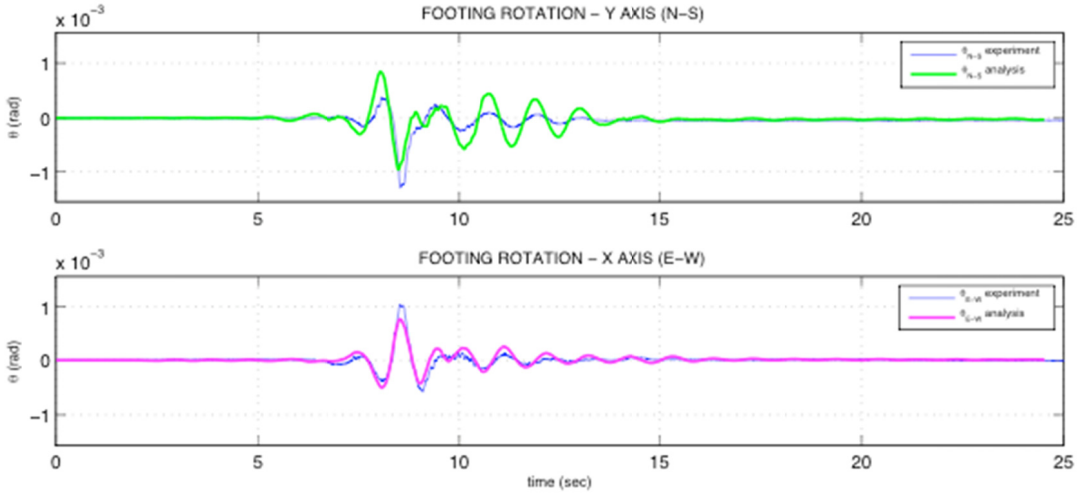

Figure 5.47 Footing rotation – elastic column neoprene springs (A2R).

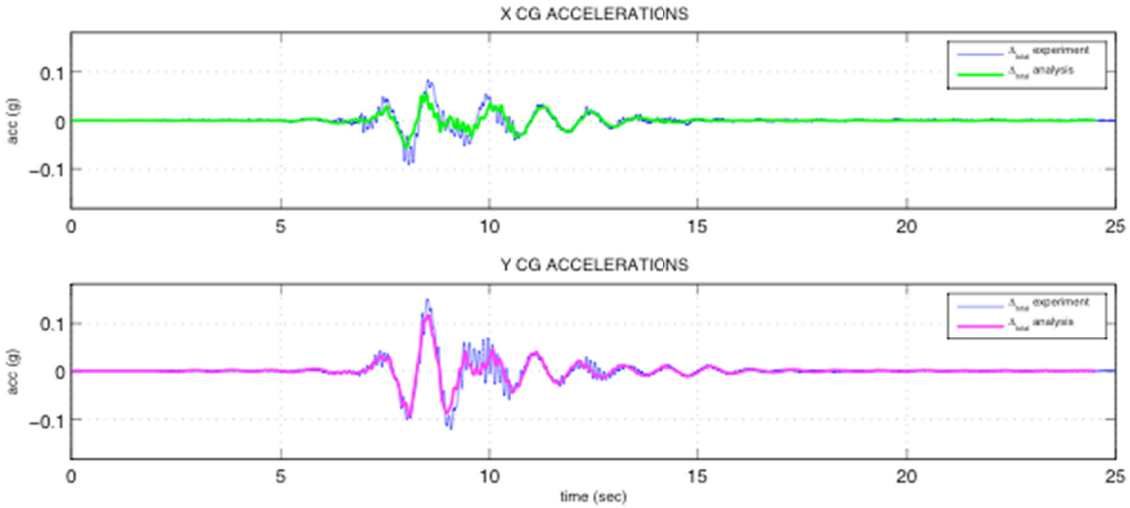

Figure 5.48 Center mass acceleration – elastic column ENT springs (A2R).

5.5.5.1 Forces and Moments

Comparison of the column base moment versus curvature (M-ϕ) and column base moment versus footing rotation (M-θ) are presented below.

Column Moment-Curvature: Figure 5.49 compares the analytical model versus observed response for test A2R in. In general, the prediction was reasonably good; the peak values of moment and curvature matched. As expected, the elastic column did not capture the cycle where a small amount of inelastic action occurred in the east-west direction.

Column Moment- Footing Rotation: Figure 5.50 compares the column base moment footing rotation predicted by the analytical model compared to the experimental results for test A2R. In the north-south narrow footing direction ($3D_c$), the experimental response was rotationally stiffer than the analytic prediction. In the wider footing direction the observed and analytic models agreed reasonably well.

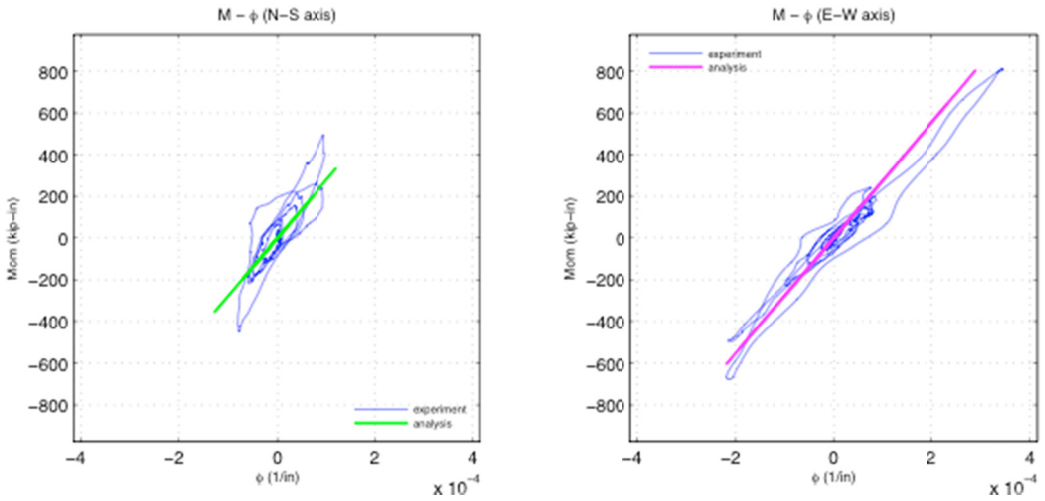

Figure 5.49 Column base M-ϕ – elastic column ENT springs (A2R).

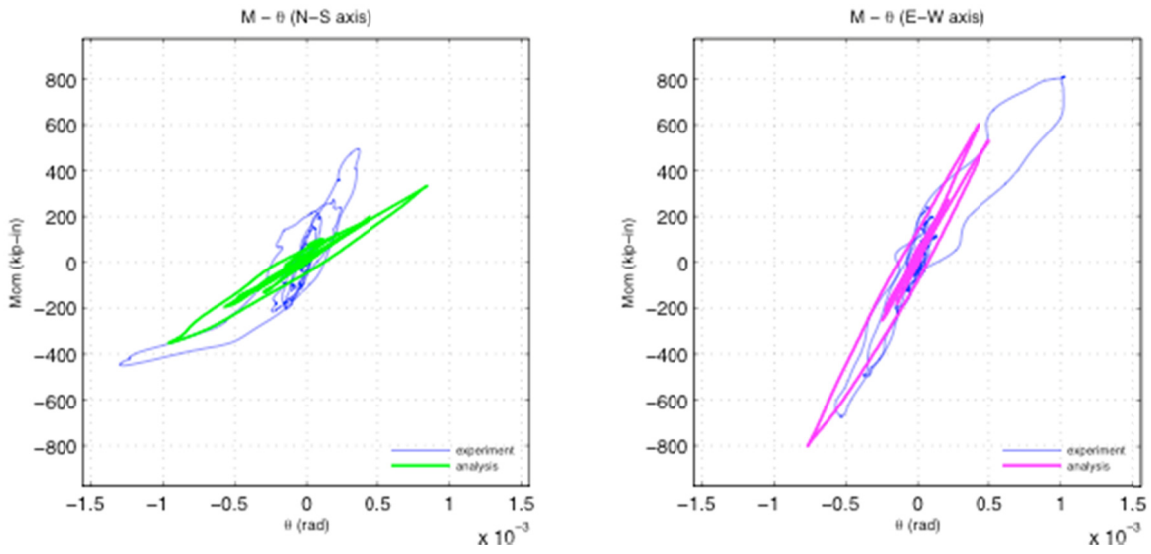

Figure 5.50 Footing moment rotation *M-θ* – elastic column ENT springs (A2R).

5.6 COMPARISON OF NONLINEAR ANALYSIS AND EXPERIMENTAL RESULTS

5.6.1 Design Axial Load and 5Dx x 3Dc Footing

Several analytical models were evaluated for their ability to predict the inelastic specimen response. The analysis models considered here have the ability to respond inelastically with an elastic footing and supporting soil. The goal here was to model a column footing system with simultaneous footing uplift and column yielding. The inelastic yielding of the column includes crushing of the core and cover concrete and/or yielding and fracture of the steel reinforcing bars. These combinations often lead to permanent drifts or residual displacements of the column center of mass. As noted previously, inelastic column response was observed during test runs A3R and A4R. The column model options for inelastic response are described in Section 5.3.2. In the experimental program the footing uplifted but remained elastic (see Section 5.4).

Initial efforts to model column yielding have focused on using fiber sections with distributed plasticity column elements (see Berry and Eberhard [2006] and Jeong et al. [2008)]. Results have shown there is a limited ability to accurately predict peak and residual displacements unless the initial stiffness accurately matches the observed initial stiffness. Even under these conditions, the magnitude of residual displacement is difficult to match. Recent work by Jeong et al. [2008] has shown improved prediction capabilities when using a concentrated plasticity column model that has fiber sections over a finite plastic hinge length at the column ends and elastic column response in between; this column model had been calibrated to the observed initial stiffness with a bilinear steel model or nonlinear backbone curve.

Properties of Nonlinear Column Models: All of the nonlinear models described herein use an elastic footing and soil model with a column model that uses fiber sections. The uplifting footing and column model with modeling options is shown in Figure 5.12.

1. Footing and soil uses a BNWF model.
2. Concrete using Kent-Park model with tension.
3. Steel modeled using bilinear or nonlinear backbone curve.
4. Fiber element model with distributed plasticity column model and five integration points along the column length.
5. Fiber element model with concentrated plasticity column model. One finite length plastic hinge at column base with two integration points. Remainder of column is elastic with effective column properties EI_{eff}.

Each of the models described above was used to predict the response of the specimen. The recorded three-dimensional (X+Y+Z) shake table accelerations were used as input ground motions. During the discussion of results the peak and residual displacements reported refer to the incremental change measured from the start of the given test run.

5.6.1.1 Displacements

Figure 5.51 to Figure 5.59 compare the analytical displacement time histories to experimental results for the multi-direction input accelerations of the center of mass and footing uplift, which is described herein via the footing rotation. The accuracy of the different models in predicting the column response and the footing uplift response is evaluated.

The base model used was the distributed plasticity column model (Nonlinear Beam Column) with a bilinear steel model option (**Steel02**) concrete modeled using **Concrete02** and neoprene springs. Using the measured material properties, Figure 5.51 shows the center-of-mass displacements for this model. The analysis of the design level earthquake (A3R) was repeated three times while varying either the column plasticity or steel model assumption. Results are shown in Figure 5.52 through Figure 5.54. Each model was reviewed and investigated to achieve best agreement possible between analysis and observed results. Evaluation was based on the initial stiffness, total displacement, column flexural, and rocking displacements at center of mass, footing uplift, and corresponding force deformation relationships.

Ultimately, the lumped plasticity column model with reinforcing steel provided the best approximation of the observed results. Figure 5.55 shows column flexural displacements for the design-level earthquake (A3R) and Figure 5.56 shows footing rotation displacements. Center-of-mass displacements for the maximum level earthquake (A4R) are presented in Figure 5.57. The column flexural displacements are presented in Figure 5.58. The corresponding footing rotation displacements are shown in Figure 5.59. Damping was observed to be low for this system (approximately 3.0%).

The residual displacements for the design-level earthquake (A3R) were approximately 1/2 in. and 1 in. in the X- and Y-directions, respectively, with a flexural ductility of approximately 6 (μ=u_{flex}/u_{yield}). The analytic model predicted 1/4 in. and 1/2 in., respectively in the X- and Y-directions. Considering the complexity of rocking system and large displacements, this seemed to be a reasonable approximation of the observed behavior. The maximum-level earthquake (A4R) with a residual displacement of 9 in. and 12 in. was more difficult to model. The most appropriate model predicted approximately 4 in. and 6 in. Several options were investigated to better capture the residual displacements, including modifying the concrete

descending region, steel hardening ratio, and the damping ratio. At this time no modifications appropriately captured the residual displacements while maintaining the observed current stiffness and damping qualities. Further work is warranted.

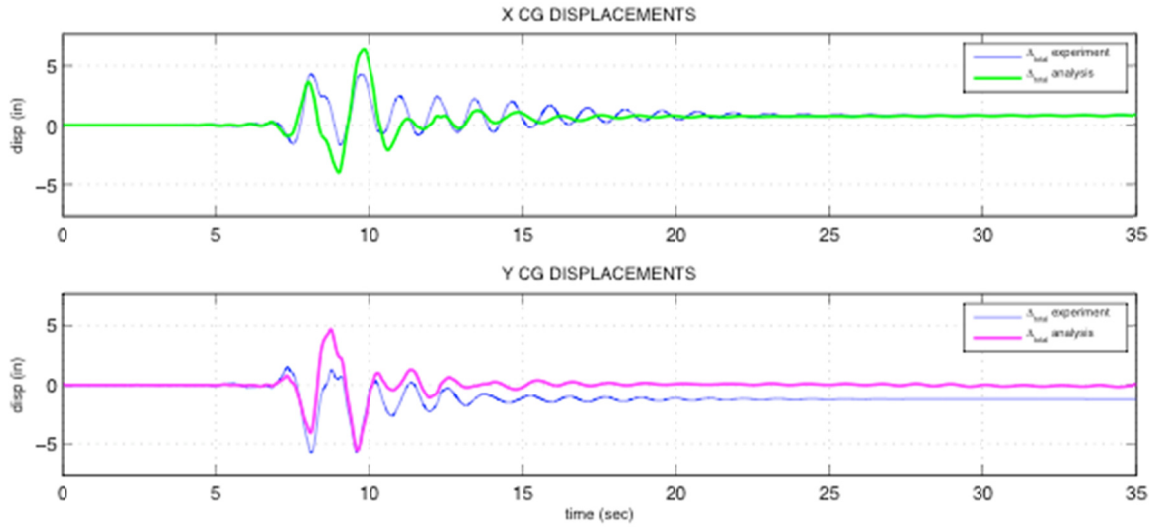

Figure 5.51 **Design .level earthquake – distributed plasticity column with neoprene springs CG displacements, bilinear steel (A3R).**

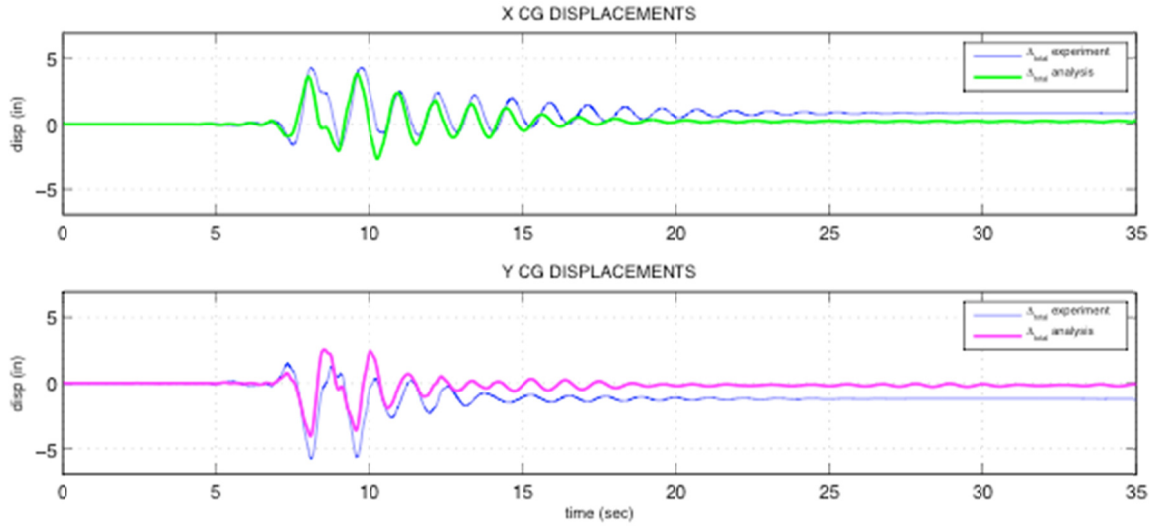

Figure 5.52 **Design-level earthquake - distributed plasticity column with neoprene springs CG displacements, reinforcing steel (A3R).**

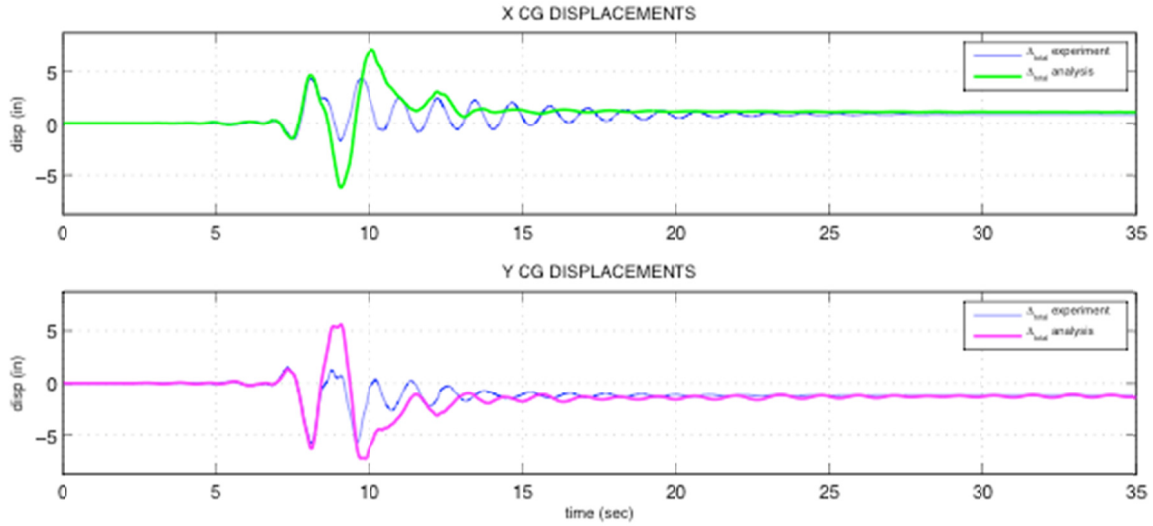

Figure 5.53 **Design-level earthquake concentrated plasticity column with neoprene springs CG displacements, bilinear steel (A3R).**

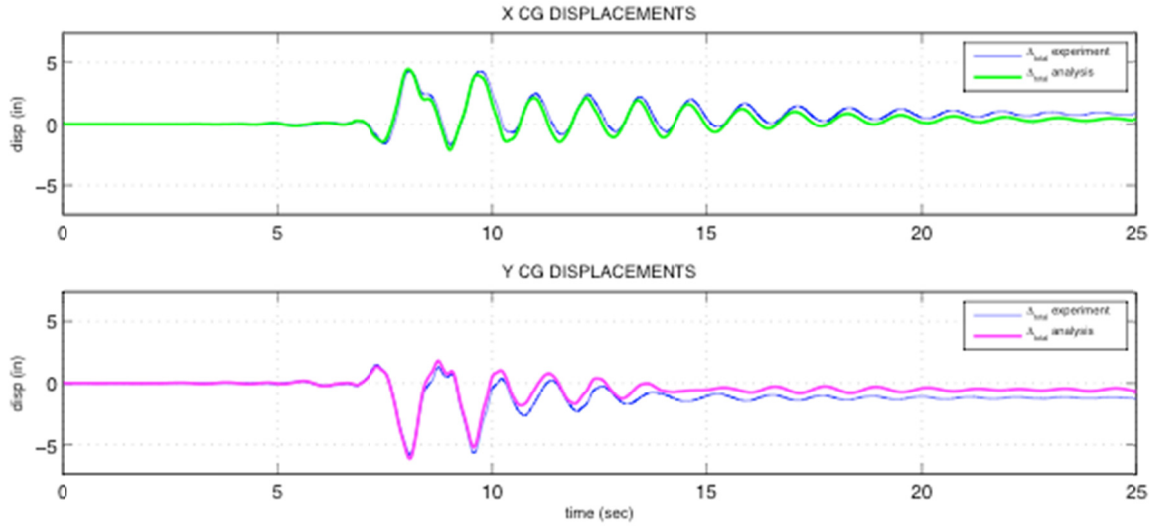

Figure 5.54 **Design-level earthquake concentrated plasticity column with neoprene springs CG displacements, reinforcing steel (A3R).**

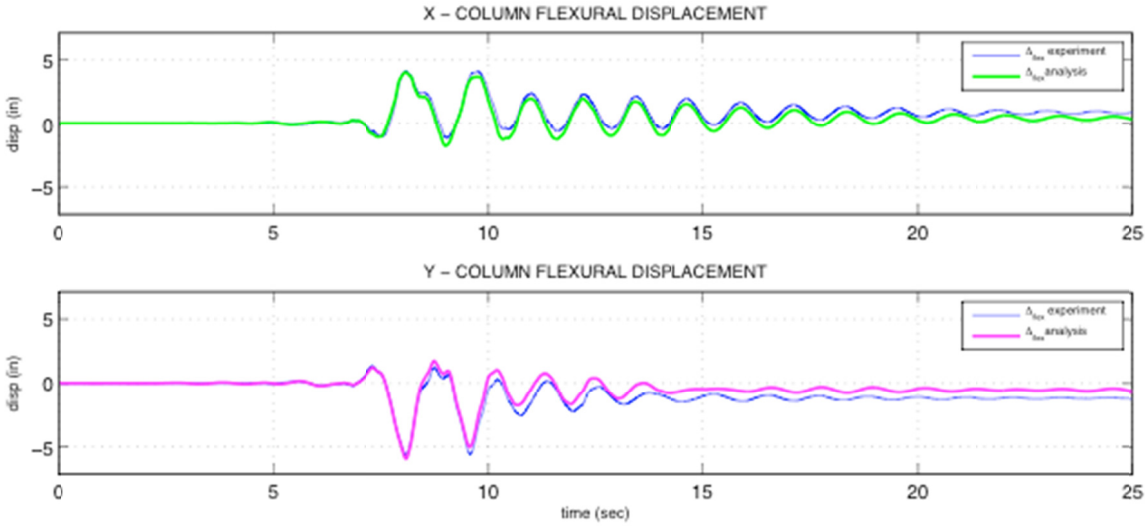

Figure 5.55 **Design-level earthquake concentrated plasticity column with neoprene springs column flexural displacements (A3R).**

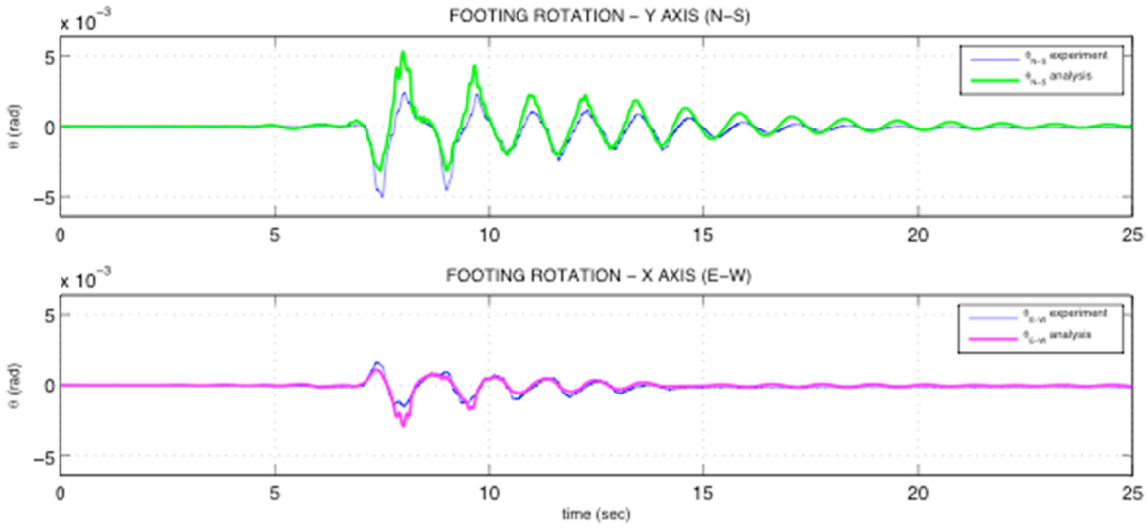

Figure 5.56 **Design-level earthquake concentrated plasticity column with neoprene springs footing rotation (A3R).**

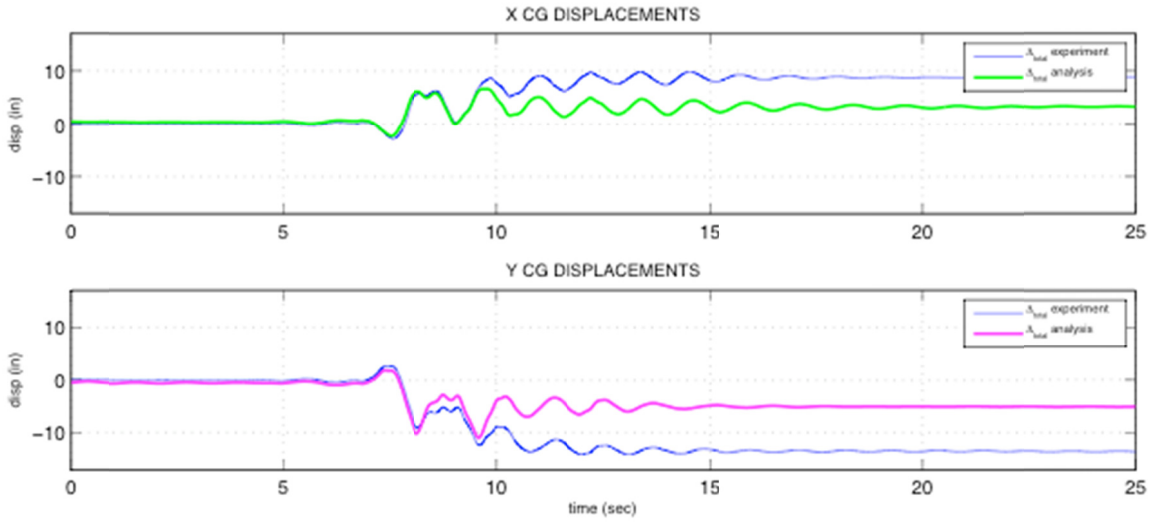

Figure 5.57 **Maximum-level earthquake concentrated plasticity column with neoprene springs CG displacements (A4R).**

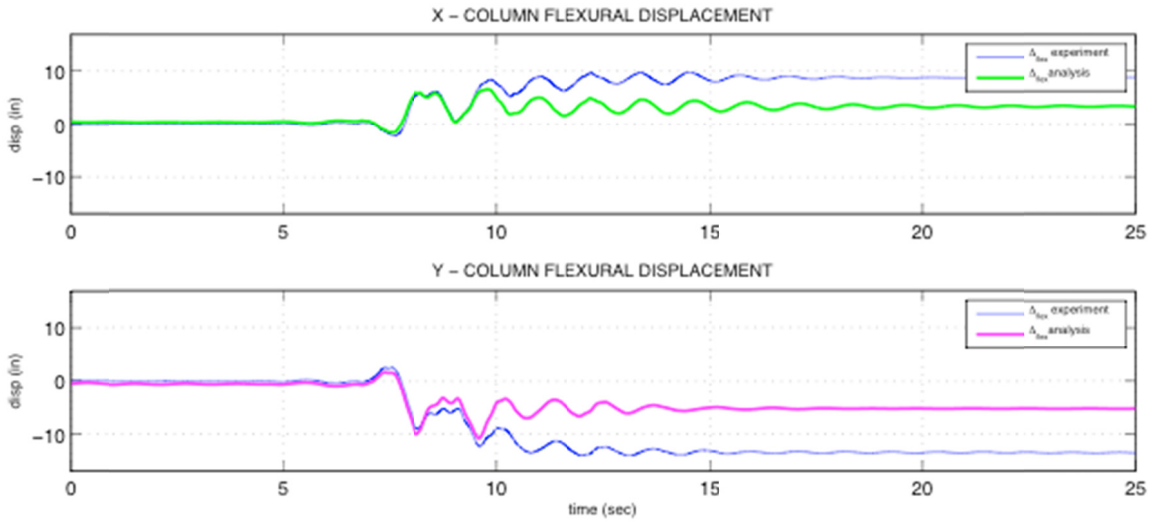

Figure 5.58 **Maximum-level earthquake concentrated plasticity column with neoprene springs column flexural displacements (A4R).**

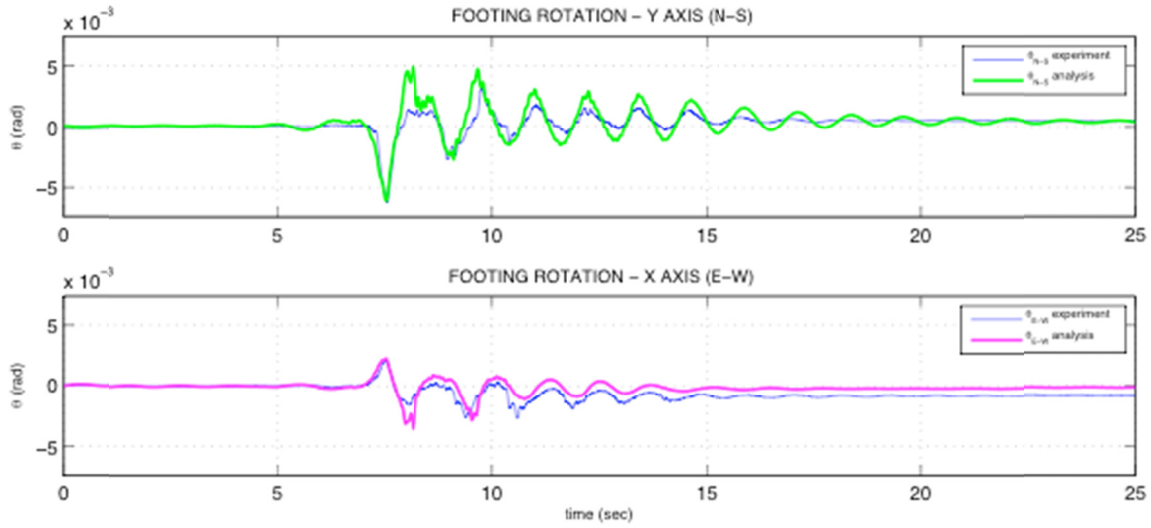

Figure 5.59 Maximum-level earthquake concentrated plasticity column with neoprene springs footing rotation (A4R).

5.6.1.2 Accelerations

The comparison of displacement response for the experiment and analysis shows that the Concentrated Plasticity column model with Reinforcing Steel provided the best approximation of the observed response. This best approximation is limited to the column and footing models discussed herein. In the interest of limited space, only the accelerations responses are shown. Figure 5.60 shows the acceleration time-history comparison for the design-level test A3R. The peak value magnitudes were approximately the same. Figure 5.61 shows the acceleration time history for the maximum level test A4R. The magnitudes of accelerations did not track well once the column experienced significant inelastic action. (See Section 5.6.1.1 for a discussion on modeling the inelastic response.) The residual acceleration of the experiment was not an observed behavior but rather a by-product of the accelerometer recording method.

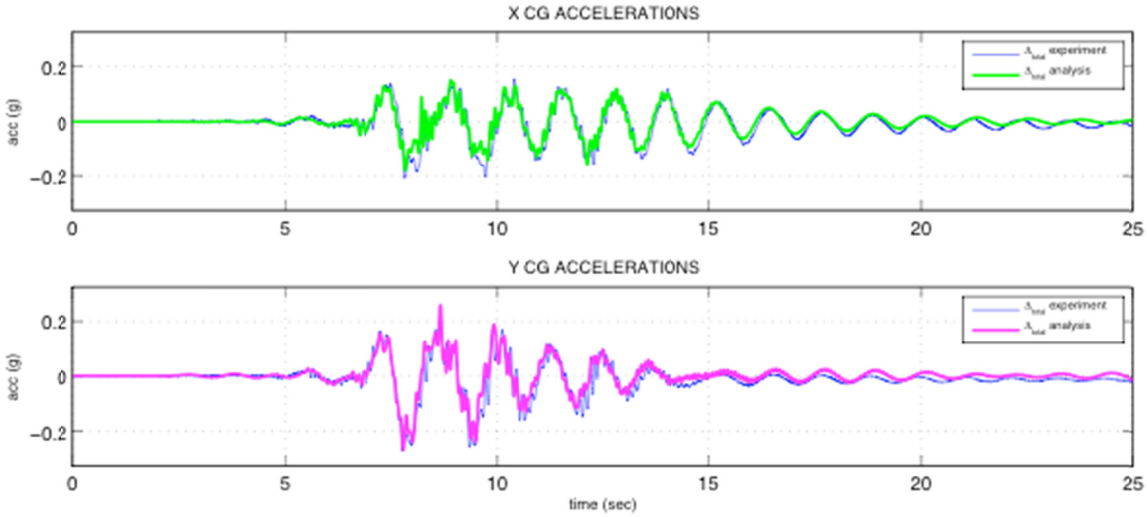

Figure 5.60 **Design-level earthquake concentrated plasticity column with neoprene springs CG accelerations (A3R).**

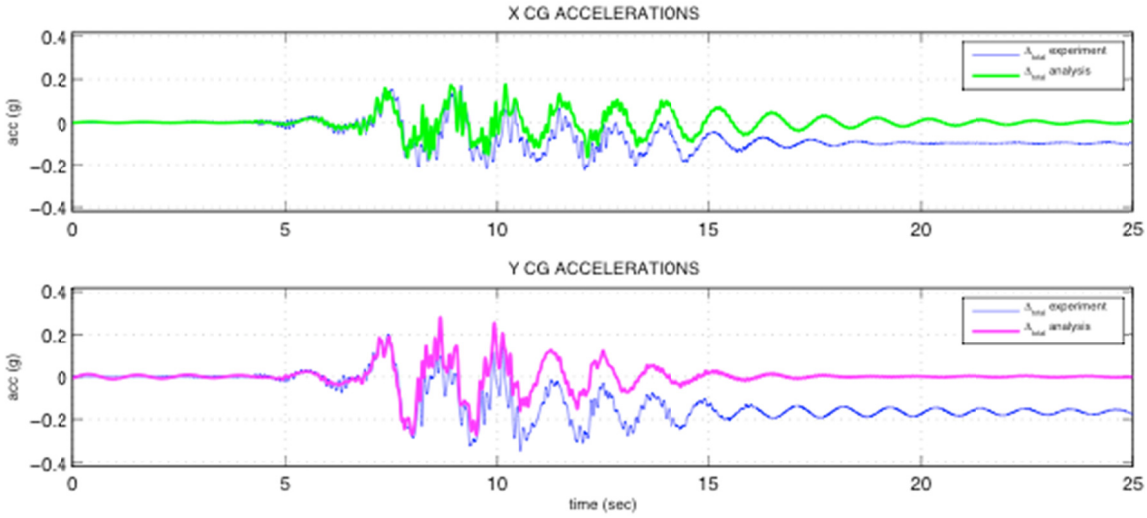

Figure 5.61 **Maximum-level earthquake concentrated plasticity column with neoprene springs CG accelerations (A4R).**

5.6.1.3 Forces and Moments

The inelastic response relationship of the column base moment to column base curvature and the footing rotation are shown in Figure 5.62 through Figure 5.65. Test A3R was set to the design-level acceleration and test A4R was set to the maximum-level acceleration. A comparison of displacement response for the experimental versus analytical response shows that the Concentrated Plasticity column model with Reinforcing Steel provided the best approximation of the observed response. Modeling of the inelastic response is especially complex when considering uplifting of the footing, requiring capturing accurately the stress-strain relationships that cause concrete crushing, reinforcement yielding, strain hardening, and buckling. Secondary P-Δ effects are significant here due to the large displacements of the center of mass.

The lumped plasticity column model with **ReinforcingSteel** material is the best option for modeling the column behavior because it allows for calibrating the column stiffness to the observed stiffness using effective properties. The distributed plasticity model does not allow for an adjustment of the observed effective column properties caused by cracks as a result of, among other things, small level earthquakes experienced by the system. The **ReinforcingSteel** option better captures the nonlinear behavior of yielding steel than the bilinear **Steel02** uniaxial material.

Column Moment-Curvature: The column base moment versus curvature response for the design-level test (A3R) is presented in Figure 5.62. The east-west axis experienced more significant inelastic response during testing, which was captured relatively well by the lumped plasticity column model with the reinforcing steel assumption; also predicted relationship well were the peak moment and peak curvature values. The moment at the column base due to residual displacement of the center of mass was not captured well by the analytic model, with the experimental results and analytic results being centered on differing values of M-ϕ at the end of the test. Although the north-south axis tracked relatively well, there was evidence of inelastic response in the analytic model that was not observed in the experimental test. The maximum-level test (A4R) moment curvature response is presented in Figure 5.63. The analytical versus experimental responses diverged due to the significant residual displacement not captured by the analytic model.

Footing Moment-Rotation: A comparison of column base moment to footing rotation is presented in Figure 5.64 for the design-level test (A3R) and Figure 5.65 for the maximum-level test (A4R). Although the responses tracked reasonably well, they were affected by the inability of the analytic model to capture the residual displacement. The residual displacement affected the column base moment calculation, which fundamentally altered the moment-footing rotation relationship.

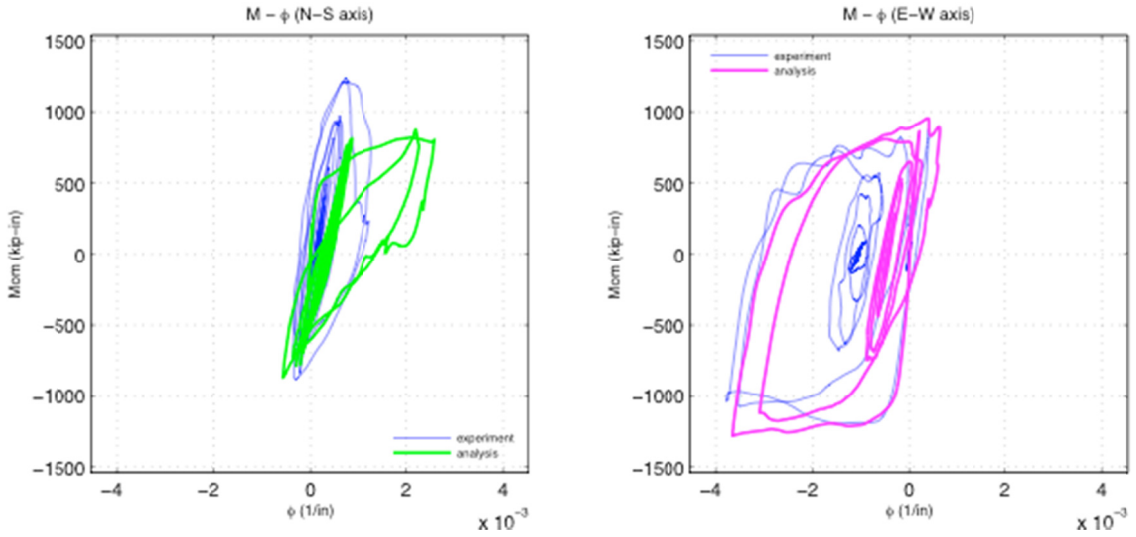

Figure 5.62 **Design-level earthquake concentrated plasticity column with neoprene springs column base *M*-ϕ (A3R).**

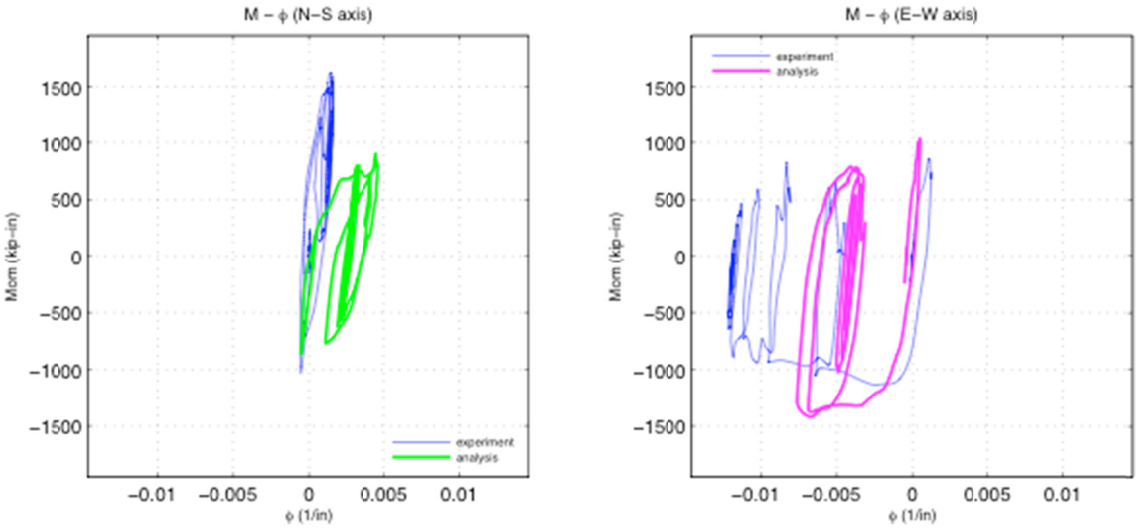

Figure 5.63 **Maximum-level earthquake concentrated plasticity column with neoprene springs column base *M*-ϕ (A4R).**

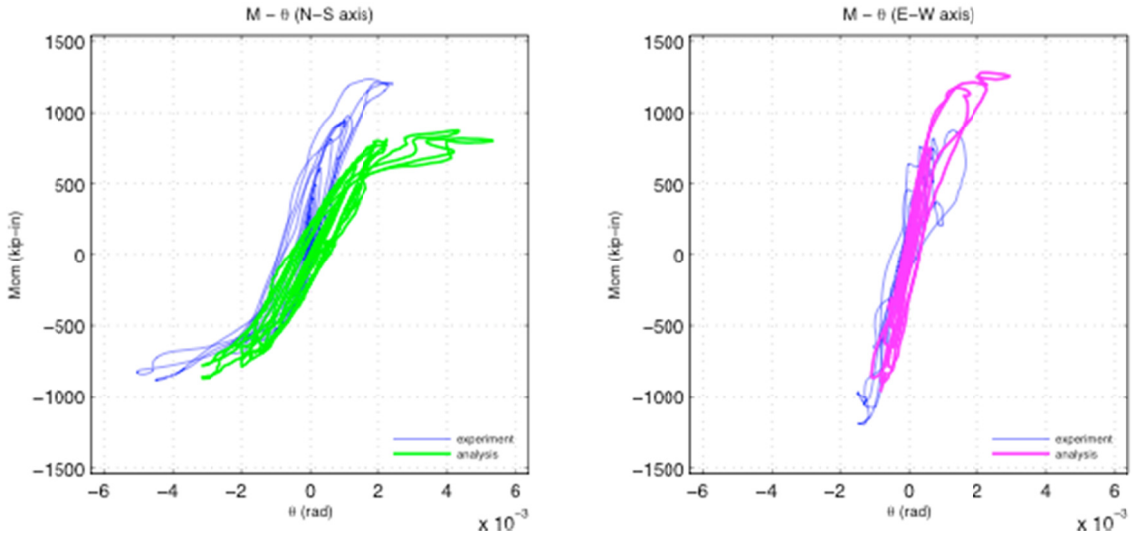

Figure 5.64 **Design-level earthquake concentrated plasticity column with neoprene springs footing moment rotation *M*-θ (A3R).**

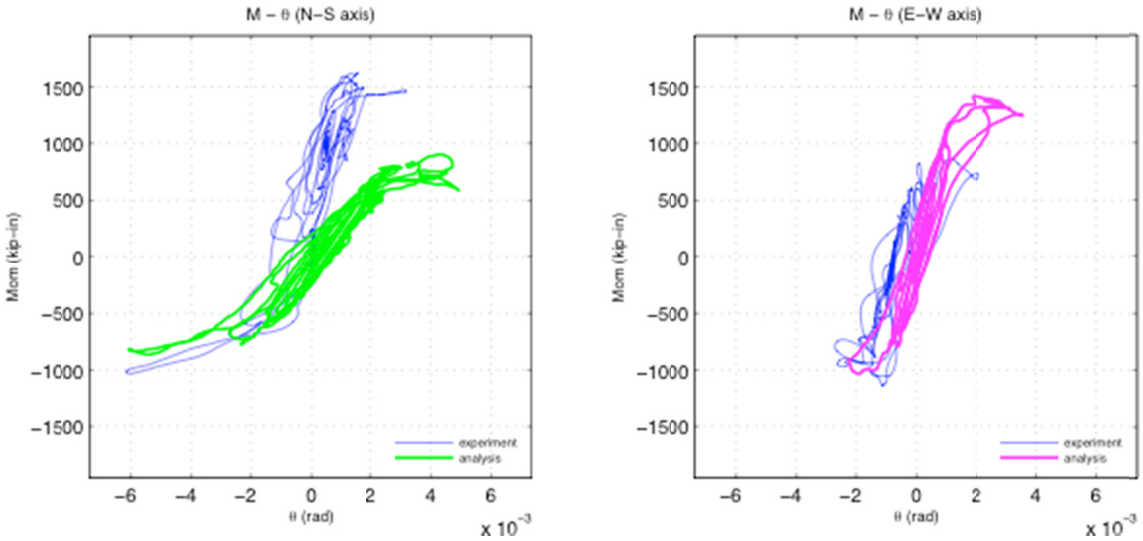

Figure 5.65 **Maximum-level earthquake concentrated plasticity column with neoprene springs footing moment rotation *M*-θ (A4R).**

5.7 SUMMARY AND CONCLUSIONS

A comparison of analytic models versus the observed experimental response was performed to reliably predict the seismic performance of RC bridge piers allowed to uplift. Global and local response parameters were compared to the observed displacements, accelerations, and force deformation relationships of the uplifting system. The open-source structural analysis platform OpenSees was used to conduct both linear and nonlinear analysis. A summary of the analysis performed is given in Section 5.7.1. Conclusions about the analytic models are presented in Section 5.7.2.

5.7.1 Summary

Several analytic models were developed and calibrated to the observed specimen characteristics. These models varied the column type, soil spring type, soil spring spacing, and column reinforcement type to match the column initial stiffness, footing rotational stiffness, footing vertical stiffness, footing uplift relationship, etc. Only experimental test runs with significant displacement and/or uplift response were presented in this chapter. Response parameters compared include column total displacement and the contribution of flexural column displacement and lateral translation due to footing rocking to the total displacement, as well as column accelerations, column moment curvature and footing moment rotation relationships.

Column

- The distributed plasticity option did not model system response well because of the inability to model effective section properties of concrete columns. The elastic and lumped plasticity options both were adequate for modeling the elastic response of the system. The lumped plasticity model is a valid option for modeling the inelastic response of the system.
- A plastic hinge length calculated using the Priestley method for estimating the plastic hinge length, provided reasonable results on the yielding of the column.

Footing

- Elastic-No-Tension and neoprene soil springs modelled with an acceptable degree of accuracy the observed rotational and vertical stiffness of the footing.
- The number of springs used for the best model comparison was a 6 x 6 grid (36 total). More refined grids were unwarranted, because they provided a small improvement in accuracy at a significant increase in computational expense.

Materials

- Column Steel Reinforcement – The **ReinforcingSteel** model proved to be the most appropriate choice for modeling the inelastic response of the column in part because it better captured the post-yield behavior of the reinforcement.
- Soil Springs: Both the ENT and neoprene material modelled with a degree of accuracy the vertical and rotational stiffness of the footing. The neoprene

material was deemed the better option because of the hysteretic damping properties that were similar to the observed elastomeric pad response.

Damping

- Rayleigh damping applied to the entire system was used for the analytic modeling. At significant levels of uplift the analytic damping level was 5–6%. When there was less uplift, lower values of damping, approximately 3%, were warranted.

5.7.2 Conclusions

Through use of OpenSees, analytical models predicted with a reasonable degree of accuracy the seismic response of uplifting bridge pier systems.. The analytic models were idealizations of the superstructure mass, column, footing, and elastomeric pad the footing rested upon. The evaluation criteria were based on observed results of natural properties and dynamic response to multi-directional input earthquake accelerations. Linear and nonlinear models were used based on the observed system response.

The linear models used were able to predict the peak displacements to within 20–25% for the square configuration footing ($3D_c$ x $3D_c$) tests with nominal design axial load ($10\%f'_cA_g$) and the rectangular footing ($3D_c$ x $5D_c$) tests with the equal design axial load. In general, the linear models used were able to predict the observed response with a high degree of confidence.

The nonlinear models used were able to predict the design-level (flexural ductility μ=6) test peak displacements to within 20% of the observed values. The residual displacements were under predicted by approximately 100%. However, given the small value of residual displacements (less than 1 in.), the most appropriate model predicted the amount of rocking and uplifting, column flexural displacements, and column total displacements very well for the design-level earthquake. For the maximum-level earthquake (μ=8), the analytic model predicted the initial cycles of displacement well but deviated once the column experienced significant residual displacements. When discounting the effect residual displacements had on total displacement, the model was still able to reasonably predict the peak displacements, which occurred at approximately a column flexural ductility of 10. Additionally, the model still was able to predict approximately 50% of the observed residual displacement and appeared to exhibit similar post-yield stiffness response despite not having the same amount of yielding.

The column center of mass accelerations were predicted to within 25% for the linear and nonlinear analysis models. The column base moment curvature prediction for the linear response was predicted reasonably well. The nonlinear analytic model performed reasonably well for the design-level earthquake but did not completely predict the residual displacements observed as discussed. Because of this, the analytic model moment-curvature relationship did not show the shift in origin due to the residual displacements of the column. The analytic model needs further refinement for the maximum-level test in part because of its inability to capture residual displacements. The permanent column offset created a shift in the origin that affected the system displacement and thus acceleration and moment response.

The footing rotational stiffness and subsequent softening during uplift were predicted reasonably well by the numerical models for the linear analysis cases. The neoprene springs for the elastomeric pad provided good approximations of the static displacement, rotational stiffness, moment, and rotation at first footing edge uplift and the softening behavior. The footing response under nonlinear analysis was affected by the discrepancy in predicted residual displacements, which caused a permanent shift in the origin of the footing moment rotation relationship.

The more uplift expected in a system, the higher the value of Rayleigh damping that should be used. Analytic models showed that damping values of 5–6% should be used for systems with significant uplift and approximately 3–4% for yielding systems with less uplift.

Based on these comparisons, the recommended analysis models for the uplifting bridge pier system predicted with sufficient accuracy the global responses of linear uplifting systems and design- and maximum-level uplifting systems. Additional research is needed to improve modeling of the free vibration phase of uplifting systems subjected to multi-directional input excitation and residual displacements in columns allowed to uplift.

6 Parametric Investigation of Uplifting Bridge Piers

6.1 INTRODUCTION

The experimental and analytic work presented herein is intended to provide the basis for developing guidelines for designing traditional RC bridge columns on competent soil that may be allowed to uplift on competent soil. As noted in Chapter 1, much analytic work and some experimental work has been done previously to devise simplified guidelines. Considerable research, including that carried out in this study, demonstrates that rocking and uplift may provide a useful form of seismic isolation for bridge piers supported on narrow foundations. Furthermore, narrow foundations may be sufficient to develop yielding in the column plastic hinge region. However, few studies have developed guidelines for bridge footings and superstructures that could be integrated within existing design methods. The methodology proposed by Priestly et al. [1996] is perhaps the most widely referenced, including within the Federal Highway Administration Bridge Design Manual. However, as noted previously, it has a number of important limitations, and may be difficult to apply to more general multi-directional excitations.

Past experimental tests and analytic research found that there are a few important parameters that control the characteristics of a rocking bridge pier system. These include the dimensions of the footing, ratio of superstructure height to footing width, the weight acting on the footing, allowable bearing pressure of the soil, the fixed-base period of the pier, and the effective period of the pier resulting from the flexibility of the supporting soil. Simplified theories such as those by Yim and Chopra [1983] and Meek [1975] appear to be adequate to predict whether a foundation will uplift, However, these early studies focused on the beneficial effects of uplift on reducing base shear rather than on predicting the lateral displacement of the system and the amount of uplift required. Methods such as those by Priestley et al. appear to be based on available evidence [Harden et al. 2005], resulting in significantly over or under conservative estimates of lateral displacements.

The uplifting system parameters of investigation are discussed in Section 6.3. These include analytic assumptions for the superstructure, column, footings, soil, soil springs, and effective natural period. Sections 6.4 through 6.6 describe the parametric investigation of uplifting systems and spectral acceleration and displacement. Section 6.7 compares the response of fixed-base and uplifting systems. Guideline development, based on the parametric investigation, including observed characteristics of uplifting systems and potential benefits and negative consequences of allowing uplift is described in Section 6.8.

6.2 SUMMARY OF OBJECTIVES

First, an assessment must be made to determine the benefits of designing a bridge with a spread footing foundation allowed to uplift compared to a traditional fixed base design with large spread footings. The question to be answered is thus: will designing a footing to uplift provide a reliable and appreciable seismic isolation mechanism and/or energy dissipation, such that demand levels for design earthquakes would be significantly reduced to below inelastic levels or a reduced damage state? Criteria to determine if global instability would be likely to occur by allowing uplift are also needed.

Previous chapters have shown that allowing bridge piers to uplift is a valid mode of response for the column system considered. However, the experimental testing was limited in scope to a single column, with two-footing configurations, and one soil medium considered. Analytic models developed in Chapter 5 will be used to perform a parametric investigation. The purpose here is to determine the response of a wide variety of bridge pier systems allowed to uplift and then compare the response of these systems to a traditional fixed-base bridge pier design. The parameterization includes the natural period of the pier, column response type, footing width, soil response, ground motions, allowable soil pressure, and column displacement demands versus capacity. Uplifting systems have been seen to act as seismic isolators of sorts, with a noticeable elongation of the natural period directly correlated to the footing and soil stiffness. The parametric investigation will illustrate the differences between fixed and uplifting systems by plotting the response variable of interest for the uplifting systems against the corresponding fixed-base response.

The second objective is to assess the benefits and drawbacks of allowing traditional bridge piers to uplift in design. This is accomplished by evaluating traditional design metrics including total displacement, acceleration, and local demands on deformation and forces. A comparison of existing design methods for columns allowed to uplift is performed and compared to the dynamic time-history method used herein.

6.3 UPLIFTING BRIDGE PIER SYSTEM

The uplifting bridge pier system was designed according to the criteria described in the Caltrans BDS and the SDC. This study focused on piers with spread footings resting on competent soil. A traditional fixed-base design would select footing dimensions sufficient to prevent measurable uplift compared to the column displacement and also maintain soil pressures well below the allowable limits. Figure 6.1 illustrates the uplifting bridge pier model and the parameters of interest. The following sections described the notation used to describe the uplifting system and the analytic modeling of the various components.

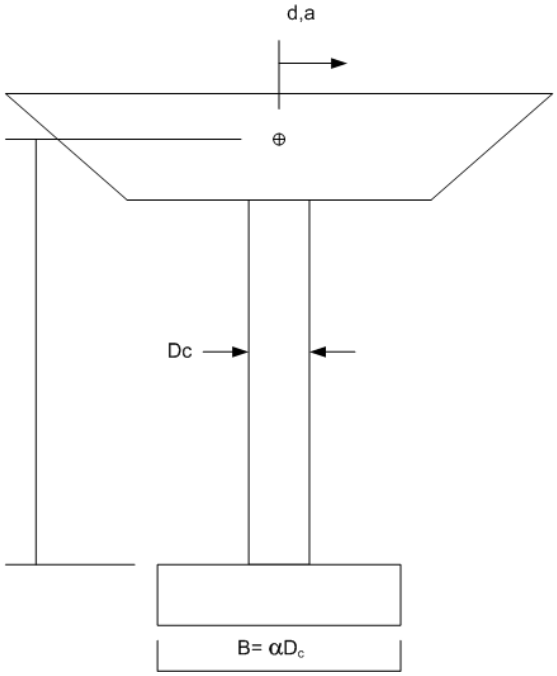

Figure 6.1 Prototype column.

6.3.1 Notation

Below is a description of the parameters used in the parametric investigation as well as response variables used to describe the uplifting system. Some of these are repeated from Chapter 4.

D_c = column diameter
α = ratio of footing length to column diameter
T_{nf} = fundamental period of fixed base system
T_{nr} = fundamental period of uplifting system
S_{AF} = a_{max} fixed-base system at column center of mass
S_{AR} = a_{max} uplifting system at column center of mass
S_{DF} = d_{max} fixed-base pier at column center of mass
S_{DR} = d_{max} of uplifting system at column center of mass = $d_f + d_r$
S_{DRF} = peak column flexural displacement of uplifting system at column center of mass
S_{DRR} = peak column translation displacement of uplifting system at column center of mass due to footing rotation

6.3.2 Column and Superstructure

The prototype column and superstructure were designed according to Caltrans BDS. For the parametric investigation, the column was modeled for both elastic and inelastic response. Superstructure mass was idealized as a lumped mass as this investigation used an inverted pendulum parametric model.

The column was modeled as a RC section with a fixed column diameter of 6 ft. The reinforcement ratio was selected to 1.5% for longitudinal reinforcing and 0.6% for the volumetric spiral reinforcement. Longitudinal bars were selected to be No. 7 and No. 5 bars selected for the spiral reinforcement. The concrete was assumed to have a compressive strength of f'_c = 4 ksi. Steel reinforcing tensile yield strength was assumed to be f_y = 60 ksi. The column height measured from top of footing to center of column mass varied to provide a range of periods from 0.1 sec to 3.0 sec for the fixed base system. The axial dead load was assumed to be 10% of $f'_c A_g$.

The column was modeled as either an elastic beam-column element or a nonlinear beam-column element. Effective section properties as recommended by the Caltrans SDC were used in modifying the concrete flexural stiffness. For nonlinear response the column plastic hinge length was estimated using the Priestly equation (Eqn. 7.25) in the SDC.

6.3.3 Footing

The footing was assumed to be rigid relative to the column and soil response during rocking and uplifting. It was assumed to be square with dimensions $B = L$ determined by the column to footing width ratio $\alpha = B/D_c = L/D_c$. Footing width ratios of 3, 4, 5, and 6 were used for the analysis. Footing ratios less than 3 tended to have bearing pressures much larger than allowable. Footing width ratios larger than 6 tended to be too conservative for design when considering effective fixed base response and bearing pressures.

When considering uplifting systems the footing depth was an important parameter because the footing uplifts about the bottom of the footing face affecting the effective column height. Compared to the column heights used for this investigation, the amount of footing height was small and was not considered.

Embedment and lateral translation were not considered in the investigation. The purpose was to remove any negligible response mode that might distort the effect of uplift on the column response. The analytic model allows the footing to translate vertically and rotate about the two horizontal axes, as shown in Figure 5.11.

6.3.4 Soil

This investigation focused on footings resting on competent soil. A representative sandy medium dense soil was selected to model the soil of a system allowed to uplift. Several sources are available to determine appropriate soil engineering properties, including allowable bearing pressure, shear modulus, friction angle of sand, and soil factor of safety. The study by Harden et al. [2005], ASCE 41, and the Caltrans BDS were consulted to determine suitable soil engineering properties.

The representative medium dense sandy soil was selected to have the properties ϕ=35 degrees, unit weight of 130 pcf, a Poisson's ratio of 0.3, and a shear wave velocity of 600 ft/sec, which is comparable to a NEHRP soil site class *D*. Allowable bearing pressure design values for spread footings are listed in the Caltrans BDS Table 4.11.4.1.4-1 and ASCE 41 (Table 4-2); for medium dense sands Caltrans recommends allowable bearing pressures of 4.0–6.0 ksf and ASCE 41 recommends approximately 3–4 ksf. A representative value of q_{allow} was selected based on the

Caltrans recommendation. The factor of safety for soil bearing pressure was selected to be FS_v = 3.0, which is the BDS recommended value.

The shear modulus (G) estimation was determined by procedures in ASCE 41 *Shallow Bearing Foundations Methods* (4.4.2.1). Using the recommended effective modulus ratio G/G_o = 0.5, the calculated initial shear modulus G_o = 662 ksf, and the effective shear modulus used was G=331 ksf. The soil properties are listed in Table 6.1.

6.3.5 Soil Springs

Soil springs for modeling the footing as a BNWF were implemented as described in Section 5.3.3. Global vertical and rotational stiffness of the footing needed to be established prior to discretizing the footing into middle and end regions with associated spring stiffnesses. The ASCE 41 recommended method by Gazetas [1991] used in Harden et al. [2005] (with modifications) for modeling shallow bearing foundations with rigid footings and flexible soil was used here to estimate the global vertical and rotational stiffness. The Gazetas method calculates the vertical and rotational stiffness of a footing $B \times L$ as a function of dimensions, shear modulus, and Poisson's ratio. Table 6.1 lists the calculations for vertical and rotational stiffness. The recommended embedment correction factors were not used because the footing embedment effects are not considered in this study.

As expected for a uniform soil, the vertical and rotational stiffness increase as the footing dimensions increases. The discretized middle and end region spring stiffness were calculated as described in Section 5.3.3. Table 6.1 lists the relative soil spring information.

Table 6.1 Parametric soil spring model parameters.

Column-Footing Width Ratio	$\alpha = 3, 4, 5, 6$
Footing Width	$L = \alpha D_c$
Footing Length	$B = \alpha D_c$
Effective Shear Modulus Ratio	$G/G_o = 0.5$
Initial Shear Modulus	$G_o = 662$ ksf
Allowable Bearing Pressure	$q_{\text{allow}} = 5.0$ ksf
Global Vertical Stiffness	$K_z = \frac{GB}{1-v}\left[1.55\left(\frac{L}{B}\right)^{0.75} + 0.8\right]$
Global Rotational Stiffness	$K_{\theta x} = \frac{GB^3}{1-v}\left[0.4\left(\frac{L}{B}\right) + 0.1\right]$ $K_{\theta y} = \frac{GB^3}{1-v}\left[0.47\left(\frac{L}{B}\right)^{2.4} + 0.034\right]$

6.3.6 Natural Period

The natural period of elastic response can be calculated using the methods described in Chapter 5. The initial fundamental period of the uplifting system before uplift is a function of the column fixed-base fundamental period T_{nf} and a factor related inversely to the footing rotational stiffness. As the footing width increased in this study, the rotational stiffness increased given the consistent soil assumption. Consequently, the fundamental period of uplifting decreased until it reached the asymptote defined by the fixed-base fundamental period. The fundamental period of uplifting system is repeated here in Equation (6.1).

$$T_{nr} = T_{nf}\sqrt{1 + \frac{k_{col} \cdot H_{col}^{\ 2}}{K_{\theta}}} \tag{6.1}$$

6.3.7 Damping

Damping for uplifting system was estimated using the methods described in ASCE 41. The uplifting system experienced damping from hysteretic response of the column and the radiation damping from the footing interacting with the underlying soil. In contrast, the fixed-base system experiences damping from the hysteretic column response only.

The hysteretic damping of the column was assumed to be ξ_o = 5%. This is the typical value used for elastic response spectra analysis. The uplifting system damping, ξ, is calculated as a function of the column damping and soil radiation damping, ξ_f. Equation (6.2) below shows the calculation for system damping for soil-structure interaction.

$$\xi = \xi_f + \frac{\xi_o}{\left(T_{nr} / T_{nf}\right)^3} \tag{6.2}$$

The range of damping for uplifting systems is 5%–7.5% using the soils and footing configurations described above.

6.3.8 Ground Motions

In order to facilitate a direct comparison between the two system, ground motions for the investigation of uplifting systems were selected based on relevant criteria used to design fixed-base bridge piers,. The ground motions were selected from the PEER Transportation System Ground Motion Studies program [Baker et al. 2011]. One set considered the directivity effects from near-fault earthquakes and the other considered site specific target hazard levels.

The near-fault records chosen have significant velocity pulses in the fault-normal component of the record. In most cases, the fault-parallel component had a noticeable velocity pulse with smaller velocity. In general, the range of periods of velocity pulses for the motions considered is from 0–5 sec. None of the ground motions were amplitude scaled. All were recorded within 11 km of the fault rupture.

Three site specific hazards levels typically used for design of structures were selected for analyzing uplifting systems. They corresponded a to 2%, 10%, and 50% 50-year probability of exceedance. The site specific ground motions used were those selected for the I880 Testbed program in Oakland, California (37.803N, 122.287W) described in Baker et al. [2011]. The target PGA for the three hazard levels was 0.94g, 0.60g, and 0.27g for the 2%, 10%, and 50% probability of exceedance. Some of the ground motions considered had directivity effects like velocity pulses due to their proximity to the Hayward fault line.

For each of the four groups described above, 10 ground motions were selected for analysis of uplifting and fixed-base systems. Ground motions selected were not scaled beyond that described in the Baker et al. [2011]. Table 6.2 list the ground motions used in the parametric investigation.

Table 6.2 Parametric investigation ground motions.

No.	Hazard Level	Name[1]	Record
1	2% in 50yr	Oak_2_50_1	Imperial Valley-02 (1940)
2	2% in 50yr	Oak_2_50_2	Imperial Valley-06 (1979)
3	2% in 50yr	Oak_2_50_3	Chalfant Valley-02 Bishop (1986)
4	2% in 50yr	Oak_2_50_4	Superstition Hills-02 (1987)
5	2% in 50yr	Oak_2_50_5	Loma Prieta-Gilroy (1989)
6	2% in 50yr	Oak_2_50_6	Erzican, Turkey (1992)
7	2% in 50yr	Oak_2_50_7	Northridge-01 Sylmar (1994)
8	2% in 50yr	Oak_2_50_8	Kobe (1995)
9	2% in 50yr	Oak_2_50_9	Duzce, Turkey (1999)
10	2% in 50yr	Oak_2_50_10	Chi-Chi, Taiwan (1999)
11	10% in 50yr	Oak_10_50_1	Imperial Valley-02 (1940)
12	10% in 50yr	Oak_10_50_2	Victoria, Mexico (1980)
13	10% in 50yr	Oak_10_50_3	Westmoreland (1981)
14	10% in 50yr	Oak_10_50_4	Chalfant Valley-02 Bishop (1986)
15	10% in 50yr	Oak_10_50_5	Superstition Hills-02 (1987)
16	10% in 50yr	Oak_10_50_6	Loma Prieta-Gilroy (1989)
17	10% in 50yr	Oak_10_50_7	Northridge-01 Sepulveda (1994)
18	10% in 50yr	Oak_10_50_8	Northridge-01 Sylmar (1994)
19	10% in 50yr	Oak_10_50_9	Duzce, Turkey (1999)
20	10% in 50yr	Oak_10_50_10	Chi-Chi, Taiwan (1999)
21	50% in 50yr	Oak_50_50_1	Imperial Valley-02 (1940)
22	50% in 50yr	Oak_50_50_2	San Fernando (1971)
23	50% in 50yr	Oak_50_50_3	Imperial Valley-06 (1979)
24	50% in 50yr	Oak_50_50_4	Chalfant Valley-02 Bishop (1986)
25	50% in 50yr	Oak_50_50_5	Superstition Hills-02 (1987)
26	50% in 50yr	Oak_50_50_6	Loma Prieta-Gilroy (1989)
27	50% in 50yr	Oak_50_50_7	Landers (1992)
28	50% in 50yr	Oak_50_50_8	Northridge-01 Sepulveda (1994)
29	50% in 50yr	Oak_50_50_9	Duzce, Turkey (1999)
30	50% in 50yr	Oak_50_50_10	Chi-Chi, Taiwan (1999)
31	near fault	PL_1	Imperial Valley-06 (1979)
32	near fault	PL_2	Morgan Hill (1984)
33	near fault	PL_3	Loma Prieta-LGPC (1989)
34	near fault	PL_4	Landers-Lucerne (1992)
35	near fault	PL_5	Northridge-01 Newhall (1994)
36	near fault	PL_6	Northridge-01 Sylmar (1994)
37	near fault	PL_7	Kobe (1995)
38	near fault	PL_8	Kocaeli, Turkey (1999)
39	near fault	PL_9	Chi-Chi, Taiwan (1999)
40	near fault	PL_10	Chi-Chi, Taiwan (1999)

[1] Ten files selected for each group from Baker et al. were renumbered from 1-10. Do not match original numbering.

6.4 PERFORMANCE EVALUATION OF UPLIFTING BRIDGE PIER SYSTEM

The rocking system column response and its components were described in Section 4.2. The relationship of column displacement is repeated in Equation (6.3).

$$\Delta_T = \Delta_{flex} + \Delta_{rock}$$

$$\{or\} \tag{6.3}$$

$$d = d_f + d_r$$

A representative system with a fixed-base natural period equal to 1.0 sec was used to evaluate the performance of a system allowed to uplift. The representative ground motion was selected based on seismic design requirements of RC columns. For this system, a ground motion was selected to reach the target ductility for a design-level earthquake (10% in 50 year probability of exceedance).

Three types of analysis were performed to evaluate the system: pushover, dynamic, and spectral analysis. Three combinations of column and footing modeling assumptions were presented: elastic column and soil, nonlinear column and elastic soil, and nonlinear column and soil. The same column characteristics were used for all systems. The footing width was chosen as 3, 4, 5, or 6 times the column diameter.

As will be shown, a footing to column width of 5 has a significant amount of yielding. For this system to realize the benefits of rocking, the footing/column ratio needs to be less than 5. In particular, the footing to column width of 4 also has a displacement contribution from yielding. To reduce the amount of inelastic response the footing needs to be approximately 3 to 4 times the column diameter.

6.4.1 Pushover Analysis

A pushover analysis of uplifting systems provides an enveloped response of systems allowed to uplift. It also facilitates a relative comparison of design variables and their sensitivity on key response parameters such as total column displacement. This section describes and illustrates the pushover response of the three types of modeling assumptions used. Some of the key response parameters include: footing uplift, column yield, soil yield, column shear, column base moment, total column displacement, and column displacement from flexure. To gauge the performance of uplifting systems, these parameters will be compared to the fixed-base system response of the same column.

6.4.1.1 Column Force Displacement

The applied lateral force versus total column displacement is shown in Figure 6.2(a) for an elastic column-soil modeling assumption. The three curves show the force versus column displacement for the fixed column, and uplifting columns with footing-to-column width ratios of 3 and 5. As expected, the footing uplifts at larger applied loads for increasing footing widths. The applied force to uplift a footing with α=3.0 is approximately one-half that of the α=5.0 assumption.

Figure 6.2(b) shows the system response assuming a nonlinear column - elastic soil for the fixed column, α=3.0, and α=5.0 assumptions. The yield displacement of the fixed-base column is approximately 3.5 in. The figure shows α=3.0 footing uplifts before it yields and α=5.0 footing yields before it uplifts. The α=3.0 footing uplifts at total displacement of 2.8 in. and yields at 8.6 in. The α=5.0 footing uplifts at 10.6 in. and yields at 4.1 in. Table 6.3 lists some of the values for these uplifting systems, indicating that the α=3.0 footing will uplift well before it yields and that the total displacement at yield will be approximately 2.5 times larger than that of the fixed-base column. This shows there should be a reduction in nonlinear behavior for the α=3.0 footing. The α=5.0 footing will yield before it uplifts and the displacement at uplift will be approximately 3.0 times that of the yield displacement. Hence the column will have an approximate displacement ductility of 3 before the footing uplifts. Figure 6.3 shows the response of the system assuming a nonlinear column and soil model. As stated previously, it was assumed that the yield soil bearing pressure is three times greater than the system vertical bearing pressure. The α=3.0 soil yields before the column reaches the yield point, which is evident in the figure by the negatives slope. The α=5.0 does not reach soil yield until well after the column has yielded.

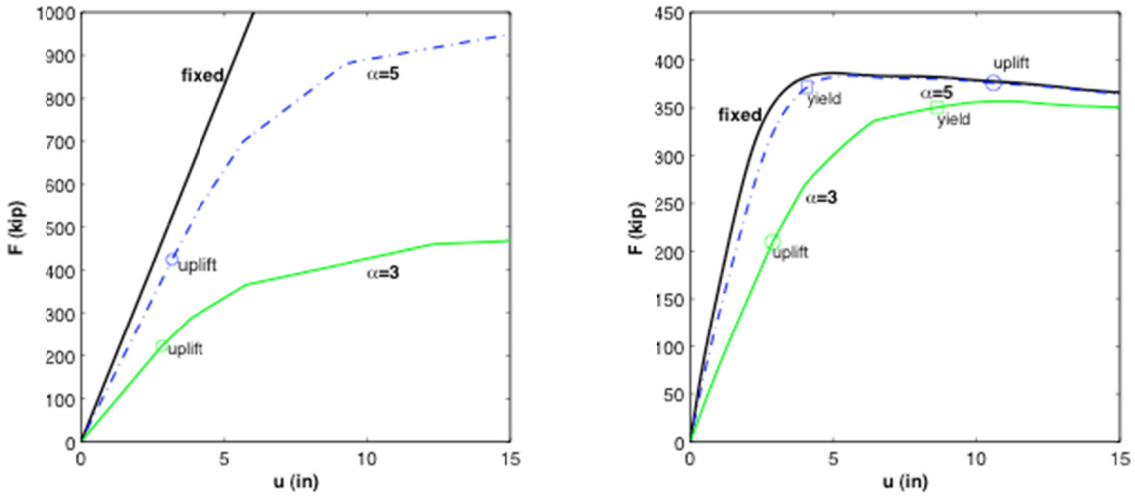

(a) elastic column – elastic soil (b) nonlinear column – elastic soil

Figure 6.2 Pushover analysis (elastic or nonlinear column – elastic soil).

Table 6.3 Uplifting system response values.

Response Parameter	α=3		α=5		Fixed
	Elastic	Nonlinear	Elastic	Nonlinear	
u_{up} (in.)	2.8	2.8	3.1	10.6	-
u_{flex} at u_{up} (in.)	1.3	1.4	2.5	10.0	-
θ_{up} (rad)	0.0042	0.0042	0.0017	0.0017	-
F_{up} (kip)	222	209	425	376	-
M_{up} (k-ft)	6,490	6500	12,405	12,406	-
u_{yield} (in.)	-	8.6	-	4.1	3.51
M_{yield} (k-ft)	-	11,400	-	11,400	11,400
F_{yield} (kip)	-	351	-	372	374

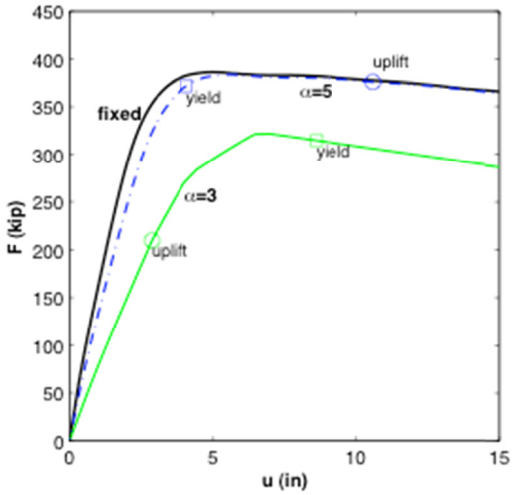

Figure 6.3 Pushover analysis (nonlinear column-soil).

6.4.1.2 *Footing Moment Rotation*

The footing moment rotation response for the same modeling assumptions discussed in the column force displacement section is shown in this section. Figure 6.4 shows the elastic column-soil model and nonlinear column-elastic soil model moment rotation response of the footing. The nonlinear column-soil model response is shown in Figure 6.5. The relationship between the various modeling assumptions is very similar to the column force-displacement curves.

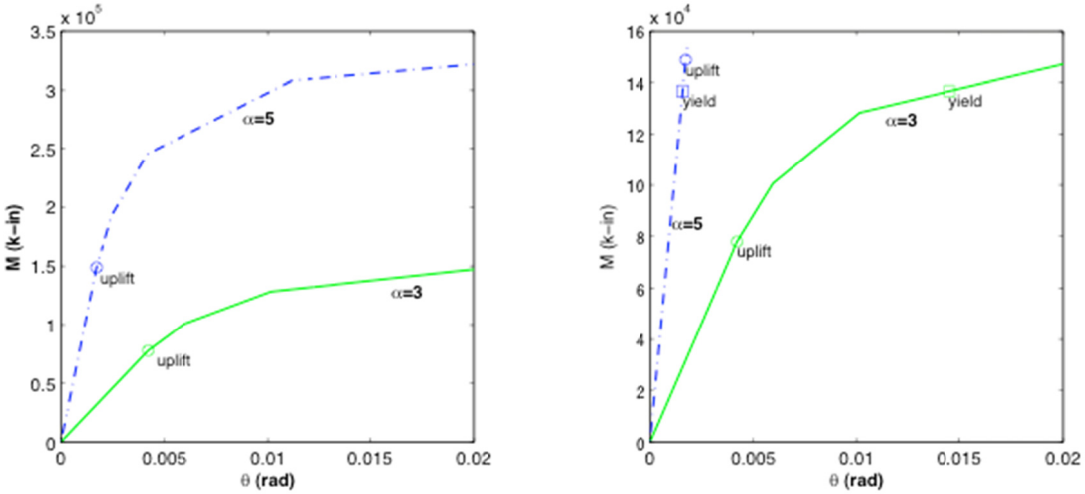

(a) elastic column – elastic soil **(b) nonlinear column – elastic soil**

Figure 6.4 Footing moment rotation (elastic or nonlinear column – elastic soil).

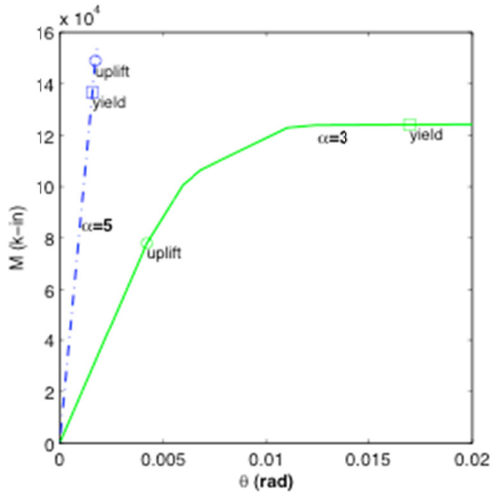

Figure 6.5 Footing moment rotation (nonlinear column-soil).

6.4.1.3 Moment-Curvature Relationship

The moment-curvature response is similar for the nonlinear column assumptions because the axial load is relatively uniform. For a more detailed discussion on the dynamic response of column moment curvature, see Section 6.4.2.5.

6.4.1.4 Soil Springs

The soil spring bearing pressure versus footing rotation is shown in Figure 6.6 for the elastic column-soil and nonlinear column-elastic soil model assumptions. The nonlinear column-soil model is shown in Figure 6.7.

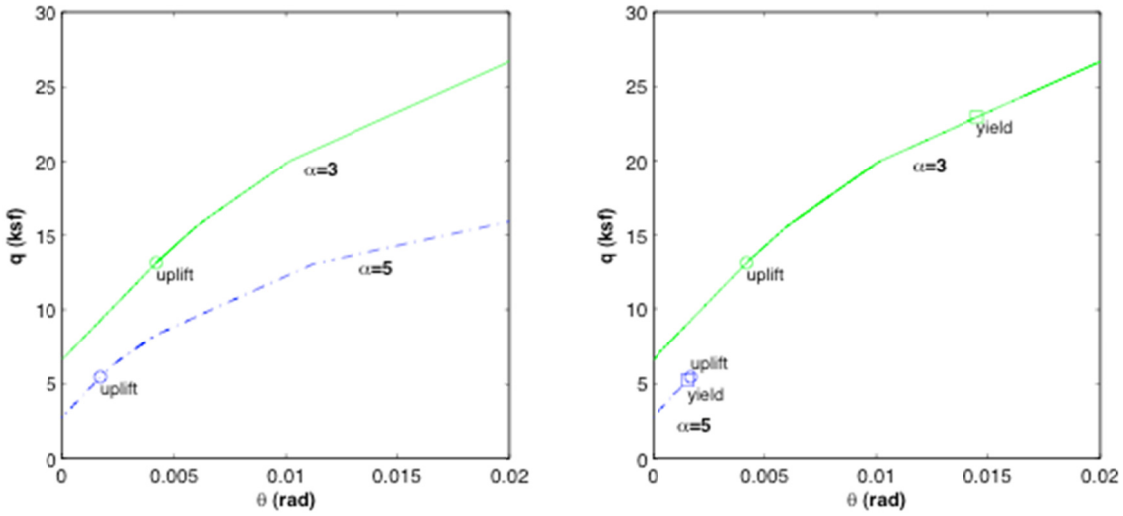

(a) elastic column – elastic soil (b) nonlinear column – elastic soil

Figure 6.6 Soil springs versus rotation (elastic or nonlinear column – elastic soil).

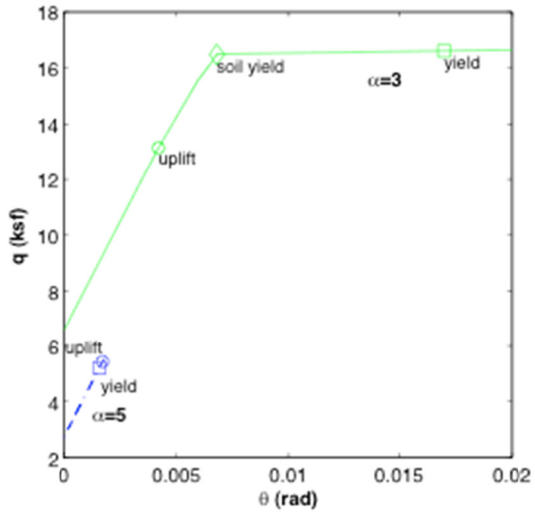

Figure 6.7 Soil springs versus rotation (nonlinear column-soil).

6.4.2 Dynamic Analysis

The dynamic response of the fixed-base and uplifting system are compared to illustrate the relative differences between the assumptions. The ground motion, fixed-base natural period, and footing widths are the same as those described in the previous section. Time histories of acceleration, total displacement, column flexural displacement, and moment are compared, as are the force deformation relationships for column base moment versus footing rotation and column base moment versus column curvature.

6.4.2.1 Acceleration

Figure 6.8 compares the fixed-base column acceleration to the uplifting system in for the elastic column and soil model assumption. Figure 6.8(a) shows that the acceleration of α=3.0 footing width is consistently smaller than the fixed-base response and longer period of motion. The peak acceleration of the uplifting system is approximately 90% the fixed-base response. The α=5.0 footing width has a similar acceleration response as α=3.0 footing width. The peak acceleration of the uplifting system is approximately 95% of the fixed-base response.

For the nonlinear column and elastic soil the acceleration response of the uplifting and fixed-based systems are similar. Figure 6.9(a) shows the α=3.0 footing width response. Figure 6.9(b) shows the α=5.0 footing width response. The accelerations for both footings are very similar especially after the column reaches yield. Essentially the uplifting and fixed-base responses were identical once the column reaches the yield point.

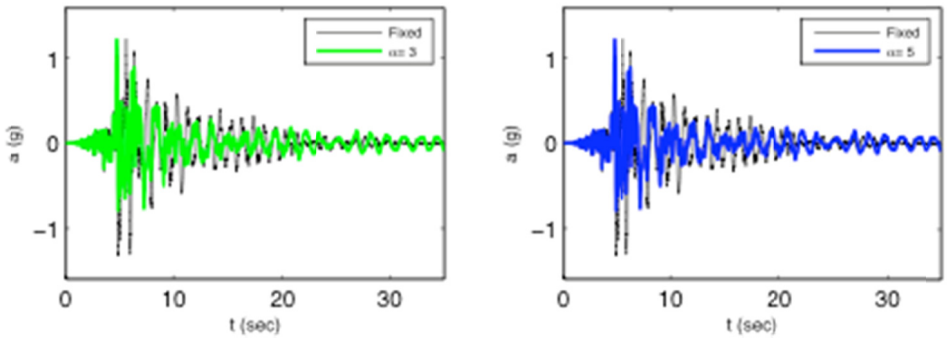

(a) α = 3.0 **(b) α = 5.0**

Figure 6.8 Acceleration time history (elastic column and soil).

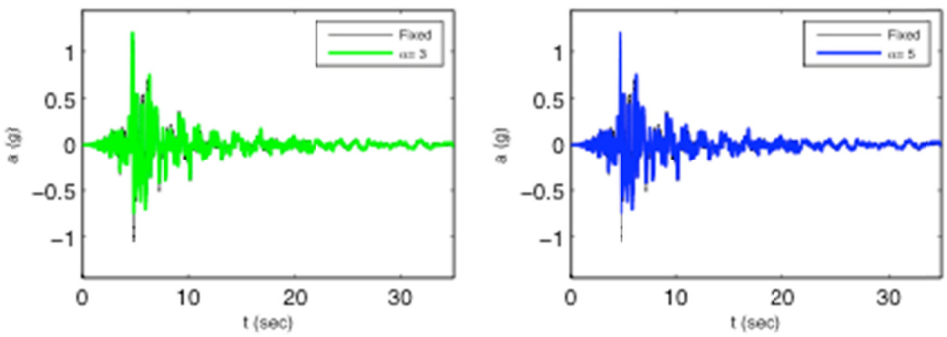

(a) α = 3.0 (b) α = 5.0

Figure 6.9 Acceleration time history (nonlinear column-elastic soil).

6.4.2.2 Displacement

The displacement time history of the uplifting footing is shown in Figure 6.10 and Figure 6.11. To illustrate the general displacement response of uplifting systems, the total displacement and column flexural displacement are shown. The column displacement due to rocking is not presented for simplicity. The quantity of uplift can be inferred from the difference between total and column flexural displacement. Figure 6.10 shows the displacement time history of the elastic column-soil system. For the α=3.0 footing width the peak total displacement and column flexural displacement are approximately 14.3 in. and 3.0 in. For the α=5.0 footing width the peak total displacement and column flexural displacement are approximately 9.2 in. and 5.5 in. The fixed-base response peak is 7.6 in., indicating that there is a significant contribution from rocking for the smaller footing width; for the larger footing width uplifting occurs, but it is less pronounced.

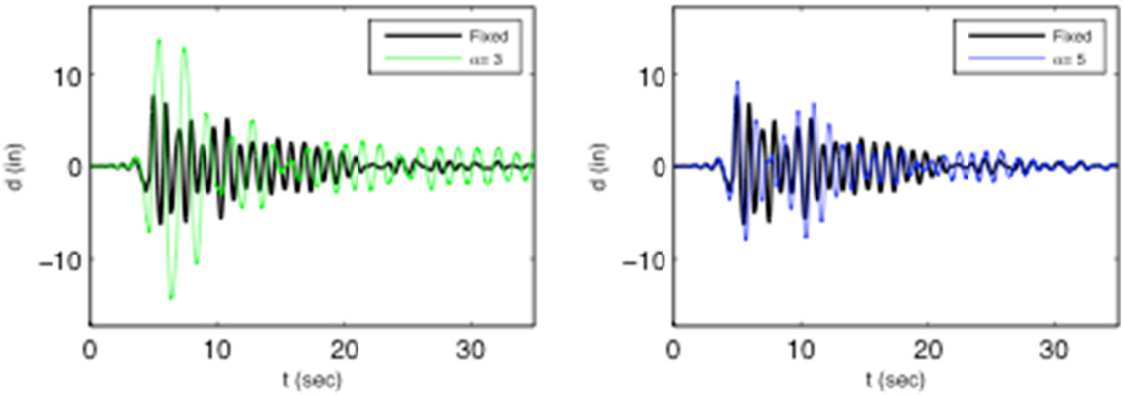

(a) α = 3.0

(b) α = 5.0

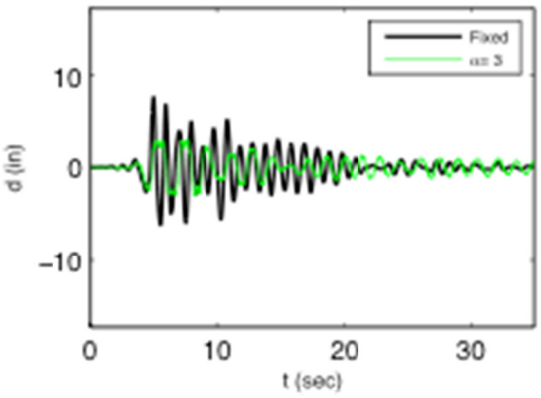

(c) α = 3.0

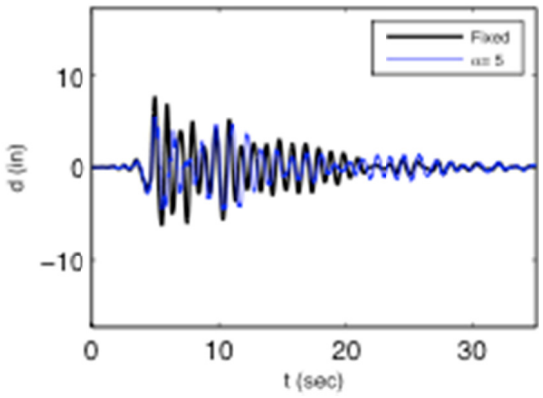

(d) α = 5.0

Figure 6.10 Displacement rime history (elastic column and soil).

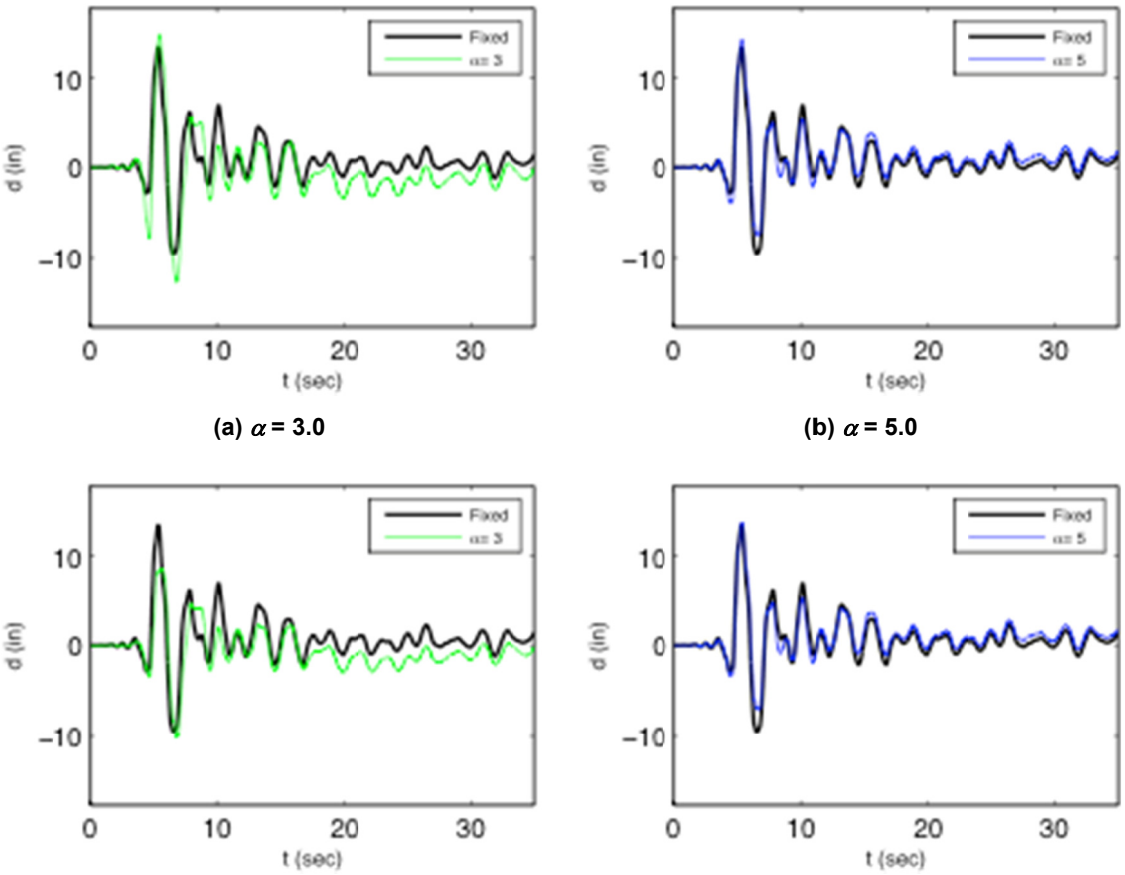

(a) $\alpha = 3.0$ (b) $\alpha = 5.0$

(c) $\alpha = 3.0$ (d) $\alpha = 5.0$

Figure 6.11 Displacement time history (nonlinear column-elastic soil).

6.4.2.3 Moment

The moment time histories for the elastic column-soil models are presented in Figure 6.12. The α=3.0 footing has consistently smaller moment demands compared to the fixed-base response, while the α=5.0 footing is very similar to the fixed-base response. The ratios of uplifting system peak moment to fixed-base systems are 0.40 and 0.72, respectively.

Nonlinear column-elastic soil model time histories are presented in Figure 6.13. Due to the nonlinear response of the column, the moment demands for the uplifting and fixed-base responses are very similar. . The ratios of uplifting system peak moment to fixed-base systems are 0.96 and 0.97, respectively. The column demands for uplifting and fixed systems both reached yield during excitation.

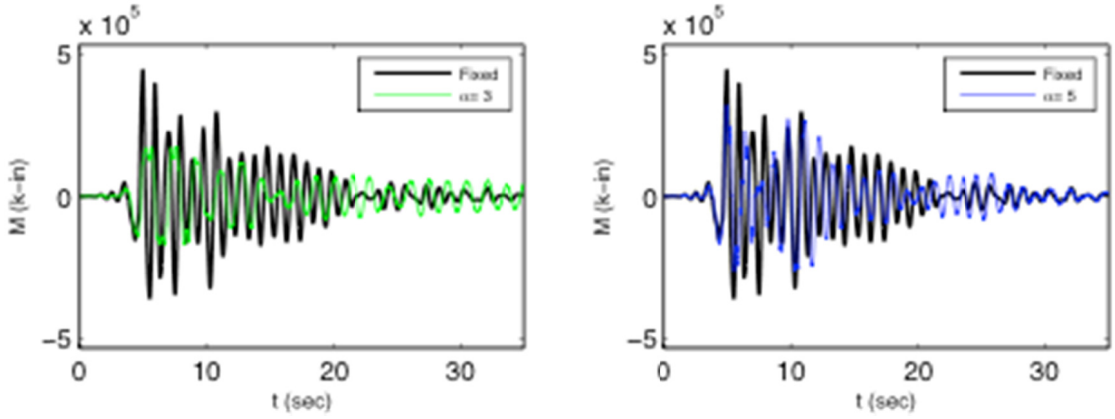

(a) α = 3.0 (b) α = 5.0

Figure 6.12 Moment time history (elastic column and soil).

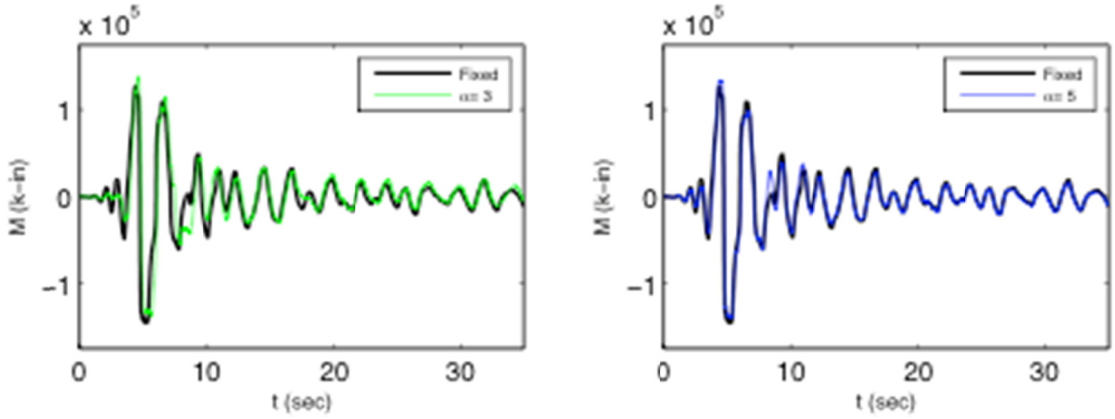

(a) α = 3.0 (b) α = 5.0

Figure 6.13 Moment time history (nonlinear column-elastic soil).

6.4.2.4 Moment-Rotation

Footing moment-rotation response for the elastic column-soil model assumption is presented in Figure 6.14, showing that uplift occurs for both footings but that the α=3.0 footing experienced much more uplift than the α=5.0 footing. The footing moment-rotation response of the nonlinear column model is presented in Figure 6.14. For this case the α=3.0 footing uplifts, however the total rotation is smaller and the number of cycles of uplift is less. The footing uplifts before the column yields; however, once uplift occurs, the column yields and does not significantly uplift subsequently. The α=5.0 footing does not uplift for the nonlinear column-elastic soil model. In this case the column yields before uplift and the moment required to uplift to footing does not occur.

6.4.2.5 Moment Curvature

Figure 6.15 presents the moment curvature response of the column for the nonlinear column-elastic soil model case. The α=3.0 footing and the α=5.0 footing both experience nonlinear response; however, the amount of nonlinearity is smaller for the α=3.0 footing, indicating a benefit by allowing the footing to uplift.

The ductility demands can also be estimated by the curvature values, which are more representative of system response since they are the result of moment demand, which includes P-Δ effects. The ratios of peak curvatures for the two footings are 0.76 and 1.02, respectively. For the α=3.0 and α=5.0 footing widths the ductility demands $\mu=\phi_r/\phi_f$ are 4.7 and 6.3, respectively, which are similar, but not exactly the same as the calculated displacement ductility demand in Section 6.4.2.2.

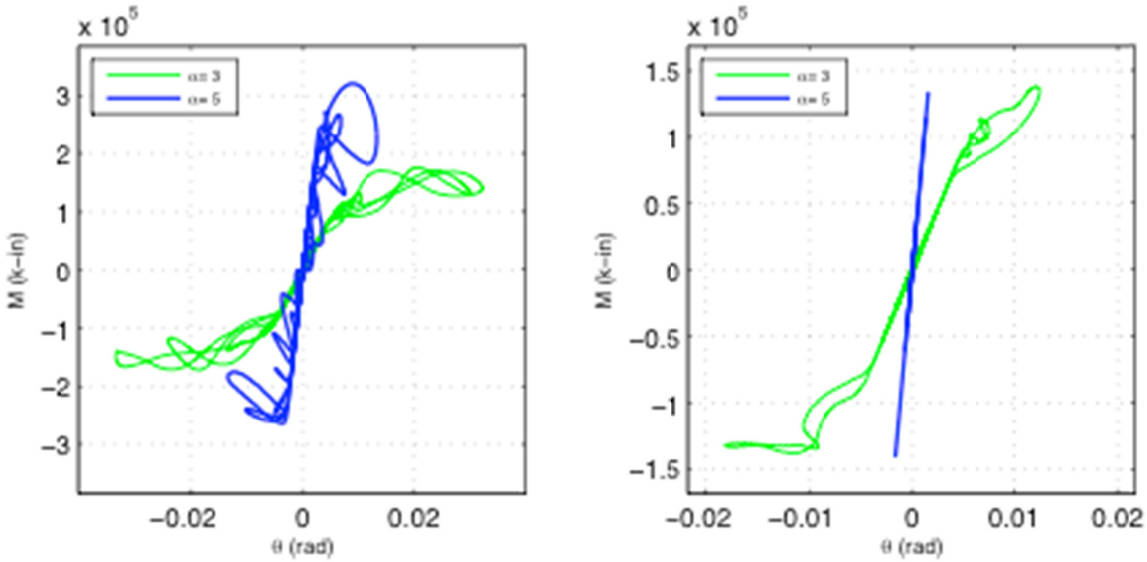

(a) elastic column-soil **(b) nonlinear column-elastic soil**

Figure 6.14 Moment-footing rotation (elastic column and soil).

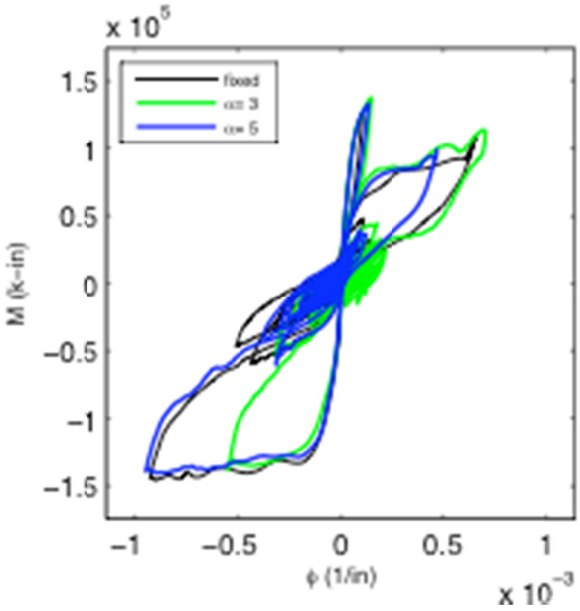

Figure 6.15 Moment curvature (nonlinear column-elastic soil).

6.4.3 Spectral Analysis

For the single ground motion considered, the spectral response of an uplifting column is plotted for two footing widths and compared to the fixed-base response. All spectral response quantities of the uplifting systems are plotted using the corresponding cantilever column fixed-base period T_{nf}, not the effective rocking period, T_{nr}. For example, the spectral acceleration of an uplifting system is plotted as a function of T_{nf} and S_{AR}. Spectral accelerations, total spectral displacement, and column flexure spectral displacement response are compared to the fixed-base response. The two modeling assumptions presented are elastic column-soil and nonlinear column and elastic soil. Only the one-dimensional directional excitation is shown for illustrative purposes.

6.4.3.1 Acceleration

Elastic column and soil spectral acceleration response to the selected ground motion is show in Figure 6.16. A narrow footing width (α=3.0) shows peak accelerations consistently smaller than the fixed-base period system (Figure 6.16a). For the same ground motion and a larger footing width (α=5.0), the response more closely represents that of a fixed-base system. However, the total acceleration is still less than the fixed-base response. The predicted peak acceleration for both systems is less than or equal to the fixed-base response.

The nonlinear column and elastic soil spectral acceleration response to the selected ground motion is show in Figure 6.17. A narrow footing width (α=3.0) shows peak accelerations approximately equal for all periods considered except the short-period range. For natural periods less than approximately 0.25 sec, the peak acceleration exceeds that of the fixed-base system (Figure 6.17a). The larger footing width (α=5.0) has a spectral response almost identical to the fixed-base response for the nonlinear column and elastic soil model, except for the very short-period range in which the uplifting response is much larger.

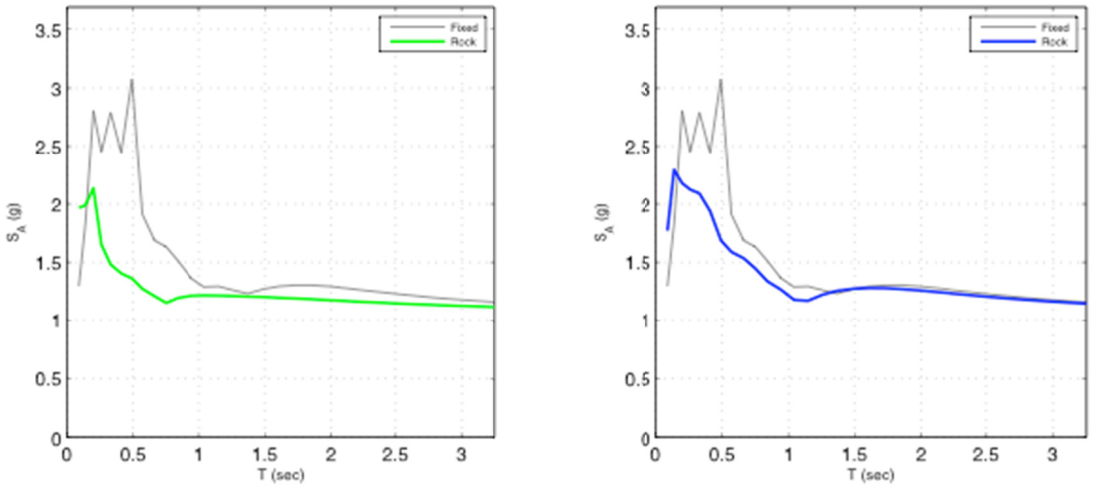

(a) $\alpha = 3.0$ (b) $\alpha = 5.0$

Figure 6.16 Spectral acceleration; elastic column and soil 1D excitation (Oak_10_50_6).

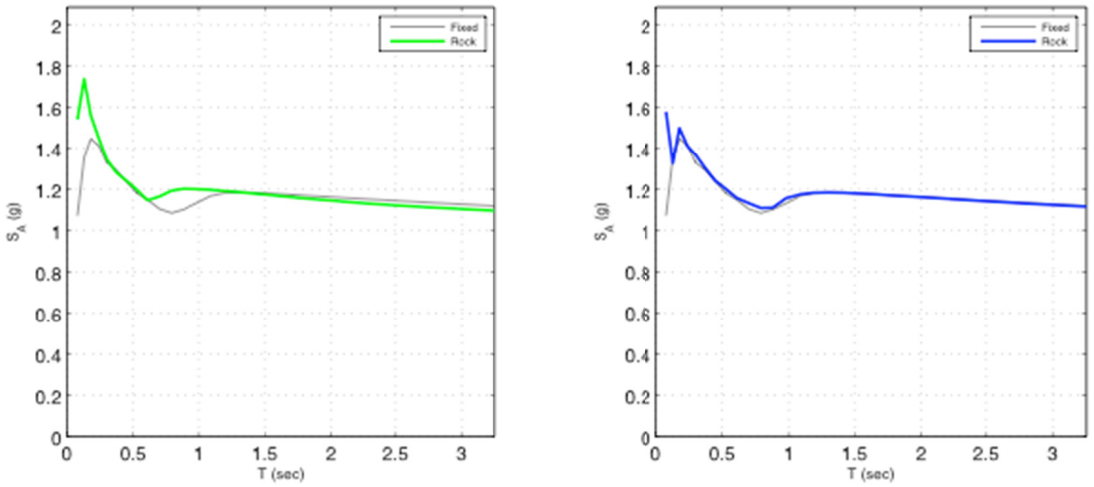

(a) $\alpha = 3.0$ (b) $\alpha = 5.0$

Figure 6.17 Spectral acceleration; nonlinear column-elastic soil 1D excitation. (Oak_10_50_6).

6.4.3.2 Displacement

Figure 6.18 and Figure 6.19 show the displacement spectral response of the uplifting versus the rocking system. Response of the two footing widths for total rocking displacement, column flexural displacement, and fixed-base displacement response are shown.

The elastic column-soil model spectral displacement is shown in Figure 6.18. Figure 6.18(a) shows the fixed-base response versus the total uplifting column displacement for α=3.0 and Figure 6.18(b) shows the same response for α=5.0. The fixed base response versus column flexural displacement component is shown in Figure 6.18 (c) for α=3.0 and Figure 6.18 (d) for α=50.

In general for the period ranges considered, the α=3 footing width has larger total displacements for T_{nf} <1.5 sec. At a natural period of 0.8 sec, the ratio of total column displacement for rocking versus fixed is a maximum of 2.0; everywhere else it is less. However, inspection of the rocking column flexural displacement shows this component is about one-half the fixed-base response indicating that the system will not have significant flexural response while uplifting when in the elastic range.

The nonlinear column-soil model spectral displacement is shown in Figure 6.19. The fixed-base response versus the total uplifting column displacement for α= 3.0 is shown in Figure 6.19(a) and Figure 6.19(b) for α=5.0. The fixed base response versus column flexural displacement component is shown in Figure 6.19(c) for α =3.0 and Figure 6.19(d) for α=5.0.

Compared to the fixed base nonlinear column response, total displacements for the α=3.0 footing width are greater for T_n < 1.0 sec and then become smaller for larger periods. The column flexural response is approximately the same as the fixed-base response for T_{nf} less than or equal to 0.75 sec and then significantly less. The α=5.0 footing is very similar to the fixed-base response for total and column flexural displacements., indicating there is not significant rocking response for this footing width except for periods larger than 1 sec when there is a slight reduction.

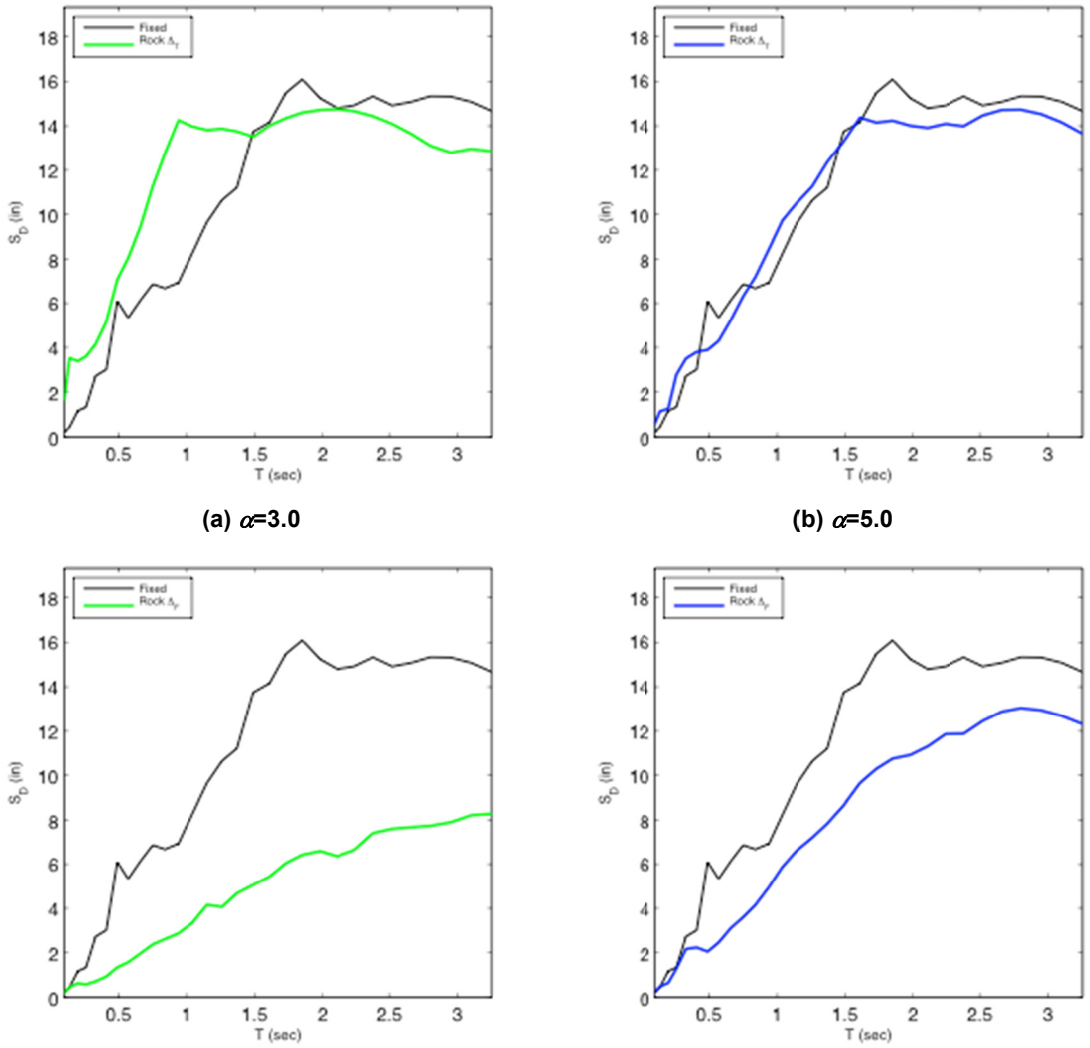

(a) α=3.0 (b) α=5.0

(c) α=3.0 (d) α=5.0

Figure 6.18 Spectral displacement; elastic column-soil 1D excitation (Oak_10_50_6).

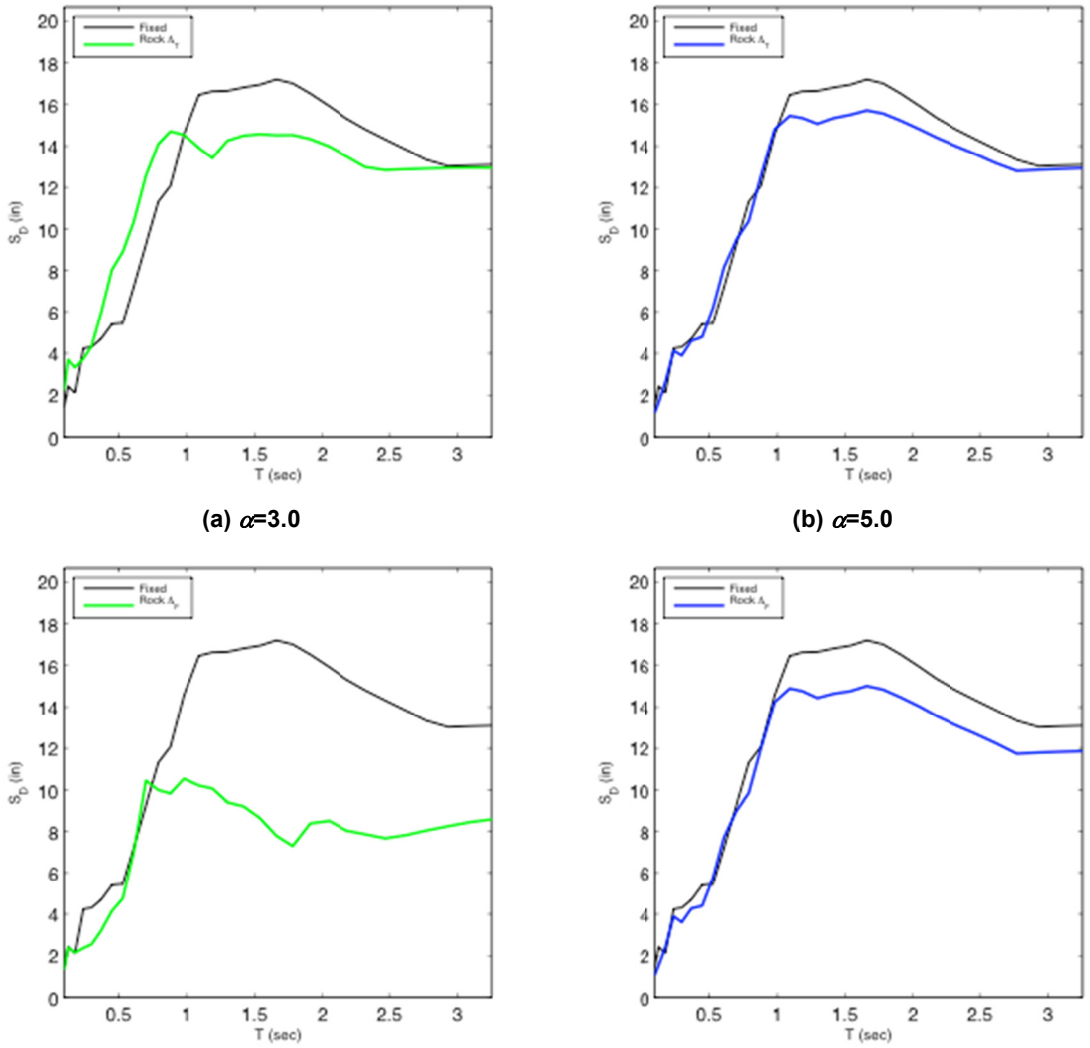

(a) α=3.0 (b) α=5.0

(c) α=3.0 (d) α=5.0

Figure 6.19 Spectral displacement; nonlinear column-elastic soil 1D excitation (Oak_10_50_6).

6.5 SPECTRAL ACCELERATION RESPONSE OF UPLIFTING BRIDGE PIER SYSTEM

The spectral acceleration response of uplifting bridge pier systems and the response for two combinations of analytic assumptions for column and is presented next. The first is elastic column and soil where there is no yielding in either element (Section 6.5.1). The second is a nonlinear column assumption with elastic soil. In this case the column may yield while the footing uplifts (Section 6.5.2). The nonlinear column-soil is not presented since significant yielding was found for only α=4.0 footing widths or smaller. The goal of this investigation is to compare a variety of uplifting systems to fixed-base response. Future work on this topic is warranted. The spectral acceleration response quantity is measured at the center of mass of the superstructure for both *x*- and *y*-directions of the cantilevered system.

Ground motions used are those presented in Section 6.3.8. A more thorough description of the spectral response variables was given in Section 6.4.3 for a single ground motion. This section presents the median response for all hazard levels and ground motions considered. The following sections discuss the two types of uplifting systems analytic models subjected to one-dimensional and three-dimensional input excitation. To assess the spectral response of uplifting systems, the mean response for each group of ground motions is presented. The mean response for spectral acceleration is plotted against individual dynamic test runs to illustrate the group response for a select ground motion group initially before displaying all mean group responses.

6.5.1 Elastic Column and Soil

The spectral acceleration response of uplifting bridge piers assuming elastic column and soil response is presented in the following sections. The total acceleration of the uplifting and corresponding fixed-based systems are plotted to illustrate the amplification or reduction of the peak column acceleration as a function of column natural period. Figure 6.20 illustrates the individual ground motion spectral acceleration mean responses and the response of the ten motions for the 10% in 50 year probability of exceedance for one-dimensional ground motions. The fixed base response is shown in Figure 6.20(a) and uplifting system response with a footing to column width ratio of 3.0 as an example is shown in Figure 6.20(b). Figure 6.21 through Figure 6.25 compares the mean responses for the four ground motion groups to the fixed-base response. Each group has four associated footing widths related to uplifting footings.

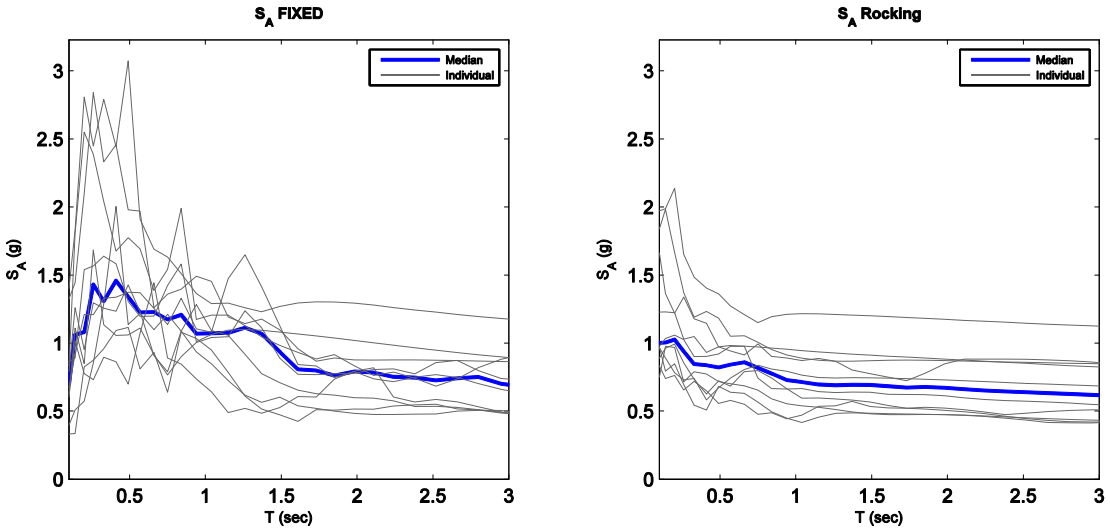

(a) fixed base (b) uplifting system α=3.0

Figure 6.20 S_A representative mean response (10% in 50 years 1D).

6.5.1.1 1D Excitation

The spectral acceleration response of the single-degree-of-freedom system fixed at the base and allowed to uplift is presented in Figure 6.21. The ground motions evaluated are the *X* component of the four groups described in Section 6.3.8. Typically, the magnitude of acceleration is smaller across all groups for smaller footing widths. As footing size decreases, the reduction in acceleration relative to fixed-base response increases. This observation does not hold for very short-period, stiff structures ranges. The near fault, 2% in 50, 10% in 50, and 50% in 50 year probability of exceedance, groups all have accelerations larger than the fixed base at 0.25 sec or less [Figure 6.21 (a)– (d)].

The uplifting system amplifies the acceleration in the short-period range. For longer period structures (T_{nf} = 2.0 sec.), the uplifting response approaches the fixed-base response. As the footing width increases, the reduction in acceleration decreases. However, even for large footing widths (α=6) where there is not significant uplift, the rocking motion of the system still dissipates some of the energy. The figures show that as the magnitude of the input excitation increases the amount of acceleration reduction is increased.

6.5.1.2 3D Excitation

The spectral acceleration response of the single-degree-of-freedom system to three-dimensional input accelerations of the four ground motion groups is presented in Figure 6.22 through Figure 6.25. Typically, allowing the footing to uplift reduces the peak accelerations; the smaller the footing the more the amount of reduction. As shown for the one-dimensional input excitation at periods less than approximately 0.25 sec, the acceleration of uplifting systems is actually larger. At periods of approximately 2.0 sec or longer, the uplifting response approaches the fixed-base response.

Figure 6.22 illustrates the *X* and *Y* response of the near fault inputs. In the *X*-direction there appears to be more acceleration reduction than the *Y*-direction. However, they both present

acceleration reductions when allowed to uplift. For example, at T=1.0 sec for the α=3.0 footing the X and Y acceleration reduction is 1.3g/0.8g = 1.6 and 1.0g/0.6g = 1.67, respectively. In this case, the magnitudes of reduction are actually quite similar. The one-dimensional X response [Figure 6.21(a)] and three-dimensional X response are very similar, indicating there may be little interaction for the near-fault records.

The 2% in 50 acceleration response to three-dimensional input is shown in Figure 6.23. There is a significant reduction in acceleration when allowing the footing to uplift especially for the α=3.0 footing. The 10% in 50 acceleration response is shown in Figure 6.24. The 50% in 50 years is shown in Figure 6.25. The three-dimensional input excitation does not seem to significantly alter the X-direction magnitudes (Figure 6.21) for the elastic column-soil assumption. See Section 6.7 for a discussion on the ratio of amplification of uplifting footings to fixed base response.

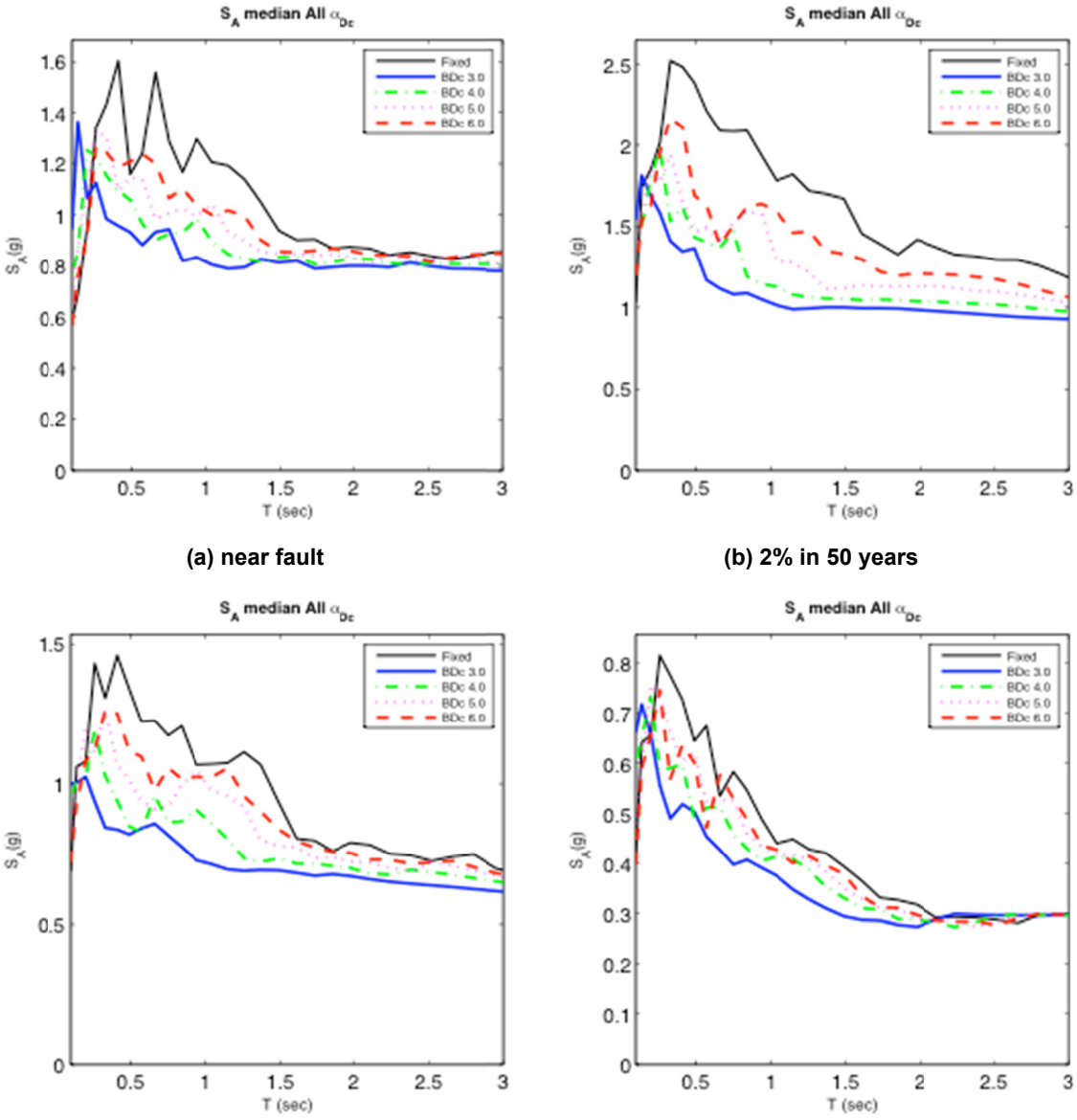

(a) near fault

(b) 2% in 50 years

(c) 10% in 50 years

(d) 50% in 50 years

Figure 6.21 S_A **mean response; elastic column-soil (all ground motions 1D).**

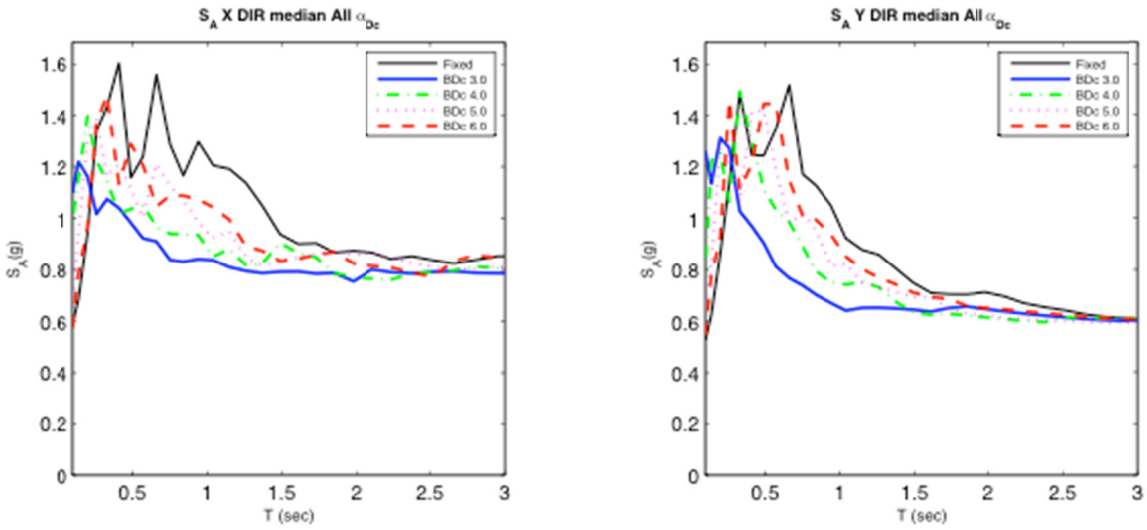

Figure 6.22 S_A **mean response; elastic column-soil (near fault 3D).**

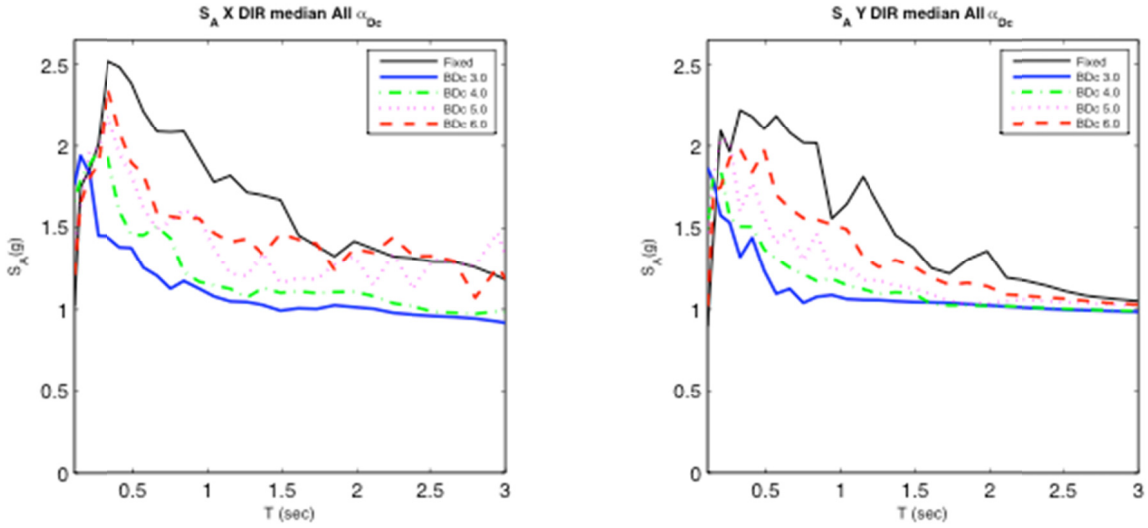

Figure 6.23 S_A **mean response; elastic column-soil (2% in 50 years 3D).**

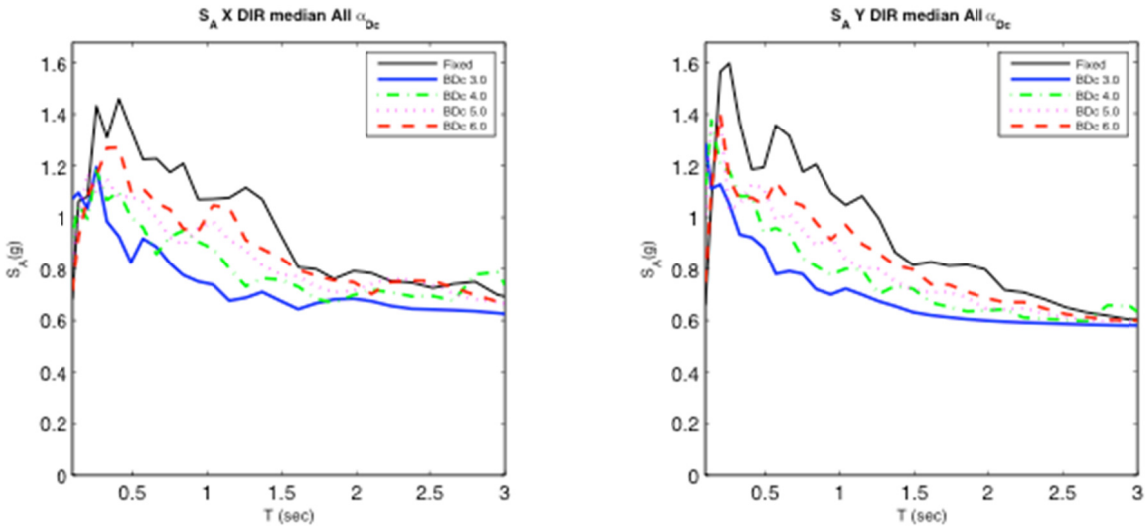

Figure 6.24 S_A **mean response; elastic column-soil (10% in 50 years 3D).**

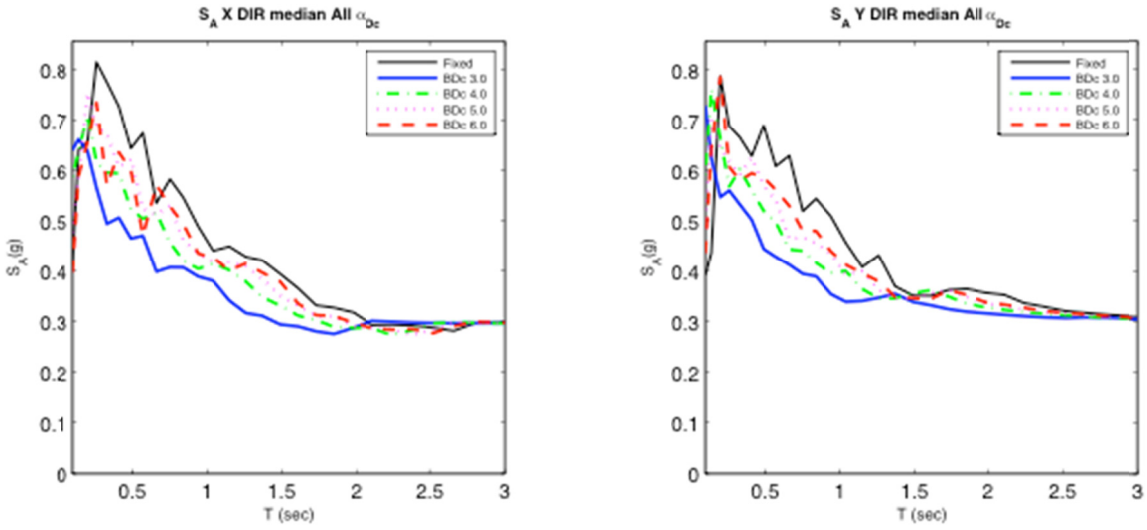

Figure 6.25 S_A **mean response; elastic column-soil (50% in 50 years 3D).**

6.5.2 Inelastic Column and Elastic Soil

Spectral acceleration response of the single-degree-of-freedom system with nonlinear column and elastic soil model assumption is presented next. Figure 6.26 through Figure 6.29 show the one-dimensional and three-dimensional input excitation response for the three ground motion groups and the three footing widths. The 50% in 50 year probability of exceedance motions were not presented in this section because the magnitude of nonlinear behavior was small. The α=6.0 footing width group is not presented either because the footing essentially acts as a fixed-base system when nonlinear response is evaluated. The total displacements, moment-curvature, and base shear are all very similar to the fixed-base response for this footing width.

6.5.2.1 One-Dimensional Excitation

The one-dimensional spectral acceleration response for nonlinear column and soil is presented in Figure 6.26. Plots (a)-(c) show the near fault, 2% in 50 years, and 10% in 50 years acceleration responses. Typically, these footings all have identical acceleration at periods of 1.0 sec or larger, which differs from the elastic column-soil assumption (Section 6.5.1). It can be inferred that the uplifting systems are reaching the acceleration at which yield occurs and no more force is being developed in the system.

For period ranges less than 1.0 sec, typically the uplifting systems are developing slightly larger accelerations, especially for the α=3.0 footing widths. The α=4.0 and α=5.0 footing widths approach the fixed-base response. The increase in this range is on the order of 30%–100%. While these are relatively large percentage increases, they may be small for the system. A refined analysis that includes displacements of the system for this period range will assist in answering if uplifting of nonlinear columns-elastic soil is viable. See Section 6.7 for more discussion.

6.5.2.2 Three-Dimensional Excitation

The acceleration response of the nonlinear column-elastic soil model subjected to three-dimensional input excitation is presented in Figure 6.27 through Figure 6.29 for the three ground motion groups. Typically, the fixed-base and uplifting systems have very similar responses for the periods of 1.0 sec or larger. At less than 1.0 sec, the uplifting systems have slightly larger accelerations. The peak percentage increase is approximately 20%–30% for the three-dimensional input excitation, which is less than the one-dimensional input excitation. The α=3.0 footing width appears to have the largest increase relative to the fixed base. The α=4.0 and α=5.0 widths more closely resemble the fixed base. When compared to the one-dimensional input excitation, the magnitude of acceleration is reduced, indicating the *Y* component affects the response of the column. This is likely due to more inelastic response occurring in the *Y*-direction and further dissipating the input energy.

It appears that for the three ground motion groups in both directions of input the column is reaching the acceleration at which yield occurs and developing no further acceleration. This does not answer how much inelastic action occurs, only that there is some. The amount of inelasticity may better be answered by evaluating displacements of the system. For example, the ductility of the uplifting and fixed-base systems may be different. See Section 6.7 and 6.8 for a discussion of displacement response for uplifting and fixed-base systems.

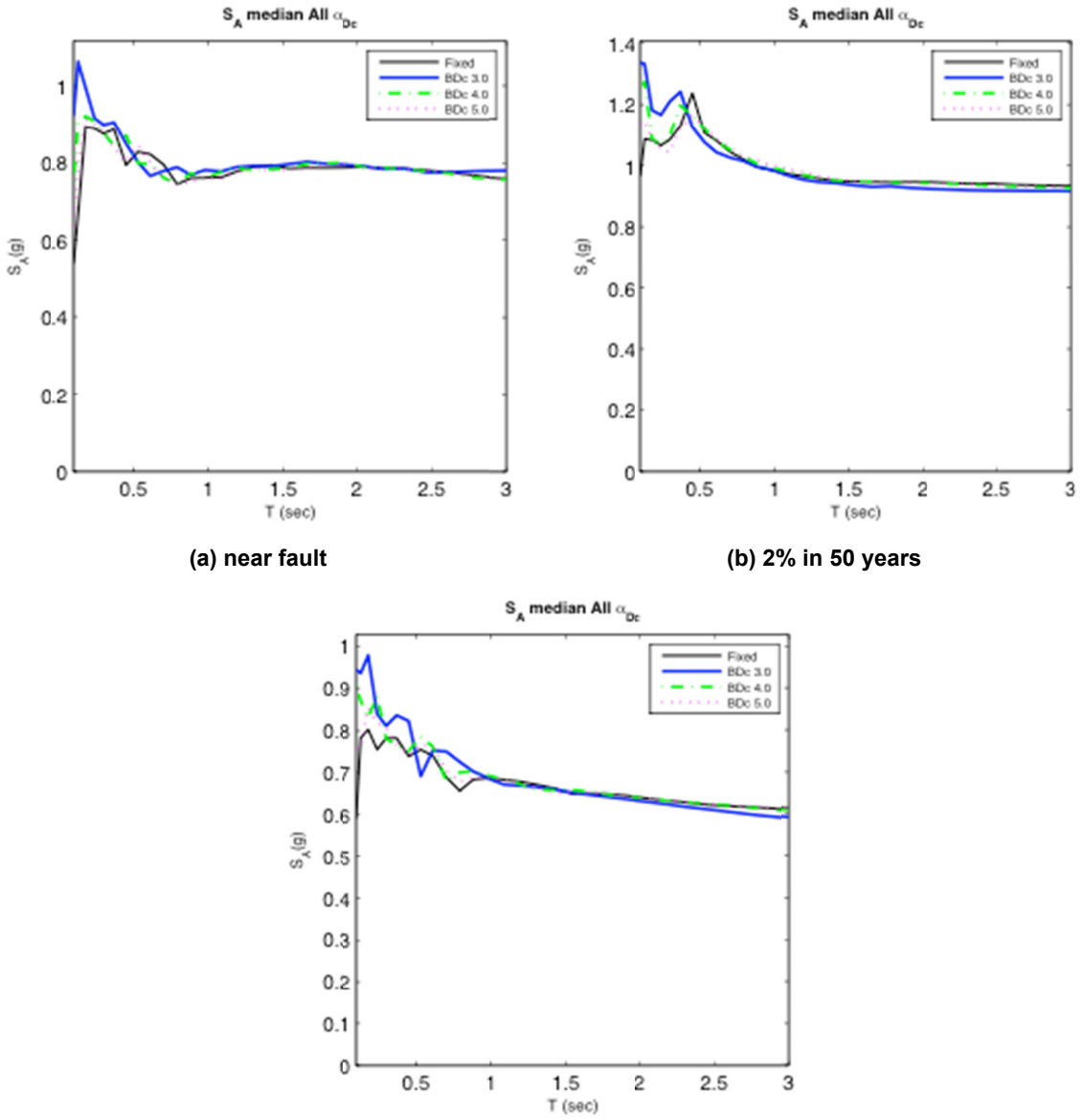

(a) near fault

(b) 2% in 50 years

(c) 10% in 50 years

Figure 6.26 S_A **mean response; nonlinear column-elastic soil (all ground motions 3D).**

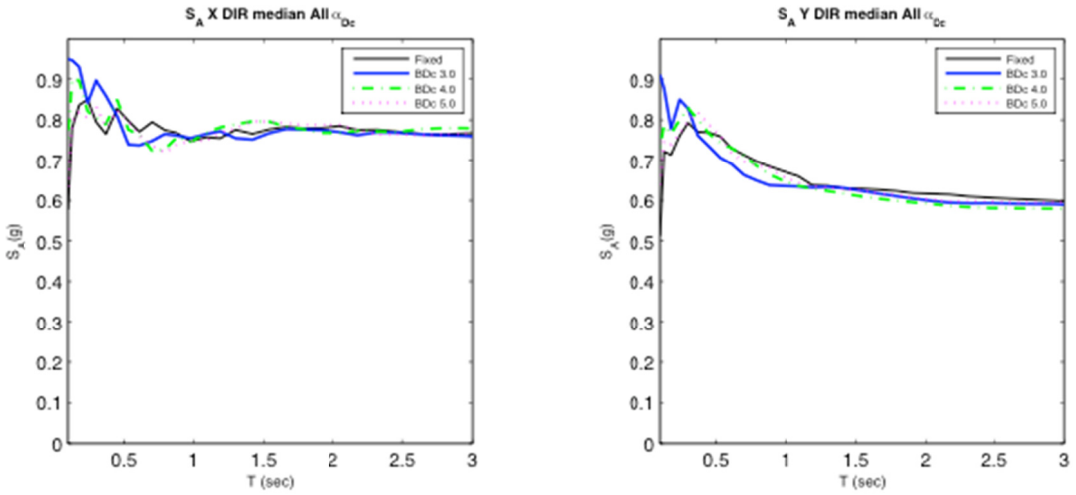

Figure 6.27 S_A **mean response; nonlinear column-elastic soil (near fault 3D).**

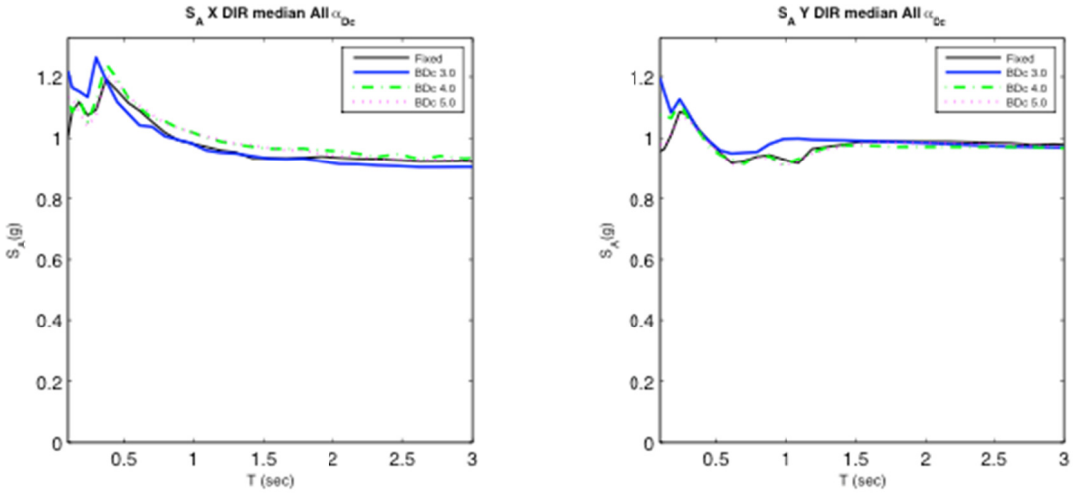

Figure 6.28 S_A **mean response; nonlinear column-elastic soil (2% in 50 years 3D).**

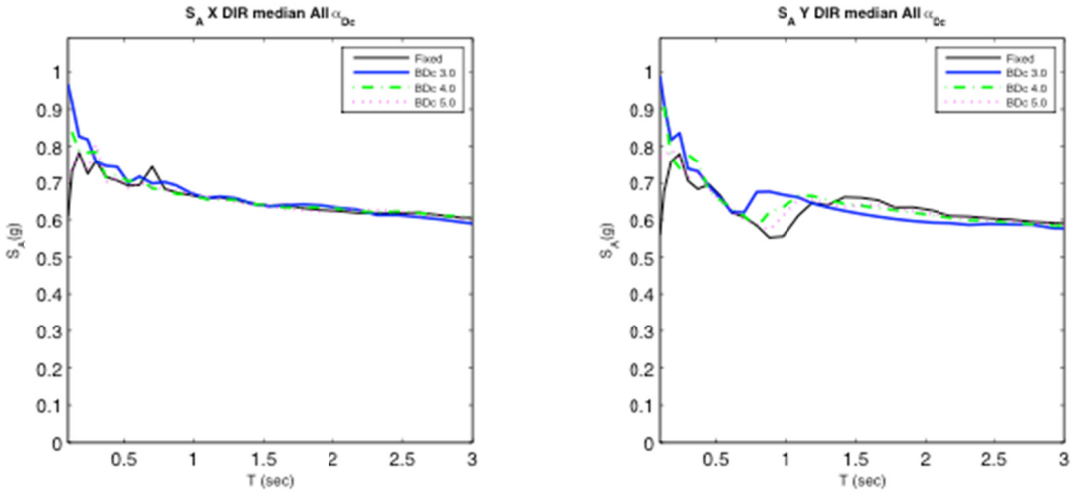

Figure 6.29 S_A **mean response; nonlinear column-elastic soil (10% in 50 years 3D).**

The spectral displacement response of the uplifting system for the two analytic column and soil combinations considered is presented next. As described in the representative case in Section 6.4.3, the two types of column displacement of uplifting systems are compared to the fixed-base response. The intent is to illustrate the relative response between the uplifting and fixed-base response and highlight benefits and drawbacks. As is expected, the rocking response will approach the fixed-base response as the footing width increases. To simplify the presentation, only the total and flexural rocking components will be shown compared to the fixed base. The rocking component of response may be inferred from the total and flexural column displacement presented. Also the response for each footing width will be presented on one plot for each ground motion group.

6.5.3 Elastic Column and Soil

Figure 6.30 shows the mean response determination for the 10% in 50 year probability of exceedence group assuming a footing to column width ratio of 3.0. The plot in Figure 6.30(a) shows the fixed base response; Figure 6.30(b) the total rocking response; Figure 6.30(c) the flexural component of total rocking response; and Figure 6.30(d) the rocking component of total rocking response. Note that the amount of flexural column displacement for uplift is very uniform despite the wide variance of total rocking displacement and column displacement from footing uplift.

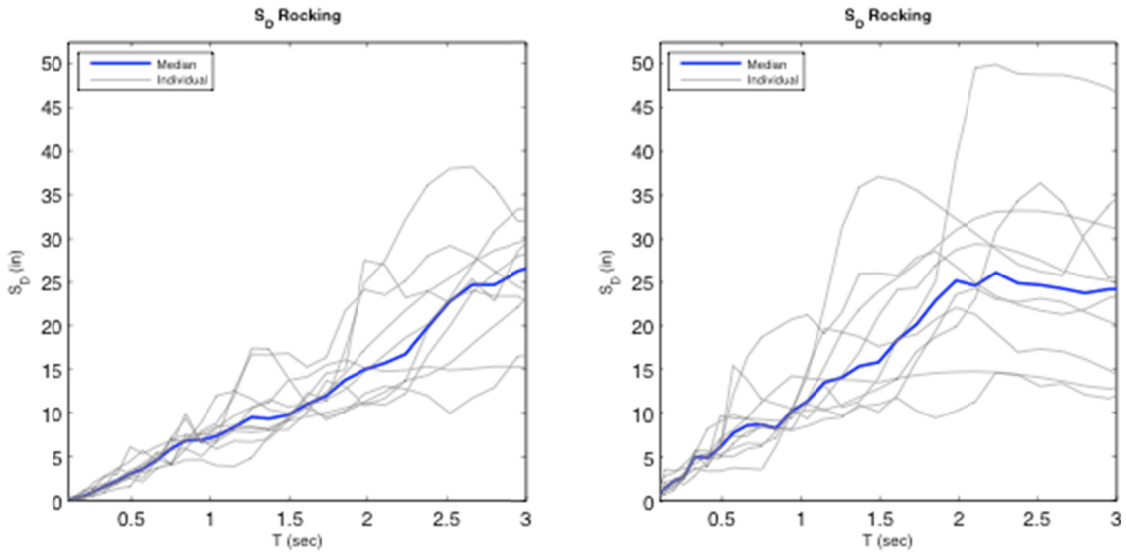

(a) fixed S_{DF}

(b) rocking S_{DR}

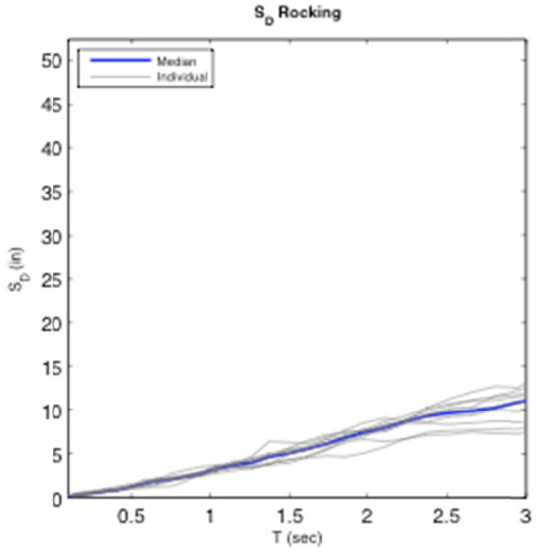

(c) flexural S_{DRF}

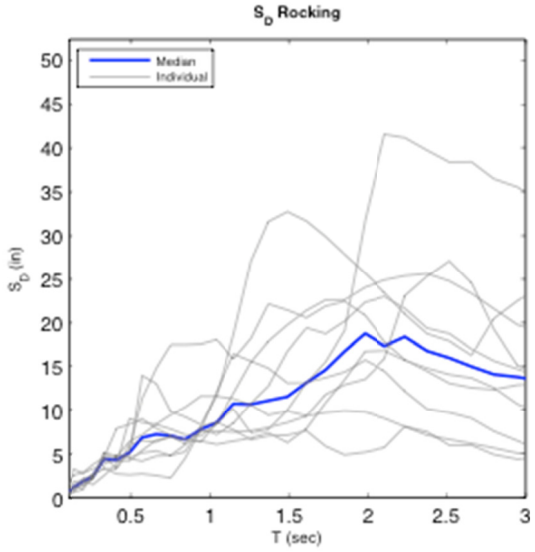

(d) rocking S_{DRR}

Figure 6.30 S_D representative mean response (10% in 50 years 1D).

6.5.3.1 One-Dimensional Excitation

The uplifting system displacement response for the four ground motion groups subject to the one-dimensional X input excitation is presented in Figure 6.31 through Figure 6.34. The total displacements are compared in the (a) figure and the column flexural displacements are presented in the (b) figure. Total column displacements of the uplifting systems are typically larger than the fixed-base response. Figure 6.31(a) shows the near-fault ground motion group. The α=3.0 footing is larger for the period range, shown while the α=6.0 is approximately the same as fixed base. The 2% in 50 year response also has larger total displacements than the fixed base; however, they converge at approximately 2.5 sec at which point the magnitude of rocking response becomes smaller. The 10% in 50 and 50% in 50 year cases also have larger uplifting

response, e.g., for a structure with T_{nf}=1.5 sec, the ratio of uplifting to fixed base total displacement for α=3.0 is approximately 1.18–2.31, for the four footing groups. As the footing width increases, all total displacements approach the fixed-base response.

The amount of column flexural displacement is consistently less than the fixed base-response, indicating that allowing uplift reduces the amount of column flexural displacement and likely the inelastic response for a wide range of footing widths. This shows that if the fixed-base system can accommodate the total predicted displacement when uplifting, there is a likely benefit in reduced column response. See Section 6.8 for the comparison of rocking displacement to fixed base ratios as a function of period.

6.5.3.2 Three-Dimensional Excitation

The spectral displacement response to the three-dimensional input excitation for the four ground motion groups is presented in Figure 6.35 through Figure 6.38. The (a) plot shows the *X* and *Y* total displacements and the (b) plots shows the *X* and *Y* column flexural displacements. Typically, the total displacement of uplifting systems is greater than the fixed-base response. As was shown in the discussion of one-dimensional displacements, the α=3.0 footing has more total displacement than the α=6.0 footing for all ground motions. The amount of displacement amplification appears to be similar to the one-dimensional response; on the order of 1–2 times larger. Column flexural displacement is consistently less than the fixed-base response, indicating less flexural demand on the column and a likely reduction in inelastic response.

The interaction of displacements from multi-directional input is not readily apparent. It appears that the one-dimensional and three-dimensional *X* response are relatively similar. Section 6.8 will discuss in greater details the comparison of the ratios of uplift to fixed-base displacements. It appears that the smaller the excitation, the less the amount of uplift that occurs. The 2% in 50 year results appear to have more uplift than the 10% in 50 year ones, which in turn have more than the 50% in 50 year response. The near-fault motions seem to have larger rocking response in the period range matching the pulse period of the near-fault motions.

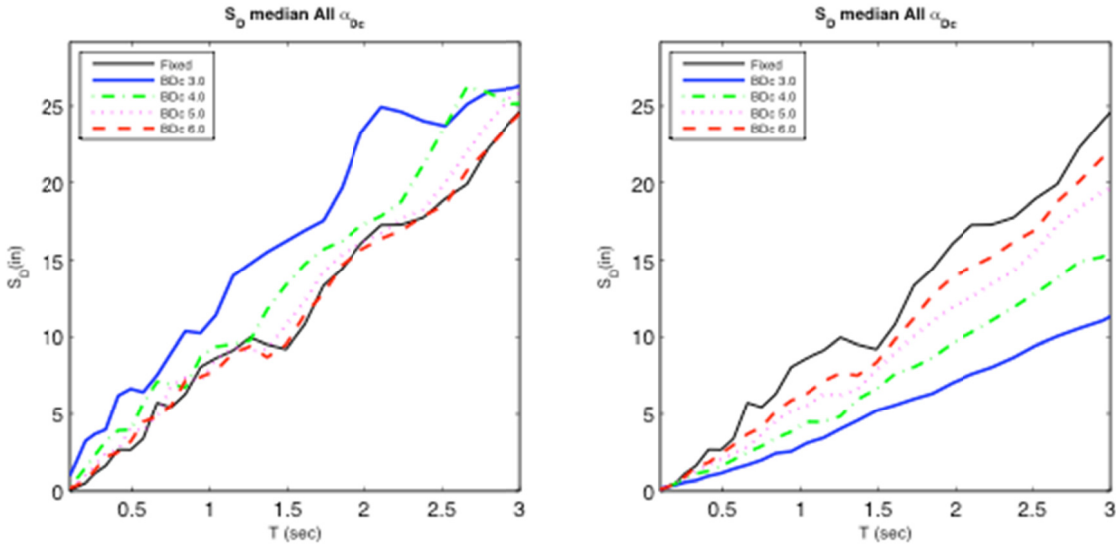

(a) S_{DR} (b) S_{DRF}

Figure 6.31 S_D mean response; elastic column-soil (near fault 1D).

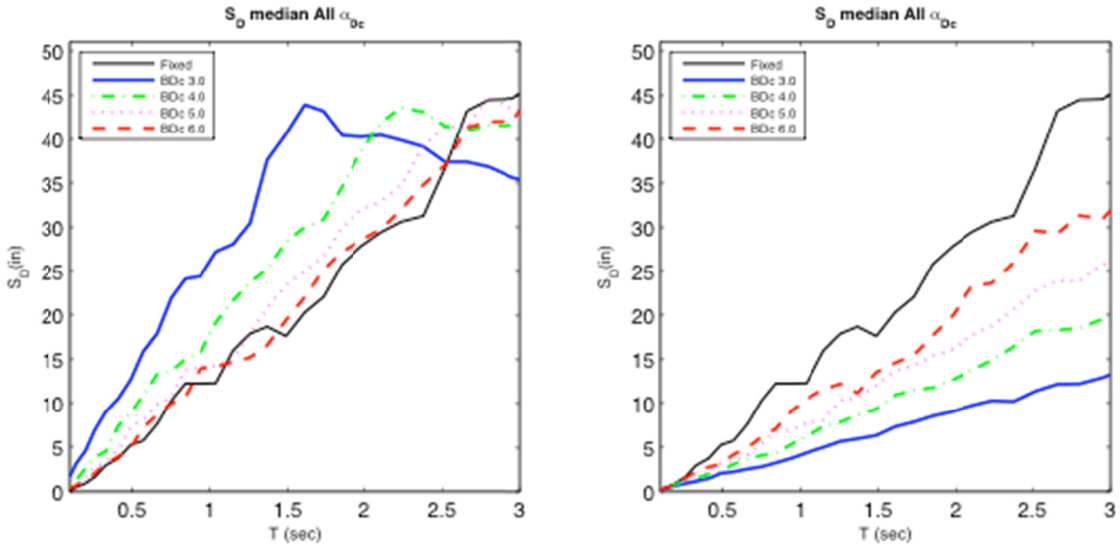

(a) S_{DR} (b) S_{DRF}

Figure 6.32 S_D mean response; elastic column-soil (2% in 50 years 1D).

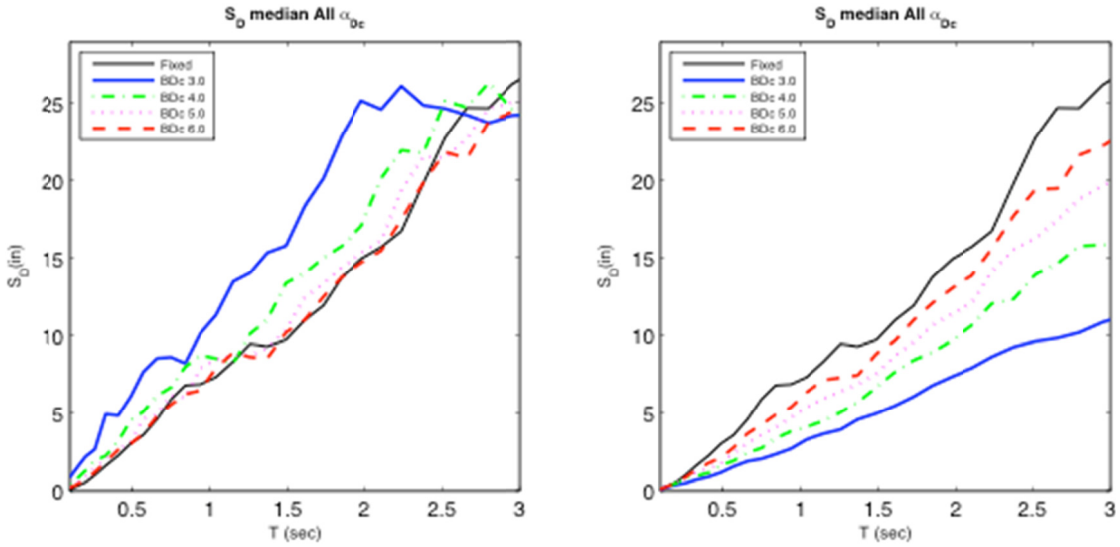

(a) S_{DR} **(b) S_{DRF}**

Figure 6.33 S_D **mean response; elastic column-soil (10% in 50 years 1D).**

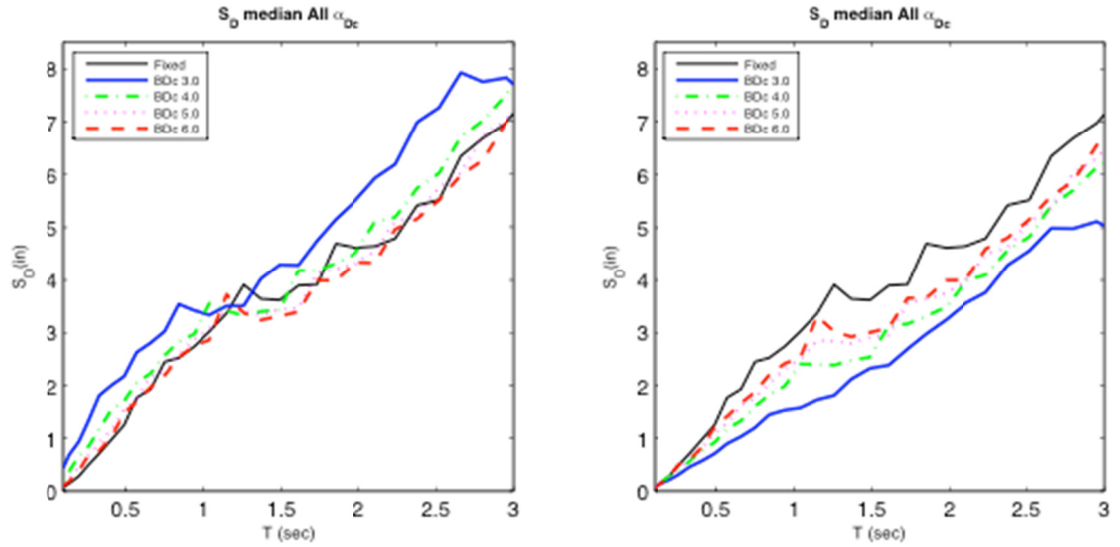

(a) S_{DR} **(b) S_{DRF}**

Figure 6.34 S_D **mean response; elastic column-soil (50% in 50 years 1D).**

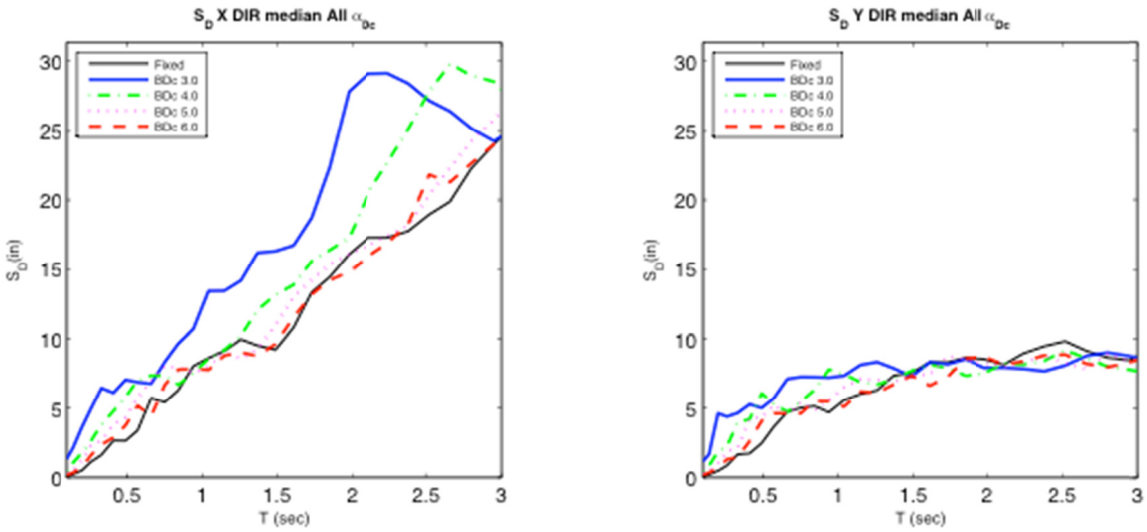

(a) S_{DR}

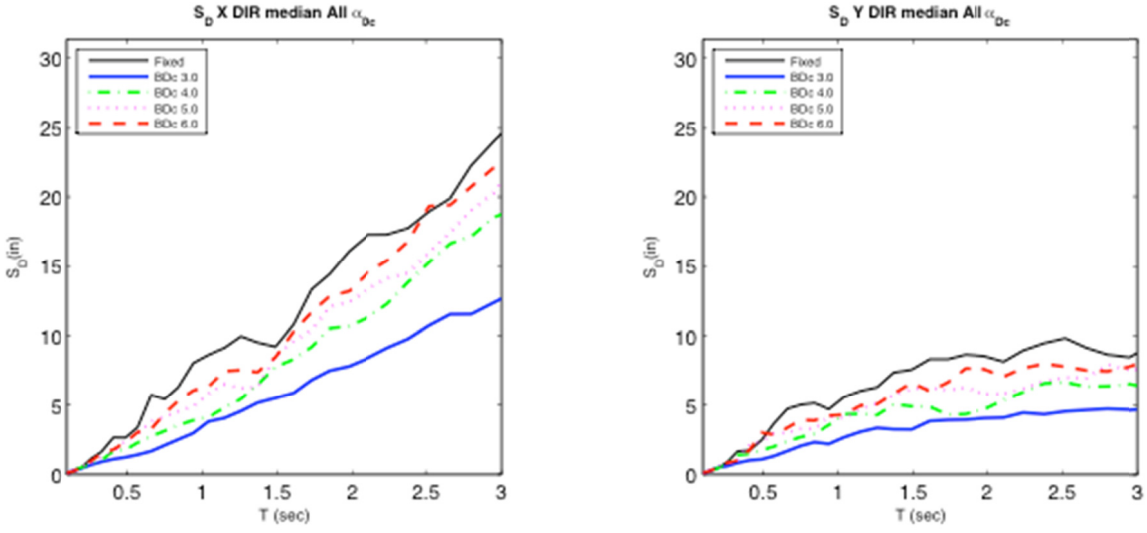

(b) S_{DRF}

Figure 6.35 S_D Mean response; elastic column-soil (near fault 3D).

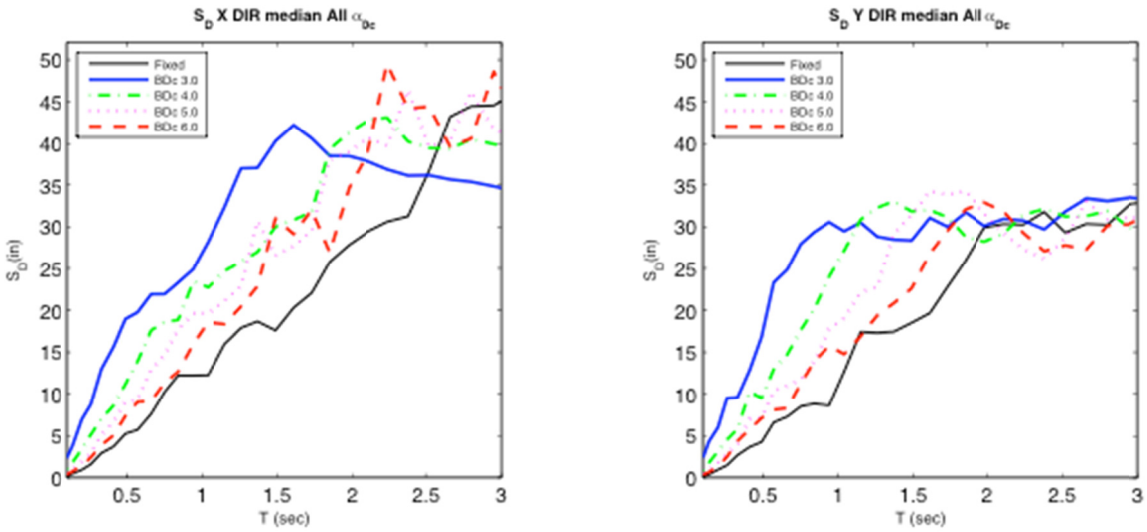

(a) S_{DR}

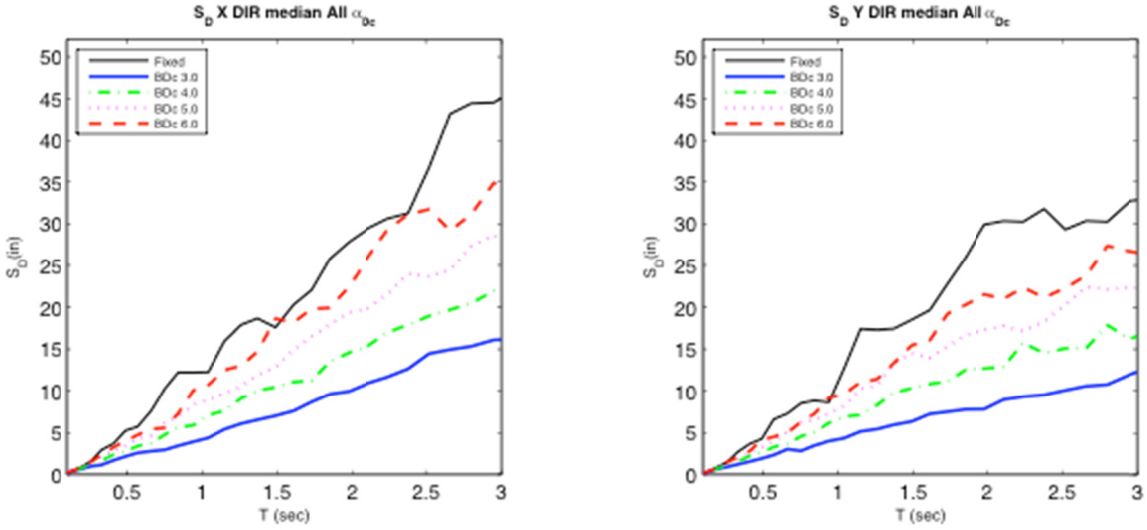

(b) S_{DRF}

Figure 6.36 S_D mean response; elastic column-soil (2% in 50 years 3D).

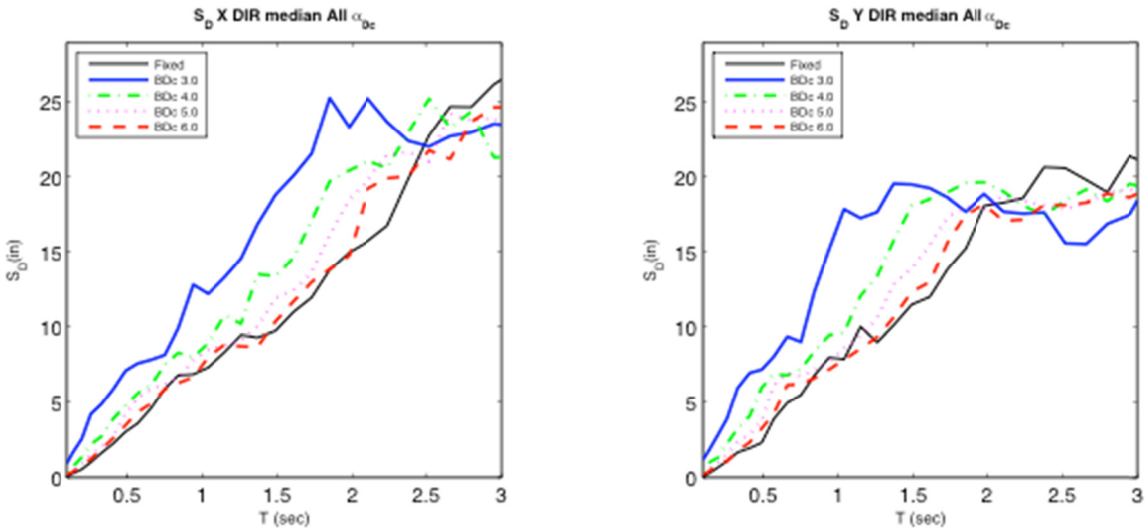

(a) S_{DR}

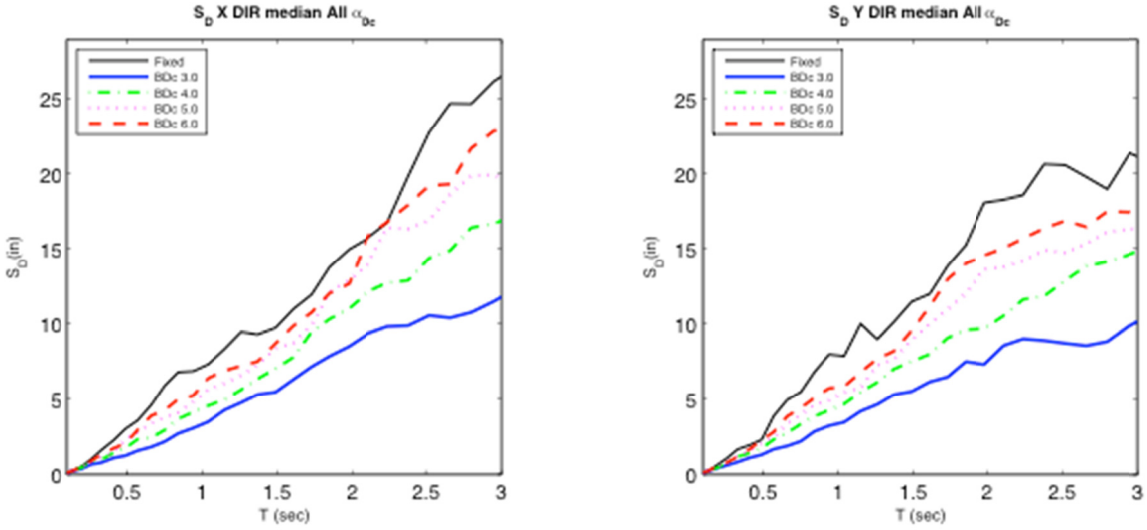

(b) S_{DRF}

Figure 6.37 S_D mean response; elastic column-soil (10% in 50 years 3D).

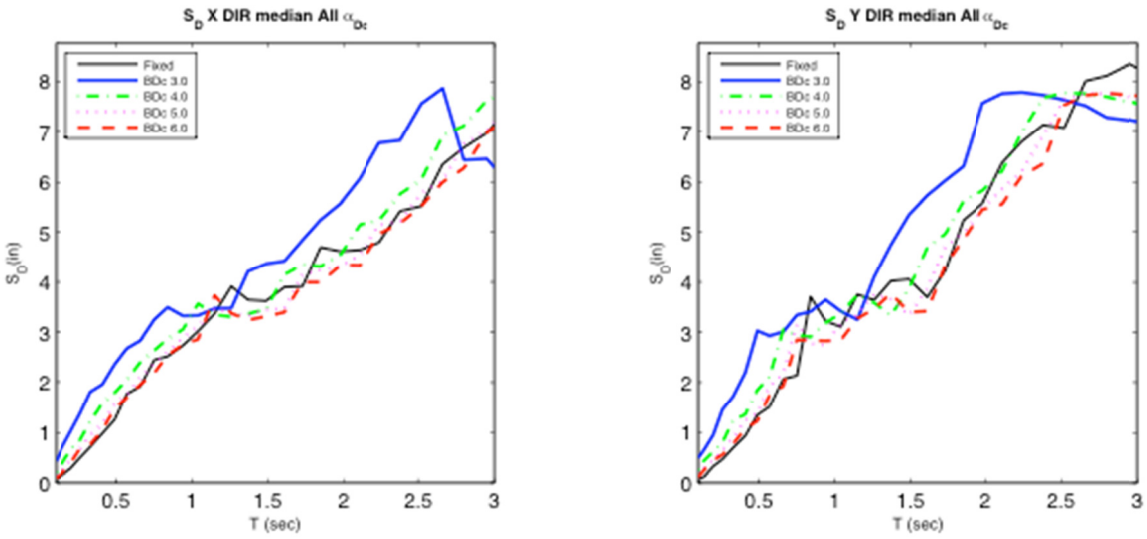

(a) S_{DR}

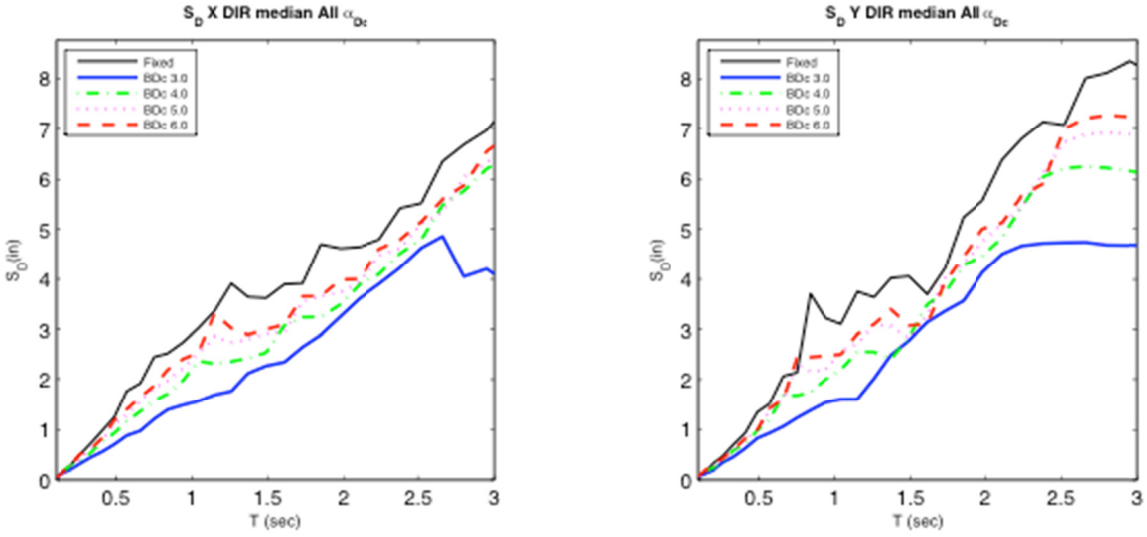

Figure 6.38 S_D mean response; elastic column-soil. (50% in 50 years 3D).

6.5.4 Inelastic Column and Elastic Soil

The response of uplifting footings assuming nonlinear column and elastic soil model assumption is presented next. The ground motions used are the same as described in the Section 6.6.1. The total and column flexural displacements of uplifting systems are plotted against the fixed-base response. As was discussed in Section 6.5.2.2, the 50% in 50 year ground motion is not presented and the α=6.0 footing width is excluded.

6.5.4.1 One-Dimensional Excitation

Displacement response of the uplifting system to one-dimensional *X* input excitation is presented in Figure 6.39 through Figure 6.41. The consideration of inelastic action appears to alter the response of the total displacement, which is shown in plot (a). For each ground motion group the total displacements are approximately equal for the 0 to 1.5 sec range. However, for the 2% in 50 year and 10% in 50 year motions, the total displacement of uplifting systems is less than the fixed-base response at periods greater than 1.5 sec.

The column flexural displacements are also very similar for periods less than or equal to 1.5 sec, as shown in the (b) plots. At periods larger than 1.5 sec, the amount of column displacement is less than the fixed-base response, indicating a reduction in inelastic action at this range. In general, the α=3.0 footings have the smallest column flexural displacements, which increases as the footing width increases; however they do not reach the level of fixed-base response for these footing widths. Section 6.7 presents the ductility response of uplifting columns, and Section 6.8 presents the ratio of displacements for uplifting and fixed base response.

6.5.4.2 Three-Dimensional Excitation

The displacement response of uplifting footing to three-dimensional input excitation is presented in Figure 6.42 through Figure 6.44. The (a) plots show the total response and the (b) plots show the column flexural displacement. The *X* and *Y* components of displacement are presented for each ground motion group.

The total displacements are similar for the *X*- and *Y*-direction for the fixed base and the three footing widths considered. Typically the α=3.0 footing width has smaller displacements but not significantly smaller than the other footing widths and fixed-base response. The exception is the *Y*-direction of the 2% in 50 year group, which has a larger discrepancy compared to fixed base response than the others.

The column flexural displacements in the *X*-direction are similar to the one-dimensional excitation response. The fixed-base and uplifting systems are approximately the same for 0 to 1.5 sec period structures. At periods larger than 1.5 sec, the uplifting footing systems have smaller displacements; the *Y*-direction is similar although the amount of reduction at 1.5 sec appears to be less. This may be due to smaller excitation accelerations in the *Y*-direction. This result is also observed for the difference between ground motion groups 2%, 10%, and 50% probability of exceedance. Sections 6.8 and 6.9 have further discussion on the relationship between displacement demands of uplifting and fixed base systems.

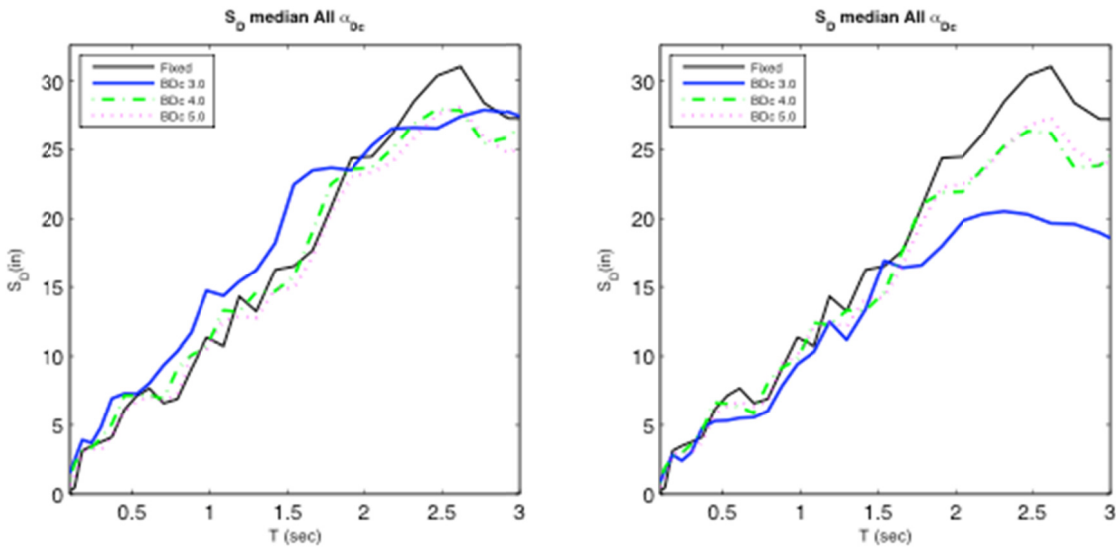

(a) S_{DR} (b) S_{DRF}

Figure 6.39 S_D **mean response; nonlinear column-elastic soil. (near fault 1D)**

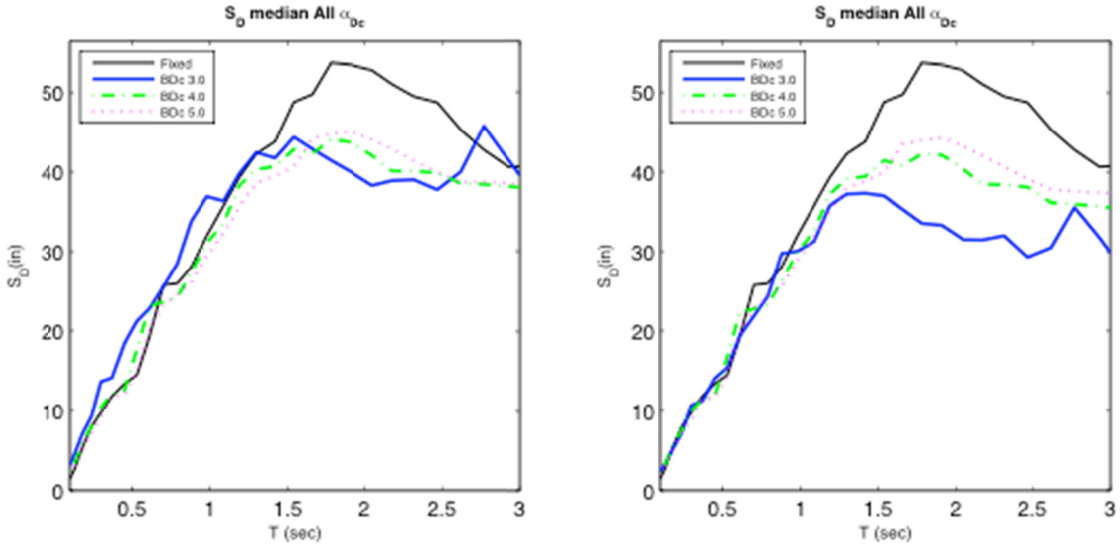

(a) S_{DR} (b) S_{DRF}

Figure 6.40 S_D **mean response; nonlinear column-elastic soil. (2% in 50 years 1D).**

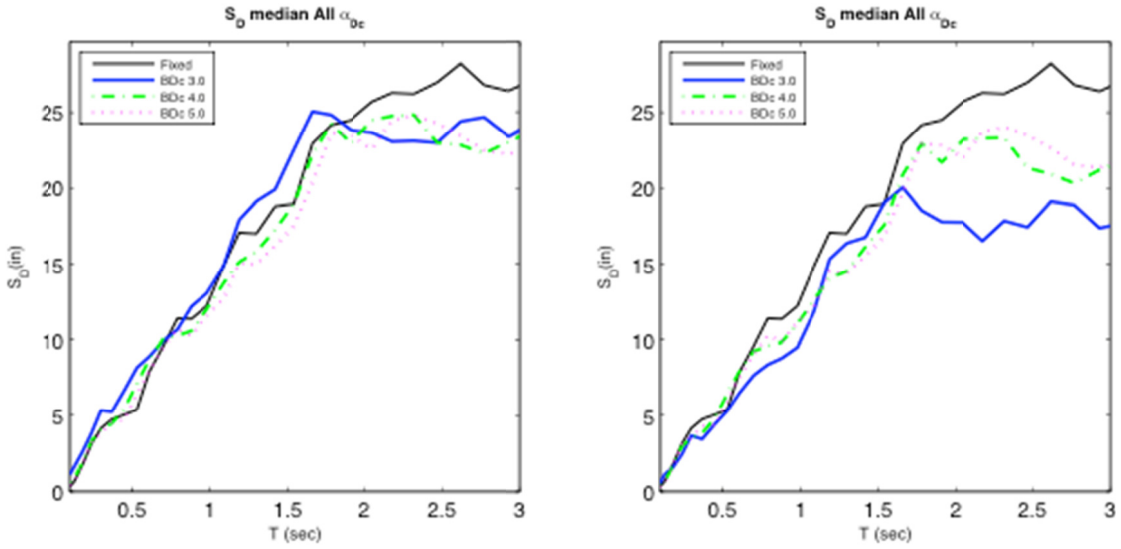

(a) S_{DR} **(b) S_{DRF}**

Figure 6.41 S_D mean response; nonlinear column-elastic soil. (10% in 50 years 1D).

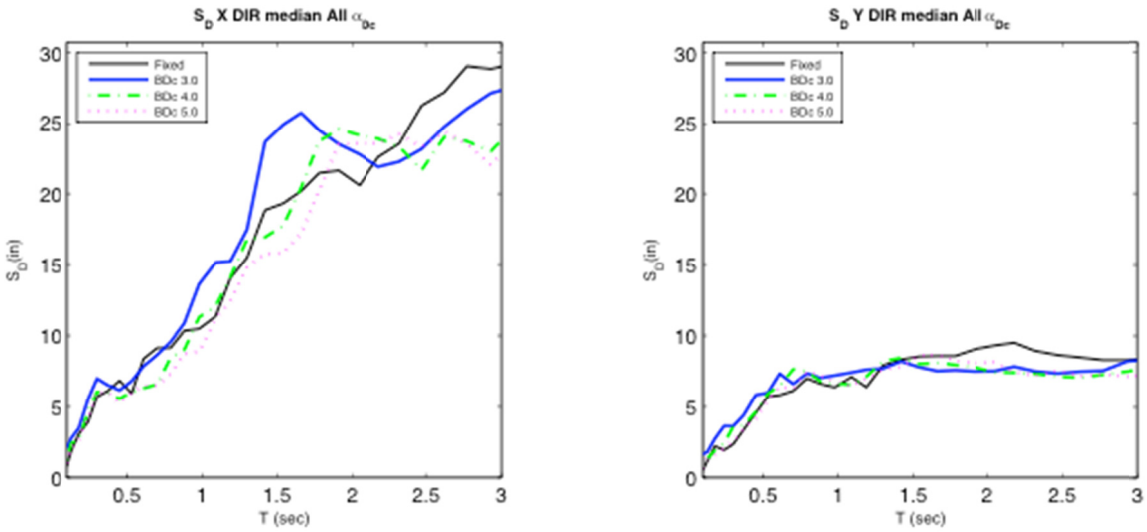

(a) S_{DR}

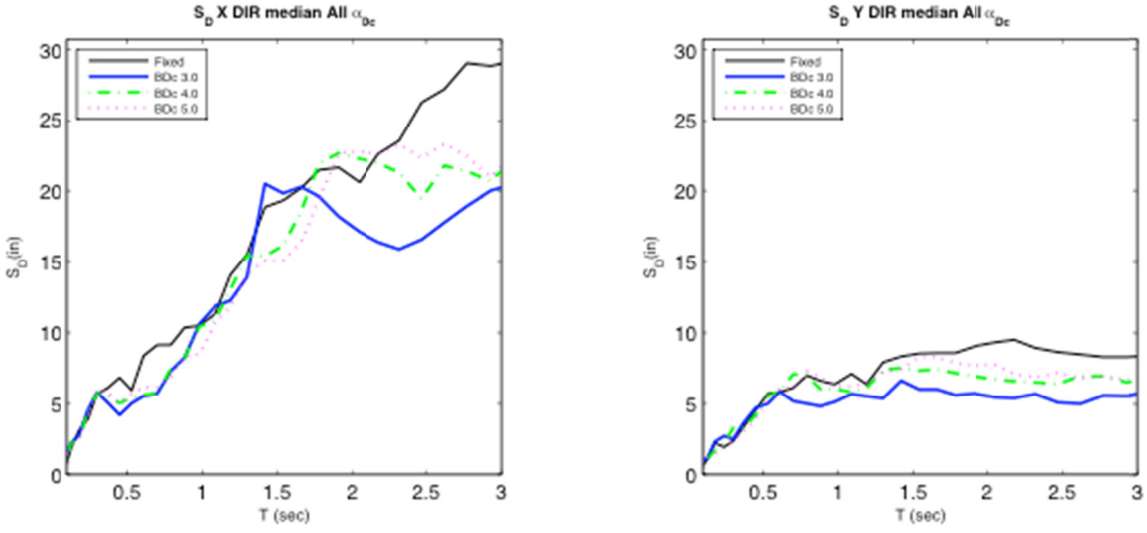

(b) S_{DRF}

Figure 6.42 S_D mean response; nonlinear column-elastic soil (near-fault 3D).

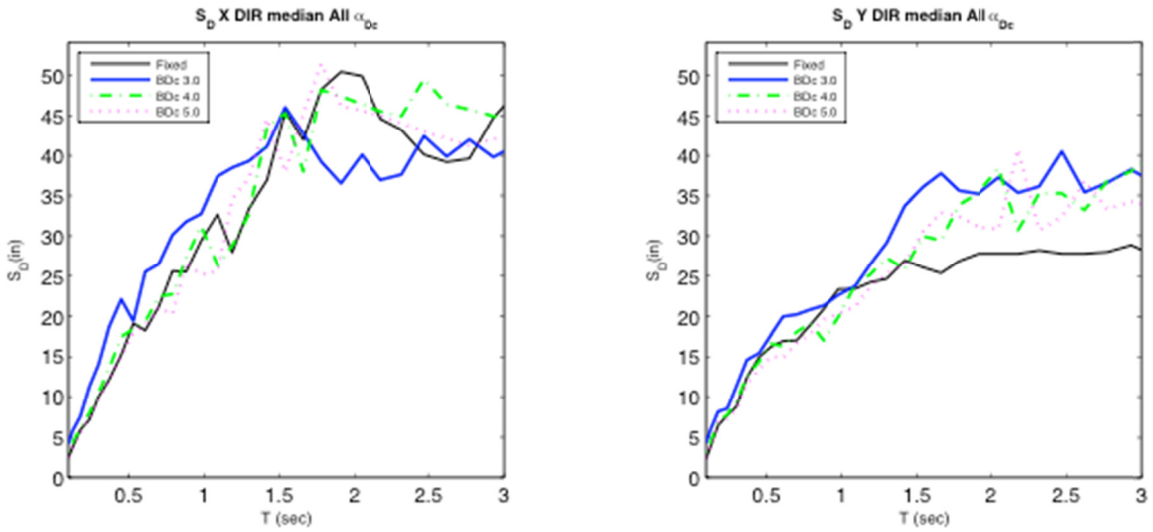

(a) *SDR*

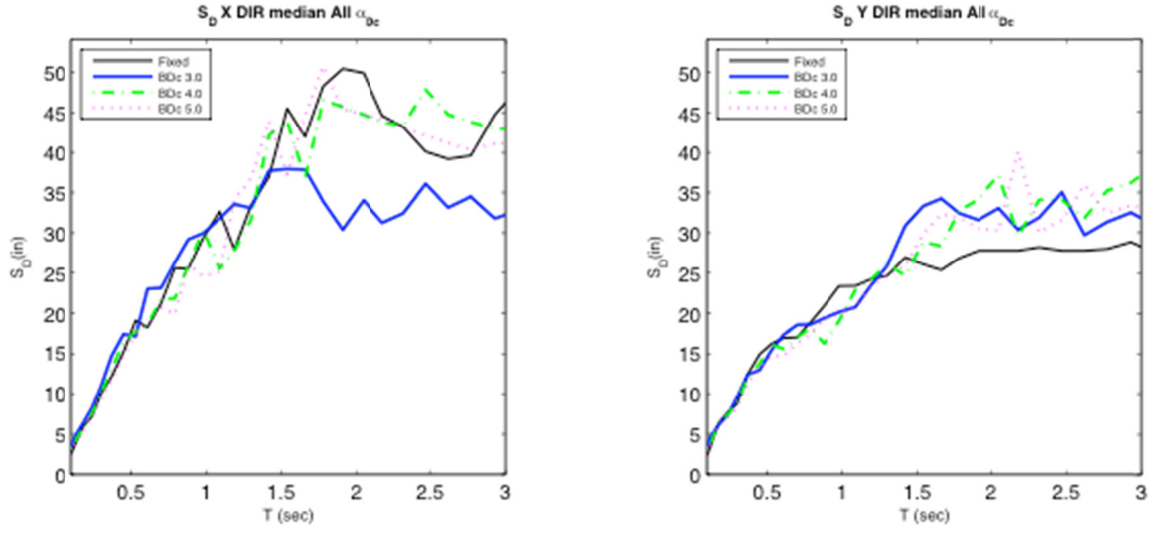

(b) S_{DRF}

Figure 6.43 S_D mean response; nonlinear column-elastic soil (2% in 50 years 3D).

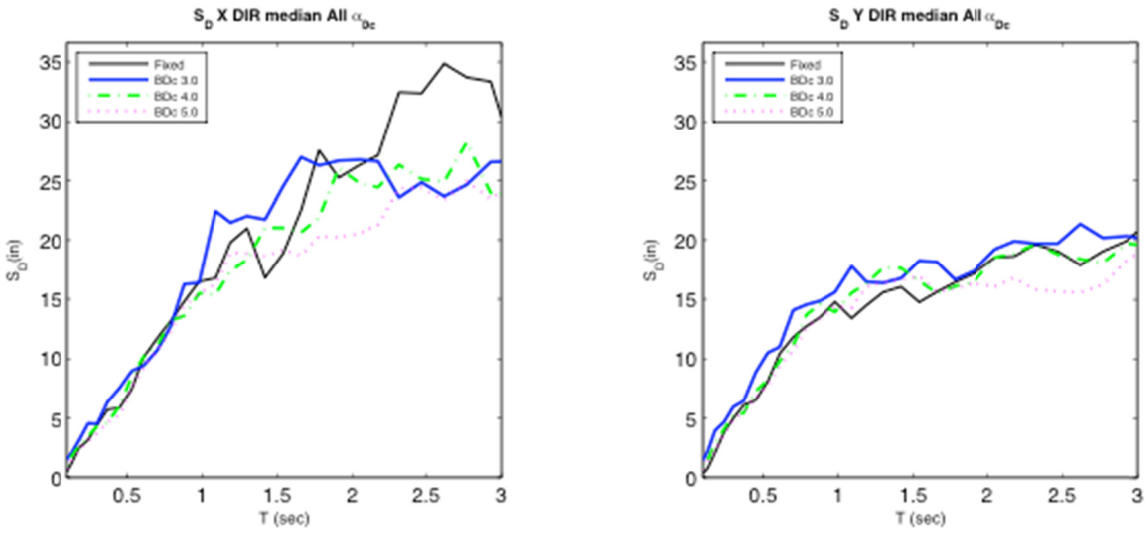

(a) S_{DR}

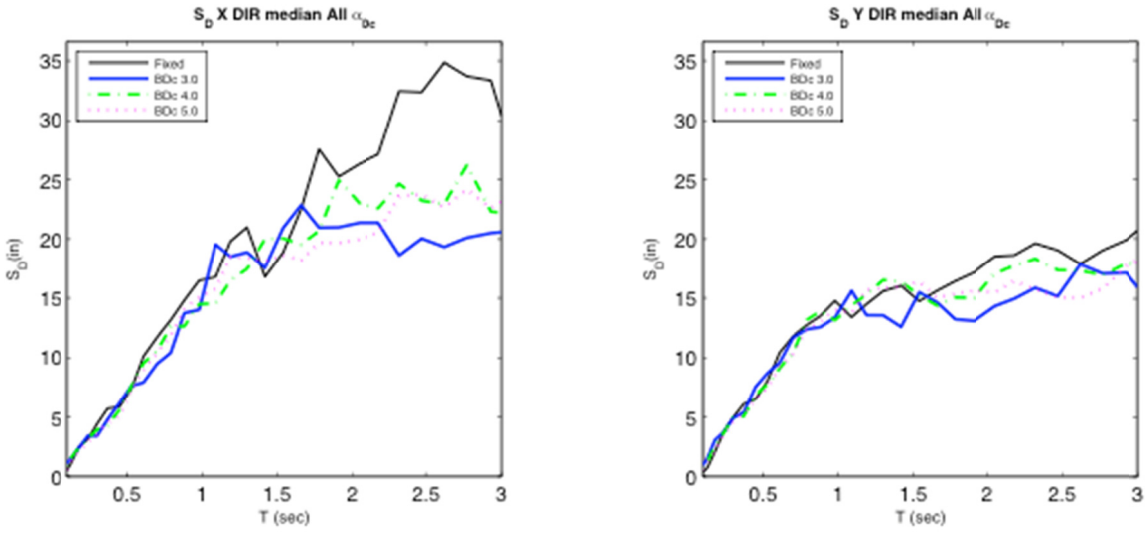

(b) S_{DRF}

Figure 6.44 S_D mean response; nonlinear column-elastic soil (10% in 50 years 3D).

6.6 DISPLACEMENT DUCTILITY RESPONSE OF UPLIFTING BRIDGE PIER SYSTEM

Ductility response of the uplifting and fixed column bases are compared in this section for the nonlinear column - elastic soil model. Ductility values for the three ground motion groups and footing widths are plotted in Figure 6.45 based on the mean spectral displacement presented in Section 6.7. The displacement ductility of the fixed base column is calculated using the standard ratio of total column displacement to column yield displacement [Equation (6.4)].

$$\mu = \frac{u_{total}}{u_{yield}} \tag{6.4}$$

The uplifting system displacement ductility is estimated in Equation (6.5) as the ratio of column flexural displacement to column yield displacement. It is more accurate to use the column curvature deformation ductility [Equation (6.6)] since it accurately captures the moment and resulting curvature demand for the uplifting system with earthquake loading and overturning P-Δ effects. In this case, the uplifting system column displacement ductility will under predict the ductility value, but the difference is on the order of 10%. This is a reasonable approximation for this comparison.

$$\mu = \frac{u_{flexural}}{u_{yield}} \tag{6.5}$$

$$\mu_{\phi} = \frac{\phi_u}{\phi_y} \tag{6.6}$$

Figure 6.45 (a)-(c) shows the ductility demands for the near-fault group for the one-dimensional *X* and three-dimensional *X* and *Y* components. Figure 6.45(d)-(f) shows the ductility demands for the 2% in 50 years group for the one-dimensional *X* and three-dimensional *X* and *Y* components. Figure 6.45(g)-(i) shows the ductility demands for the 2% in 50 group for the one-dimensional *X* and three-dimensional *X* and *Y* components.

Inspection of the plots shows that there is not a significant difference in ductility between the fixed-base system and any of the uplifting footing systems. All of the ground motion groups are very similar in the short- and medium-period range. At the long-period ranges, a select number of the α=3.0 footing widths have smaller ductilities than the fixed-base response, particularly for periods greater than 1.5 sec. The ratio of ductilities in Section 6.7.3 provides more critique of the demand ductilities of uplifting systems.

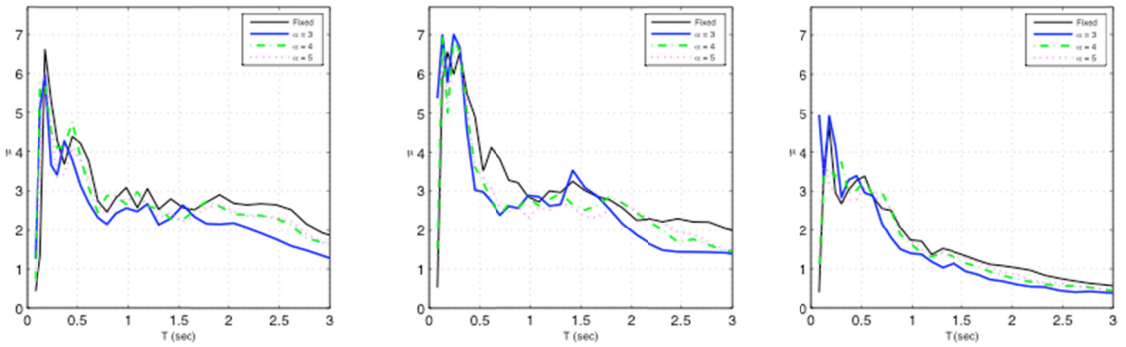

near fault

(a) 1D - *X* **(b) 3D - *X*** **(c) 3D - *Y***

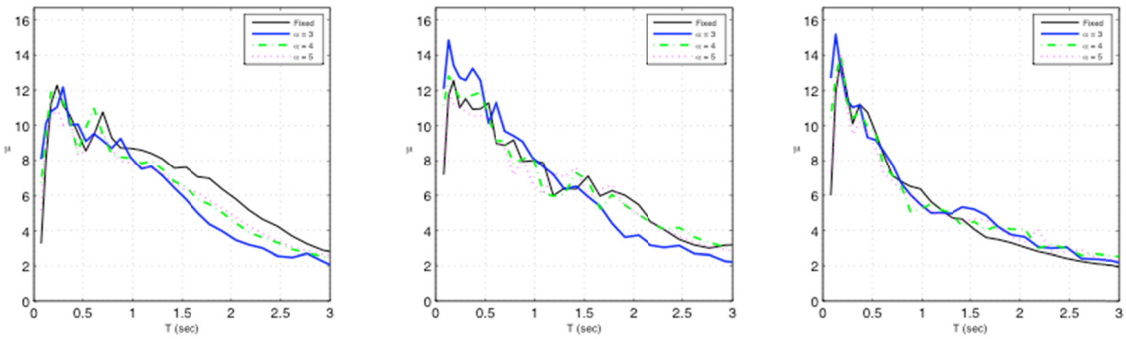

2% in 50 years

(d) 1D - *X* **(e) 3D - *X*** **(f) 3D - *Y***

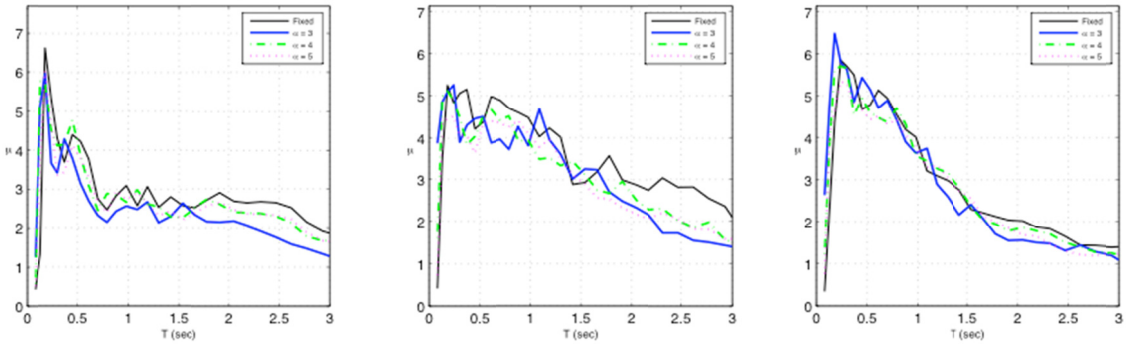

10% in 50 years

(g) 1D - *X* **(h) 3D - *X*** **(i) 3D - *Y***

Figure 6.45 Displacement ductility response.

6.7 SPECTRAL RELATIONSHIP OF UPLIFTING TO FIXED BASE SYSTEMS

The spectral analysis of Sections 6.5 to 6.7 was used to compare uplifting and fixed-base systems and evaluate the benefits and drawbacks of uplifting systems. Periods of all systems are plotted as a function of the corresponding fixed-base period.

6.7.1 Acceleration

The ratio of fixed base to uplifting peak accelerations is calculated as R_R using Equation (6.7). For values of $R_R > 1$ the uplifting systems have a reduced acceleration. Values of $R_R < 1$ indicate the uplifting systems amplify the peak acceleration. Figure 6.46 shows the elastic column-elastic soil R_R values. Mean responses of the 1D*X*, 3D*X*, and 3D*Y* input motions are plotted for each footing width and ground motion group. Figure 6.47 shows the R_R values for the nonlinear column-elastic soil.

$$R_R = \frac{S_{A\ fixed}}{S_{A\ uplift}} \tag{6.7}$$

Elastic column-soil uplifting models have reduced accelerations in the medium period range from 0.5 to 1.5 sec; narrower footing widths have a more significant reduction in acceleration. Also larger magnitude excitations tend to have a larger reduction in accelerations. For the shorter period range, less than 0.5 sec, the uplifting systems amplify the acceleration relative to fixed-base response. For longer period structures, the ratio of uplift to fixed response converges towards unity. Nonlinear column-elastic soil uplifting accelerations are virtually identical to fixed-base response (R_R=1) for periods of 0.5 sec or greater, indicating that the nonlinear uplifting systems reach the same yield acceleration as the fixed-base system. At the short-period range, the uplifting systems also amplify the peak accelerations.

6.7.2 Displacement

The ratio of uplifting total column and flexural column displacement to fixed-base displacement is calculated as γ_R [Equation (6.8)] and γ_{RF} [Equation (6.9)]. Magnitudes < 1 indicate a reduction in displacement for the uplifting system and values > 1 indicate amplification in uplifting systems.

$$\gamma_R = \frac{S_{DR\ total}}{S_{D\ fixed}} \tag{6.8}$$

$$\gamma_{RF} = \frac{S_{DRColFlexural}}{S_{D\ fixed}} \tag{6.9}$$

Figure 6.48 and Figure 6.49 show the elastic column-soil and nonlinear column-elastic soil displacement amplification ratios. The elastic column-soil models show that narrower footing widths tend to have larger total displacements; however, the amount of column flexural displacement is typically about one-half the fixed base displacement. Typically, the greater the magnitude of excitation, the greater is the displacement of the uplifting system. At very short periods, both the total and column flexural displacement of uplifting systems is larger than the fixed base. Longer period structures (> 2.0 sec) tend to have similar displacements, indicated by displacement amplification ratios converging on 1.0. Nonlinear column-elastic soil displacement amplification ratios are approximately 1.0 for the larger footing widths (α=4.0 and α=5.0), except for very stiff structures with $T < 0.25$ sec. The narrow footing width (α=3.0) has a slight

increase in total displacement and a reduction in column flexural displacement, especially for longer period ranges. Short-period structures have significant displacement amplification.

6.7.3 Ductility

Ratio of displacement ductilities for uplifting to fixed-base systems is calculated as μ_R [Equation (6.10)]. Values < 1 indicate a reduction in ductility demand of uplifting systems and >1 indicate an increase in ductility. Rocking can be beneficial or neutral when μ_R is less than or equal to 1, which means reduced inelastic action.

$$\mu_R = \frac{\mu_{uplift}}{\mu_{fixed}} \tag{6.10}$$

Figure 6.50 shows the ductility amplification ratio. For the footing widths and ground motion groups shown, there is a reduction in the ductility demand for medium and long-period ranges. Short periods have a significant increase in the ductility demand. The narrow footing width (α=3.0) has approximately a 25% reduction in the ductility demand for medium and long periods. Wider footings (α=4.0 and α=5.0) have approximately a 10% reduction.

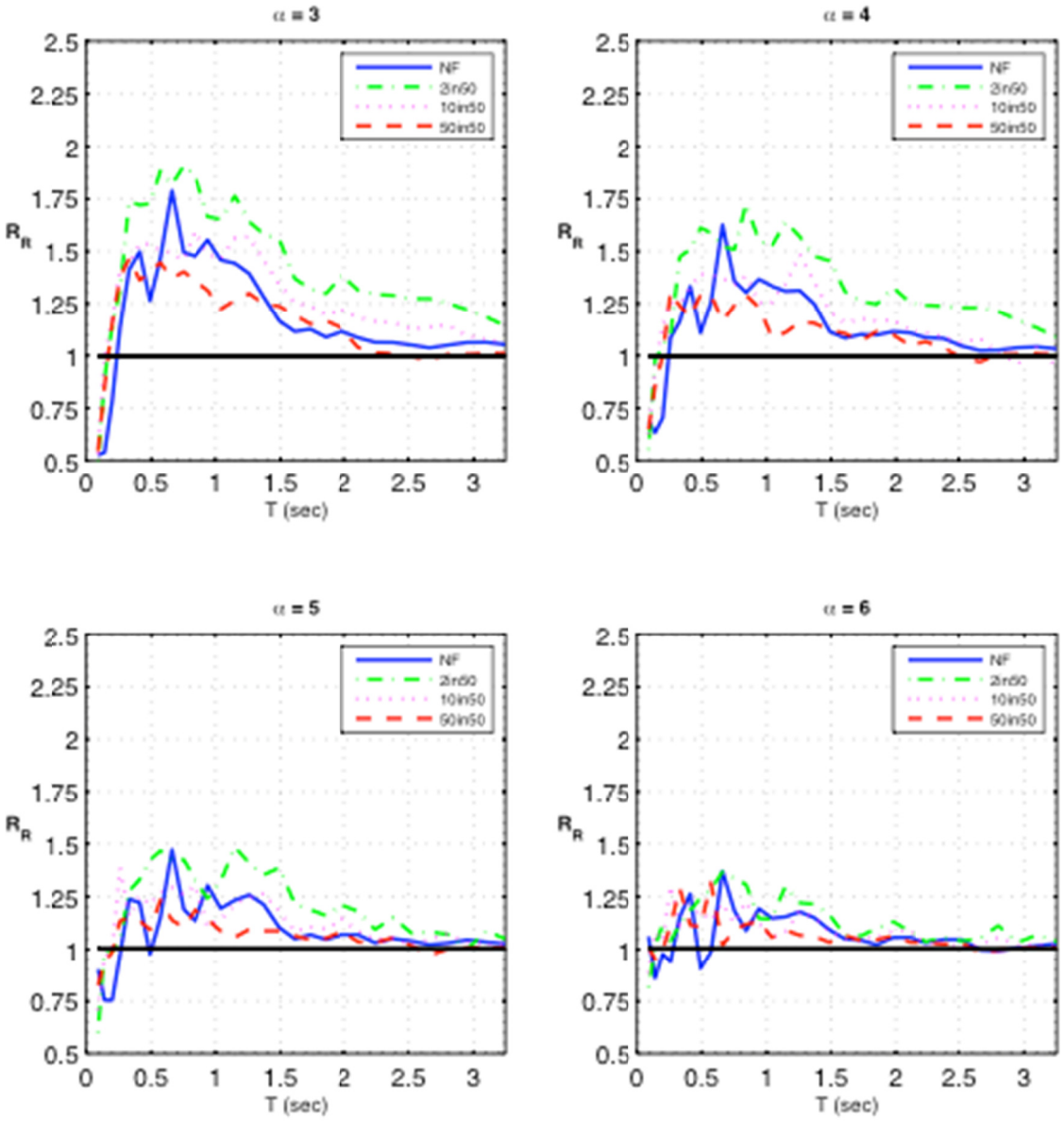

Figure 6.46 R_R **elastic column-elastic soil.**

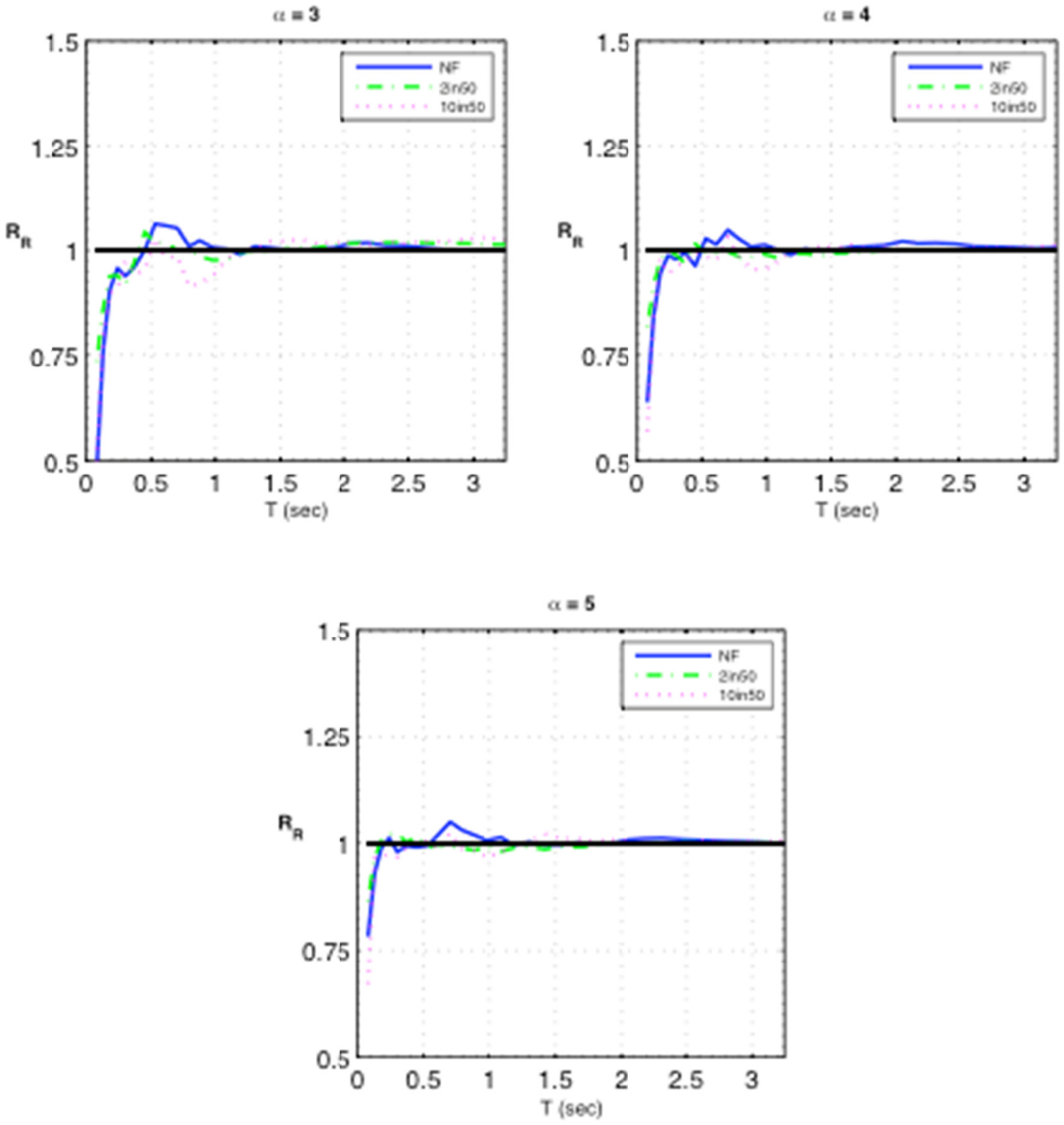

Figure 6.47 R_R **nonlinear column-elastic soil.**

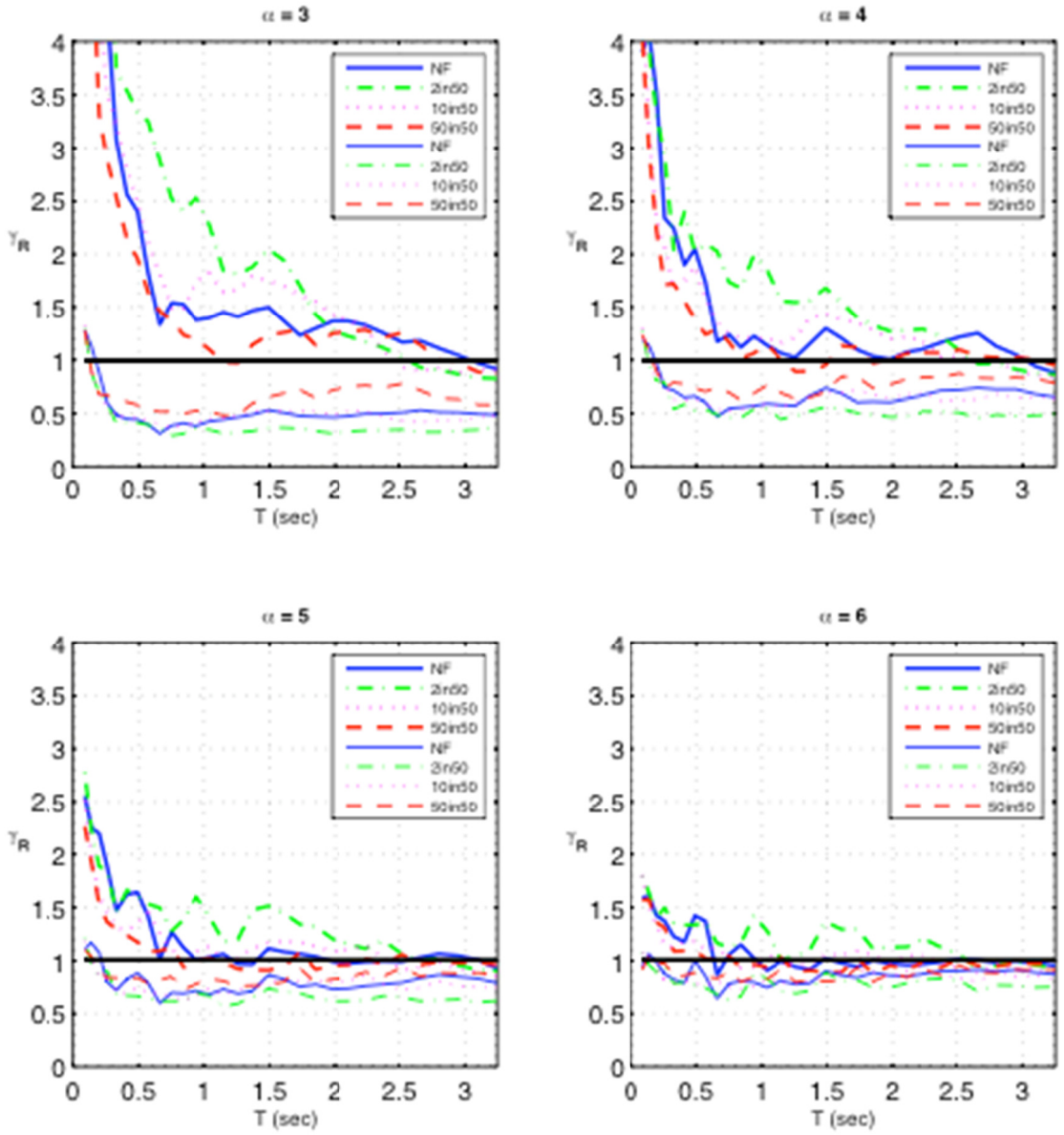

Figure 6.48 γ_R and γ_{RF} elastic column-elastic soil.

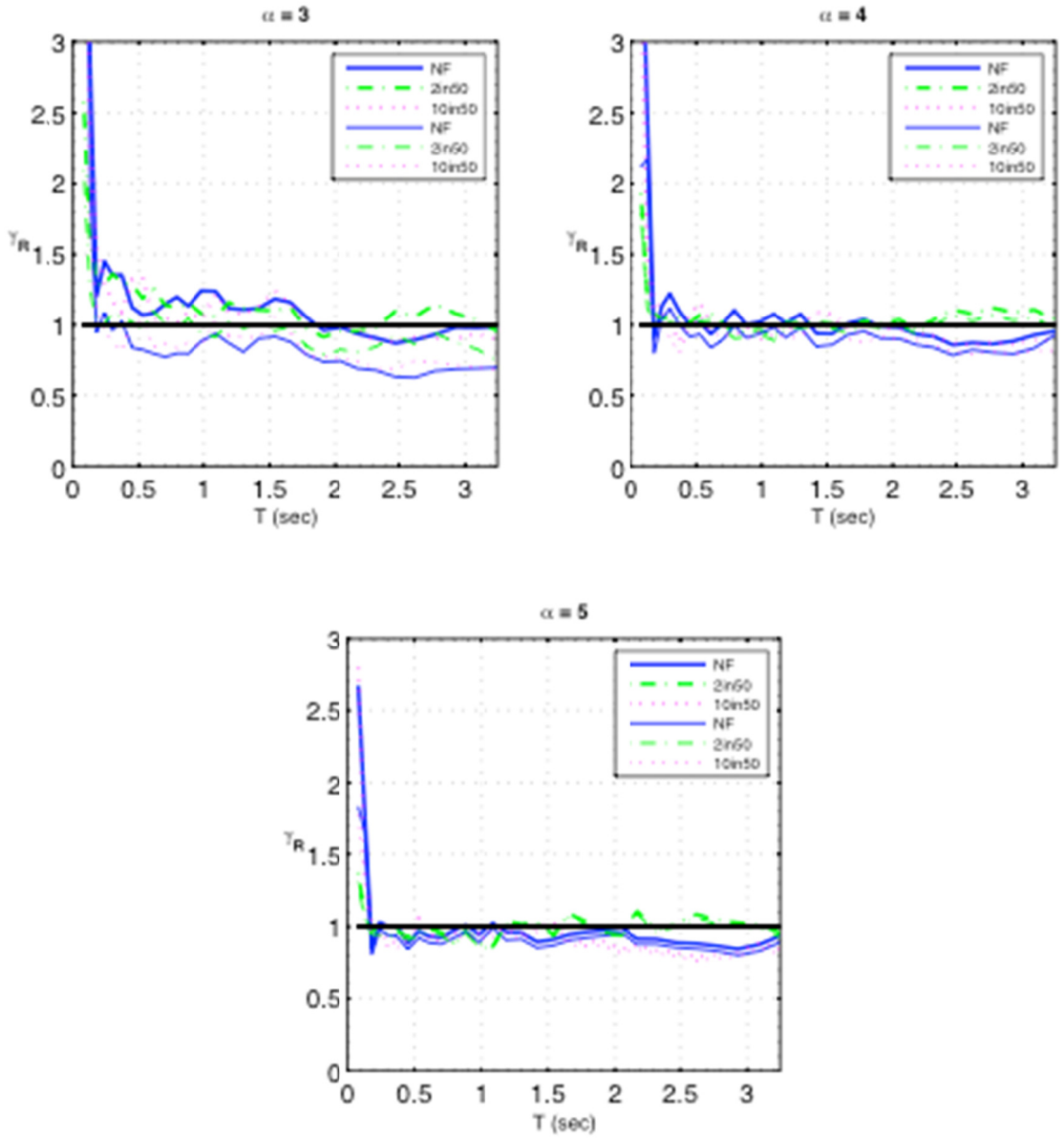

Figure 6.49 γ_R and γ_{RF} nonlinear column-elastic soil.

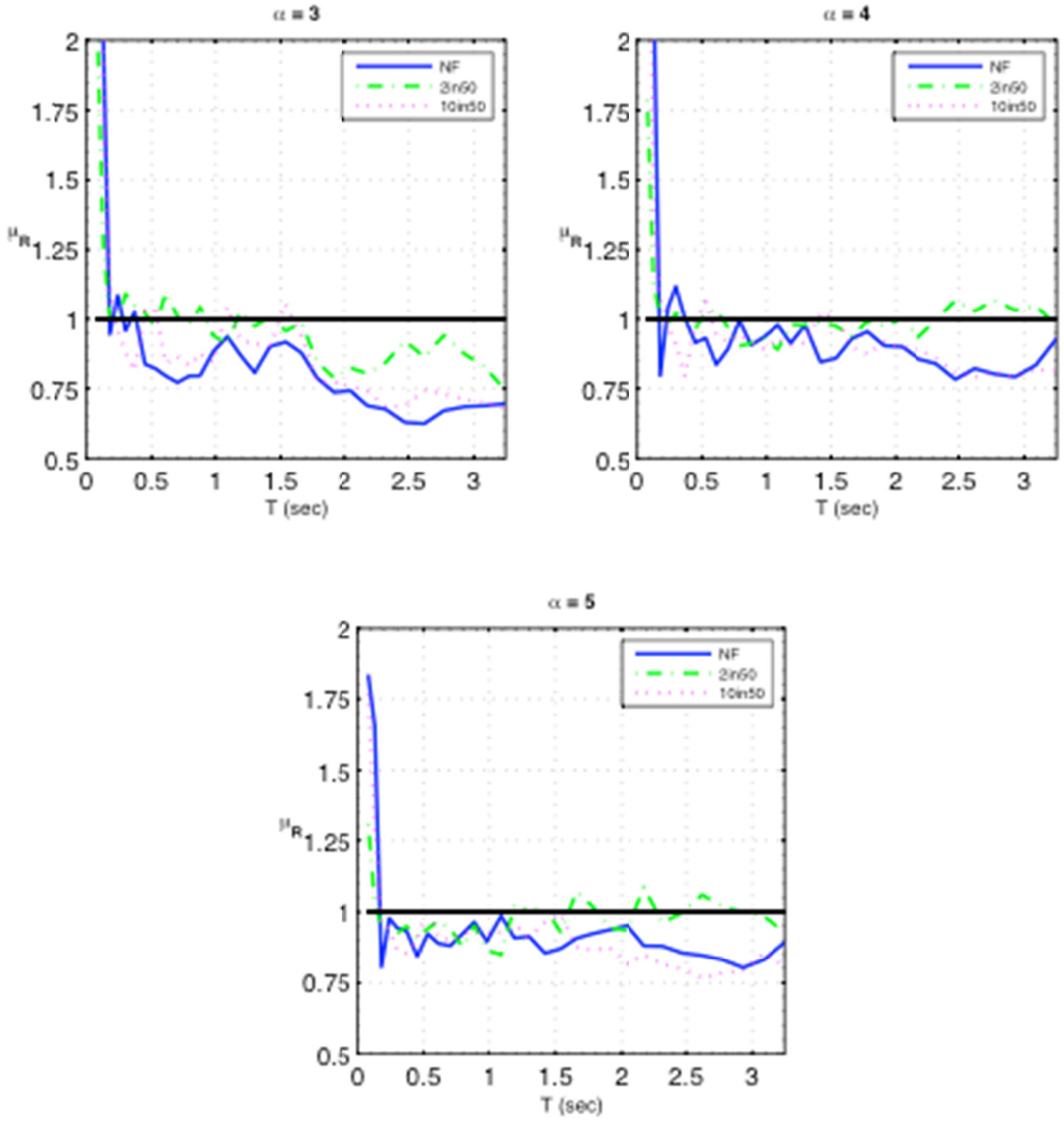

Figure 6.50 μ_R **ductility ratio.**

6.8 UPLIFTING BRIDGE PIER GUIDELINE RECOMMENDATIONS

Design of bridge piers was evaluated for systems allowed to uplift. Using predictions developed for when uplift will occur and the resulting effects of uplift on column accelerations, displacements, and inelastic response, these are compared to response of traditional fixed-base design systems. Design guidance, benefits, drawbacks, and a comparison to existing methods are provided next.

6.8.1 Design Guidance

Use of spread footings to support new bridge piers is a viable, economical approach in many situations. Agencies such as Caltrans will typically use spread footings where the soil has a high bearing capacity and is not susceptible to consolidation. Footings are designed as capacity protected elements with widths selected so that plastic hinging occurs in the base of the column. The influence of foundation uplift on seismic response raises sufficient concerns such that design engineers often provide wider footings or even piles to provide assurance that uplift cannot occur. The parametric investigation conduct here has demonstrated that allowing uplift may reduce inelastic response or at least identify where plastic hinging will occur in the column base in spite of uplifting footings.

From the analytic and experimental results provided herein, basic equations can be used with confidence to predict the lateral force on the column at the onset of uplift. Thus, the ratio β of the moment capacity of the column to the gravity load restoring moment can be used to determine whether uplift will occur. Equation (6.11) is repeated from Chapter 4.

$$\beta_i = \frac{M_{col}}{M_i} = \frac{3M_{n\,col}}{(W + W_o)b} \tag{6.11}$$

where W is the weight of the inertial mass of the system, and W_o represents the weight of the footing, surcharge, and other loads acting on the footing not associated with the inertial mass of the bridge deck. If $\beta < 1$ and M_n is used for the column moment, the column would be expected to develop its full nominal moment capacity prior to uplift.

6.8.2 Benefits

As presented in the experimental investigation and parametric study, uplift can have a beneficial effect on the behavior of a bridge by providing a means of seismic isolation. Also it has been shown that plastic hinging in column bases can occur for smaller footing widths than typically considered in design. The overall displacement of the structure may be increased depending on the degree of energy dissipation in the soil that accompanies the uplift, and the damage in the column may be reduced. A word of caution: designing for uplift may not necessarily be beneficial because in certain configurations there may be amplification or displacement demands when compared to fixed-base systems.

If the total displacements are acceptable or contained by abutments or other restraints, piers supported on spread footings that uplift might not mean that the expected performance is

inadequate. In faction, reduction of damaged to the column and the tendency of narrow footings to re-center following an earthquake when situated on soils with high gravity load factors of safety may result in superior performance.

Retrofit strategies of existing bridge piers have been undertaken to increase the footing width and ensure plastic hinging occurs in the column base. In situations where the total displacements are acceptable and soils have sufficient strength against bearing failure, the parametric investigation conducted herein has shown that the hinge can occur at the column base for narrow footing widths of α=3.0 and α=4.0. This may prevent the need to incur costly retrofit schemes to widen the footings.

Table 6.4 provides the ratios of column acceleration, total displacement, column flexural displacement, and ductilities for uplifting systems. In general, $R_R > 1$ indicates a reduction in peak acceleration—which is desirable—$R_R < 1.0$ indicates an increase. Displacement and ductility values < 1.0 indicate a reduction in uplifting system response. The shaded regions of the table indicate that period ranges where the uplifting response is amplified relative to the fixed-base response.

Table 6.4 Uplifting system ratios of response parameters.

Period	Elastic Column-Soil			Nonlinear Column-Elastic Soil			
	R_R	γ_R	γ_{RF}	R_R	γ_R	γ_{RF}	μ_R
Short T < 0.5 sec	< 1.0	1.5-4.0	0.5-1.25	< 1.0	1.0-4.0	0.9-3.0	1.0-3.0
Medium T= 0.5-1.5 sec	1.0-1.80	1.5-3.0	0.5-1.0	1.0-1.08	0.8-1.4	0.8-1.0	0.75-1.0
Long T > 1.5 sec	1.0-1.25	1.0-1.5	0.5-1.0	1.0	1.0-1.2	0.7-1.0	0.65-1.0

6.8.3 Negative Consequences

Evaluation of the potential use of uplift in bridge pier seismic design the consideration is based on a neutral or reduced response compared to fixed-base systems or a small increase in some response parameters where appropriate. The comparison of response parameters shown in Section 6.8 provides guidance on negative effects of uplift. Table 6.4 in the previous section provides a summary of the ratios of uplifting to fixed-base response and the ranges where uplift significantly amplifies response.

In general, acceleration amplification occurs for uplifting systems with corresponding fixed-base periods (T_{nf}, less than 0.5 sec) when considering elastic or nonlinear column modeling response (Figure 6.46 and Figure 6.47). Total displacements of uplifting systems are increased for short-period fixed-based structures (T_{nf} < 0.3 sec) even though column flexural displacements of the uplifting systems in question are less than fixed-base response (Figure 6.48 and Figure 6.49). The amount of total displacement amplification increases as the footing width becomes narrower. For example, the total displacement of the α=3.0 footings for elastic systems, for periods less than 1.0 sec, is 2.0 times greater than the fixed-base response. For the nonlinear

system, with α=3.0, the total displacements are up to 1.25 times greater than the fixed-base response.

Where uplift is not desired, several checks should be done. The effect of realistic material properties and deformation hardening should be considered in evaluation of M_n. Solution of Equation (6.11) should be based on ϕM_n or alternately M_u obtained from a section analysis of the column based on material properties and detailing. Soil properties should be checked to determine if soil would be overstressed due to footing rotation loading and vertical bearing pressures. Finally, the rotational and translational stiffness of the footing should be determined and used to assess the effect of the footing flexibility on the effective period and dynamic response of the pier. Lastly, the column and footing should be designed and detailed in accordance with standard Caltrans practices.

6.8.4 Recommendations

The Winkler spring foundation models presented in Chapter 5 and 6 give a reasonable prediction of response consistent with emerging trends in bridge analysis practice. Performing nonlinear column and soil analysis via the foundation model and fiber sections for the column appears to provide reasonable predictions. Recommendations and conclusions can be made for bridge piers designed to uplift on the basis of the analytical and parametric investigations performed.

The following conclusions on typical response parameters of bridge pier design are helpful in making the accompanying recommendations for when uplift should and should not be considered:

1. Similarly to fixed base response, larger ground motion excitations tend to create more displacement response of uplifting systems when compared to smaller motions for similar structures. Rocking and uplifting, as a percentage of the total displacement response increased as the magnitude of excitation increased, indicating that allowing uplift for smaller magnitude design earthquakes does not increase instability of the system because the amount of uplift is small.
2. Footing rotations were found to increase for similar magnitude earthquakes as the footing size is reduced. Increasing footing rotation leads to greater possibility of soil yielding and a subsequent reduced effective footing width post-seismic event. Hence, effective footing sizes may be less than desired for footings designed with minimum dimensions, which may decrease system stability.

From the parametric investigation it was found that certain uplift bridge pier design ranges (noted by the corresponding fixed-base period) had harmful response compared to traditional fixed-base piers. For these ranges, uplift should be prevented:

1. The displacement, acceleration, and ductility demands for short-period columns supported on footings that uplift tend to be significantly amplified. The short-period range is for columns with fixed-base natural periods ($T_{nf} < 0.5$ sec). Uplift should not be considered unless detailed nonlinear dynamic analyses are undertaken.

Using the parametric investigation and above discussion on uplifting bridge piers, the following recommendations are made on when uplift should be considered as a potential benefit in the design and response of traditional fixed-base bridge piers:

1. Design of bridge piers in regions of low seismicity should be considered because while the amount of rocking is small, it can still prove beneficial. The parametric study has shown that the overall stability of the system is sufficient.
2. Given the observed response, retrofit schemes for widening footings that do not consider uplift should be revisited after detailed nonlinear dynamic analysis of uplifting footings has been performed. The analysis should determine if the plastic hinge can form and if the total displacements are acceptable for uplifting response.
3. Acceptable uplifting behavior was observed both experimentally on the shake table and numerically for the parametric investigation for footing sizes $3D_c$ or larger. This is for competent soils with gravity load factors of safety 3 or larger. Uplift should be considered for footings meeting these conditions.
4. Uplifting systems tend to have larger global displacements. As such, clearances between columns and the surrounding environment should be sufficiently designed to accommodate anticipated displacement amplification. For the cases considered herein with fixed-base periods greater than 0.5 sec, the amplification ranged from 1.0 to 3.0.
5. In spite of the potential benefit of reduced moments and damage in columns of uplifting systems, it is recommended that columns and footings be detailed for ductile behavior with a plastic hinge occurring at the base of the column. Skewed bending and bi-directional loading of the column into the inelastic range can increase the uplift resistance of the footing and reduce the moment capacity of the column, which may result in column yielding not anticipated based on uni-directional excitation analysis. Also, uplift resistance may be increased by construction of roadways, barriers, and other structures over a footing. As such, use of ductile details and capacity design on the basis of a fixed footing condition is considered prudent unless special efforts are taken to mitigate these conditions.

7 Conclusions

The seismic response of traditional reinforced concrete bridge piers supported on shallow foundations allowed to uplift during seismic events has been evaluated as part of a research program to determine the response and potential benefits of uplifting foundations. This research has consisted of an experimental program, development of analytic models, and a parametric investigation based on the validated analytic models. The general intent was to identify traditional fixed-base piers which may benefit from the consideration of uplift during seismic events.

The specific research objectives were to develop and validate analytic models of bridge piers on shallow foundations allowed to uplift. Typically, the fixed-base design approach assumes a significant inelastic response during seismic events and corresponding displacement ductilities demands. The benefit of uplifting systems is that the mode of uplift may dissipate energy, thereby reducing inelastic demands and damage related to seismic events. The experimental and analytic validation program focused on two-footing configurations and two earthquake excitations. The parametric investigation built upon the analytic models to consider a wide range of ground motions, column height to diameter ratios, footing widths, and elastic and inelastic response.

7.1 EXPERIMENTAL INVESTIGATION OF UPLIFTING SYSTEMS

A bridge pier typically designed as a fixed-based system was tested through a series of shaking table tests to evaluate the response of bridge piers uplifting during seismic events. The specific objective was to validate that rocking is a valid mode of response, and that the rocking motion dissipates some of the energy typically associated with inelastic response thereby reducing plastic deformations. The single column system modelled was a conventional reinforced concrete column with typical axial load and a footing smaller than standard design dimensions. The footing was designed to be expandable and as a capacity protected element to ensure plastic behavior occurred at the column base.

Three test groups were conducted to assess the response of uplifting systems. Groups 1 and 2 had footing to column width ratios of 3 and axial loads of 33% and 100% of the design axial load. Test Group 3 had a footing width of 5 × 3 column diameters with 100% of the column design axial load.

Test Groups 1 and 2 each were tested using motions scaled to keep the column in the elastic demand level range. Various combinations of one-dimensional, two-dimensional, and three-dimensional excitations were input. Test Group 3 was tested using motions that were scaled to achieve column yield and displacement ductility demands of 1, 4, and 6–8, which correspond to yield, design, and maximum credible earthquake loading levels. At the conclusion of the maximum credible earthquake, the column was significantly damaged and no further testing was feasible.

Measured base moment versus footing rotation behavior typically followed the response predicted by the simple analysis model using a Winkler foundation. For the sufficiently narrow footings, uplift occurred and exhibited a nonlinear elastic type hysteresis with some energy dissipation from the supporting elastomeric pad. In this case, the overturning moment exceeded the restoring capacity of the footing and the column behaved elastically, illustrating the potential benefits of allowing uplift. The comparison of one-dimensional, two-dimensional, and three-dimensional input excitations revealed that interaction may reduce the amount of uplift.

The wider footing and larger excitations of Test Group 3 were expected to induce yielding of the column prior to uplift of the foundation in the $5D_c$ footing width direction. It was observed that bi-directional moments in the column reduced the effective moment capacity of the column in the narrow footing direction such that yielding occurred earlier than expected on the basis of the uni-directional excitation. Multi-directional response appeared to increase the effective width of the footing (due to skew), which resulted in less rocking and uplift than expected. Note that for Test Group 3 the column plastic hinge occurred in spite of the smaller than typical footing dimensions. For design applications, in cases where competent soils are available, a column with footing dimension $3D_c$ or larger and typical axial load, no tie-downs or footing increase is necessary to induce energy dissipation through plastic hinging of the column. The final test run at the maximum credible earthquake illustrated that the column was able to develop a full plastic hinge, dissipate earthquake energy, and remain stable without the need for vertical restraint.

In conclusion, the limited run of experimental testing shows the design performance of traditional fixed-base bridge piers may be met when rocking and uplift occur without the added cost of piles or alternative methods. These shake table tests used an elastomeric pad beneath the footing in place of soil. Consequently, the tests were used to validate a numerical model for spread footings resting on competent soil.

7.2 ANALYTICAL MODELING OF UPLIFTING SYSTEMS

Analytic models have the capability to reasonably predict the seismic response of uplifting bridge pier systems with the use of the open-source structural analysis platform OpenSees. Idealizations of the superstructure mass, column, footing, and elastomeric pad were used in the analytic models. Evaluation of the analytic models through linear and nonlinear model assumptions was based on the observed dynamic response to multi-direction input earthquake accelerations and natural properties of the systems.

Linear models used to model the elastic response behavior of the uplifting systems were able to predict the observed response with a high degree of confidence. The models were found

to predict peak displacements to within 25% for the uplifting systems with design axial load (10% $f'_c A_g$) and square ($3D_c \times 3D_c$) or rectangular ($5D_c \times 3D_c$) footings.

Nonlinear models were able to predict the design level (μ=6) test peak displacements to within 20% of the observed response. Residual displacements were under predicted by 100%; however, the observed magnitude was small (less than 1 in.). Given this response, the observed model predicted with a good degree of accuracy the amount of rock, uplift, column flexural displacements, and column total displacements for the design-level earthquake. For the maximum-level earthquake (μ=8), the analytical model predicted with an acceptable degree of accuracy the initial cycles of displacement, but deviated once the column experienced significant residual displacements. In-spite of this, the model was still able to reasonably predict the peak displacements that occurred at a column flexural displacement ductility of μ=10. In addition, the model was able to predict approximately 50% of the observed residual displacement and had a similar post-yield stiffness to the observed response.

Column center of mass accelerations were predicted to within 25% for the linear and nonlinear analytic models. For the linear response, the column base moment curvature prediction was reasonable. For the nonlinear analytic model, the design-level earthquake moment-curvature response was reasonable but did not show the shift in origin due to residual displacements, which caused a permanent overturning moment at the column base. This permanent column offset created a shift in the origin that affected the system displacement and corresponding acceleration and moment response.

The footing rotational stiffness was modeled reasonably well by the numerical models for the linear analysis cases. The Winkler foundation used to model the neoprene springs provided a good approximation of the static displacement, rotational stiffness, moment and rotation at initial footing uplift, and the softening behavior as the footing uplifts. Nonlinear response predicted by the analysis was affected by the discrepancy in residual displacements, which caused a permanent shift in the origin of the footing moment-rotation relationship. Analytic models showed 5–6% Rayleigh damping was effective for systems with significant uplift and 3–4% was effective for yielding systems with less uplift.

Based on these comparisons, the analytic models of uplifting bridge pier systems on shallow foundations using linear and nonlinear column assumptions and a Winkler spring foundation predict with sufficient accuracy the global response of linear uplifting systems and yielding systems tested to design and maximum earthquake levels.

7.3 PARAMETRIC STUDY

Using the uplifting analytical model developed in the analytical validation, parametric studies were performed to evaluate the effects of different ground motions, footing widths, column height to diameter ratios, and column model assumptions. Accelerations, displacement, and displacement ductility responses were determined for various combinations of these uplifting systems and compared to fixed-base response. The following observations and conclusions of typical response parameters used in the design of fixed-base bridge piers, for uplifting bridge piers are as follows:

1. The amount of uplift and rocking varies based on the magnitude of excitation. For smaller magnitude seismic events, such as 50% in 50 year probability of exceedance, the rocking and fixed-base responses were similar. Larger events, such as the 2% in 50 year probability of exceedance, caused larger rocking response. In general, the percentage of rocking displacement relative to the total displacement increased as the seismic excitation increased.
2. The observed accelerations of elastic column and soil models were reduced for uplifting systems relative to the similar fixed-base systems, with the exception of the short-period range, $T_{nf} < 0.5$ sec, where the response was amplified. The medium-period range of 0.5–1.5 sec had the most significant reduction. At longer periods the uplifting response tended to be similar to the fixed based response, however, the magnitude was still greater.
3. The observed accelerations of the nonlinear column and elastic soil models were approximately equal for periods typically greater than 0.5 sec. Uplifting systems reached the acceleration at which column yield occurred for the near-fault, 2% in 50 year, and 10% in 50 year events. This was observed for all footing widths used in the nonlinear column and elastic soil model parametric investigation (i.e., $3D_c$ to $5D_c$). At periods less than 0.5 sec, the observed accelerations of the uplifting systems were much greater than the corresponding fixed base acceleration.
4. Elastic column and soil model total displacements were typically larger than the fixed-base response. In the medium- and long-period ranges, the increase varied according to footing width. In general, the amount of increase was 1 to 3 times larger. The short-period ranges significantly amplified the motion, by up as much as four times. The associated column flexural displacement component of the total displacement for these ranges was typically less than the fixed-base response, indicating that the rocking response was primarily responsible for the total displacement increase. This suggests that short-period structures whose design is sensitive to total displacement should not consider rocking in design evaluation.
5. Typically, total displacements of the nonlinear column and elastic soil models were equal for the short- and medium-period ranges. Uplift was observed for these model assumptions, indicating that the total flexural displacement on the column was reduced when allowing uplift. At longer period ranges of 2.0 sec or greater, the uplifting system total displacements were slightly less.
6. The displacement ductility demands of uplifting systems are an indicator of the amount of inelastic action and response that occurs during seismic excitation. For the nonlinear column and elastic soil models, the ductility demands were typically less than the fixed-base system for structural fixed-base periods greater than 0.5 sec. The amount of reduction was up to 25% less than the fixed-base response. In the short-period range, the ductility demands on the uplifting bridge pier were significantly increased relative to the fixed-base period structures. The range was 1.0 to 3.0 times as much. For these expected ductility demands, bridge piers designed to uplift would need to be reassessed to ensure that adequate detailing for ductile response was provided.

7. A reduction in column inelastic action was observed and the comparison on ductility demands described in No. 6 above. Reduction by up to 25% of the displacement ductility demands indicates that the permanent displacements in the system may be reduced compared to a fixed-base system, a factor that can be very beneficial in the function of bridge piers following seismic events. However, allowing uplift did not eliminate inelastic column response relative to corresponding fixed-base bridge piers.

Allowing uplift on bridge piers typically designed as fixed based appears to have a beneficial or neutral response when compared to fixed-base systems. The exception is short-period fixed-base structures allowed to uplift where the system response is amplified. Neutral or beneficial behavior was observed for a wide variety of footing widths, column natural periods, and ground motions. Based on the observed parametric investigation results described above, the following conclusions and recommendations are made for when to allow bridge piers typically designed as fixed base (thus preventing uplift) to uplift, thereby utilizing potential damage reduction characteristics:

1. Current practice evaluates existing bridges for increasing seismic demands and determines if retrofits of footings are necessary to prevent uplift and ensure plastic hinging can be confined to the column base. Given the observed response, these footing widening schemes, should be revisited after detailed nonlinear dynamic analysis of uplifting footings has been performed to determine if the plastic hinge can form and if the total displacements are acceptable for the bridge pier response.
2. Uplift should be considered for footing sizes $3D_c$ or larger supported by competent soils with gravity load factors of safety 3 or larger. These uplifting systems were found to have acceptable uplifting behavior on traditional fixed-base bridge pier design metrics.
3. For systems where uplift is to be utilized in design, clearances between columns and the surrounding environment should be sufficiently designed to accommodate anticipated displacement amplification. For the cases considered herein with fixed-bases periods greater than 0.5 sec, the amplification ranged from 1.0 to 3.0.
4. Columns and footings should be detailed for ductile behavior, in spite of the potential benefit of reduced inelastic column response of uplifting systems. Columns should be detailed such that a plastic hinge occurs at the base of the column for a variety of reasons, including skewed bending and bi-directional loading of the column into the inelastic range, which can increase the uplift resistance of the footing and reduce the moment capacity of the column. Also, uplift resistance may be increased by construction of roadways, barriers, and other structures over a footing. Hence, use of ductile details and capacity design on the basis of a fixed footing condition is considered prudent unless special efforts are taken to mitigate these conditions.

7.4 FUTURE RESEARCH

This study has provided insight on the seismic response of uplifting bridge piers through a series of experiments and the development of analytic models. There are additional items that require further investigation in order to apply to the design of bridge piers allowed to uplift:

1. More extensive parametric studies to examine a broader range of soil conditions should be conducted. The parametric studies undertaken herein should be expanded to consider a broader range of soil types and mechanical characteristics.
2. Additional parametric studies on the bridge pier response when soil yields during excitation are warranted. In particular, focus should be paid to the amount of yielding and the effective footing width following yielding due to both uni-directional and multi-directional excitation, which will have an effect on post-seismic event footing stiffness (rotational and translational).
3. Residual displacements of uplifting footings are an important design consideration for bridge pier design. Further work is warranted to assess the magnitude of residual displacements compared to fixed-base design.
4. For locations with poorer soil conditions, reducing damage to the column and re-centering of the bridge system may be achieved by supporting the pier footing on piles, where the pile cap is allowed to uplift from the pier. An option would be to place the pile into a socket cast on the bottom of the pile cap so that lateral load can be transferred from the pile cap to the pile during uplift. Elastomeric pads or some type of yielding device might be installed in the socket between the pile cap and the pile so that energy is dissipated during uplift and reseating.
5. Bridge systems where the effect of the vertical movement of the column associated with rocking is considered should be evaluated. Uplift behavior causes the bridge deck to raise and lower on opposite ends. For cases where restraints are provided to prevent this uplift movement, the uplift behavior may be prevented or greater soil yielding may be achievable. For example, the bridge deck may be vertically restrained at the abutments, and a stiff bridge deck will tend to resist the upward movement of the deck associated with uplift of the footings. Similarly, where columns of different length support a bridge or the individual footings have different widths, the amount of vertical movement during uplift will differ. As such, the resistance of the footing to vertical movement at the column lines will result in different vertical forces in each column. As such, the rocking and uplift behavior will differ from what is observed here. In the case of curved or skewed bridges, the different principal axes of the footings may result in behaviour not considered herein. Thus it is strongly recommended that this work be extended to consider bridge systems having columns supported on spread footings susceptible to uplift. Testing on a geotechnical centrifuge and shake table would be desirable, as would numerical simulations.

REFERENCES

Alameddine, F, Imbsen, R. (2002). Rocking of bridge piers under earthquake loading, *Proc.,* 3rd Nat. Seismic Conf. and Workshop on Bridges and Highways, Portland, OR.

Algie, T.B., Deng, L., Erduran, E., Kutter, B.L., Kunnath, S. (2008). Centrifuge modeling of innovative foundation systems to optimize seismic behavior of bridge structures, *Proc.*, 14th World Conf. on Earthq. Engrg., Beijing, China.

American Society of Civil Engineers (2007). *Seismic Rehabilitation of Existing Buildings*, ASCE-41, Reston, VA.

Baker, J.W., Lin, T., Shahi, S.K., Jayaram, N. (2011). New ground motion selection procedures and selected motions for the PEER Transportation Research Program, *Technical Report PEER 2011/03,* Pacific Earthquake Engineering Research Center, University of California, Berkeley, CA.

Berry, M.P., Eberhard, M.O. (2006). Modeling of reinforced concrete bridge columns, Presentation at the PEER Annual Meeting, San Francisco, CA.

Boulanger, R.W., Curras, C.J., Kutter, B.L., Wilson, D.W., Abghari, A. (1999). Seismic soil-pile structure interaction experiments and analyses, ASCE, *J. Geotech. GeoEnviro. Engrg.,*125(9):750–759.

California Department of Transportation (2004a). *Seismic Design Criteria,* Version 1.4, Sacramento, CA.

California Department of Transportation (2004b). *Bridge Design Specifications,* Version 1.4, Sacramento, CA.

Chang, G., Mander, J. (1994). Seismic energy-based fatigue damage analysis of bridge columns: Part I – evaluation of seismic capacity, *Report No. NCEER-94-0006*, Department of Civil and Environmental Engineering, State University of New York, Buffalo, NY.

Chopra, A.K., Yim, C (1983). Simplified earthquake analysis of structures with foundation uplift, ASCE, *J. Struct. Engrg.*, 111(4):906-930.

Chopra, A.K., Goel, R.K. (1999). Capacity-demand-diagram methods for estimating seismic deformation of inelastic structures: SDF systems, *Technical Report PEER-1999/02,* Pacific Earthquake Engineering Research Center, University of California, Berkeley, CA, 67 pgs.

Deng, L., Kutter, B.L., Kunnath, S., Algie, T. (2010). Centrifuge modeling of bridge system with rocking footings, *Proc.,* Intl. Conf. on Physical Modeling in Geotechnics, Zurich, Switzerland. A.A. Balkema Publishers, Rotterdam, Netherlands.

Deng, L., Kutter, B.L. (2011). Characterization of rocking shallow foundations using centrifuge model tests, *Earthq. Engrg. Struct. Dyn.,* doi: 10.1002/eqe.1181.

Federal Emergency Management Agency (2000). *Pre-standard and Commentary for the Seismic Rehabilitation of Buildings, FEMA Publication No. 356,* prepared by the American Society of Civil Engineers for the Federal Emergency Management Agency, Washington, D.C.

Gazetas, G. (1991). Displacement and soil-structure interaction under dynamic and cyclic loading, *Proc*., 10th Eur. Conf. on Soil Mechanics and Foundation Engrg., Florence, Italy.

Hachem, M., Mahin, S., Moehle, J. (2003). Performance of circular reinforced concrete bridge columns under bidirectional earthquake loading, *Technical Report PEER 2003/06,* Pacific Earthquake Engineering Research Center, University of California, Berkeley, Calif.

Harden, C., Hutchinson, T., Martin, G., Kutter, B.L. (2005). Numerical modeling of the nonlinear cyclic response of shallow foundations, *Technical Report PEER 2005/04,* Pacific Earthquake Engineering Research Center, University of California, Berkeley, CA.

Housner G.W. (1963). The behavior of inverted pendulum structures during earthquakes, *Bull. Seismo. Soc. Am.,* 53(2):403–417.

Jeong, H., Sakai, J., Mahin, S.A. (2008). Shaking table tests and numerical investigation of self-centering reinforced concrete bridge columns, *Technical Report PEER 2008/06,* Pacific Earthquake Engineering Research Center, University of California, Berkeley, CA.

Karsan, I.D., Jirsa, J.O. (1969). Behavior of concrete under compressive loading, ASCE*, J. Struct. Div.*, 95(ST-12).

Kawashima, K., Hosoiri, K. (2003). Rocking response of bridge columns on direct foundations, *Proc.,* Symp. on Concrete Structures in Seismic Regions, Paper No. 118, FIB, Athens, Greece.

Kawashima, K., Nagai, T., Sakellaraki, D. (2007). Rocking seismic isolation of bridges supported by spread foundations, *Proc.,* 2nd Japan-Greece Workshop on Seismic Design, Observation and Retrofit of Foundations, pp. 254-265, Japan Society of Civil Engineers, Tokyo, Japan.

Krawinkler, H., Moncarz, P.D. (1982). Similitude requirements for dynamic models, *Dynamic Modeling of Concrete Structures, ACI SP 73-1*, Detroit, MI, pp. 1–22.

Meek, J. (1975). Effects of foundation tipping on dynamic response, ASCE, *J. Struct. Div.,* 101(ST7):1297–1311.

Miranda, E., Ruiz-Garcia, J. (2002). Evaluation of approximate methods to estimate maximum inelastic displacement demands, *Earthq. Engrg Struct. Dyn*., 31:539–560.

Nagai, T., Kawashima, K. (2006). Effect of bilateral excitation on the rocking seismic isolation of foundations, ASCE, *J. Struct. Engrg.,* 52(2):499–509.

Newmark, N., Rosenblueth, E. (1971). *Fundamentals of Earthquake Engineering*, Prentice Hall, New York, NY.

OpenSees Development Team (Open Source Project). OpenSees: open system for the earthquake engineering simulations, http://opensees.berkeley.edu/, 1998–2003.

Phalen, J.D. (2003). Physical modeling of the soil-foundation interaction of spread footings subjected to lateral cyclic loading, *M.S. Thesis,* University of California, Davis, CA.

PEER NGA Database (2005). "NGA Database Record Number NGA0779." Pacific Earthquake Engineering Research Center. http://peer.berkeley.edu/nga/data?doi=NGA0779 .

Priestley, N.M.J., Evison, R.J., Carr, A.J. (1978). Seismic response of structures free to rock on their foundations, *Bull. New Zealand Nat. Soc. Earthq. Engrg.*, 11(3):141–150.

Priestley, N.M.J., Seible, F. (1991). Seismic assessment and retrofit of bridges, *Technical Report SSRP-91/03,* University of California, San Diego, CA.

Priestley, N.M.J, Seible, F., Calvi, G.M. (1996). *Seismic Design and Retrofit of Bridges,* John Wiley & Sons, New York.

Rosebrook, KR (2001). Moment loading on shallow foundations: Centrifuge test data archives, *M.S. Thesis,* Department of Civil and Environmental Engineering, University of California, Davis, CA.

Rutenberg, A., Jennings, P.C., Housner, G.W. (1982). The response of Veterans Hospital Building 41 in the San Fernando earthquake, *Earthq. Engrg. Struct. Dyn.*, 10(3):359–380.

SAC Steel Project (2006). Impulsive Near-Field Earthquake Ground Motions http://nisee.berkeley.edu/data /strong_motion/sacsteel/motions/nearfault.html

Sakai, J., Mahin, S.A. (2006). Earthquake simulation tests on reducing residual displacements of reinforced concrete bridge columns. *Technical Report PEER* 2006/13, Pacific Earthquake Engineering Research Center, University of California, Berkeley, CA.

Sakellaraki, D., Watanabe, G., Kawashima, K. (2005). Experimental rocking response of direct foundations of bridges, *Proc.,* 2nd Int. Conf. on Urban Earthq. Engrg., Tokyo Inst. of Technology, Tokyo, Japan.

Sakellaraki, D., Kawashima, K. (2006). Effectiveness of seismic rocking isolation of bridges based on shake table test, *Proc.,* 1st Eur. Conf. Earthq. Engrg. and Seismo., Paper No. 364, pp. 1–10, Geneva, Switzerland

Scott, M.H., Fenves, G.L. (2006). Plastic hinge integration methods for force- based beam-column elements, ASCE*, J. Struct. Engrg.*, 132(2):244–252.

Taucer, F.F., Spacone, E., Filippou, F.C. (1991). A fiber beam-column element for seismic response analysis of reinforced concrete structures, *Report No. UCB/EERC-91/17*, Earthquake Engineering Research Center, University of California, Berkeley, CA.

Wang, S., Kutter, B.L., Chacko, J.M., Wilson, D.W., Boulanger, R.W., Abghari, A. (1998). Nonlinear seismic soil-pile structure interaction, *Earthq. Spectra,* 14(2):377–396.

Werner, S.D, Nisar, A., Beck, J.L. (1992). Assessment of UBC seismic design provisions using recorded building motions, *Proc.*, Tenth World Conf. Earthq. Engrg., Vol 10, pp. 5723–5728.

WINROCK: Computer program to estimate displacement of bridge piers allowed to rock on their foundations, Caltrans (Version 1.1.2 – 5/25/05).

Yim, C.-S., Chopra, A.K. (1983). Effects of transient foundation uplift on earthquake response of structures, *Report No. UCB/EERC-83/09,* Earthquake Engineering Research Center, University of California, Berkeley, CA, 134 pgs.

Yim, C.-S., Chopra, A.K. (1984a). Dynamics of structures on two-spring foundation allowed to uplift, ASCE, *J. Engrg. Mech.,* 110(7):1124–1146.

Yim, C.-S., Chopra, A.K. (1984b). Earthquake response of structures with partial uplift on Winkler foundation, *Earthq. Engrg. Struc. Dyn.,* 12(2):263–281.

Appendix A Experimental Test Schedule

Three test groups were run on the shaking table. Each of the test groups had several variations of loading direction, earthquake, and excitation amplitude or time scaling. The test schedule including run identification numbers is outlined in this Appendix.

Test Group	Test	Level[1]	Earthquake	Amplitude Scale	Loading Input	$dt=dt_o/\sqrt{S_d}$
1 (nominal $3\%f'_cA_g$ & $3D_c$ x $3D_{c)}$	A1	Elastic	Los Gatos	8%	1D-X	$0.02/\sqrt{(4.5)}$
	A2	Elastic	Los Gatos	8%	1D-Y	$0.02/\sqrt{(4.5)}$
	A3	Elastic	Los Gatos	8%	2D-X+Y	$0.02/\sqrt{(4.5)}$
	A4	Elastic	Los Gatos	8%	2D-X+Z	$0.02/\sqrt{(4.5)}$
	A5	Elastic	Los Gatos	8%	3D-X+Y+Z	$0.02/\sqrt{(4.5)}$
	B1	Elastic	Los Gatos	32%	1D-X	$0.02/\sqrt{(4.5)}$
	B2	Elastic	Los Gatos	32%	1D-Y	$0.02/\sqrt{(4.5)}$
	B3	Elastic	Los Gatos	32%	2D-X+Y	$0.02/\sqrt{(4.5)}$
	B4	Elastic	Los Gatos	32%	2D-X+Z	$0.02/\sqrt{(4.5)}$
	B5	Elastic	Los Gatos	32%	3D-X+Y+Z	$0.02/\sqrt{(4.5)}$
	C1	Elastic	Tabas	8%	1D-X	$0.01/\sqrt{(4.5)}$
	C2	Elastic	Tabas	8%	1D-Y	$0.01/\sqrt{(4.5)}$
	C3	Elastic	Tabas	8%	2D-X+Y	$0.01/\sqrt{(4.5)}$
	C4	Elastic	Tabas	8%	2D-X+Z	$0.01/\sqrt{(4.5)}$
	C5	Elastic	Tabas	8%	3D-X+Y+Z	$0.01/\sqrt{(4.5)}$
	D1	Elastic	Tabas	32%	1D-X	$0.01/\sqrt{(4.5)}$
	D2	Elastic	Tabas	32%	1D-Y	$0.01/\sqrt{(4.5)}$
	D3	Elastic	Tabas	32%	2D-X+Y	$0.01/\sqrt{(4.5)}$
	D4	Elastic	Tabas	32%	2D-X+Z	$0.01/\sqrt{(4.5)}$
	D5	Elastic	Tabas	32%	3D-X+Y+Z	$0.01/\sqrt{(4.5)}$
	E1	Elastic	Los Gatos	32%	1D-X	$\sqrt{(2)}*0.02/\sqrt{(4.5)}$
	E2	Elastic	Los Gatos	32%	1D-Y	$\sqrt{(2)}*0.02/\sqrt{(4.5)}$
	E3	Elastic	Los Gatos	32%	2D-X+Y	$\sqrt{(2)}*0.02/\sqrt{(4.5)}$
	E4	Elastic	Los Gatos	32%	2D-X+Z	$\sqrt{(2)}*0.02/\sqrt{(4.5)}$
	E5	Elastic	Los Gatos	32%	3D-X+Y+Z	$\sqrt{(2)}*0.02/\sqrt{(4.5)}$
	F1	Elastic	Tabas	42%	1D-X	$0.01/\sqrt{(4.5)}$
	F2	Elastic	Tabas	42%	1D-Y	$0.01/\sqrt{(4.5)}$
	F3	Elastic	Tabas	42%	2D-X+Y	$0.01/\sqrt{(4.5)}$
	F4	Elastic	Tabas	42%	2D-X+Z	$0.01/\sqrt{(4.5)}$
	F5	Elastic	Tabas	42%	3D-X+Y+Z	$0.01/\sqrt{(4.5)}$
2 (nominal $10\%f'_cA_g$ & $3D_c$ x $3D_{c)}$	A1S	Elastic	Los Gatos	15%	1D-X	$\sqrt{(2)}*0.02/\sqrt{(4.5)}$
	A2S	Elastic	Los Gatos	15%	1D-Y	$\sqrt{(2)}*0.02/\sqrt{(4.5)}$
	A3S	Elastic	Los Gatos	15%	2D-X+Y	$\sqrt{(2)}*0.02/\sqrt{(4.5)}$
	A4S	Elastic	Los Gatos	15%	2D-X+Z	$\sqrt{(2)}*0.02/\sqrt{(4.5)}$
	A5S	Elastic	Los Gatos	15%	3D-X+Y+Z	$\sqrt{(2)}*0.02/\sqrt{(4.5)}$
	B1S	Elastic	Tabas	15%	1D-X	$0.01/\sqrt{(4.5)}$
	B2S	Elastic	Tabas	15%	1D-Y	$0.01/\sqrt{(4.5)}$
	B3S	Elastic	Tabas	15%	2D-X+Y	$0.01/\sqrt{(4.5)}$
	B4S	Elastic	Tabas	15%	2D-X+Z	$0.01/\sqrt{(4.5)}$
	B5S	Elastic	Tabas	15%	3D-X+Y+Z	$0.01/\sqrt{(4.5)}$
	C1S	Elastic	Los Gatos	15%	1D-X	$0.02/\sqrt{(4.5)}$
	C2S	Elastic	Los Gatos	15%	1D-Y	$0.02/\sqrt{(4.5)}$
	C3S	Elastic	Los Gatos	15%	2D-X+Y	$0.02/\sqrt{(4.5)}$
	C4S	Elastic	Los Gatos	15%	2D-X+Z	$0.02/\sqrt{(4.5)}$
	C5S	Elastic	Los Gatos	15%	3D-X+Y+Z	$0.02/\sqrt{(4.5)}$
	D1S	Elastic	Los Gatos	25%	1D-X	$0.02/\sqrt{(4.5)}$
	D2S	Elastic	Los Gatos	25%	1D-Y	$0.02/\sqrt{(4.5)}$
	D3S	Elastic	Los Gatos	25%	2D-X+Y	$0.02/\sqrt{(4.5)}$

	D4S	Elastic	Los Gatos	25%	2D-X+Z	0.02/√(4.5)
	D5S	Elastic	Los Gatos	25%	3D-X+Y+Z	0.02/√(4.5)
	E1S	Elastic	Los Gatos	15%	3D-X+Y+Z	0.02/√(4.5)
	E2S	Elastic	Los Gatos	25%	3D-X+Y+Z	0.02/√(4.5)
	F1S	Elastic	Tabas	25%	1D-X	0.01/√(4.5)
	F2S	Elastic	Tabas	25%	1D-Y	0.01/√(4.5)
	F3S	Elastic	Tabas	25%	2D-X+Y	0.01/√(4.5)
	F4S	Elastic	Tabas	25%	2D-X+Z	0.01/√(4.5)
	F5S	Elastic	Tabas	25%	3D-X+Y+Z	0.01/√(4.5)
	G1S	Elastic	Tabas	25%	1D-X	√(2)*0.01/√(4.5)
	G2S	Elastic	Tabas	25%	1D-Y	√(2)*0.01/√(4.5)
	G3S	Elastic	Tabas	25%	2D-X+Y	√(2)*0.01/√(4.5)
	G4S	Elastic	Tabas	25%	2D-X+Z	√(2)*0.01/√(4.5)
	G5S	Elastic	Tabas	25%	3D-X+Y+Z	√(2)*0.01/√(4.5)
	H1S	Elastic	Los Gatos	25%	1D-X	0.02/√(4.5)
	H2S	Elastic	Los Gatos	25%	3D-X+Y+Z	0.02/√(4.5)
3 (nominal $10\%f'_cA_g$ $5D_cx3D_c$)	A1R	Elastic	Los Gatos	10%	3D-X+Y+Z	0.02/√(4.5)
	A2R	Yield	Los Gatos	25%	3D-X+Y+Z	0.02/√(4.5)
	A3R	Design	Los Gatos	90%	3D-X+Y+Z	0.02/√(4.5)
	A4R	MCE	Los Gatos	120%	3D-X+Y+Z	0.02/√(4.5)

[1]loading level defined by flexural ductility demands

Appendix B Experimental Test Results

Some of the experimental results from selected tests listed in Appendix A are displayed on the following pages. The general behavior of a system allowed to uplift are shown. Plots presented include the center of mass translational components, footing uplift displacement, the moment demand at base of column versus the rotation of the footing and the column base moment versus average curvature demands.

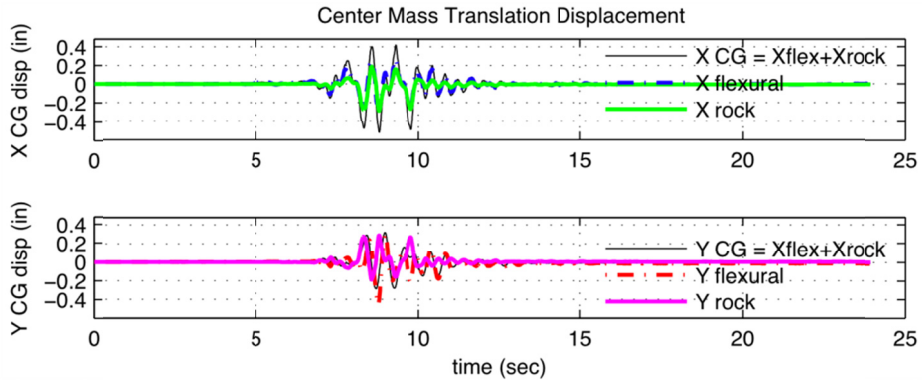

(a) X center mass translation (b) Y center mass translations

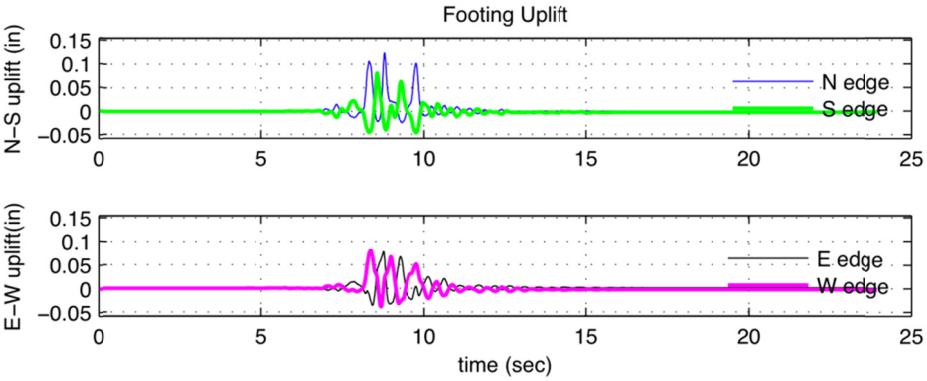

(c) N-S footing uplift (d) E-W footing uplift

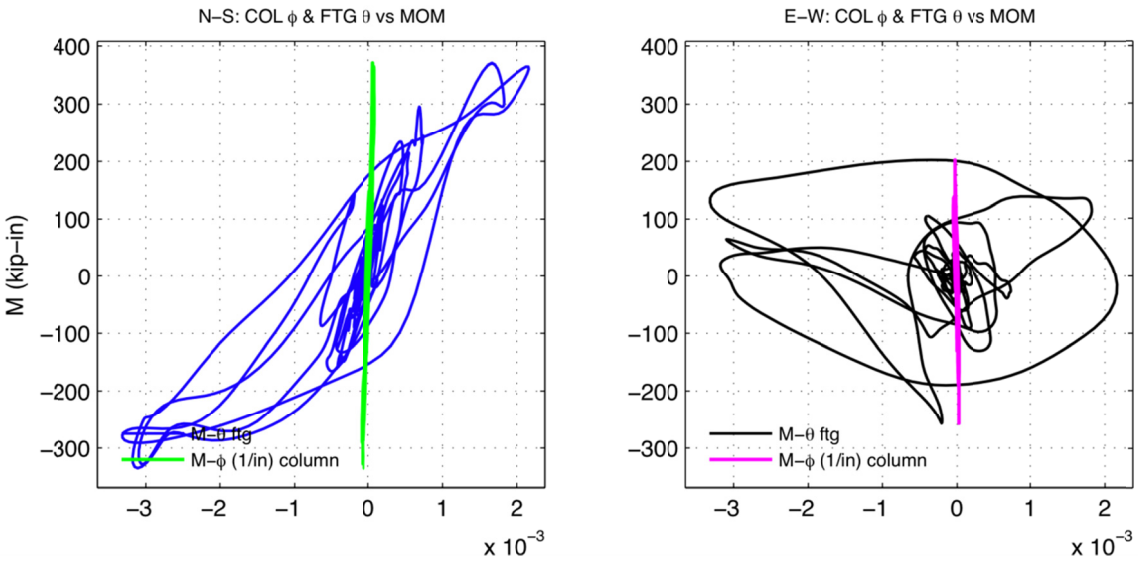

(e) N-S: Mom. vs Col ϕ (1/in) and FTG θ (f) E-W: Mom. vs Col ϕ (1/in) and FTG

Figure B.1 B1 experimental results.

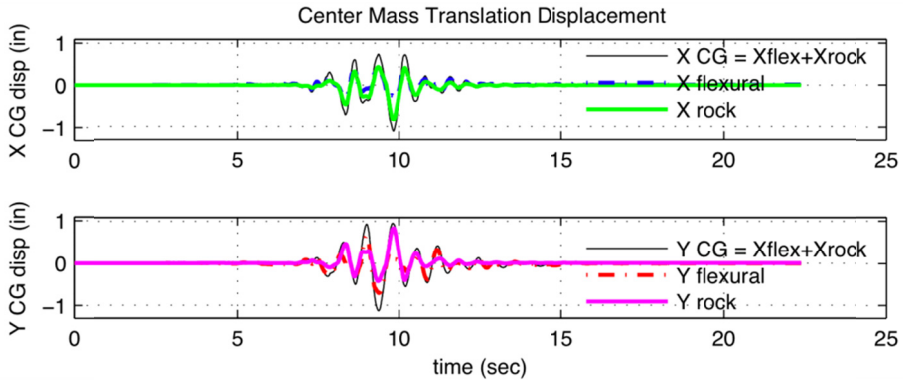

(a) X center mass translation (b) Y center mass translations

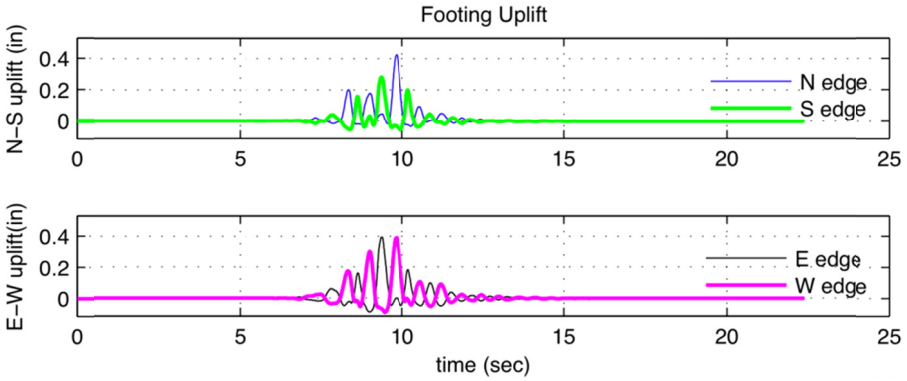

(c) N-S footing uplift (d) E-W footing uplift

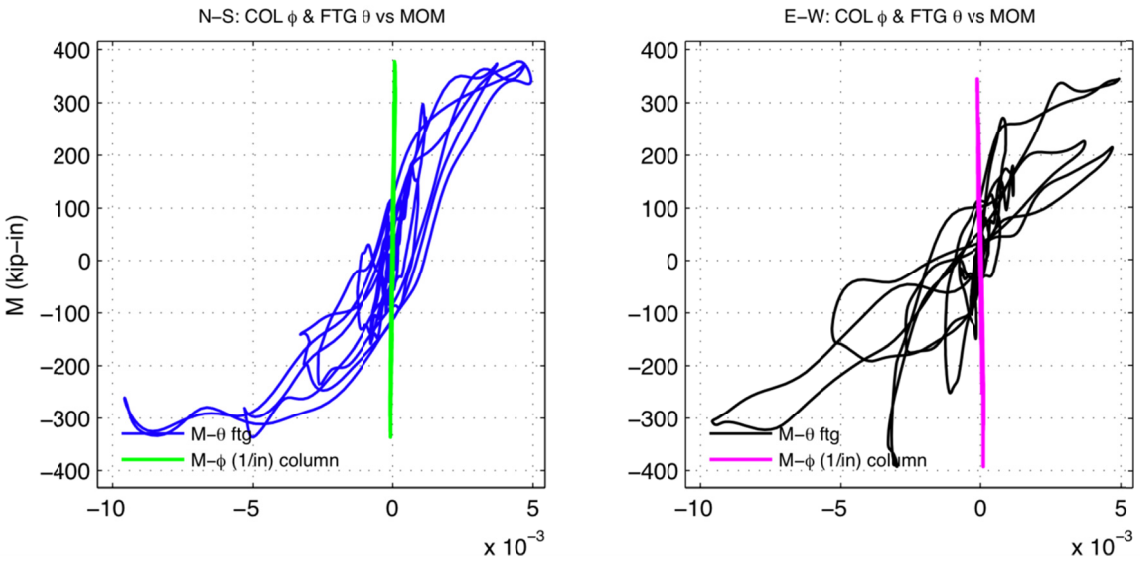

(e) N-S: Mom. vs Col ϕ (1/in) and FTG θ (f) E-W: Mom. vs Col ϕ (1/in) and FTG

Figure B.2 B3 experimental results.

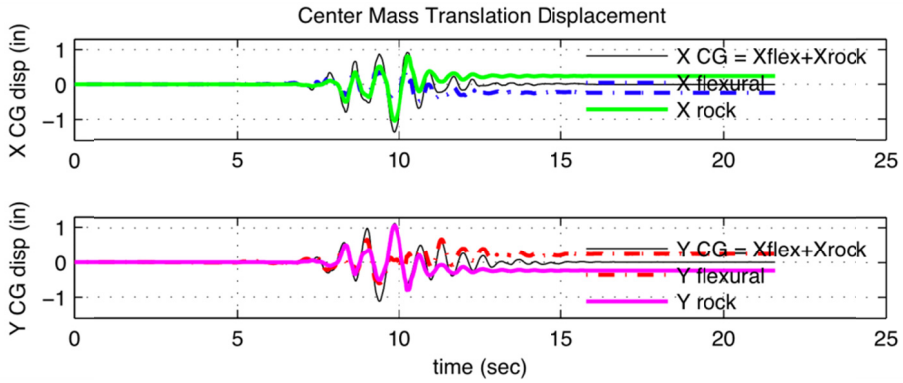

(a) X center mass translation (b) Y center mass translations

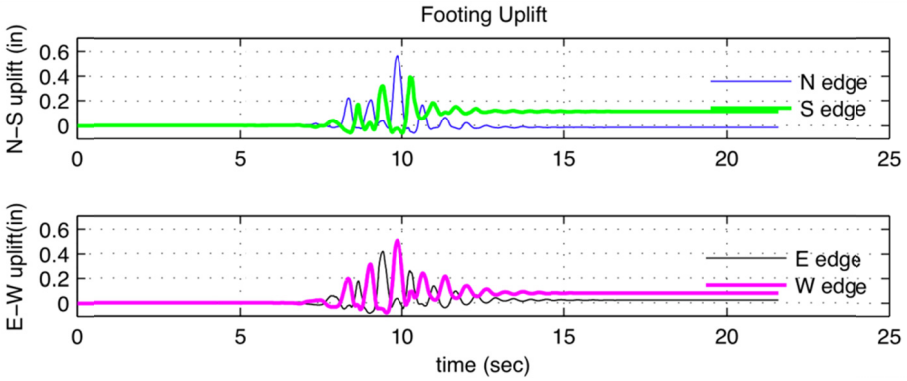

(c) N-S footing uplift (d) E-W footing uplift

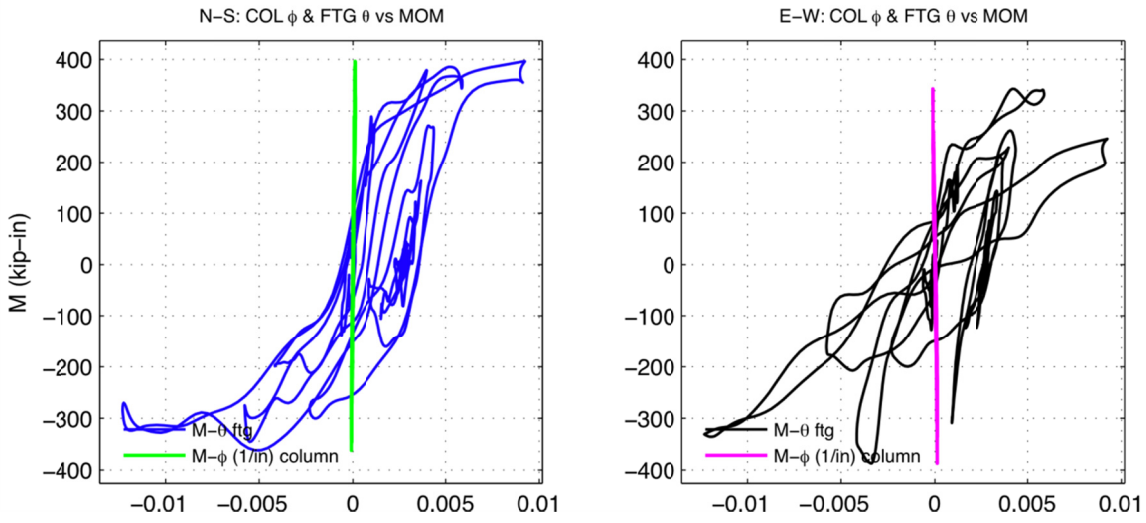

(e) N-S: Mom. vs Col ϕ (1/in) and FTG θ (f) E-W: Mom. vs Col ϕ (1/in) and FTG

Figure B.3 B5 experimental results.

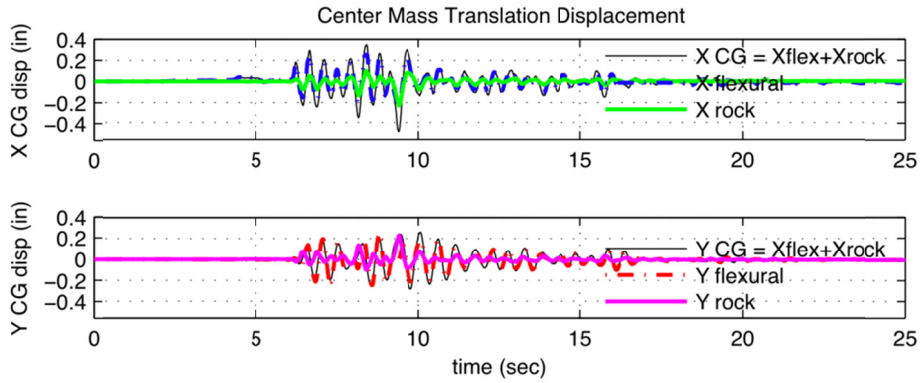

(a) X center mass translation (b) Y center mass translations

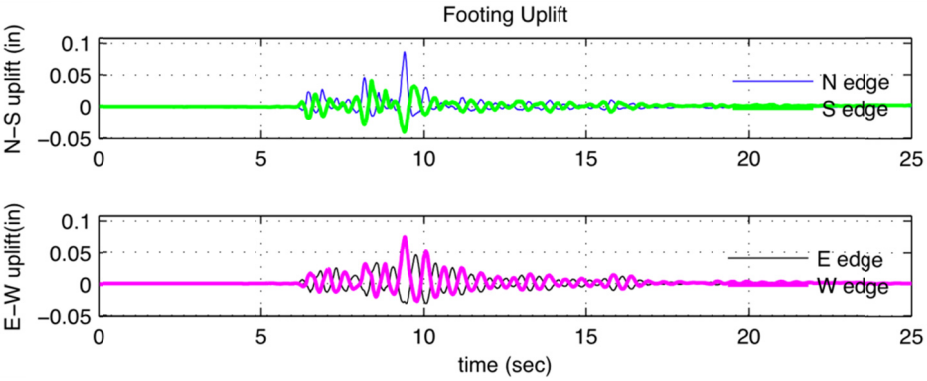

(c) N-S footing uplift (d) E-W footing uplift

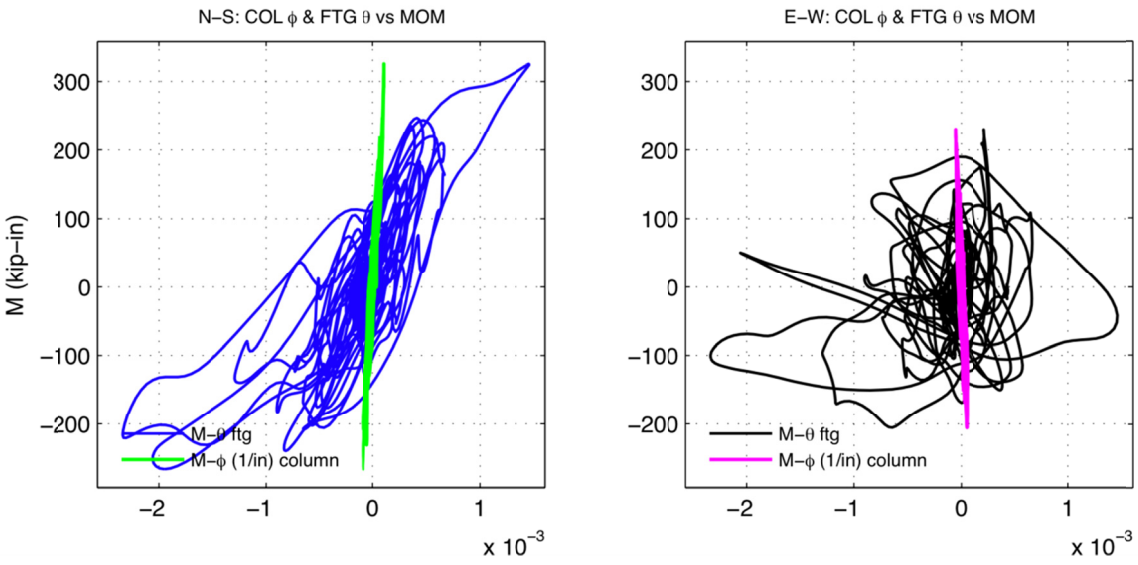

(e) N-S: Mom. vs Col ϕ (1/in) and FTG θ (f) E-W: Mom. vs Col ϕ (1/in) and FTG

Figure B.4 D1 experimental results.

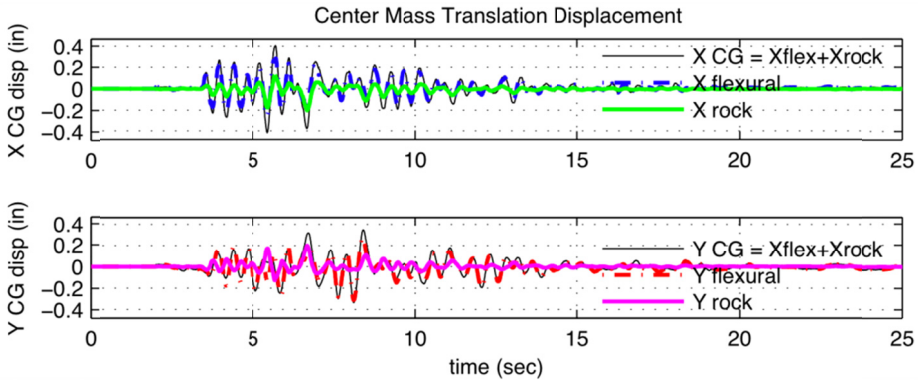

(a) X center mass translation (b) Y center mass translations

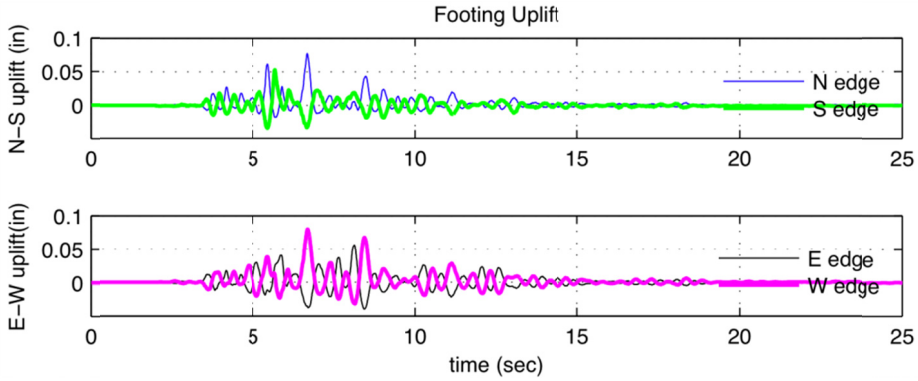

(c) N-S footing uplift (d) E-W footing uplift

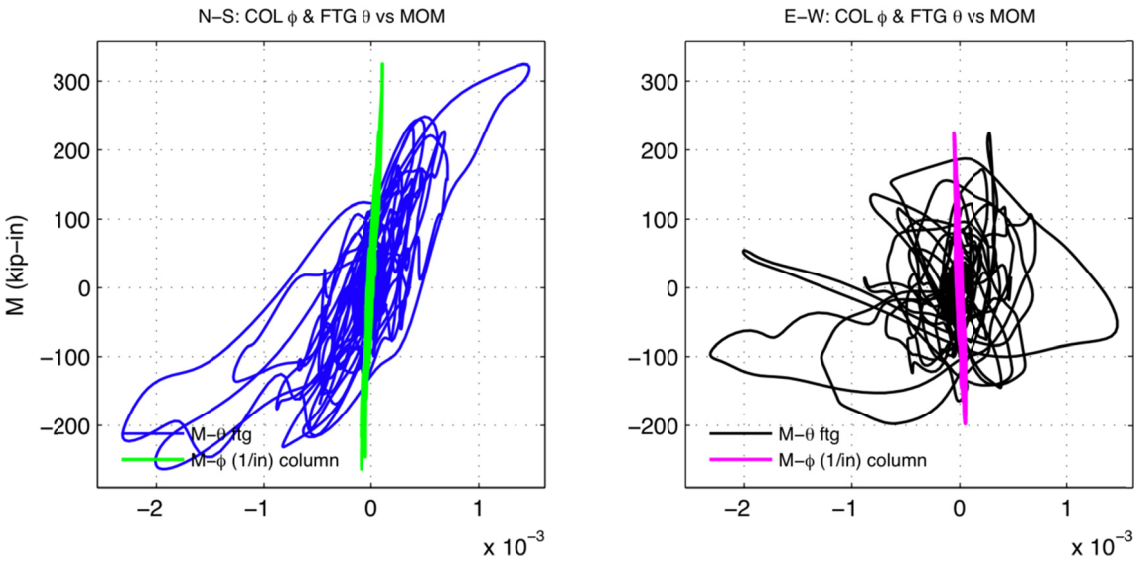

(e) N-S: Mom. vs Col ϕ (1/in) and FTG θ (f) E-W: Mom. vs Col ϕ (1/in) and FTG

Figure B.5 D3 experimental results.

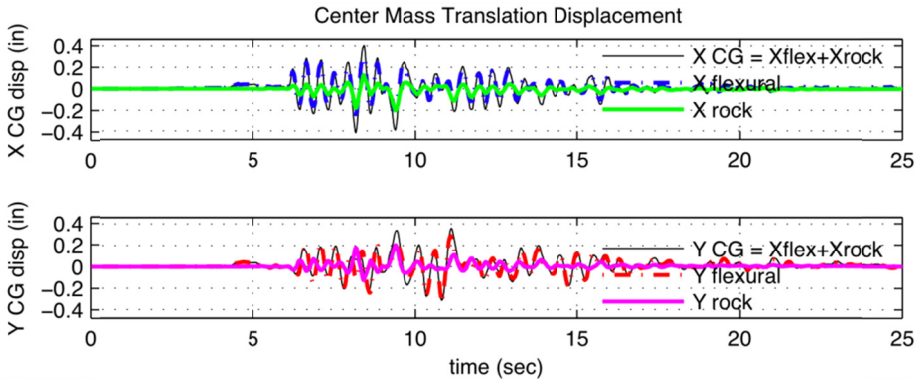

(a) X center mass translation (b) Y center mass translations

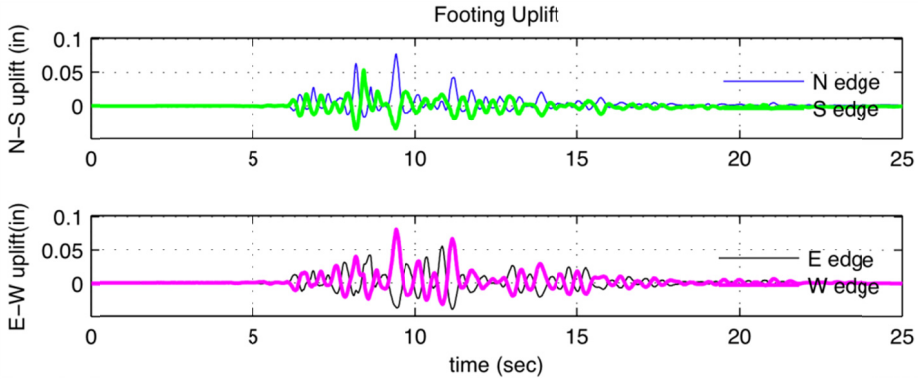

(c) N-S footing uplift (d) E-W footing uplift

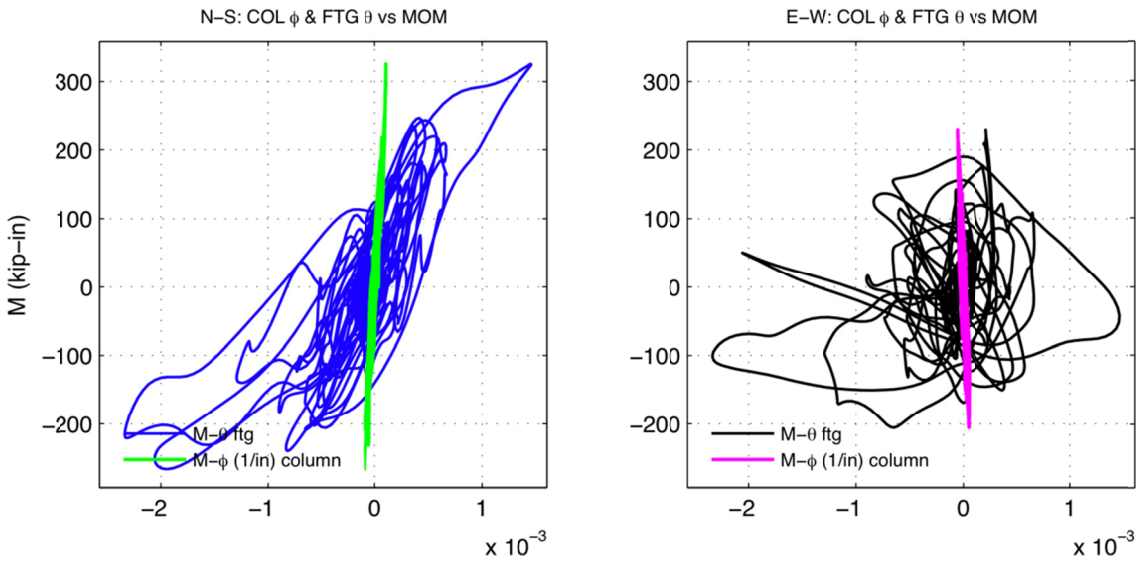

(e) N-S: Mom. vs Col ϕ (1/in) and FTG θ (f) E-W: Mom. vs Col ϕ (1/in) and FTG

Figure B.6 D5 experimental results.

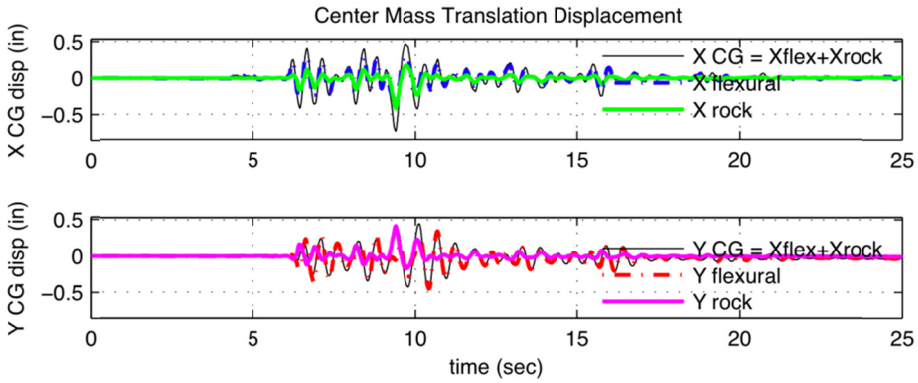

(a) X center mass translation (b) Y center mass translations

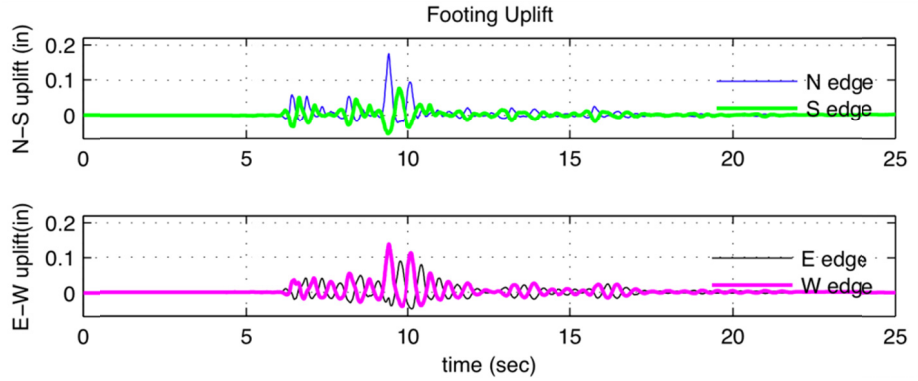

(c) N-S footing uplift (d) E-W footing uplift

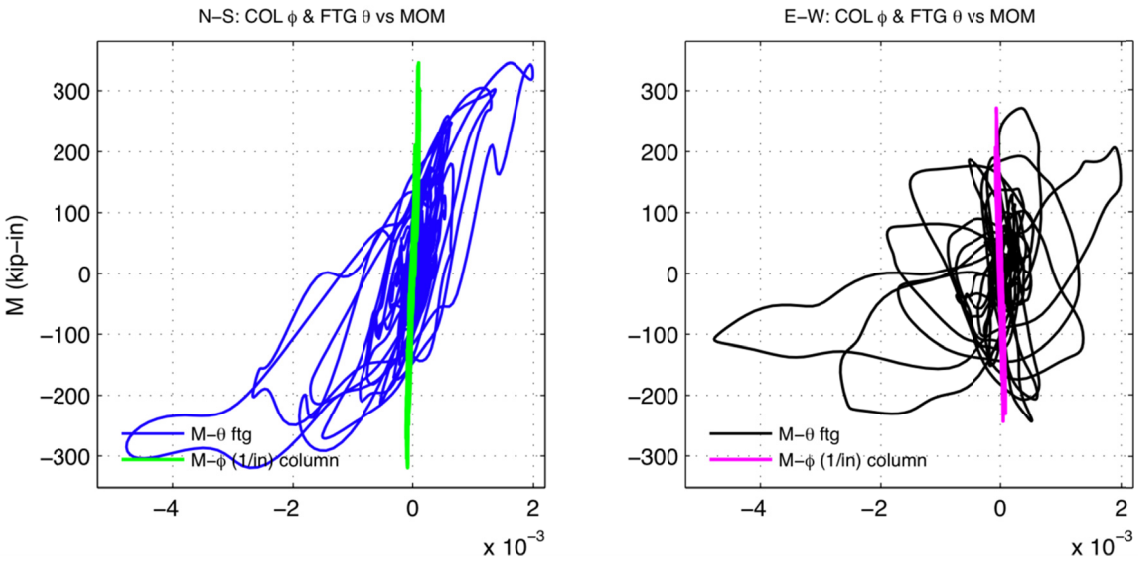

(e) N-S: Mom. vs Col ϕ (1/in) and FTG θ (f) E-W: Mom. vs Col ϕ (1/in) and FTG

Figure B.7 F1 experimental results.

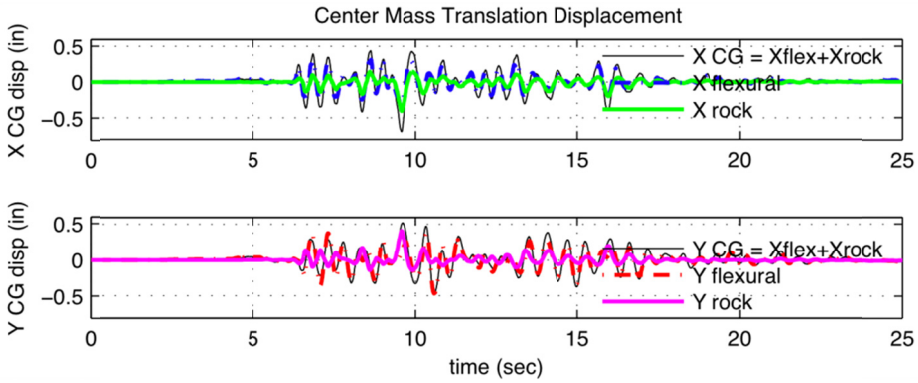

(a) X center mass translation (b) Y center mass translations

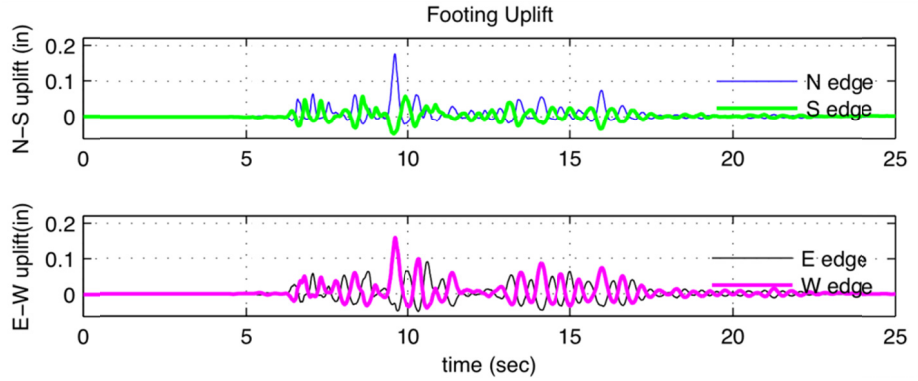

(c) N-S footing uplift (d) E-W footing uplift

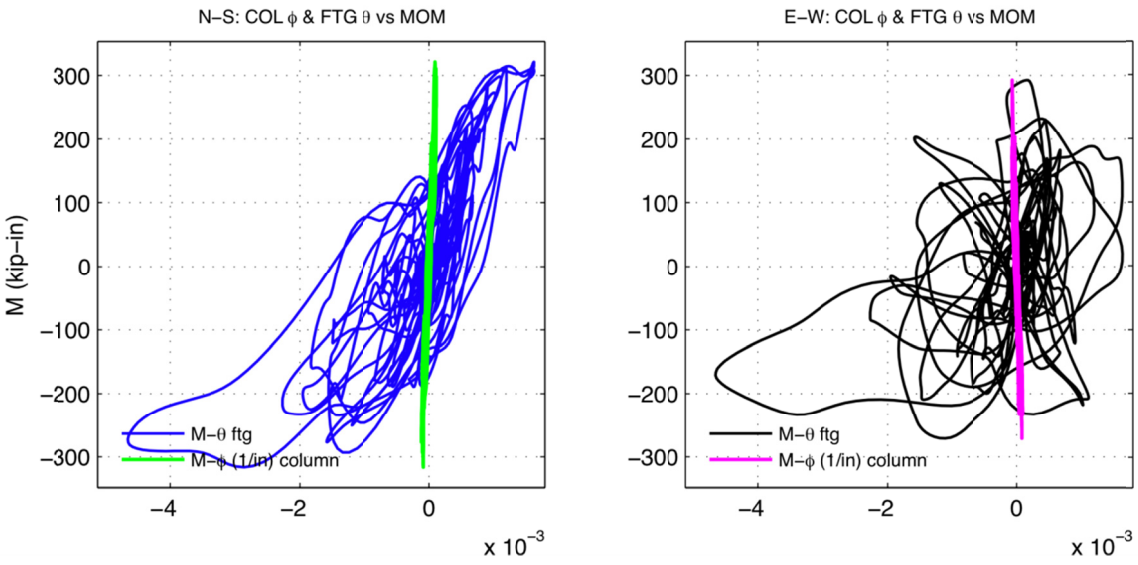

(e) N-S: Mom. vs Col ϕ (1/in) and FTG θ (f) E-W: Mom. vs Col ϕ (1/in) and FTG

Figure B.8 F3 experimental results.

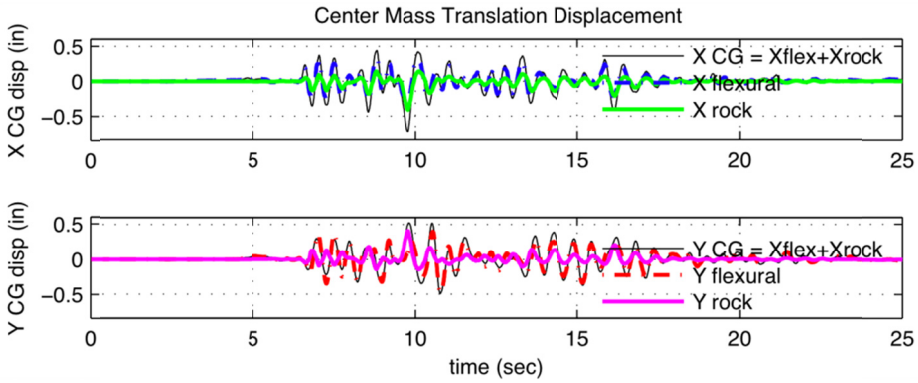

(a) X center mass translation (b) Y center mass translations

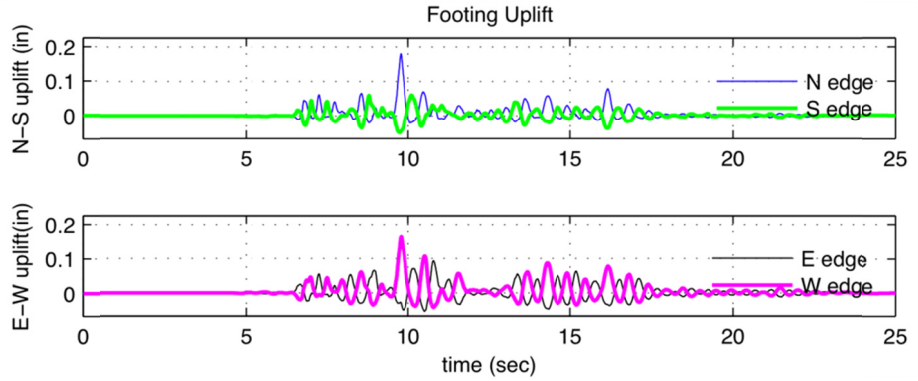

(c) N-S footing uplift (d) E-W footing uplift

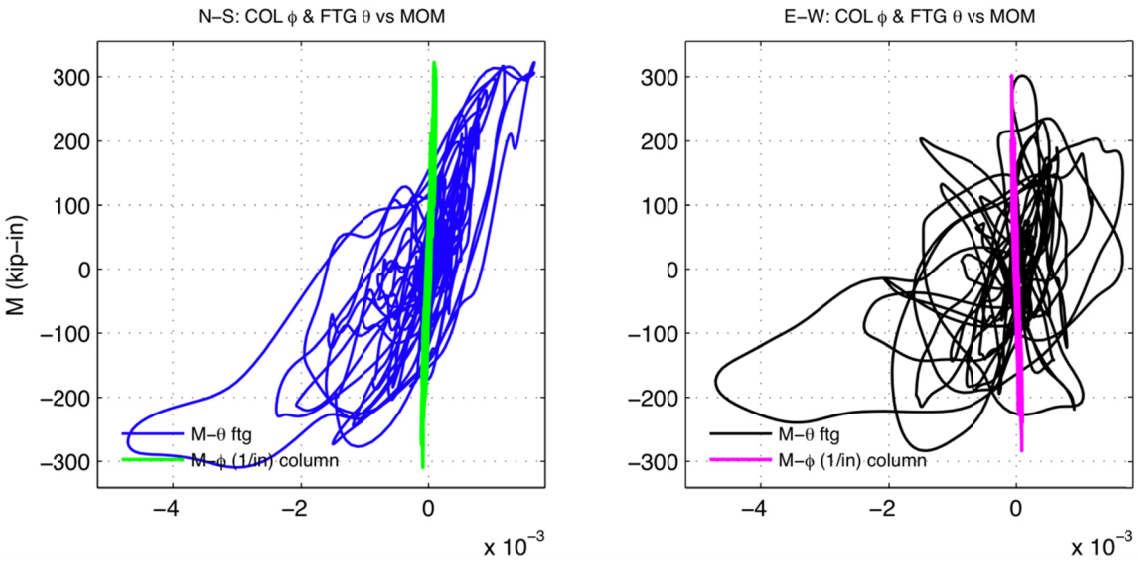

(e) N-S: Mom. vs Col ϕ (1/in) and FTG θ (f) E-W: Mom. vs Col ϕ (1/in) and FTG

Figure B.9 F5 experimental results.

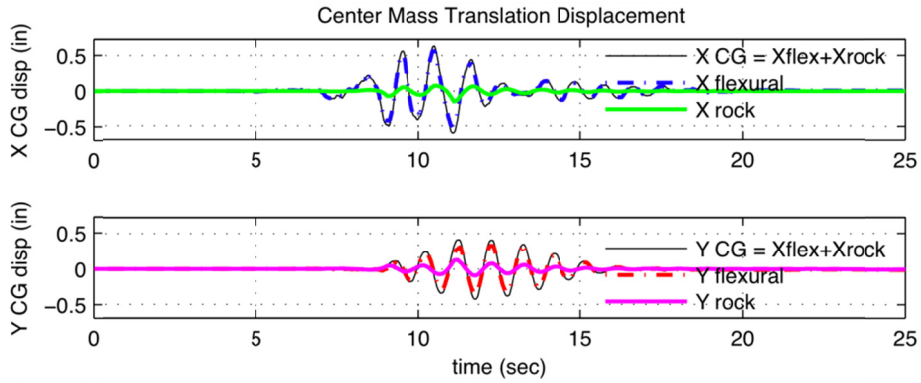

(a) X center mass translation (b) Y center mass translations

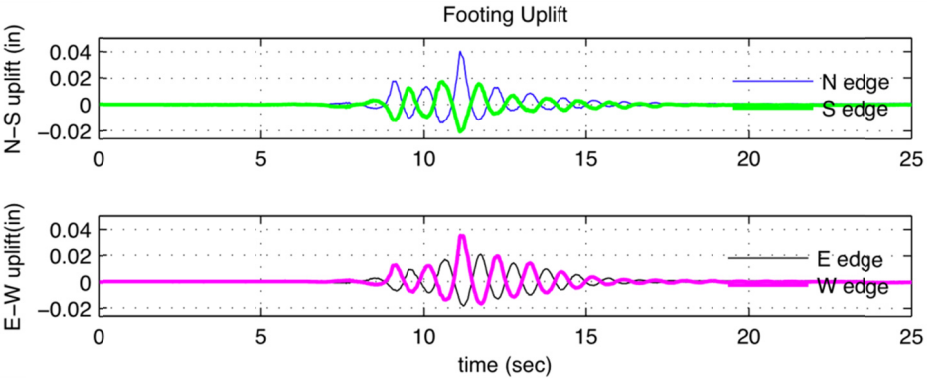

(c) N-S footing uplift (d) E-W footing uplift

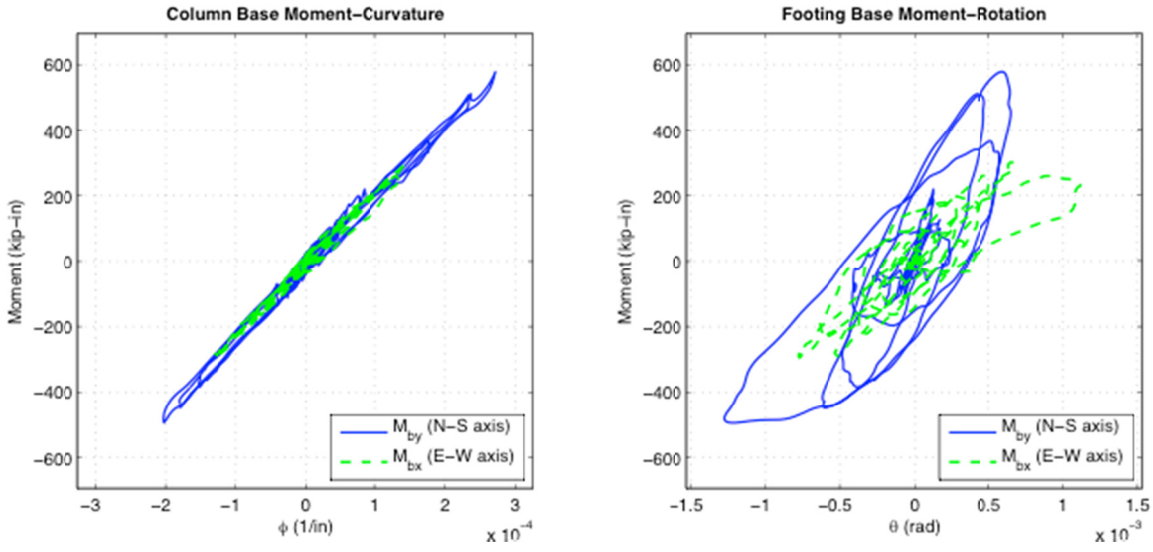

(e) Mom. vs Col ϕ (1/in) (f) Mom. vs FTG θ (rad)

Figure B.10 A1S experimental results.

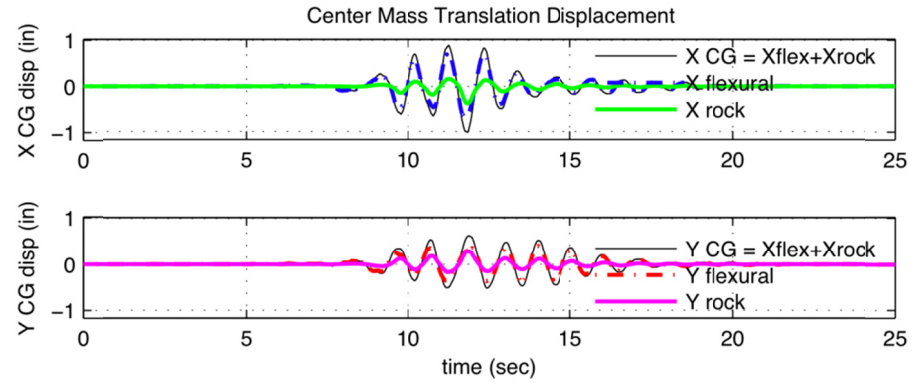

(a) X center mass translation (b) Y center mass translations

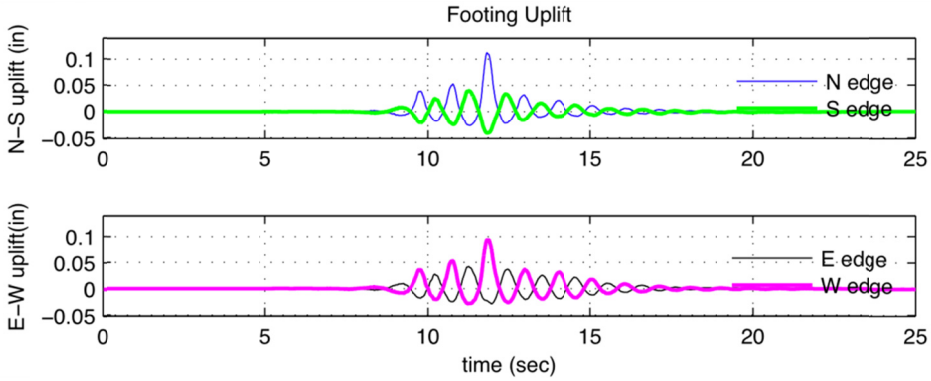

(c) N-S footing uplift (d) E-W footing uplift

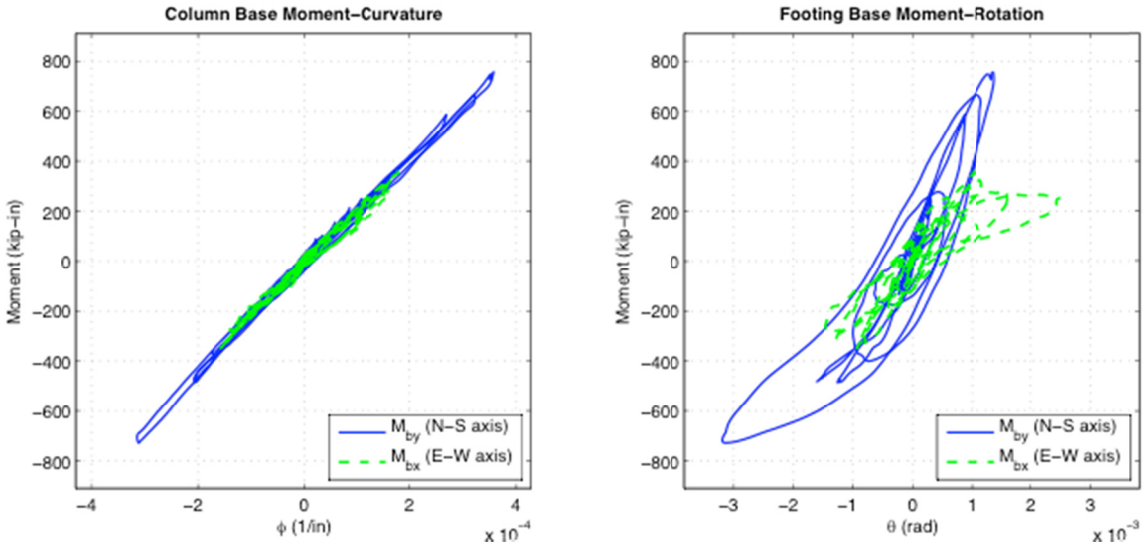

(e) Mom. vs Col ϕ (1/in) (f) Mom. vs FTG θ (rad)

Figure B.11 A3S experimental results.

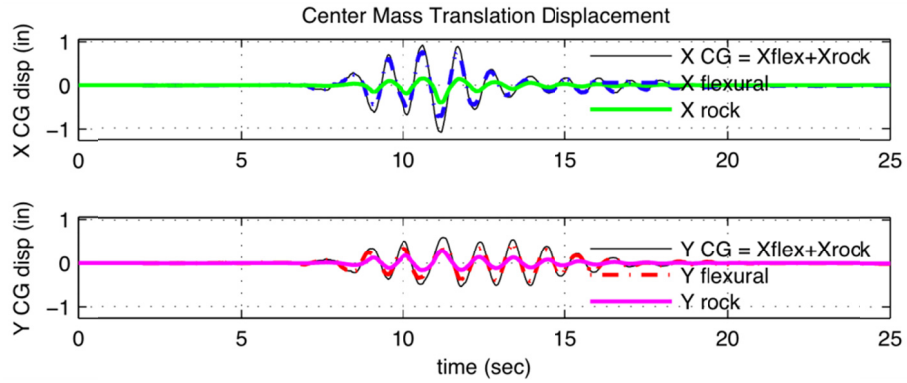

(a) X center mass translation (b) Y center mass translations

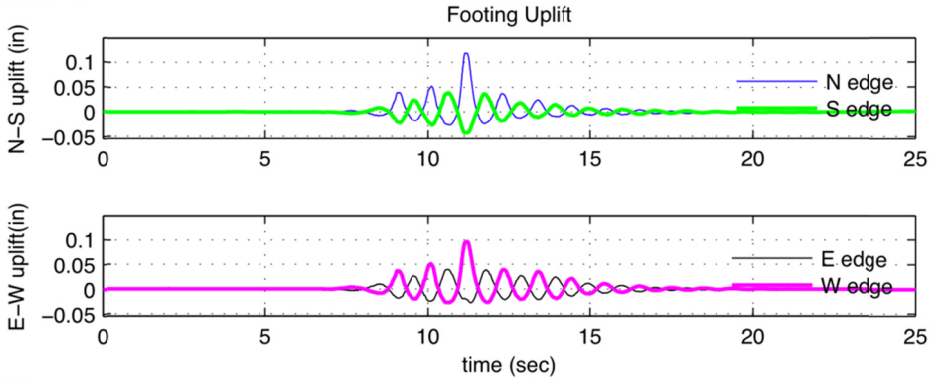

(c) N-S footing uplift (d) E-W footing uplift

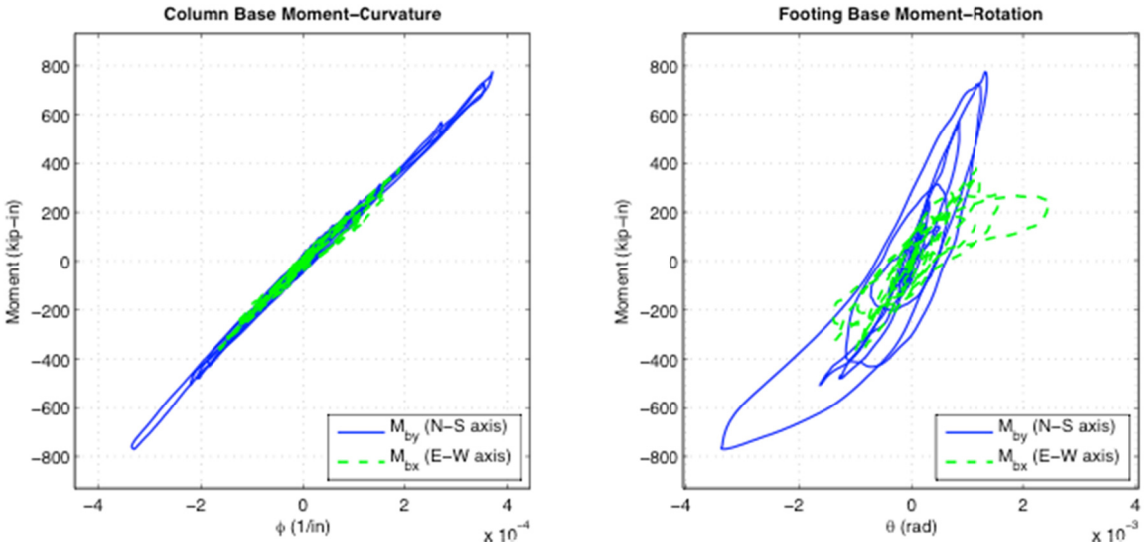

(e) Mom. vs Col ϕ (1/in) (f) Mom. vs FTG θ (rad)

Figure B.12 A5S experimental results.

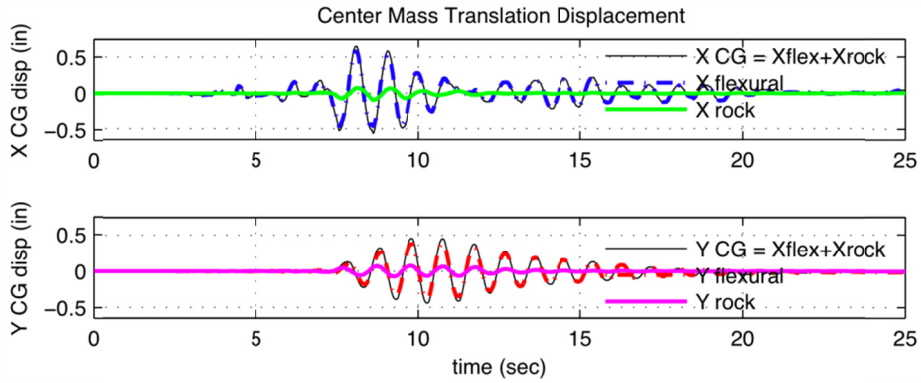

(a) X center mass translation (b) Y center mass translations

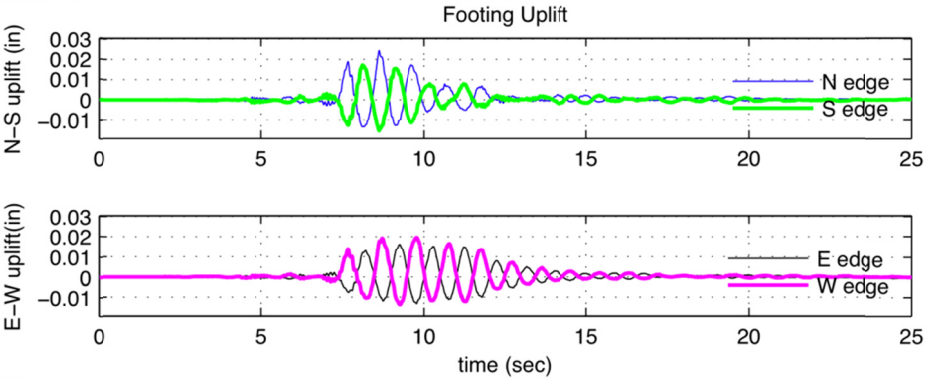

(c) N-S footing uplift (d) E-W footing uplift

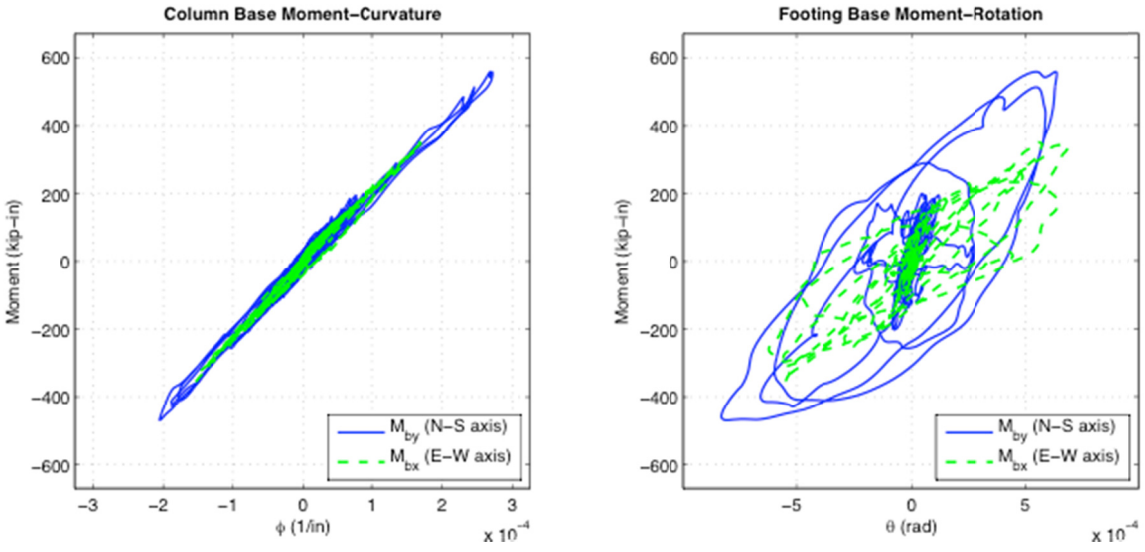

(e) Mom. vs Col ϕ (1/in) (f) Mom. vs FTG θ (rad)

Figure B.13 B1S experimental results.

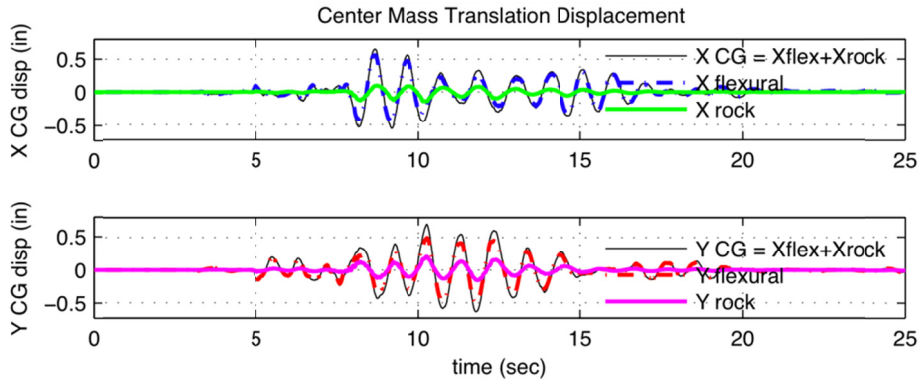

(a) X center mass translation (b) Y center mass translations

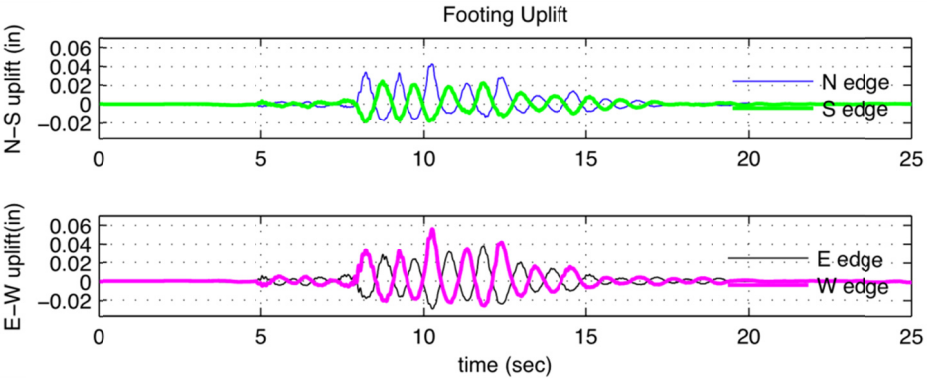

(c) N-S footing uplift (d) E-W footing uplift

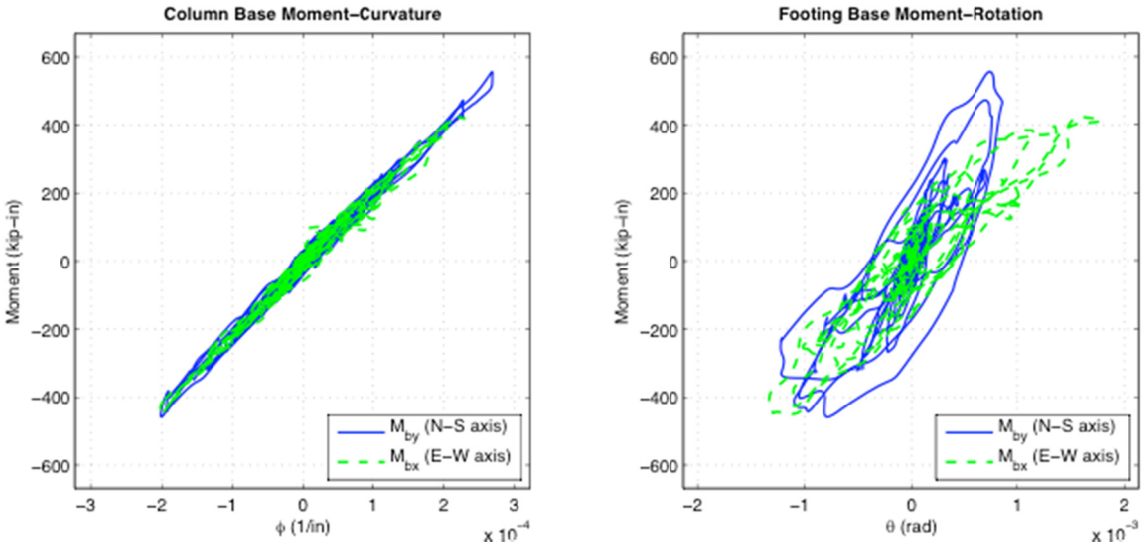

(e) Mom. vs Col ϕ (1/in) (f) Mom. vs FTG θ (rad)

Figure B.14 B3S experimental results.

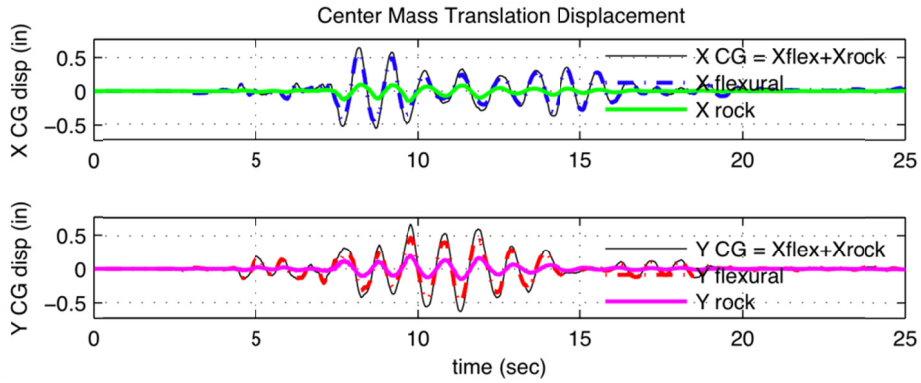

(a) X center mass translation (b) Y center mass translations

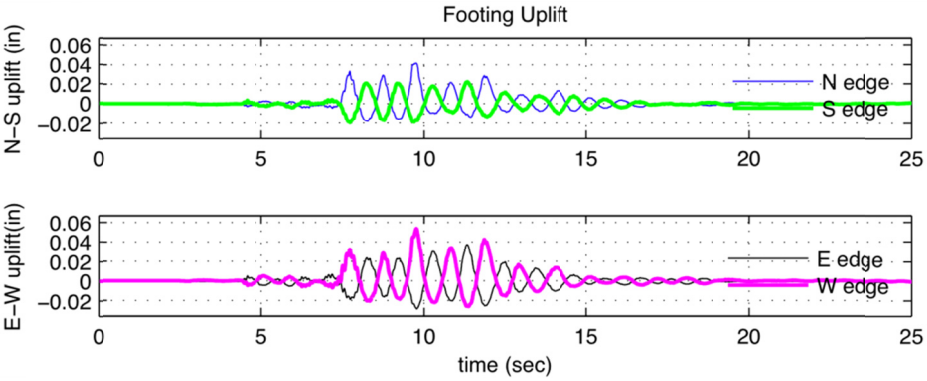

(c) N-S footing uplift (d) E-W footing uplift

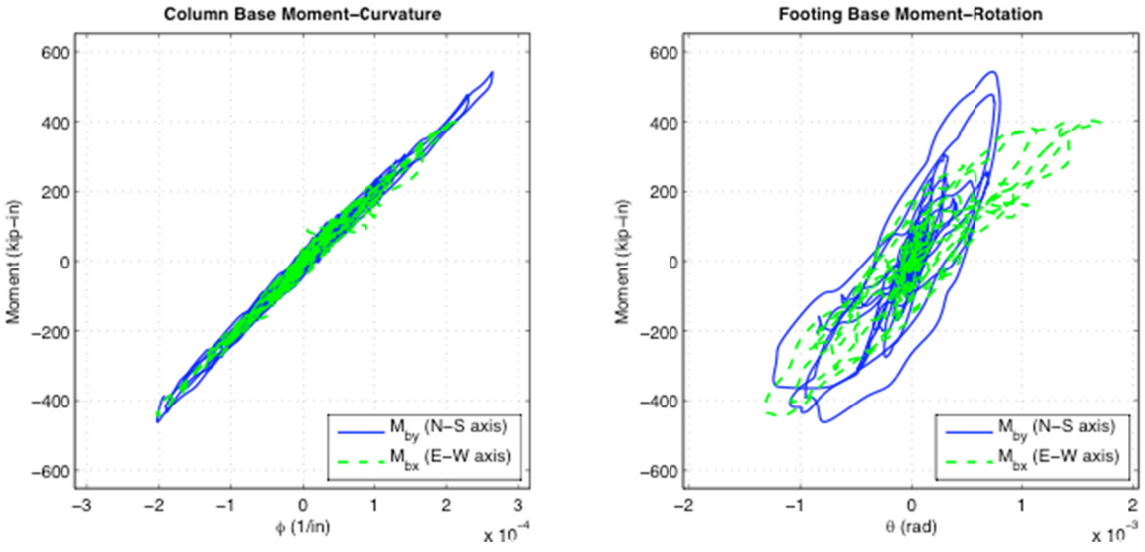

(e) Mom. vs Col ϕ (1/in) (f) Mom. vs FTG θ (rad)

Figure B.15 B5S experimental results.

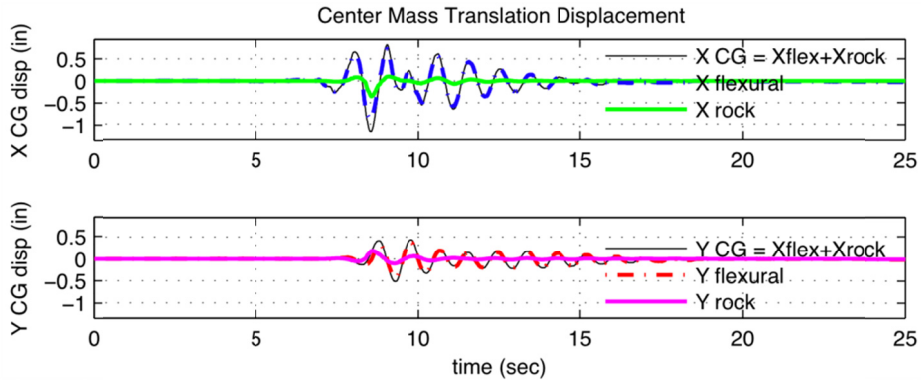

(a) X center mass translation (b) Y center mass translations

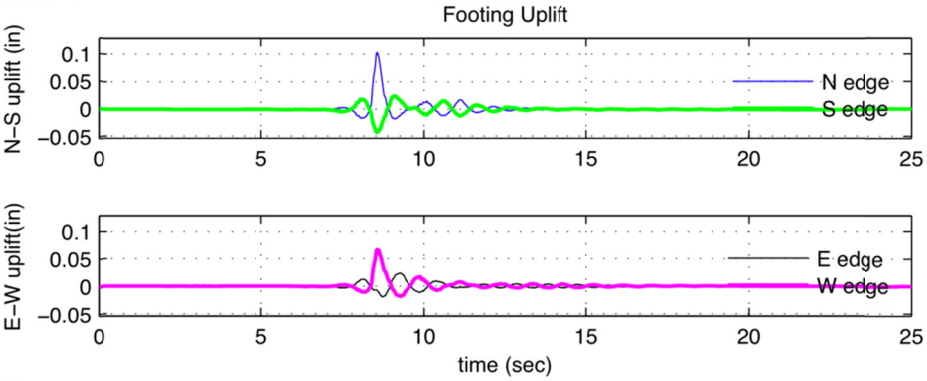

(c) N-S footing uplift (d) E-W footing uplift

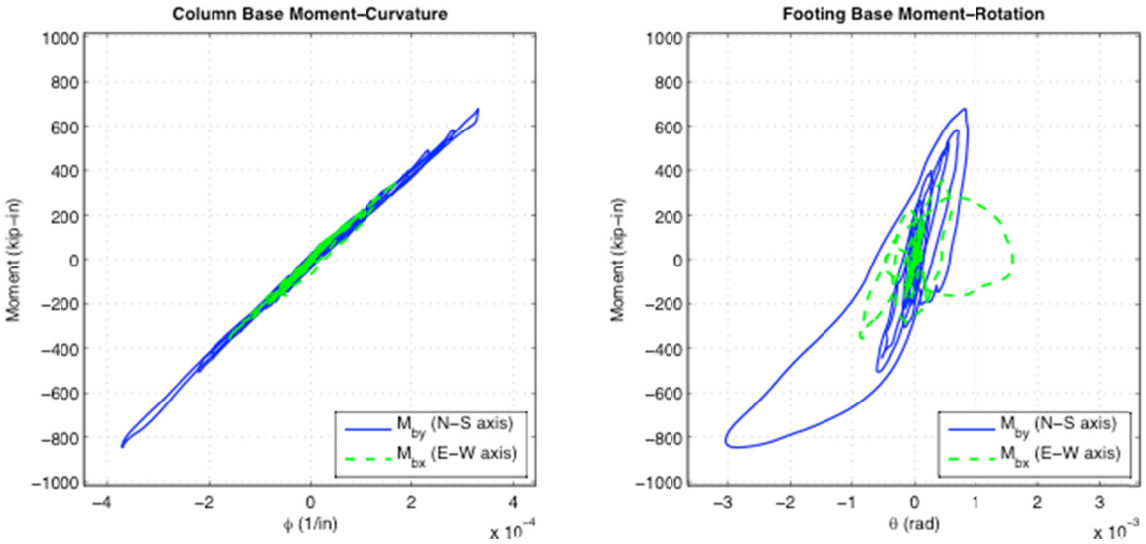

(e) Mom. vs Col ϕ (1/in) (f) Mom. vs FTG θ (rad)

Figure B.16 C1S Experimental Results.

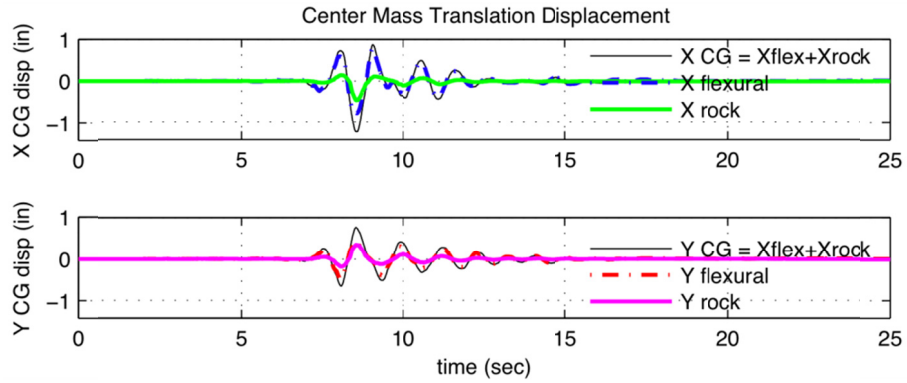

(a) X center mass translation (b) Y center mass translations

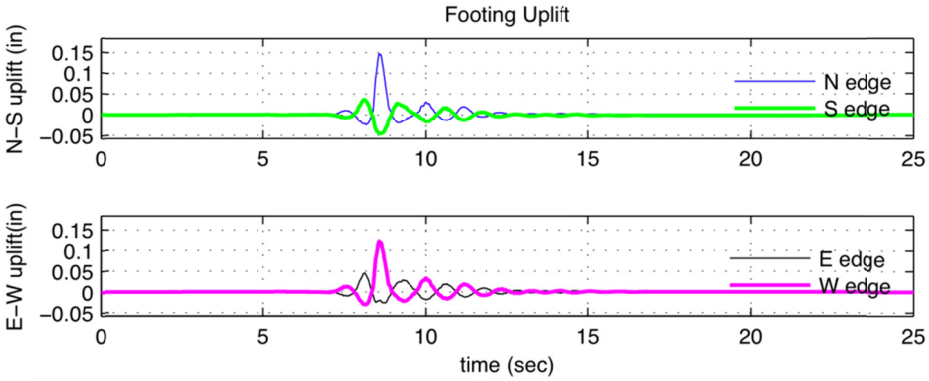

(c) N-S footing uplift (d) E-W footing uplift

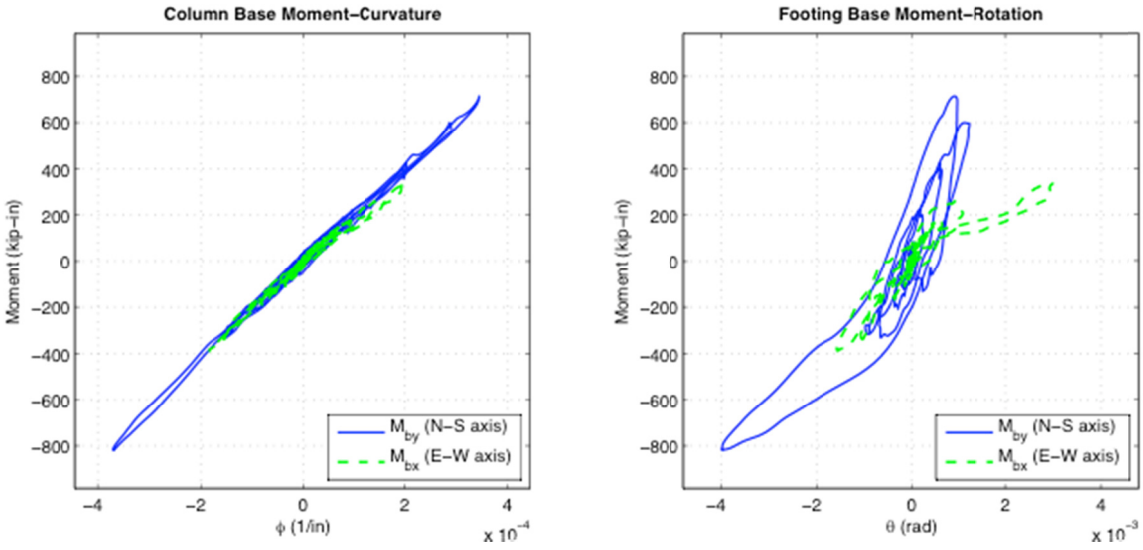

(e) Mom. vs Col ϕ (1/in) (f) Mom. vs FTG θ (rad)

Figure B.17 C3S experimental results.

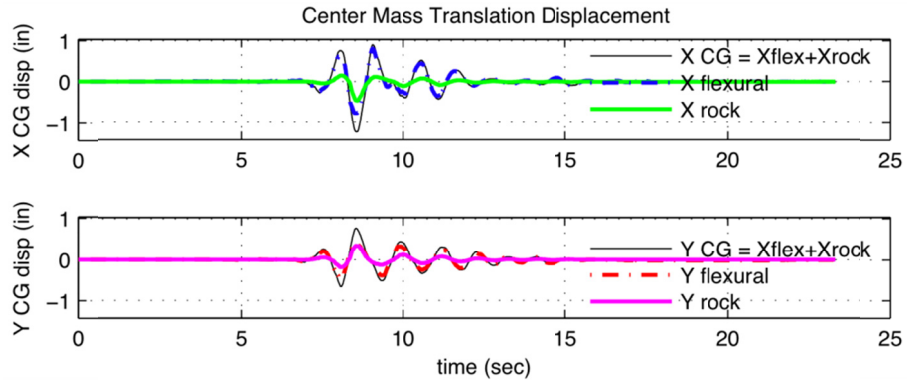

(a) X center mass translation (b) Y center mass translations

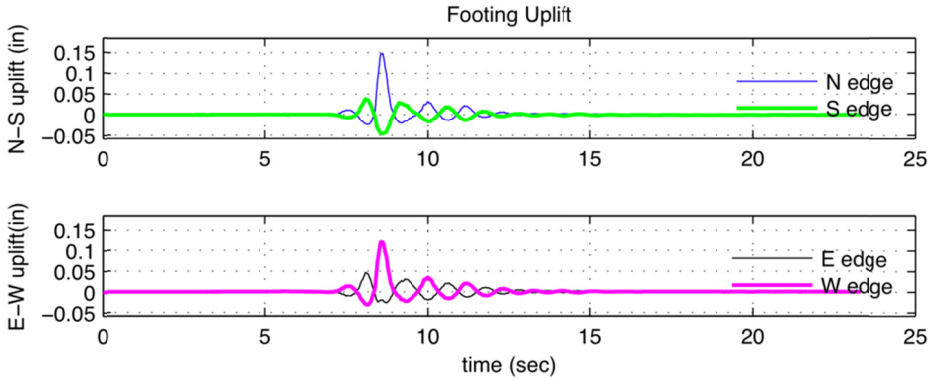

(c) N-S footing uplift (d) E-W footing uplift

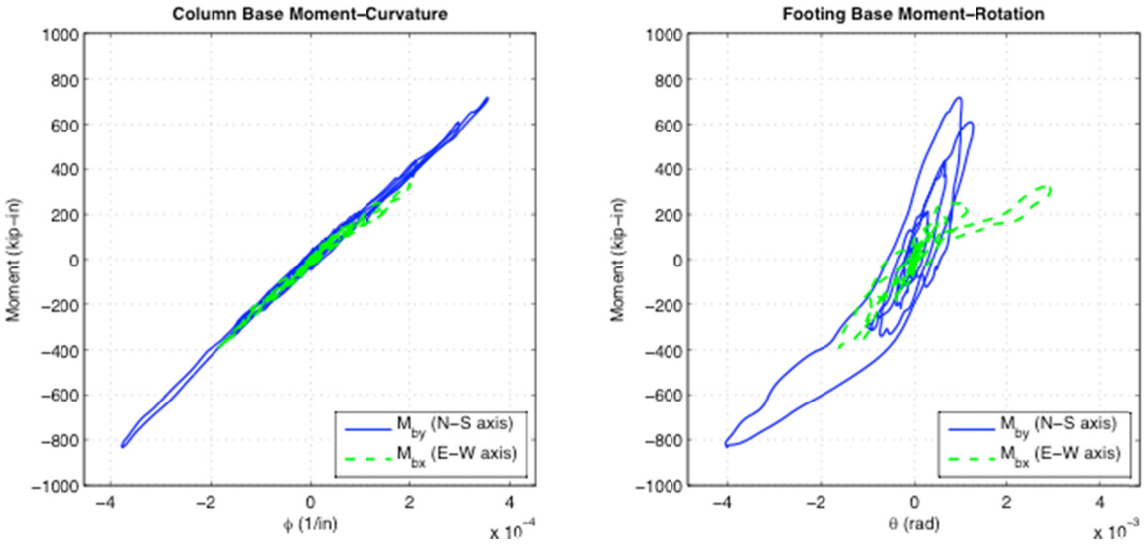

(e) Mom. vs Col ϕ (1/in) (f) Mom. vs FTG θ (rad)

Figure B.18 C5S experimental results.

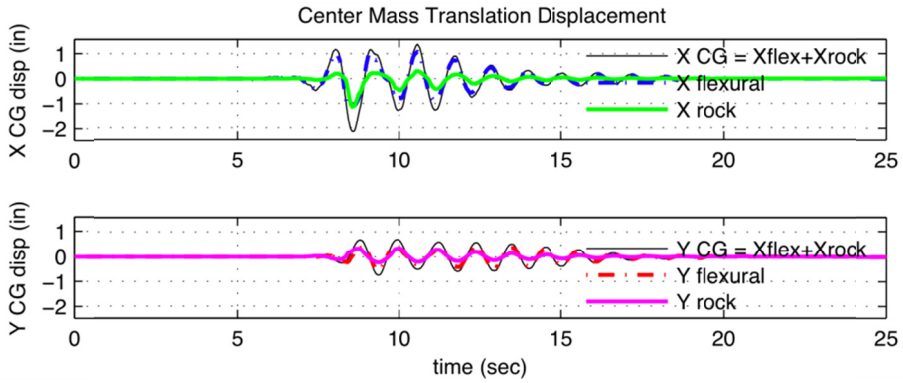

(a) X center mass translation (b) Y center mass translations

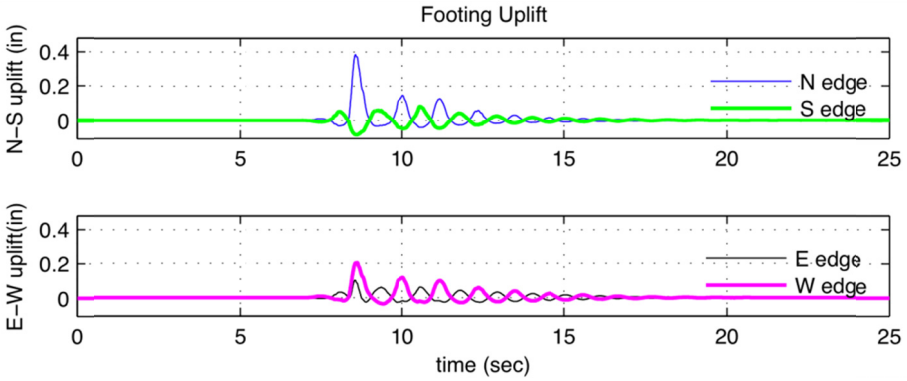

(c) N-S footing uplift (d) E-W footing uplift

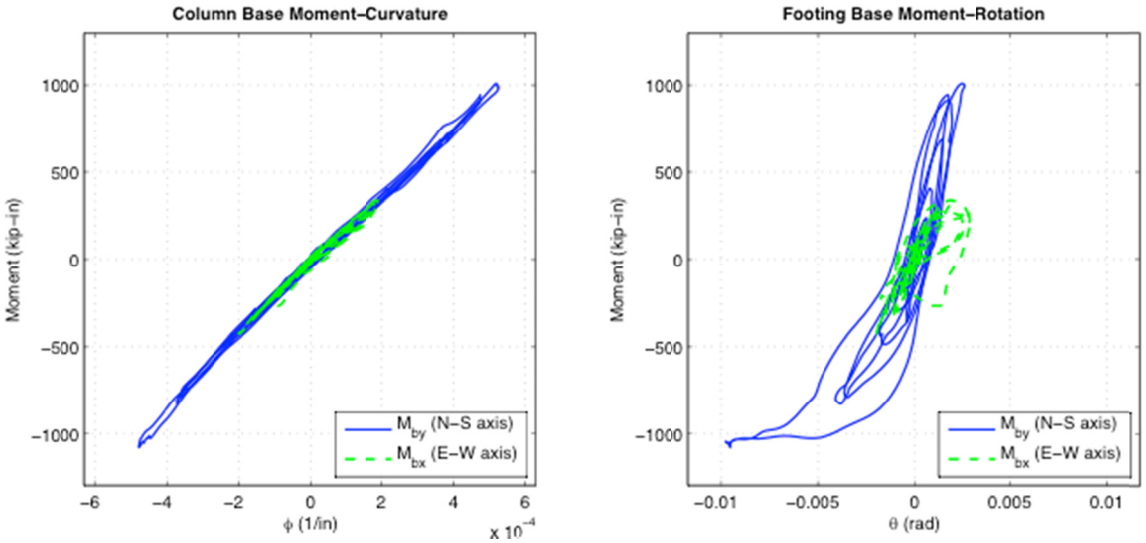

(e) Mom. vs Col ϕ (1/in) (f) Mom. vs FTG θ (rad)

Figure B.19 D1S experimental results.

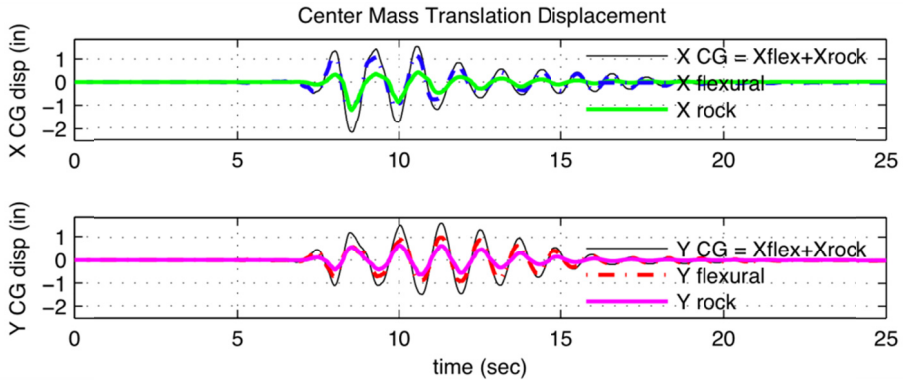

(a) X center mass translation (b) Y center mass translations

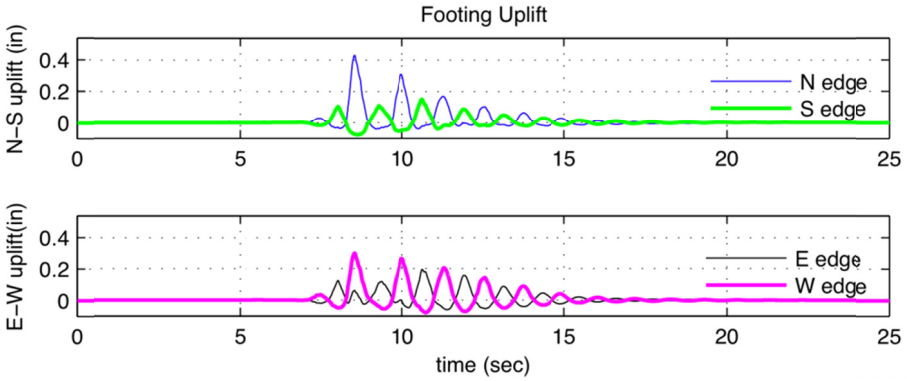

(c) N-S footing uplift (d) E-W footing uplift

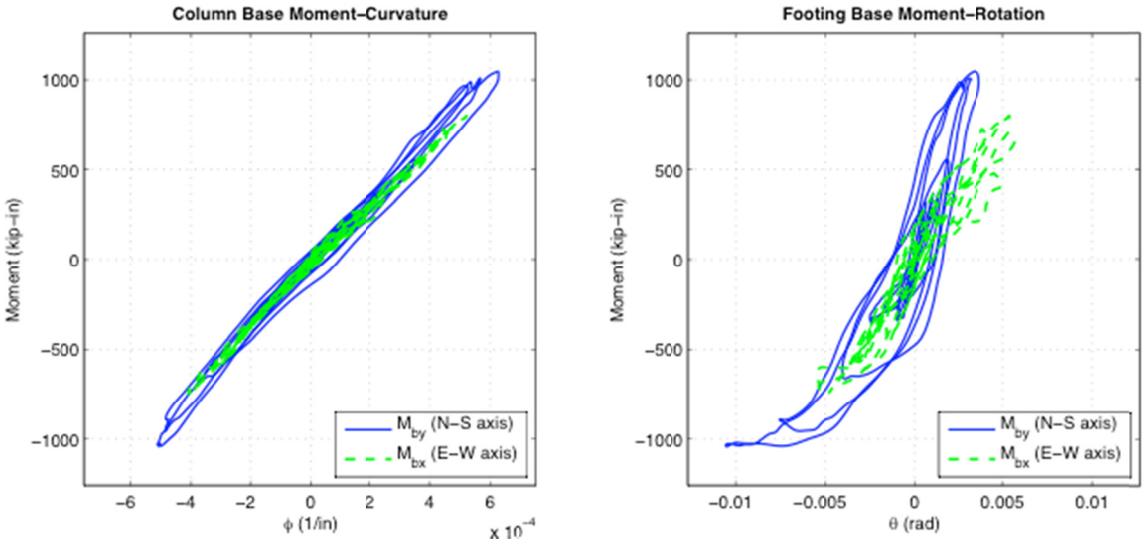

(e) Mom. vs Col ϕ (1/in) (f) Mom. vs FTG θ (rad)

Figure B.20 D3S experimental results.

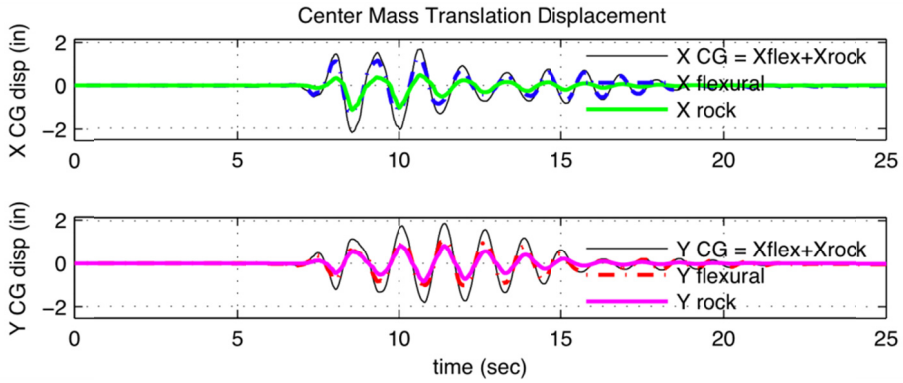

(a) X center mass translation (b) Y center mass translations

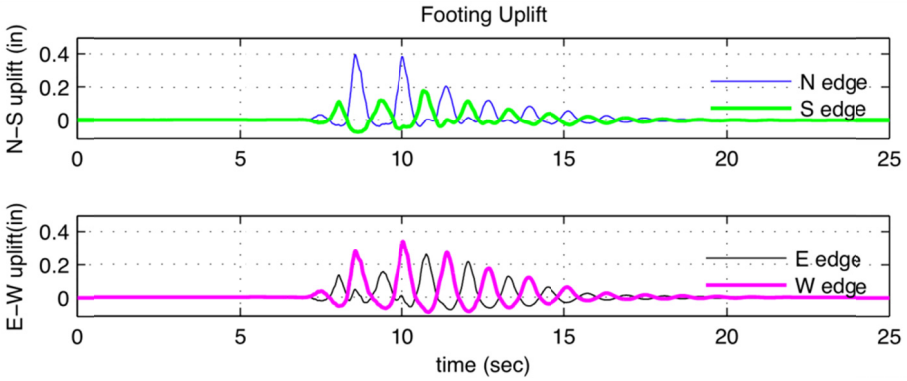

(c) N-S footing uplift (d) E-W footing uplift

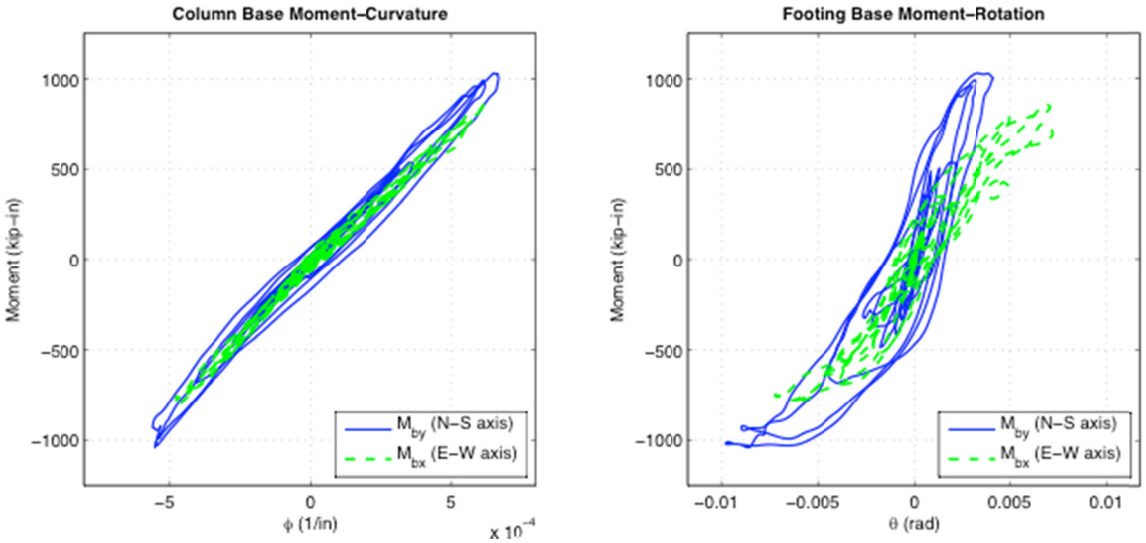

(e) Mom. vs Col ϕ (1/in) (f) Mom. vs FTG θ (rad)

Figure B.21 D5S experimental results.

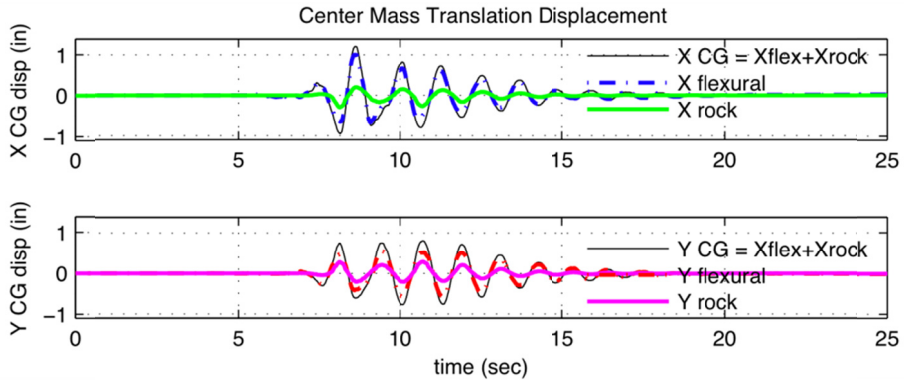

(a) X center mass translation (b) Y center mass translations

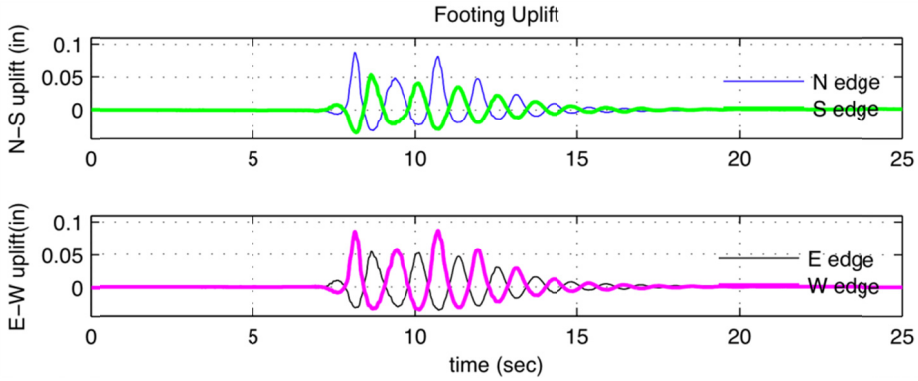

(c) N-S footing uplift (d) E-W footing uplift

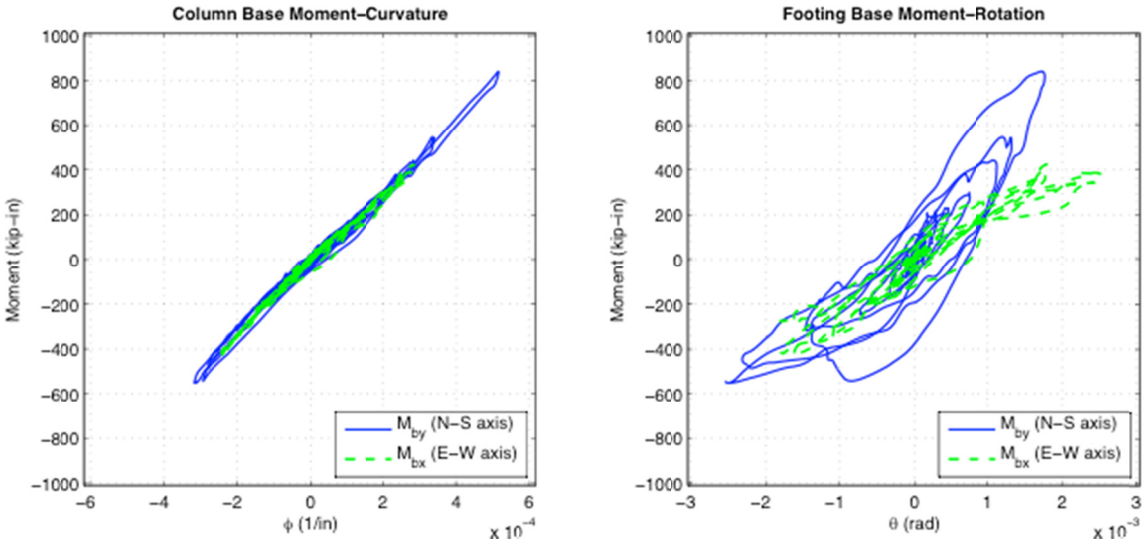

(e) Mom. vs Col ϕ (1/in) (f) Mom. vs FTG θ (rad)

Figure B.22 E1S experimental results.

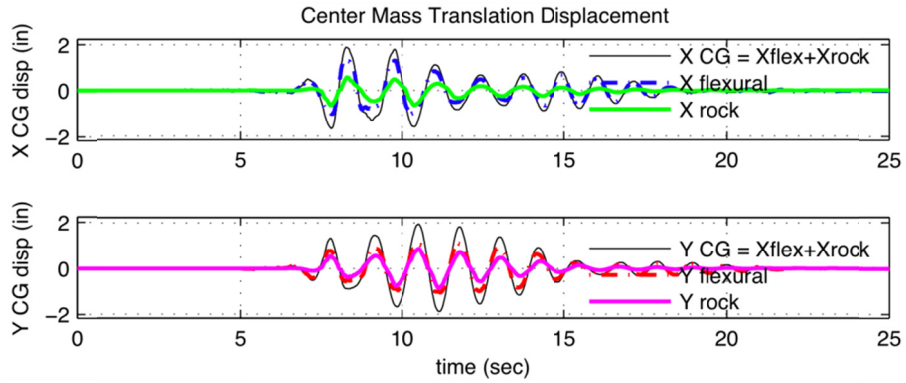

(a) X center mass translation (b) Y center mass translations

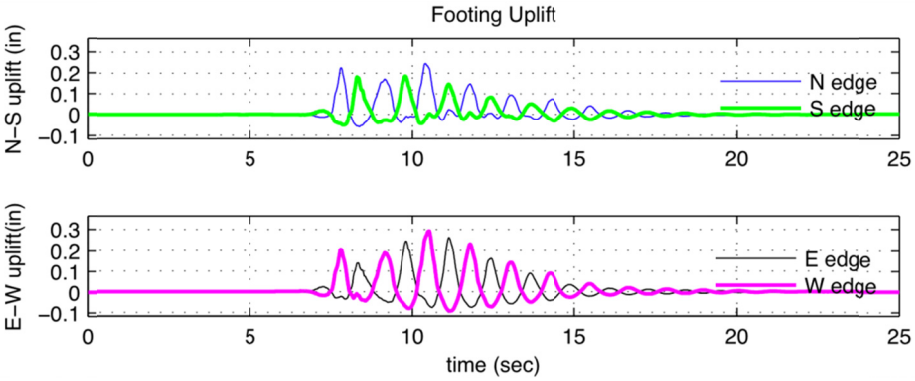

(c) N-S footing uplift (d) E-W footing uplift

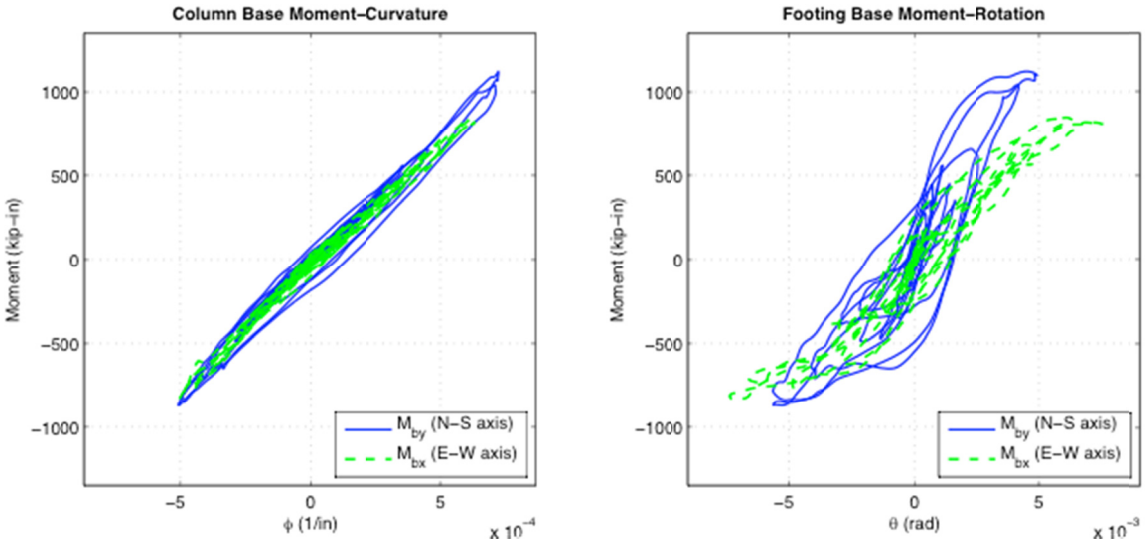

(e) Mom. vs Col ϕ (1/in) (f) Mom. vs FTG θ (rad)

Figure B.23 E2S experimental results.

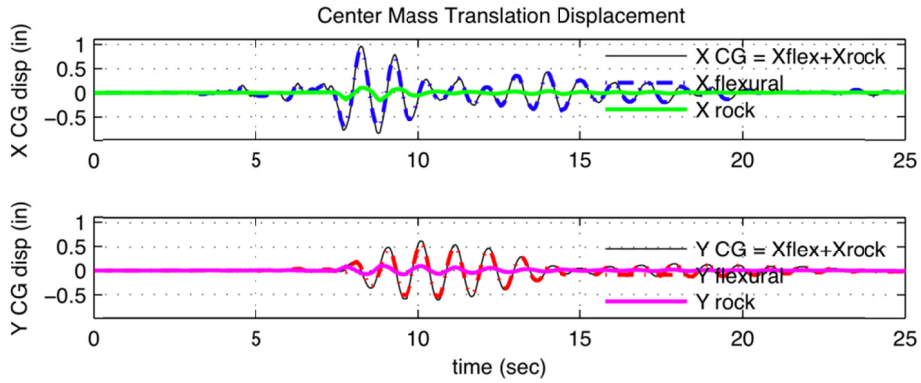

(a) X center mass translation (b) Y center mass translations

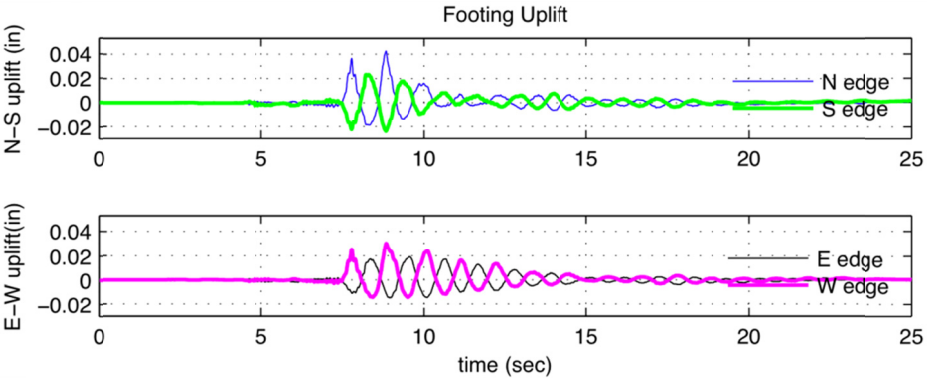

(c) N-S footing uplift (d) E-W footing uplift

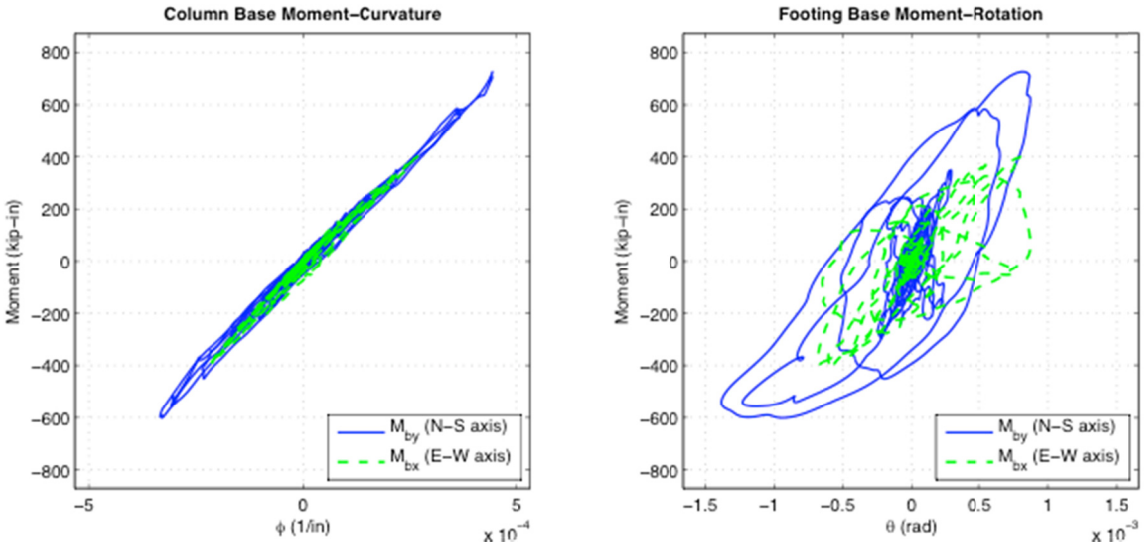

(e) Mom. vs Col ϕ (1/in) (f) Mom. vs FTG θ (rad)

Figure B.24 F1S experimental results.

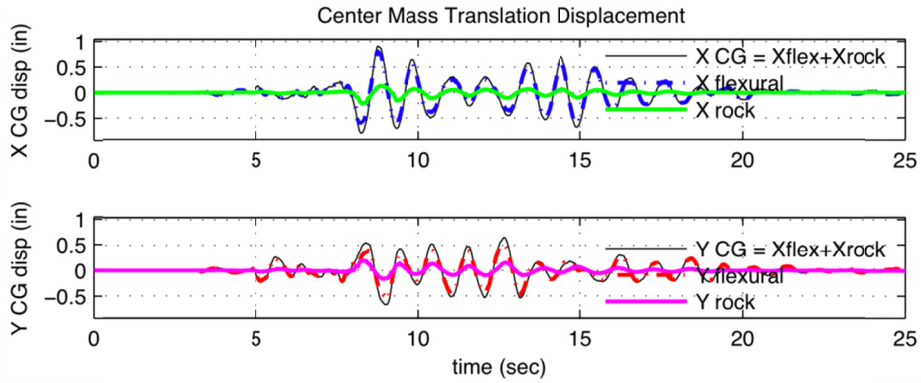

(a) X center mass translation (b) Y center mass translations

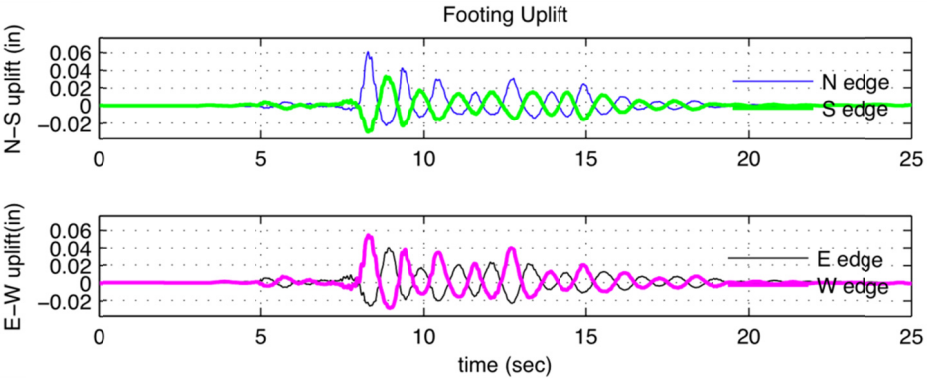

(c) N-S footing uplift (d) E-W footing uplift

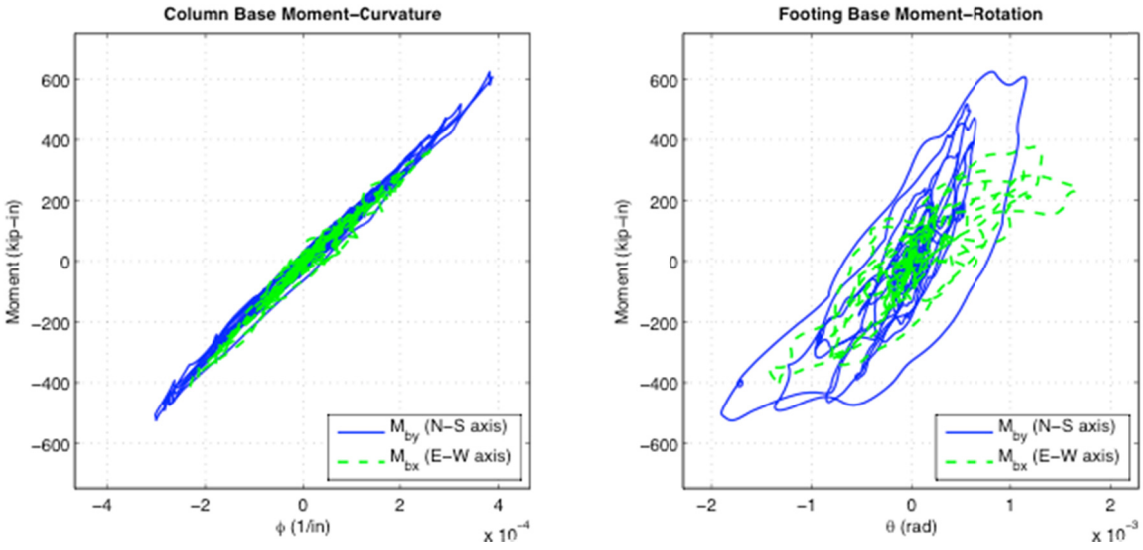

(e) Mom. vs Col ϕ (1/in) (f) Mom. vs FTG θ (rad)

Figure B.25 F3S experimental results.

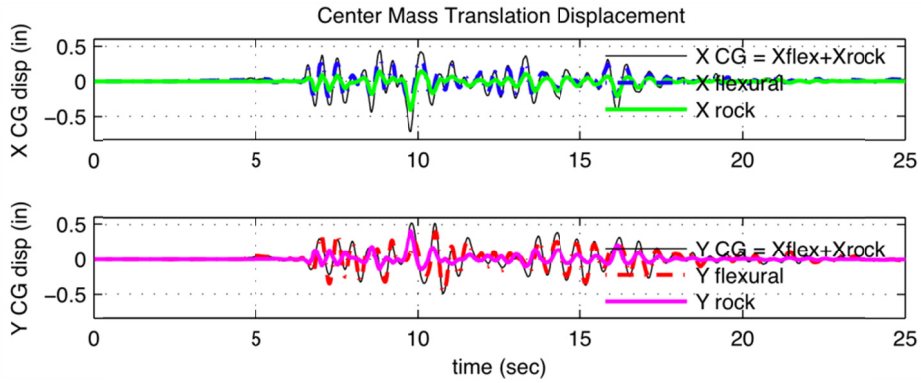

(a) X center mass translation (b) Y center mass translations

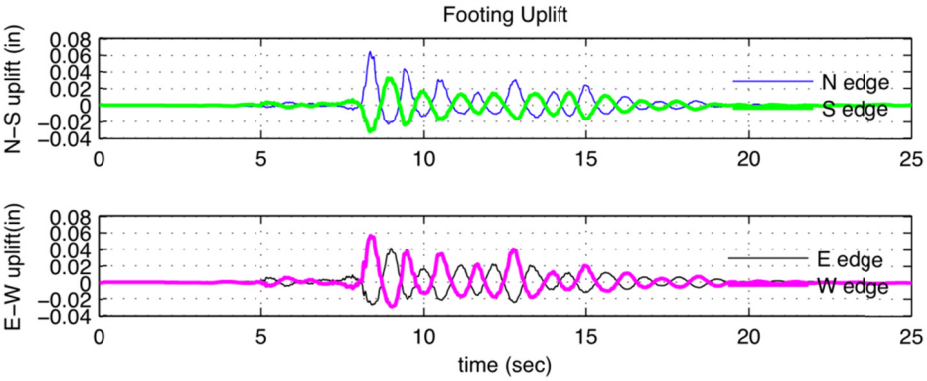

(c) N-S footing uplift (d) E-W footing uplift

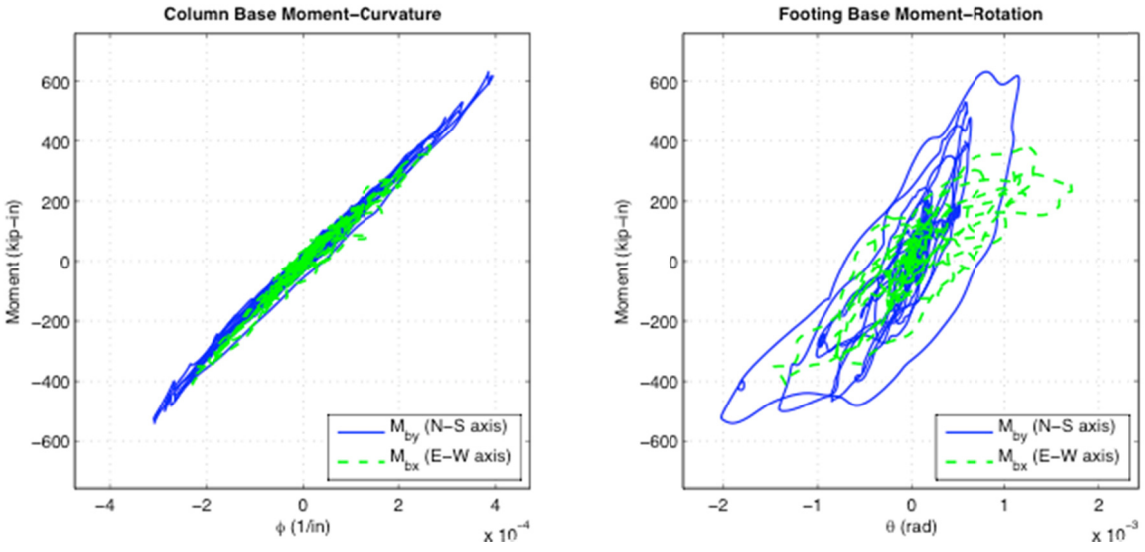

(e) Mom. vs Col ϕ (1/in) (f) Mom. vs FTG θ (rad)

Figure B.26 F5S experimental results.

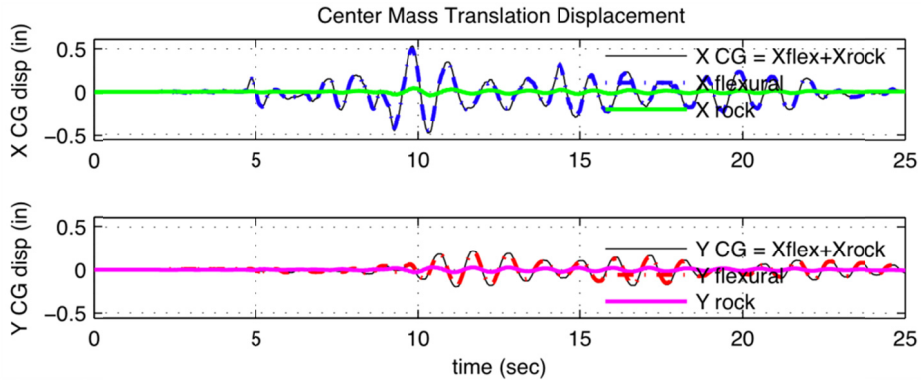

(a) X center mass translation (b) Y center mass translations

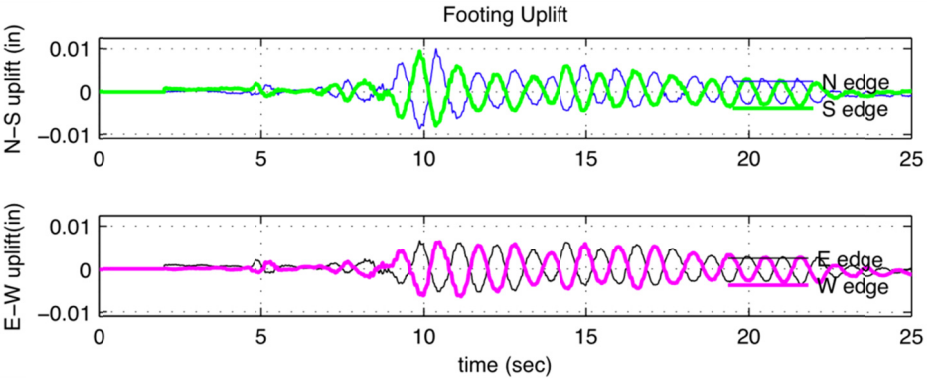

(c) N-S footing uplift (d) E-W footing uplift

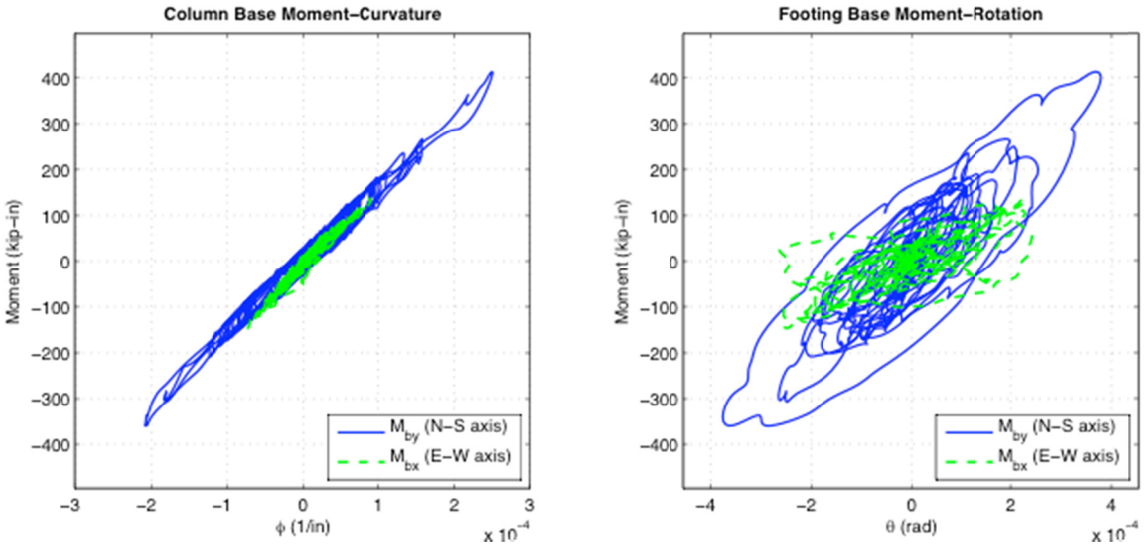

(e) Mom. vs Col ϕ (1/in) (f) Mom. vs FTG θ (rad)

Figure B.27 G1S experimental results.

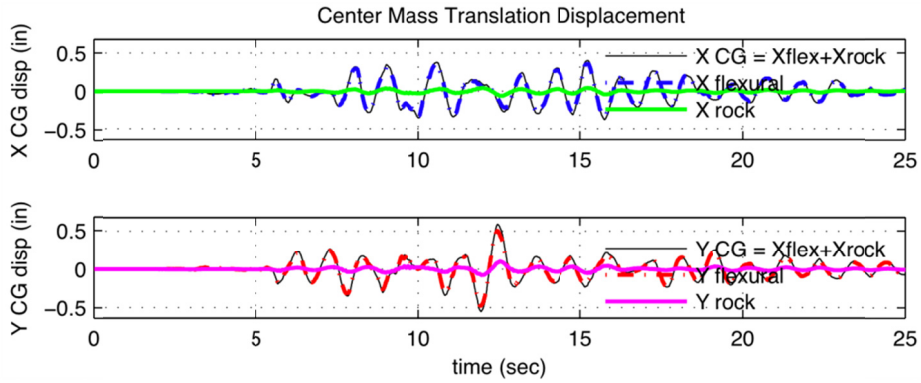

(a) X center mass translation (b) Y center mass translations

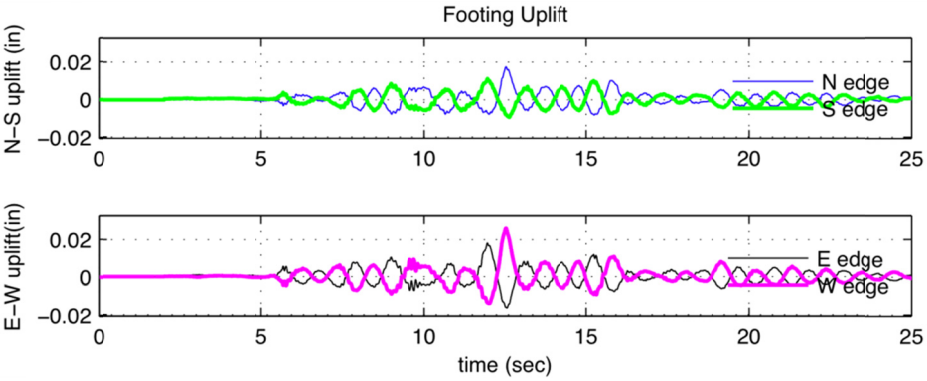

(c) N-S footing uplift (d) E-W footing uplift

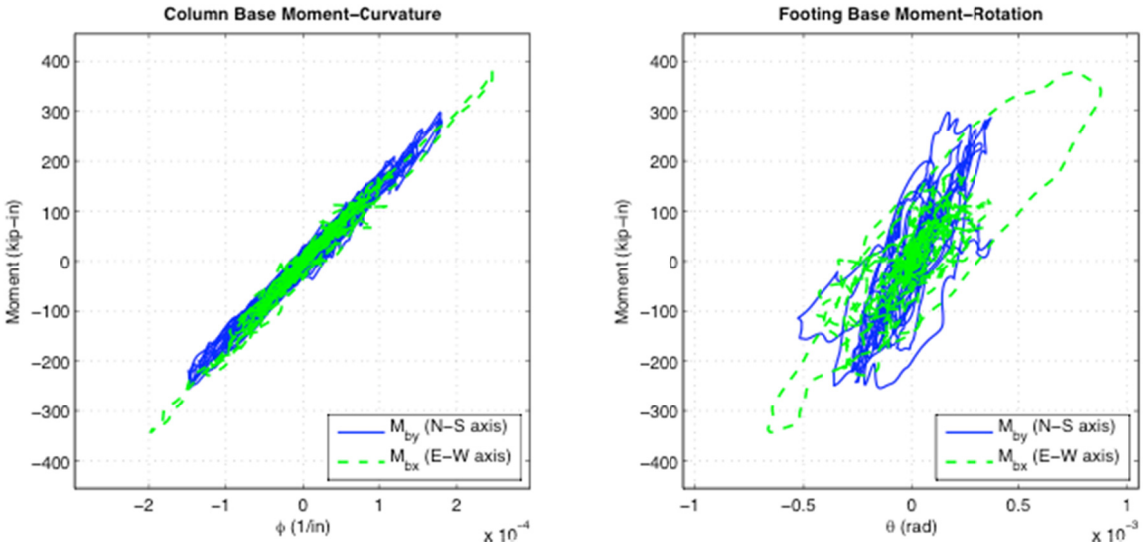

(e) Mom. vs Col ϕ (1/in) (f) Mom. vs FTG θ (rad)

Figure B.28 G3S experimental results.

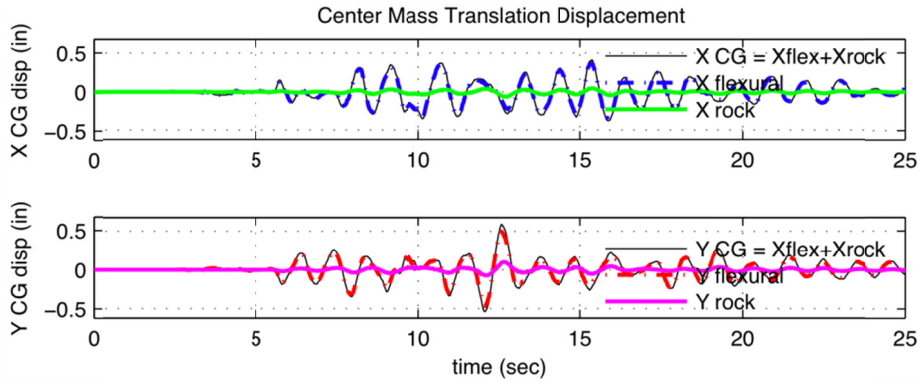

(a) X center mass translation (b) Y center mass translations

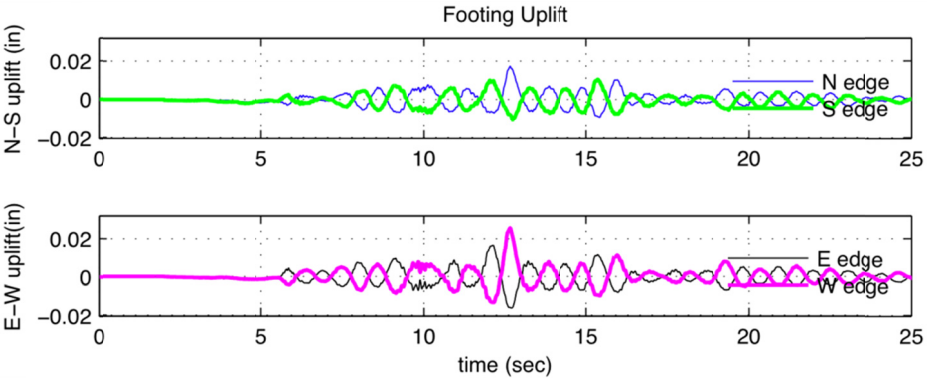

(c) N-S footing uplift (d) E-W footing uplift

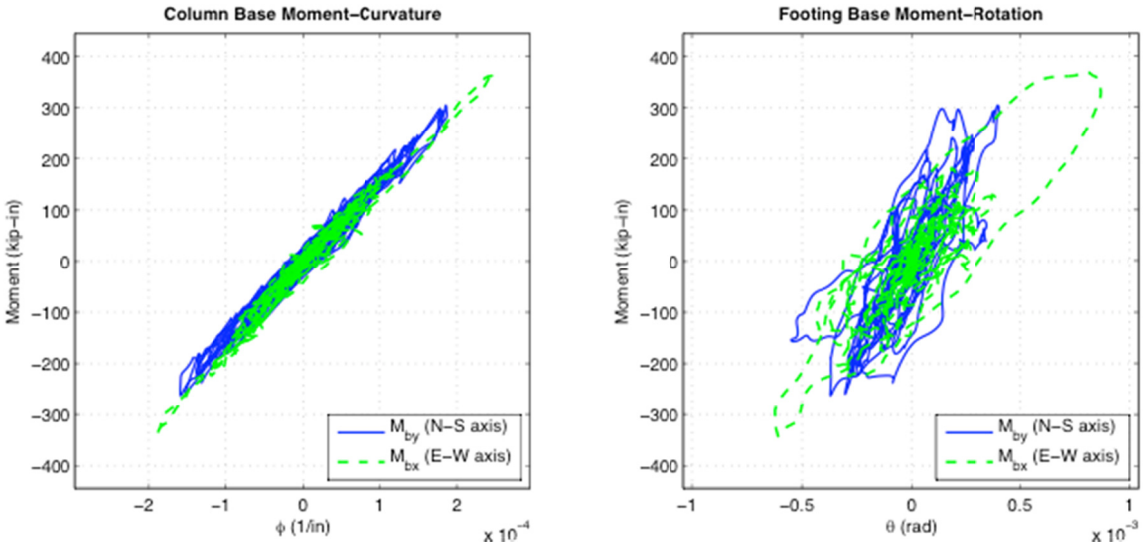

(e) Mom. vs Col ϕ (1/in) (f) Mom. vs FTG θ (rad)

Figure B.29 G5S experimental results.

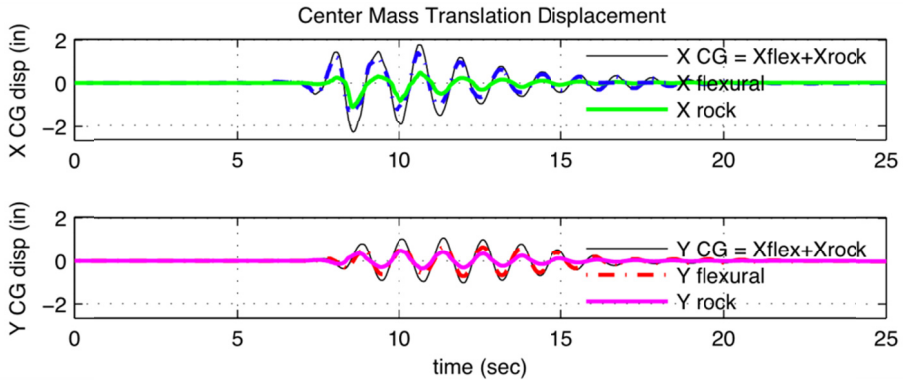

(a) X center mass translation (b) Y center mass translations

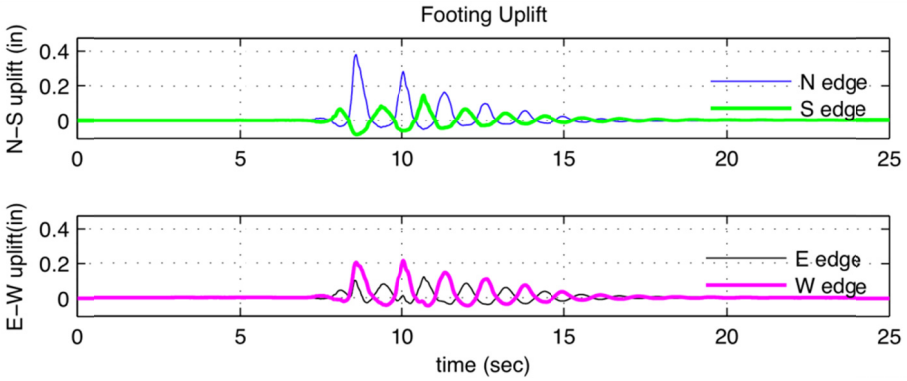

(c) N-S footing uplift (d) E-W footing uplift

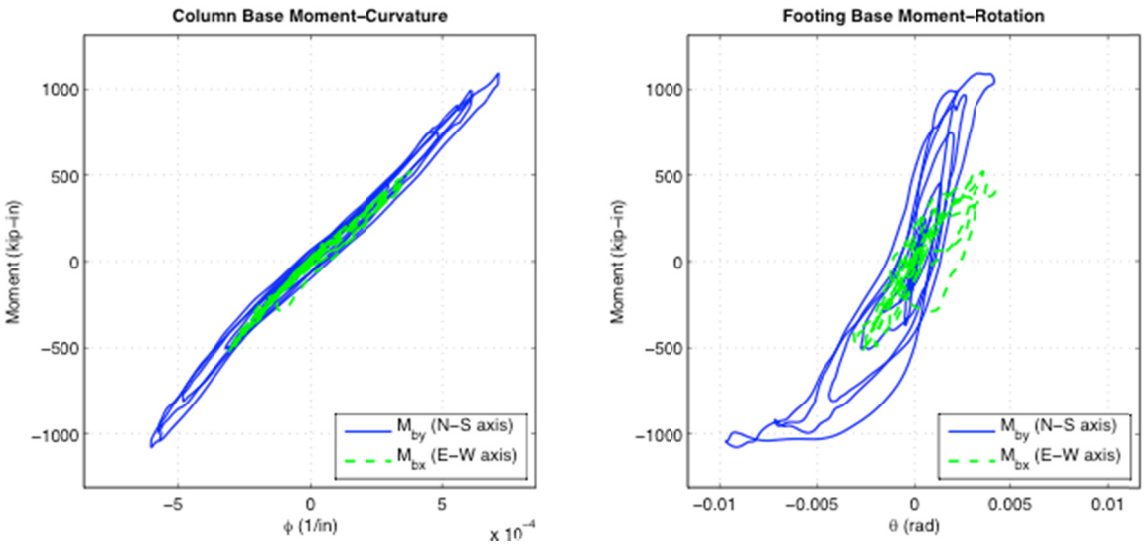

(e) Mom. vs Col ϕ (1/in) (f) Mom. vs FTG θ (rad)

Figure B.30 H1S experimental results.

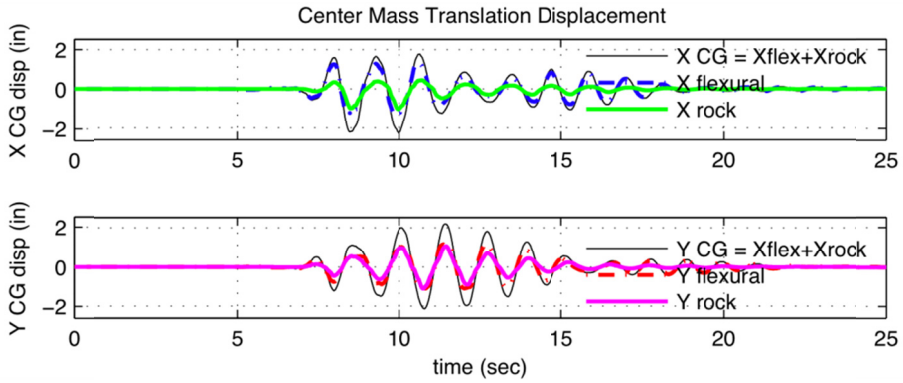

(a) X center mass translation (b) Y center mass translations

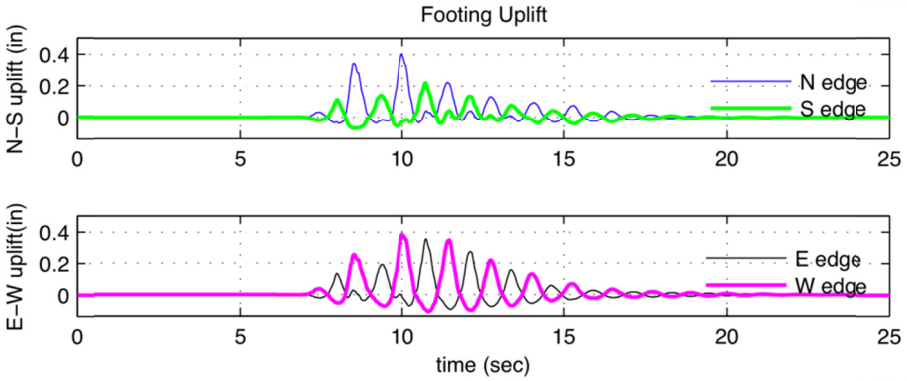

(c) N-S footing uplift (d) E-W footing uplift

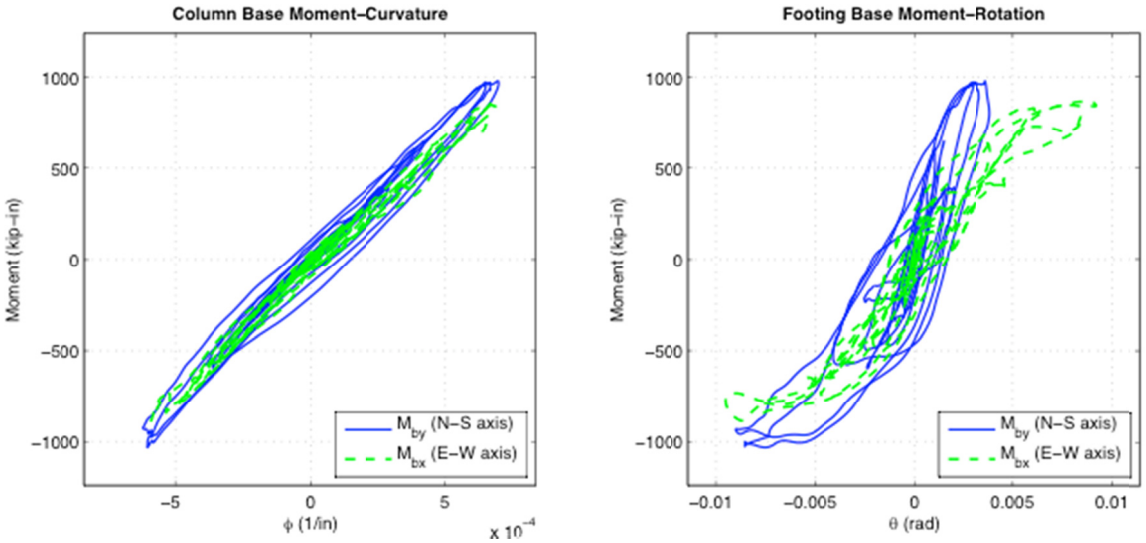

(e) Mom. vs Col ϕ (1/in) (f) Mom. vs FTG θ (rad)

Figure B.31 H2S experimental results.

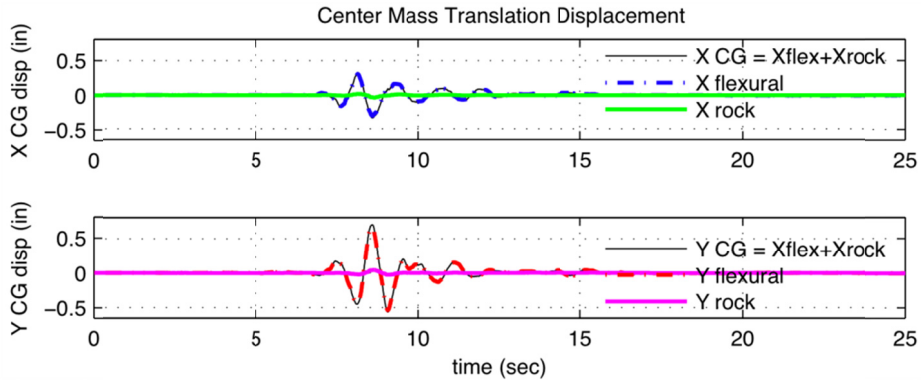

(a) X center mass translation (b) Y center mass translations

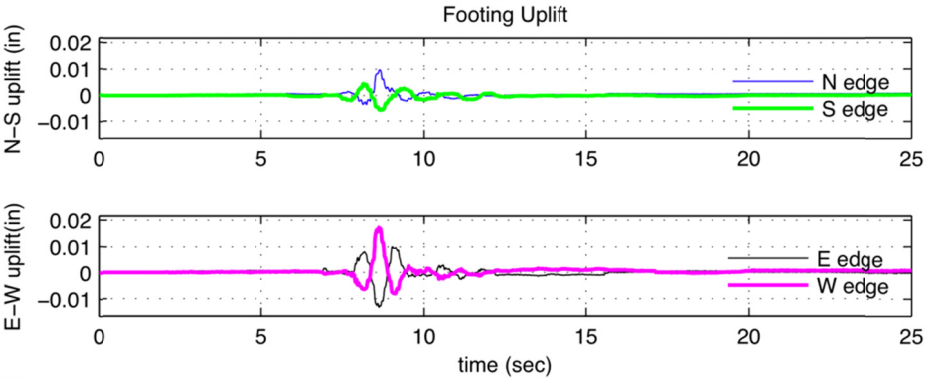

(c) N-S footing uplift (d) E-W footing uplift

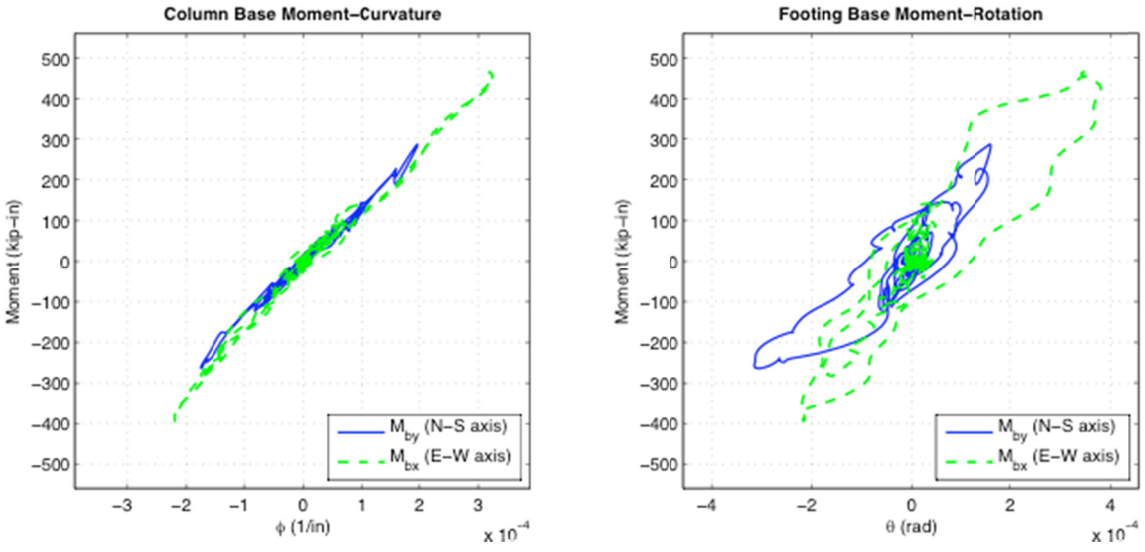

(e) Mom. vs Col ϕ (1/in) (f) Mom. vs FTG θ (rad)

Figure B.32 A1R experimental results.

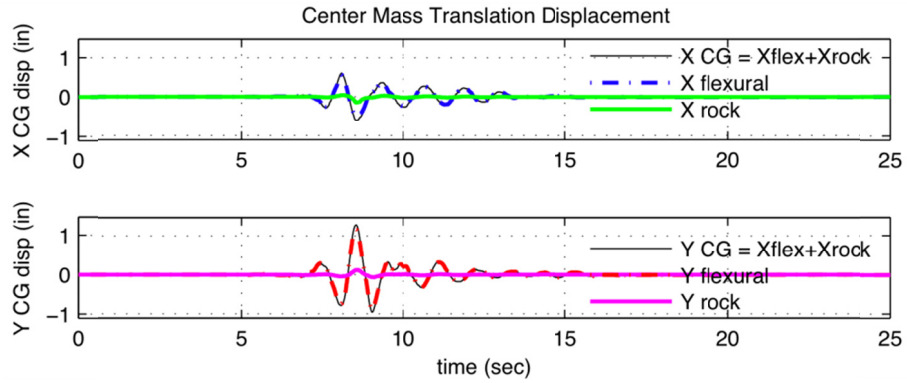

(a) X center mass translation (b) Y center mass translations

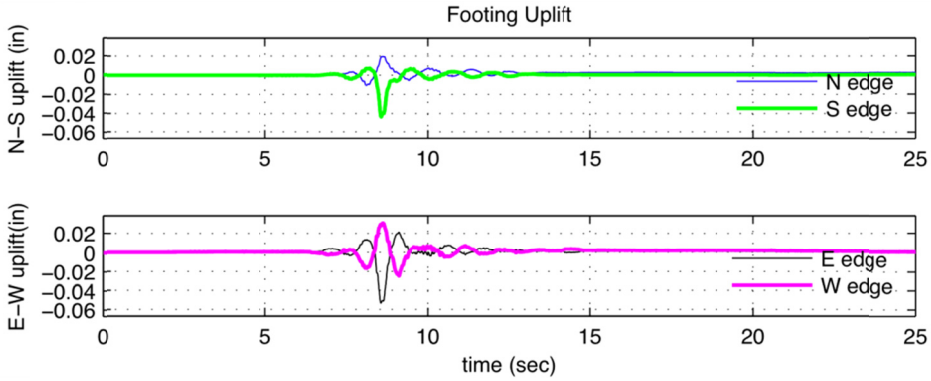

(c) N-S footing uplift (d) E-W footing uplift

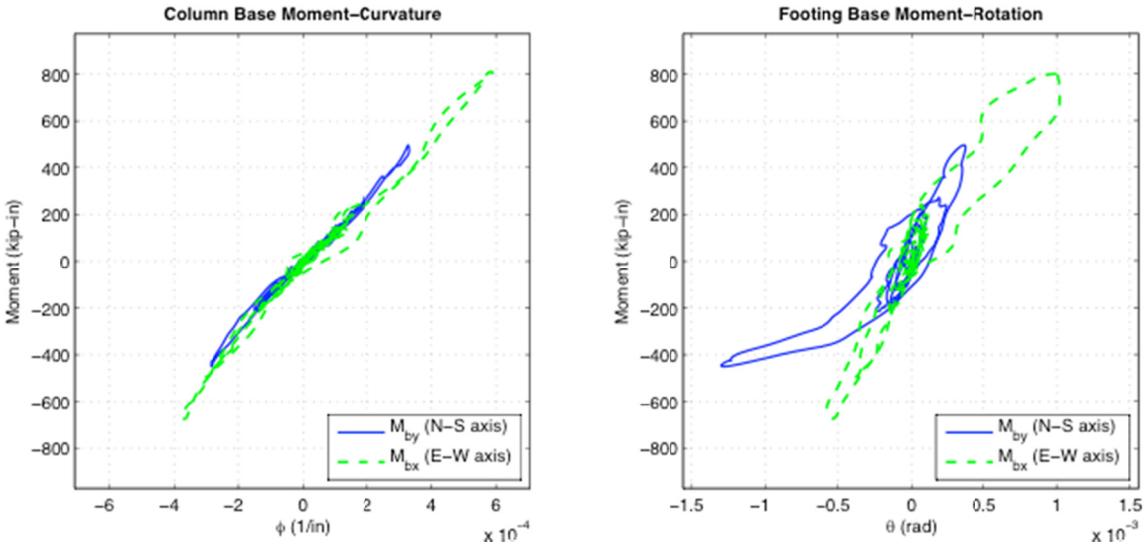

(e) Mom. vs Col ϕ (1/in) (f) Mom. vs FTG θ (rad)

Figure B.33 A2R experimental results.

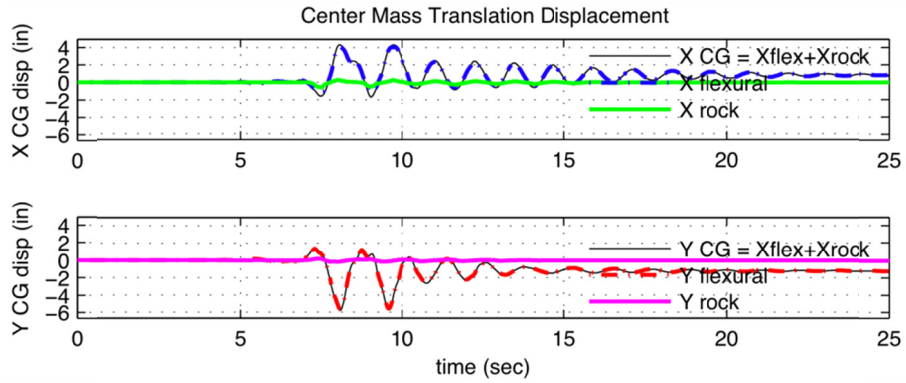

(a) X center mass translation (b) Y center mass translations

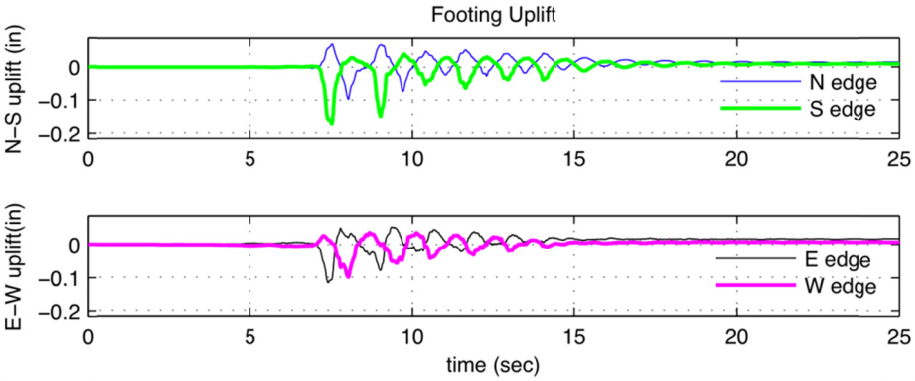

(c) N-S footing uplift (d) E-W footing uplift

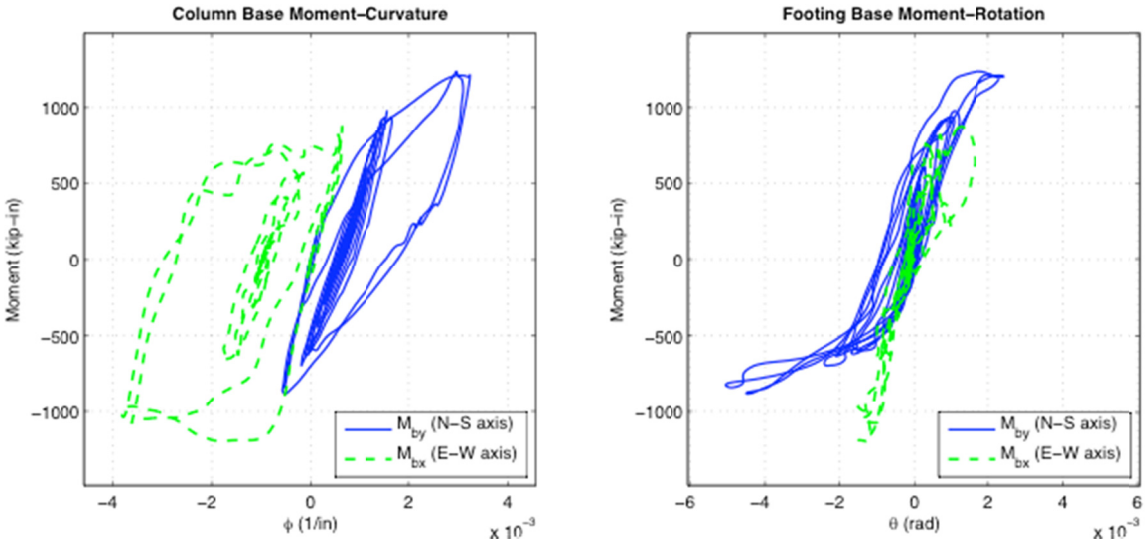

(e) Mom. vs Col ϕ (1/in) (f) Mom. vs FTG θ (rad)

Figure B.34 A3R experimental results.

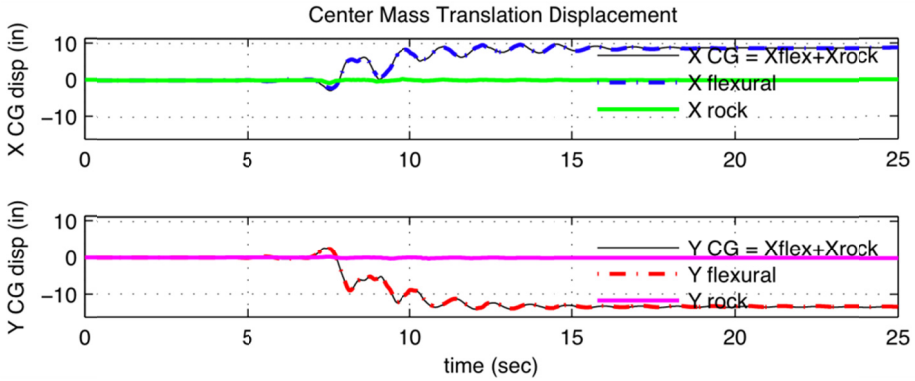

(a) X center mass translation (b) Y center mass translations

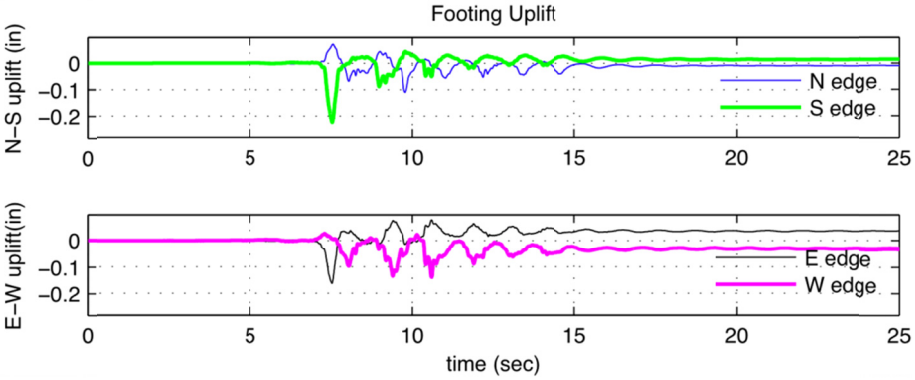

(c) N-S footing uplift (d) E-W footing uplift

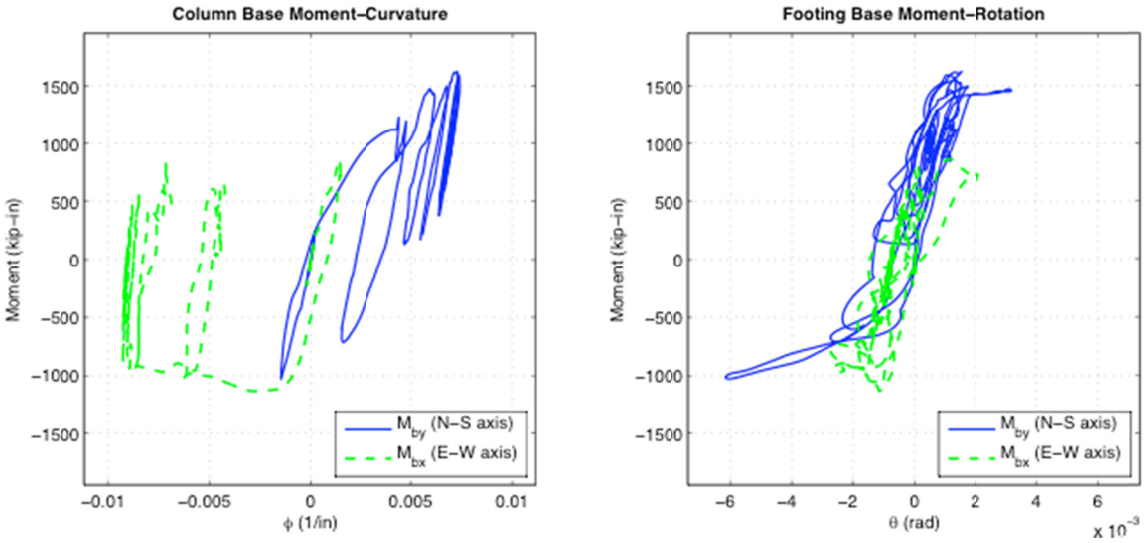

(e) Mom. vs Col ϕ (1/in) (f) Mom. vs FTG θ (rad)

Figure B.35 A4R experimental results.

Appendix C Tcl Code – 3D Shallow Foundations Allowed to Uplift

The script included here is intended for use with the tcl based structural and geotechnical analysis platform OpenSees (Open System for Earthquake Engineering Simulation). The purpose is to model a spread footing on flexible underlying soil that is allowed to uplift. The footing is modeled as a three-dimensional Nonlinear Winkler Beam Foundation (NWBF) with springs and dashpots. The code builds the physical representation of the footing and calls a second sequence that assigns material properties to each spring being created.

```
##############################################################################################
BUILDFOUNDATION_F.tcl
##
##  Developed by Andres Espinoza ,Ph.D. Candidate at the Univ. of California, Berkeley.
##  Work supported by Caltrans under a grant for Development of Design Guidelines for Foundation Uplift
##
##  Coding was derived from work done by :
##  Harden et al. (2005) PEER Report 2005/04
## "Numerical Modeling of the Nonlinear Cyclic Response of Shallow Foundation"
##############################################################################################

proc BuildFOUNDATION_F { sn tn qult Kzm Kze Kr L B Lep Bep rmx rmy rex rey type FEmat soiltype gap qip
z50 Cr crad Kf Qf KPEP QPEP VISC VC Valpha FSECTION Wf TP} {

  variable node1
  variable node2
  variable node3
  variable node4

  set depth 0.0
  set matdir 3

# CALCULATION FOR SPRING SPACING
  ################################

        if {$rmx > 0.5} {set $rmx 0.5; puts "RATIOMX TOO LARGE -- RESET TO O.5"}
        if {$rmy > 0.5} {set $rmy 0.5; puts "RATIOMY TOO LARGE -- RESET TO O.5"}
        if {$rex > 0.5} {set $rex 0.5; puts "RATIOEX TOO LARGE -- RESET TO O.5"}
        if {$rey > 0.5} {set $rey 0.5; puts "RATIOEY TOO LARGE -- RESET TO O.5"}

  set Lmp         [expr 1-2*$Lep]
  set Lmid        [expr $Lmp*$L]
  set Lend        [expr $Lep*$L]

  set Bmp         [expr 1-2*$Bep]
  set Bmid        [expr $Bmp*$B]
  set Bend        [expr $Bep*$B]

  set nmx         [expr int(pow($rmx,-1))]
  set nmy         [expr int(pow($rmy,-1))]

  if {$Lend != 0} {
    set nex       [expr int(pow($rex,-1))]
    set ney       [expr int(pow($rey,-1))]
  } elseif {$Lend == 0} {
    set nex 0;
    set ney 0
  }


        # CHECK FOR ODD NUMBER OF  NODES
        # CHANGE TO EVEN IF NECESSARY
        ################################
        set rtmx [expr $nmx*0.5 - int($nmx*0.5)]
        set rtmy [expr $nmy*0.5 - int($nmy*0.5)]
        set rtex [expr $nex*0.5 - int($nex*0.5)]
```

```
        set rtey [expr $ney*0.5 - int($ney*0.5)]

        if {$rtmx == 0.5} {set nmx [expr $nmx+1]}; puts "NODESMX = $nmx"
        if {$rtmy == 0.5} {set nmy [expr $nmy+1]}; puts "NODESMY = $nmy"
        if {$rtex == 0.5} {set nex [expr $nex+1]}; puts "NODESEX = $nex"
        if {$rtey == 0.5} {set ney [expr $ney+1]}; puts "NODESEY = $ney"


set rmx [expr 1.0/$nmx];  puts "RATIOMX = $rmx"
set rmy [expr 1.0/$nmy];  puts "RATIOMY = $rmy"
if {$Lend != 0} {
  set rex [expr 1.0/$nex];  puts "RATIOEX = $rex"
  set rey [expr 1.0/$ney];  puts "RATIOEY = $rey"
} elseif {$Lend == 0} {
  set rex 0
  set rey 0
}

set Aratiom       [expr $rmx*$rmy*$Lmid*$Bmid/$L/$B]; puts "Aratiom  = $Aratiom"
set Aratioe  [expr $rex*$rey*$Lend*$Bend/$L/$B]; puts "Aratioe  = $Aratioe"
set AratioXe [expr $rex*$rmy*$Lend*$Bmid/$L/$B]; puts "AratioXe = $AratioXe"
set AratioYe [expr $rmx*$rey*$Lmid*$Bend/$L/$B]; puts "AratioYe = $AratioYe"

set nodesx [expr $nmx + 2*$nex] ; puts "NODESX = $nodesx"
set nodesy [expr $nmy + 2*$ney] ; puts "NODESY = $nodesy"
set nodes  [expr $nodesx*$nodesy]            ; puts "NODES  = $nodes"

## FOUNDATION SECTION
if {$FSECTION == 0} {
        set Efoundation [expr 1.0e10]
        section Elastic 100 $Efoundation [expr pow($L,2)] [expr pow($L,3)]
        set FSECTION 100
}


### CREATE NODES AND ELEMENTS FROM CENTER TO EDGES
### OVER ALL Y FOR EACH X STRIP
set a(1) 1;   set a(2) -1;  set a(3)  1;  set a(4) -1;  # toggle axis postion
set b(1) 1;   set b(2)  1;  set b(3) -1;  set b(4) -1;  # for symmetric nodes

set Aratio         $Aratiom
set kzi $Kzm

set fLx  [expr $Lmid/$nmx]
set fLy  [expr $Bmid/$nmy]

set x    [expr $fLx*0.5]
set y    [expr $fLy*0.5]
set mc   1000

        ## OPEN FILE TO RECORD NODE COORDINATES & SPRING CONSTANTS
        set h1       [open "NODEXYZ.txt" w]
        set h2    [open "ELEMENTid.txt" w]
        set h3       [open "ELEMENTxy.txt" w]
        puts $h1  [format "iNODE \t Xi \t Yi \t Zi \t jNODE \t Xj \t Yj \t Zj \t Aratio \t kzi"]
```

```
puts $h1  [format "%4.0f  %6.2f  %6.2f  %6.2f  %4.0f  %6.2f  %6.2f  %6.2f  %6.4f\
                                %6.2f"  $sn 0 0 0 $sn 0 0 $depth 0 0]
puts $h2  [format "ELEMENT\tiNODE\tjNODE\tTYPE (0=zeroLength\, 1=ElasticBeam)\tX\tY "]


  set node0   [expr $tn+1]
  set Atotal  0.0

  set node4    [expr $tn+2*$nodes-1]
  set node3    [expr $node4-2]
  set node2    [expr $node3-2]
  set node1    [expr $node2-2]

  set mF              [expr $Wf/$nodes/386.4]

  ## VISCOUS DAMPING MATERIAL
  if {$VISC == 1} {
   set matVISC $nodes
   uniaxialMaterial Viscous $matVISC $VC $Valpha
  }


  ## START LOOPING OVER ALL NODES
  for {set j 1} {$j <= [expr 0.5*$nodesy]} {incr j} {
   for {set i 1} {$i <= [expr 0.5*$nodesx]} {incr i} {

               source BUILD_MAT_F.tcl;       # CALL MATERIAL CONSTANTS
# FOR 4 SYMMETRIC NODES

           for {set k 1} {$k <=4} {incr k} {
             node [expr $node0]    [expr $a($k)*$x] [expr $b($k)*$y] $depth
             node [expr $node0+1]  [expr $a($k)*$x] [expr $b($k)*$y] $depth
             fix  [expr $node0+1] 1 1 1 1 1 1

             mass $node0 $mF $mF $mF 1e-6 1e-6 1e-6

             element zeroLength $mc  [expr $node0+1] [expr $node0] -mat $mati -dir $matdir

 if {$VISC == 1} {
   puts "ADDING VISCOUS MATERIAL -- VC=$VC  Valpha=$Valpha"
   element zeroLength [expr $mc+10*$nodes] [expr $node0+1] [expr $node0] -mat $matVISC -dir $matdir
 }

  puts $h1 [format "%4.0f   %6.2f   %6.2f   %6.2f   %4.0f   %6.2f   %6.2f   %6.2f  %6.4f  %6.2f" \
   $node0 [expr $a($k)*$x] [expr $b($k)*$y] $depth [expr $node0+1] [expr $a($k)*$x] \   [expr $b($k)*$y] $depth
$Aratio $Ki ]

  puts  $h2 [format "%d\t%d\t%d\t%d" $mc [expr $node0] [expr $node0+1] 0 ]
  puts $h3 [format "%d\t%d\t%d\t%6.4f\t%6.4f" $mc [expr $node0] [expr $node0+1] [expr $a($k)*$x] \
   [expr $b($k)*$y]]

 set mc    [expr $mc+1]
 set node0 [expr $node0+2]

}
```

```
set Atotal [expr $Atotal + 4*$Aratio]

set x [expr $x+$fLx]

 if {$Lend != 0} {
 if {$i == [expr int($nmx*0.5)]} {

   set fLx [expr $Lend/$nex]
              set x     [expr 0.5*$Lmid+$fLx*0.5]

    if {$j <= 0.5*$nmy} {set Aratio $AratioXe;     set kzi    $Kze       }
              if {$j >  0.5*$nmy} {set Aratio $Aratioe;          set kzi    $Kze       }
 }
 }

};   # END OF LOOP OVER i

     if {$j < 0.5*$nmy}   {set Aratio $Aratiom;       set kzi    $Kzm        }
     if {$j >= 0.5*$nmy} {set Aratio $AratioYe;    set kzi    $Kze        }

     set fLx   [expr $Lmid/$nmx]
     set x       [expr 0.5*$fLx];

     set y [expr $y+$fLy];
     if {$Bend != 0 } {
     if {$j == [expr int($nmy*0.5)]} {

           set fLy [expr $Bend/$ney]
           set y     [expr 0.5*$Bmid+$fLy*0.5]

     }
     }
  }; # END OF LOOP OVER j

  puts "ATOTAL = $Atotal"


 ################################################
 ## BUILD ELASTIC BEAMS AND CONNECT            ##
 ## TO SPECIFIED SPRING LOCATIONS              ##
 ################################################
 set xTf  50;
 set yTf  [expr $xTf+1];

 geomTransf Linear $xTf  0 0 1
 geomTransf Linear $yTf  0 0 1


 set Af  1e10;
 set Ef  1e12;    set Gf  1e8;
 set Jf  1e8;   set Iyf 1e6;   set Izf 1e6;
```

```
   set node0 [expr $tn+1];


   # CONNECT STARTING NODE SN TO FOUNDATION
   ########################################

  for {set k 1} {$k <= 4 } {incr k} {

     set iN $sn;
     set jN [expr $node0];

     element elasticBeamColumn $mc $iN $jN $Af $Ef $Gf $Jf $Iyf $Izf $xTf

     puts $h2 [format "%d\t%d\t%d\t%d" $mc $iN $jN 1]

     set mc    [expr $mc+1]
               set node0 [expr $node0+2]
  }


  # LOOP OVER ALL X AND Y NODES TO CREATE
  # ELASTIC BEAM ELEMENTS
  #######################################
  set node0 [expr $tn+1]

 # BUILD BEAMS IN X-DIRECTION
############################

for {set j 1} {$j<=0.5*$nodesy} {incr j} {

  set nc [expr 4*$nodesx*($j-1)]

  for {set i 1} {$i<= 0.5*$nodesx-1} {incr i} {

          if {$i==1} {
             set ap 0

            for {set k 1} {$k <= 2} {incr k} {
        set iN [expr $node0+$nc+ $ap   ]
        set jN [expr $node0+$nc+ $ap +2]

                  element elasticBeamColumn $mc $iN $jN $Af $Ef $Gf $Jf $Iyf $Izf $xTf

        puts $h2 [format "%d\t%d\t%d\t%d" $mc $iN $jN 1]

        set mc [expr $mc+1]
                  set ap [expr $ap+4]

            }
   }


   for {set k 1} {$k <= 4} {incr k} {
        set iN [expr $node0+$nc+8*($i-1)+2*($k-1) ]
         set jN [expr $node0+$nc+8*($i)  +2*($k-1) ]
```

```
            element elasticBeamColumn $mc $iN $jN $Af $Ef $Gf $Jf $Iyf $Izf $xTf

            puts $h2 [format "%d\t%d\t%d\t%d" $mc $iN $jN 1]

          set mc [expr $mc+1]
 }

}
}


# BUILD BEAMS IN Y-DIRECTION
############################

for {set i 1} {$i<=0.5*$nodesx} {incr i} {
    set nc  [expr 8*($i-1)]

    for {set j 1} {$j<= 0.5*$nodesy-1} {incr j} {
        set nc2 [expr $nc+4*$nodesx*($j-1)]
        set nc3 [expr $nc+4*$nodesx*($j)]

if {$j==1} {
   set ap 0
   for {set k 1} {$k <= 2} {incr k} {
          set iN [expr $node0+$nc+ $ap   ];
          set jN [expr $node0+$nc+ $ap +4];

          element elasticBeamColumn $mc $iN $jN $Af $Ef $Gf $Jf $Iyf $Izf $yTf

          puts $h2 [format "%d\t%d\t%d\t%d" $mc $iN $jN 1]

          set mc [expr $mc+1]
          set ap [expr $ap+2]
  }
          }

         for {set k 1} {$k <= 4} {incr k} {
 set iN [expr $node0+$nc2+2*($k-1) ]
 set jN [expr $node0+$nc3+2*($k-1) ]

            element elasticBeamColumn $mc $iN $jN $Af $Ef $Gf $Jf $Iyf $Izf $xTf

            puts $h2 [format "%d\t%d\t%d\t%d" $mc $iN $jN 1]

 set mc [expr $mc+1]
       }
    }
  }
 ##############################################

 close $h1
 close $h2
 close $h3

};  # END OF PROCEDURE....BUILDFOUNDATION_F.tcl
```

```
##############################################################################################
##  BUILD_MAT_F.tcl
##
## Source code for subgrade reaction elements. Zerolength springs of varied materials.
## Either linear elastic or nonlinear
##
##          Written:
##             Andres Espinoza
##             AUGUST 2006;  based on work done by Harden et al. (2005) PEER REPORT 2005/04
##############################################################################################


set qi [expr $qip*$qult]


##   PRESSURE DISTRIBUTION SPECIFICATION
#####################################################
 if {$type == 1} {              ;# Uniform Pressure Distribution
   set qx $qult
 }
 if {$type ==2} { ;# Triangular Distribution
   # nothing for this yet
 }
if {$type ==3} {  ;# Trapezoidal Distribution
    # nothing for this yet
 }
 if {$type ==4} { ;# Parabolic Distribution
    # nothing for this yet
 }
 if {$type ==5} { ;# Inverse Distribution
     # nothing for this yet
 }
#####################################################


            ## CHECK FOR ZER0/NEGATIVE qx
            ###################################
            if {$qx == 0} {
              set qx 0.0001;  puts "qx zero, set=0.0001 for material $mati"
            }
            if {$qx < 0.0} {
              set qx 0.0001;  puts "qx negative, set=0.0001 for material $mati"
            }
            ###################################


# CALCULATE ULTIMATE BEARING FORCE/NODE FOR WHEN REQ'D
set Qultx [expr $L*$B*$Aratio*$qx]



## SOIL FOUNDATION SPRINGS MODEL SELECTION
#############################################

set Ki [expr $kzi*$Aratio]
```

```
if {$FEmat == 8} {                                          ;## ELASTIC NO TENSION SPRINGS
  set mati [expr $mc+1000]
  uniaxialMaterial ENT $mati $Ki
 }

if {$FEmat == 9} {                                           ; ## ELASTIC SPRINGS
  set mati [expr $mc+1000]
  uniaxialMaterial Elastic $mati $Ki
 }

    ###############################
    ##  QZ CONSTANTS           ##
    ###############################
    if {$soiltype == 1} {;  #clay soil
          set qzType 1;
       set c 0.35
          set n 1.2
       set Kfar 0.525
    }
    if {$soiltype == 2} {;  #sand soil
       set qzType 2;
       set c 12.3
          set n  5.5
       set Kfar 1.39
     }

if {$FEmat == 10} {                                          ; ## QzSimple1 SPRING
  set mati [expr $mc+1000]

  set QultQZ [expr $Qultx]
  set z50i   [expr $Kfar*$Qultx*pow($Ki,-1)]

  uniaxialMaterial QzSimple1 $mati $qzType $QultQZ $z50i $TP $crad
}

if {$FEmat == 11} {                                          ; ## PySimple1 SPRING
  set mati [expr $mc+1000]

  set QultPy [expr $Qultx]
  set y50i [expr $Kfar*$Qultx*pow($Ki,-1)]

  uniaxialMaterial PySimple1 $mati $qzType $QultPy $y50i $TP $crad
}

if {$FEmat == 12} {                                          ; ## ELASTICPPGAP SPRINGS
  set mati [expr $mc+1000]
  uniaxialMaterial ElasticPPGap $mati $Ki -$Qultx -$gap  0.01 damage
 }
```

PEER REPORTS

PEER reports are available individually or by yearly subscription. PEER reports can be ordered at http://peer.berkeley.edu/publications/peer_reports.html or by contacting the Pacific Earthquake Engineering Research Center, 325 Davis Hall mail code 1792, Berkeley, CA 94720. Tel.: (510) 642-3437; Fax: (510) 665-1655; Email: peer_editor@berkeley.edu

PEER 2012/02 *Seismic Performance of Reinforced Concrete Bridges Allowed to Uplift during Multi-Directional Excitation.* Andres Oscar Espinoza and Stephen A. Mahin. July 2012.

PEER 2012/01 *Spectral Damping Scaling Factors for Shallow Crustal Earthquakes in Active Tectonic Regions.* Sanaz Rezaeian, Yousef Bozorgnia, I. M. Idriss, Kenneth Campbell, Norman Abrahamson, and Walter Silva. July 2012.

PEER 2011/10 *Earthquake Engineering for Resilient Communities: 2011 PEER Internship Program Research Report Collection.* Eds. Heidi Faison and Stephen A. Mahin. December 2011.

PEER 2011/09 *Calibration of Semi-Stochastic Procedure for Simulating High-Frequency Ground Motions.* Jonathan P. Stewart, Emel Seyhan, and Robert W. Graves. December 2011.

PEER 2011/08 *Water Supply in regard to Fire Following Earthquake.* Charles Scawthorn. November 2011.

PEER 2011/07 *Seismic Risk Management in Urban Areas. Proceedings of a U.S.-Iran-Turkey Seismic Workshop.* September 2011.

PEER 2011/06 *The Use of Base Isolation Systems to Achieve Complex Seismic Performance Objectives.* Troy A. Morgan and Stephen A. Mahin. July 2011.

PEER 2011/05 *Case Studies of the Seismic Performance of Tall Buildings Designed by Alternative Means.* Task 12 Report for the Tall Buildings Initiative. Jack Moehle, Yousef Bozorgnia, Nirmal Jayaram, Pierson Jones, Mohsen Rahnama, Nilesh Shome, Zeynep Tuna, John Wallace, Tony Yang, and Farzin Zareian. July 2011.

PEER 2011/04 *Recommended Design Practice for Pile Foundations in Laterally Spreading Ground.* Scott A. Ashford, Ross W. Boulanger, and Scott J. Brandenberg. June 2011.

PEER 2011/03 *New Ground Motion Selection Procedures and Selected Motions for the PEER Transportation Research Program.* Jack W. Baker, Ting Lin, Shrey K. Shahi, and Nirmal Jayaram. March 2011.

PEER 2011/02 *A Bayesian Network Methodology for Infrastructure Seismic Risk Assessment and Decision Support.* Michelle T. Bensi, Armen Der Kiureghian, and Daniel Straub. March 2011.

PEER 2011/01 *Demand Fragility Surfaces for Bridges in Liquefied and Laterally Spreading Ground.* Scott J. Brandenberg, Jian Zhang, Pirooz Kashighandi, Yili Huo, and Minxing Zhao. March 2011.

PEER 2010/05 *Guidelines for Performance-Based Seismic Design of Tall Buildings.* Developed by the Tall Buildings Initiative. November 2010.

PEER 2010/04 *Application Guide for the Design of Flexible and Rigid Bus Connections between Substation Equipment Subjected to Earthquakes.* Jean-Bernard Dastous and Armen Der Kiureghian. September 2010.

PEER 2010/03 *Shear Wave Velocity as a Statistical Function of Standard Penetration Test Resistance and Vertical Effective Stress at Caltrans Bridge Sites.* Scott J. Brandenberg, Naresh Bellana, and Thomas Shantz. June 2010.

PEER 2010/02 *Stochastic Modeling and Simulation of Ground Motions for Performance-Based Earthquake Engineering.* Sanaz Rezaeian and Armen Der Kiureghian. June 2010.

PEER 2010/01 *Structural Response and Cost Characterization of Bridge Construction Using Seismic Performance Enhancement Strategies.* Ady Aviram, Božidar Stojadinović, Gustavo J. Parra-Montesinos, and Kevin R. Mackie. March 2010.

PEER 2009/03 *The Integration of Experimental and Simulation Data in the Study of Reinforced Concrete Bridge Systems Including Soil-Foundation-Structure Interaction.* Matthew Dryden and Gregory L. Fenves. November 2009.

PEER 2009/02 *Improving Earthquake Mitigation through Innovations and Applications in Seismic Science, Engineering, Communication, and Response. Proceedings of a U.S.-Iran Seismic Workshop.* October 2009.

PEER 2009/01 *Evaluation of Ground Motion Selection and Modification Methods: Predicting Median Interstory Drift Response of Buildings.* Curt B. Haselton, Ed. June 2009.

PEER 2008/10 *Technical Manual for Strata.* Albert R. Kottke and Ellen M. Rathje. February 2009.

PEER 2008/09 *NGA Model for Average Horizontal Component of Peak Ground Motion and Response Spectra.* Brian S.-J. Chiou and Robert R. Youngs. November 2008.

PEER 2008/08 *Toward Earthquake-Resistant Design of Concentrically Braced Steel Structures.* Patxi Uriz and Stephen A. Mahin. November 2008.

PEER 2008/07 *Using OpenSees for Performance-Based Evaluation of Bridges on Liquefiable Soils.* Stephen L. Kramer, Pedro Arduino, and HyungSuk Shin. November 2008.

PEER 2008/06 *Shaking Table Tests and Numerical Investigation of Self-Centering Reinforced Concrete Bridge Columns.* Hyung IL Jeong, Junichi Sakai, and Stephen A. Mahin. September 2008.

PEER 2008/05 *Performance-Based Earthquake Engineering Design Evaluation Procedure for Bridge Foundations Undergoing Liquefaction-Induced Lateral Ground Displacement.* Christian A. Ledezma and Jonathan D. Bray. August 2008.

PEER 2008/04 *Benchmarking of Nonlinear Geotechnical Ground Response Analysis Procedures.* Jonathan P. Stewart, Annie On-Lei Kwok, Yousseff M. A. Hashash, Neven Matasovic, Robert Pyke, Zhiliang Wang, and Zhaohui Yang. August 2008.

PEER 2008/03 *Guidelines for Nonlinear Analysis of Bridge Structures in California.* Ady Aviram, Kevin R. Mackie, and Božidar Stojadinović. August 2008.

PEER 2008/02 *Treatment of Uncertainties in Seismic-Risk Analysis of Transportation Systems.* Evangelos Stergiou and Anne S. Kiremidjian. July 2008.

PEER 2008/01 *Seismic Performance Objectives for Tall Buildings.* William T. Holmes, Charles Kircher, William Petak, and Nabih Youssef. August 2008.

PEER 2007/12 *An Assessment to Benchmark the Seismic Performance of a Code-Conforming Reinforced Concrete Moment-Frame Building.* Curt Haselton, Christine A. Goulet, Judith Mitrani-Reiser, James L. Beck, Gregory G. Deierlein, Keith A. Porter, Jonathan P. Stewart, and Ertugrul Taciroglu. August 2008.

PEER 2007/11 *Bar Buckling in Reinforced Concrete Bridge Columns.* Wayne A. Brown, Dawn E. Lehman, and John F. Stanton. February 2008.

PEER 2007/10 *Computational Modeling of Progressive Collapse in Reinforced Concrete Frame Structures.* Mohamed M. Talaat and Khalid M. Mosalam. May 2008.

PEER 2007/09 *Integrated Probabilistic Performance-Based Evaluation of Benchmark Reinforced Concrete Bridges.* Kevin R. Mackie, John-Michael Wong, and Božidar Stojadinović. January 2008.

PEER 2007/08 *Assessing Seismic Collapse Safety of Modern Reinforced Concrete Moment-Frame Buildings.* Curt B. Haselton and Gregory G. Deierlein. February 2008.

PEER 2007/07 *Performance Modeling Strategies for Modern Reinforced Concrete Bridge Columns.* Michael P. Berry and Marc O. Eberhard. April 2008.

PEER 2007/06 *Development of Improved Procedures for Seismic Design of Buried and Partially Buried Structures.* Linda Al Atik and Nicholas Sitar. June 2007.

PEER 2007/05 *Uncertainty and Correlation in Seismic Risk Assessment of Transportation Systems.* Renee G. Lee and Anne S. Kiremidjian. July 2007.

PEER 2007/04 *Numerical Models for Analysis and Performance-Based Design of Shallow Foundations Subjected to Seismic Loading.* Sivapalan Gajan, Tara C. Hutchinson, Bruce L. Kutter, Prishati Raychowdhury, José A. Ugalde, and Jonathan P. Stewart. May 2008.

PEER 2007/03 *Beam-Column Element Model Calibrated for Predicting Flexural Response Leading to Global Collapse of RC Frame Buildings.* Curt B. Haselton, Abbie B. Liel, Sarah Taylor Lange, and Gregory G. Deierlein. May 2008.

PEER 2007/02 *Campbell-Bozorgnia NGA Ground Motion Relations for the Geometric Mean Horizontal Component of Peak and Spectral Ground Motion Parameters.* Kenneth W. Campbell and Yousef Bozorgnia. May 2007.

PEER 2007/01 *Boore-Atkinson NGA Ground Motion Relations for the Geometric Mean Horizontal Component of Peak and Spectral Ground Motion Parameters.* David M. Boore and Gail M. Atkinson. May. May 2007.

PEER 2006/12 *Societal Implications of Performance-Based Earthquake Engineering.* Peter J. May. May 2007.

PEER 2006/11 *Probabilistic Seismic Demand Analysis Using Advanced Ground Motion Intensity Measures, Attenuation Relationships, and Near-Fault Effects.* Polsak Tothong and C. Allin Cornell. March 2007.

PEER 2006/10 *Application of the PEER PBEE Methodology to the I-880 Viaduct.* Sashi Kunnath. February 2007.

PEER 2006/09 *Quantifying Economic Losses from Travel Forgone Following a Large Metropolitan Earthquake.* James Moore, Sungbin Cho, Yue Yue Fan, and Stuart Werner. November 2006.

PEER 2006/08 *Vector-Valued Ground Motion Intensity Measures for Probabilistic Seismic Demand Analysis.* Jack W. Baker and C. Allin Cornell. October 2006.

PEER 2006/07 *Analytical Modeling of Reinforced Concrete Walls for Predicting Flexural and Coupled–Shear-Flexural Responses.* Kutay Orakcal, Leonardo M. Massone, and John W. Wallace. October 2006.

PEER 2006/06 *Nonlinear Analysis of a Soil-Drilled Pier System under Static and Dynamic Axial Loading.* Gang Wang and Nicholas Sitar. November 2006.

PEER 2006/05 *Advanced Seismic Assessment Guidelines.* Paolo Bazzurro, C. Allin Cornell, Charles Menun, Maziar Motahari, and Nicolas Luco. September 2006.

PEER 2006/04 *Probabilistic Seismic Evaluation of Reinforced Concrete Structural Components and Systems.* Tae Hyung Lee and Khalid M. Mosalam. August 2006.

PEER 2006/03 *Performance of Lifelines Subjected to Lateral Spreading.* Scott A. Ashford and Teerawut Juirnarongrit. July 2006.

PEER 2006/02 *Pacific Earthquake Engineering Research Center Highway Demonstration Project.* Anne Kiremidjian, James Moore, Yue Yue Fan, Nesrin Basoz, Ozgur Yazali, and Meredith Williams. April 2006.

PEER 2006/01 *Bracing Berkeley. A Guide to Seismic Safety on the UC Berkeley Campus.* Mary C. Comerio, Stephen Tobriner, and Ariane Fehrenkamp. January 2006.

PEER 2005/16 *Seismic Response and Reliability of Electrical Substation Equipment and Systems.* Junho Song, Armen Der Kiureghian, and Jerome L. Sackman. April 2006.

PEER 2005/15 *CPT-Based Probabilistic Assessment of Seismic Soil Liquefaction Initiation.* R. E. S. Moss, R. B. Seed, R. E. Kayen, J. P. Stewart, and A. Der Kiureghian. April 2006.

PEER 2005/14 *Workshop on Modeling of Nonlinear Cyclic Load-Deformation Behavior of Shallow Foundations.* Bruce L. Kutter, Geoffrey Martin, Tara Hutchinson, Chad Harden, Sivapalan Gajan, and Justin Phalen. March 2006.

PEER 2005/13 *Stochastic Characterization and Decision Bases under Time-Dependent Aftershock Risk in Performance-Based Earthquake Engineering.* Gee Liek Yeo and C. Allin Cornell. July 2005.

PEER 2005/12 *PEER Testbed Study on a Laboratory Building: Exercising Seismic Performance Assessment.* Mary C. Comerio, editor. November 2005.

PEER 2005/11 *Van Nuys Hotel Building Testbed Report: Exercising Seismic Performance Assessment.* Helmut Krawinkler, editor. October 2005.

PEER 2005/10 *First NEES/E-Defense Workshop on Collapse Simulation of Reinforced Concrete Building Structures.* September 2005.

PEER 2005/09 *Test Applications of Advanced Seismic Assessment Guidelines.* Joe Maffei, Karl Telleen, Danya Mohr, William Holmes, and Yuki Nakayama. August 2006.

PEER 2005/08 *Damage Accumulation in Lightly Confined Reinforced Concrete Bridge Columns.* R. Tyler Ranf, Jared M. Nelson, Zach Price, Marc O. Eberhard, and John F. Stanton. April 2006.

PEER 2005/07 *Experimental and Analytical Studies on the Seismic Response of Freestanding and Anchored Laboratory Equipment.* Dimitrios Konstantinidis and Nicos Makris. January 2005.

PEER 2005/06 *Global Collapse of Frame Structures under Seismic Excitations*. Luis F. Ibarra and Helmut Krawinkler. September 2005.

PEER 2005//05 *Performance Characterization of Bench- and Shelf-Mounted Equipment*. Samit Ray Chaudhuri and Tara C. Hutchinson. May 2006.

PEER 2005/04 *Numerical Modeling of the Nonlinear Cyclic Response of Shallow Foundations.* Chad Harden, Tara Hutchinson, Geoffrey R. Martin, and Bruce L. Kutter. August 2005.

PEER 2005/03 *A Taxonomy of Building Components for Performance-Based Earthquake Engineering.* Keith A. Porter. September 2005.

PEER 2005/02 *Fragility Basis for California Highway Overpass Bridge Seismic Decision Making*. Kevin R. Mackie and Božidar Stojadinović. June 2005.

PEER 2005/01 *Empirical Characterization of Site Conditions on Strong Ground Motion.* Jonathan P. Stewart, Yoojoong Choi, and Robert W. Graves. June 2005.

PEER 2004/09 *Electrical Substation Equipment Interaction: Experimental Rigid Conductor Studies.* Christopher Stearns and André Filiatrault. February 2005.

PEER 2004/08 *Seismic Qualification and Fragility Testing of Line Break 550-kV Disconnect Switches.* Shakhzod M. Takhirov, Gregory L. Fenves, and Eric Fujisaki. January 2005.

PEER 2004/07 *Ground Motions for Earthquake Simulator Qualification of Electrical Substation Equipment.* Shakhzod M. Takhirov, Gregory L. Fenves, Eric Fujisaki, and Don Clyde. January 2005.

PEER 2004/06 *Performance-Based Regulation and Regulatory Regimes.* Peter J. May and Chris Koski. September 2004.

PEER 2004/05 *Performance-Based Seismic Design Concepts and Implementation: Proceedings of an International Workshop.* Peter Fajfar and Helmut Krawinkler, editors. September 2004.

PEER 2004/04 *Seismic Performance of an Instrumented Tilt-up Wall Building.* James C. Anderson and Vitelmo V. Bertero. July 2004.

PEER 2004/03 *Evaluation and Application of Concrete Tilt-up Assessment Methodologies.* Timothy Graf and James O. Malley. October 2004.

PEER 2004/02 *Analytical Investigations of New Methods for Reducing Residual Displacements of Reinforced Concrete Bridge Columns.* Junichi Sakai and Stephen A. Mahin. August 2004.

PEER 2004/01 *Seismic Performance of Masonry Buildings and Design Implications.* Kerri Anne Taeko Tokoro, James C. Anderson, and Vitelmo V. Bertero. February 2004.

PEER 2003/18 *Performance Models for Flexural Damage in Reinforced Concrete Columns.* Michael Berry and Marc Eberhard. August 2003.

PEER 2003/17 *Predicting Earthquake Damage in Older Reinforced Concrete Beam-Column Joints.* Catherine Pagni and Laura Lowes. October 2004.

PEER 2003/16 *Seismic Demands for Performance-Based Design of Bridges.* Kevin Mackie and Božidar Stojadinović. August 2003.

PEER 2003/15 *Seismic Demands for Nondeteriorating Frame Structures and Their Dependence on Ground Motions.* Ricardo Antonio Medina and Helmut Krawinkler. May 2004.

PEER 2003/14 *Finite Element Reliability and Sensitivity Methods for Performance-Based Earthquake Engineering.* Terje Haukaas and Armen Der Kiureghian. April 2004.

PEER 2003/13 *Effects of Connection Hysteretic Degradation on the Seismic Behavior of Steel Moment-Resisting Frames.* Janise E. Rodgers and Stephen A. Mahin. March 2004.

PEER 2003/12 *Implementation Manual for the Seismic Protection of Laboratory Contents: Format and Case Studies.* William T. Holmes and Mary C. Comerio. October 2003.

PEER 2003/11 *Fifth U.S.-Japan Workshop on Performance-Based Earthquake Engineering Methodology for Reinforced Concrete Building Structures.* February 2004.

PEER 2003/10 *A Beam-Column Joint Model for Simulating the Earthquake Response of Reinforced Concrete Frames.* Laura N. Lowes, Nilanjan Mitra, and Arash Altoontash. February 2004.

PEER 2003/09 *Sequencing Repairs after an Earthquake: An Economic Approach.* Marco Casari and Simon J. Wilkie. April 2004.

PEER 2003/08 *A Technical Framework for Probability-Based Demand and Capacity Factor Design (DCFD) Seismic Formats*. Fatemeh Jalayer and C. Allin Cornell. November 2003.

PEER 2003/07 *Uncertainty Specification and Propagation for Loss Estimation Using FOSM Methods.* Jack W. Baker and C. Allin Cornell. September 2003.

PEER 2003/06 *Performance of Circular Reinforced Concrete Bridge Columns under Bidirectional Earthquake Loading*. Mahmoud M. Hachem, Stephen A. Mahin, and Jack P. Moehle. February 2003.

PEER 2003/05 *Response Assessment for Building-Specific Loss Estimation.* Eduardo Miranda and Shahram Taghavi. September 2003.

PEER 2003/04 *Experimental Assessment of Columns with Short Lap Splices Subjected to Cyclic Loads*. Murat Melek, John W. Wallace, and Joel Conte. April 2003.

PEER 2003/03 *Probabilistic Response Assessment for Building-Specific Loss Estimation.* Eduardo Miranda and Hesameddin Aslani. September 2003.

PEER 2003/02 *Software Framework for Collaborative Development of Nonlinear Dynamic Analysis Program.* Jun Peng and Kincho H. Law. September 2003.

PEER 2003/01 *Shake Table Tests and Analytical Studies on the Gravity Load Collapse of Reinforced Concrete Frames.* Kenneth John Elwood and Jack P. Moehle. November 2003.

PEER 2002/24 *Performance of Beam to Column Bridge Joints Subjected to a Large Velocity Pulse.* Natalie Gibson, André Filiatrault, and Scott A. Ashford. April 2002.

PEER 2002/23 *Effects of Large Velocity Pulses on Reinforced Concrete Bridge Columns.* Greg L. Orozco and Scott A. Ashford. April 2002.

PEER 2002/22 *Characterization of Large Velocity Pulses for Laboratory Testing.* Kenneth E. Cox and Scott A. Ashford. April 2002.

PEER 2002/21 *Fourth U.S.-Japan Workshop on Performance-Based Earthquake Engineering Methodology for Reinforced Concrete Building Structures*. December 2002.

PEER 2002/20 *Barriers to Adoption and Implementation of PBEE Innovations.* Peter J. May. August 2002.

PEER 2002/19 *Economic-Engineered Integrated Models for Earthquakes: Socioeconomic Impacts.* Peter Gordon, James E. Moore II, and Harry W. Richardson. July 2002.

PEER 2002/18 *Assessment of Reinforced Concrete Building Exterior Joints with Substandard Details.* Chris P. Pantelides, Jon Hansen, Justin Nadauld, and Lawrence D. Reaveley. May 2002.

PEER 2002/17 *Structural Characterization and Seismic Response Analysis of a Highway Overcrossing Equipped with Elastomeric Bearings and Fluid Dampers: A Case Study.* Nicos Makris and Jian Zhang. November 2002.

PEER 2002/16 *Estimation of Uncertainty in Geotechnical Properties for Performance-Based Earthquake Engineering.* Allen L. Jones, Steven L. Kramer, and Pedro Arduino. December 2002.

PEER 2002/15 *Seismic Behavior of Bridge Columns Subjected to Various Loading Patterns.* Asadollah Esmaeily-Gh. and Yan Xiao. December 2002.

PEER 2002/14 *Inelastic Seismic Response of Extended Pile Shaft Supported Bridge Structures.* T.C. Hutchinson, R.W. Boulanger, Y.H. Chai, and I.M. Idriss. December 2002.

PEER 2002/13 *Probabilistic Models and Fragility Estimates for Bridge Components and Systems.* Paolo Gardoni, Armen Der Kiureghian, and Khalid M. Mosalam. June 2002.

PEER 2002/12 *Effects of Fault Dip and Slip Rake on Near-Source Ground Motions: Why Chi-Chi Was a Relatively Mild M7.6 Earthquake.* Brad T. Aagaard, John F. Hall, and Thomas H. Heaton. December 2002.

PEER 2002/11 *Analytical and Experimental Study of Fiber-Reinforced Strip Isolators*. James M. Kelly and Shakhzod M. Takhirov. September 2002.

PEER 2002/10 *Centrifuge Modeling of Settlement and Lateral Spreading with Comparisons to Numerical Analyses***.** Sivapalan Gajan and Bruce L. Kutter. January 2003.

PEER 2002/09 *Documentation and Analysis of Field Case Histories of Seismic Compression during the 1994 Northridge, California, Earthquake.* Jonathan P. Stewart, Patrick M. Smith, Daniel H. Whang, and Jonathan D. Bray. October 2002.

PEER 2002/08 *Component Testing, Stability Analysis and Characterization of Buckling-Restrained Unbonded Braces™.* Cameron Black, Nicos Makris, and Ian Aiken. September 2002.

PEER 2002/07 *Seismic Performance of Pile-Wharf Connections.* Charles W. Roeder, Robert Graff, Jennifer Soderstrom, and Jun Han Yoo. December 2001.

PEER 2002/06 *The Use of Benefit-Cost Analysis for Evaluation of Performance-Based Earthquake Engineering Decisions*. Richard O. Zerbe and Anthony Falit-Baiamonte. September 2001.

PEER 2002/05 *Guidelines, Specifications, and Seismic Performance Characterization of Nonstructural Building Components and Equipment*. André Filiatrault, Constantin Christopoulos, and Christopher Stearns. September 2001.

PEER 2002/04 *Consortium of Organizations for Strong-Motion Observation Systems and the Pacific Earthquake Engineering Research Center Lifelines Program: Invited Workshop on Archiving and Web Dissemination of Geotechnical Data, 4–5 October 2001*. September 2002.

PEER 2002/03 *Investigation of Sensitivity of Building Loss Estimates to Major Uncertain Variables for the Van Nuys Testbed.* Keith A. Porter, James L. Beck, and Rustem V. Shaikhutdinov. August 2002.

PEER 2002/02 *The Third U.S.-Japan Workshop on Performance-Based Earthquake Engineering Methodology for Reinforced Concrete Building Structures*. July 2002.

PEER 2002/01 *Nonstructural Loss Estimation: The UC Berkeley Case Study.* Mary C. Comerio and John C. Stallmeyer. December 2001.

PEER 2001/16 *Statistics of SDF-System Estimate of Roof Displacement for Pushover Analysis of Buildings.* Anil K. Chopra, Rakesh K. Goel, and Chatpan Chintanapakdee. December 2001.

PEER 2001/15 *Damage to Bridges during the 2001 Nisqually Earthquake.* R. Tyler Ranf, Marc O. Eberhard, and Michael P. Berry. November 2001.

PEER 2001/14 *Rocking Response of Equipment Anchored to a Base Foundation.* Nicos Makris and Cameron J. Black. September 2001.

PEER 2001/13 *Modeling Soil Liquefaction Hazards for Performance-Based Earthquake Engineering.* Steven L. Kramer and Ahmed-W. Elgamal. February 2001.

PEER 2001/12 *Development of Geotechnical Capabilities in OpenSees.* Boris Jeremić. September 2001.

PEER 2001/11 *Analytical and Experimental Study of Fiber-Reinforced Elastomeric Isolators*. James M. Kelly and Shakhzod M. Takhirov. September 2001.

PEER 2001/10 *Amplification Factors for Spectral Acceleration in Active Regions.* Jonathan P. Stewart, Andrew H. Liu, Yoojoong Choi, and Mehmet B. Baturay. December 2001.

PEER 2001/09 *Ground Motion Evaluation Procedures for Performance-Based Design.* Jonathan P. Stewart, Shyh-Jeng Chiou, Jonathan D. Bray, Robert W. Graves, Paul G. Somerville, and Norman A. Abrahamson. September 2001.

PEER 2001/08 *Experimental and Computational Evaluation of Reinforced Concrete Bridge Beam-Column Connections for Seismic Performance*. Clay J. Naito, Jack P. Moehle, and Khalid M. Mosalam. November 2001.

PEER 2001/07 *The Rocking Spectrum and the Shortcomings of Design Guidelines.* Nicos Makris and Dimitrios Konstantinidis. August 2001.

PEER 2001/06 *Development of an Electrical Substation Equipment Performance Database for Evaluation of Equipment Fragilities*. Thalia Agnanos. April 1999.

PEER 2001/05 *Stiffness Analysis of Fiber-Reinforced Elastomeric Isolators.* Hsiang-Chuan Tsai and James M. Kelly. May 2001.

PEER 2001/04 *Organizational and Societal Considerations for Performance-Based Earthquake Engineering.* Peter J. May. April 2001.

PEER 2001/03 *A Modal Pushover Analysis Procedure to Estimate Seismic Demands for Buildings: Theory and Preliminary Evaluation.* Anil K. Chopra and Rakesh K. Goel. January 2001.

PEER 2001/02 *Seismic Response Analysis of Highway Overcrossings Including Soil-Structure Interaction.* Jian Zhang and Nicos Makris. March 2001.

PEER 2001/01 *Experimental Study of Large Seismic Steel Beam-to-Column Connections.* Egor P. Popov and Shakhzod M. Takhirov. November 2000.

PEER 2000/10 *The Second U.S.-Japan Workshop on Performance-Based Earthquake Engineering Methodology for Reinforced Concrete Building Structures.* March 2000.

PEER 2000/09 *Structural Engineering Reconnaissance of the August 17, 1999 Earthquake: Kocaeli (Izmit), Turkey*. Halil Sezen, Kenneth J. Elwood, Andrew S. Whittaker, Khalid Mosalam, John J. Wallace, and John F. Stanton. December 2000.

PEER 2000/08 *Behavior of Reinforced Concrete Bridge Columns Having Varying Aspect Ratios and Varying Lengths of Confinement.* Anthony J. Calderone, Dawn E. Lehman, and Jack P. Moehle. January 2001.

PEER 2000/07 *Cover-Plate and Flange-Plate Reinforced Steel Moment-Resisting Connections.* Taejin Kim, Andrew S. Whittaker, Amir S. Gilani, Vitelmo V. Bertero, and Shakhzod M. Takhirov. September 2000.

PEER 2000/06 *Seismic Evaluation and Analysis of 230-kV Disconnect Switches.* Amir S. J. Gilani, Andrew S. Whittaker, Gregory L. Fenves, Chun-Hao Chen, Henry Ho, and Eric Fujisaki. July 2000.

PEER 2000/05 *Performance-Based Evaluation of Exterior Reinforced Concrete Building Joints for Seismic Excitation.* Chandra Clyde, Chris P. Pantelides, and Lawrence D. Reaveley. July 2000.

PEER 2000/04 *An Evaluation of Seismic Energy Demand: An Attenuation Approach.* Chung-Che Chou and Chia-Ming Uang. July 1999.

PEER 2000/03 *Framing Earthquake Retrofitting Decisions: The Case of Hillside Homes in Los Angeles.* Detlof von Winterfeldt, Nels Roselund, and Alicia Kitsuse. March 2000.

PEER 2000/02 *U.S.-Japan Workshop on the Effects of Near-Field Earthquake Shaking.* Andrew Whittaker, ed. July 2000.

PEER 2000/01 *Further Studies on Seismic Interaction in Interconnected Electrical Substation Equipment.* Armen Der Kiureghian, Kee-Jeung Hong, and Jerome L. Sackman. November 1999.

PEER 1999/14 *Seismic Evaluation and Retrofit of 230-kV Porcelain Transformer Bushings*. Amir S. Gilani, Andrew S. Whittaker, Gregory L. Fenves, and Eric Fujisaki. December 1999.

PEER 1999/13 *Building Vulnerability Studies: Modeling and Evaluation of Tilt-up and Steel Reinforced Concrete Buildings.* John W. Wallace, Jonathan P. Stewart, and Andrew S. Whittaker, editors. December 1999.

PEER 1999/12 *Rehabilitation of Nonductile RC Frame Building Using Encasement Plates and Energy-Dissipating Devices.* Mehrdad Sasani, Vitelmo V. Bertero, James C. Anderson. December 1999.

PEER 1999/11 *Performance Evaluation Database for Concrete Bridge Components and Systems under Simulated Seismic Loads.* Yael D. Hose and Frieder Seible. November 1999.

PEER 1999/10 *U.S.-Japan Workshop on Performance-Based Earthquake Engineering Methodology for Reinforced Concrete Building Structures.* December 1999.

PEER 1999/09 *Performance Improvement of Long Period Building Structures Subjected to Severe Pulse-Type Ground Motions*. James C. Anderson, Vitelmo V. Bertero, and Raul Bertero. October 1999.

PEER 1999/08 *Envelopes for Seismic Response Vectors*. Charles Menun and Armen Der Kiureghian. July 1999.

PEER 1999/07 *Documentation of Strengths and Weaknesses of Current Computer Analysis Methods for Seismic Performance of Reinforced Concrete Members*. William F. Cofer. November 1999.

PEER 1999/06 *Rocking Response and Overturning of Anchored Equipment under Seismic Excitations.* Nicos Makris and Jian Zhang. November 1999.

PEER 1999/05 *Seismic Evaluation of 550 kV Porcelain Transformer Bushings.* Amir S. Gilani, Andrew S. Whittaker, Gregory L. Fenves, and Eric Fujisaki. October 1999.

PEER 1999/04 *Adoption and Enforcement of Earthquake Risk-Reduction Measures.* Peter J. May, Raymond J. Burby, T. Jens Feeley, and Robert Wood.

PEER 1999/03 *Task 3 Characterization of Site Response General Site Categories*. Adrian Rodriguez-Marek, Jonathan D. Bray, and Norman Abrahamson. February 1999.

PEER 1999/02 *Capacity-Demand-Diagram Methods for Estimating Seismic Deformation of Inelastic Structures: SDF Systems*. Anil K. Chopra and Rakesh Goel. April 1999.

PEER 1999/01 *Interaction in Interconnected Electrical Substation Equipment Subjected to Earthquake Ground Motions.* Armen Der Kiureghian, Jerome L. Sackman, and Kee-Jeung Hong. February 1999.

PEER 1998/08 *Behavior and Failure Analysis of a Multiple-Frame Highway Bridge in the 1994 Northridge Earthquake.* Gregory L. Fenves and Michael Ellery. December 1998.

PEER 1998/07 *Empirical Evaluation of Inertial Soil-Structure Interaction Effects.* Jonathan P. Stewart, Raymond B. Seed, and Gregory L. Fenves. November 1998.

PEER 1998/06 *Effect of Damping Mechanisms on the Response of Seismic Isolated Structures.* Nicos Makris and Shih-Po Chang. November 1998.

PEER 1998/05 *Rocking Response and Overturning of Equipment under Horizontal Pulse-Type Motions.* Nicos Makris and Yiannis Roussos. October 1998.

PEER 1998/04 *Pacific Earthquake Engineering Research Invitational Workshop Proceedings, May 14–15, 1998: Defining the Links between Planning, Policy Analysis, Economics and Earthquake Engineering.* Mary Comerio and Peter Gordon. September 1998.

PEER 1998/03 *Repair/Upgrade Procedures for Welded Beam to Column Connections.* James C. Anderson and Xiaojing Duan. May 1998.

PEER 1998/02 *Seismic Evaluation of 196 kV Porcelain Transformer Bushings.* Amir S. Gilani, Juan W. Chavez, Gregory L. Fenves, and Andrew S. Whittaker. May 1998.

PEER 1998/01 *Seismic Performance of Well-Confined Concrete Bridge Columns.* Dawn E. Lehman and Jack P. Moehle. December 2000.

ONLINE REPORTS

The following PEER reports are available by Internet only at http://peer.berkeley.edu/publications/peer_reports.html

PEER 2012/101 *Mechanics of Fiber Reinforced Bearings.* James M. Kelly and Andrea Calabrese. February 2012.

PEER 2011/107 *Nonlinear Site Response and Seismic Compression at Vertical Array Strongly Shaken by 2007 Niigata-ken Chuetsu-oki Earthquake.* Eric Yee, Jonathan P. Stewart, and Kohji Tokimatsu. December 2011.

PEER 2011/106 *Self Compacting Hybrid Fiber Reinforced Concrete Composites for Bridge Columns.* Pardeep Kumar, Gabriel Jen, William Trono, Marios Panagiotou, and Claudia Ostertag. September 2011.

PEER 2011/105 *Stochastic Dynamic Analysis of Bridges Subjected to Spacially Varying Ground Motions.* Katerina Konakli and Armen Der Kiureghian. August 2011.

PEER 2011/104 *Design and Instrumentation of the 2010 E-Defense Four-Story Reinforced Concrete and Post-Tensioned Concrete Buildings.* Takuya Nagae, Kenichi Tahara, Taizo Matsumori, Hitoshi Shiohara, Toshimi Kabeyasawa, Susumu Kono, Minehiro Nishiyama (Japanese Research Team) and John Wallace, Wassim Ghannoum, Jack Moehle, Richard Sause, Wesley Keller, Zeynep Tuna (U.S. Research Team). June 2011.

PEER 2011/103 *In-Situ Monitoring of the Force Output of Fluid Dampers: Experimental Investigation.* Dimitrios Konstantinidis, James M. Kelly, and Nicos Makris. April 2011.

PEER 2011/102 *Ground-motion prediction equations 1964 - 2010.* John Douglas. April 2011.

PEER 2011/101 *Report of the Eighth Planning Meeting of NEES/E-Defense Collaborative Research on Earthquake Engineering.* Convened by the Hyogo Earthquake Engineering Research Center (NIED), NEES Consortium, Inc. February 2011.

PEER 2010/111 *Modeling and Acceptance Criteria for Seismic Design and Analysis of Tall Buildings.* Task 7 Report for the Tall Buildings Initiative - Published jointly by the Applied Technology Council. October 2010.

PEER 2010/110 *Seismic Performance Assessment and Probabilistic Repair Cost Analysis of Precast Concrete Cladding Systems for Multistory Buildlings.* Jeffrey P. Hunt and Božidar Stojadinovic. November 2010.

PEER 2010/109 *Report of the Seventh Joint Planning Meeting of NEES/E-Defense Collaboration on Earthquake Engineering. Held at the E-Defense, Miki, and Shin-Kobe, Japan, September 18–19, 2009.* August 2010.

PEER 2010/108 *Probabilistic Tsunami Hazard in California.* Hong Kie Thio, Paul Somerville, and Jascha Polet, preparers. October 2010.

PEER 2010/107 *Performance and Reliability of Exposed Column Base Plate Connections for Steel Moment-Resisting Frames.* Ady Aviram, Božidar Stojadinovic, and Armen Der Kiureghian. August 2010.

PEER 2010/106 *Verification of Probabilistic Seismic Hazard Analysis Computer Programs.* Patricia Thomas, Ivan Wong, and Norman Abrahamson. May 2010.

PEER 2010/105 *Structural Engineering Reconnaissance of the April 6, 2009, Abruzzo, Italy, Earthquake, and Lessons Learned.* M. Selim Günay and Khalid M. Mosalam. April 2010.

PEER 2010/104 *Simulating the Inelastic Seismic Behavior of Steel Braced Frames, Including the Effects of Low-Cycle Fatigue.* Yuli Huang and Stephen A. Mahin. April 2010.

PEER 2010/103 *Post-Earthquake Traffic Capacity of Modern Bridges in California.* Vesna Terzic and Božidar Stojadinović. March 2010.

PEER 2010/102 *Analysis of Cumulative Absolute Velocity (CAV) and JMA Instrumental Seismic Intensity (I_{JMA}) Using the PEER–NGA Strong Motion Database.* Kenneth W. Campbell and Yousef Bozorgnia. February 2010.

PEER 2010/101 *Rocking Response of Bridges on Shallow Foundations.* Jose A. Ugalde, Bruce L. Kutter, and Boris Jeremic. April 2010.

PEER 2009/109 *Simulation and Performance-Based Earthquake Engineering Assessment of Self-Centering Post-Tensioned Concrete Bridge Systems.* Won K. Lee and Sarah L. Billington. December 2009.

PEER 2009/108 *PEER Lifelines Geotechnical Virtual Data Center.* J. Carl Stepp, Daniel J. Ponti, Loren L. Turner, Jennifer N. Swift, Sean Devlin, Yang Zhu, Jean Benoit, and John Bobbitt. September 2009.

PEER 2009/107 *Experimental and Computational Evaluation of Current and Innovative In-Span Hinge Details in Reinforced Concrete Box-Girder Bridges: Part 2: Post-Test Analysis and Design Recommendations.* Matias A. Hube and Khalid M. Mosalam. December 2009.

PEER 2009/106 *Shear Strength Models of Exterior Beam-Column Joints without Transverse Reinforcement.* Sangjoon Park and Khalid M. Mosalam. November 2009.

PEER 2009/105 *Reduced Uncertainty of Ground Motion Prediction Equations through Bayesian Variance Analysis.* Robb Eric S. Moss. November 2009.

PEER 2009/104 *Advanced Implementation of Hybrid Simulation.* Andreas H. Schellenberg, Stephen A. Mahin, Gregory L. Fenves. November 2009.

PEER 2009/103 *Performance Evaluation of Innovative Steel Braced Frames.* T. Y. Yang, Jack P. Moehle, and Božidar Stojadinovic. August 2009.

PEER 2009/102 *Reinvestigation of Liquefaction and Nonliquefaction Case Histories from the 1976 Tangshan Earthquake.* Robb Eric Moss, Robert E. Kayen, Liyuan Tong, Songyu Liu, Guojun Cai, and Jiaer Wu. August 2009.

PEER 2009/101 *Report of the First Joint Planning Meeting for the Second Phase of NEES/E-Defense Collaborative Research on Earthquake Engineering.* Stephen A. Mahin et al. July 2009.

PEER 2008/104 *Experimental and Analytical Study of the Seismic Performance of Retaining Structures.* Linda Al Atik and Nicholas Sitar. January 2009.

PEER 2008/103 *Experimental and Computational Evaluation of Current and Innovative In-Span Hinge Details in Reinforced Concrete Box-Girder Bridges. Part 1: Experimental Findings and Pre-Test Analysis.* Matias A. Hube and Khalid M. Mosalam. January 2009.

PEER 2008/102 *Modeling of Unreinforced Masonry Infill Walls Considering In-Plane and Out-of-Plane Interaction.* Stephen Kadysiewski and Khalid M. Mosalam. January 2009.

PEER 2008/101 *Seismic Performance Objectives for Tall Buildings.* William T. Holmes, Charles Kircher, William Petak, and Nabih Youssef. August 2008.

PEER 2007/101 *Generalized Hybrid Simulation Framework for Structural Systems Subjected to Seismic Loading.* Tarek Elkhoraibi and Khalid M. Mosalam. July 2007.

PEER 2007/100 *Seismic Evaluation of Reinforced Concrete Buildings Including Effects of Masonry Infill Walls.* Alidad Hashemi and Khalid M. Mosalam. July 2007.

The Pacific Earthquake Engineering Research Center (PEER) is a multi-institutional research and education center with headquarters at the University of California, Berkeley. Investigators from over 20 universities, several consulting companies, and researchers at various state and federal government agencies contribute to research programs focused on performance-based earthquake engineering.

These research programs aim to identify and reduce the risks from major earthquakes to life safety and to the economy by including research in a wide variety of disciplines including structural and geotechnical engineering, geology/seismology, lifelines, transportation, architecture, economics, risk management, and public policy.

PEER is supported by federal, state, local, and regional agencies, together with industry partners.

PEER Core Institutions:
University of California, Berkeley (Lead Institution)
California Institute of Technology
Oregon State University
Stanford University
University of California, Davis
University of California, Irvine
University of California, Los Angeles
University of California, San Diego
University of Southern California
University of Washington

PEER reports can be ordered at http://peer.berkeley.edu/publications/peer_reports.html or by contacting

Pacific Earthquake Engineering Research Center
University of California, Berkeley
325 Davis Hall, mail code 1792
Berkeley, CA 94720-1792
Tel: 510-642-3437
Fax: 510-642-1655
Email: peer_editor@berkeley.edu

ISSN 1547-0587X